EPIGENETIC REGULATION IN CARDIOVASCULAR DISEASES

EDITED BY: Zhihua Wang, Indulekha C. L. Pillai, Christoph D. Rau and Suowen Xu

PUBLISHED IN: Frontiers in Cardiovascular Medicine, Frontiers in Genetics and Frontiers in Cell and Developmental Biology

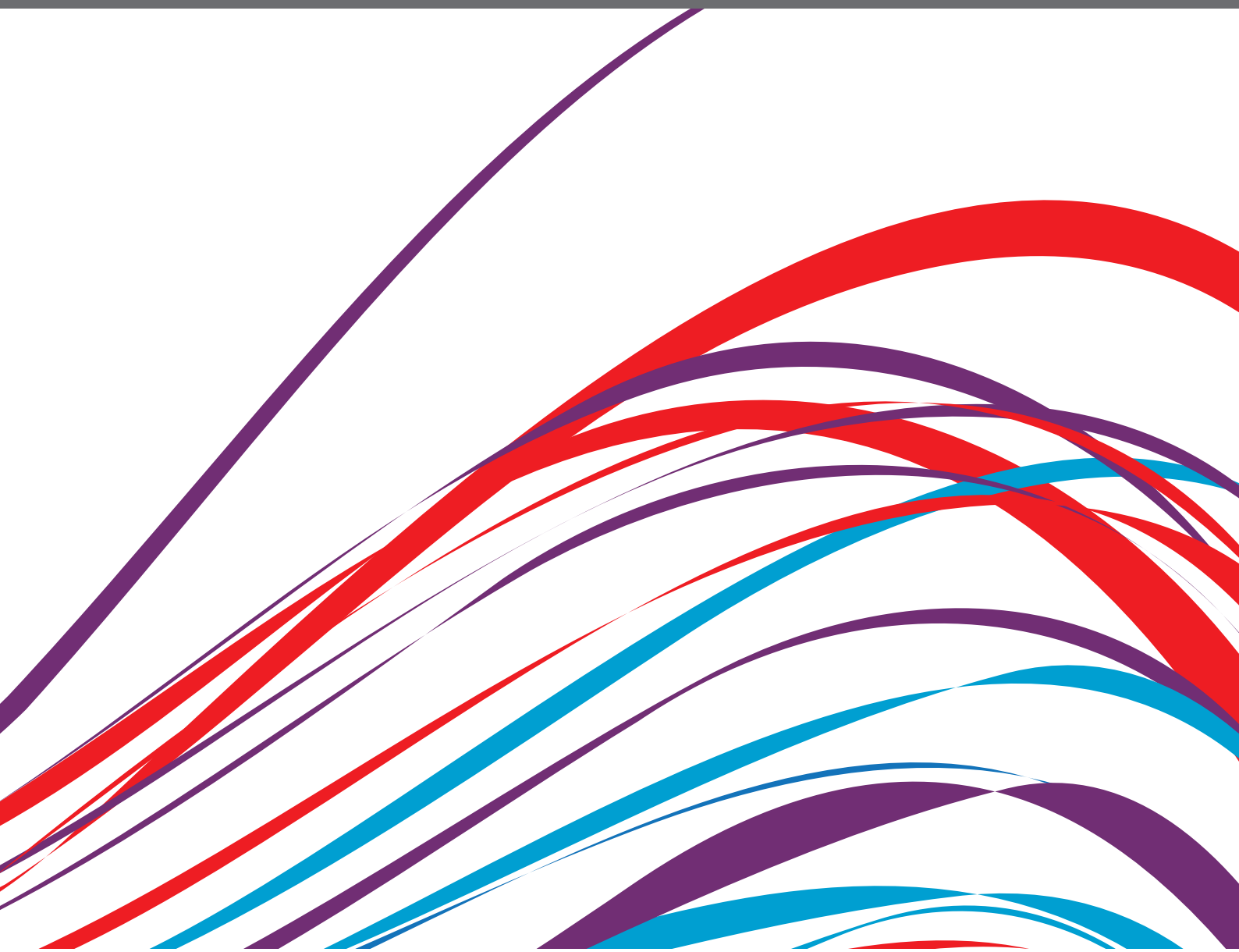

frontiers Research Topics

frontiers

ISSN 1664-8714
ISBN 978-2-88974-416-9
DOI 10.3389/978-2-88974-416-9

About Frontiers

Frontiers is more than just an open-access publisher of scholarly articles: it is a pioneering approach to the world of academia, radically improving the way scholarly research is managed. The grand vision of Frontiers is a world where all people have an equal opportunity to seek, share and generate knowledge. Frontiers provides immediate and permanent online open access to all its publications, but this alone is not enough to realize our grand goals.

Frontiers Journal Series

The Frontiers Journal Series is a multi-tier and interdisciplinary set of open-access, online journals, promising a paradigm shift from the current review, selection and dissemination processes in academic publishing. All Frontiers journals are driven by researchers for researchers; therefore, they constitute a service to the scholarly community. At the same time, the Frontiers Journal Series operates on a revolutionary invention, the tiered publishing system, initially addressing specific communities of scholars, and gradually climbing up to broader public understanding, thus serving the interests of the lay society, too.

Dedication to Quality

Each Frontiers article is a landmark of the highest quality, thanks to genuinely collaborative interactions between authors and review editors, who include some of the world's best academicians. Research must be certified by peers before entering a stream of knowledge that may eventually reach the public - and shape society; therefore, Frontiers only applies the most rigorous and unbiased reviews.
Frontiers revolutionizes research publishing by freely delivering the most outstanding research, evaluated with no bias from both the academic and social point of view. By applying the most advanced information technologies, Frontiers is catapulting scholarly publishing into a new generation.

What are Frontiers Research Topics?

Frontiers Research Topics are very popular trademarks of the Frontiers Journals Series: they are collections of at least ten articles, all centered on a particular subject. With their unique mix of varied contributions from Original Research to Review Articles, Frontiers Research Topics unify the most influential researchers, the latest key findings and historical advances in a hot research area! Find out more on how to host your own Frontiers Research Topic or contribute to one as an author by contacting the Frontiers Editorial Office: frontiersin.org/about/contact

EPIGENETIC REGULATION IN CARDIOVASCULAR DISEASES

Topic Editors:
Zhihua Wang, Chinese Academy of Medical Sciences and Peking Union Medical College, China
Indulekha C. L. Pillai, Amrita Vishwa Vidyapeetham University, India
Christoph D. Rau, University of North Carolina at Chapel Hilll, United States
Suowen Xu, University of Science and Technology of China, China

Citation: Wang, Z., Pillai, I. C. L., Rau, C. D., Xu, S., eds. (2022). Epigenetic Regulation in Cardiovascular Diseases. Lausanne: Frontiers Media SA.
doi: 10.3389/978-2-88974-416-9

Table of Contents

frontiers in Cardiovascular Medicine

EDITORIAL
published: 11 January 2022
doi: 10.3389/fcvm.2021.831851

Editorial: Epigenetic Regulation in Cardiovascular Diseases

Indulekha C. L. Pillai[1], *Suowen Xu*[2], *Christoph D. Rau*[3] *and Zhihua Wang*[4,5]*

[1] Stem Cells and Regenerative Biology Laboratory, School of Biotechnology, Amrita Vishwa Vidyapeetham, Kollam, India, [2] Institute of Endocrine and Metabolic Diseases, The First Affiliated Hospital of USTC, University of Science and Technology of China, Hefei, China, [3] Computational Medicine Program and Department of Genetics, The University of North Carolina at Chapel Hill, Chapel Hill, NC, United States, [4] Shenzhen Key Laboratory of Cardiovascular Disease, Fuwai Hospital Chinese Academy of Medical Sciences, Shenzhen, China, [5] State Key Laboratory of Cardiovascular Disease, National Center for Cardiovascular Disease, Fuwai Hospital, Chinese Academy of Medical Sciences and Peking Union Medical College, Beijing, China

Keywords: epigenetics, cardiovascular disease, DNA methylation, histone modification, non-coding RNA

Editorial on the Research Topic

Epigenetic Regulation in Cardiovascular Diseases

Cardiovascular disease (CVD) is the leading cause of death globally. Progress in the diagnosis, prevention, and treatment of CVD is contingent on the advancement of our knowledge to explain the complex pathophysiology underlying CVD in which gene expression re-programming plays a fundamental role. Emerging evidence highlights the impact of epigenetic regulation on the transition of gene expression patterns from physiological to pathological states. Epigenetics, originally defined as stably heritable phenotypes resulting from changes in a chromosome without alterations in the DNA sequence, is now more broadly understood to encompass any modification to DNA structure or function that influences phenotypes related to development or disease other than an actual change to the sequence. The epigenetic environment of a gene is mostly determined by DNA methylation, histone modifications, and chromatin remodeling. Various writers, readers, and erasers for different epigenetic marks have been discovered, and their dysfunction tightly correlates with the development of CVD. Research elucidating epigenetic regulations in this field have, in turn, promoted novel drug discoveries to treat CVD. The identification of novel epigenetic players in CVD and how they act to fine-tune molecular processes would help expand our understanding of the complexity of cardiovascular pathophysiology. In the current Research Topic, we have collected 16 high-quality studies that cover promising, recent, and novel research trends in the epigenetic regulation of CVD.

Using an integrated approach with gene expression and DNA methylation profiles, Zhang et al. identify novel biomarkers, including FN1, PTEN, and POLR3A, for coronary artery disease. Li et al. find that the co-occurrence of chronic hepatitis B and fibrosis is associated with a decrease in hepatic global DNA methylation levels in patients with non-alcoholic fatty liver disease. A review by Xu et al. summarize the roles and mechanisms of DNA methylation in vascular aging and related diseases. Furthermore, Ju et al. find that diabetic cardiomyopathy is accompanied by global changes in m^6A RNA modification, possibly due to the alteration of FTO expression.

By combining RNA-seq with ChIP-seq, Wang et al. systematically investigated the genome-wide profiles of five histone marks (H3K27ac, H3K9ac, H3K4me3, H3K9me3, and H3K27me3) in the early stage of myocardial infarction, and clarify a H3K27ac-related gene expression pattern associated with angiogenesis. Greenway et al. profile histone modification patterns in aortic tissues during abdominal aortic aneurysms formation in two distinct mouse models, angiotensin II infusion and calcium chloride overload. A review by Li et al. links epigenetic mechanisms with oxidative stress-induced ferroptosis in CVD.

OPEN ACCESS

Edited and reviewed by:
Silvio Zaina,
University of Guanajuato, Mexico

***Correspondence:**
Zhihua Wang
treerwang@163.com

Specialty section:
This article was submitted to Cardiovascular Genetics and Systems Medicine, a section of the journal Frontiers in Cardiovascular Medicine

Received: *09 December 2021*
Accepted: *17 December 2021*
Published: *11 January 2022*

Citation:
Pillai ICL, Xu S, Rau CD and Wang Z (2022) Editorial: Epigenetic Regulation in Cardiovascular Diseases. Front. Cardiovasc. Med. 8:831851. doi: 10.3389/fcvm.2021.831851

By screening patients with atherosclerosis, Gao et al. identify miR-135a-5p as a protective factor against atherosclerosis development by directly targeting JAK2. Wang et al. identify novel non-coding RNAs, especially a class of snoRNAs, being dynamically associated with a H3K27 methyltransferase EZH2 at the early phase of cardiac hypertrophy. A review by Saadat et al. summarizes emerging evidence that non-coding RNAs, including miRNAs, circRNAs and lncRNAs, modify the TGF-β/Smad Signaling during the progression of cardiac fibrosis.

Wei et al. sequenced individuals with or without hypertension from an ethnic minority of China, and finds that haplotypes of CYP17A1 and ATP2B1 are correlated with hypertension risks. Yang et al. find that GRB10 rs1800504 polymorphism is associated with the risk of coronary heart disease in patients with type 2 diabetes mellitus. Liu et al. unveil a causal effect of statin use on type 2 diabetes and related traits through epigenetic mechanisms, specifically, DNA methylation at cg06500161 of ABCG1. Kashyap et al. find that antiretroviral drug treatment significantly reduces acetylation at H3K9 and H3K27 and promotes methylation at H3K9 and H3K27 possibly through regulating the expression of SIRT1, SUV39H1, and EZH2. A review by Chen et al. presents an updated summary on the roles of HDACs and HDAC inhibitors in vascular dysfunction with an emphasis on therapeutic targets and agents in atherosclerotic cardiovascular diseases. Finally, Ahmed et al. develops a network-based approach using a novel algorithm, IVI (Integrated Value of Influence), to dissect genes with important roles in cardiovascular disease and chronic kidney disease.

Taken together, the present Research Topic represents an important source of up-to-date information, covering most aspects of epigenetics in the CVD field with a broad view from basic research to clinical trials and from fundamental mechanisms to precision medicine. More comprehensive knowledge based on these discoveries may bring about new diagnostic and therapeutic approaches.

AUTHOR CONTRIBUTIONS

All authors listed have made an equal, substantial, direct, and intellectual contribution to the work and approved it for publication.

Conflict of Interest: The authors declare that the research was conducted in the absence of any commercial or financial relationships that could be construed as a potential conflict of interest.

Publisher's Note: All claims expressed in this article are solely those of the authors and do not necessarily represent those of their affiliated organizations, or those of the publisher, the editors and the reviewers. Any product that may be evaluated in this article, or claim that may be made by its manufacturer, is not guaranteed or endorsed by the publisher.

frontiers in Genetics

ORIGINAL RESEARCH
published: 16 June 2020
doi: 10.3389/fgene.2020.00622

Statin Use Associates With Risk of Type 2 Diabetes via Epigenetic Patterns at *ABCG1*

*Yuwei Liu[1,2], Yu Shen[2], Tao Guo[2,3], Laurence D. Parnell[4], Kenneth E. Westerman[2], Caren E. Smith[2], Jose M. Ordovas[2,5,6] and Chao-Qiang Lai[4]**

[1] School of Public Health, Fudan University, Shanghai, China, [2] Nutrition and Genomics Laboratory, JM-USDA Human Nutrition Research Center on Aging at Tufts University, Boston, MA, United States, [3] Department of Cardiology, Zhongnan Hospital of Wuhan University, Wuhan, China, [4] USDA Agricultural Research Service, Nutrition and Genomics Laboratory, JM-USDA Human Nutrition Research Center on Aging at Tufts University, Boston, MA, United States, [5] IMDEA Food Institute, CEI UAM + CSIC, Madrid, Spain, [6] Centro Nacional de Investigaciones Cardiovasculares (CNIC), Madrid, Spain

OPEN ACCESS

Edited by:
Suowen Xu,
University of Science and Technology of China, China

Reviewed by:
Wilfried Le Goff,
Institut National de la Santé et de la Recherche Médicale (INSERM), France
Line Hjort,
Rigshospitalet, Denmark
Michinori Matsuo,
Kyoto Women's University, Japan

***Correspondence:**
Chao-Qiang Lai
chaoqiang.lai@usda.gov

Specialty section:
This article was submitted to Epigenomics and Epigenetics, a section of the journal Frontiers in Genetics

Received: 18 February 2020
Accepted: 22 May 2020
Published: 16 June 2020

Citation:
Liu Y, Shen Y, Guo T, Parnell LD, Westerman KE, Smith CE, Ordovas JM and Lai C-Q (2020) Statin Use Associates With Risk of Type 2 Diabetes via Epigenetic Patterns at ABCG1. Front. Genet. 11:622. doi: 10.3389/fgene.2020.00622

Statin is the medication most widely prescribed to reduce plasma cholesterol levels. Yet, how the medication contributes to diabetes risk and impaired glucose metabolism is not clear. This study aims to examine the epigenetic mechanisms of *ABCG1* through which statin use associates with risk of type 2 diabetes. We determined the association between the statin use, DNA methylation at *ABCG1* and type 2 diabetes/glycemic traits in the Framingham Heart Study Offspring (FHS, $n = 2741$), with validation in the Women's Health Initiative Study (WHI, $n = 2020$). The causal effect of statin use on the risk of type 2 diabetes was examined using a two-step Mendelian randomization approach. Next, based on transcriptome analysis, we determined the links between the medication-associated epigenetic status of *ABCG1* and biological pathways on the pathogenesis of type 2 diabetes. Our results showed that DNA methylation levels at cg06500161 of *ABCG1* were positively associated with the use of statin, type 2 diabetes and related traits (fasting glucose and insulin) in FHS and WHI. Two-step Mendelian randomization suggested a causal effect of statin use on type 2 diabetes and related traits through epigenetic mechanisms, specifically, DNA methylation at cg06500161. Our results highlighted that gene expression of *ABCG1, ABCA1* and *ACSL3*, involved in both cholesterol metabolism and glycemic pathways, was inversely associated with statin use, CpG methylation, and diabetic signatures. We concluded that DNA methylation site cg06500161 at *ABCG1* is a mediator of the association between statins and risk of type 2 diabetes.

Keywords: statin, *ABCG1*, methylation, type 2 diabetes, cg06500161

INTRODUCTION

Dyslipidemia is a major risk factor for cardiovascular disease (CVD), which remains the leading cause of mortality worldwide. Lipid-lowering drugs, like statins, are the medication most widely prescribed to reduce plasma cholesterol levels (Chou et al., 2016; Zhan et al., 2018). With common and long-term use of such medications, a number of adverse effects have been reported. Specifically,

statins have been associated with liver damage (Aguirre et al., 2013), muscle discomfort (Pirillo and Catapano, 2015) and diabetes (Kim D. W. et al., 2019; Kim Y. S. et al., 2019). Yet, how the medication contributes to diabetes risk and impaired glucose metabolism is not clear.

Type 2 diabetes is a complex disease that results from genetic and environmental factors and their interactions. Environmental factors, including diet, lifestyle and medications, may modify epigenetic status affecting the risk of type 2 diabetes (Vickers, 2014; Nilsson and Ling, 2017). Epigenome-wide association studies in several cohorts have shown strong associations between DNA methylation at CpG sites in ATP binding cassette subfamily G member 1 (*ABCG1*) and risk of type 2 diabetes (Hidalgo et al., 2014; Dayeh et al., 2016; Davegardh et al., 2018). ABCG1, a member of the ATP-binding cassette (ABC) protein family, functions in removing excess cholesterol from peripheral tissues and transporting it to the liver (Matsuo, 2010). *ABCG1* expression has been reported to be regulated by statins in Caco-2 cells and COPD patients (Genvigir et al., 2011; Obeidat et al., 2015). Thus, we hypothesized statin use induces epigenetic changes that affect gene expression to increase the risk of type 2 diabetes.

This study aims to characterize the association between the use of statins, DNA methylation at *ABCG1* and glycemic traits. For this purpose, we used the Framingham Heart Study Offspring (FHS) as the discovery population and validated the findings in the Women's Health Initiative Study (WHI). We then determined if statin use had causal effects on the risk of type 2 diabetes using a two-step Mendelian randomization approach (Relton and Davey Smith, 2012; Caramaschi et al., 2017; Zhu et al., 2018). Furthermore, we determined whether altered DNA methylation at CpGs contributed to specific metabolic pathways on the pathogenesis of type 2 diabetes.

MATERIALS AND METHODS

Framingham Heart Study (FHS)

The FHS follows several community dwelling generations of participants recruited in Framingham, MA, since 1948 (Dawber et al., 1951). In 1971, 5124 offspring, self-identified as European ancestry, from the original cohort and spouses were recruited (Kannel et al., 1979). In exam 8 (2005–2008) of this offspring cohort, participants completed a comprehensive set of dietary and health assessment questionnaires. The use of statins was obtained from the questionnaires. Statin users were defined as participants who took any type of statins, whereas non-statin users were those who did not use statin, but might or might not have taken other lipid-lowering drugs. LDL-C was estimated using Friedewald equation (Lindsey et al., 2004). DNA methylome and transcriptome analyses were performed on blood samples collected from 2741 participants (Marioni et al., 2015). These data were obtained from dbGaP (accession: phs000007.v29.p10; downloaded on September 27, 2017).

Women's Health Initiative Study (WHI)

Starting from 1993, the WHI study recruited over 160,000 women into a long-term national health study that focuses on strategies for preventing heart disease, breast and colorectal cancer, and osteoporosis in postmenopausal women The Women's Health Initiative Study Group (1998). Participants (n = 2020) from a combined case-control and pseudo-case-cohort were included in this study. Blood samples used for measurement of DNA methylation and clinical biochemistry were taken at Exam 1. Data was requested from dbGaP (accession: phs000200.v11.p3; downloaded on September 27, 2017). At Exam 1, participants also completed a comprehensive set of dietary and health assessment questionnaires. The use of statins was obtained from the questionnaires. The same definition of statin users and non-statin users in FHS was applied to WHI.

DNA Methylation Analysis

Raw IDAT files of DNA methylation analysis were quality-controlled and processed as described (Hidalgo et al., 2014; Marioni et al., 2015; Lai et al., 2018). Briefly, we used a β score to measure methylation signal as the proportion of the total methylation-specific signal, and the detection P-value as the probability that the total intensity for a given probe fell within the background signal intensity. Then, we excluded any CpG probes with a detection P-value > 0.01 and missing sample percentage $> 1.5\%$, or $> 10\%$ of samples lacking sufficient intensity. We performed normalization on the filtered β scores using the ComBat package in R (Morris et al., 2014). Principal components were calculated on the β scores of samples that passed quality control using the prcomp function in R.

Genotyping

Genotypes for 2176 individuals from FHS were requested from dbGaP (accession: phs000342.v18.p11) as part of the NHLBI SNP Health Association Resource (SHARe) project, with initial QC and imputation having been performed previously. Briefly, approximately 500,000 SNPs were genotyped on the Affymetrix500k and Affymetrix50k chips and filtered for Hardy-Weinberg equilibrium, call rate, and minor allele frequency. These genotypes were then phased using MACH and imputed to the November 2010 release of 1000 Genomes using Minimac. Additional filters were applied to the imputed dosage data as follows: only samples associated with subjects who also had methylation data available were retained, and SNPs were filtered for an imputation quality score (R^2) > 0.9. Dosages were converted to hard-calls if the dosage was within 0.2 of an integer allele count (0/1/2) and otherwise were set as missing.

Genotypes for 1966 individuals from WHI were available from dbGaP (accession: phs000746.v2.p3) as part of an imputation and harmonization effort across six GWAS sub-studies. Quality control and preprocessing steps were applied in each of the sub-studies prior to imputation (details available at dbGaP). Genotypes were then phased and aligned to the 1000 Genomes reference panel using BEAGLE and Minimac. The imputed dosages of 5,298,674 SNPs were retrieved from dbGaP and filtered for imputation quality score > 0.3, converted to hard-calls within 0.1 of an integer allele count (otherwise set as missing), and merged across sub-studies.

For both genotyped cohorts, SNP IDs, loci, and allelic information were annotated using the 1000 Genomes Phase

3 download from dbSNP (download date: April 13, 2018). Genotype processing was performed using PLINK 1.9 and 2.0 [URL[1]; (Chang et al., 2015)].

Transcriptome Analysis

We obtained FHS transcriptome data from dbGaP under accession phe00002.v6. Transcriptome analysis was conducted in exam 8 using the Affymetrix Human Exon 1.0 ST array for 17873 probes with mRNA from whole blood samples collected from 1616 participants from the Offspring Cohort after overnight fasting. Detailed descriptions of transcriptome analysis procedures are available (Katz et al., 2006).

Statistical Methods

Associations Between Statin Use and DNA Methylation of ABCG1

Focusing on *ABCG1*, we investigated all 31 CpG sites (cg00177237, cg00222799, cg01176028, cg01289965, cg01881899, cg02241241, cg02316713, cg02370100, cg02473680, cg05046272, cg0544165, cg05639842, cg06030219, cg06500161, cg07397296, cg07875759, cg08663969, cg08841829, cg10192877, cg11662315, cg14982472, cg16068063, cg17526396, cg20214535, cg21410080, cg23245768, cg25615529, cg26519745, cg26767954, cg26768067, cg27243685) that are in or near the *ABCG1* gene. In the discovery stage in FHS, we modeled the association between statin use and methylation score at these *ABCG1* CpG sites in (i) all participants and (ii) the participants who were not using antidiabetic medications using a generalized linear model, adjusting for family relationship, sex, age, smoking, alcohol and cell-type heterogeneity (basic model). Moreover, we used an LDL-C and TG adjusted model in which low density lipoprotein cholesterol (LDL-C) and triglycerides (TG) were added to the basic model. The analysis was implemented by the log link function in a GENMOD Procedure in SAS studio (University Edition). We fitted the identical model to the replication samples in WHI using the statistically significant CpG sites identified in FHS (*P*-value cut-off was set as 1.6E-3, Bonferroni correction), where adjustment for family relationship and gender were not needed, as WHI is an un-related female cohort.

Correlations Between DNA Methylation of ABCG1 and Diabetic Traits

In the discovery stage, we examined the association between methylation of *ABCG1* CpG that were associated with statin use (*P*-value $<$ 1.6E-3 in basic model) in both cohorts for diabetes-related traits. A generalized linear model was implemented with methylation measures as dependent variables and type 2 diabetes (selection criteria: fasting glucose $\geq$ 126 mg/dL, or use of diabetic medication) as the predictor using logit link function in a GENMOD Procedure in SAS, adjusting for family relationship, sex, age, smoking, alcohol use and cell-type heterogeneity. Participants without diabetes were included for a similar association study in the Log-Linear Model of GENMOD Procedure with methylation measures as dependent variables, while log-transformed glucose or insulin levels were used as predictors, adjusting for family relationship, sex, age, smoking, alcohol use and cell-type heterogeneity. We fitted the identical models in the replication samples in the WHI study. As noted previously, family relationship and gender were not adjusted in WHI because it is an un-related female cohort.

Two-Step Mendelian Randomization (MR) Approach

We performed a two-step MR approach to test the causal role of statin use on diabetic traits (fasting glucose and insulin) in the non-diabetic population and type 2 diabetes in the whole population. The first step MR analysis was implemented in the FHS study with the second in the WHI cohort using GSMR (Generalized Summary-data-based on Mendelian randomization) in GCTA (Zhu et al., 2018). In the first step, genome-wide SNPs were first tested for association with the statin use (exposure) and cg06500161 methylation (outcome) using a mixed linear model association (GCTA-MLMA), adjusting for sex, age, smoking, alcohol use, cell-type heterogeneity, and family relationship (Yang et al., 2014). These tests were repeated in the LDL-C and TG adjusted models. Then, the summary data from MLMA were used to estimate the causal effect of statin use on cg06500161 using GSMR. We selected the genome-wide significant SNPs (*P*-value $<$ 5E-5) associated with the exposures as the instrumental variable in the basic and LDL-C and TG adjusted models, respectively. We used the HEIDI-outlier approach to remove SNPs that have effects on both the exposures and the outcomes. The remaining SNPs were then tested for the association with the outcomes for causal effect.

In the second step, SNPs were firstly tested in the identical models for association with cg06500161 methylation (exposure) as well as diabetes, log-transformed fasting glucose and insulin levels (outcomes), separately. In this step, the sex, age, smoking, and alcohol use, were adjusted. Next, the summary data from MLMA were utilized to calculate the causal effect of cg06500161 on type 2 diabetes and related traits using GSMR. We selected the genome-wide significant SNPs (*P*-value $<$ 5E-5) associated with the exposures as the instrumental variable in diabetes, glucose and insulin models, respectively. We also used the HEIDI-outlier approach to remove SNPs that have effects on both the exposures and the outcomes. The remaining SNPs were then tested for the association with the outcomes for causal effect. Then the causal effects of statins on type 2 diabetes and related phenotypes through cg06500161 methylation were calculated by multiplying the causal effect of statin use on cg06500161 from Step 1 and the causal effect of cg06500161 on the outcomes (type 2 diabetes and related traits) from Step 2.

Gene Sets Analysis

To uncover the connection among statins, epigenomic modification and transcriptional network, we conducted gene set enrichment analysis (GSEA) in light of the identified methylation sites in the selected non-diabetic participants of the FHS study. Firstly, we performed separate association analyses between all transcripts and statins, cg06500161 methylation, log-transformed glucose as well as insulin levels using a default mixed linear model in OSCA (OmicS-data-based Complex Trait Analysis, version 0.42), adjusting for sex, age, smoking, alcohol,

[1]https://www.cog-genomics.org/plink/2.0/

and cell-type heterogeneity in the LDL-C and TG adjusted model (Zhang et al., 2018). The CpG-associated (P-value < 0.05) genes were then evaluated for overlaps with those genes correlating (at P-value < 0.05) with statins, glucose or insulin levels. The number of overlapped genes was counted within each pathway. P-values and FDR q values were calculated for both KEGG and Reactome pathway data using GSEA with 45956 gene entries.

RESULTS

Statin Use Is Associated With ABCG1 CpG Methylation

Clinical characteristics for all participants in both FHS and WHI cohorts are listed according to statin-use status and T2D in **Table 1**. Using an independent t-test or Fisher's exact test, we examined the differences between statin and non-statin groups, excluding participants taking antidiabetic medication, and between T2D and non-T2D groups in both populations. In both cohorts (**Table 1**), participants who took statins or those with T2D, tended to have an increased risk for abnormal lipid profile, except for cholesterol (total cholesterol and LDL-C), compared to non-statin users or non-T2D participants (**Table 1**). One important observation was the percentage of T2D patients who took statin was about twice that of non-T2D participants in both FHS (56% vs 28%) and WHI (21% vs 10%). This suggests that T2D risk is strongly associated with statin use.

To examine the association of statins with *ABCG1* methylation, we examined DNA methylation of *ABCG1* on the Infinium 450K array using the FHS cohort as a discovery set, with the WHI cohort used for validation. **Table 2** lists CpGs that were associated with statin use in all participants of FHS, adjusting for age, sex, smoking, alcohol use, cell-type heterogeneity, and family relationship. After filtering out highly correlated CpG sites based on pairwise Pearson correlation tests ($r \geq 0.5$), five CpGs were significantly associated with statin use, with cg06500161 (β = 0.0320, P-value = 1.00E-32) being the most significant. After additionally adjusting for serum low density lipoprotein cholesterol (LDL-C) and total triglycerides (TG), the association remained significant for cg06500161 (β = 0.0252, P- value = 1.55E-15). We then sought replication in the WHI cohort, observing that only cg06500161 (β = 0.0143, P-value = 3.15E-3) and cg05639842 (β = 0.0484, P-value = 6.15E-3) were significantly associated with statin use (**Table 2**). Thus, both CpGs remained statistically significant in the LDL-C and TG adjusted model in both FHS and WHI (**Table 2**). We found a similar association of statin use with *ABCG1* methylation in participants who were not using antidiabetic medication in both FHS and WHI cohorts (**Table 3**).

ABCG1 CpG Methylation Is Associated With Type 2 Diabetes and Related Traits

Because epigenetic analysis of other cohorts identified associations between DNA methylation at *ABCG1* and type 2 diabetes phenotypes, we tested both cg06500161 and cg05639842 for association with type 2 diabetes in the FHS cohort. Replication was sought in the WHI cohort. We observed greater type 2 diabetes prevalence with higher DNA methylation levels at cg06500161 (β = 12.4, P-value = 1.33E-10) in FHS (**Table 4**). Similar results with cg06500161 were found in WHI (β = 11.7, P-value = 4.70E-11). However, cg05639842 was not associated with type 2 diabetes in either FHS or WHI (**Table 4**).

For the prediction of type 2 diabetes, we investigated DNA methylation at cg06500161 and cg05639842 with common risk factors for type 2 diabetes (fasting blood glucose and insulin levels) in non-diabetic participants in both cohorts. DNA methylation at cg06500161 was positively correlated with fasting glucose (β = 0.504, P-value = 1.02E-7) and insulin levels (β = 4.85, P-value = 4.44E-16) in FHS, adjusting for age, sex, smoking, alcohol, cell-type heterogeneity and family relationship, while DNA methylation at cg05639842 was not correlated with fasting glucose or insulin levels in the same model (**Table 4**). We found similar associations between cg06500161 methylation and fasting glucose (β = 0.853, P-value = 9.22E-7) and insulin levels (β = 4.05, P-value = 3.86E-21) in the WHI study (**Table 4**).

Causal Effect of Statin Use on Type 2 Diabetes and Related Traits Through Epigenetics of *ABCG1* DNA Methylation

To determine the causal effect of statin use on type 2 diabetes risk/status and its related traits through DNA methylation at cg06500161, we conducted a two-step epigenetic Mendelian randomization (MR) approach in FHS and WHI consecutively. In the first step performed in FHS, SNPs were tested for associations with statin use and cg06500161 methylation, respectively, in (a) all participants and (b) non-diabetic participants. GSMR models then were implemented based on the summary results from GWAS, adjusting for sex, age, smoking, alcohol use, and cell-type heterogeneity. In this step, SNPs that were only associated with statin use were used to calculate a genetic score as the instrumental variable. For all participants, statin use was validated as a significant causal factor with cg06500161 methylation as the outcome (basic model: β = 0.0186, P-value = 2.56E-35; LDL-C and TG adjusted model: β = 0.0157, P-value = 1.05E-19; **Table 5**). We obtained similar results in the non-diabetic participants (basic model: β = 0.0179, P-value = 9.64E-31; LDL-C and TG adjusted model: β = 0.0142, P-value = 2.12E-19; **Table 5**).

In the second step of the MR analysis, conducted in WHI, we fitted a similar basic model for associations between cg06500161 methylation and type 2 diabetes in all participants, as well as cg06500161 and fasting glucose, cg06500161 and fasting insulin in the non-diabetic participants. Similar GSMR models were also implemented (diabetes: β = 1.13, P-value = 1.16E-4; glucose: β = 0.246, P-value = 3.87E-04; insulin: β = 1.47, P-value = 4.72E-10; **Table 5**). In this GSMR model, we used 59, 79 and 79 SNPs (**Supplementary Table S1**) as the instrumental variables in diabetes, glucose and insulin models, respectively. CpG cg06500161 methylation was validated as the causal factor with type 2 diabetes, glucose and insulin as the outcomes.

TABLE 1 | Clinical characteristics of participants from the FHS and WHI studies.

	A[1]		*B*[2]	
	Statin[3]	**Non-Statin**	**T2D**[4]	**Non-T2D**
FHS				
N	654	1287	318	1858
Age, years	68.0 ± 8.2	64.6 ± 9.0*	68.7 ± 8.4	65.7 ± 8.9*
Female (%)	319(49)	766(60)*	135(43)	1055(57)*
Statin user (%)	654(100)	0*	179(56)	514(28)*
Smoker (%)	45(7)	119(9)	21(6.6)	161(9)
Drinker (%)	553(85)	1062(83)	223(70)	1554(84)*
TC (mg/dL)	167.7 ± 30.7	198.9 ± 33.8*	165.9 ± 35.1	189.0 ± 36.0*
HDL-C (mg/dL)	54.4 ± 15.0	60.7 ± 19.0*	48.8 ± 16.6	59.0 ± 17.9*
LDL-C (mg/dL)	89.6 ± 25.3	115.9 ± 29.0*	87.5 ± 28.7	107.4 ± 30.5*
TG (mg/dL)	118.5 ± 61.3	111.6 ± 63.1*	146.2 ± 91.4	112.4 ± 69.2*
Glucose (mg/dL)	103.7 ± 11.9	101.0 ± 13.4*	139.3 ± 39.1	100.4 ± 9.3*
Insulin (pmol/L)	83.2 ± 58.6	65.7 ± 43.5*	111.0 ± 78.3	69.8 ± 49.0*
WHI				
N	190	1339	258	1762
Age (years)	66.6 ± 6.2	64.7 ± 7.1*	63.9 ± 6.7	64.5 ± 7.1
Female (%)	190(100)	1339(100)	258(100)	1762(100)
Statin user (%)	190 (100)	0*	53(21)	182(10)*
Smoker (%)	88(47)	627(48)	111(44)	811(47)
Drinker (%)	54(28)	381(29)	20(8)	511(29)*
TC (mg/dL)	249.6 ± 44.2	231.9 ± 42.2*	231.5 ± 46.2	234.0 ± 42.7
HDL-C (mg/dL)	50.7 ± 12.1	52.3 ± 12.7*	46.8 ± 11.9	52.4 ± 12.8*
LDL-C (mg/dL)	164.9 ± 41.4	151.1 ± 38.2*	148.7 ± 42.8	152.8 ± 38.9
TG (mg/dL)	174.8 ± 90.3	139.9 ± 73.5*	189.4 ± 133.5	141.2 ± 76.4*
Glucose (mg/dL)	100.1 ± 25.6	101.0 ± 29.0	173.7 ± 66.6	99.4 ± 26.0*
Insulin (pmol/L)	61.5 ± 38.7	60.5 ± 50.0	144.1 ± 330.9	59.2 ± 48.2*

*[1]Participants who are not using antidiabetic medicines. [2]All participants. [3]Statin: Participants who are using statins. [4]T2D: Participants who have type 2 diabetes. * Statistically significantly different between statin and non-statin groups, or between T2D and non-T2D groups in both FHS and WHI using independent t-test or Fisher's exact test, P < 0.05.*

TABLE 2 | *ABCG1* CpG sites associated with statin use in all participants from the FHS and WHI studies.

		FHS (Discovery)				**WHI (Validation)**			
CpG	**Chr: Position**[†]	***N***	**B***	**SE**	***P*-value***	***N***	**B***	**SE**	***P*-value***
Basic model									
cg06500161	21:42236477	2157	0.0320	3.02E-3	1.00E-32	1702	0.0143	4.83E-3	3.15E-3
cg01881899	21:42232595	2157	0.0749	0.0165	5.93E-6	1702	0.0138	0.0261	0.596
cg05639842	21:42219330	2157	0.0693	0.0196	3.98E-4	1702	0.0484	0.0177	6.15E-3
cg01176028	21:42233124	2157	0.0283	6.05E-3	2.88E-6	1702	6.85E-3	0.0167	0.682
cg02370100	21:42235147	2157	0.0373	0.0108	5.92E-4	1702	0.0257	0.0149	0.0846
LDL-C and TG adjusted model									
cg06500161	21:42236477	2153	0.0252	3.16E-3	1.55E-15	1564	0.0134	5.10E-3	8.36E-3
cg01881899	21:42232595	2153	0.0502	0.0173	3.76E-3	1564	0.0108	0.0265	0.684
cg05639842	21:42219330	2153	0.0582	0.0220	8.16E-3	1564	0.0470	0.0187	0.0121
cg01176028	21:42233124	2153	0.0183	6.86E-3	7.82E-3	1564	-0.0134	0.0173	0.437
cg02370100	21:42235147	2153	0.0344	0.0119	3.72E-3	1564	0.0215	0.0160	0.178

*[†]The physical positions of CpG sites are based on GRCh38.p12. *Adjusted for age, sex (for FHS), smoking, alcohol use, cell-type heterogeneity, and family relationship (for FHS).*

TABLE 3 | *ABCG1* CpG sites associated with statin use in participants who are not using antidiabetic medication from the FHS and WHI studies.

		WHI (Validation)				FHS (Discovery)			
CpG	**Chr: Position†**	***N***	**β**	**SE**	***P*-value**	***N***	**β**	**SE**	***P*-value**
Basic model									
cg06500161	21:42236477	1923	0.0317	3.25E-3	1.00E-32	1502	0.0114	5.34E-3	0.0325
cg01881899	21:42232595	1923	0.0738	0.0187	8.08E-5	1502	4.78E-5	2.97E-2	0.999
cg05639842	21:42219330	1923	0.0765	0.0212	3.00E-4	1502	0.0621	0.0191	1.13E-3
cg01176028	21:42233124	1923	0.0273	6.73E-3	2.07E-5	1502	0.0192	0.0188	0.306
cg02370100	21:42235147	1923	0.0392	0.0115	6.51E-4	1502	0.0275	0.0165	0.0957
LDL-C and TG adjusted model									
cg06500161	21:42236477	1922	0.0257	3.29E-3	6.22E-15	1390	8.53E-3	5.54E-3	0.123
cg01881899	21:42232595	1922	0.0453	0.0204	0.0261	1390	-7.06E-4	0.0299	0.813
cg05639842	21:42219330	1922	0.0664	0.0236	4.97E-3	1390	0.0630	0.0202	1.85E-3
cg01176028	21:42233124	1922	0.0206	7.15E-3	3.97E-3	1390	-0.0241	0.0194	0.214
cg02370100	21:42235147	1922	0.0345	0.0124	5.52E-3	1390	0.0209	0.0177	0.238

†*The physical positions of CpG sites are based on GRCh38.p12.*

TABLE 4 | *ABCG1* CpG sites associated with type 2 diabetes, fasting glucose and fasting insulin in participants from the FHS and WHI studies.

			FHS (Discovery)				WHI (Validation)			
	CpG	**Chr: Position†**	***N***	**β**	**SE**	***P*-value**	***N***	**β**	**SE**	***P*-value**
All participants										
Type 2 diabetes	cg06500161	21:42236477	2176	12.4	1.93	1.33E-10	2020	11.7	1.77	4.70E-11
	cg05639842	21:42219330	2176	1.69	3.71	0.648	2020	16.0	11.73	0.172
Non-diabetic participants										
Blood glucose	cg06500161	21:42236477	1858	0.504	0.0946	1.02E-7	1762	0.853	0.174	9.22E-7
	cg05639842	21:42219330	1858	0.117	0.169	0.489	1762	−1.30	1.22	0.287
Blood insulin	cg06500161	21:42236477	1858	4.85	0.594	4.44E-16	1762	4.05	0.429	3.86E-21
	cg05639842	21:42219330	1858	1.42	1.20	0.0760	1762	0.842	3.21	0.793

†*The physical positions of CpG sites are based on GRCh38.p12.*

TABLE 5 | Two-step Mendelian randomization (MR) analysis in participants from the FHS and WHI studies.

		Exposure	**Outcome**	**# SNP (Instrument variable)**	**β**	**SE**	***P*-value**	**GWAS-threshold**	**MED effect via CpG methylation‡**
All participants									
Step 1	FHS (Basic model)	Statin	cg06500161	200	0.0186	1.50E-3	2.56E-35	5E-5	
	FHS (LDL-C and TG adjusted)	Statin	cg06500161	162	0.0157	1.72E-3	1.05E-19	5E-5	
Step 2	WHI	cg06500161	T2D†	59	1.13	0.292	1.16E-4	5E-5	0.0177
Non-diabetic participants									
Step 1	FHS (Basic model)	Statin	cg06500161	177	0.0179	1.55E-3	9.64E-31	5E-5	
	FHS (LDL-C and TG adjusted)	Statin	cg06500161	171	0.0142	1.58E-3	2.12E-19	5E-5	
Step 2	WHI	cg06500161	Glucose	79	0.246	0.0693	3.87E-4	5E-5	3.49E-3
	WHI	cg06500161	Insulin	79	1.47	0.237	4.72E-10	5E-5	0.0209

†*T2D: Type 2 diabetes.* ‡*The causal effect of statin use on type 2 diabetes and related phenotypes through cg06500161 methylation was calculated by multiplying the genetic score estimates of step 2 MR by the genetic score estimate of step 1 MR in the LDL-C and TG adjusted model.*

TABLE 6 | Overlaps for doubly-associated gene expression in non-diabetic participants from the FHS study (genes in overlap ≥ 5, LDL-C and TG adjusted model).

Gene set name	Genes in overlap	*P*-value	FDR *q*-value
***Statin and CpG*†**			
Reactome: NR1H2 and NR1H3-mediated signaling	5	2.70E-8	4.14E-5
Reactome: plasma lipoprotein assembly, remodeling, and clearance	5	2.22E-7	1.70E-4
Reactome: signaling by nuclear receptors	7	1.34E-6	6.86E-4
CpG and Glucose			
Reactome: metabolism of lipids and lipoproteins	5	5.49E-4	0.0787
CpG and Insulin			
Reactome: metabolism of lipids and lipoproteins	7	1.48E-5	6.38E-3
Reactome: transmembrane transport of small molecules	6	6.53E-5	0.0112

†*CpG: DNA methylation at cg06500161.*

Combining results from the first and second steps of MR, the causal effect of statins on type 2 diabetes, glucose, and insulin through cg06500161 methylation was calculated as 0.0177, 3.49E-3 and 0.0209, respectively (**Table 5**).

Links Between Statin Use and DNA Methylation, and Gene Expression

To examine potential mechanisms through which statins mediated DNA methylation at cg06500161 that led to increased risk of diabetes, we separately correlated gene expression levels with statin use, cg06500161 methylation and fasting glucose and insulin levels. This was done with available gene expression data from all non-diabetic FHS participants. As shown in **Supplementary Table S2**, seventy-seven transcripts were correlated with both statin use and cg06500161 methylation. Fifty-six transcripts were found to be correlated with both fasting glucose and DNA methylation of cg06500161, and 80 transcripts were associated with both fasting insulin and cg06500161 methylation (**Supplementary Table S2**). Gene set enrichment analysis conducted with both KEGG and REACTOME gene-pathway assignments at an FDR of 10% suggested that the genes doubly associated with cg06500161 methylation and insulin are primarily involved in cholesterol and lipoprotein metabolic pathways (**Table 6**).

When combining the transcripts whose expression in whole blood associated significantly with statin use, cg06500161 methylation and insulin level, 16 genes were found correlated with each of three different outcomes, with the greatest responses involved in cholesterol, fatty acid and lipid transport and homeostasis (**Figure 1**). Specifically, it should be noted that *ABCG1*, *ABCA1* and *ACSL3* were negatively, while *KAT2B* positively, associated with all signatures of statin use, CpG methylation and diabetes risk/status (**Supplementary Tables S3, S4**).

DISCUSSION

Our findings imply that statin use mediates DNA methylation at cg06500161 of *ABCG1* and this contributes to increased risk of type 2 diabetes. Firstly, we have shown that statin use was associated with DNA methylation modifications of *ABCG1* and such methylation patterns are correlated with the risk of type 2 diabetes. Secondly, Mendelian randomization demonstrates that statin use has moderate causal effects on type 2 diabetes and diabetes-related traits through differential methylation at cg06500161. Moreover, our results suggest that statin use and the methylation modifications in *ABCG1* are correlated with the expression of genes involved in both lipid metabolism and glycemic pathways.

This study reveals a potential epigenetic mechanism mediating the effect of statin use on glycemic signatures. The associations between epigenetic variants at *ABCG1* and diabetic traits have been observed previously (Hidalgo et al., 2014; Chambers et al., 2015; Dayeh et al., 2016), but little is known about the association between lipid-lowering medications and DNA methylation of *ABCG1*. Because DNA methylation at cg06500161 of *ABCG1* in blood has been associated positively with triglyceride levels and negatively with HDL-C levels (Dekkers et al., 2016; Braun et al., 2017), it is plausible that blood lipids have a causal effect on the epigenetic status at *ABCG1*. For this reason, in this study, we controlled for blood LDL cholesterol and triglyceride levels in our analyses. Importantly, our data from the LDL-C and TG adjusted model remained significant, indicating that statin use is an independent factor of higher cg06500161 methylation and consequently increased diabetic risk. Hence, the results from MR analysis have demonstrated that statin use is highly likely the causal factor of increased cg06500161 methylation and diabetic risk.

ABCG1 encodes a protein member in the ATP-binding cassette (ABC) transporters superfamily, which transports specific intracellular sterols away from the endoplasmic reticulum (Tarling and Edwards, 2011). *ABCG1* has shown an allelic imbalance of expression in human pancreatic islet cells suggesting both genetic and epigenetic roles in altering the allelic expression of *ABCG1* (Serre et al., 2008). Indeed, genetic variants contribute to differences in *ABCG1* expression (Matsson et al., 2012). Does genetic variation impart stronger regulation of *ABCG1* expression than epigenetic modification? Previous GWAS have reported negative results in the associations between *ABCG1* and risk for type 2 diabetes (Vattikuti and Towler, 2004; Saxena et al., 2010). Coding SNPs in *ABCG1* were found not to be associated with risks for type 2 diabetes in the Copenhagen General Population Study (Schou et al., 2012). Frisdal et al. further demonstrated that *ABCG1* SNPs (rs1893590 and rs1378577) in severely obese individuals were not associated with the presence of diabetes or HOMA-IR (Frisdal et al., 2015). In the present study, we did not find any significant association between *ABCG1* SNPs with T2D, fasting glucose, or insulin levels in either FHS or WHI cohorts. The mechanisms of genetic variants on *ABCG1* and type 2 diabetes remain unclear and controversial, suggesting that epigenetic processes might be involved in the regulation of *ABCG1* and downstream

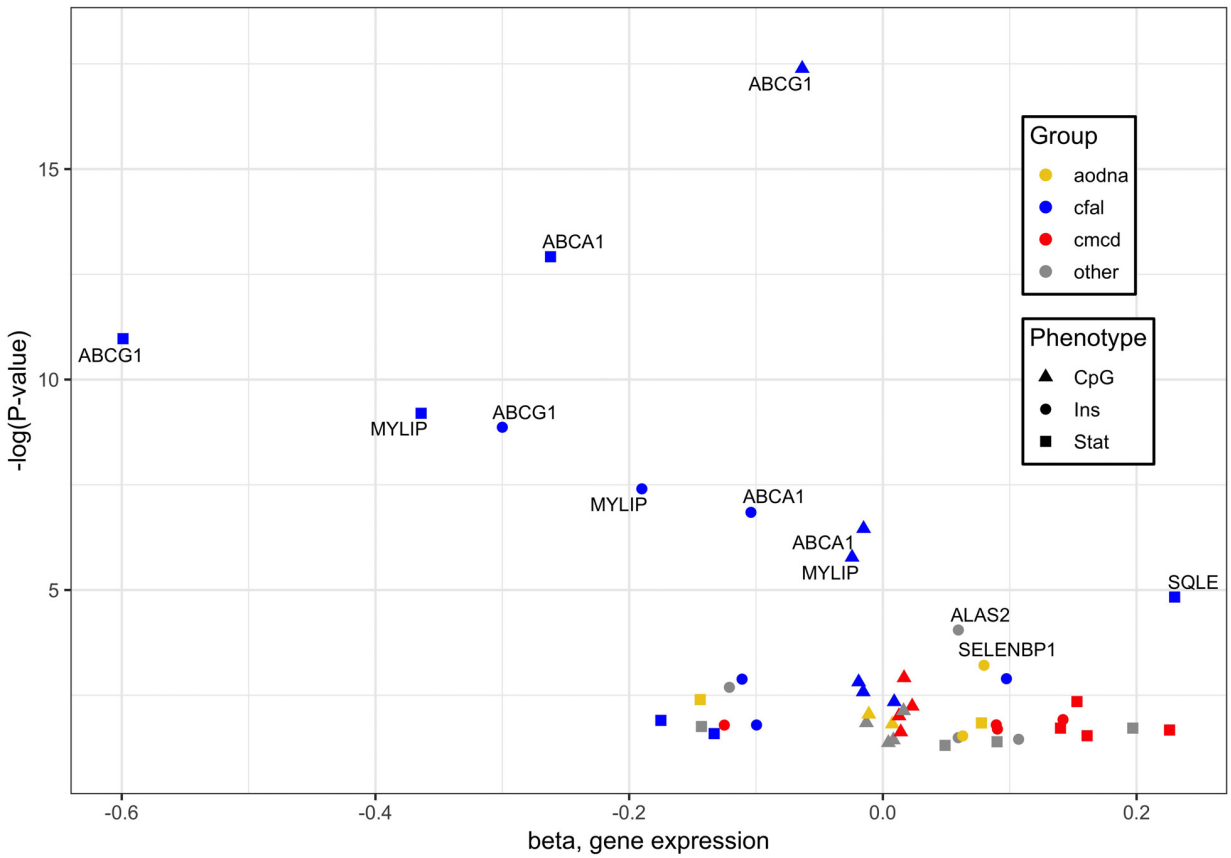

FIGURE 1 | Genes whose expression associated significantly with cg06500161 methylation, glycemic traits and statin use. Of 16 genes whose expression in whole blood associated significantly with each of three different outcomes, those with the greatest responses are involved in cholesterol, fatty acid and lipid transport and homeostasis (blue). Associations were derived from methylation at *ABCG1* CpG cg06500161, glycemic factors, and statin use, designated by triangles, circles and squares, respectively. Other notable functional groups include cell migration and cytoskeletal dysnamics (red) and antioxidant defense and DNA damage response (orange). Plotted data taken from **Supplementary Table S3**.

gene expression, and ultimately diabetic signatures. Our results and those of others (Dayeh et al., 2016) show that increased DNA methylation at *ABCG1* was positively associated with diabetic signatures providing substantial evidence in support of these correlations between *ABCG1* and type 2 diabetes from an epigenetic perspective.

ABCG1 is a central regulator of cellular lipid homeostasis (Schmitz et al., 2001). Recently, several reports also suggest that ABCG1 may be involved in glucose metabolism. ABCG1 has been reported to mediate cholesterol transport and thus influence insulin secretion in pancreatic β-cells (Sturek et al., 2010; Kruit et al., 2012). Decreased *ABCG1* expression has been found in skeletal muscle from subjects with type 2 diabetes (Dayeh et al., 2016). In order to investigate possible methylation-driven gene expression changes and uncover the potential mechanism of diabetes risk mediated by statins, we examined the correlation of the transcriptome with statins, cg06500161 methylation status, and glucose and insulin levels in all non-diabetic participants in FHS. The expressions of *ABCG1, ABCA1, ACSL3* were negatively, while *KAT2B* positively, associated with the medication, cg06500161 methylation, and glucose and insulin levels. KAT2B (lysine acetyltransferase 2B), functions as a histone acetyltransferase to promote transcriptional activation (Ogryzko et al., 1996), has been reported to stimulate hepatic gluconeogenesis and increase circulating blood glucose concentrations, whereas inhibition of KAT2B improves glucose balance in insulin-resistant mice (Ravnskjaer et al., 2013). ABCA1 (ATP binding cassette subfamily A member 1), which normally moves cholesterol and phospholipids across cell membranes, could increase insulin secretion in pancreatic β-cells (Kruit et al., 2012). Additionally, silencing *ACSL3* and *ACSL4* (Long-chain acyl-CoA synthetases), which are responsible for activation of long-chain fatty acids, have been found to inhibit glucose-stimulated insulin release in pancreatic β-cells (Ansari et al., 2017). Meanwhile, previous findings, as illustrated in **Figure 2**, also have shown that reduced *ABCA1* and *ACSL3* expression impairs the phosphorylation of AKT, resulting in insulin resistance (de Haan et al., 2014; Li et al., 2018). Thus, decreased expression of *ABCG1*, *ABCA1*, and *ACSL3* could impair insulin secretion and lead to insulin resistance. All this supports the positive correlations observed here between statin use and insulin levels as well as glucose levels, which result in

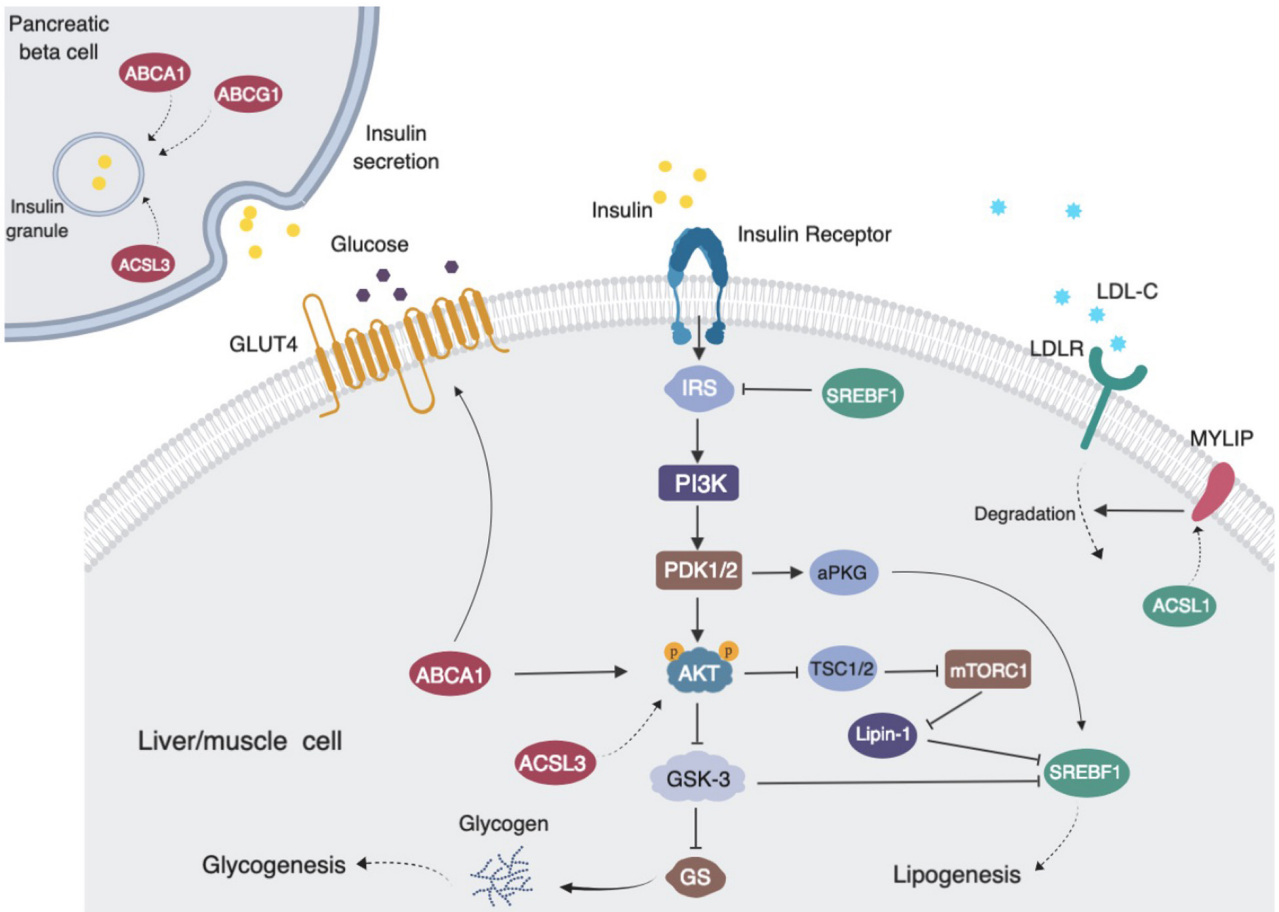

FIGURE 2 | Proposed pathways of statin use associating with cg06500161 methylation, fasting blood glucose and fasting blood insulin levels (LDL-C and TG adjusted model). *ABCG1*, *ABCA1, ACSL3* and *MYLIP* (dark red) expression levels were negatively associated with medication use, CpG methylation and diabetic signatures. *SREBF1* and *ACSL3* (dark green) expression levels were inversely associated with medication use and CpG methylation. Statin use induced *ABCG1* methylation that leads to decreased expression of *ABCG1*, then altered insulin sensitivity and insulin secretion and increased risk of diabetes.

an increased risk of type 2 diabetes. It is also worth noting that other mechanisms such as epigenetic changes on non-coding RNAs and histone modifications might also affect the association between the statin use and T2D risk (Muka et al., 2016; Sun and Wong, 2016), and further studies are warranted to elucidate these mechanisms.

Some limitations should be acknowledged when interpreting the results of this study. First, there were differences in gender distribution between the two cohorts, in particular, WHI includes females only, which might contribute to slight inconsistencies in associations between statin use and methylation at *ABCG1*. Second, some glucose and insulin metabolism take place in the liver, pancreatic islet, adipose tissue, and skeletal muscle, but the available data permitted investigation of the mechanisms only in blood. This limitation in the sample type should not undermine the link between statin use and diabetes risk, as DNA methylation status in blood often reflects the epigenetic status in other tissues (Bysani et al., 2016; Crujeiras et al., 2017). Nevertheless, our findings suggest that further investigation is warranted in order to further characterize the molecular mechanism of increased diabetes risk with specific statin use.

In summary, we report DNA methylation site cg06500161 at *ABCG1* as a mediator of the association between statins and type 2 diabetes. These findings provide insights into the epigenetic mechanisms of statins influencing glycemic traits and further, type 2 diabetes pathogenesis. We show evidence for cg06500161 as a potential predictor or therapeutic target for prevention of type 2 diabetes. Implementation of functional studies of cg06500161 will uncover the precise molecular mechanisms. The eventual goal is to translate this information into clinical use, specifically, to develop useful prediction and prevention strategies for type 2 diabetes.

DATA AVAILABILITY STATEMENT

Publicly available datasets were analyzed in this study. These data can be found here: dbGaP: phs000200.v11.p3, phs000746.v2.p3, phs000342.v18.p11, phs000007.v29.p10, and phe00002.v6.

ETHICS STATEMENT

The studies involving human participants were reviewed and approved by the Institutional Review Board (IRB) at Tufts University. The patients/participants provided their written informed consent to participate in this study.

AUTHOR CONTRIBUTIONS

C-QL and YL conceptualized and designed the study. YL, YS, TG, and LP contributed to data analysis. KW contributed to the processing and quality control of imputed genotypes of acquired through dbGaP. LP, JO, YS, TG, and CS critically evaluated the manuscript. JO is responsible for the funding and supervision of the study. YL and C-QL wrote and edited the manuscript. All authors read and approved the final manuscript.

FUNDING

This work was partially supported by grant 201806105018 from the China Scholarship Council (CSC), and by the United States Department of Agriculture, under agreement no. 8050-51000-098-00D.

ACKNOWLEDGMENTS

The Genotype-Tissue Expression (GTEx) Project was supported by the Common Fund of the Office of the Director of the National Institutes of Health, and by NCI, NHGRI, NHLBI, NIDA, NIMH, and NINDS. Any opinions, findings, conclusion, or recommendations expressed in this publication are those of the authors and do not necessarily reflect the view of the United States Department of Agriculture. None of the authors had a conflict of interest. Mention of trade names or commercial products in this publication is solely for the purpose of providing specific information and does not imply recommendation or endorsement by the United States Department of Agriculture. The USDA is an equal opportunity provider and employer.

SUPPLEMENTARY MATERIAL

The Supplementary Material for this article can be found online at: https://www.frontiersin.org/articles/10.3389/fgene.2020.00622/full#supplementary-material

REFERENCES

Aguirre, L., Hijona, E., Macarulla, M. T., Gracia, A., Larrechi, I., Bujanda, L., et al. (2013). Several statins increase body and liver fat accumulation in a model of metabolic syndrome. *J. Physiol. Pharmacol.* 64, 281–288.

Ansari, I. H., Longacre, M. J., Stoker, S. W., Kendrick, M. A., O'Neill, L. M., Zitur, L. J., et al. (2017). Characterization of Acyl-CoA synthetase isoforms in pancreatic beta cells: gene silencing shows participation of ACSL3 and ACSL4 in insulin secretion. *Arch. Biochem. Biophys.* 618, 32–43. doi: 10.1016/j.abb.2017.02.001

Braun, K. V. E., Dhana, K., de Vries, P. S., Voortman, T., van Meurs, J. B. J., Uitterlinden, A. G., et al. (2017). Epigenome-wide association study (EWAS) on lipids: the Rotterdam Study. *Clin. Epigenet.* 9:15.

Bysani, M., Perfilyev, A., de Mello, V. D., Rönn, T., Nilsson, E., Pihlajamäki, J., et al. (2016). Epigenetic alterations in blood mirror age-associated DNA methylation and gene expression changes in human liver. *Epigenomics* 9, 105–122. doi: 10.2217/epi-2016-0087

Caramaschi, D., Sharp, G. C., Nohr, E. A., Berryman, K., Lewis, S. J., Davey Smith, G., et al. (2017). Exploring a causal role of DNA methylation in the relationship between maternal vitamin B12 during pregnancy and child's IQ at age 8, cognitive performance and educational attainment: a two-step Mendelian randomization study. *Hum. Mol. Genet.* 26, 3001–3013. doi: 10.1093/hmg/ddx164

Chambers, J. C., Loh, M., Lehne, B., Drong, A., Kriebel, J., Motta, V., et al. (2015). Epigenome-wide association of DNA methylation markers in peripheral blood from Indian Asians and Europeans with incident type 2 diabetes: a nested case-control study. *Lancet Diabetes Endocrinol.* 3, 526–534.

Chang, C. C., Chow, C. C., Tellier, L. C., Vattikuti, S., Purcell, S. M., and Lee, J. J. (2015). Second-generation PLINK: rising to the challenge of larger and richer datasets. *Gigascience* 4:7.

Chou, R., Dana, T., Blazina, I., Daeges, M., and Jeanne, T. L. (2016). Statins for prevention of cardiovascular disease in adults: evidence report and systematic review for the US preventive services task force. *JAMA* 316, 2008–2024. doi: 10.1001/jama.2015.15629

Crujeiras, A. B., Diaz-Lagares, A., Sandoval, J., Milagro, F. I., Navas-Carretero, S., Carreira, M. C., et al. (2017). DNA methylation map in circulating leukocytes mirrors subcutaneous adipose tissue methylation pattern: a genome-wide analysis from non-obese and obese patients. *Sci. Rep.* 7:41903. doi: 10.1038/srep41903

Davegardh, C., Garcia-Calzon, S., Bacos, K., and Ling, C. (2018). DNA methylation in the pathogenesis of type 2 diabetes in humans. *Mol. Metab.* 14, 12–25. doi: 10.1016/j.molmet.2018.01.022

Dawber, T. R., Meadors, G. F., and Moore, F. E. Jr. (1951). Epidemiological approaches to heart disease: the Framingham Study. *Am. J. Public Health* 41, 279–281.

Dayeh, T., Tuomi, T., Almgren, P., Perfilyev, A., Jansson, P. A., de Mello, V. D., et al. (2016). DNA methylation of loci within ABCG1 and PHOSPHO1 in blood DNA is associated with future type 2 diabetes risk. *Epigenetics* 11, 482–488. doi: 10.1080/15592294.2016.1178418

de Haan, W., Bhattacharjee, A., Ruddle, P., Kang, M. H., and Hayden, M. R. (2014). ABCA1 in adipocytes regulates adipose tissue lipid content, glucose tolerance, and insulin sensitivity. *J. Lipid Res.* 55, 516–523. doi: 10.1194/jlr.M045294

Dekkers, K. F., van Iterson, M., Slieker, R. C., Moed, M. H., Bonder, M. J., van Galen, M., et al. (2016). Blood lipids influence DNA methylation in circulating cells. *Genome Biol.* 17:138.

Frisdal, E., Le Lay, S., Hooton, H., Poupel, L., Olivier, M., Alili, R., et al. (2015). Adipocyte ATP-binding cassette G1 promotes triglyceride storage, fat mass growth, and human obesity. *Diabetes* 64, 840–855. doi: 10.2337/db14-0245

Genvigir, F. D., Rodrigues, A. C., Cerda, A., Hirata, M. H., Curi, R., and Hirata, R. D. (2011). ABCA1 and ABCG1 expressions are regulated by statins and ezetimibe in Caco-2 cells. *Drug Metabol. Drug Interact.* 26, 33–36. doi: 10.1515/DMDI.2011.101

Hidalgo, B., Irvin, M. R., Sha, J., Zhi, D., Aslibekyan, S., Absher, D., et al. (2014). Epigenome-wide association study of fasting measures of glucose, insulin, and HOMA-IR in the genetics of lipid lowering drugs and diet network study. *Diabetes* 63, 801–807. doi: 10.2337/db13-1100

Kannel, W. B., Feinleib, M., McNamara, P. M., Garrison, R. J., and Castelli, W. P. (1979). An investigation of coronary heart disease in families: the Framingham offspring study. *Am. J. Epidemiol.* 110, 281–290. doi: 10.1093/oxfordjournals.aje.a112813

Katz, S., Irizarry, R. A., Lin, X., Tripputi, M., and Porter, M. W. (2006). A summarization approach for Affymetrix GeneChip data using a reference

training set from a large, biologically diverse database. *BMC Bioinformatics* 7:464. doi: 10.1186/1471-2105-7-464

Kim, D.-W., Kim, D.-H., Park, J.-H., Choi, M., Kim, S., Kim, H., et al. (2019). Association between statin treatment and new-onset diabetes mellitus: a population based case–control study. *Diabetol. Metab. Syndr.* 11:30.

Kim, Y. S., Han, Y. E., Choi, E. A., You, N. Y., Lee, J. W., You, H. S., et al. (2019). Statin use increased new-onset diabetes in hypercholesterolemic individuals: data from the Korean National Health Insurance Service-National Health Screening Cohort database (NHIS-HEALS). *Prim Care Diabetes* 14, 246–253. doi: 10.1016/j.pcd.2019.08.005

Kruit, J. K., Wijesekara, N., Westwell-Roper, C., Vanmierlo, T., de Haan, W., Bhattacharjee, A., et al. (2012). Loss of both ABCA1 and ABCG1 results in increased disturbances in islet sterol homeostasis, inflammation, and impaired β-cell function. *Diabetes* 61, 659–664. doi: 10.2337/db11-1341

Lai, C.-Q., Smith, C. E., Parnell, L. D., Lee, Y.-C., Corella, D., Hopkins, P., et al. (2018). Epigenomics and metabolomics reveal the mechanism of the APOA2-saturated fat intake interaction affecting obesity. *Am. J. Clin. Nutr.* 108, 188–200. doi: 10.1093/ajcn/nqy081

Li, K., Mao, Y.-H., Qiu, W.-H., He, J.-W., Wang, D.-J., Hu, C., et al. (2018). Acyl-CoA synthetase long-chain 3 regulates AKT phosphorylation and the functional activity of human prostate cancer cells. *J. BioX Res.* 1, 56–61. doi: 10.1097/jbr.0000000000000009

Lindsey, C. C., Graham, M. R., Johnston, T. P., Kiroff, C. G., and Freshley, A. (2004). A clinical comparison of calculated versus direct measurement of low-density lipoprotein cholesterol level. *Pharmacotherapy* 24, 167–172. doi: 10.1592/phco.24.2.167.33142

Marioni, R. E., Shah, S., McRae, A. F., Chen, B. H., Colicino, E., Harris, S. E., et al. (2015). DNA methylation age of blood predicts all-cause mortality in later life. *Genome Biol.* 16:25.

Matsson, P., Yee, S. W., Markova, S., Morrissey, K., Jenkins, G., Xuan, J., et al. (2012). Discovery of regulatory elements in human ATP-binding cassette transporters through expression quantitative trait mapping. *Pharmacogenomics J.* 12, 214–226. doi: 10.1038/tpj.2011.8

Matsuo, M. (2010). ATP-binding cassette proteins involved in glucose and lipid homeostasis. *Biosci. Biotechnol. Biochem.* 74, 899–907. doi: 10.1271/bbb.90921

Morris, T. J., Butcher, L. M., Feber, A., Teschendorff, A. E., Chakravarthy, A. R., Wojdacz, T. K., et al. (2014). ChAMP: 450k chip analysis methylation pipeline. *Bioinformatics* 30, 428–430. doi: 10.1093/bioinformatics/btt684

Muka, T., Nano, J., Voortman, T., Braun, K. V. E., Ligthart, S., Stranges, S., et al. (2016). The role of global and regional DNA methylation and histone modifications in glycemic traits and type 2 diabetes: a systematic review. *Nutr. Metab. Cardiovasc. Dis.* 26, 553–566. doi: 10.1016/j.numecd.2016.04.002

Nilsson, E., and Ling, C. (2017). DNA methylation links genetics, fetal environment, and an unhealthy lifestyle to the development of type 2 diabetes. *Clin. Epigenetics* 9:105.

Obeidat, M., Fishbane, N., Nie, Y., Chen, V., Hollander, Z., Tebbutt, S. J., et al. (2015). The effect of statins on blood gene expression in COPD. *PLoS One* 10:e0140022. doi: 10.1371/journal.pone.0140022

Ogryzko, V. V., Schiltz, R. L., Russanova, V., Howard, B. H., and Nakatani, Y. (1996). The transcriptional coactivators p300 and CBP are histone acetyltransferases. *Cell* 87, 953–959. doi: 10.1016/s0092-8674(00)82001-2

Pirillo, A., and Catapano, A. L. (2015). Statin intolerance: diagnosis and remedies. *Curr. Cardiol. Rep.* 17:27. doi: 10.1007/s11886-015-0582-z

Ravnskjaer, K., Hogan, M. F., Lackey, D., Tora, L., Dent, S. Y., Olefsky, J., et al. (2013). Glucagon regulates gluconeogenesis through KAT2B- and WDR5-mediated epigenetic effects. *J. Clin. Invest.* 123, 4318–4328. doi: 10.1172/jci69035

Relton, C. L., and Davey Smith, G. (2012). Two-step epigenetic Mendelian randomization: a strategy for establishing the causal role of epigenetic processes in pathways to disease. *Int. J. Epidemiol.* 41, 161–176. doi: 10.1093/ije/dyr233

Saxena, R., Hivert, M. F., Langenberg, C., Tanaka, T., Pankow, J. S., Vollenweider, P., et al. (2010). Genetic variation in GIPR influences the glucose and insulin responses to an oral glucose challenge. *Nat. Genet.* 42, 142–148. doi: 10.1038/ng.521

Schmitz, G., Langmann, T., and Heimerl, S. (2001). Role of ABCG1 and other ABCG family members in lipid metabolism. *J. Lipid Res.* 42, 1513–1520.

Schou, J., Tybjaerg-Hansen, A., Moller, H. J., Nordestgaard, B. G., and Frikke-Schmidt, R. (2012). ABC transporter genes and risk of type 2 diabetes: a study of 40,000 individuals from the general population. *Diabetes Care* 35, 2600–2606. doi: 10.2337/dc12-0082

Serre, D., Gurd, S., Ge, B., Sladek, R., Sinnett, D., Harmsen, E., et al. (2008). Differential allelic expression in the human genome: a robust approach to identify genetic and epigenetic cis-acting mechanisms regulating gene expression. *PLoS Genet.* 4:e1000006. doi: 10.1371/journal.pgen.1000006

Sturek, J. M., Castle, J. D., Trace, A. P., Page, L. C., Castle, A. M., Evans-Molina, C., et al. (2010). An intracellular role for ABCG1-mediated cholesterol transport in the regulated secretory pathway of mouse pancreatic beta cells. *J. Clin. Invest.* 120, 2575–2589. doi: 10.1172/JCI41280

Sun, X., and Wong, D. (2016). Long non-coding RNA-mediated regulation of glucose homeostasis and diabetes. *Am. J. Cardiovasc. Dis.* 6, 17–25.

Tarling, E. J., and Edwards, P. A. (2011). ATP binding cassette transporter G1 (ABCG1) is an intracellular sterol transporter. *Proc. Natl. Acad. Sci. U.S.A.* 108, 19719–19724. doi: 10.1073/pnas.1113021108

The Women's Health Initiative Study Group, (1998). Design of the Women's Health Initiative clinical trial and observational study. The Women's Health Initiative Study Group. *Control. Clin. Trials* 19, 61–109. doi: 10.1016/s0197-2456(97)00078-0

Vattikuti, R., and Towler, D. A. (2004). Osteogenic regulation of vascular calcification: an early perspective. *Am. J. Physiol. Endocrinol. Metab.* 286, E686–E696. doi: 10.1152/ajpendo.00552.2003

Vickers, M. H. (2014). Early life nutrition, epigenetics and programming of later life disease. *Nutrients* 6, 2165–2178. doi: 10.3390/nu6062165

Yang, J., Zaitlen, N. A., Goddard, M. E., Visscher, P. M., and Price, A. L. (2014). Advantages and pitfalls in the application of mixed-model association methods. *Nat. Genet.* 46, 100–106. doi: 10.1038/ng.2876

Zhan, S., Tang, M., Liu, F., Xia, P., Shu, M., and Wu, X. (2018). Ezetimibe for the prevention of cardiovascular disease and all-cause mortality events. *Cochrane Database Syst. Rev.* 11:Cd012502. doi: 10.1002/14651858.CD012502.pub2

Zhang, F., Chen, W., Zhu, Z., Zhang, Q., Deary, I. J., Wray, N. R., et al. (2018). OSCA: a tool for omic-data-based complex trait analysis. *bioRxiv [Preprint]* doi: 10.1101/445163

Zhu, Z., Zheng, Z., Zhang, F., Wu, Y., Trzaskowski, M., Maier, R., et al. (2018). Causal associations between risk factors and common diseases inferred from GWAS summary data. *Nat. Commun.* 9:224.

Conflict of Interest: The authors declare that the research was conducted in the absence of any commercial or financial relationships that could be construed as a potential conflict of interest.

frontiers in Genetics

ORIGINAL RESEARCH
published: 09 September 2020
doi: 10.3389/fgene.2020.00778

Identification of Potential Biomarkers for CAD Using Integrated Expression and Methylation Data

*Xiaokang Zhang, Yang Xiang, Dingdong He, Bin Liang, Chen Wang, Jing Luo and Fang Zheng**

Department of Clinical Laboratory Medicine and Center for Gene Diagnosis, Zhongnan Hospital of Wuhan University, Wuhan, China

DNA methylation plays an essential role in the pathogenesis of coronary artery disease (CAD) through regulating mRNA expressions. This study aimed to identify hub genes regulated by DNA methylation as biomarkers of CAD. Gene expression and methylation datasets of peripheral blood leukocytes (PBLs) of CAD were downloaded from the Gene Expression Omnibus (GEO) database. Subsequently, multiple computational approaches were performed to analyze the regulatory networks and to recognize hub genes. Finally, top hub genes were verified in a case-control study, based on their differential expressions and methylation levels between CAD cases and controls. In total, 535 differentially expressed-methylated genes (DEMGs) were identified and partitioned into 4 subgroups. TSS200 and 5′UTR were confirmed as high enrichment areas of differentially methylated CpGs sites (DMCs). The function of DEMGs is enriched in processes of histone H3-K27 methylation, regulation of post-transcription and DNA-directed RNA polymerase activity. Pathway enrichment showed DEMGs participated in the VEGF signaling pathway, adipocytokine signaling pathway, and PI3K-Akt signaling pathway. Besides, expressions of hub genes fibronectin 1 (FN1), phosphatase (PTEN), and tensin homolog and RNA polymerase III subunit A (POLR3A) were discordantly expressed between CAD patients and controls and related with DNA methylation levels. In conclusion, our study identified the potential biomarkers of PBLs for CAD, in which FN1, PTEN, and POLR3A were confirmed.

Keywords: coronary artery disease, methylation, FN1, PTEN, POLR3A

OPEN ACCESS

Edited by:
Indulekha C. L. Pillai, Amrita Vishwa Vidyapeetham, India

Reviewed by:
Shabeesh Balan, RIKEN Center for Brain Science, Japan
Srimonta Gayen, Indian Institute of Science, India

***Correspondence:**
Fang Zheng
zhengfang@whu.edu.cn

Specialty section:
This article was submitted to Epigenomics and Epigenetics, a section of the journal Frontiers in Genetics

Received: *13 February 2020*
Accepted: *30 June 2020*
Published: *09 September 2020*

Citation:
Zhang X, Xiang Y, He D, Liang B, Wang C, Luo J and Zheng F (2020) Identification of Potential Biomarkers for CAD Using Integrated Expression and Methylation Data. Front. Genet. 11:778. doi: 10.3389/fgene.2020.00778

INTRODUCTION

Coronary artery disease (CAD), as the main type of cardiovascular disease, has become one of the leading causes of morbidity and mortality in both developed and developing countries (Wood and Eisele, 2017). This acute tendency is due to the population aging. According to the CAD prediction model, in China, more than 20 million deaths and 16 million instances of labor loss will be attributed to CAD from 2000 to 2029 (Moran et al., 2008). The total attributed to the social economy connected with CAD in developing countries was estimated to be approximately 3.7 trillion dollars in 2010, which is roughly equal to 1–3% of Gross Domestic Product (GDP) across developing countries (Gaziano et al., 2017).

Coronary arteriography (CAG) is the gold standard of CAD diagnosis, but the high cost and invasiveness limit its application (De Marco et al., 2018), whereas the cheaper cost and less invasive nature of blood biomarker detection make it easier to promote (Rusnak et al., 2017). Epigenetics is defined as the heritable transcriptional modifications that are not induced by the nucleotide sequence alterations of DNA (Duan et al., 2018). Multiple factors such as environment, diet, oxidative stress, and inflammatory stimuli influence epigenetic contents, including DNA methylation, RNA methylation, chromatin histone modification, non-coding RNA and DNA methylation, among which DNA methylation is the most indagated (Xu et al., 2019). For example, prolonged hypoxia can induce epigenetic modifications in myocardial fibroblasts, since methylation status of the genome and specific genes are affected by DNA methyltransferase (DNMT), which is regulated by a hypoxia inducible factor 1α (HIF-1α) (Watson et al., 2014). While studies have shown that in women who lost weight by lowering their calorie intake, the DNA methylation levels of Leptin and TNF-α promoters were significantly reverse modified, and the risk of CAD was significantly reduced (Cordero et al., 2011).

Aberrant DNA methylation participates in various processes of CAD development by regulating the mRNA expression of interrelated genes. For instance, ABCA1 plays an essential part in reverse cholesterol transport (RCT) by combining with apoA-I to form high-density lipoprotein (HDL) in the cell membrane and promoting the excretion of free cholesterol and phospholipids from cells. ABCA1 weakens the chemotactic ability of macrophages by reducing the content of free cholesterol in the cell membrane and delays the pathological progress of CAD (Bashore et al., 2019). The demethylation of the ABCA1 promotor has been verified to be related to the high expression of ABCA1, which can accelerate the process of CAD by expediting the formation of foam cells and thrombogenesis (Peng et al., 2014; Ghaznavi et al., 2018). Intriguingly, there is a conspicuous correlation between the methylation status of the ABCA1 promoter and physiological age. The ABCA1 promoter is hypermethylated in aged CAD patients, which can be partially illustrated by the accumulation of aberrant epigenetic changes during the long-term disease states (Ghaznavi et al., 2018). Cystathionine gamma-lyase, encoded by *CTH*, is a crucial part of the homocysteine metabolism pathway (Szijarto et al., 2018). Previous studies have found that hypermethylation of the *CTH* promotor in hyperhomocysteinemia in mice can lead to the decrease of *CTH* expression, which in turn prevents homocysteine from being catabolized and causes vascular endothelial cells injury, eventually results in CAD (Li et al., 2015; Giannakopoulou et al., 2017). A similar phenomenon has been observed in male CAD patients, while the methylation level of *CTH* promotor in female patients is not different from normal controls (Latini et al., 2004). Aberrant methylation status of the promoter has also been proved to impact the inflammatory pathways, which are well known to participate in the progress of CAD by regulating the number, ratio, and function of immune cells. PTX3 accelerates the formation of atherosclerotic plaques by enhancing the migration and chemotactic ability of macrophages, promotes vascular endothelial damage, and exacerbates vascular inflammation. The methylation level of the PTX3 promoter in CAD patients is much lower compared with controls, while higher PTX3 concentration and neutrophil to lymphocyte ratio (NLR) are detected in CAD patients. It indicates that the methylation level of the PTX3 promoter impacts the expression of PTX3 and regulates the number and classification ratio of white blood cells, aggravates an inflammatory response, and then participates in the progress of CAD (Guo et al., 2016).

However, in the past a few years, research on DNA methylation has mainly focused on the connection between methylation conditions of promoter regions and the expression of genes. Recently the aberrant methylation status of other gene regions has also been identified to be associated with CAD, but these complex regulatory networks remain largely unexplored (Oudejans et al., 2016; Nakatochi et al., 2017; Yamada et al., 2018). Therefore, an integrative research study was required, combining both genomic expression profile and epigenomic DNA methylation of PBLs in CAD in Chinese populations. In our study, we calculated the methylation status of 5′-C-phosphate-G-3′ (CpGs) sites in different intragenic gene regions, including TSS1500, TSS200, 5′UTR, 1stExon, body, and 3′UTR. Besides, we consolidated DNA methylation and mRNA expression data to recognize genes functioning in CAD and regulated by DNA methylation, which might be potential PBLs biomarkers. We identified hub genes that were both aberrantly methylated and differentially expressed in CAD patients compared with controls. Vital hub genes were validated in a case-control study to enhance the reliability of bioinformatics analysis. Based on the combined results of bioinformatics analysis and clinical sample validation, we aimed to ascertain novel feasible PBLs biomarkers and shed light on their possible roles in the pathogenesis of CAD.

MATERIALS AND METHODS

The methods used in our study mainly contained microarray data collection, differential expression, and methylation analysis, functional and pathway enrichment analysis, Protein-protein interaction (PPI) network establishment, module analysis, and hub genes identification, followed by experimental validation in PBLs, correlation analysis, and multivariate stepwise linear regression analysis. The research flow diagram of this study is shown in **Supplementary Figure S1**.

Microarray Data Collection

We retrieved GEO of The National Center for Biotechnology Information (NCBI) to screen datasets that contained profiling information about mRNA expressions and DNA methylations in CAD patients versus controls. A series of datasets were obtained and only those that met both the inclusion and exclusion criteria were analyzed. The detailed inclusion criteria were as follows: (Wood and Eisele, 2017) datasets involved mRNA expression information or DNA methylation status detected from PBLs; (Moran et al., 2008) those that contained both CAD patients and controls; (Gaziano et al., 2017) sample size was no less than 5 of each subgroup. Besides, datasets were

excluded if the specimen type was one of the components of PBLs, such as monocytes, granulocytes, or platelets. Only two datasets were up to the selection criteria, GSE42148, and GSE107143. Gene expression profiling array (GSE42148), measured by the Agilent-028004 SurePrint G3 Human GE 8 × 60K Microarray, provided mRNA expression data from 11 controls with normal electrocardiogram diagnoses and 13 CAD patients. The series matrix and platform files (GPL13607) were downloaded from the GEO database. The genome-wide DNA methylation profiling array (GSE107143) contained information on DNA methylation status from 8 controls with normal physical conditions and 8 CAD patients. The data were measured by Illumina HumanMethylation450 BeadChip and the series matrix file, as well as the platform file (GPL13534), which were obtained from the GEO database. In consideration of mRNA expression array, GSE71226 did not meet the inclusion criteria with a small sample size of 3 CAD patients and 3 controls, meaning we only used it to evaluate the discriminating ability of candidate gene mining.

Differential Expression Analysis

The R package named "limma" was utilized to select differentially expressed genes (DEGs) from the series matrix file downloaded from the GEO database (Ritchie et al., 2015). Probes without matching gene symbols were deleted and genes with multiple probes were averaged in the subsequent analysis. We took $P < 0.05$ and absolute value of $\log_2$FC (fold change) > 0.3 as the threshold of significant DEGs. A heatmap based on the expression data was drawn using the R package "pheatmap."

Differential DNA Methylation Analysis

AS, one of the mainstream detection platforms for DNA methylation, Illumina HumanMethylation450 BeadChip covered roughly 450,000 CpGs that randomly separate in different gene regions, including TSS1500, TSS200, 5′UTR, 1stExon, body, 3′UTR, and intergenic regions. TSS1500 and TSS200 are regions from 201 to 1500 bases and 1 to 200 bases of the upstream of transcriptional start site (TSS), respectively. The "5′UTR (5′ untranslated region)" is considered as the region between TSS and the first initiation codon. "1stExon (the first exon)" is one of the most extensively studied translated regions that is generally influenced by methylation status. "Body" stands for the sequence from the first initiation codon to the stop codon of a gene. The "3′UTR (3′ untranslated region)" is the area between the stop codon and poly-A tail. The 6 intragenic regions mentioned above are the main components of a gene and we took the average of the beta value of CpGs from the same region as the comprehensive methylation level of each intragenic region. The limma package of R was used for identification of differentially methylated CpGs sites (DMCs), differentially methylated regions (DMRs), and differentially methylated genes (DMGs) with the threshold $P < 0.05$ and $\log_2$FC > 0.3. Single CpGs met the threshold were taken as DMCs, meanwhile, intragenic regions that matched the threshold were identified as DMRs. Genes with one or more DMRs that differentially methylated in the same direction were considered as DMGs. We defined genes that were identified both as DEGs and DMGs as differentially expressed-methylated genes (DEMGs). The Upset plot performed by R package "UpSetR" was utilized to describe the distribution of DMCs in different intragenic regions (Conway et al., 2017). The locations of DMCs on chromosomes were visualized by R package "RIdeogram" (Zhaodong et al., 2019).

Functional and Pathway Enrichment Analysis

The r package "clusterProfiler" was USED to implement Gene ontology (GO) enrichment analysis and the Kyoto Encyclopedia of Genes and Genomes (KEGG) for pathway analysis (Kanehisa and Goto, 2000; Gene Ontology Consortium, 2006). More precisely, GO enrichment analysis was carried out within 3 classical subschemas: biological process (BP), cellular component (CC), and molecular function (MF). Subsequently, we utilized "ggplot2" for visualization of the results. The cutoff value of statistical significance was set as $P < 0.05$.

PPI Network Establishment, a Module Analysis, and Hub Gene Identification

A PPI network was preliminarily constructed through the Search Tool for the Retrieval of Interacting Genes (STRING) database, as a way to explore the inherent relation and regularity of DEMGs. The cutoff value of the interaction score in the STRING database was set at 0.4. To make the PPI network more legible, we used Cytoscape to visualize the network based on interaction information calculated from STRING (Shannon et al., 2003). An auxiliary application named Molecular Complex Detection (MCODE) from Cytoscape was used for module analysis to identify modules with significant interaction under threshold MCODE scores > 3, k-score $= 2$ and nodes numbers > 4. CytoHubba, another application from Cytoscape, provided 12 algorithms to estimate evidence levels of interaction within genes from the PPI network (Chin et al., 2014). We summarized these 12 evaluation scores as the comprehensive assessment standard for screening top hub genes.

Study Population and PBLs Collection

We performed a case-control study to consolidate the expression status of hub genes filtered through bioinformatics analysis. PBLs of 40 CAD patients from Zhongnan Hospital of Wuhan University (Wuhan, China) were collected from December 2018 and July 2019. The diagnostic criterion for CAD was based on coronary angiography that showed stenosis caused by atherosclerotic plaque was more than 50% in at least one coronary artery. Meanwhile, 36 age and sex matched people who were negative in the examination of ultrasound or coronary CTA or coronary angiography were enrolled as controls. None of the participants were diagnosed with the following diseases: cancer, acute inflammation, hematological system disorders, congenital heart disease, history of previous myocardial infarction (MI), hepatic failure, or other severe disorders. The basic information and clinical characteristics of participants are shown in **Table 1**. Our study was authorized by the Medical Ethics Committee of Zhongnan Hospital of Wuhan University.

TABLE 1 | Clinical characteristics of subjects in validation study.

Characteristic	Controls	CAD patients	*P* value
Demographics			
Male/Female	17/13	22/8	0.2789
Age (year)	55.27 ± 9.03	59.80 ± 9.26	0.0598
Risk factors			
History of HP (yes/no)	9/21	20/10	**0.0092**
History of DM (yes/no)	1/29	8/22	**0.0257**
Clinical parameters			
TC (mmol/L)	4.25 ± 0.72	4.53 ± 1.45	0.3429
TG (mmol/L)	1.14 ± 0.39	1.89 ± 1.43	**<0.001**
LDL-C (mmol/L)	2.60 ± 0.60	2.80 ± 1.08	0.3701
HDL-C (mmol/L)	1.41 ± 0.34	1.30 ± 0.47	0.2964
FPG (mmol/L)	5.48 (5.03, 5.73)	5.69 (5.18, 6.90)	0.0740
WBC ($\times 10^9$)	5.84 ± 1.33	6.33 ± 1.77	0.2290
Monocyte ($\times 10^9$)	0.43 ± 0.11	0.58 ± 0.21	**<0.001**
Neutrophil ($\times 10^9$)	3.31 ± 1.03	3.97 ± 1.28	**0.0315**
Lymphocyte ($\times 10^9$)	1.93 ± 0.51	1.60 ± 0.61	**0.0250**
LMR (ratio)	4.68 ± 1.17	2.98 ± 1.21	**<0.001**
NMR (ratio)	7.70 (6.13, 8.85)	6.48 (5.53, 8.90)	0.1973
NLR (ratio)	1.68 (1.30, 2.05)	2.58 (1.94, 3.20)	**<0.001**

Data were showed as mean ± SD, median (25 percentiles, 75 percentiles). HP, hypertension; DM, diabetes mellitus; TC, total cholesterol; TG, triglycerides; LDL-C, low-density lipoprotein cholesterol; HDL-C, high-density lipoprotein cholesterol; FPG, fasting plasma glucose; WBC, white blood cell; LMR, lymphocyte to monocyte ratio; NMR, neutrophil to monocyte ratio; NLR, neutrophil to lymphocyte ratio. Entries in bold font indicate statistically significant (P < 0.05).

The mRNA Expression Analysis

RNA was isolated from PBLs of 30 CAD patients and 30 controls using TRIZOL reagent (Life Technologies, United States). To assess the concentration and purity of RNA, NanoDrop 2000C was applied. About 1 microgram RNA of each sample was used for reverse transcription into complementary DNA (cDNA) through the PrimeScript^{TM} RT reagent kit with gDNA Remover (Takara, Japan). The qPCR was carried out using SYBR Green I UltraSYBR Mixture (CWBIO, China) on Bio-Rad CFX96 (Bio-Rad Laboratories, United States). We took *glyceraldehyde 3-phosphate dehydrogenase (GAPDH)* as an endogenous reference gene to normalize the expression level among multiple samples. The specific sequences of each pair of primers were available in **Supplementary Table S1**. All experiments were performed twice. Relative gene expression status was calculated by the $2^{-\Delta Cq}$ method, in which ΔCq stands for the difference between the mean Cq (quantification cycle) of a target gene and the endogenous reference gene (*GAPDH*).

The DNA Methylation Analysis

Genomic DNA was extracted from the PBLs of 30 CAD patients and 30 controls using standard phenol/chloroform extraction. DNA was quantified by the NanoDrop-2000C (Thermo Fisher Scientific, United States) and stored at -20°C until use. Due to the limited volume of the PBLs, PBLs from 10 CAD patients and 6 controls were only utilized to extract DNA, and PBLs from 10 CAD patients and 6 controls were only used to extract RNA. PBLs from 20 CAD patients and 24 controls were used to extract both DNA and RNA. Methylation-dependent restriction enzyme digestion based quantitative PCR (MDRE-qPCR) and methylation-sensitive restriction enzyme digestion based quantitative PCR (MSRE-qPCR) were adopted in methylation detection (Redshaw et al., 2014). Methylation-dependent restriction enzyme MspJI and FspEI (New England Biolabs, United States) were used in the analysis of FN1 and PTEN, respectively. POLR3A was detected using methylation-sensitive restriction enzyme Hin6I (SibEnzyme, China). The sequences of primers used in the experiments were listed in **Supplementary Table S1**. The methylation level was calculated by $100\% \times [1-2^{\Delta Cq(\text{undigested}-\text{digested})}]$ in MDRE-qPCR, while $100\% \times 2^{\Delta Cq(\text{undigested}-\text{digested})}$ was the formula used in MSRE-qPCR (Zhang et al., 2015). To verify the efficacy of enzyme digestion, Methylated HCT116 gDNA, and Unmethylated HCT116 DKO gDNA (Takara, China) was adopted as the positive control and the negative control, respectively, in each experiment. Only when the methylation levels of positive controls were close to 1 and the methylation levels of negative controls were close to zero, the enzyme digestion could be taken as eligible. All experiments were performed twice to enhance the dependability.

Statistical Analysis

Mean ± standard deviation (SD) was utilized to describe the basic information and clinical characteristics that were normal distributed continuous variables. Abnormal distributed continuous variables were depicted as the median and inter-quartile range. Categorical variables were exhibited by frequencies. We applied a student's *t* test or Mann-Whitney *U* tests to compare the difference between 2 groups based on the distribution type. Chi-square test or Fisher's exact test were performed, enabling comparison of categorical variables between groups. The Pearson or Spearman test was used for correlation analysis. We utilized multivariate stepwise linear regression to eliminate interference factors in regression analysis. The receiver operation curve (ROC) was drawn to appraise the diagnostic value of hub genes. Youden's index was used to screen out the optimum cutoff point of sensitivity (Se) and specificity (Sp). All statistical analyses of this research were conducted through SPSS version 25.0 (SPSS Inc., United States) and GraphPad Prism 8.0 (GraphPad Inc., United States). A statistically significant threshold of two-sided *P* value was set at 0.05.

RESULTS

General Characteristics of DEGs, DMCs, DMGs, and DEMGs

A total of 3351 DEGs were identified, among which 1863 genes were up-regulated, and 1488 genes were down-regulated in CAD patients' PBLs compared with controls'. Another microarray dataset from GEO (GSE107143) was used to explore DMCs among approximately 450, 000 CpGs in 8 CAD patients and 8 controls. In aggregate, 7694 DMCs were identified and 3362 of DMCs were hypermethylated, and the other 4332 DMCs were hypomethylated according to the $\log_2$FC of delta of beta value. The distribution of DMCs on chromosomes is exhibited

in **Figure 1**. Interestingly, none of DMCs were found on sex chromosomes nor the short arms of chromosomes 13, 14, 15, 21, and 22. Meanwhile, it could be observed that DMCs in regions around centromeres were relatively sparse compared to other chromosome regions. To further investigate whether the difference in DMCs density distribution was significant statistically, we calculated the DMCs density in centromere regions and other chromosome regions. We took the 11.1 subbands from both the short arm and the long arm of one chromosome as the centromere region based on genome version GRCh37.p13. As shown in **Table 2**, the DMCs density was much lower in centromere when compared with other regions ($P < 0.001$), which indicates that there might be a correlation between chromosome regions and gene methylation status.

To probe into the potential effect of the whole intragenic regions' methylation status on gene function, we considered genes with one or more DMRs that differentially methylated in the same direction as DMGs. About 2413 hypermethylated genes and 2952 hypomethylated genes were classified based on DMRs. Subsequently, 135 genes were identified as up-regulated and hypermethylated (up-hyper genes), 212 genes were confirmed as up-regulated and hypomethylated (up-hypo genes), 100 genes were taken as down-regulated and hypermethylated (down-hyper genes), 88 genes were considered as down-regulated and hypomethylated (down-hypo genes) by overlapping DEGs and DMGs (**Figure 2A**).

Our integration analysis combined both expression and methylation data. The sensitivity and specificity of identifying potential functional genes might be affected when compared with traditional one type microarray data mining. Another expression microarray GSE71226 was analyzed as a quality assessment. As displayed in **Figure 2B**, there were 281 (2.2%) overlapped up-regulated genes, and 234 (1.8%) overlapped down-regulated genes in overlaps of GSE42148 and GSE71226 expression arrays. By contrast, a combination of expression and methylation arrays identified overlapped DEMGs with 135 (1.7%) up-hyper genes and 88 (1.1%) down-hypo genes (**Figure 2A**).

In total, 535 differentially expressed and methylated genes were screened out as DEMGs. It was worth noting that up-hyper genes and down-hypo genes occupied virtually half of DEMGs, which indicated the multidirectional regulation of methylation on gene function that is worth further study. Heatmaps were formed according to the hierarchical clustering of gene expressions or methylations levels to exhibit the top 50 ranked DEMGs by $\log_2$FC, respectively (**Figures 2C,D**). The full list of DEGs, DMCs, DMGs, and DEMGs can be found in **Supplementary Table S2**.

Distributions of DMCs in Intragenic Regions

DMCs were inhomogenously distributed in 6 intragenic regions of DMGs and DEMGs. As **Figure 3A,B** show, DMCs located in TSS1500 and the body of both DMGs and DEMGs accounted for over 50% of the total DMCs numbers. In contrast, there was less than 3% DMCs distributed in 3′UTR. In terms of linear lengths, the TSS1500 body is much longer than TSS200 and 5′UTR, and it is more reasonable to take TSS200 and 5′UTR as the high enrichment areas of DMCs. These results indicated the significant correlation of TSS200 and 5′UTR methylation status and gene expression. A similar distribution mode can be found in 4 kinds of DEMGs (**Figure 3C**). It can be observed

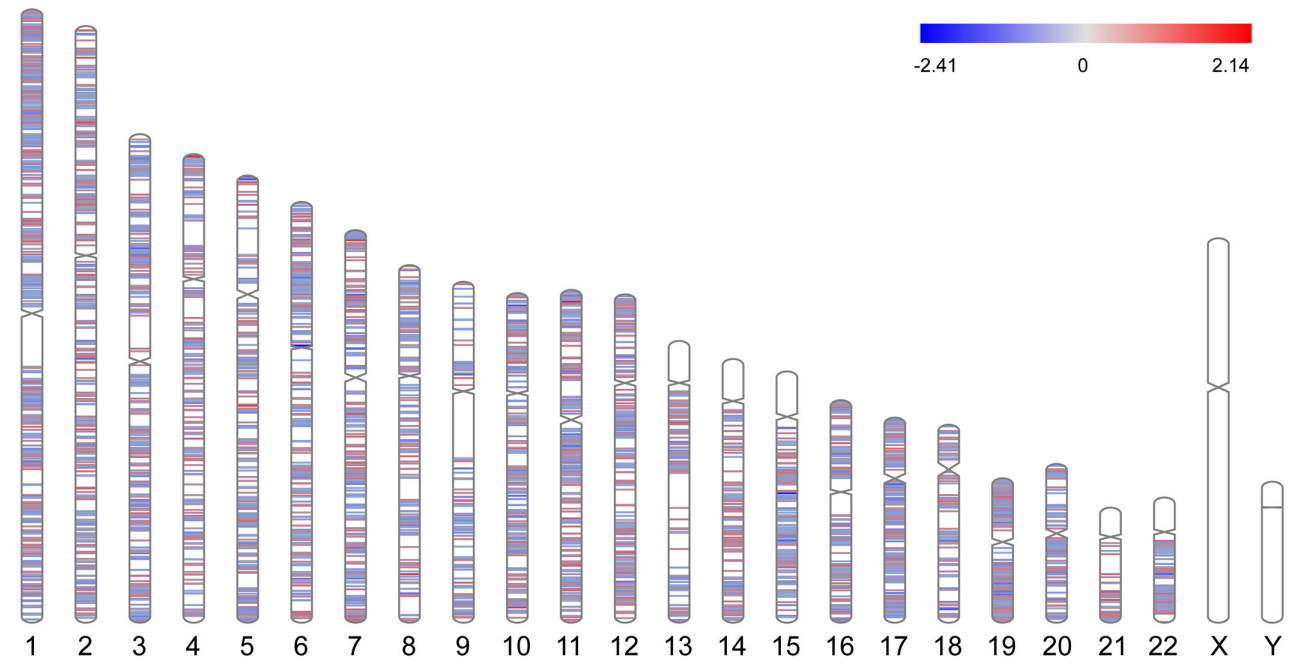

FIGURE 1 | Chromosome distributions of DMCs. Hypermethylated DMCs were marked in red, hypomethylated DMCs were marked in blue.

TABLE 2 | Density distribution of intragenic DMCs in centromere and other chromosome regions.

Chromosome ID	Centromere length (Mb)	Other regions length (Mb)	DMCs in centromere	DMCs in other regions	DMCs density in centromere (n/Mb)	DMCs density in other regions (n/Mb)	*P* value
1	7.40	241.85	0	805	0.00	3.33	**<0.001***
2	6.30	236.68	1	486	0.16	2.05	
3	6.00	192.02	2	465	0.33	2.42	
4	4.50	186.65	1	294	0.22	1.58	
5	4.60	176.32	0	445	0.00	2.52	
6	4.60	166.52	0	607	0.00	3.65	
7	3.70	155.44	0	440	0.00	2.83	
8	5.00	141.36	1	257	0.20	1.82	
9	3.40	137.81	0	172	0.00	1.25	
10	4.30	131.23	2	355	0.47	2.71	
11	4.10	130.91	0	483	0.00	3.69	
12	4.90	128.95	1	422	0.20	3.27	
13	3.20	111.97	0	149	0.00	1.33	
14	3.00	104.35	0	213	0.00	2.04	
15	4.90	97.63	0	238	0.00	2.44	
16	4.00	86.35	0	322	0.00	3.73	
17	3.60	77.60	2	476	0.56	6.13	
18	3.60	74.48	1	109	0.28	1.46	
19	4.20	54.93	1	519	0.24	9.45	
20	3.80	59.23	1	215	0.26	3.63	
21	3.40	44.73	0	53	0.00	1.18	
22	5.70	45.60	4	152	0.70	3.33	

**Paired t test between DMCs density in centromere and DMCs density in other regions. Mb, million base pair.*

that DMCs in 6 intragenic regions were mostly possessed by up-hypo genes, which manifested up-hypo genes as major roles in epigenetic regulation of CAD. These results indicate a significant correlation between TSS200 and 5′UTR methylation status and gene expression.

To demonstrate relevance among intragenic regions, UpSet plots were drawn to describe the methylation status of a certain DMGs with one or more DMRs. Over 70% of both hypermethylated genes and hypomethylated genes were single region-specific in TSS1500, TSS200, 5′UTR, or body (**Figures 3D,E**), while DMGs with multiple DMRs were mainly occupied by 5′UTR and 1stExon, TSS1500 and TSS200, TSS200, and 5′UTR. Even more noteworthy is the fact that approximately 6% of DMGs had 3 or more differentially methylated regions, which represented a general differential methylation status of a certain gene in CAD patients compared to controls.

GO Functional and KEGG Pathway Enrichment Analysis of DEMGs

We performed GO functional and KEGG pathway enrichment analysis on up-hyper, up-hypo, down-hyper, down-hypo genes separately to explore the inner connection of DEMGs. The top 5 GO enrichment terms were illustrated in **Table 3**, from which we could find DEMGs enriched in numerous processes. Up-hyper genes were enriched in the biological process and 2 terms were associated with actin cytoskeleton reorganization. Four-fifths of terms enriched on up-hypo genes were related to organelle membrane or granule membrane. Notably, the rest 1 term of up-hypo genes was neutrophil activation, which enriched most genes among the top 5 terms. AS for down-hyper genes, GO terms were majorly centered on DNA-directed RNA polymerase activity, which indicates a potential connection between DNA methylation and mRNA expression. Besides, 2 terms of down-hypo genes were involved in the regulation of calcium ion transportation.

Table 4 exhibits top KEGG pathways of 4 kinds DEMGs. Enrichment analysis suggested up-hyper genes were significantly enriched in the VEGF signaling pathway and adipocytokine signaling pathway that might link with blood lipids. Up-hypo genes are mainly enriched in autophagy, vitamin digestion and absorption, and PI3K-Akt signaling pathway. There were fewer KEGG pathways enriched in down-hyper and down-hypo genes by comparison with up-regulated DEMGs. Only RNA polymerase and Fanconi anemia pathways, were identified in down-hyper genes. Down-hypo genes were associated with other types of O-glycan biosynthesis, cytosolic DNA-sensing pathway, mRNA surveillance pathway, and non-homologous end-joining.

PPI Network Establishment, a Module Analysis, and Hub Genes Identification

To excavate the interaction among DEMGs, PPI networks based on STRING were visualized by Cytoscape for 4 kinds

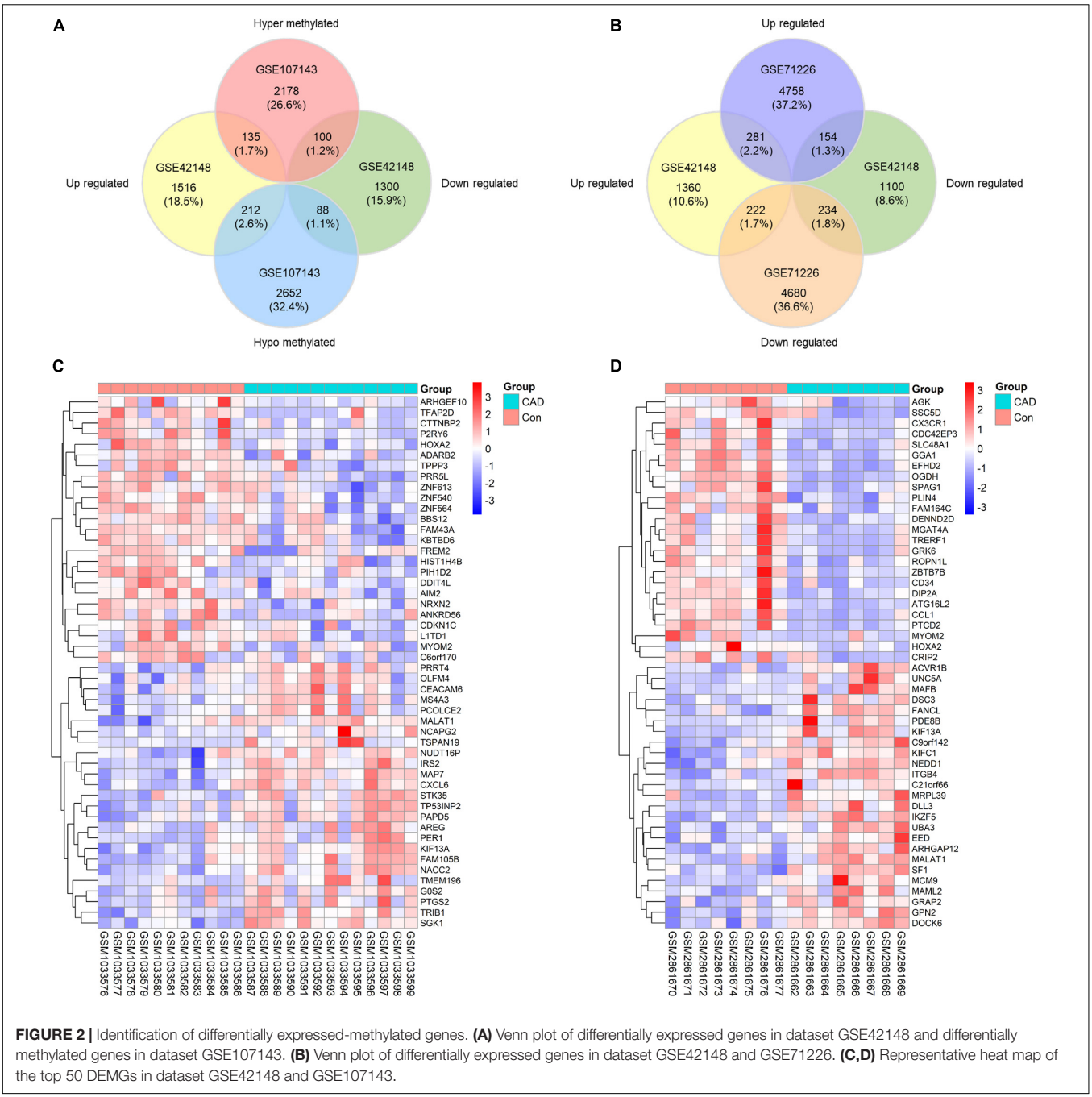

FIGURE 2 | Identification of differentially expressed-methylated genes. **(A)** Venn plot of differentially expressed genes in dataset GSE42148 and differentially methylated genes in dataset GSE107143. **(B)** Venn plot of differentially expressed genes in dataset GSE42148 and GSE71226. **(C,D)** Representative heat map of the top 50 DEMGs in dataset GSE42148 and GSE107143.

of DEMGs, respectively. The radius of each gene circle in the PPI network was positively associated with the absolute value of $\log_2$FC of mRNA expression between CAD patients and controls. Analogously, the color depth of each gene circle represents the methylation status of genes in the PPI network. The darker the color, the greater the difference of methylation levels between 2 study populations. Module analysis was performed to simplify the PPI network and focus on certain modules with stronger interactions. Subsequently, hub genes were filtered by 12 algorithms based on the bioinformatics analysis.

As displayed in **Figure 4A,B**, the top 10 hub genes of up-hyper genes are FN1, STAT3, CDC42, DDX5, ABL1, PTGS2, PCSK2, PNISR, XRN2, and SF1. PPI network, top 3 modules, and top 10 up-hypo hub genes were shown in **Figures 4C,D**. More precisely, the top 10 hub genes of up-hypo genes including PTEN, KRAS, MMP9, MAP1LC3A, ITCH, TGOLN2, CD34, KIT, WDFY4, and SPTBN1. The same module analysis and hub gene screening were performed on down-hyper genes, identifying the top 10 hub genes were POLR3A, HIST1H4B, CTTNBP2, EED, CETN3, TUBE1, FHL2, GRID2, GMNN, and MRPL39 (**Figures 4E,F**). While the top

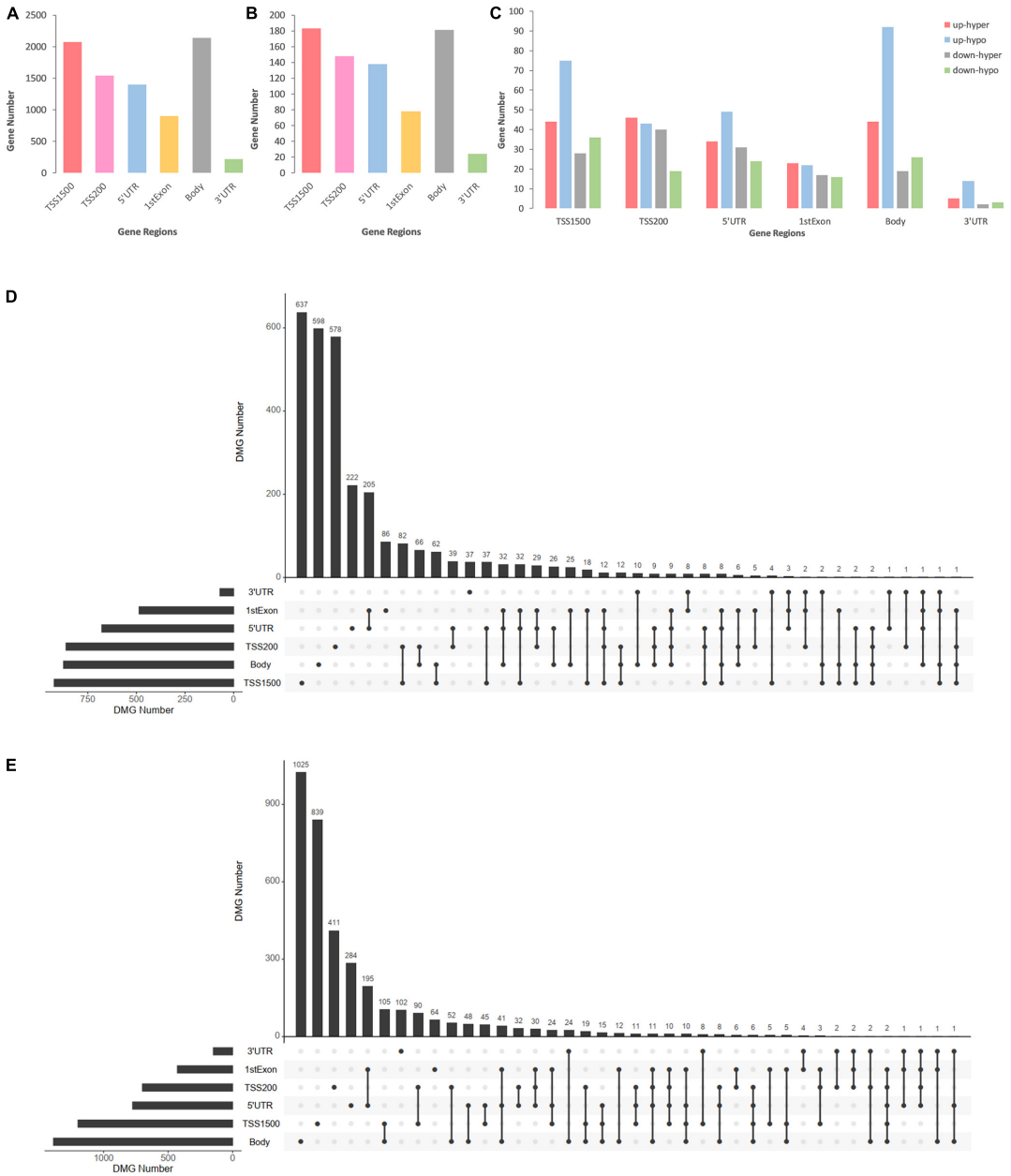

FIGURE 3 | Consolidation analysis results of gene region distributions of intragenic DMCs. **(A)** Bar plot for intragenic DMCs in different regions of DMGs. **(B)** Bar plot for intragenic DMCs in different regions of DEMGs. **(C)** Bar plot for intragenic DMCs in different regions of four DEMGs groups. **(D)** UpSet plot for intragenic DMCs in different regions of hypermethylated genes. **(E)** UpSet plot for intragenic DMCs in different regions of hypomethylated genes.

10 hub genes based on interaction information from the PPI network of down-hypo genes were UBR1, TREX1, CDKN1C, UBE2T, ID3, DHX36, LFNG, LIMD1, EPHB3, and AIM2 (**Figures 4G,H**).

GO Functional Enrichment Analysis of Hub Genes

To illustrate the functional interrelation of hub genes, GO enrichment analysis was conducted in the top 10 hub genes of 4 DEMGs subgroups (**Figure 5**). Up-hyper hub genes were majorly enriched in terms of acute-phase response and positive regulation of the post-transcription. Regulation of synaptic function and membrane biogenesis were the main terms enriched in up-hypo genes. Intriguingly, down-hyper genes were observed to be associated with the regulation of histone H3-K27 methylation and participated in the regulation of postsynaptic in ways that were similar to up-hypo genes. Terms enriched in down-hypo genes were mostly related to response to interferons and urogenital system development.

TABLE 3 | List of top enriched GO terms of 4 DEMGs groups.

Category	Terms	ID	Description	Gene count	%	*P* value	Genes
Up-hyper genes	BP	GO:0034446	Substrate adhesion-dependent cell spreading	6	5.77	2.02E-05	ABL1, CDC42, FER, FN1, MICALL2, TRIOBP
	BP	GO:2000251	Positive regulation of actin cytoskeleton reorganization	3	2.88	1.52E-04	ABL1, BAIAP2L1, CDC42
	BP	GO:0042749	Regulation of circadian sleep/wake cycle	3	2.88	2.08E-04	CHRNB2, NR1D1, PER3
	BP	GO:0031532	Actin cytoskeleton reorganization	5	4.81	2.52E-04	ABL1, BAIAP2L1, CDC42, FER, MICALL2
	BP	GO:2000637	Positive regulation of gene silencing by miRNA	3	2.88	2.74E-04	DDX5, STAT3, TRIM71
Up-hypo genes	CC	GO:0016323	Basolateral plasma membrane	11	6.01	6.06E-06	ABCC1, AQP9, ATP6V1B1, B4GALT1, CD34, EZR, FLOT2, KCNQ1, MAP7, SLC19A1, SLC23A1
	CC	GO:0035579	Specific granule membrane	7	3.83	2.22E-05	CD59, MMP25, MS4A3, PLAUR, PLD1, PTPRJ, VAMP1
	CC	GO:0030667	Secretory granule membrane	12	6.56	2.33E-05	B4GALT1, CD59, CEACAM6, FLOT2, ICA1, MMP25, MS4A3, PLAUR, PLD1, PTPRJ, SLC11A1, VAMP1
	CC	GO:0033116	Endoplasmic reticulum Golgi intermediate compartment membrane	6	3.28	5.11E-05	AREG, CD59, CSNK1D, ERGIC1, MPPE1, NAT8
	BP	GO:0042119	Neutrophil activation	15	8.62	6.84E-05	B4GALT1, CAP1, CD59, CEACAM6, CXCL6, IMPDH1, MMP25, MMP9, MPO, MS4A3, OLFM4, PLAUR, PLD1, PTPRJ, SLC11A1
Down-hyper genes	MF	GO:0003899	DNA-directed 5′-3′ RNA polymerase activity	3	3.53	9.99E-04	CD3EAP, POLR3A, ZNRD1
	CC	GO:0030008	TRAPP complex	2	2.30	1.23E-03	TRAPPC4, TRAPPC5
	CC	GO:0055029	Nuclear DNA-directed RNA polymerase complex	4	4.60	1.29E-03	CD3EAP, POLR3A, RPRD1A, ZNRD1
	MF	GO:0034062	5′-3′ RNA polymerase activity	3	3.53	1.31E-03	CD3EAP, POLR3A, ZNRD1
	MF	GO:0097747	RNA polymerase activity	3	3.53	1.31E-03	CD3EAP, POLR3A, ZNRD1
Down-hypo genes	BP	GO:0034644	Cellular response to UV	4	5.80	2.40E-04	CRIP1, DHX36, TREX1, TRIAP1
	BP	GO:0002244	Hematopoietic progenitor cell differentiation	5	7.25	3.71E-04	C12orf29, DHX36, TCF12, TREX1, ZBTB24
	BP	GO:0051281	Positive regulation of release of sequestered calcium ion into cytosol	3	4.35	4.33E-04	F2RL3, P2RY6, TRPC1
	BP	GO:0045668	Negative regulation of osteoblast differentiation	3	4.35	8.86E-04	HOXA2, ID3, LIMD1
	BP	GO:0010524	Positive regulation of calcium ion transport into cytosol	3	4.35	1.05E-03	F2RL3, P2RY6, TRPC1

TABLE 4 | List of top enriched KEGG terms of 4 DEMGs groups.

Category	ID	Description	Gene count	%	*P* value	Genes
Up-hyper genes	hsa04370	VEGF signaling pathway	5	9.80	3.44E-05	AKT2, CDC42, KDR, PPP3CA, PTGS2
	hsa05206	MicroRNAs in cancer	8	15.69	7.21E-04	ABL1, IRS2, MARCKS, PTGS2, RPS6KA5, SOX4, STAT3, TRIM71
	hsa04722	Neurotrophin signaling pathway	5	9.80	9.38E-04	ABL1, AKT2, CDC42, IRAK3, RPS6KA5
	hsa04920	Adipocytokine signaling pathway	4	7.84	9.57E-04	AKT2, IRS2, RXRG, STAT3
	hsa05165	Human papillomavirus infection	8	15.69	1.08E-03	AKT2, CDC42, FN1, ITGB4, MAML2, MAML3, PTGS2, THBS4
Up-hypo genes	hsa04140	Autophagy - animal	7	7.87	8.25E-04	ATG16L2, CAMKK2, CFLAR, KRAS, PPP2CA, PTEN, TP53INP2
	hsa04977	Vitamin digestion and absorption	3	3.37	2.32E-03	ABCC1, SLC19A1, SLC23A1
	hsa04710	Circadian rhythm	3	3.37	4.87E-03	BHLHE40, CSNK1D, PER1
	hsa04151	PI3K-Akt signaling pathway	10	11.24	6.00E-03	AREG, CSF3R, IFNAR2, KIT, KRAS, MYB, PIK3R6, PPP2CA, PTEN, SGK1
	hsa05221	Acute myeloid leukemia	4	4.49	6.59E-03	KIT, KRAS, MPO, RUNX1
Down-hyper genes	hsa03020	RNA polymerase	2	7.41	4.87E-03	POLR3A, ZNRD1
	hsa03460	Fanconi anemia pathway	2	7.41	1.43E-02	FANCF, FANCL
Down-hypo genes	hsa00514	Other types of O-glycan biosynthesis	2	6.90	1.21E-02	GALNT3, LFNG
	hsa04623	Cytosolic DNA-sensing pathway	2	6.90	2.19E-02	AIM2, TREX1
	hsa03015	mRNA surveillance pathway	2	6.90	4.31E-02	PPP2R2B, RNGTT
	hsa03450	Non-homologous end-joining	1	3.45	4.65E-02	RAD50

Clinical Characteristics of Subjects in the Validation Study

The clinical parameters of CAD patients and controls are summarized in **Table 1**. Groups of participants were matched in terms of gender and age. More CAD patients suffered from hypertension (HP) (P = 0.009) and diabetes mellitus (DM) (P = 0.025) compared with the controls. Among the serum lipid parameters, no conspicuous differences were observed in total cholesterol (TC), low density lipoprotein cholesterol (LDL-C), high density lipoprotein cholesterol (HDL-C). While the level of triglyceride (TG) was much higher in CAD patients ($P < 0.001$), the leucocyte differential count revealed a significant increase of monocytes ($P < 0.001$) and neutrophils (P = 0.031), but a prominent decrease of lymphocytes (P = 0.025) in CAD patients. Parameters based on leucocyte differential counts such as the lymphocyte to monocyte ratio (LMR) ($P < 0.001$) were decreased while the neutrophil to lymphocyte ratio (NLR) ($P < 0.001$) was increased in CAD patients.

Hub Genes' Expression and Methylation Status in the Validation Study

In order to validate the significance of the hub genes identified during bioinformatics analysis, the mRNA expression levels of top 1 hub genes from 4 DEMGs groups were detected by qPCR. In accord with the bioinformatics results, the FN1 (P = 0.001) from up-hyper genes and PTEN ($P < 0.001$) belonged to up-hypo genes and were remarkably upregulated in CAD patients when compared with controls (**Figures 6A,B**). The mRNA expression level of POLR3A, the top 1 hub gene of down-hyper genes, was conspicuously decreased in patients with CAD, which was also consistent with the bioinformatics results (P = 0.004, **Figure 6C**). Nevertheless, the foremost hub gene UBR1 from down-hypo genes was not differentially expressed between CAD patients and controls (P = 0.687, **Figure 6D**).

When considering the hub genes from DEMGs, we speculated that the significant expression differences of FN1, PTEN, and POLR3A were correlated with the aberrant DNA methylation status in CAD patients. According to the results of our bioinformatics analysis, FN1 was hypermethylated in 5′UTR, PTEN was hypomethylated in 5′UTR, and POLR3A was hypermethylated in TSS200. We detected the methylation status of corresponding regions by MDRE-qPCR and MSRE-qPCR. As displayed in **Figure 6E**, the 5′UTR of FN1 was prominently hypermethylated in CAD patients ($P < 0.001$). The methylation level was lower in the 5′UTR of PTEN in patients with CAD (P = 0.014, **Figure 6F**). TSS200 of POLR3A showed higher methylation status in CAD patients (P = 0.031, **Figure 6G**).

Meanwhile, the methylation of FN1 was positively related with the expression level (r = 0.379, P = 0.011, **Figure 6H**). Negative correlation between PTEN methylation and expression was demonstrated in **Figure 6I** ($r = -0.338$, P = 0.025). However, no obvious correlation was found in the methylation and expression of POLR3A ($r = -0.125$, P = 0.418, **Figure 6J**).

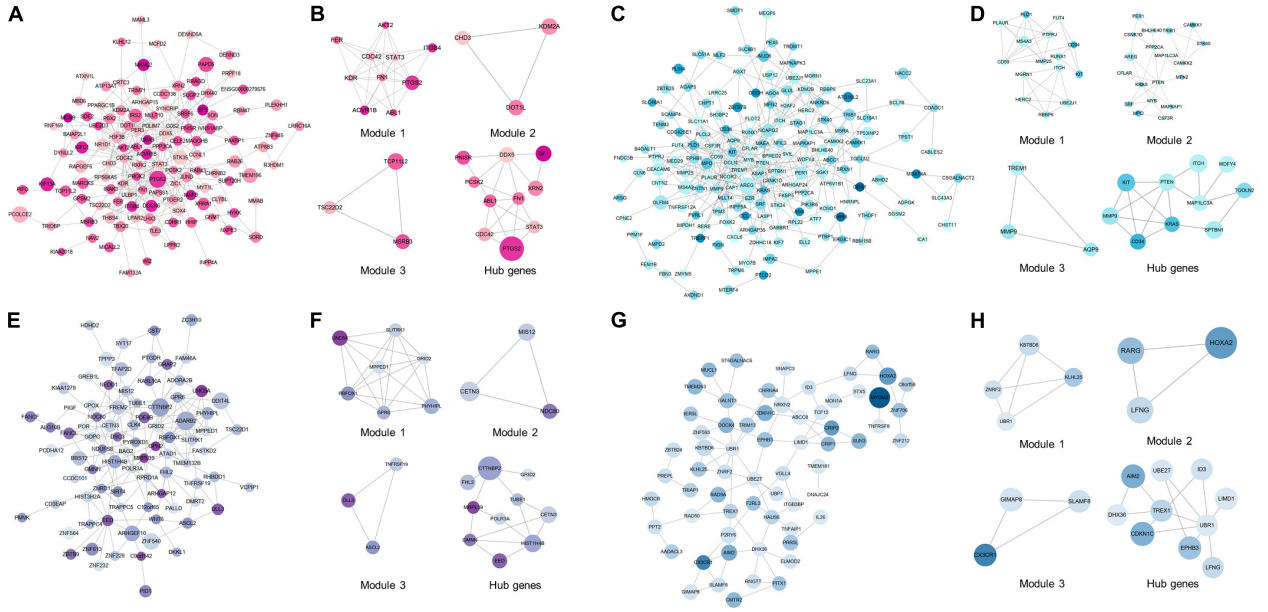

FIGURE 4 | PPI network, top 3 modules, and top 10 hub genes of 4 DEMGs groups. **(A,B)** Up-hyper genes. **(C,D)** Up-hypo genes. **(E,F)** Down-hyper genes. **(G,H)** Down-hypo genes.

Predictive Validity of Hub Genes

To evaluate the predictive validity of hub genes as potential biomarkers in CAD, ROC analysis was performed based on the mRNA expression and DNA methylation levels of hub genes separately or combinedly. As displayed in **Figure 6K** and **Table 5**, the expression (AUC = 0.738, $P = 0.002$) and methylation (AUC = 0.839, $P < 0.001$) of FN1 were with moderate diagnostic value. The predictive validity of FN1 was improved with the combination of expression and methylation data (AUC = 0.894, $P < 0.001$). Moderate diagnostic value was verified in the expression of PTEN (AUC = 0.776, $P < 0.001$, **Figure 6L**). Although the methylation of PTEN had lower predictive value (AUC = 0.683, $P = 0.015$), the predictive value was remarkably increased when combined with the expression data (AUC = 0.856, $P < 0.001$). POLR3A showed comparatively lower diagnostic validity in both expression (AUC = 0.691, $P = 0.011$) and methylation levels (AUC = 0.662, $P = 0.031$, **Figure 6M**). The diagnostic ability of POLR3A was improved by taking expression and methylation data into integration (AUC = 0.779, $P = 0.002$).

Correlations Between Hub Genes Expressions and Clinical Characteristics

Correlation analysis and multivariate stepwise linear regression analysis were performed to investigate the underlying connection between the clinical characteristics of all enrolled subjects and expression levels of hub genes. As displayed in **Table 6**, both FN1 ($r = 0.268$, $P = 0.039$) and PTEN ($r = 0.326$, $P = 0.011$) were identified as positively correlated with monocyte counts. LMR was observed to be negatively related with FN1 ($r = -0.255$, $P = 0.049$) and PTEN ($r = -0.315$, $P = 0.014$), and positively correlated with POLR3A ($r = 0.288$, $P = 0.026$). Besides, PTEN was reversely associated with NMR ($r = -0.311$, $P = 0.016$) and the expression of POLR3A decreased with aging ($r = -0.320$, $P = 0.013$). In addition, although the expression of UBR1 was not confirmed to be different between CAD patients and controls, a prominent reverse correlation was verified between UBR1 and TG when all subjects were involved ($r = -0.312$, $P = 0.012$).

After adjustment of LMR by multivariate stepwise linear regression, there still existed a positive correlation of FN1 with monocyte counts ($\beta = 0.268$, $P = 0.039$). When eliminated the interference of LMR and NMR, PTEN was still associated with monocyte amounts ($\beta = 0.326$, $P = 0.011$), while POLR3A remained related to age ($\beta = -0.320$, $P = 0.013$) after adjusting LMR.

DISCUSSION

Identify epigenetic regulation patterns and certain biomarkers from PBLs would be conducive to the diagnosis, therapy, and monitor of CAD in a non-invasive approach. In this study, we filtrated genes that were both discrepantly expressed and methylated in CAD patients compared with controls. Pathways enriched by these genes were demonstrated and hub genes were screened out based on the PPI network. To verify the results of bioinformatics data analysis, expression and methylation levels of top hub genes were experimentally compared in CAD patients and controls. Furthermore, we investigated methylation patterns of different gene regions and gave evidence of the most vulnerable region to methylation in CAD. The differential expressions of top hub genes filtered from DEMGs were associated with altered DNA methylation status, which shed light on the underlying regulatory mechanism of

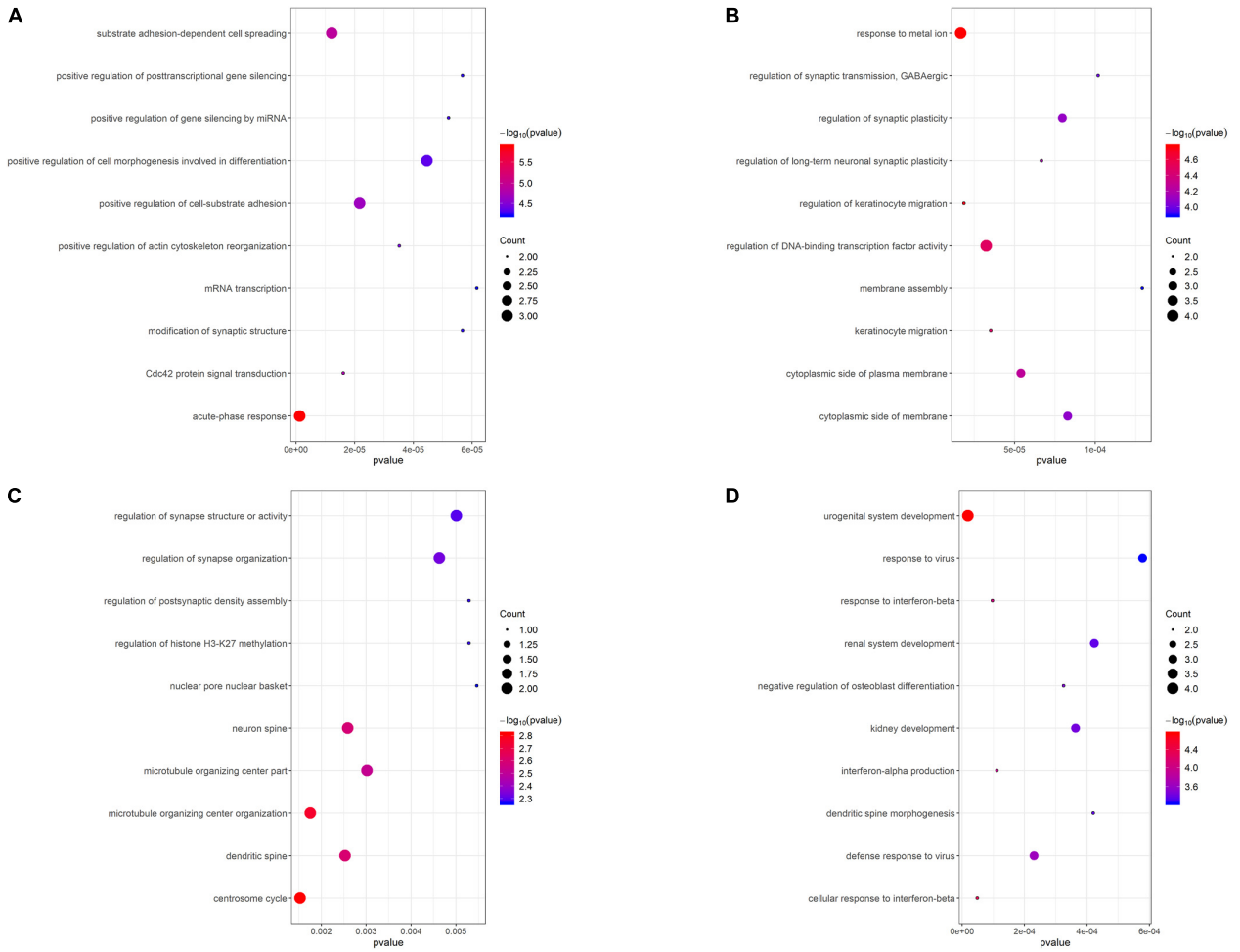

FIGURE 5 | GO functional enrichment analysis of the top 10 hub genes of 4 DEMGs groups. **(A)** Up-hyper hub genes. **(B)** Up-hypo hub genes. **(C)** Down-hyper hub genes. **(D)** Down-hypo hub genes.

DNA methylation in CAD and helped identify the novel nucleic acid biomarkers.

As the chromosome distribution map exhibited, differentially methylated CpGs covered almost every region of each chromosome. This can be regarded as the universality of methylated regulation in the pathogenesis of CAD (Deng et al., 2018). However, no DMCs were observed on sex chromosomes in our study, and a similar phenomenon was also observed in another published study of Parkinson's disease (Wang et al., 2019). We speculated this was partly due to the relatively short liner length and fewer CpG sites on sex chromosomes. Meanwhile, it is interesting to note that DMCs distributed in regions near centromeres were relatively fewer than other regions. The phenomenon might be partly attributed to the supercoiling structure and hyper-reiterated DNA sequence around the centromeres (Ichikawa et al., 2017).

Numerous published studies took promoters as key differentially methylated regions in CAD, while other intragenic regions were less concerned (Heidari et al., 2019; Indumathi et al., 2019). Recently, a few studies have demonstrated methylation sites in the gene body or TSS1500 were also essential to the pathogenesis of CAD (Liu et al., 2017). Our research confirmed that the gene body and TSS1500 possessed almost half of DMCs, no matter in DMGs or DEMGs. Nevertheless, TSS200 and 5′UTR were the most enriched intragenic areas of DMCs when we considered the linear length. A portion of hypermethylation and hypomethylation genes showed discrepant methylation status in both 5′UTR and 1stExon, or TSS1500 and TSS200, or TSS200 and 5′UTR. Given the adjacent spatial positions of the 3 pairs regions, a rational inference could be raised that the methylation status of CpGs was spatiality and regionality. We divided DEMGs into 4 groups and demonstrated up-hypo genes as the major part functioning in the progress of CAD.

Contrary to the conventional concept that DNA methylation always negatively regulates gene expression, our study found that up-hyper genes and down-hypo genes made up 42% of DEMGs. The up-hyper and down-hypo genes have been reported in a few published studies. About 43% of 32 prognostic genes showed a significant positive correlation between the expression level and the DNA methylation status in breast

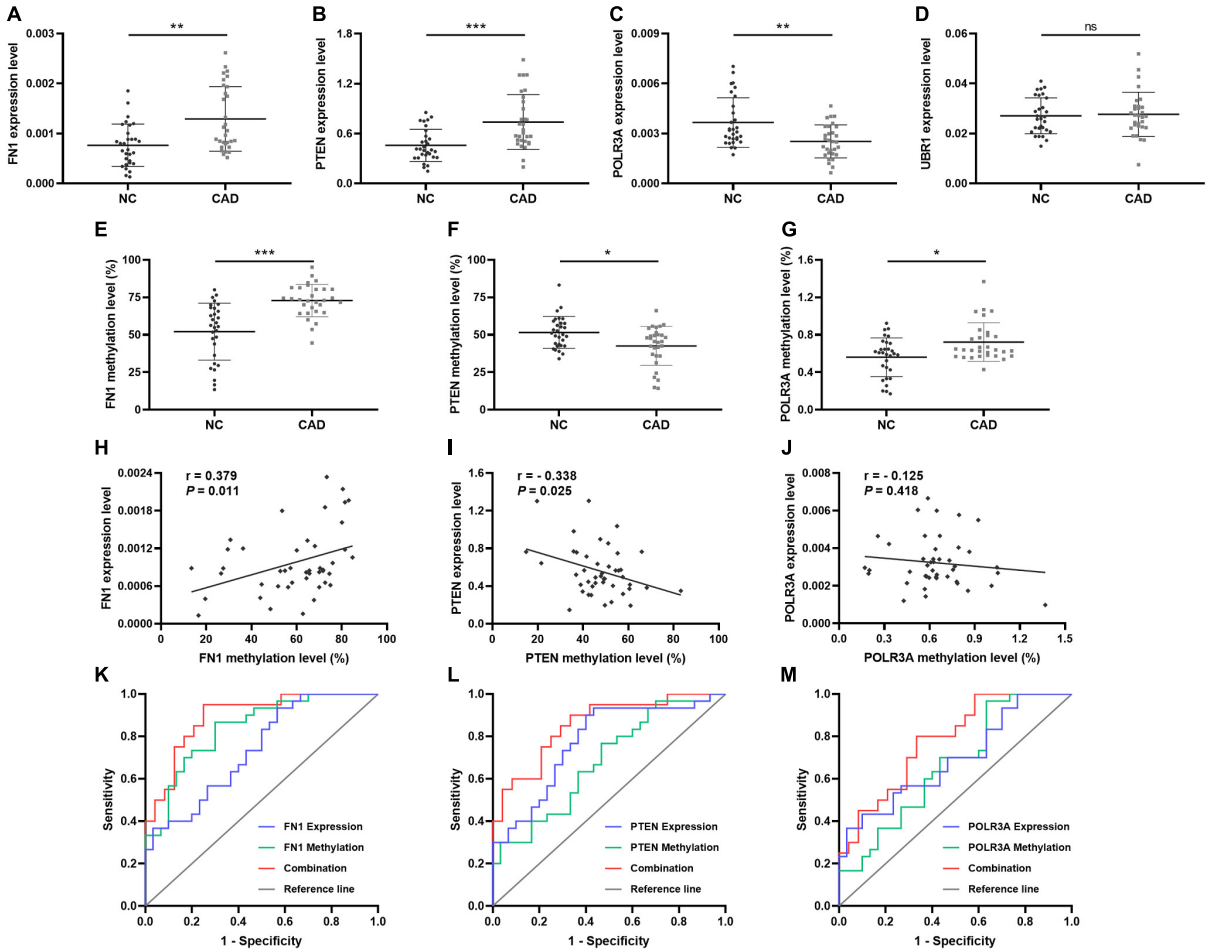

FIGURE 6 | Relative expression, methylation, and ROC of top hub genes from 4 DEMGs subgroups. Expression level in 30 CAD patients and 30 controls. **(A)** FN1. **(B)** PTEN. **(C)** POLR3A. **(D)** UBR1. Methylation levels in 30 CAD patients and 30 controls. **(E)** FN1. **(F)** PTEN. **(G)** POLR3A. Correlation between expression and methylation. **(H)** FN1. **(I)** PTEN. **(J)** POLR3A. ROC is based on expression and methylation separately or combined. **(K)** FN1. **(L)** PTEN. **(M)** POLR3A. All experiments were performed twice. $^{*}P < 0.05$, $^{**}P < 0.01$, $^{***}P < 0.001$.

cancer (Győrffy et al., 2016). In another report of lung cancer, the correlations between DNA methylation and gene expression were detected for approximately 750 genes, but for one-third of these, the correlations were positive (Bjaanæs et al., 2016). More than 30% of significant methylation-expression correlations were positive in human monocytes (Liu et al., 2013), however, no convincing explanation for this has yet been raised. We speculate that the aberrant methylated regions might encompass potential *cis*-acting elements, such as enhancers and silencers. The interaction between *cis*-acting elements and *trans*-acting elements can be multidirectional, depending on their characters in gene expression regulations. The regulatory mechanisms will become more complicated when the *cis*-acting elements have a different methylation status, given that methylation may influence the combining capacity of transcription factors through the changes of DNA spatial structure. These findings and hypotheses suggest a great diversity and complexity of epigenetic regulatory mechanisms and highlight the need for further molecular investigations.

Kyoto Encyclopedia of Genes and Genomes pathway enrichment analysis suggested up-hyper genes mainly enriched in adipocytokine signaling pathway and VEGF signaling pathway. This was consistent with previous studies in which increased expression of the adipocytokine omentin was detected in the epicardial adipose tissue of CAD patients and the unbalance of isoforms of VEGF was associated with the complexity and severity of CAD (Harada et al., 2016; Shibata et al., 2018). Up-hypo genes are primarily enriched in neutrophil activation and it has been confirmed in several studies that an increased neutrophil count was connected with the severity of CAD (Li et al., 2018). Intriguingly, hub genes belonged to down-hyper genes and were directly correlated with the regulation of histone H3-K27 methylation according to GO enrichment analysis, which indicated an underlying association between DNA methylation and histone methylation. Regulation of calcium ion transport into the cytosol was the term enriched by down-hypo genes and has been proved to affect the

TABLE 5 | ROC analysis based on the expression and methylation status of hub genes.

Hub gene	Classification	AUC	95% CI	*P* value	Se (%)	Sp (%)
FN1	Expression	0.738	0.614–0.861	0.002	93.333	43.333
	Methylation	0.839	0.740–0.938	<0.001	86.667	70.000
	Combination	0.894	0.801–0.987	<0.001	95.000	75.000
PTEN	Expression	0.776	0.656–0.895	<0.001	93.333	56.667
	Methylation	0.683	0.549–0.817	0.015	76.667	53.333
	Combination	0.856	0.746–0.967	<0.001	90.000	66.667
POLR3A	Expression	0.691	0.558–0.824	0.011	36.667	96.667
	Methylation	0.662	0.525–0.800	0.031	96.667	36.667
	Combination	0.779	0.645–0.913	0.002	80.000	66.667

AUC, area under the receiver operating characteristic curves; Se, sensitivity; Sp, specificity.

progress of CAD through the coronary smooth muscle (Badin et al., 2018).

Protein-protein interaction networks were established to excavate the interaction among DEMGs and filtrate the most central 10 hub genes from each group. Although these top hub genes were only enriched in several items from GO enrichment analysis, many of these enriched items were validated by published large-scale transcriptomics sequencing and DNA methylation studies in CAD. For instance, dysregulation of cell-substrate adhesion has been demonstrated to accelerate the progress of CAD by promoting macrophages migration in both peripheral blood and aortic tissue, which was accordant with our findings in up-hyper hub genes (Sinnaeve et al., 2009; Rask-Andersen et al., 2016). We observed that up-hypo hub genes were enriched in response to metal ion, a response also found in both peripheral blood and adipose tissue from CAD patients (Ek et al., 2016; Vacca et al., 2016). Besides, activation of the immune system was the main item that down-hypo hub genes enriched in, and similar results were indicated in plaques from the internal mammary artery, coronary artery, and great saphenous vein (Elashoff et al., 2011; Nazarenko et al., 2015). These findings indicate the molecular mechanism intercommunity in various tissues when organisms suffer from CAD.

Because of the small sample size of datasets obtained from the GEO database and accumulative deviation from bioinformatics analysis, we performed laboratory verification with a considerable sample size for each top 1 hub genes in each DEMGs subgroup. The results suggested accordant expression and methylation levels of FN1, PTEN, and POLR3A in comparison with bioinformatics analysis results. The expression of FN1 was positively related to the methylation level. Negative relevance was found between the expression and methylation status of PTEN. These significant correlations hinted that aberrant DNA methylation was involved in the regulation of FN1 and PTEN expression in CAD patients. To further investigate the mechanism of FN1, PTEN, and POLR3A in the pathogenesis of CAD, correlation analysis and multivariate stepwise linear regression analysis were performed. FN1 was positively correlated with monocyte counts. A positive correlation was also observed in PTEN with monocyte amounts. POLR3A was negatively related to age. These results indicated that FN1 and PTEN might function in the system infection since the monocytosis was the acknowledged systemic infection index.

Inflammatory cytokines activated TGF-β signaling pathway, which promoted the expression of FN1 in human endothelial cells (Chen et al., 2015). Fibronectin, encoded by FN1, was enriched in vascular subendothelial basement membrane during the early process of atherosclerotic plaque formation and aggravated the monocytes recruitment (Al-Yafeai et al., 2018). The significant up-regulation of FN1 was positively related to monocyte amounts in CAD patients. In considering the significant correlation between the expression and 5′UTR methylation of FN1, it could be inferred that the aberrant 5′UTR methylation status of FN1 induced the over expression of FN1 and triggered the recruitment of monocytes in CAD patients. However, the methylation status of 5′UTR of FN1 was positively related to the expression level, which was opposite to the conventional concept that DNA methylation was always negatively correlated with gene expressions. Since the 5′UTR of FN1 was hypermethylated, the upstream of FN1 might also be hypermethylated. We speculated the upstream of FN1 encompassed silencers, which were incapacitated due to hypermethylation. Further studies are needed to verify the hypothesis. Vascular endothelial cell injury, caused by chronic inflammation in atherosclerosis, accelerated atherosclerotic plaque formation. A series of microRNAs could bind to the 3′UTR of PTEN, altering the proliferation of vascular endothelial cells through the PI3K-Akt pathway and influencing the procession of CAD (Wang et al., 2017). Previous reports have suggested that PTEN was up-regulated in the peripheral blood mononuclear cells of CAD patients, which was consistent with our findings in PBLs and confirmed the reliability of our research (Nariman-Saleh-Fam et al., 2019). Besides the involvement of microRNAs in the regulation of PTEN, we proved that the 5′UTR methylation of PTEN might also participate in the regulation network. Currently, no study was carried out to research the function of POLR3A in CAD or atherosclerosis. POLR3A was reported to mainly trigger leukodystrophy (Choquet et al., 2017). The correlation between POLR3A methylation and expression was not statistically significant, hinting there might be other elements that participated in the expression regulation of POLR3A, such as the wildly reported POLR3A mutations, miRNAs and transcript factors. The aberrant expression and

TABLE 6 | Correlation analysis and multivariate stepwise linear regression analysis of gene expression with clinical parameters of all participants.

Characteristics	FN1 (*n* = 60)				PTEN (*n* = 60)				POLR3A (*n* = 60)				UBR1 (*n* = 60)			
	r	***P* value**	**β**	***P* value**	**r**	***P* value**	**β**	***P* value**	**r**	***P* value**	**β**	***P* value**	**r**	***P* value**	**β**	***P* value**
Age	0.221	0.090			0.134	0.308			**−0.320**	**0.013**	**−0.320**	**0.013**	−0.223	0.087		
Gender	−0.114	0.385			−0.087	0.508			0.030	0.817			0.099	0.449		
History of HP	0.083	0.530			0.141	0.284			−0.219	0.093			−0.140	0.285		
History of DM	0.151	0.250			0.019	0.884			0.050	0.707			−0.143	0.276		
TC	0.092	0.494			0.037	0.784			0.124	0.358			0.164	0.224		
TG	0.192	0.153			0.123	0.361			−0.071	0.598			**−0.312**	**0.012**	**−0.312**	**0.012**
LDL-C	0.052	0.701			0.014	0.918			0.145	0.283			0.132	0.327		
HDL-C	−0.129	0.341			−0.150	0.267			0.042	0.759			0.194	0.148		
WBC	−0.086	0.512			−0.066	0.619			−0.021	0.871			−0.030	0.818		
Monocyte	**0.268**	**0.039**	**0.268**	**0.039**	**0.326**	**0.011**	**0.326**	**0.011**	−0.089	0.497			0.022	0.866		
Neutrophil	0.004	0.974			0.070	0.593			−0.102	0.439			−0.102	0.440		
Lymphocyte	0.144	0.271			0.089	0.500			0.207	0.113			0.113	0.390		
LMR	**−0.255**	**0.049**	−0.216	0.055	**−0.315**	**0.014**	−0.203	0.086	**0.288**	**0.026**	0.104	0.128	0.075	0.568		
NMR	−0.125	0.342			**−0.311**	**0.016**	−0.235	0.069	0.046	0.730			−0.136	0.301		
NLR	0.230	0.077			0.025	0.847			−0.185	0.157			−0.120	0.361		

Entries in bold font indicate statistically significant (P < 0.05).

methylation of POLR3A may indicate a new target for CAD, while the regulatory mechanisms still need further investigation.

In summary, our study consolidated both mRNA expression and DNA methylation microarrays of PBLs in CAD into bioinformatics analysis and executed experimental validation. The methylation patterns of CAD were profiled based on the distribution of DMCs in intragenic regions. FN1, PTEN, and POLR3A were screened as top hub genes through bioinformatics analysis and were confirmed through subsequent experimental verification in a Chinese case-control study. Further molecular and clinical experiments with a larger sample size are needed to illuminate the underlying mechanism of the differential expression and methylation of FN1, PTEN, and POLR3A in the pathogenesis of CAD.

PRE-PRINT

This manuscript has been released as a pre-print at Research Square (Zhang XK, Xiang Y, He DD, et al.) (Zhang et al., 2020).

DATA AVAILABILITY STATEMENT

Gene Expression omnibus (GEO) was the source of the primary data. The gene expression data can be found at https://www.ncbi.nlm.nih.gov/geo/query/acc.cgi?acc=GSE42148 and https://www.ncbi.nlm.nih.gov/geo/query/acc.cgi?acc=GSE71226. DNA methylation data can be downloaded at https://www.ncbi.nlm.nih.gov/geo/query/acc.cgi?acc=GSE107143.

ETHICS STATEMENT

The studies involving human participants were reviewed and approved by Medical Ethics Committee of Zhongnan Hospital of Wuhan University. Written informed consent for participation was not required for this study in accordance with the national legislation and the institutional requirements.

AUTHOR CONTRIBUTIONS

FZ conceived and designed the workflow. XZ performed the experiments and analyzed the data. XZ and FZ wrote the manuscript. YX collected the samples. DH analyzed the data and created the figures. BL, CW, and JL revised the manuscript. All authors approved the final manuscript.

FUNDING

This work was supported by grants from the National Natural Science Foundation of China (Grant No. 81871722) and the Science, Technology and Innovation Seed Fund of Wuhan University Zhongnan Hospital (Grant Nos. znpy2019054 and znpy2019049).

SUPPLEMENTARY MATERIAL

The Supplementary Material for this article can be found online at: https://www.frontiersin.org/articles/10.3389/fgene.2020.00778/full#supplementary-material

FIGURE S1 | Flow diagram of the analysis process.

TABLE S1 | Primer sequences and Tm for qPCR.

TABLE S2 | Full list of DEGs, DMCs, DMGs, and DEMGs.

REFERENCES

Al-Yafeai, Z., Yurdagul, A., Jr., Peretik, JM., Alfaidi, M., Murphy, P. A., Orr, A. W. (2018). Endothelial FN (Fibronectin) Deposition by alpha5beta1 Integrins Drives Atherogenic Inflammation. *Arterioscler. Thromb. Vasc. Biol.* 38(11), 2601–2614. doi: 10.1161/atvbaha.118.311705

Badin J. K, Bruning R. S., and Sturek M. (2018). Effect of metabolic syndrome and aging on Ca(2+) dysfunction in coronary smooth muscle and coronary artery disease severity in Ossabaw miniature swine. *Exp. Gerontol.* 108, 247–255. doi: 10.1016/j.exger.2018.04.024

Bashore, A. C., Liu, M., Key, C. C., Boudyguina, E., Wang, X., Carroll, C. M. et al. (2019). Targeted Deletion of Hepatocyte Abca1 Increases Plasma HDL (High-Density Lipoprotein) Reverse Cholesterol Transport via the LDL (Low-Density Lipoprotein) Receptor. *Arterioscler. Thromb. Vasc. Biol.* 39(9):1747–1761. doi: 10.1161/atvbaha.119.312382

Bjaanæs, M. M., Fleischer, T, Halvorsen. A. R., Daunay, A., Busato, F., Solberg, S. et al. (2016). Genome-wide DNA methylation analyses in lung adenocarcinomas: Association with EGFR, KRAS and TP53 mutation status, gene expression and prognosis. *Mol. Oncol.* 10(2), 330–343. doi: 10.1016/j.molonc.2015.10.021

Chen, P. Y., Qin, L., Baeyens, N., Li, G., Afolabi, T., Budatha, M. et al. (2015). Endothelial-to-mesenchymal transition drives atherosclerosis progression. *J. Clin. Invest.* 125(12), 4514–4528. doi: 10.1172/jci82719

Chin, C. H., Chen, S. H., Wu, H. H., Ho, C. W., Ko, M. T., Lin, C. Y. (2014). cytoHubba: identifying hub objects and sub-networks from complex interactome. *BMC Sys. Biol.* 4:S11. doi: 10.1186/1752-0509-8-s4-s11

Choquet, K., Yang, S., Moir, R. D., Forget, D., Lariviere, R., Bouchard, A. et al. (2017). Absence of neurological abnormalities in mice homozygous for the Polr3a G672E hypomyelinating leukodystrophy mutation. *Mole. Brain* 10(1), 1–13. doi: 10.1186/s13041-017-0294-y

Conway, J. R., Lex, A., Gehlenborg, N. (2017). UpSetR: an R package for the visualization of intersecting sets and their properties. *Bioinformatics* 33(18), 2938–2940. doi: 10.1093/bioinformatics/btx364

Cordero, P., Campion, J., Milagro, F. I., Goyenechea, E., Steemburgo, T., Javierre, B. M. et al. (2011). Leptin and TNF-alpha promoter methylation levels measured by MSP could predict the response to a low-calorie diet. *J. Physiol. Biochem.* 67(3), 463–470. doi: 10.1007/s13105-011-0084-4

De Marco, E., Vacchiano, G., Frati, P., La Russa, R., Santurro, A., Scopetti, M. et al. (2018). Evolution of post-mortem coronary imaging: from selective coronary arteriography to post-mortem CT-angiography and beyond. *La Radiologia medica* 123(5), 351–358. doi: 10.1007/s11547-018-0855-x

Deng, Q., Huang, W., Peng, C., Gao, J., Li, Z., Qiu, X. et al. (2018). Genomic 5-mC contents in peripheral blood leukocytes were independent protective factors for coronary artery disease with a specific profile in different leukocyte subtypes. *Clin. Epigenetics* 10:9. doi: 10.1186/s13148-018-0443-x

Duan, L., Liu, C., Hu, J., Liu, Y., Wang, J., Chen, G. et al. (2018). Epigenetic mechanisms in coronary artery disease: The current state and prospects. *Trend Cardiovascul. Med.* 28(5), 311–319. doi: 10.1016/j.tcm.2017.12.012

Ek, W. E., Hedman, A. K., Enroth, S., Morris, A. P., Lindgren, C. M., Mahajan, A. et al. (2016). Genome-wide DNA methylation study identifies genes associated with the cardiovascular biomarker GDF-15. *Hum. Mol. Genet.* 25(4), 817–827. doi: 10.1093/hmg/ddv511

Elashoff, M. R., Wingrove, J. A., Beineke, P., Daniels, S. E., Tingley, W. G., Rosenberg, S. et al. (2011). Development of a blood-based gene expression algorithm for assessment of obstructive coronary artery disease in non-diabetic patients. *BMC Med. Genom.* 4:26. doi: 10.1186/1755-8794-4-26

Gaziano, T. A., Suhrcke, M., Brouwer, E., Levin, C., Nikolic, I., Nugent, R. (2017). "Costs and Cost-Effectiveness of Interventions and Policies to Prevent and Treat Cardiovascular and Respiratory Diseases," in *Disease Control Priorities (third edition): Volume 5, Cardiovascular, Respiratory, and Related Disorders*. eds D. Prabhakaran, S. Anand, T. A, Gaziano, J. C, Mbanya Y, Wu (Washington, DC: The International Bank for Reconstruction and Development).

Gene Ontology Consortium (2006). The Gene Ontology (GO) project in 2006. *Nucleic Acids Res.* 34, D322–D326. doi: 10.1093/nar/gkj021

Ghaznavi, H., Mahmoodi, K., Soltanpour, M. S. (2018). A preliminary study of the association between the ABCA1 gene promoter DNA methylation and coronary artery disease risk. *Mol. Biol. Res. Commun.* 7(2), 59–65. doi: 10.22099/mbrc.2018.28910.1312

Giannakopoulou, E., Konstantinou, F., Ragia, G., Tavridou, A., Karaglani, M., Chatzaki, E. et al. (2017). Epigenetics-by-Sex Interaction for Coronary Artery Disease Risk Conferred by the Cystathionine gamma-Lyase Gene Promoter Methylation. *Omics J. Integr. Biol.* 21(12), 741–748. doi: 10.1089/omi.2017.0149

Guo, T. M., Huang, L. L., Liu, K., Ke, L., Luo, Z. J., Li, Y. Q. et al. (2016). Pentraxin 3 (PTX3) promoter methylation associated with PTX3 plasma levels and neutrophil to lymphocyte ratio in coronary artery disease. *J. Geriatr. Cardiol.* 13(8), 712–717. doi: 10.11909/j.issn.1671-5411.2016.08.010

Győrffy, B., Bottai, G., Fleischer, T, Munkácsy, G., Budczies, J., Paladini, L. et al. (2016). Aberrant DNA methylation impacts gene expression and prognosis in breast cancer subtypes. *Int. J. Cancer* 138(1), 87–97. doi: 10.1002/ijc.29684

Harada, K., Shibata, R., Ouchi, N., Tokuda, Y., Funakubo, H., Suzuki, M. et al. (2016). Increased expression of the adipocytokine omentin in the epicardial adipose tissue of coronary artery disease patients. *Atherosclerosis* 251, 299–304. doi: 10.1016/j.atherosclerosis.2016.07.003

Heidari, L., Ghaderian, S. M. H., Vakili, H., Salmani, T. A. (2019). Promoter methylation and functional variants in arachidonate 5-lipoxygenase and forkhead box protein O1 genes associated with coronary artery disease. *J. Cell. Biochem.* 120(8), 12360–12368.

Ichikawa, K., Tomioka, S., Suzuki, Y., Nakamura, R., Doi, K., Yoshimura, J. et al. (2017). Centromere evolution and CpG methylation during vertebrate speciation. *Nat. Commun.* 8(1):1833. doi: 10.1038/s41467-017-01982-1987

Indumathi, B., Katkam, S. K., Krishna, L. S. R., Kutala, V. K. (2019). Dual Effect of IL-6 -174 G/C Polymorphism and Promoter Methylation in the Risk of Coronary Artery Disease Among South Indians. *Indian J. Clin. Biochem.* 34(2), 180–187. doi: 10.1007/s12291-018-0740-743

Kanehisa, M., and Goto, S. (2000). KEGG: kyoto encyclopedia of genes and genomes. *Nucleic Acids Res.* 28(1):27–30. doi: 10.1093/nar/28.1.27

Latini, R., Maggioni, A. P., Peri, G., Gonzini, L., Lucci, D., Mocarelli, P. et al. (2004). Prognostic significance of the long pentraxin PTX3 in acute myocardial infarction. *Circulation* 110(16), 2349–2354. doi: 10.1161/01.Cir.0000145167.30987.2e

Li, J. J., Li, Q., Du, H. P., Wang, Y. L., You, S. J., Wang, F. et al. (2015). Homocysteine Triggers Inflammatory Responses in Macrophages through Inhibiting CSE-H2S Signaling via DNA Hypermethylation of CSE Promoter. *Int. J. Mol. Sci.* 16(6), 12560–12577. doi: 10.3390/ijms160612560

Li, X., Ji, Y., Kang, J., Fang, N. (2018). Association between blood neutrophil-to-lymphocyte ratio and severity of coronary artery disease: Evidence from 17 observational studies involving 7017 cases. *Medicine* 97(39):e12432. doi: 10.1097/md.0000000000012432

Liu, Y., Ding, J., Reynolds, L. M., Lohman, K., Register, T. C., De La Fuente, A. et al. (2013). Methylomics of gene expression in human monocytes. *Hum. Mol. Genet.* 22(24), 5065–5074. doi: 10.1093/hmg/ddt356

Liu, Y., Reynolds, L. M., Ding, J., Hou, L., Lohman, K., Young, T. et al. (2017). Blood monocyte transcriptome and epigenome analyses reveal loci associated with human atherosclerosis. *Nat. Commun.* 8(1):393. doi: 10.1038/s41467-017-00517-514

Moran, A., Zhao, D., Gu, D., Coxson, P., Chen, C. S., Cheng, J. et al. (2008). The future impact of population growth and aging on coronary heart disease in China: projections from the Coronary Heart Disease Policy Model-China. *BMC Pub. Health* 8:394. doi: 10.1186/1471-2458-8-394

Nakatochi, M., Ichihara, S., Yamamoto, K., Naruse, K., Yokota, S., Asano, H. et al. (2017). Epigenome-wide association of myocardial infarction with DNA methylation sites at loci related to cardiovascular disease. *Clin. Epigenet.* 9:54. doi: 10.1186/s13148-017-0353-353

Nariman-Saleh-Fam, Z., Vahed, S. Z., Aghaee-Bakhtiari, S. H., Daraei, A., Saadatian, Z., Kafil, H. S. et al. (2019). Expression pattern of miR-21, miR-25 and PTEN in peripheral blood mononuclear cells of patients with significant or insignificant coronary stenosis. *Gene* 698, 170–178. doi: 10.1016/j.gene.2019.02.074

Nazarenko, M. S., Markov, A. V., Lebedev, I. N., Freidin, M. B., Sleptcov, A. A., Koroleva, I. A. et al. (2015). A comparison of genome-wide DNA methylation patterns between different vascular tissues from patients with coronary heart disease. *PLoS One* 10(4):e0122601. doi: 10.1371/journal.pone.0122601

Oudejans, C., Poutsma, A., Michel, O., Mulders, J., Visser, A., van Dijk, M. et al. (2016). Genome-Wide Identification of Epigenetic Hotspots Potentially Related to Cardiovascular Risk in Adult Women after a Complicated Pregnancy. *PLoS One* 11(2):e0148313. doi: 10.1371/journal.pone.0148313

Peng, P., Wang, L., Yang, X., Huang, X., Ba, Y., Chen, X. et al. (2014). A preliminary study of the relationship between promoter methylation of the ABCG1, GALNT2 and HMGCR genes and coronary heart disease. *PLoS One* 9(8):e102265. doi: 10.1371/journal.pone.0102265

Rask-Andersen, M., Martinsson, D., Ahsan, M, Enroth, S., Ek, W. E., Gyllensten, U. et al. (2016). Epigenome-wide association study reveals differential DNA methylation in individuals with a history of myocardial infarction. *Hum. Mol. Genet.* 25(21), 4739–4748. doi: 10.1093/hmg/ddw302

Redshaw, N., Huggett, J. F., Taylor, M. S., Foy, C. A., Devonshire, A. S. (2014). Quantification of epigenetic biomarkers: an evaluation of established and emerging methods for DNA methylation analysis. *BMC Genom.* 15(1):1174. doi: 10.1186/1471-2164-15-1174

Ritchie, M. E., Phipson, B., Wu, D., Hu, Y., Law, C. W., Shi, W. et al. (2015). limma powers differential expression analyses for RNA-sequencing and microarray studies. *Nucleic Acids Res.* 43(7):e47. doi: 10.1093/nar/gkv007

Rusnak, J., Fastner, C., Behnes, M., Mashayekhi, K., Borggrefe, M., Akin, I. (2017). Biomarkers in Stable Coronary Artery Disease. *Curr. Pharm. Biotechnol.* 18(6), 456–471. doi: 10.2174/1389201018666170630120805

Shannon, P., Markiel, A., Ozier, O., Baliga, N. S., Wang, J. T., Ramage, D. et al. (2003). Cytoscape: a software environment for integrated models of biomolecular interaction networks. *Genome Res.* 13(11), 2498–2504. doi: 10.1101/gr.1239303

Shibata, Y., Kikuchi, R., Ishii, H., Suzuki, S., Harada, K., Hirayama, K. et al. (2018). Balance between angiogenic and anti-angiogenic isoforms of VEGF-A is associated with the complexity and severity of coronary artery disease. *J. Clin. Chem.* 478, 114–119. doi: 10.1016/j.cca.2017.12.042

Sinnaeve, P. R., Donahue, M. P., Grass, P., Seo, D., Vonderscher, J., Chibout, S. D. et al. (2009). Gene expression patterns in peripheral blood correlate with the extent of coronary artery disease. *PLoS One* 4(9):e7037. doi: 10.1371/journal.pone.0007037

Szijarto, I. A., Marko, L., Filipovic, M. R., Miljkovic, J. L., Tabeling, C., Tsvetkov, D. et al. (2018). Cystathionine gamma-Lyase-Produced Hydrogen Sulfide Controls Endothelial NO Bioavailability and Blood Pressure. *Hypertension* 71(6), 1210–1217. doi: 10.1161/hypertensionaha.117.10562

Vacca, M., Di Eusanio, M., Cariello, M., Graziano, G., D'Amore, S., Petridis, F. D. et al. (2016). Integrative miRNA and whole-genome analyses of epicardial adipose tissue in patients with coronary atherosclerosis. *Cardiovasc. Res.* 109(2), 228–239. doi: 10.1093/cvr/cvv266

Wang, C., Chen, L., Yang, Y., Zhang, M., Wong, G. (2019). Identification of potential blood biomarkers for Parkinson's disease by gene expression and DNA methylation data integration analysis. *Clin. Epigenetics* 11(1):24. doi: 10.1186/s13148-019-0621-5

Wang, D., Wang, Y., Ma, J., Wang, W., Sun, B., Zheng, T. et al. (2017). MicroRNA-20a participates in the aerobic exercise-based prevention of coronary artery disease by targeting PTEN. *Biomed. Pharmacother. Biomed. Pharmacother.* 95, 756–763. doi: 10.1016/j.biopha.2017.08.086

Watson, C. J., Collier, P., Tea, I., Neary, R., Watson, J. A., Robinson, C. et al. (2014). Hypoxia-induced epigenetic modifications are associated with cardiac tissue fibrosis and the development of a myofibroblast-like phenotype. *Hum. Mol. Genet.* 23(8), 2176–2188. doi: 10.1093/hmg/ddt614

Wood, D., and Eisele, J. L. (2017). A global coalition for the fight against heart disease and stroke. *Lancet* 390, 2130–2131. doi: 10.1016/s0140-6736(17)32676-32674

Xu, S., Kamato, D., Little, P. J., Nakagawa, S., Pelisek, J., Jin, Z. G. (2019). Targeting epigenetics and non-coding RNAs in atherosclerosis: from mechanisms to therapeutics. *Pharmacol. Therapeut.* 196, 15–43. doi: 10.1016/j.pharmthera.2018.11.003

Yamada, Y., Horibe, H., Oguri, M., Sakuma, J., Takeuchi, I., Yasukochi, Y., et al. (2018). Identification of novel hyper- or hypomethylated CpG sites and genes associated with atherosclerotic plaque using an epigenome-wide association study. *Int. J. Mol. Med.* 41(5), 2724–2732. doi: 10.3892/ijmm.2018.3453

Zhang, X. K., Xiang, Y., He, D. D., Liang, B., Wang, C., Luo, J. et al. (2020). *Identification of potential biomarkers for CAD using integration with expression and methylation data and validation by case-control study. Research Square [Preprint]*. Available online at: https://doi.org/10.21203/rs.2.23331/v1 [accessed February 13, 2020].

Zhang, X., Liu, S., Shen, C., Wu, Y., Zhang, L., Chen, X. et al. (2015). DNA methylation consistency implicates the primary tumor cell origin of recurrent hepatocellular carcinoma. *Epigenomics* 7(4), 581–592. doi: 10.2217/epi.15.23

Zhaodong, H., Dekang, L., Ying, G., Jisen, S., Dolf, W., Guangchuang, Y. et al. (2019). *RIdeogram: drawing SVG graphics to visualize and map genome-wide data on idiograms*. Available online at:https://cran.r-project.org/web/packages/RIdeogram [accessed October 06, 2019].

Conflict of Interest: The authors declare that the research was conducted in the absence of any commercial or financial relationships that could be construed as a potential conflict of interest.

frontiers in Cardiovascular Medicine

ORIGINAL RESEARCH
published: 30 October 2020
doi: 10.3389/fcvm.2020.595011

Profiling of Histone Modifications Reveals Epigenomic Dynamics During Abdominal Aortic Aneurysm Formation in Mouse Models

Jacob Greenway[1,2†], Nicole Gilreath[1,2†], Sagar Patel[1,2†], Tetsuo Horimatsu[1,2], Mary Moses[1,2], David Kim[1,2], Lauren Reid[1,2], Mourad Ogbi[1,2], Yang Shi[3,4], Xin-Yun Lu[4], Mrinal Shukla[5], Richard Lee[5], Yuqing Huo[2,6], Lufei Young[7], Ha Won Kim[1,2] and Neal L. Weintraub[1,2]*

[1] Departments of Medicine, College of Nursing at Augusta University, Augusta, GA, United States, [2] Vascular Biology Center, Medical College of Georgia, College of Nursing at Augusta University, Augusta, GA, United States, [3] Department of Population Health Sciences, College of Nursing at Augusta University, Augusta, GA, United States, [4] Department of Neuroscience and Regenerative Medicine, College of Nursing at Augusta University, Augusta, GA, United States, [5] Department of Surgery, College of Nursing at Augusta University, Augusta, GA, United States, [6] Department of Cell Biology and Anatomy, College of Nursing at Augusta University, Augusta, GA, United States, [7] Department of Physiological and Technological Nursing, College of Nursing at Augusta University, Augusta, GA, United States

OPEN ACCESS

Edited by:
Zhihua Wang,
Wuhan University, China

Reviewed by:
Jing Jing Tong,
Central China Normal University, China
Peijing Zhang,
Huazhong University of Science and Technology, China

***Correspondence:**
Neal L. Weintraub
nweintraub@augusta.edu

[†] These authors have contributed equally to this work

Specialty section:
This article was submitted to Cardiovascular Genetics and Systems Medicine, a section of the journal Frontiers in Cardiovascular Medicine

Received: *14 August 2020*
Accepted: *08 October 2020*
Published: *30 October 2020*

Citation:
Greenway J, Gilreath N, Patel S, Horimatsu T, Moses M, Kim D, Reid L, Ogbi M, Shi Y, Lu X-Y, Shukla M, Lee R, Huo Y, Young L, Kim HW and Weintraub NL (2020) Profiling of Histone Modifications Reveals Epigenomic Dynamics During Abdominal Aortic Aneurysm Formation in Mouse Models. Front. Cardiovasc. Med. 7:595011. doi: 10.3389/fcvm.2020.595011

Introduction: Abdominal aortic aneurysms (AAA) are characterized by localized inflammation, extracellular matrix degradation, and apoptosis of smooth muscle cells, which together lead to progressive and irreversible aortic dilation. Major risk factors for AAA include smoking and aging, both of which prominently alter gene expression via epigenetic mechanisms, including histone methylation (me) and acetylation (ac).However, little is known about epigenomic dynamics during AAA formation. Here, we profiled histone modification patterns in aortic tissues during AAA formation in two distinct mouse models; (1) angiotensin II (AngII) infusion in low density lipoprotein receptor (LDLR) knockout (KO) mice, and (2) calcium chloride ($CaCl_2$) application in wild type mice.

Methods and Results: AAA formed in both models, in conjunction with enhanced macrophage infiltration, elastin degradation and matrix metalloproteinases expression as evaluated by immunohistochemistry. To investigate the histone modification patterns during AAA formation, total histone proteins were extracted from AAA tissues, and histone H3 modifications were quantified using profiling kits. Intriguingly, we observed dynamic changes in histone H3 modifications of lysine (K) residues at different time points during AAA formation. In mature aneurysmal tissues at 3 weeks after AngII infusion, we detected reduced K4/K27/K36 monomethylation, K9 trimethylation K9, and K9/K56 acetylation (<70%), and increased K4 trimethylation (>130%). Conversely, in $CaCl_2$-induced AAA, K4/K9/K27/K36/K79 monomethylation and K9/K18/K56 acetylation were reduced in AAA tissues, whereas K27 di-/tri-methylation and K14 acetylation were upregulated. Interestingly, K4/K27/K36 monomethylation, K9 trimethylation, and K9/K56 acetylation were commonly downregulated in both animal models, while no H3 modifications were uniformly upregulated. Western blot of AAA tissues confirmed

markedly reduced levels of key H3 modifications, including H3K4me1, H3K9me3, and H3K56ac. Furthermore, pathway enrichment analysis using an integrative bioinformatics approach identified specific molecular pathways, including endocytosis, exon guidance and focal adhesion signaling, that may potentially be linked to these histone H3 modifications during AAA formation.

Conclusions: Dynamic modifications of histone H3 occur during AAA formation in both animal models. We identified 6 discreet H3 modifications that are consistently downregulated in both models, suggesting a possible role in AAA pathobiology. Identifying the functional mechanisms may facilitate development of novel strategies for AAA prevention or treatment.

Keywords: abdominal aortic aneurysm, angiotensin II, calcium chloride, histone modification, methylation, acetylation

INTRODUCTION

Abdominal aortic aneurysms (AAA) are a relatively common cause of death and are frequently asymptomatic until rupture occurs (1, 2). AAA repair is associated with significant morbidity and mortality, particularly when performed emergently; thus far, no medical therapy has proven effective in preventing AAA growth or rupture (3). Human AAA are typically characterized by elastin degradation, loss of vascular smooth muscle cells (VSMCs), and immune cell infiltration (4). Smoking, age, male sex, hypertension, and hypercholesterolemia are important risk factors for AAA, but the underlying mechanisms that lead to AAA formation are incompletely defined.

Epigenetic regulation refers to potentially stable and heritable changes in gene expression that arise independent of alterations in the primary DNA sequences. Epigenetic modifications occur dynamically in response to various environmental stimuli, and recent studies have shown that several risk factors for AAA, including smoking and aging, can dysregulate gene expression through epigenetic mechanisms (5, 6). Major processes associated with epigenetic control of gene expression include DNA methylation, histone modifications and non-coding RNA (7). Among these epigenetic mechanisms, histone (H) modifications fundamentally change chromatin structure and gene transcription, thereby regulating key cellular mechanisms and functions. Histone methylation is a post-translational process whereby methyl groups are attached to H3 and H4 proteins by enzyme histone methyltransferases (HMTs), thus altering the histone's interactions with DNA and nuclear proteins. Either transcriptional repression or activation can occur, depending on the site of methylation and its impact on chromatin structure. Histone acetylation refers to the process whereby acetyl groups are added to histone proteins, specifically to the lysine residues, by histone acetyltransferase (HAT). Histone acetylation typically leads to a transcriptionally active chromatin structure. Separate groups of enzymes, termed histone demethylases and deacetylases, remove the methyl and acetyl groups, respectively, thus allowing for dynamic regulation of gene expression. Epigenetic mechanisms are associated with many human diseases, including cardiovascular disease, cancer and metabolic disease (8–10). However, epigenetic mechanisms associated with AAA have not been extensively investigated, and most available data have been inferred from studies of other types of vascular disease or pathology. Hence, understanding the epigenetic mechanisms that are operative in AAA could potentially lead to development of novel therapeutics that ameliorate AAA growth and rupture.

Several animal models have been developed to study AAA formation. Angiotensin II (AngII) infusion by osmotic minipump and periaortic calcium chloride ($CaCl_2$) application are well-established animal models of AAA. The presentation of AAA in these models is not identical to the human disease, but they serve as valuable models that share key features of human AAA (11). The AngII model is characterized by elastic degradation, macrophage infiltration, thrombus formation, aortic dissection, and rupture. However, these mice typically develop aneurysms in the suprarenal aorta, as opposed to the infrarenal aorta in humans. In addition, aortic rupture is an early event in the AngII-infusion model, associated with medial dissection, while in human AAA, rupture is most often a late event associated with pronounced dilation. On the other hand, the $CaCl_2$ application model induces markedly dilated AAA in the infrarenal location. $CaCl_2$-induced AAA also exhibit many pathological characteristics observed in human AAA, including calcification, profound neutrophil infiltration and elastin degradation, neovascularization, and VSMC apoptosis. However, the aneurysms do not rupture or develop thrombus formation, nor are they associated with atherosclerosis, which are typical features of human AAA (11).

Here, using two distinct animal models of AAA, we focused on profiling aortic histone H3 modifications during AAA formation.

Abbreviations: AAA, Abdominal aortic aneurysms; ac, acetylation; Acta2, smooth muscle alpha-2 actin; AngII, Angiotensin II; $CaCl_2$, calcium chloride; Chip-Seq, chromatin immunoprecipitation followed by sequencing; GO, Gene Ontology; H&E, hematoxylin and eosin; Ilk, intergrin-linked kinase; K, lysine; KEGG, Kyoto Encyclopedia of Genes and Genomes; KO, knockout; LDLR, low density lipoprotein receptor; LRP1, identified low density lipoprotein receptor-related protein 1; me, methylation; MMP, matrix metalloproteinase; P, phosphorylation; Sirt1, silent mating type information regulation 2 homolog 1; TAA, thoracic aortic aneurysm; VVG, Verhoeff van Gieson; VSMC, vascular smooth muscle cells.

We detected dynamic histone modification patterns occurring in a time- and model-dependent fashion, and we identified several H3 modifications that were highly conserved between the two models. Furthermore, pathway enrichment analysis using an integrative bioinformatics approach identified specific molecular signaling pathways that may potentially be linked to these histone H3 modifications during AAA formation. Our findings set the stage for future investigations into the role of these dynamic histone H3 modifications in AAA pathogenesis.

MATERIALS AND METHODS

AngII-Induced AAA Model

Animal experimental protocols were approved by the Institutional Animal Care and Use Committee at the Medical College of Georgia at Augusta University and complied with National Institute of Health guidelines. Low density lipoprotein receptor (LDLR) knockout (KO) mice were purchased from Jackson Laboratory. Ang II (1,000 ng/kg/min, Enzo Life Sciences) was infused into male LDLR KO mice via osmotic minipumps (ALZET Model 2004) as previously reported (12, 13). One to three weeks after minipump implantation, mice were euthanized and aortic outer diameter was measured. Aortic tissues were harvested for immunohistochemical analysis, histone H3 analysis and Western blot.

$CaCl_2$-Induced AAA Model

Male C57Bl/6 mice (Jackson Laboratory) were treated with $CaCl_2$ (0.5 mol/L, Sigma-Aldrich) for AAA induction as described previously (12). After 1–3 weeks, animals were anesthetized, aortic outer diameter was measured, and aortas were harvested for further analysis.

Aortic Tissue Collection

Aortic tissue samples were harvested as described previously (12). Briefly, after blood was withdrawn from the right ventricle, aortas were irrigated with cold PBS through the left ventricle, and the peri-adventitial tissue was dissected carefully from the wall of the aorta. The abdominal aorta, from the last intercostal artery to the ileal bifurcation, was sectioned and the aneurysmal areas were fixed in paraformaldehyde (4% wt/vol) for immunohistochemistry, or processed for histone extraction as described below.

Immunohistochemistry

Paraffin-embedded cross sections of aortas were used for hematoxylin and eosin (H&E), Verhoeff van Gieson (VVG) and immunostaining staining for Mac-3, matrix metalloproteinase (MMP)-2 and−9. Antibodies for Mac-3 (BD Pharmingen) and MMP-2/-9 (Calbiochem) were used with the HistoMouse-SP kit (Invitrogen) or DAB Substrate kit (Vector Labs).

Histone Extraction and Quantification of Histone Modifications

Total histone proteins were extracted from aortas using EpiQuik™ Total Histone Extraction Kit (Epigentek). Major histone H3 modifications were quantified using EpiQuik™ Histone H3 Modification Multiplex Assay Kit (Epigentek). Pooled aortic histone extracts from three mice were subjected to the assay and 100 ng of total histone proteins were used.

Western Blotting

Protein extraction and western blotting were performed as described previously (12). H3K4me1, H3K9me3, H3K56ac and total histone H3 antibodies were purchased from Cell Signaling Technology. Pooled aortic histone extracts from three mice were subjected to the assay.

Quantitative PCR

Total RNA was extracted from whole aortas using QIAzol lysis reagent and purified with the RNeasy lipid tissue mini kit (Qiagen) per manufacturer's protocol. Real-time quantification of mRNA was performed using Power SYBR® Green RNA-to-CT™ 1-Step Kit (Applied Biosystems). Normalized Ct values were subjected to statistical analysis, and the fold difference was calculated by the ΔΔCt method.

Bioinformatic Analysis

Chromatin immunoprecipitation followed by sequencing (ChIP-Seq) data for mouse heart and human aorta were downloaded from the website of the Encyclopedia of DNA Elements (ENCODE) project (14). The R package ChIPseeker (15) was used to retrieve the nearest genes around the peak and to annotate the genomic region of the peak, while the UCSC build hg19 and mm10 annotations were used to annotate the known genes for human and mouse data, respectively. The transcription start site (TSS) region of each gene was defined from −3kb to +3kb. Next, the annotated genes were used as an input for functional enrichment analysis, which was performed using the Gene Ontology (GO) terms, Kyoto Encyclopedia of Genes and Genomes (KEGG) pathways and Reactome pathways databases, respectively.

Statistical Analysis

All statistical analysis was performed using Graphpad Software and results are expressed as mean ± SEM. Differences between

TABLE 1 | Phenotypic differences of AAA between two animal models.

Human AAA features	AngII model	$CaCl_2$ model
Medial degeneration	X	X
Inflammatory cell infiltration	X	X
VSMC apoptosis	X	X
Oxidative stress	X	X
Thrombus formation	X	
Aortic rupture	X	
Neutrophil infiltration		X
Anatomic location (infrarenal)		X
Risk factors: hypertension, atherosclerosis, male predisposition	X X X	

two groups were analyzed by Student's *t*-test. *P*-values <0.05 were considered to be significant.

RESULTS

AAA Formation by AngII Infusion and Periaortic $CaCl_2$ Application in Mice

To induce AAA in mice, we employed two distinct animal models, AngII infusion and $CaCl_2$ application. Phenotypic differences of AAA between two animal models are summarized in the **Table 1**. As shown in **Figure 1**, AngII infusion for 3 weeks induced AAA in nearly 80% of the LDLR KO mice, resulting in a significant increase in suprarenal aortic diameter as visualized macroscopically and confirmed by H&E staining (**Figures 1A–D**). Elastin degradation, MMP expression and vascular inflammation were markedly increased in aortas of mice infused with AngII as compared to control (saline infusion) as evaluated by VVG staining, MMP-2/-9 staining, and MAC-3 staining (**Figure 1D**).

We also confirmed that infrarenal aortic diameter was significantly increased by periaortic $CaCl_2$ application in wild-type (C57Bl/6) mice after 3 weeks (**Figures 2A,B**), in conjunction with severe elastin degradation (VVG staining), increased macrophage infiltration (Mac-3 staining) and MMP-2/-9 expression (MMP-2/-9 staining, **Figure 2C**).

Profiling of Histone H3 Modifications in AngII-Induced AAA

In the AngII infusion model, we identified a unique H3 modification profile at each time point (1, 2, and 3 weeks

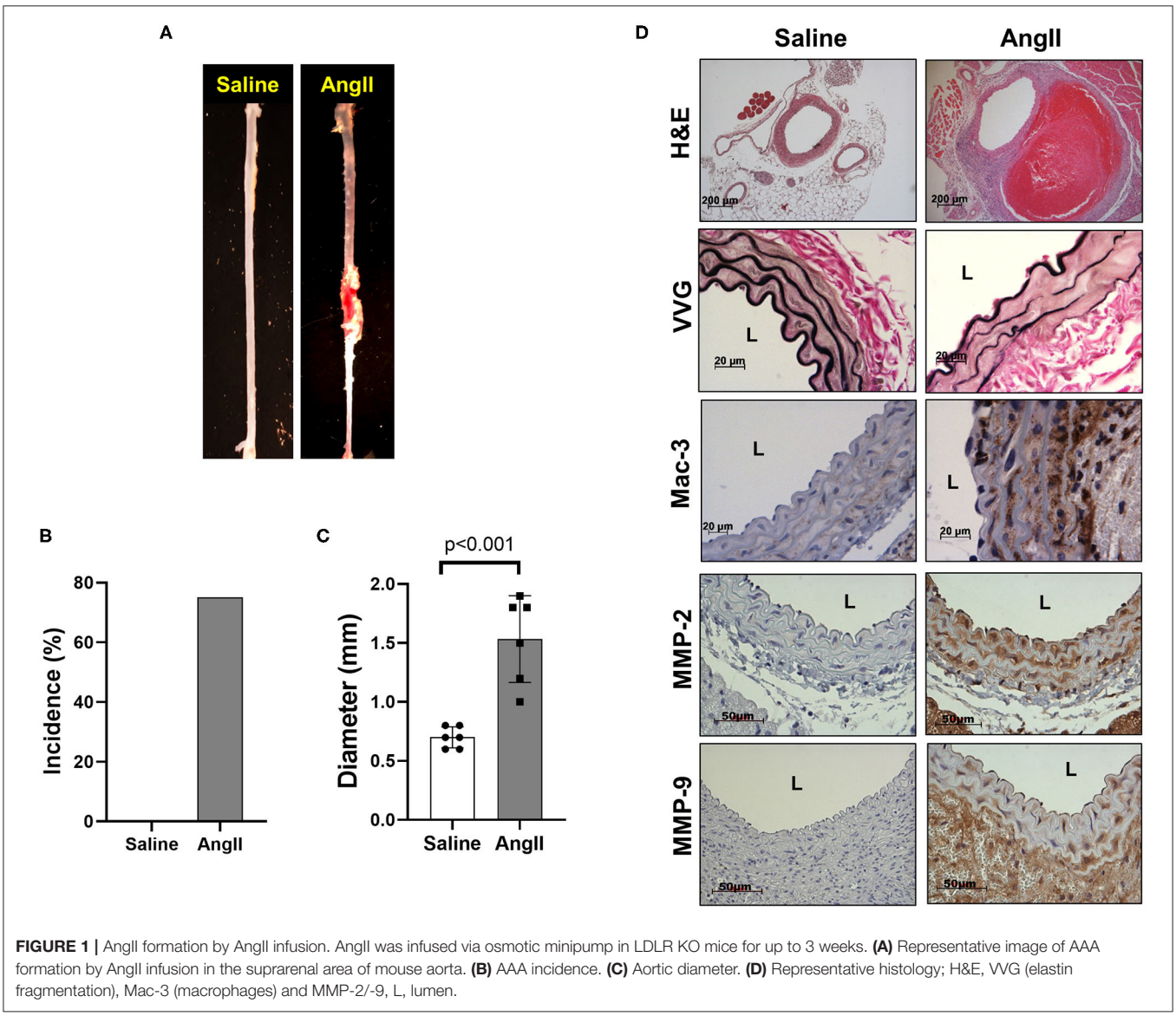

FIGURE 1 | AngII formation by AngII infusion. AngII was infused via osmotic minipump in LDLR KO mice for up to 3 weeks. **(A)** Representative image of AAA formation by AngII infusion in the suprarenal area of mouse aorta. **(B)** AAA incidence. **(C)** Aortic diameter. **(D)** Representative histology; H&E, VVG (elastin fragmentation), Mac-3 (macrophages) and MMP-2/-9, L, lumen.

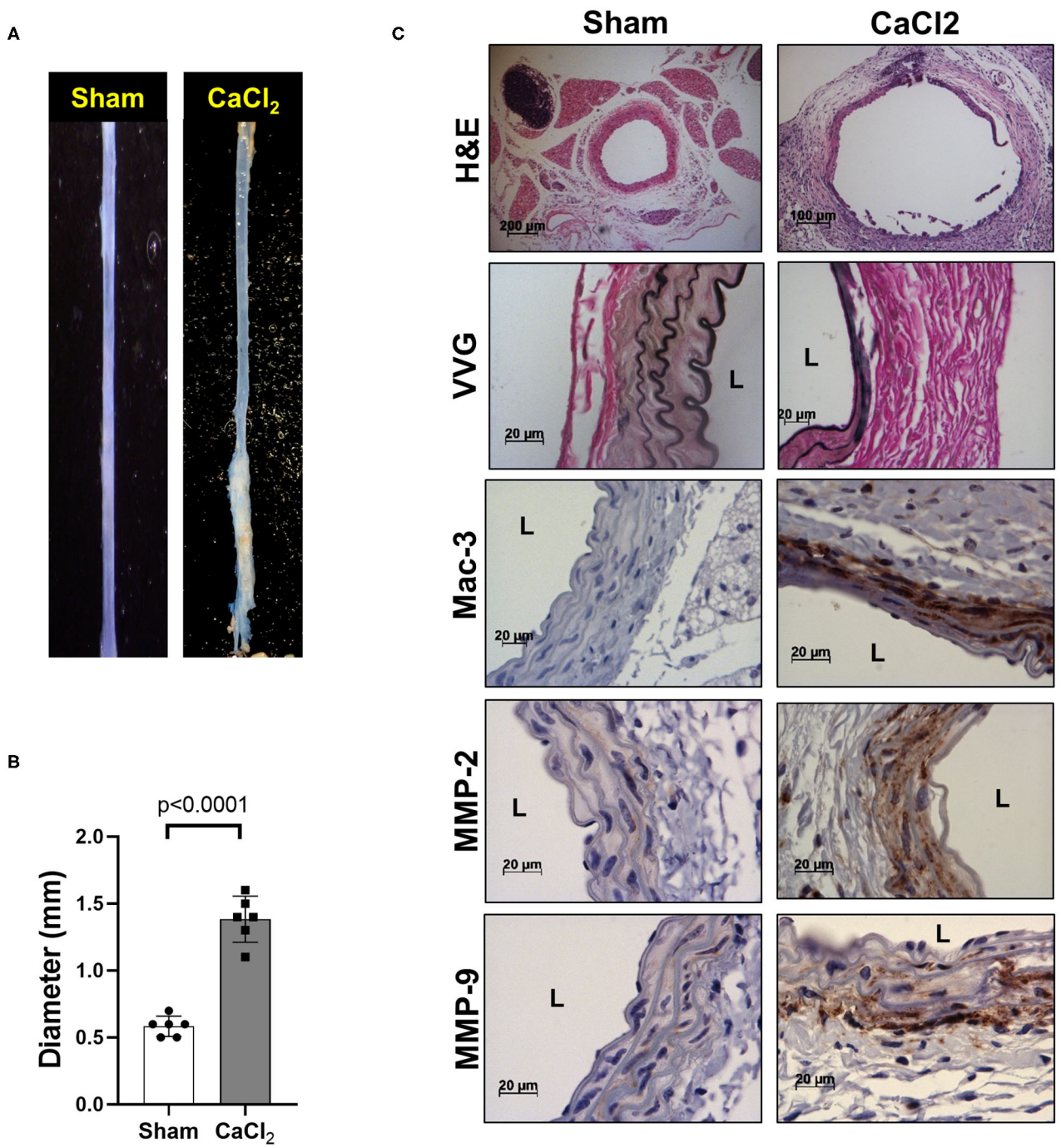

FIGURE 2 | AAA formation by periaortic $CaCl_2$ application. $CaCl_2$ was applied to the infrarenal aorta of C57Bl/6 mice, which were sacrificed at 3 weeks after $CaCl_2$ application. **(A)** Representative image of AAA formation by $CaCl_2$ application in infrarenal area of mouse aorta. **(B)** Aortic diameter. **(C)** Representative histology; H&E, VVG (elastin fragmentation), Mac-3 (macrophages) and MMP-2/-9, L, lumen.

after AngII infusion). At 1 week after AngII infusion, when inflammation and oxidative stress are prevalent and preceed the formation of AAA, we observed significant upregulation (>130%) of methylation of K4, K9, K27, K79 (H3K4me3, H3K9me2, H3K27me3, H3K79me1/me3), acetylation of K9, K18 (H3K9ac, H3K18ac) and phosphorylation of ser10 (H3ser10P), while there was significant downregulation (<70%) of H3K9me1, H3K36me1, and H3K56ac (**Figures 3A,B**). At 2 weeks after AngII infusion, which represents the middle stage of AAA formation, mono- and try-methylation of K79 (H3K79me1/me3) and

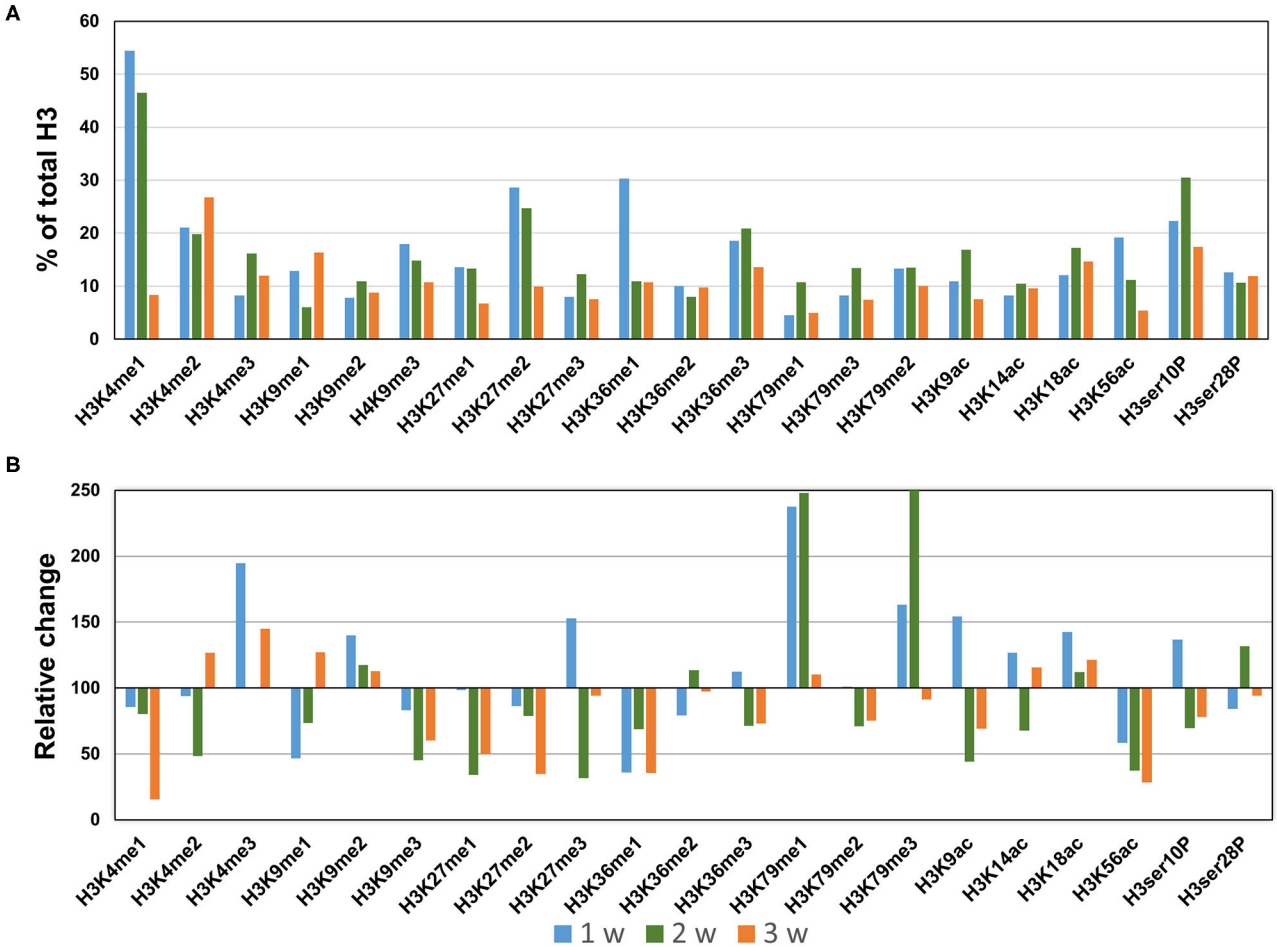

FIGURE 3 | Profiling of major histone H3 modifications in AngII-induced AAA tissues. Total histone proteins were extracted from AAA tissues (at 1, 2, 3 weeks, respectively), and histone H3 modifications were quantified using profiling kits. Pooled aortic histone extracts from three mice were subjected to the assay. **(A)** Percentage of total histone H3. **(B)** Relative changes of histone H3 modifications.

phosphorylation of ser28 (H3ser28P) was upregulated, whereas methylation (H3K4me2, H3K9me3, H3K36me1, H3K27me1, H3K27me3, H3K36me1) and acetylation (H3K9ac, H3ser10P, H3K9ac, H3K14ac, H3K56ac) were largely downregulated (**Figures 3A,B**). At 3 weeks after AngII infusion, at which time the AAA is mature, only H3K4me3 was upregulated, while H3K27me2, H3K4me1, H3K9me3, H3K27me1, H3K36me1, H3K9ac, and H3K56ac were downregulated (**Figures 3A,B**). These results demonstrate that dynamic H3 modifications occur during AAA formation induced by AngII.

Profiling of Histone H3 Modifications in $CaCl_2$-Induced AAA

Next, we profiled the histone H3 modifications in $CaCl_2$-induced AAA. In contrast to the AngII-induced AAA model, H3 modifications were neither significantly upregulated nor downregulated at 1 week after $CaCl_2$ application (**Figures 4A,B**). At 2 weeks after $CaCl_2$ application, downregulation of K4/K9/K27/K36/K79 monomethylation, K9/K18/K56 acetylation, and H3ser28P phosphorylation was detected (**Figures 4A,B**). Additional histone modifications (H3K4me1/2/3, H3K9me1/2/3, H3K27me1, H3K36me1/2/3, H3K79me1/2/3, H3K9ac, H3K18ac, H3K56ac, H3ser10P, H3ser28P) were observed to be downregulated 3 weeks after $CaCl_2$ application (**Figures 4A,B**). On the other hand, only H3K27me2/3 and H3K14ac were found to be upregulated at this latter time point.

Comparing H3 Modifications Between AngII- and $CaCl_2$-Induced AAA

As described above, the two animal models we employed exhibit both overlapping and contrasting pathophysiological features, which presumably result from common and distinct biochemical and molecular mechanisms, respectively. Thus, we sought to identify overlapping histone H3 modifications observed in both models. Interestingly, we found that the overlapping H3 modifications between the models were all downregulated (**Figures 5A,B**). Four modifications (H3K27me1/me3, H3K14ac,

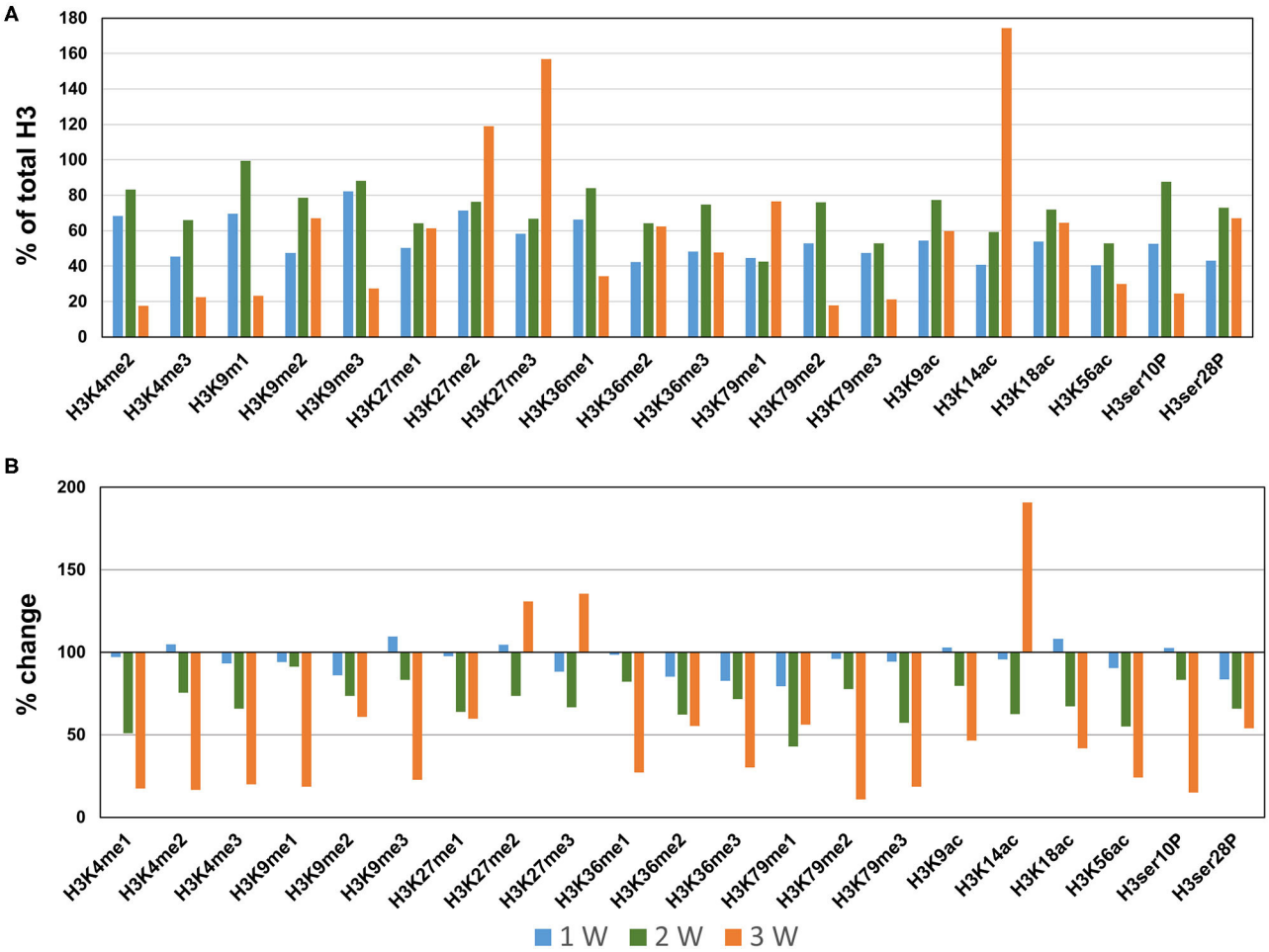

FIGURE 4 | Profiling of major histone H3 modifications in $CaCl_2$-induced AAA tissues. Total histone proteins were extracted from AAA tissues (at 1, 2, 3 weeks, respectively), and histone H3 modifications were quantified using profiling kits. Pooled aortic histone extracts from three mice were subjected to the assay. **(A)** Percentage of total histone H3. **(B)** Relative changes of histone H3 modifications.

and H3K56ac) were found to be commonly downregulated 2 weeks after AAA induction, and six discreet modifications (H3K4me1, H3K9me3, H3K27me1, H3K36me1, H3K9ac, and H3K56ac) were uniformly downregulated at 3 weeks (**Figure 5B**). Western blot was performed to verify key H3 modifications (H3K4me1, H3K9me3, and H3K56ac) consistently downregulated in both models at 3 weeks after AAA induction (**Figures 5C,D**).

Functional Enrichment Analysis of Genes With H3 Modifications

To predict the molecular mechanisms and biological functions of H3 modifications in AAA pathogenesis, we performed pathways and GO terms enrichment analyses using publicly available ChIP-Seq data from the ENCODE project. Since no Chip-seq data from mouse aorta are available, we examined the pathways and GO terms that are enriched in genes with H3K4me1, H3K9m3, and H3K9ac in mouse heart tissue and genes with H3K4me1 and H3K9m3 in human aorta tissue (**Figure 6** and **Supplementary Figures 1–7**). Interestingly, some pathways and GO terms were found to be common in both mouse and human tissues. For instance, the KEGG pathways such as endocytosis, axon guidance, regulation of actin cytoskeleton and focal adhesion were significantly enriched of genes with H3K4me1, while pathways such as calcium signaling, glutamatergic synapse and Herpes simplex virus 1 infection were significantly enriched of genes with H3K9m3 (**Figure 6**). In support of our bioinformatics data, we measured mRNA expression of several genes which were randomly selected from the proposed signaling pathways. Interestingly, we found that gene expression of smooth muscle alpha-2 actin (*Acta2*), which is associated with actin cytoskeleton regulation, was significantly reduced in AngII-induced AAA tissues as compared to saline control. Furthermore, expression of integrin-linked kinase (*Ilk*), a focal adhesion and cytoskeleton-associated molecule, showed a trend toward reduced expression in AAA tissues (**Supplementary Figure 8**).

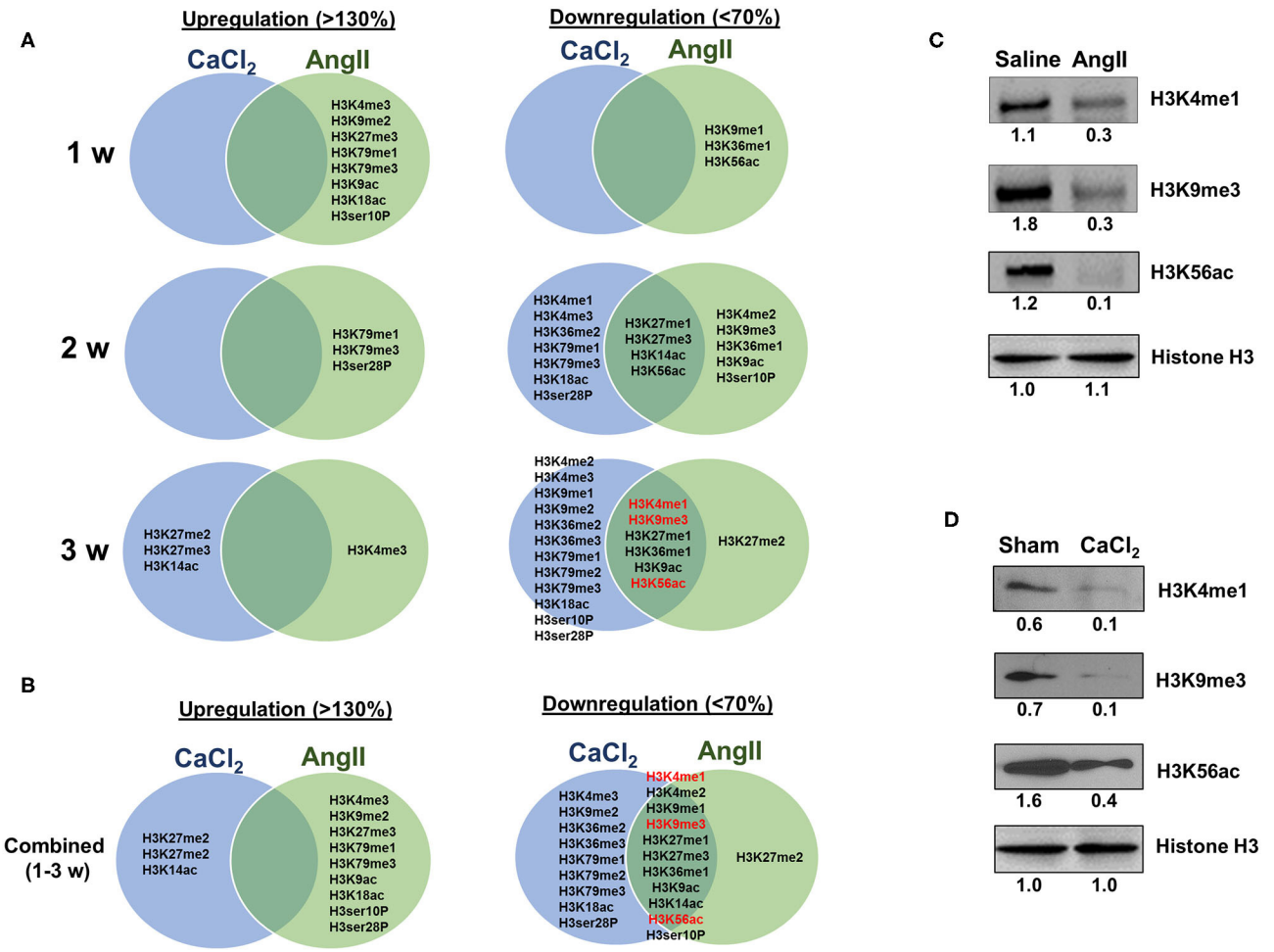

FIGURE 5 | Comparing H3 modifications between AngII- and $CaCl_2$-induced AAA. **(A)** Summary of upregulated (>130%) and downregulated (<70%) histone H3 modifications in AngII- and $CaCl_2$-induced AAA tissues in each time point (1, 2, 3 weeks, respectively). Venn diagram was used to demonstrate the overlapping histone H3 modifications between the two animal models of AAA. **(B)** Combined data at all time points (1–3 weeks). Key overlapping H3 modifications (H3K4me1, H3K9me3, and H3K56ac) in AngII-induced **(C)** and $CaCl_2$-induced AAA **(D)** were verified by Western blot. Pooled aortic histone extracts from three mice were subjected to Western blot. Number represents the quantitative expression levels, normalized by histone H3 in saline or sham group.

DISCUSSION

AAA pathogenesis is influenced by environmental, genetic and epigenetic regulatory mechanisms. Two of the major risk factors for AAA, smoking and age, prominently alter gene expression via epigenetic mechanisms, including histone methylation and acetylation (16–18). However, little is known regarding the epigenomics of AAA formation. In this study, using two dinstinct animal models of AAA, we profiled histone H3 modifications and analyzed their dynamic changes during AAA formation. Moreover, we identified those histone H3 modifications which overlapped in the two animal models of AAA. Interestingly, we detected consistent downregulation of H3K4me1, H3K9me3, H3K56ac levels in both animal models, while no H3 modifications were found to be consistently upregulated. Furthermore, pathway enrichment analysis of genes by integrative bioinformatics approach suggested that specific functional pathways, including endocytosis, exon guidance and focal adhesion signaling, may be associated with these overlapping histone H3 modifications during AAA formation.

Histone modifications are known to be key epigenetic mechanisms associated with vascular diseases such as atherosclerosis. However, the association of histone modifications with AAA pathogenesis is not well defined. A previous study showed that global acetylation rates of H3, and specific acetylation at H3K9, were lower in regulatory T cells of patients with established AAA, which was speculated to be associated with reduced T cell numbers and transcriptional activity (19). These results are consistent with our data from animal models in that acetylation at H3K9 was also decreased in mature AAA tissues. In contrast, Han et al. detected increased expression of histone acetyltransferase enzymes, along with increased histone acetylation modifications, in human AAA tissues obtained during elective surgical repair as compared

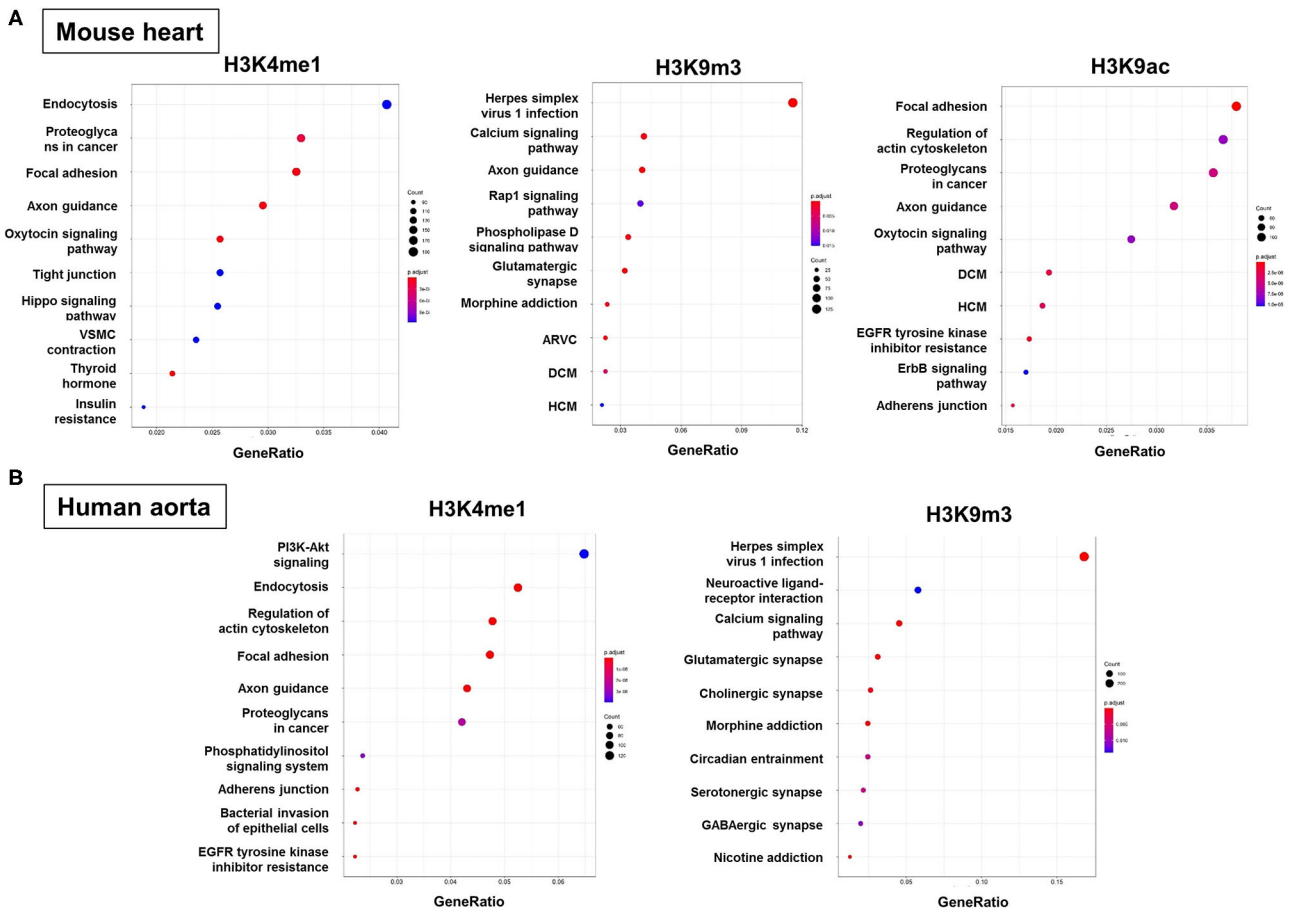

FIGURE 6 | Functional enrichment analysis of genes with H3 modifications. GO terms, KEGG pathways and Reactome pathways databases were used as an input for functional enrichment analysis. Pathways and GO terms that are enriched for genes with H3K4me1, H3K9m3, and H3K9ac in mouse heart tissue **(A)** and genes with H3K4me1 and H3K9m3 in human aorta tissue **(B)**. The results of GO terms and Reactome pathways are shown in **Supplemental Materials**. GO, gene ontology; KEGG, kyoto encyclopedia of genes and genomes; ARVC, arrhythmogenic right ventricular cardiomyopathy; DCM, dilated cardiomyopathy; HCM, hypertrophic cardiomyopathy.

to healthy control aorta obtained from organ donors suffering traumatic injury (20). Moreover, Gomez et al. showed that H3K9 acetylation and H3K4 methylation were increased at the Smad2 promoter of VSMCs derived from thoracic aortic aneurysm tissues as compared to control aorta from organ transplant donors (21). These human studies are not strictly comparable to our animal study, with principal differences not only related to species, but also to disease chronicity, associated medical conditions, predisposing risk factors, control tissues, etc. Further in-depth studies are required to resolve these differences and define the processes that regulate histone methylation and acetylation patterns in AAA.

Acetylation of H3K4 and H3K9 is in part regulated by silent mating type information regulation 2 homolog 1 (Sirt1), an NAD^+-dependent class III histone deacetylase that plays an important role in genome stability through deacetylation of N-terminus tails of acetylated histones. We recently reported that Sirt1 activity is significantly reduced in AAA tissues and is mechanistically linked to AAA pathogenesis (22). Interestingly, Sirt1 was also reported to regulate histone methyltransferase SUV39H1-dependent H3K9me3 (23), levels of which are reduced by smoking and aging, key risk factors for AAA (24, 25). Our observation that H3K9me3 is one of the most downregulated H3 modifications in AAA potentially implicates dysregulation of the Sirt1/SUV39H1/H3K9me3 axis as a mechanism involved in AAA pathogenesis, which warrants further investigation.

In this study, we performed functional enrichment analysis of genes associated with histone H3 modifications to predict the cellular pathways involved in AAA pathogenesis. Since mouse aorta ChIP-seq databases do not exist, we probed databases of human aorta and mouse heart. Using the human aorta database, we identified putative signaling pathways that could be potentially regulated by H3 modifications during AAA formation (e.g., PI3K-Akt pathway, endocytosis, actin cytoskeleton, focal adhesion for H3K4me1 and calcium signaling, glutamatergic synapse, cholinergic synapse, associated with

H3K9me3). Interestingly, some pathways and GO terms were found to be common in both mouse heart and human aorta. (e.g., endocytosis, focal adhesion and exon guidance pathways, associated with H3K4me1). Previously, genome-wide association studies (GWAS) carried out by an international consortia on large sample sets of AAA cases has identified low density lipoprotein receptor-related protein 1 (LRP1) as one of the most significantly associated genes for AAA (26). Interestingly, LRP1 is known to be associated with VSMC and macrophage endocytosis, both of which were also predicted to be involved in AAA formation by our functional enrichment analysis (27). Our bioinformatic data also indicate that focal adhesion pathway may be involved in AAA; a previous study likewise reported that focal adhesion kinase, a cytoplasmic tyrosine kinase, plays an important role in the progression of aortic aneurysm by modulating macrophage behavior (28). Our data also predicted that actin cytoskeleton regulation may be a signaling pathway associated with AAA, and in keeping with this notion, we showed that expression of Acta2, a gene involved in actin cytoskeleton regulation, was significantly reduced in AAA tissues. Interestingly, Acta2 was previously reported to contribute to AngII-induced thoracic aortic aneurysms (TAA) and dissections (29). Moreover, mutations in Acta2 are associated with TAA in humans (30). We also detected a non-significant trend toward reduced expression of Ilk, a focal adhesion and actin cytoskeleton-associated gene, in AAA tissues. A previous study demonstrated that VSMC-specific deletion of Ilk increased TAA formation (31). Taken together, these findings suggest that Acta2 and Ilk can regulate not only TAA, but also AAA formation. Collectively, the data suggest that these key signaling pathways associated with histone H3 modifications may be linked to epigenetic regulatory mechanisms involved in AAA pathogenesis. However, these bioinformatic data need to be further verified experimentally in future studies.

Mechanisms of AAA formation are complex, and distinct cell types and molecular pathways are associated with different stages of AAA pathogenesis (e.g., initiation vs. progression). For example, extracellular matrix degradation is observed early in the initiation of AAA, while intraluminal thrombus formation and angiogenesis occur primarily in the progression and maturation stages. Although immune cell recruitment can be observed in all stages, innate immune responses, mainly mediated by neutrophils, are an initiating mechanism of AAA. Our results demonstrate that certain histone modifications are upregulated in the initiation stage, but downregulated in the maturation stage (e.g., H3K79me1/me3). These temporal changes in histone modifications may reflect the distinct cell types and molecular pathways involved at different stages of AAA formation, a hypothesis which will need to be addressed in future studies.

In conclusion, despite the limitations of this exploratory study, our results demonstrate the dynamic changes of histone H3 modifications occurring duing AAA formation and suggest underlying mechanisms that could serve as novel targets for AAA treatment. In future studies, ChIP-seq will be required to gain more insight into mechanisms of epigenetic regulation of AAA. Moreover, future studies are also required to identify specific cell types which are responsible for individual histone modifications detected in the whole aorta, which consists of numerous cell types, including VSMCs, endothelial cells, fibroblasts, immune cells, etc., which together orchestrate AAA formation. Finally, further investigations into histone H4 modifications and histone-modifying enzymes are required to fully define the epigenetic landscape associated with AAA formation.

DATA AVAILABILITY STATEMENT

The raw data supporting the conclusions of this article will be made available by the authors, without undue reservation.

ETHICS STATEMENT

The animal study was reviewed and approved by Institutional Animal Care and Use Committee at the Medical College of Georgia at Augusta University.

AUTHOR CONTRIBUTIONS

HK and NW developed the conception and design of the study. JG, NG, SP, TH, MM, DK, LR, MO, and HK performed experiments and collected data. JG, YS, X-YL, MS, RL, YH, LY, HK, and NW analyzed, interpreted, and discussed data. JG, YS, HK, and NW wrote the manuscript. All authors contributed to the article and approved the submitted version.

FUNDING

This study was funded by grants HL124097, HL126949, HL134354, AR070029, and AG064895 (NW) from the National Institutes of Health.

SUPPLEMENTARY MATERIAL

The Supplementary Material for this article can be found online at: https://www.frontiersin.org/articles/10.3389/fcvm.2020.595011/full#supplementary-material

REFERENCES

1. Diehm N, Dick F, Schaffner T, Schmidli J, Kalka C, Di Santo S, et al. Novel insight into the pathobiology of abdominal aortic aneurysm and potential future treatment concepts. *Prog Cardiovasc Dis.* (2007) 50:209–17. doi: 10.1016/j.pcad.2007.05.001
2. Sakalihasan N, Limet R, Defawe OD. Abdominal aortic aneurysm. *Lancet.* (2005) 365:1577–89. doi: 10.1016/S0140-6736(05)66459-8
3. Silaghi H, Branchereau A, Malikov S, Andercou A. Management of small asymptomatic abdominal aortic aneurysms–a review. *Int J Angio.* (2007) 16:121–7. doi: 10.1055/s-0031-1278264
4. Thompson RW, Curci JA, Ennis TL, Mao D, Pagano MB, Pham CT. Pathophysiology of abdominal aortic aneurysms: insights from the elastase-induced model in mice with different genetic backgrounds. *Ann N Y Acad Sci.* (2006) 1085:59–73. doi: 10.1196/annals.1383.029

5. Kim HW, Stansfield BK. Genetic and epigenetic regulation of aortic aneurysms. *BioMed Res Int.* (2017) 2017:7268521. doi: 10.1155/2017/7268521
6. Boileau A, Lindsay ME, Michel JB, Devaux Y. Epigenetics in ascending thoracic aortic aneurysm and dissection. *Aorta.* (2018) 6:1. doi: 10.1055/s-0038-1639610
7. Gibney E, Nolan C. Epigenetics and gene expression. *Heredity.* (2010) 105:4–13. doi: 10.1038/hdy.2010.54
8. Ordovás JM, Smith CE. Epigenetics and cardiovascular disease. *Nat Rev Cardiol.* (2010) 7:510–9. doi: 10.1038/nrcardio.2010.104
9. Esteller M. Epigenetics in cancer. *N Engl J Med.* (2008) 358:1148–59. doi: 10.1056/NEJMra072067
10. Gluckman PD, Hanson MA, Buklijas T, Low FM, Beedle AS. Epigenetic mechanisms that underpin metabolic and cardiovascular diseases. *Nat Rev Endocrinol.* (2009) 5:401. doi: 10.1038/nrendo.2009.102
11. Poulsen JL, Stubbe J, Lindholt J. Animal models used to explore abdominal aortic aneurysms: a systematic review. *Eur J Vasc Endovasc Surg.* (2016) 52:487–99. doi: 10.1016/j.ejvs.2016.07.004
12. Kim HW, Blomkalns AL, Ogbi M, Thomas M, Gavrila D, Neltner BS, et al. Role of myeloperoxidase in abdominal aortic aneurysm formation: mitigation by taurine. *Am J Physiol Heart Circ Physiol.* (2017) 313:H1168–H1179. doi: 10.1152/ajpheart.00296.2017
13. Tunaru S, Kero J, Schaub A, Wufka C, Blaukat A, Pfeffer K, et al. PUMA-G and HM74 are receptors for nicotinic acid and mediate its anti-lipolytic effect. *Nat Med.* (2003) 9:352–5. doi: 10.1038/nm824
14. Stanford University. *Encyclopedia of DNA Elements 2020.* (2020). Available online at: https://www.encodeproject.org/ (accessed August 12, 2020).
15. Yu G, Wang LG, He QY. ChIPseeker: an R/Bioconductor package for ChIP peak annotation, comparison and visualization. *Bioinformatics.* (2020) 31:2382–3. doi: 10.1093/bioinformatics/btv145
16. Kent KC, Zwolak RM, Egorova NN, Riles TS, Manganaro A, Moskowitz AJ, et al. Analysis of risk factors for abdominal aortic aneurysm in a cohort of more than 3 million individuals. *J Vasc Surg.* (2010) 52:539–48. doi: 10.1016/j.jvs.2010.05.090
17. Joehanes R, Just AC, Marioni RE, Pilling LC, Reynolds LM, Mandaviya PR, et al. Epigenetic signatures of cigarette smoking. *Circ Cardiovasc Genet.* (2016) 9:436–47. doi: 10.1161/CIRCGENETICS.116.001506
18. Ding YN, Tang X, Chen HZ, Liu DP. Epigenetic regulation of vascular aging and age-related vascular diseases. *Adv Exp Med Biol.* (2018) 1086:55–75. doi: 10.1007/978-981-13-1117-8_4
19. Xia Q, Zhang J, Han Y, Zhang X, Jiang H, Lun Y, et al. Epigenetic regulation of regulatory T cells in patients with abdominal aortic aneurysm. *FEBS Open Bio.* (2019) 9:1137–43. doi: 10.1002/2211-5463.12643
20. Han Y, Tanios F, Reeps C, Zhang J, Schwamborn K, Eckstein HH, et al. Histone acetylation and histone acetyltransferases show significant alterations in human abdominal aortic aneurysm. *Clin Epigenetics.* (2016) 8:3. doi: 10.1186/s13148-016-0169-6
21. Gomez D, Coyet A, Ollivier V, Jeunemaitre X, Jondeau G, Michel JB, et al. Epigenetic control of vascular smooth muscle cells in Marfan and non-Marfan thoracic aortic aneurysms. *Cardiovasc Res.* (2011) 89:446–56. doi: 10.1093/cvr/cvq291
22. Horimatsu T, Blomkalns AL, Ogbi M, Moses M, Kim D, Patel S, et al. Niacin protects against abdominal aortic aneurysm formation via GPR109A independent mechanisms: role of NAD+/nicotinamide. *Cardiovasc Res.* (2019) cvz303. doi: 10.1093/cvr/cvz303. [Epub ahead of print].
23. Vaquero A, Scher M, Erdjument-Bromage H, Tempst P, Serrano L, Reinberg D. SIRT1 regulates the histone methyl-transferase SUV39H1 during heterochromatin formation. *Nature.* (2007) 450:440–4. doi: 10.1038/nature06268
24. Djeghloul D, Kuranda K, Kuzniak I, Barbieri D, Naguibneva I, Choisy C, et al. Age-associated decrease of the histone methyltransferase SUV39H1 in HSC perturbs heterochromatin and B lymphoid differentiation. *Stem Cell Reports.* (2016) 6:970–84. doi: 10.1016/j.stemcr.2016.05.007
25. Chen TT, Wu SM, Ho SC, Chuang HC, Liu CY, Chan YF, et al. SUV39H1 reduction is implicated in abnormal inflammation in COPD. *Sci Rep.* (2017) 7:46667. doi: 10.1038/srep46924
26. Bown MJ, Jones GT, Harrison SC, Wright BJ, Bumpstead S, Baas AF, et al. Abdominal aortic aneurysm is associated with a variant in low-density lipoprotein receptor-related protein 1. *Am J Hum Genet.* (2011) 89:619–27. doi: 10.1016/j.ajhg.2011.10.002
27. Actis Dato V, Chiabrando GA. The role of low-density lipoprotein receptor-related protein 1 in lipid metabolism, glucose homeostasis and inflammation. *Int J Mol Sci.* (2018) 19:1780. doi: 10.3390/ijms19061780
28. Harada T, Yoshimura K, Yamashita O, Ueda K, Morikage N, Sawada Y, et al. Focal adhesion kinase promotes the progression of aortic aneurysm by modulating macrophage behavior. *Arterioscler Thromb Vasc Biol.* (2017) 37:156–65. doi: 10.1161/ATVBAHA.116.308542
29. Cheng J, Zhou X, Jiang X, Sun T. Deletion of ACTA2 in mice promotes angiotensin II induced pathogenesis of thoracic aortic aneurysms and dissections. *J Thorac Dis.* (2018) 10:4733. doi: 10.21037/jtd.2018.07.75
30. Guo DC, Pannu H, Tran-Fadulu V, Papke CL, Robert KY, Avidan N, et al. Mutations in smooth muscle α-actin (ACTA2) lead to thoracic aortic aneurysms and dissections. *Nat Genet.* (2007) 39:1488–93. doi: 10.1038/ng.2007.6
31. Shen D, Li J, Lepore JJ, Anderson TJ, Sinha S, Lin AY, et al. Aortic aneurysm generation in mice with targeted deletion of integrin-linked kinase in vascular smooth muscle cells. *Circ Res.* (2011) 109:616–28. doi: 10.1161/CIRCRESAHA.110.239343

Conflict of Interest: The authors declare that the research was conducted in the absence of any commercial or financial relationships that could be construed as a potential conflict of interest.

frontiers in Cell and Developmental Biology

REVIEW
published: 12 November 2020
doi: 10.3389/fcell.2020.581015

Histone Deacetylases (HDACs) and Atherosclerosis: A Mechanistic and Pharmacological Review

Xiaona Chen[1,2], Yanhong He[2], Wenjun Fu[2], Amirhossein Sahebkar[3,4,5], Yuhui Tan[1,2], Suowen Xu[6] and Hong Li[1,2]**

[1] Department of Medical Biotechnology, School of Basic Medical Sciences, Guangzhou University of Chinese Medicine, Guangzhou, China, [2] The Research Center of Basic Integrative Medicine, Guangzhou University of Chinese Medicine, Guangzhou, China, [3] Biotechnology Research Center, Pharmaceutical Technology Institute, Mashhad University of Medical Sciences, Mashhad, Iran, [4] Neurogenic Inflammation Research Center, Mashhad University of Medical Sciences, Mashhad, Iran, [5] Polish Mother's Memorial Hospital Research Institute, Łódź, Poland, [6] Department of Endocrinology, First Affiliated Hospital, Division of Life Sciences and Medicine, University of Science and Technology of China, Hefei, China

OPEN ACCESS

Edited by:
Nejat Dalay, Istanbul University, Turkey

Reviewed by:
Silvio Zaina, University of Guanajuato, Mexico
Amy Tsurumi, Massachusetts General Hospital and Harvard Medical School, United States

***Correspondence:**
Suowen Xu
sxu1984@ustc.edu.cn; suowen.xu@gmail.com
Hong Li
lihgzucm@foxmail.com

Specialty section:
This article was submitted to Epigenomics and Epigenetics, a section of the journal Frontiers in Cell and Developmental Biology

Received: *07 July 2020*
Accepted: *14 October 2020*
Published: *12 November 2020*

Citation:
Chen X, He Y, Fu W, Sahebkar A, Tan Y, Xu S and Li H (2020) Histone Deacetylases (HDACs) and Atherosclerosis: A Mechanistic and Pharmacological Review. Front. Cell Dev. Biol. 8:581015. doi: 10.3389/fcell.2020.581015

Atherosclerosis (AS), the most common underlying pathology for coronary artery disease, is a chronic inflammatory, proliferative disease in large- and medium-sized arteries. The vascular endothelium is important for maintaining vascular health. Endothelial dysfunction is a critical early event leading to AS, which is a major risk factor for stroke and myocardial infarction. Accumulating evidence has suggested the critical roles of histone deacetylases (HDACs) in regulating vascular cell homeostasis and AS. The purpose of this review is to present an updated view on the roles of HDACs (Class I, Class II, Class IV) and HDAC inhibitors in vascular dysfunction and AS. We also elaborate on the novel therapeutic targets and agents in atherosclerotic cardiovascular diseases.

Keywords: atherosclerosis, endothelial dysfunction, smooth muscle cells, macrophage, epigenetic, histone deacetylation, HDAC inhibitors

INTRODUCTION

Atherosclerosis (AS) is the critical underlying pathology of CVD, which ranks the first on the morbidity and mortality of diseases (Fanelli et al., 2017; Libby et al., 2019; Niu et al., 2019; Wang et al., 2019). It lessens the elasticity of the arteries and may lead to myocardial infraction, ischemic stroke, cerebrovascular incidents, and peripheral vascular disease (Ziegler et al., 2019). The most prominent characteristic of AS is plaque formation in the arteries. Although the cause of the spontaneous AS and its initially characteristic focal plaque morphology has not been well understood, the histology and the progression of the advanced plaque have been identified (Ross, 1993; Poston, 2019). The progression of AS includes low-density lipoprotein (LDL) oxidation, endothelial activation, monocytes recruitment, macrophage-derived foam cell formation, VSMC proliferation, and thrombus formation (Poston, 2019).

Among the multiple mechanisms that exist in the development of AS, endothelial dysfunction has been recognized as one of the major cardiovascular risk factors (Arcaro et al., 1995). The healthy endothelium is important to maintain vascular homeostasis. It possesses the function of generating bioactive NO, regulating vascular tone, protecting the endothelial cell (EC) integrity,

repairing the injury and inducing angiogenesis (Huynh and Heo, 2019). However, impaired NO bioavailability, oxidative stress, inflammation cytokines, and vascular tone potentially disrupt the endothelium homeostasis with consequence of endothelial dysfunction. Once the endothelium function is altered, followed by increased permeability to lipoprotein that attracts more leukocytes, induced secretion of inflammation cytokines and ROS, but less NO production (Poston, 2019); it exacerbates the pathology lesion of the arteries. Ensuing events of endothelial dysfunction include the proliferation and migration of VSMCs and formation of foam cell (Tian K.et al., 2019).

The epigenetic modification on genes is a crucial mechanism for many diseases, including cancer and CVDs (Xu et al., 2018, 2019; Khan et al., 2020). As one of histone modifications, histone acetylation plays an important role in altering the condensation of chromatin (which is mainly composed of DNA and histones in the nucleus of cells) without changing DNA sequences and has been regarded as the potential therapeutic targets. Acetylation of histones and nonhistone proteins is achieved by histone acetylases but removed by HDACs, which can regulate the transcriptional activities of the specific genes via interaction with the histones and transcription factors (Shirodkar and Marsden, 2011). In fact, the role of HDACs in cancer has been extensively studied *in vivo* and *in vitro*. Particularly, there are several HDAC inhibitors (HDACi) that have been approved by the Food and Drug Administration (FDA) for clinical application in cancer. During last two decades, much attention has been focused on the critical involvement of HDACs in CVD. The purpose of this article is to provide a systematic review on the role of HDACs and their inhibitors in vascular function and the progression of AS and highlight the potential application of HDACi in treating AS.

Abbreviations: ABCA1, ATP-binding cassette subfamily A1; ABCG1, ATP-binding cassette subfamily G1; AKT, protein kinase B; AMPK, adenosine 5′-monophosphate (AMP)-activated protein kinase; AngII, angiotensin II; ApoE$^{-/-}$, apolipoprotein E knockout; AS, atherosclerosis; Bcl-2, B-cell lymphoma-2; BH_4, tetrahydrobiopterin; BuA, butyric acid; CAT, catalase; CD16, cluster of differentiation 16; cdk2, cyclin-dependent kinase2; cdk4, cyclin-dependent kinase4; cdk6, cyclin-dependent kinase6; COX-2, cyclooxygenase 2; CSE, cigarette smoke extract; CVD, cardiovascular disease; CYR61, cysteine rich angiogenic inducer 61; E2F1, E2F transcription factor 1; ECM, extracellular matrix; ECs, endothelial cells; ECV304 cells, human umbilical vein endothelial 304; eNOS, nitric oxide synthase; ERK 1/2, extracellular regulated protein kinases1/2; ET-1, endothelin 1; FSTL1, follistatin like 1; GLUT-1/4, glucose transport protein 1/4; H3K9, histone H3 lysine 9; HAECs, human aortic endothelial cells; HDAC6$^{-/-}$, HDAC6 knockout; HDACi, histone deacetylases inhibitors; HDACs, histone deacetylases; HIF-1α, hypoxia inducible factor-1; HoxA9, homeobox A9; HPAECs, human pulmonary artery endothelial cells; HUVECs, human umbilical vein endothelial cells; ICAM-1, intercellular cell adhesion molecule 1; Id2, inhibitor of DNA binding 2; IGF-1, insulin-like growth factor 1; IKBα, NF-κB inhibitor; IL-10, interleukin 10; JNK, c-Jun N-terminal kinase; KLF2/4, Krüppel-like factor 2/4; LPS, lipopolysaccharide; MAPK, mitogen-activated protein kinase; MCP1, monocyte chemoattractant protein-1; MDR1, multidrug resistance protein 1; MEF2, myocyte enhancer factor 2; MMPs, matrix metalloproteinase; MS-275, entinostat; NAD+, nicotinamide adenine dinucleotide; NE-Y, nuclear factor-Y; NF-κB, nuclear factor κB; NO, nitric oxide; Nox, NADPH oxidase; $ONOO^-$, peroxynitrite; OSS, oscillatory shear stress; ox-LDL, oxidized low density lipoprotein; PAECs, pulmonary artery vascular cells; PAH, pulmonary arterial hypertension; PAI-1, plasminogen activator inhibitor type 1; PCAF, p300/CBP-associated factor; PPARγ, peroxisome proliferator-activated receptors; PVRL2, poliovirus receptor related protein 2; ROS, reactive oxygen species; SAHA, varinostat; sGC, soluble guanylyl cyclase; SIRT, sirtuin; Slc2a1, solute carrier family 2 member 1; Slit2, Slit homolog 2 protein; SMC, smooth muscle cell; SOD, superoxide dismutase; SP1, Specificity Protein 1; STAT1, signal transducers and activators of transcription 1; TF, tissue factor; TIMP, the tissue inhibitor of metalloproteinase; TLR4, toll like receptor 4; TNF-α, tumor necrosis factor α; t-PA, tissue-type plasminogen activator; TSA, trichostatin; VCAM-1, vascular cell adhesion molecule 1; VEGF, vascular endothelial growth factor; VEGFR, vascular endothelial growth factor receptor; VPA, valproic acid; VSMC, vascular smooth muscle cells; vWF, von-Willebrand factor.

HISTONE DEACETYLASES

Histone deacetylases remove the acetylated residues at lysine, redense the chromatin structures, and inhibit the transcription of target genes (Bae et al., 2009). They are divided into two families, HDAC family and sirtuin family, including 18 members. These members are characterized into four groups: Classes I, II, III, and IV (Parra and Verdin, 2010) (**Figure 1**). Class III consists of the sirtuin family (SIRT1-7), which has been identified since 21st century. They differ from other groups because of their specific conserved catalytic core domain that requires the binding of NAD^+/NADH, whereas the others require zinc molecule as an activator (Mihaylova and Shaw, 2013). Correspondingly, HDACs in Classes I, II, and IV, other than Class III, are referred to as the classical HDACs. Class I (HDAC1/2/3/8) HDACs are similar to the yeast Rpd3 and mostly locate in the nucleus, except that HDAC3 can export to the cytoplasm. In addition, Class II HDACs were subclassified into Classes IIa and IIb based on their primary structures. Class IIa (HDAC4/5/7/9) subfamily contains only an N-terminal regulatory domain, whereas Class IIb (HDAC6/10) subfamily has two catalytic domains (Gray and Ekström, 2001). All Class IIa members shuttle between the nucleus and the cytoplasm, which interact with the kinase families such as the calcium-independent protein kinase and the MAPK, acting as a signal transducer, but Class IIb (HDAC6/10) is mainly located in the cytoplasm (Fischle et al., 2002). As for Class III, SIRT1/2 are located in both the nucleus and cytoplasm, SIRT6/7 are in the nucleus, and SIRT 3/4/5 are in the mitochondria (Luo et al., 2014) (**Figure 1**). Of note, the location of HDACs might vary from different types of cells. HDAC11 is the only member of Class IV, and it is a negative regulator of interleukin (IL) 10 and the activity of T cells, indicating the potential role of HDAC11 in treating AS, which occurs as an inflammatory process (Yanginlar and Logie, 2018).

Although HDACs were primarily identified as enzymes that deacetylate histones, further studies have identified many other nonhistone protein substrates, especially transcription factors such as the p65 subunit of NF-κB, E2F1, SP1, KLF 2/4, and signal transducers and activators of transcription 1 (STAT1) (Lyu et al., 2019). Because of multifunctional properties of HDACs, they have been involved in many cellular activities, tissue development, and various diseases, including embryonic development, tissue function, viral infections, CVD, cancer, kidney diseases, and autoimmune diseases (Gatla et al., 2019). Of note, the sirtuin family is well known for their effects in regulating vascular health, which have been deeply analyzed in recent reviews (Kane and Sinclair, 2018; Zhang et al., 2020). Hence, in this review, we mainly focus the role of classical HDACs in vascular function and AS, as well as the pharmacological effects of HDACi on AS.

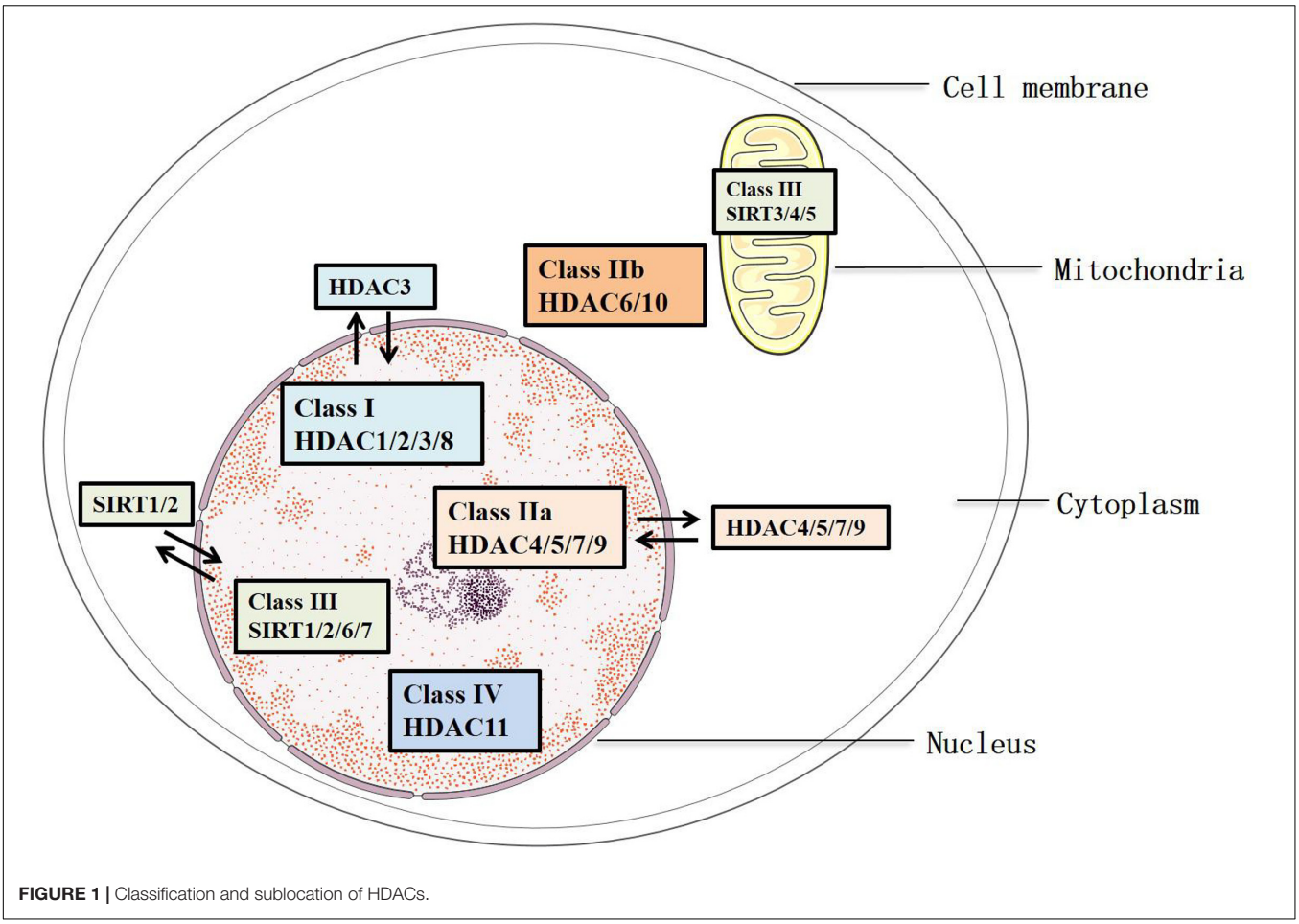

FIGURE 1 | Classification and sublocation of HDACs.

HDAC INHIBITORS

Because of the fact that HDACs are implicated in triggering the development of some diseases, especially cancer, HDACi have been designed or investigated. These inhibitors mainly bind with the catalytic sites of HDACs, resulting in genes re-expression (Zhang et al., 2018). Although HDACi are specific for HDACs, most of them are not specific to the HADC subclass. Based on their chemical structures, HDACi can be classified into four groups: short-chain fatty acids, benzamides, hydroxamic acids, and cyclic peptides (Marks, 2010). To date, five HDACi (SAHA, LBH589, PXD101, VPA, romidepsin) have been approved by the FDA for clinical treatment of cancer (Gatla et al., 2019). In addition, some HDACi are also in clinical trials for other diseases such as human immunodeficiency virus infection (Elliott et al., 2014), sickle cell disease (Okam et al., 2015), Duchenne muscular dystrophy (Bettica et al., 2016), polycythemia vera (Finazzi et al., 2013), and myeloproliferative diseases (Rambaldi et al., 2010). Although currently there is still no clinical usage of HDACi in CVD, plenty of evidence has shown the great potential of some HDACi in inhibiting endothelial dysfunction and AS (Zheng et al., 2015; Xu et al., 2017; Lee and Chiu, 2019). Notably, as some HDACs protect vascular cells against injury triggered by proatherogenic stimuli, it is necessary to clarify the specific role of each HDAC in different cellular context and activities in the vasculature, so that HDACi could be better repurposed for cardiovascular therapeutics.

ROLE OF HDACs IN ATHEROSCLEROSIS

HDACs Are Involved in Endothelial Function and Dysfunction

HDACs and NO Production

Nitric oxide is a catalytic product of endothelial NO synthase (eNOS) in the endothelium, with the L-arginine as the substrate and BH_4 as the cofactor (Förstermann et al., 2017). NO production can be inhibited by arginase 2 or AngII from VSMCs (Krause et al., 2016; Ryu et al., 2019). Once NO diffuses across the EC membrane, it can activate the sGC rapidly in VSMCs. The activated sGC catalyzes GTP to generate cGMP, a second messenger mediating the PKC signaling pathway, which results in a decline of the intracellular concentration of calcium and triggers the vasodilation of the VSMCs (Feil et al., 2003). The endogenous NO not only decreases the vascular tone but also inhibits the progression of the inflammation and the angiogenesis. Interestingly, HDACs and their inhibitors have been found to modulate the production of NO.

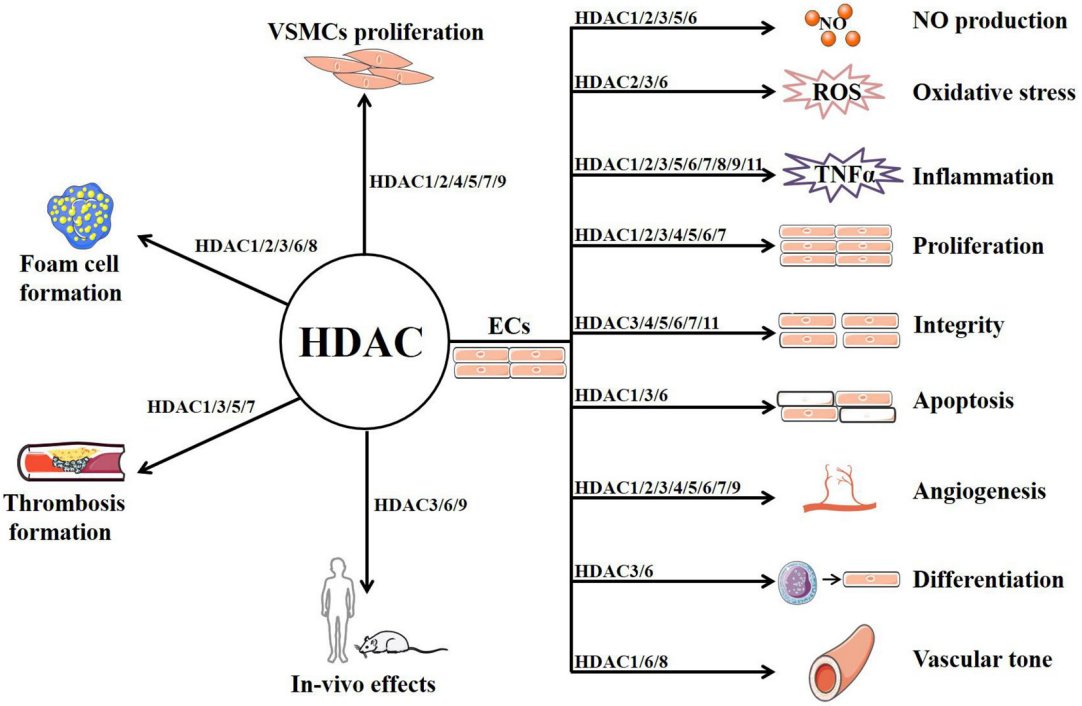

FIGURE 2 | The potential mechanism of HDACs in atherosclerosis.

On the one hand, HDACs regulate the expression of eNOS. For example, HDAC1 was recruited at eNOS promoters and impaired eNOS expression in ECs subject to ischemic/reperfusion insult, leading to decrease in NO formation, which was ameliorated by the HDACi TSA treatment (Yang et al., 2012). In ECs from DJ-1/park7$^{-/-}$ mice, HDAC1 also inhibited eNOS transcription by inhibiting histone acetylation at the eNOS promoter (Won et al., 2014). HDAC3 (Zhang et al., 2008) and HDAC6 (Chen et al., 2019) had similar effects in inhibiting eNOS expression, and the effects could be reversed by tubacin, a selective inhibitor of HDAC6. By contrast, fluid shear stress induced phosphorylation of HDAC5, which was subsequently exported from nucleus and was involved in increased eNOS expression (Wang W.et al., 2010; Kwon et al., 2014). However, both of the HDACi-BuA and entinostat (MS-275) caused a decrease in eNOS protein (Rossig et al., 2002). In addition, the authors found that although TSA increased the eNOS promoter transcriptional activity, it reduced the production of NO through posttranscriptional suppression of eNOS protein levels. On the other hand, eNOS activity was regulated by HDACs via posttranslational modifications. HDAC1 (Hyndman et al., 2014) and HDAC3 (Jung et al., 2010) could reduce the lysine acetylation of eNOS and blocked NO expression. On the contrary, VPA could improve NO production by influencing eNOS phosphorylation (Cho et al., 2014). Of note, overexpression of HDAC2 could suppress the expression of arginase 2, a protein that counteracts eNOS activity, and the effect was reversed by TSA through increasing levels of H3K9 and H4K12 acetylation at arginase 2 proximal and core promoter (Pandey et al., 2014; Krause et al., 2016), indicating a protective role of HDAC2 in endothelial dysfunction and AS.

HDACs and Endothelial Oxidative Stress

BH_4, the coactivator of the eNOS, can be easily oxidized to dihydrobiopterin, resulting in uncoupling of eNOS, leading to superoxide rather than NO production (Stocker and Keaney, 2004). Superoxide interacts with NO to produce $ONOO^-$, which reduces the bioavailability of NO. In general, superoxide is mainly derived from the process when the membrane oxidase Nox transfers the electrons from NADPH to oxygen (Craige et al., 2015). Among the members of Nox family, Nox1/2/4/5 are expressed in the cardiovascular system with abundant expression of Nox4.

It was reported that the pan-HDACi varinostat (SAHA) reduced expression of Nox1/2/4 in the aorta of *ApoE*$^{-/-}$ mice, which contributed to its anti-AS effect (Manea et al., 2020). Recruitment of HDAC abolishes the interaction of RNA polymerase II and p300 to the promoter sites of Nox2/4/5, respectively, which inhibited the activation at those promoter regions and resulted in a decline of ROS (Chen et al., 2016; Hakami et al., 2016). In addition, HDAC3 could ameliorate the oxidative stress induced by AngII or disturbed flow (Martin et al., 2014). In another aspect, HDAC1 and HDACi could regulate the antioxidant enzymes including SOD and CAT, which scavenge the superoxide *in vivo* or *in vitro*. HDAC1 dissociation from SOD3 promoter was critically involved in SOD3 expression elicited by caffeic acid phenethyl ester (Ohashi et al., 2017). It is reported that TSA could induce the expression of SOD3 and

TABLE 1 | Effect of HDAC members in endothelial (dys)function and atherosclerosis.

Class	Subtypes	Endothelial (dys)function and atherosclerosis (AS)													Included inhibitors	
		ECs									VSMCs	Macrophages	In vessel	*In vivo*		
		NO production	Oxidative stress	Inflammation	Proliferation	Integrity	Apoptosis	Angiogenesis	Differentiation	Vascular tone	proliferation	Foam cell formation	Thrombosis formation	Overall effects of AS	Selective inhibitors	Other specificity
I	HDAC1	−	*	−	+	*	−	+	*	−	+	+	−	*	*	Pan-HDAC: SAHA TSA ITF2357 Tributyrin Class I: MS-275 Butyrate Apicidin β-OHB Class I/II: VPA
	HDAC2	+	+	+/−	+	*	*	*	*	*	+	+	*	*	*	
	HDAC3	−	−	+	+	−	−	−	+	*	*	+	+	+/−	RGFP-966	
	HDAC8	*	*	+	*	*	*	*	*	−	*	+	*	*	PCI34051	
IIa	HDAC4	*	*	*	+/−	−	*	+	*	*	+	*	*	*	*	Pan-HDAC: SAHA TSA ITF2357 Tributyrin Class I/II: VPA Class IIa: TMP195
	HDAC5	+	*	−	+/−	−	*	+/−	*	*	+	*	+	*	*	
	HDAC7	*	*	+	−	+	*	+	*	*	+	*	+	*	*	
	HDAC9	*	*	+	*	*	*	+	*	*	+	*	*	+	*	
IIb	HDAC6	−	+	+	+	−	+	+	+	−	*	+	*	+	Tubacin/ tubastatin A	
	HDAC10	*	*	*	*	*	*	*	*	*	*	*	*	*	*	
IV	HDAC11	*	*	−	*	−	*	*	*	*	*	*	*	*	*	Pan-HDACi

*+, promoting; −, inhibiting; *, not clear.*

reduce NOX expression robustly in human pulmonary artery ECs exposed to scriptaid (Zelko and Folz, 2015). However, MS-275 failed to influence the expression of Nox1, Nox2, and p47phox (Ryu et al., 2019).

Reactive oxygen species are the stimuli that reduce the bioavailability of NO and induce inflammation of ECs. It was found that IGF-1 enhanced the phosphorylation of HDAC5 that is associated with AS and led to nuclear export of HDAC5, which was mediated by Nox4-dependent ROS production, as well as the phosphatidylinositol 3-kinase (PI3K)/AKT pathways (Pietruczuk et al., 2019). HDAC6 expression and activity were upregulated in ox-LDL-treated ECs, which led to decreased expression of cystathionine γ-lyase and contributed to endothelial dysfunction (Leucker et al., 2017), and knockdown of HDAC6 or pharmacological inhibition with the dietary HDACi sodium butyrate (Hou et al., 2018; Wu et al., 2018), the inhibitor of Class I HDAC, could inhibit endothelial dysfunction. Moreover, loss of HDAC2 or specific inhibition of HDAC6 was found to activate HO-1/SIRT1 pathway and inhibit oxidative stress induced by high glucose (Gao et al., 2018; Abouhish et al., 2020).

HDACs and Endothelial Inflammation

Oxidative stress, eNOS uncoupling, and inflammation are potential contributors to endothelial dysfunction. Inflammation in vasculature causes alteration of vascular wall, which can trigger the CVD especially AS (Ali et al., 2018). In the development of AS, ECs and macrophages produce the proinflammatory cytokines, such as TNF-α, IL-β, and IL-6 (Barbour and Turner, 2014). These proinflammatory molecules cause the secretion of adherent molecules, including ICAM-1, VCAM-1, and E-selectin, to recruit the leukocytes and monocytes to endothelium (Xu et al., 2017). TNF-α mediated an important signaling pathway in increasing the expression of inflammatory cytokines and superoxide, thereby attracting more monocytes into the subendothelium space (Kleinbongard et al., 2010). Accumulating studies have demonstrated that NF-κB plays a crucial role in promoting the inflammation cytokines release. Activation of NF-κB leads to the upregulation of TNF-α, IL-β, IL-6, and adherent molecules in ECs (Stein et al., 2010). In human ECs treated with ox-LDL, HDAC1 and HDAC2 were downregulated, and the effect was reversed by simvastatin, which also inhibited the NF-κB pathway (Dje N'Guessan et al., 2009). HDAC2 is also a mediator of neutrophil migration and regulated multiple MMPs and CD16 gene expression in acute ischemic stroke patients (Li et al., 2020). Similarly, phosphorylation of HDAC5 led to HDAC5 nuclear export and upregulation of KLF2 and mediated the anti-inflammatory effects of metformin in ECs (Tian R.et al., 2019). On the contrary, several HDACs were also implicated in the proinflammatory response in ECs. Bedenbender et al. (2019) reported that in TNF-α-treated human umbilical vein ECs (HUVECs), HDAC2 was recruited to the RNase I promoter and reduced the histone acetylation, leading to downregulation of RNase I, a protective molecule in vascular homeostasis. HDAC3 mediated the inflammatory response in ECs by regulating galectin-9 expression (Alam et al., 2011). In human pulmonary ECs subjected to *Staphylococcus aureus* infection, HDAC6 was upregulated followed by elevated ROS, and knockout or pharmacological inhibition of HDAC6 in mice could inhibit vascular inflammation and protect the EC integrity (Karki et al., 2019). It was suggested that the detrimental effect of HDAC6 might be mediated by microtube destabilization. Moreover, HDAC7 could induce leucocyte adhesion to ECs (Ismail et al., 2012), and HDAC8 was involved in increased secretion of ICAM-1 and VCAM-1 in the aortas of mice infused with AngII (Kee et al., 2019).

Because of the proinflammatory effects of most classical HDACs, several HDACi have been employed to determine their anti-inflammatory effects. In human lung ECs, LPS upregulated IKBα mRNA, which might be mediated by deacetylation of H3K9 and could be blocked by TSA (Thangjam et al., 2014). By contrast, TSA could suppress COX-2 expression induced by LPS through inhibiting the phosphorylation of JNK and p38 MAPK (Hsu et al., 2011). Moreover, TSA suppressed VCAM-1 (but not ICAM-1) expression in TNF-α-induced HUVECs and sickle transgenic mice, whereas MS-275 inhibited VCAM-1 and MCP-1 expression in AngII-induced hypertensive mice (Inoue et al., 2006; Hebbel et al., 2010; Ryu et al., 2019). He et al. (2011) showed that TSA inhibited the expression of TLR4 and HDAC2 induced by LPS in cultured EA.hy926 cells, which protected the EC from injury. Li et al. (2018a) found that TSA inhibited IL-8 production, and VCAM-1 expression induced by TNF-α in HUVECs, and the adhesion of peripheral blood mononuclear cell to HUVECs was also blocked. Besides, butyrate (Ogawa et al., 2003), other short-chain fatty acids (Miller et al., 2005; Vinolo et al., 2011), and HDAC8 selective inhibitor PCI34051 (Kee et al., 2019) also showed anti-inflammatory effect in ECs. It is notable that although HDACi exhibited an anti-inflammatory effect in various ECs or animal models, the inflammatory markers detected in each study varied, and the regulatory mechanism was also not well illustrated. Further study is needed to demonstrate the specific HDAC isoforms involved in and to evaluate whether the anti-inflammatory effect of HDACi is dependent on increased acetylation of histones or specific transcription/repressive factors.

HDACs Regulate EC Proliferation

Endothelium works as a selective barrier between the blood and tissue, controlling exchange of the ions and cytokines. Under healthy conditions, ECs tend to be tight and are not proliferating, but they start to migrate and proliferate when subjected to hypoxia, injury, or stress (Zeng et al., 2009). Although EC proliferation is required to response to the hypoxia, excessive EC proliferation contributes to EC turnover, which is critically associated with the endothelium permeability (Caplan and Schwartz, 1973).

β-Catenin is a signal transducer that accelerates cell proliferation and growth via activating the Id2, T cell factor/lymphoid enhancer factor, and follistatin transcription factors. Margariti et al. (2010) found that HDAC7 was important in modulating the expression of genes related to EC proliferation via regulating the transcription activity of β-catenin. Overexpression of HDAC7 suppressed HUVEC proliferation through inhibition of nuclear translocation of β-catenin and downregulation of Id2 and cyclin D1 expression, causing G1

phase elongation. The effect of HDAC7 overexpression could be abolished by the VEGF, which degraded HDAC7 via PLC-PI3K signal pathway and disrupted the complex of HDAC7 and β-catenin, leading to β-catenin released into the nucleus. It was shown that VEGF induced phosphorylation and cytoplasm translocation of HDAC7, resulting in activation of VEGF-responsive genes, and EC proliferation was enhanced (Wang et al., 2008). Similarly, HDAC4 and HDAC5 were also critical in mediating EC proliferation during cardiovascular development (Kang et al., 2013). However, in most cases, the classical HDACs were deemed to promote abnormal EC proliferation. Lee et al. (2012; Chiu and Chien, 2011) found that HDAC1/2/3-specific siRNAs reversed the increased level of cyclin A and reduction of p21 induced by OSS, which is considered to be a contributor to endothelial dysfunction of arterial branches and curvatures. Meanwhile, the HDACi VPA could suppress OSS-induced EC proliferation in BrdU-infused rats (Lee et al., 2012). HDAC4 and HDAC5 in nuclear could inhibit myocyte-enhancer factor 2 (MEF2) and KLF2/4 activity (Yang et al., 2019), whereas HDAC5 in cytoplasm mediated KLF2 expression (Wang W.et al., 2010; Kwon et al., 2014). Normal shear stress induced HDAC6 activity, which reduced tubulin acetylation and promoted ECs migration (Wang Y.H.et al., 2010). The pro-proliferation effect of VEGF could be inhibited by expressing a signal-resistant HDAC7 mutant protein in ECs (Wang et al., 2008). In parallel, the HDACi such as SAHA (Cheng and Hung, 2013), tubacin (Li et al., 2016), TSA, and apicidin (Yang et al., 2015) inhibited EC proliferation in different conditions.

HDACs and Endothelium Integrity

The endothelial barrier possesses tight junction, endothelial glycocalyx, and efflux transporters that are all essential for protecting the endothelial integrity and cell permeability and control the entry of the chemicals exchange between the blood and tissues. The endothelial glycocalyx is on the endothelial surface (Weinbaum et al., 2007). The MMPs are produced by ECs, which could degrade the ECM and connective tissue proteins, including the ones that form the glycocalyx (Haas, 2005). HDACs play a crucial role in protecting the endothelial barrier function by regulating cell permeability, chemical transporter, tight junction protein, and MMPs (Gao et al., 2008; Joshi et al., 2015; Shi et al., 2016; Castro et al., 2018). Among the classical HDACs, it seems that only HDAC7 and HDAC3 exhibit a protective effect in endothelial integrity. It was demonstrated that HDAC7 could interact with MEF2, inhibiting its transcription activity, and thus suppressed the expression of target genes such as MMP-10 (Chang et al., 2006; Gao et al., 2008; Su et al., 2013). By contrast, RGFP-966, an HDAC3-selective inhibitor, was found to significantly attenuate the oxygen–glucose deprivation/reperfusion-induced transendothelial cell permeability and downregulate the tight junction protein claudin-5 via activating PPARγ signaling pathway (Zhao et al., 2019). HDAC4 and HDAC5 regulated expression of connexin 37 and 40 in PAECs (Kim et al., 2015), and increased HDAC5 activity was essential for MMP induction, glycocalyx remodeling, and reduced expression of TIMP (Ali et al., 2019). As for HDAC6, it was a mediator leading to *S. aureus*-induced (Karki et al., 2019) or TNF-α-induced (Yu et al., 2016) endothelial permeability and could attenuate tubulin acetylation, leading to reduced cell stability (Fernandes et al., 2015). Besides, inhibition of HDAC6 could attenuate CSE-induced EC permeability and acute lung injury (Borgas et al., 2016). As the only member of class IV HDACs, HDAC11 is least studied in endothelial function. It was found that HDAC11 was upregulated in PAR2 agonist-treated ECs and mediated the impaired barrier function via modulating VE-cadherin expression (Zhang and Ge, 2017). Moreover, inhibition of HDACs via TSA or SAHA increased the protein levels of TIMP-1 and TIMP-3 (Ali et al., 2019).

The multidrug resistance protein 1 (also known as MDR1) is a crucial efflux transporter located on the top surface of capillary ECs and prevents xenobiotics accumulating in the brain (Serlin et al., 2015). You et al. (2019) showed that VPA, apicidin, and SAHA could increase MDR1 expression in human brain ECs. Glucose transporters are responsible for the energetic supply at the blood–brain barrier (Castro et al., 2016). β-Hydroxybutyrate, an HDACi, could upregulate the glucose transporter gene Slc2a1 expression in brain microvascular EC s and NB2a neuronal cells by increasing acetylation of H3K9 at the promoter site of the Slc2a1 gene (Rafehi et al., 2017). Besides, TSA, VPA, short-chain fatty acid, and the specific Class IIa HDACs inhibitor TMP269 could reverse endothelial barrier dysfunction induced by hemorrhage, lethal scald injury, and acute lung injury, respectively (Miyoshi et al., 2008; Bruhn et al., 2018; Tang et al., 2018; Kovacs-Kasa et al., 2020).

HDACs and Endothelial Apoptosis

Endothelial cell apoptosis is not active under healthy conditions, but it is activated in the development of AS and contributes to the hyperpermeability of endothelium, as well as thrombus formation on eroded plaques (Tedgui and Mallat, 2003). Li et al. (2018c) found that HDAC1 was reduced in AS lesions and ox-LDL-treated human aortic ECs (HAECs), which was regulated by miR-34a and might mediate EC apoptosis. In the process of senescence induced by radiation, HDAC1 was also reduced (Okamoto et al., 2006). Similarly, HDAC3 is critical for endothelial survival, and knockdown of HDAC3 led to apoptosis in ECs (Zampetaki et al., 2010). However, HDAC6 was implicated in apoptotic response of lung ECs induced by TNF-α (Yu et al., 2016). VPA induced the Bcl-2 phosphorylation and release of the cytochrome c via activating ERK1/2 and consequently inhibited the serum starvation-induced HUVECs apoptosis (Michaelis et al., 2006). Comparatively, VPA was found to induce apoptosis of tumor cells (Yamanegi et al., 2015).

HDACs and Angiogenesis

Angiogenesis mainly refers to the formation of functional capillaries especially in the progression of tumor, and it is a complex biological process including alterations of gene expression. Numerous studies were focused on the role of HDAC/HDACi and angiogenesis in cancer, which have been reviewed elsewhere (Mastoraki et al., 2020). Actually, the angiogenic ability of EC is also very important for maintaining the cell or tissue function during development, ischemia, hypoxia, or injury. VEGF is considered as a predominant growth factor

during the formation of capillaries, which has been a therapeutic target for tumor angiogenesis (Pepper et al., 1996). Notably, VEGF could be induced by HIF-1α activation in response to hypoxia (Ikeda, 2005). Inhibition of HDAC1/4/6/7 abolished the expression of VEGF via impairing the induction or activity of HIF-1α in hypoxia-exposed ECV304 cells, HaCaT cells, or patients with chronic obstructive pulmonary disease (Granger et al., 2008; Reynoso-Roldán et al., 2012; To et al., 2012; Kowshik et al., 2014).

Blood flow is a critical factor inducing angiogenic sprouting, in the process of which HDAC1 was phosphorylated and translocated from the nucleus to cytosol. Similarly, phosphorylation and nuclear export of HDAC5 also mediated VEGF-induced angiogenesis (Ha et al., 2008). In addition to the effect of inducing angiogenesis during myocardial infraction (Yang et al., 2019), HDAC6 also improved repair stimulated by injury (Wu et al., 2016). By targeting the antiangiogenic microRNA-17-92 cluster, HDAC9 accelerated angiogenesis in ECs (Kaluza et al., 2013). In addition, HDAC5 played an important role in inhibiting expression of the genes participating in angiogenesis including CYR61, PVRL2, FSTL1, and Slit2 in patients with systemic sclerosis, which could be reversed by silencing of HDAC5 (Urbich et al., 2009; Tsou et al., 2016). Endothelial migration is a key step of angiogenesis, and both HDAC6 (Li et al., 2011; Birdsey et al., 2012) and HDAC7 (Mottet et al., 2007; Yu et al., 2014) could promote angiogenesis by regulating cell migration. On the contrary, it was shown that HDAC3 was a negative regulator of angiogenesis (Park et al., 2014). Treatment with TSA or SAHA suppressed HIF-1α, VEGF, VEGF receptors (VEGFR1 and VEGFR2), and the formation of capillary-like structures, but increased semaphorin, a VEGF competitor, in rat lungs and cultured human pulmonary microvascular ECs (Deroanne et al., 2002; Mizuno et al., 2011). SAHA could upregulate the WNT-inducible secreted protein 1, a matricellular molecule that accelerates angiogenesis in TNF-α-stimulated HCAECs (Wright et al., 2018). Importantly, the HDACi such as VPA (Jin et al., 2011; Wang et al., 2012) and SAHA (Jin et al., 2011; Wright et al., 2018) mainly exerted proangiogenic effect, whereas TSA (Williams, 2001) could also inhibit angiogenesis.

HDACs and Cell Differentiation Into ECs

When the endothelium is damaged or nearly denuded, the circulating or local resident stem or progenitor cells would differentiate into ECs to rescue the denuded ECs (Rinkevich et al., 2011). Rossig et al. (2005) found that inhibition of HDACs abolished the endothelial differentiation from adult progenitor cells by inhibiting the expression of homeobox transcription factors HoxA9, which is a regulator of eNOS, VEGF-R2, VE-cadherin, and EC maturation induced by shear stress. TSA improved H3K9 acetylation and downregulated HDAC1 expression in bone marrow progenitor cells, which were further treated to generate cardiac progenitor cells and were able to differentiate into myocytes and ECs in the infarcted mouse heart (Rajasingh et al., 2011). Furthermore, TSA induced EC marker VE-cadherin, von Willebrand factor (vWF), and Flk in VEGF-treated multipotent adult progenitor cells and induced the differentiation into ECs (Mahapatra et al., 2010). However, in the progression of stem cell-derived ECs differentiating into ECs, TSA showed an opposite effect. While VEGF induced the differentiation accompanied by increased activity of HDAC, TSA or silence of HDAC3 reduced the EC lineage marker, indicating that the HDAC3 positively regulated the differentiation (Xiao et al., 2006; Zeng et al., 2009). Moreover, HDAC6 was important for maintaining mechanical sensing in human induced pluripotent stem cell-derived ECs (Smith et al., 2018).

HDACs and Vascular Tone

Endothelium is crucial in regulating vascular tone to control the local cardiovascular function, especially by NO, which determines the endothelium-dependent relaxation and thus, to some extent, prevents hypertension and PAH (Pan et al., 2018). PAH results in the unnatural proliferation of PAECs, triggering enhanced pulmonary vascular resistance, as well as right ventricular failure. It is recognized that PAECs, pulmonary arterial smooth muscle cells, fibroblasts, and pericytes are involved in the pathogenesis of PAH (Rabinovitch, 2012). Furthermore, the factors secreted from PAECs such as fibroblast growth factor 2, IL-6, and ET-1 induce proliferation, migration, and vascular remodeling by influencing other cells in the development of PAH (Ricard et al., 2014). Kim et al. (2015) identified that MEF2 acted as the key *cis*-acting factor that regulated the expression of target genes contributing to pulmonary vascular homeostasis, such as microRNAs-424 and -503, connexin 37, connexin 40, KLF2, and KLF4, which were evidently decreased in PAECs isolated from PAH patients. This action could be abolished by nuclear accumulation of HDAC4 and HDAC5, causing inhibition of MEF2 transcription activity. Importantly, several HDAC isoforms were upregulated in isolated pulmonary arteries in a monocrotaline-induced PAH in rat models, and HDACi inhibited Nox expression and PAH markers in isolated pulmonary arteries (Chen et al., 2016). In addition, HDAC1 was involved in increased systolic blood pressure in mice by regulating eNOS expression and NO production, which could be inhibited by VPA (Won et al., 2014). The increased NO is the major vasodilator that reduces the vascular tone, which plays a critical role in maintaining arterial patency (Nishida et al., 1992). Several studies have shown that HDAC6 was crucial in impairing vascular tone. On the one hand, HDAC6 regulated chromatin remodeling and promoted ET-1 expression (Li et al., 2016). On the other hand, it was upregulated in AngII-treated aortas and HAECs, which induced cystathionine γ-lyase ubiquitination and degradation, and was implicated in AngII-induced hypertension (Chi et al., 2019, 2020). Moreover, PAH was significantly ameliorated in HDAC6$^{-/-}$ mice. Similarly, HDAC8 was implicated in AngII-induced hypertension, and its selective inhibitor PCI34015 could reverse the effect and reduced vascular hypertrophy and inflammation (Kee et al., 2019). IGF-1 is a growth factor contributing to PAH in neonatal mice, through activating the AKT signaling pathway. Apicidin, an inhibitor of HDAC, suppressed pulmonary IGF-1/pAKT signaling pathway, which ameliorated right ventricular hypertrophy and vascular remodeling in lungs (Yang et al., 2015).

And TSA could inhibit hypertension induced by abdominal aortic constriction in rats (Kang et al., 2015).

HDACs Regulate VSMC Proliferation and Migration in Atherosclerosis

During the development of AS, VSMCs migrate to the subendothelium space and switch to a collagen-secreting synthetic phenotype (Doran et al., 2008) to form the fibrous cap, with mass of the foamy macrophages and cholesterol on the surface. Moreover, the proliferating VSMCs can also remodel the ECM by degrading the matrix components through increasing expression and activity of MMPs, which disrupts the fibrous cap of the plaque, causing plaque vulnerability (Shah, 1996).

Increasing evidence has shown the important role of HDACs in regulating VSMC proliferation and migration. Laminar flow enhanced HDAC1 activity and the interaction between HDAC1 and p53, which resulted in $p21^{WAFl}$ activation in VSMCs (Zeng et al., 2003). Sun et al. (2020) found that HDAC1 was critical for the migration and phenotypic switch of aortic VSMCs. KLF4 and KLF5 acetylation in VSMCs was regulated by phosphorylated HDAC2, which was implicated in VSMC proliferation induced by retinoic acid receptor agonist (Meng et al., 2009; Zheng et al., 2011). HDAC4 also promoted VSMC proliferation and migration (Usui et al., 2014; Li et al., 2018b; Zhang et al., 2019), whereas interfering HDAC4 could inhibit the effect (Zheng et al., 2019). HDAC5 in VSMCs could be activated by AngII, a potent stimuli for VSMC proliferation (Pang et al., 2008). Moreover, Zhou et al. (2011a) showed that by regulating β-catenin translocation, splicing of HDAC7 induced SMC proliferation. In addition, HDAC2 and HDAC5 hypoacetylated histone H4 at the promoter site of α-smooth muscle actin and decreased the expression of marker genes of SMC differentiation induced by POVPC (Yoshida et al., 2008).

It is recognized that cyclic strain regulates phenotype switch, migration, and proliferation of VSMCs in the pathogenesis of AS (Haga et al., 2007). Cyclic strain induced the secretion of transforming growth factor β1 in VSMCs and the expression of contractile phenotype markers, such as smooth muscle protein 22α, α-smooth muscle actin, and calponin (Yao et al., 2014). It was shown that the cyclic strain induced the migration of VSMCs by up-regulating HDAC7 and down-regulating the levels of HDAC3/4. Tributyrin, a pan-inhibitor of HDAC, could suppress VSMC migration accompanied by reduced expression of HDAC7 (Yan et al., 2009). TSA could inhibit VSMC proliferation by inducing expression of $p21^{WAF1}$, rather than $p16^{INK4}$, $p27^{KIP1}$, or p53, followed by cell cycle arrest through reducing Rb phosphorylation at the G1–S phase (Okamoto et al., 2006). It was reported that butyrate, a dietary HDACi, had the effect on arresting the proliferation of VSMCs. Furthermore, butyrate downregulated the G1-specfic CDKs including CDK4, CDK6, and CDK2 and induced the expression of CDK inhibitors, $p15^{INK4b}$ and $p21^{Cip1}$, leading to cell cycle arrest of VSMCs (Mathew et al., 2010). The authors also found that the effect of the butyrate was mediated by acetylating H3K and phosphorylating H3-serine10, in addition to dimethylation of H3K9 and H3K4 (Mathew et al., 2010). Besides, HDAC4 and HDAC5 was involved in vascular calcification (Abend et al., 2017; Choe et al., 2020) and inflammatory response in VSMCs (Lee et al., 2008), whereas HDAC1 (Liu and Khachigian, 2009) and HDAC5 (Pietruczuk et al., 2019) acted as a proinflammatory molecule in VSMCs. TSA could inhibit VSMC calcification (Azechi et al., 2013). All these studies revealed that the classical HDACs mediate the proliferation and migration of VSMCs, which could be blocked by HDACi.

HDACs Are Involved in Macrophage-Derived Foam Cell Formation

Macrophage-derived foam cell formation is one of the major contributors to AS development. In the early stage of plaque formation, macrophages are mainly derived from the monocytes infiltrating into subintima (Ley et al., 2007). The macrophages stimulated by ox-LDL and its lipid components produce more inflammatory factors, such as IL-α, IL-β, IL-6, IL-18, and TNF-β (Poston, 2019), which trigger adhesion molecule secretion from ECs to attract more monocytes to differentiate into macrophages (Ley et al., 2007). By uptaking ox-LDL through binding to scavenger receptors such as CD36, macrophages became lipid-laden foam cells (Orekhov, 2018). MCP-1 expressed by VSMCs guides the foam cells to the atherosclerotic plaques (Tesfamariam and DeFelice, 2007). Unfortunately, when the foam cells underwent cell death (apoptosis or necrosis), the inner cholesterol components are released to the plaque. The released cholesterol, together with the collagen-secreted VSMCs and foam cells, contributes to the early plaque (Poston, 2019).

Treatment with TSA markedly upregulated the expression of CD36 in macrophages, which increased the uptake of oxLDL and accelerated AS (Choi et al., 2005). The lipid efflux, removing redundant cholesterol from macrophage, is a vital step in suppressing the development of AS (Li et al., 2010). ATP-binding transporters (ABCA1 and ABCG1) transfer the cholesterol from macrophage to lipid-poor apolipoprotein and high-density lipoprotein (HDL). Interestingly, inhibition of HDAC with TSA, ITF2357 (pan-HDACi), or RNA interference to silence genes of HDAC 1/2/3/6/8, respectively, increased histone acetylation and ABCA1/ABCG1 expression, which suppressed the accumulation of cholesterol in macrophage, and HDAC3 silence appeared the most effective (Van den Bossche et al., 2014). The precise role of HDAC isoforms and the pharmacological effects of HDACi in foam cell formation warrant further studies. Additionally, PPARγ is a transcriptional factor critically involved in lipid metabolism and possesses anti-inflammation properties (Vallée et al., 2019). Recent study showed that, by activating PPARγ through elevating acetylation of C/EBPα (CCAAT enhancer binding protein α), TSA increased ABCA1/ABCG1 expression and reduced TNF-α/IL-1β, which contributed to the inhibition of foam cell formation and atherogenesis (Gao et al., 2020).

HDACs and Thrombus Formation

In the development of AS, both prothrombotic molecules and procoagulant molecules contribute to thrombosis formation. Tissue factor (TF) produced by plaque macrophages activates

platelets through the extrinsic pathway to initiate thrombin signaling (Collot-Teixeira et al., 2007). In addition, ox-LDL is considered to be another extrinsic factor that activates the platelets through its scavenger receptors (Ivanciu and Stalker, 2015). Thrombin activates ECs to release vWF, a factor that stimulates platelets (Spronk et al., 2013). The activated platelets potentially stimulate the platelets in a self-perpetuation manner, which produces more thrombin (Spronk et al., 2013). Wang et al. (2007) found that the HDACi (TSA, MS-275, sodium butyrate, and VPA) suppressed the expression of TF and its bioactivity. TF can enhance the release of vWF that causes platelet adhesion to ECs. The transcription factor nuclear factor Y (NE-Y) interacts with both HDAC1 and histone acetyltransferase PCAF in vWF gene promoter, causing dissociation of HDAC1 from the complex and leading to more PCAF recruited to vWF promoter, thereby promoting vWF expression (Peng et al., 2007). t-PA is generated by ECs, acting as an antithrombotic factor that is involved in clearance of intravascular fibrin deposits in ECs. The expression of t-PA could be inhibited by HDAC through deacetylating histone H3 and H4 in the t-PA gene promoter (Lappas, 2012). Furthermore, treatment with TSA, MS-275 or VPA increased the t-PA expression (Larsson et al., 2013), respectively, whereas the effect of VPA could be suppressed by knockdown of HDAC3/5/7 (Larsson et al., 2012).

HDACs Regulate Atherosclerosis in Human and Animals

Among the classical HDACs, HDAC9 is best known for its role in the development of AS. The *rs2107595* HDAC9 gene polymorphism leads to increased expression of HDAC9 in the internal carotid artery (Grbić et al., 2020) and plasma (Wang et al., 2016) and modulated gene expression in the blood of patients suffering from large vessel atherosclerotic stroke (Shroff et al., 2019). The polymorphism variant is significantly associated with AS (Prestel et al., 2019; Grbić et al., 2020) and may contribute to coronary AS and coronary artery disease risk (Wang et al., 2016). Consistently, HDAC9 deficiency in $ApoE^{-/-}$ mice resulted in evidently reduced lesion size in aortas and less advanced lesions (Azghandi et al., 2015). Further studies showed that HDAC9 could activate inhibitory κB kinase and regulate atherosclerotic plaque vulnerability (Asare et al., 2020). Moreover, HDAC9 repressed cholesterol efflux by downregulating ABCA1, ABCG1, and PPARγ and alternatively promoted macrophage activation in AS (Cao et al., 2014). On the contrary, it was demonstrated that reduced expression of HDAC9 induced by miR-182 was implicated in increased levels of cholesterol, lipoprotein lipase, and proinflammatory cytokines in oxLDL-treated human THP-1 macrophages, which the author suggested might mediate the lipid accumulation in atherosclerotic lesions and thus promoted atherogenesis in $ApoE^{-/-}$ mice administered with miR-182 agomir (Cheng et al., 2017). Moreover, it was found that HDAC1/2/3/4/6/11 were all upregulated in atherosclerotic carotid arteries and aortas from human and $ApoE^{-/-}$ mice, respectively (Manea et al., 2020). By using aortic isografted model, Zampetaki et al. (2010) found that endothelial-specific knockdown of HDAC3 in aortas from $ApoE^{-/-}$ mice robustly promoted atherosclerotic lesion formation. However, Hoeksema et al. (2014) found that HDAC3 was the only isoform upregulated in human ruptured plaques, and myeloid deletion of HDAC3 in LDL receptor knockout mice led to more stabilized atherosclerotic lesions, which might be mediated by phenotype shift of macrophages to be anti-inflammatory and less lipid accumulation. The distinct effects of HDAC3 in these two studies suggest the cell-specific function of HDAC3 during the development of AS. In ox-LDL-treated HAECs and aortas from $ApoE^{-/-}$ mice, HDAC6 was upregulated, and its selective inhibitor tubacin prevented endothelial dysfunction and the development of AS (Leucker et al., 2017). Several HDACi such as TSA (Gao et al., 2020), metacept-1 (Vinh et al., 2008), BuA (He and Moreau, 2019), and SAHA (Ye et al., 2018; Manea et al., 2020) have been demonstrated to inhibit the development of AS.

Potential Combination of BRD4 Inhibitors With HDAC Inhibitors

Recent years have witnessed the important roles of bromodomain and extra terminal (BET) proteins, which are readers of acetylated histones. The BET family comprises four members, including BRD2, BRD3, BRD4, and the testis-restricted BRDT, among which BRD4 is the most characterized and critically implicated in transcriptional regulation and atherogenesis (Lin and Du, 2020; Wang et al., 2020). Intriguingly, the BRD4 inhibitor RVX-208 (now called apabetalone) showed potent effect in increasing apolipoprotein A-I and HDL levels/particles and reducing AS (McLure et al., 2013; Jahagirdar et al., 2014; Gilham et al., 2016; Ghosh et al., 2017), and has been tested in clinical trials (Nicholls et al., 2016, 2018; Shishikura et al., 2019). Pooling completed phase 2 trial data that suggested its clinical benefits on reducing major adverse cardiovascular events in treated patients (Borck et al., 2020). However, a phase III trial (BETonMACE) completed recently showed that addition of RVX 208 to contemporary standard of care for acute coronary syndrome (ACS) did not significantly reduce major adverse cardiovascular events in patients with a recent (7–90 days) ACS, type 2 diabetes, and low HDL cholesterol (Ray et al., 2020). To date, little is known about the direct interaction of BETs and HDACs or the combinational effects of BETi and HDACi in vascular cells and AS. Nevertheless, because HDACs and BETs share many common targets and affect similar cellular activities, it will be very interesting to study their molecular interplay during AS development. Those studies will be very helpful to evaluate whether combinational strategy using specific HDACi with BETi or developing dual BET/HDACi would be promising for AS treatment, as the strategy is rational and has been suggested in cancer studies (He et al., 2020; Liu et al., 2020).

CONCLUSION AND PERSPECTIVE

As a family of enzymes critically involved in chromatin remodeling and gene transcription, HDACs have multiple functions in ECs and other vascular cells that are implicated in AS (summarized in **Figure 2** and **Table 1**) (Zhou et al., 2011b). Among the 11 classical HDACs, HDAC9 is the only subtype that has been well studied for its association with AS risk in both human and animals (Grbić et al., 2020). By

contrast, little is known about the role of HDAC10 and HDAC11. With respect to other members, HDAC6 and HDAC8 mainly exhibit the role of mediating endothelial dysfunction and AS, whereas HDAC7 is mainly recognized as a protective isoform.

As exemplified in this review, many studies have been performed to investigate the effect of HDACi in vascular dysfunction and AS. Although in most cases, HDACi could prevent the pathological process, some HDACi might exacerbate it. The reason might be attributed to the unspecific property of HDACi in either HDAC subtypes or tissues/cells, which might also limit their applications in clinic. Moreover, the dosage used in the experiments and the off-target effect would also affect the results. Interestingly, inhibitors specific to HDAC3 (Zhao et al., 2019), HDAC6 (Chen et al., 2019), and HDAC8 (Kee et al., 2019) have been found to be effective in regulating vascular homeostasis, but further studies are still required to evaluate the pharmacological and pharmacokinetic profiles. Moreover, as some HDACs exhibit protective effects, it is suggested that HDAC analogs might be designed and investigated, such as the HDAC7-derived peptide (Pan et al., 2018). Nevertheless, extensive studies are urgently needed to elucidate and validate the mechanisms of HDACs in vascular function and AS to develop the more specific and targeted HDACi with less toxicity or side effects. Furthermore, chronic toxicity studies and randomized controlled trials with optimized dosage are also required.

AUTHOR CONTRIBUTIONS

XC, YH, WF, YT, and HL wrote the manuscript. HL generated the illustration. AS revised the manuscript. SX conceptualized the manuscript, drafted the outline, and revised the manuscript. All authors contributed to the article and approved the submitted version.

FUNDING

This work was supported by National Natural Science Foundation of China (Grant No. 82070464 to SX and 81903606 to HL) and Natural Science Foundation of Guangdong Province Grant No. 2017A030310542 to HL.

REFERENCES

Abend, A., Shkedi, O., Fertouk, M., Caspi, L. H., and Kehat, I. (2017). Salt-inducible kinase induces cytoplasmic histone deacetylase 4 to promote vascular calcification. *EMBO Rep.* 18, 1166–1185. doi: 10.15252/embr.201643686

Abouhish, H., Thounaojam, M. C., Jadeja, R. N., Gutsaeva, D. R., Powell, F. L., Khriza, M., et al. (2020). Inhibition of HDAC6 attenuates diabetes-induced retinal redox imbalance and microangiopathy. *Antioxidants* 9:599. doi: 10.3390/antiox9070599

Alam, S., Li, H., Margariti, A., Martin, D., Zampetaki, A., Habi, O., et al. (2011). Galectin-9 protein expression in endothelial cells is positively regulated by histone deacetylase 3. *J. Biol. Chem.* 286, 44211–44217. doi: 10.1074/jbc.M111.242289

Ali, L., Schnitzler, J. G., and Kroon, J. (2018). Metabolism: the road to inflammation and atherosclerosis. *Curr. Opin. Lipidol.* 29, 474–480. doi: 10.1097/mol.0000000000000550

Ali, M. M., Mahmoud, A. M., Le Master, E., Levitan, I., and Phillips, S. A. (2019). Role of matrix metalloproteinases and histone deacetylase in oxidative stress-induced degradation of the endothelial glycocalyx. *Am. J. Physiol. Heart Circ. Physiol.* 316, H647–H663. doi: 10.1152/ajpheart.00090.2018

Arcaro, G., Zenere, B. M., Travia, D., Zenti, M. G., Covi, G., Lechi, A., et al. (1995). Non-invasive detection of early endothelial dysfunction in hypercholesterolaemic subjects. *Atherosclerosis* 114, 247–254. doi: 10.1016/0021-9150(94)05489-6

Asare, Y., Campbell-James, T. A., Bokov, Y., Yu, L. L., Prestel, M., El Bounkari, O., et al. (2020). Histone Deacetylase 9 activates IKK to regulate atherosclerotic plaque vulnerability. *Circ. Res.* 127, 811–823. doi: 10.1161/circresaha.120.316743

Azechi, T., Kanehira, D., Kobayashi, T., Sudo, R., Nishimura, A., Sato, F., et al. (2013). Trichostatin, A., an HDAC class I/II inhibitor, promotes Pi-induced vascular calcification via up-regulation of the expression of alkaline phosphatase. *J. Atheroscler Thromb.* 20, 538–547. doi: 10.5551/jat.15826

Azghandi, S., Prell, C., van der Laan, S. W., Schneider, M., Malik, R., Berer, K., et al. (2015). Deficiency of the stroke relevant HDAC9 gene attenuates atherosclerosis in accord with allele-specific effects at 7p21.1. *Stroke* 46, 197–202. doi: 10.1161/strokeaha.114.007213

Bae, Y. S., Lee, J. H., Choi, S. H., Kim, S., Almazan, F., Witztum, J. L., et al. (2009). Macrophages generate reactive oxygen species in response to minimally oxidized low-density lipoprotein: toll-like receptor 4- and spleen tyrosine kinase-dependent activation of NADPH oxidase 2. *Circ. Res.* 104, 210–218. 221p following 218. doi: 10.1161/circresaha.108.181040

Barbour, J. A., and Turner, N. (2014). Mitochondrial stress signaling promotes cellular adaptations. *Int. J. Cell Biol.* 2014:156020. doi: 10.1155/2014/156020

Bedenbender, K., Scheller, N., Fischer, S., Leiting, S., Preissner, K. T., Schmeck, B. T., et al. (2019). Inflammation-mediated deacetylation of the ribonuclease 1 promoter via histone deacetylase 2 in endothelial cells. *Faseb J.* 33, 9017–9029. doi: 10.1096/fj.201900451R

Bettica, P., Petrini, S., D'Oria, V., D'Amico, A., Catteruccia, M., Pane, M., et al. (2016). Histological effects of givinostat in boys with Duchenne muscular dystrophy. *Neuromuscul. Disord.* 26, 643–649. doi: 10.1016/j.nmd.2016.07.002

Birdsey, G. M., Dryden, N. H., Shah, A. V., Hannah, R., Hall, M. D., Haskard, D. O., et al. (2012). The transcription factor Erg regulates expression of histone deacetylase 6 and multiple pathways involved in endothelial cell migration and angiogenesis. *Blood* 119, 894–903. doi: 10.1182/blood-2011-04-350025

Borck, P. C., Guo, L. W., and Plutzky, J. (2020). BET epigenetic reader proteins in cardiovascular transcriptional programs. *Circ. Res.* 126, 1190–1208. doi: 10.1161/circresaha.120.315929

Borgas, D., Chambers, E., Newton, J., Ko, J., Rivera, S., Rounds, S., et al. (2016). Cigarette smoke disrupted lung endothelial barrier integrity and increased susceptibility to acute lung injury via histone deacetylase 6. *Am. J. Respir. Cell Mol. Biol.* 54, 683–696. doi: 10.1165/rcmb.2015-0149OC

Bruhn, P. J., Nikolian, V. C., Halaweish, I., Chang, Z., Sillesen, M., Liu, B., et al. (2018). Tubastatin A prevents hemorrhage-induced endothelial barrier dysfunction. *J. Trauma Acute Care Surg.* 84, 386–392. doi: 10.1097/ta.0000000000001753

Cao, Q., Rong, S., Repa, J. J., St Clair, R., Parks, J. S., and Mishra, N. (2014). Histone deacetylase 9 represses cholesterol efflux and alternatively activated macrophages in atherosclerosis development. *Arterioscler Thromb. Vasc. Biol.* 34, 1871–1879. doi: 10.1161/atvbaha.114.303393

Caplan, B. A., and Schwartz, C. J. (1973). Increased endothelial cell turnover in areas of in vivo Evans Blue uptake in the pig aorta. *Atherosclerosis* 17, 401–417. doi: 10.1016/0021-9150(73)90031-2

Castro, V., Bertrand, L., Luethen, M., Dabrowski, S., Lombardi, J., Morgan, L., et al. (2016). Occludin controls HIV transcription in brain pericytes via regulation of SIRT-1 activation. *Faseb J.* 30, 1234–1246. doi: 10.1096/fj.15-277673

Castro, V., Skowronska, M., Lombardi, J., He, J., Seth, N., Velichkovska, M., et al. (2018). Occludin regulates glucose uptake and ATP production in pericytes by influencing AMP-activated protein kinase activity. *J. Cereb. Blood Flow Metab.* 38, 317–332. doi: 10.1177/0271678x17720816

Chang, S., Young, B. D., Li, S., Qi, X., Richardson, J. A., and Olson, E. N. (2006). Histone deacetylase 7 maintains vascular integrity by repressing matrix metalloproteinase 10. *Cell* 126, 321–334. doi: 10.1016/j.cell.2006.05.040

Chen, F., Li, X., Aquadro, E., Haigh, S., Zhou, J., Stepp, D. W., et al. (2016). Inhibition of histone deacetylase reduces transcription of NADPH oxidases and ROS production and ameliorates pulmonary arterial hypertension. *Free Radic. Biol. Med.* 99, 167–178. doi: 10.1016/j.freeradbiomed.2016.08.003

Chen, J., Zhang, J., Shaik, N. F., Yi, B., Wei, X., Yang, X. F., et al. (2019). The histone deacetylase inhibitor tubacin mitigates endothelial dysfunction by up-regulating the expression of endothelial nitric oxide synthase. *J. Biol. Chem.* 294, 19565–19576. doi: 10.1074/jbc.RA119.011317

Cheng, H. P., Gong, D., Zhao, Z. W., He, P. P., Yu, X. H., Ye, Q., et al. (2017). MicroRNA-182 promotes lipoprotein lipase expression and atherogenesisby targeting histone deacetylase 9 in apolipoprotein E-Knockout Mice. *Circ. J.* 82, 28–38. doi: 10.1253/circj.CJ-16-1165

Cheng, H. T., and Hung, W. C. (2013). Inhibition of proliferation, sprouting, tube formation and Tie2 signaling of lymphatic endothelial cells by the histone deacetylase inhibitor SAHA. *Oncol. Rep.* 30, 961–967. doi: 10.3892/or.2013.2523

Chi, Z., Byeon, H. E., Seo, E., Nguyen, Q. T., Lee, W., Jeong, Y., et al. (2019). Histone deacetylase 6 inhibitor tubastatin A attenuates angiotensin II-induced hypertension by preventing cystathionine γ-lyase protein degradation. *Pharmacol. Res.* 146:104281. doi: 10.1016/j.phrs.2019.104281

Chi, Z., Le, T. P. H., Lee, S. K., Guo, E., Kim, D., Lee, S., et al. (2020). Honokiol ameliorates angiotensin II-induced hypertension and endothelial dysfunction by inhibiting HDAC6-mediated cystathionine γ-lyase degradation. *J. Cell Mol. Med.* 24, 10663–10676. doi: 10.1111/jcmm.15686

Chiu, J. J., and Chien, S. (2011). Effects of disturbed flow on vascular endothelium: pathophysiological basis and clinical perspectives. *Physiol. Rev.* 91, 327–387. doi: 10.1152/physrev.00047.2009

Cho, D. H., Park, J. H., Joo Lee, E., Jong Won, K., Lee, S. H., Kim, Y. H., et al. (2014). Valproic acid increases NO production via the SH-PTP1-CDK5-eNOS-Ser(116) signaling cascade in endothelial cells and mice. *Free Radic. Biol. Med.* 76, 96–106. doi: 10.1016/j.freeradbiomed.2014.07.043

Choe, N., Shin, S., Joung, H., Ryu, J., Kim, Y. K., Ahn, Y., et al. (2020). The microRNA miR-134-5p induces calcium deposition by inhibiting histone deacetylase 5 in vascular smooth muscle cells. *J. Cell Mol. Med.* 24, 10542–10550. doi: 10.1111/jcmm.15670

Choi, J. H., Nam, K. H., Kim, J., Baek, M. W., Park, J. E., Park, H. Y., et al. (2005). Trichostatin A exacerbates atherosclerosis in low density lipoprotein receptor-deficient mice. *Arterioscler Thromb. Vasc. Biol.* 25, 2404–2409. doi: 10.1161/01.Atv.0000184758.07257.88

Collot-Teixeira, S., De Lorenzo, F., and McGregor, J. L. (2007). Scavenger receptor A and CD36 are implicated in mediating platelet activation induced by oxidized low- density lipoproteins. *Arterioscler Thromb. Vasc. Biol.* 27, 2491–2492. doi: 10.1161/atvbaha.107.154864

Craige, S. M., Kant, S., and Keaney, J. F. Jr. (2015). Reactive oxygen species in endothelial function - from disease to adaptation. *Circ. J.* 79, 1145–1155. doi: 10.1253/circj.CJ-15-0464

Deroanne, C. F., Bonjean, K., Servotte, S., Devy, L., Colige, A., Clausse, N., et al. (2002). Histone deacetylases inhibitors as anti-angiogenic agents altering vascular endothelial growth factor signaling. *Oncogene* 21, 427–436. doi: 10.1038/sj.onc.1205108

Dje N'Guessan, P., Riediger, F., Vardarova, K., Scharf, S., Eitel, J., Opitz, B., et al. (2009). Statins control oxidized LDL-mediated histone modifications and gene expression in cultured human endothelial cells. *Arterioscler Thromb. Vasc. Biol.* 29, 380–386. doi: 10.1161/atvbaha.108.178319

Doran, A. C., Meller, N., and McNamara, C. A. (2008). Role of smooth muscle cells in the initiation and early progression of atherosclerosis. *Arterioscler Thromb. Vasc. Biol.* 28, 812–819. doi: 10.1161/atvbaha.107.159327

Elliott, J. H., Wightman, F., Solomon, A., Ghneim, K., Ahlers, J., Cameron, M. J., et al. (2014). Activation of HIV transcription with short-course vorinostat in HIV-infected patients on suppressive antiretroviral therapy. *PLoS Pathog.* 10:e1004473. doi: 10.1371/journal.ppat.1004473

Fanelli, A., Ghisi, D., Aprile, P. L., and Lapi, F. (2017). Cardiovascular and cerebrovascular risk with nonsteroidal anti-inflammatory drugs and cyclooxygenase 2 inhibitors: latest evidence and clinical implications. *Ther. Adv. Drug Saf.* 8, 173–182. doi: 10.1177/2042098617690485

Feil, R., Lohmann, S. M., de Jonge, H., Walter, U., and Hofmann, F. (2003). Cyclic GMP-dependent protein kinases and the cardiovascular system: insights from genetically modified mice. *Circ. Res.* 93, 907–916. doi: 10.1161/01.Res.0000100390.68771.Cc

Fernandes, S., Salta, S., and Summavielle, T. (2015). Methamphetamine promotes α-tubulin deacetylation in endothelial cells: the protective role of acetyl-l-carnitine. *Toxicol. Lett.* 234, 131–138. doi: 10.1016/j.toxlet.2015.02.011

Finazzi, G., Vannucchi, A. M., Martinelli, V., Ruggeri, M., Nobile, F., Specchia, G., et al. (2013). A phase II study of Givinostat in combination with hydroxycarbamide in patients with polycythaemia vera unresponsive to hydroxycarbamide monotherapy. *Br. J. Haematol.* 161, 688–694. doi: 10.1111/bjh.12332

Fischle, W., Dequiedt, F., Hendzel, M. J., Guenther, M. G., Lazar, M. A., Voelter, W., et al. (2002). Enzymatic activity associated with class II HDACs is dependent on a multiprotein complex containing HDAC3 and SMRT/N-CoR. *Mol. Cell* 9, 45–57. doi: 10.1016/s1097-2765(01)00429-4

Förstermann, U., Xia, N., and Li, H. (2017). Roles of vascular oxidative stress and nitric oxide in the pathogenesis of atherosclerosis. *Circ. Res.* 120, 713–735. doi: 10.1161/circresaha.116.309326

Gao, C., Cheng, X., Lam, M., Liu, Y., Liu, Q., Chang, K. S., et al. (2008). Signal-dependent regulation of transcription by histone deacetylase 7 involves recruitment to promyelocytic leukemia protein nuclear bodies. *Mol. Biol. Cell* 19, 3020–3027. doi: 10.1091/mbc.e07-11-1203

Gao, J., Wang, Y., Li, W., Zhang, J., Che, Y., Cui, X., et al. (2018). Loss of histone deacetylase 2 inhibits oxidative stress induced by high glucose via the HO-1/SIRT1 pathway in endothelial progenitor cells. *Gene* 678, 1–7. doi: 10.1016/j.gene.2018.07.072

Gao, Q., Wei, A., Chen, F., Chen, X., Ding, W., Ding, Z., et al. (2020). Enhancing PPARγ by HDAC inhibition reduces foam cell formation and atherosclerosis in ApoE deficient mice. *Pharmacol. Res.* 160:105059. doi: 10.1016/j.phrs.2020.105059

Gatla, H. R., Muniraj, N., Thevkar, P., Yavvari, S., Sukhavasi, S., and Makena, M. R. (2019). Regulation of chemokines and cytokines by histone deacetylases and an update on histone decetylase inhibitors in human diseases. *Int. J. Mol. Sci.* 20:1110. doi: 10.3390/ijms20051110

Ghosh, G. C., Bhadra, R., Ghosh, R. K., Banerjee, K., and Gupta, A. (2017). RVX 208: a novel BET protein inhibitor, role as an inducer of apo A-I/HDL and beyond. *Cardiovasc. Ther.* 35:e12265. doi: 10.1111/1755-5922.12265

Gilham, D., Wasiak, S., Tsujikawa, L. M., Halliday, C., Norek, K., Patel, R. G., et al. (2016). RVX-208, a BET-inhibitor for treating atherosclerotic cardiovascular disease, raises ApoA-I/HDL and represses pathways that contribute to cardiovascular disease. *Atherosclerosis* 247, 48–57. doi: 10.1016/j.atherosclerosis.2016.01.036

Granger, A., Abdullah, I., Huebner, F., Stout, A., Wang, T., Huebner, T., et al. (2008). Histone deacetylase inhibition reduces myocardial ischemia-reperfusion injury in mice. *Faseb J.* 22, 3549–3560. doi: 10.1096/fj.08-108548

Gray, S. G., and Ekström, T. J. (2001). The human histone deacetylase family. *Exp. Cell Res.* 262, 75–83. doi: 10.1006/excr.2000.5080

Grbić, E., Gorkič, N., Pleskovič, A., Zorc, M., Ljuca, F., Gasparini, M., et al. (2020). Association between rs2107595 HDAC9 gene polymorphism and advanced carotid atherosclerosis in the Slovenian cohort. *Lipids Health Dis.* 19:71. doi: 10.1186/s12944-020-01255-1

Ha, C. H., Wang, W., Jhun, B. S., Wong, C., Hausser, A., Pfizenmaier, K., et al. (2008). Protein kinase D-dependent phosphorylation and nuclear export of histone deacetylase 5 mediates vascular endothelial growth factor-induced gene expression and angiogenesis. *J. Biol. Chem.* 283, 14590–14599. doi: 10.1074/jbc.M800264200

Haas, T. L. (2005). Endothelial cell regulation of matrix metalloproteinases. *Can. J. Physiol. Pharmacol.* 83, 1–7. doi: 10.1139/y04-120

Haga, J. H., Li, Y. S., and Chien, S. (2007). Molecular basis of the effects of mechanical stretch on vascular smooth muscle cells. *J. Biomech.* 40, 947–960. doi: 10.1016/j.jbiomech.2006.04.011

Hakami, N. Y., Dusting, G. J., and Peshavariya, H. M. (2016). Trichostatin, A., a histone deacetylase inhibitor suppresses NADPH oxidase 4-Derived redox signalling and angiogenesis. *J. Cell Mol. Med.* 20, 1932–1944. doi: 10.1111/jcmm.12885

He, B., and Moreau, R. (2019). Lipid-regulating properties of butyric acid and 4-phenylbutyric acid: molecular mechanisms and therapeutic applications. *Pharmacol. Res.* 144, 116–131. doi: 10.1016/j.phrs.2019.04.002

He, H. M., Li, A., Zhang, S. W., and Duan, M. L. (2011). [The effects of a histone deacetylase (HDAC) inhibitor on endotoxin-induced endothelial cell injury]. *Zhongguo Wei Zhong Bing Ji Jiu Yi Xue* 23, 602–604.

He, S., Dong, G., Li, Y., Wu, S., Wang, W., and Sheng, C. (2020). Potent dual BET/HDAC inhibitors for efficient treatment of pancreatic cancer. *Angew. Chem. Int. Ed. Engl.* 59, 3028–3032. doi: 10.1002/anie.201915896

Hebbel, R. P., Vercellotti, G. M., Pace, B. S., Solovey, A. N., Kollander, R., Abanonu, C. F., et al. (2010). The HDAC inhibitors trichostatin A and suberoylanilide hydroxamic acid exhibit multiple modalities of benefit for the vascular pathobiology of sickle transgenic mice. *Blood* 115, 2483–2490. doi: 10.1182/blood-2009-02-204990

Hoeksema, M. A., Gijbels, M. J., Van den Bossche, J., van der Velden, S., Sijm, A., Neele, A. E., et al. (2014). Targeting macrophage Histone deacetylase 3 stabilizes atherosclerotic lesions. *EMBO Mol. Med.* 6, 1124–1132. doi: 10.15252/emmm.201404170

Hou, Q., Hu, K., Liu, X., Quan, J., and Liu, Z. (2018). HADC regulates the diabetic vascular endothelial dysfunction by targetting MnSOD. *Biosci. Rep.* 38:BSR20181042. doi: 10.1042/bsr20181042

Hsu, Y. F., Sheu, J. R., Lin, C. H., Chen, W. C., Hsiao, G., Ou, G., et al. (2011). MAPK phosphatase-1 contributes to trichostatin A inhibition of cyclooxygenase-2 expression in human umbilical vascular endothelial cells exposed to lipopolysaccharide. *Biochim. Biophys. Acta* 1810, 1160–1169. doi: 10.1016/j.bbagen.2011.08.015

Huynh, D. T. N., and Heo, K. S. (2019). Therapeutic targets for endothelial dysfunction in vascular diseases. *Arch. Pharm. Res.* 42, 848–861. doi: 10.1007/s12272-019-01180-7

Hyndman, K. A., Ho, D. H., Sega, M. F., and Pollock, J. S. (2014). Histone deacetylase 1 reduces NO production in endothelial cells via lysine deacetylation of NO synthase 3. *Am. J. Physiol. Heart Circ. Physiol.* 307, H803–H809. doi: 10.1152/ajpheart.00243.2014

Ikeda, E. (2005). Cellular response to tissue hypoxia and its involvement in disease progression. *Pathol. Int.* 55, 603–610. doi: 10.1111/j.1440-1827.2005.01877.x

Inoue, K., Kobayashi, M., Yano, K., Miura, M., Izumi, A., Mataki, C., et al. (2006). Histone deacetylase inhibitor reduces monocyte adhesion to endothelium through the suppression of vascular cell adhesion molecule-1 expression. *Arterioscler Thromb. Vasc. Biol.* 26, 2652–2659. doi: 10.1161/01.ATV.0000247247.89787.e7

Ismail, H., Mofarrahi, M., Echavarria, R., Harel, S., Verdin, E., Lim, H. W., et al. (2012). Angiopoietin-1 and vascular endothelial growth factor regulation of leukocyte adhesion to endothelial cells: role of nuclear receptor-77. *Arterioscler Thromb. Vasc. Biol.* 32, 1707–1716. doi: 10.1161/atvbaha.112.251546

Ivanciu, L., and Stalker, T. J. (2015). Spatiotemporal regulation of coagulation and platelet activation during the hemostatic response in vivo. *J. Thromb. Haemost.* 13, 1949–1959. doi: 10.1111/jth.13145

Jahagirdar, R., Zhang, H., Azhar, S., Tobin, J., Attwell, S., Yu, R., et al. (2014). A novel BET bromodomain inhibitor, RVX-208, shows reduction of atherosclerosis in hyperlipidemic ApoE deficient mice. *Atherosclerosis* 236, 91–100. doi: 10.1016/j.atherosclerosis.2014.06.008

Jin, G., Bausch, D., Knightly, T., Liu, Z., Li, Y., Liu, B., et al. (2011). Histone deacetylase inhibitors enhance endothelial cell sprouting angiogenesis in vitro. *Surgery* 150, 429–435. doi: 10.1016/j.surg.2011.07.001

Joshi, A. D., Barabutis, N., Birmpas, C., Dimitropoulou, C., Thangjam, G., Cherian-Shaw, M., et al. (2015). Histone deacetylase inhibitors prevent pulmonary endothelial hyperpermeability and acute lung injury by regulating heat shock protein 90 function. *Am. J. Physiol. Lung. Cell Mol. Physiol.* 309, L1410–L1419. doi: 10.1152/ajplung.00180.2015

Jung, S. B., Kim, C. S., Naqvi, A., Yamamori, T., Mattagajasingh, I., Hoffman, T. A., et al. (2010). Histone deacetylase 3 antagonizes aspirin-stimulated endothelial nitric oxide production by reversing aspirin-induced lysine acetylation of endothelial nitric oxide synthase. *Circ. Res.* 107, 877–887. doi: 10.1161/circresaha.110.222968

Kaluza, D., Kroll, J., Gesierich, S., Manavski, Y., Boeckel, J. N., Doebele, C., et al. (2013). Histone deacetylase 9 promotes angiogenesis by targeting the antiangiogenic microRNA-17-92 cluster in endothelial cells. *Arterioscler Thromb. Vasc. Biol.* 33, 533–543. doi: 10.1161/atvbaha.112.300415

Kane, A. E., and Sinclair, D. A. (2018). Sirtuins and NAD(+) in the development and treatment of metabolic and cardiovascular diseases. *Circ. Res.* 123, 868–885. doi: 10.1161/CIRCRESAHA.118.312498

Kang, G., Lee, Y. R., Joo, H. K., Park, M. S., Kim, C. S., Choi, S., et al. (2015). Trichostatin A modulates angiotensin II-induced vasoconstriction and blood pressure via inhibition of p66shc activation. *Korean J. Physiol. Pharmacol.* 19, 467–472. doi: 10.4196/kjpp.2015.19.5.467

Kang, Y., Kim, J., Anderson, J. P., Wu, J., Gleim, S. R., Kundu, R. K., et al. (2013). Apelin-APJ signaling is a critical regulator of endothelial MEF2 activation in cardiovascular development. *Circ. Res.* 113, 22–31. doi: 10.1161/circresaha.113.301324

Karki, P., Ke, Y., Tian, Y., Ohmura, T., Sitikov, A., Sarich, N., et al. (2019). Staphylococcus aureus-induced endothelial permeability and inflammation are mediated by microtubule destabilization. *J. Biol. Chem.* 294, 3369–3384. doi: 10.1074/jbc.RA118.004030

Kee, H. J., Ryu, Y., Seok, Y. M., Choi, S. Y., Sun, S., Kim, G. R., et al. (2019). Selective inhibition of histone deacetylase 8 improves vascular hypertrophy, relaxation, and inflammation in angiotensin II hypertensive mice. *Clin. Hypertens* 25:13. doi: 10.1186/s40885-019-0118-8

Khan, H., Belwal, T., Efferth, T., Farooqi, A. A., Sanches-Silva, A., Vacca, R. A., et al. (2020). Targeting epigenetics in cancer: therapeutic potential of flavonoids. *Crit. Rev. Food Sci. Nutr.* 1–24. doi: 10.1080/10408398.2020.1763910

Kim, J., Hwangbo, C., Hu, X., Kang, Y., Papangeli, I., Mehrotra, D., et al. (2015). Restoration of impaired endothelial myocyte enhancer factor 2 function rescues pulmonary arterial hypertension. *Circulation* 131, 190–199. doi: 10.1161/CIRCULATIONAHA.114.013339

Kleinbongard, P., Heusch, G., and Schulz, R. (2010). TNFalpha in atherosclerosis, myocardial ischemia/reperfusion and heart failure. *Pharmacol. Ther.* 127, 295–314. doi: 10.1016/j.pharmthera.2010.05.002

Kovacs-Kasa, A., Kovacs, L., Cherian-Shaw, M., Patel, V., Meadows, M. L., Fulton, D. J., et al. (2020). Inhibition of Class IIa HDACs improves endothelial barrier function in endotoxin-induced acute lung injury. *J. Cell Physiol.* doi: 10.1002/jcp.30053 [Epub ahead of print].

Kowshik, J., Giri, H., Kishore, T. K., Kesavan, R., Vankudavath, R. N., Reddy, G. B., et al. (2014). Ellagic acid inhibits VEGF/VEGFR2, PI3K/Akt and MAPK signaling cascades in the hamster cheek pouch carcinogenesis model. *Anticancer Agents. Med. Chem.* 14, 1249–1260. doi: 10.2174/1871520614666140723114217

Krause, B. J., Hernandez, C., Caniuguir, A., Vasquez-Devaud, P., Carrasco-Wong, I., Uauy, R., et al. (2016). Arginase-2 is cooperatively up-regulated by nitric oxide and histone deacetylase inhibition in human umbilical artery endothelial cells. *Biochem. Pharmacol.* 99, 53–59. doi: 10.1016/j.bcp.2015.10.018

Kwon, I. S., Wang, W., Xu, S., and Jin, Z. G. (2014). Histone deacetylase 5 interacts with Krüppel-like factor 2 and inhibits its transcriptional activity in endothelium. *Cardiovasc. Res.* 104, 127–137. doi: 10.1093/cvr/cvu183

Lappas, M. (2012). Anti-inflammatory properties of sirtuin 6 in human umbilical vein endothelial cells. *Mediators Inflamm* 2012:597514. doi: 10.1155/2012/597514

Larsson, P., Bergh, N., Lu, E., Ulfhammer, E., Magnusson, M., Wahlander, K., et al. (2013). Histone deacetylase inhibitors stimulate tissue-type plasminogen activator production in vascular endothelial cells. *J. Thromb. Thrombolysis.* 35, 185–192. doi: 10.1007/s11239-012-0831-6

Larsson, P., Ulfhammer, E., Magnusson, M., Bergh, N., Lunke, S., El-Osta, A., et al. (2012). Role of histone acetylation in the stimulatory effect of valproic acid on vascular endothelial tissue-type plasminogen activator expression. *PLoS One* 7:e31573. doi: 10.1371/journal.pone.0031573

Lee, C. W., Lin, C. C., Luo, S. F., Lee, H. C., Lee, I. T., Aird, W. C., et al. (2008). Tumor necrosis factor-alpha enhances neutrophil adhesiveness: induction of vascular cell adhesion molecule-1 via activation of Akt and CaM kinase II and modifications of histone acetyltransferase and histone deacetylase 4 in human tracheal smooth muscle cells. *Mol. Pharmacol.* 73, 1454–1464. doi: 10.1124/mol.107.038091

Lee, D. Y., and Chiu, J. J. (2019). Atherosclerosis and flow: roles of epigenetic modulation in vascular endothelium. *J. Biomed. Sci.* 26:56. doi: 10.1186/s12929-019-0551-8

Lee, D. Y., Lee, C. I., Lin, T. E., Lim, S. H., Zhou, J., Tseng, Y. C., et al. (2012). Role of histone deacetylases in transcription factor regulation and cell cycle modulation in endothelial cells in response to disturbed flow. *Proc. Natl. Acad. Sci. U.S.A.* 109, 1967–1972. doi: 10.1073/pnas.1121214109

Leucker, T. M., Nomura, Y., Kim, J. H., Bhatta, A., Wang, V., Wecker, A., et al. (2017). Cystathionine γ-lyase protects vascular endothelium: a role for

inhibition of histone deacetylase 6. *Am. J. Physiol. Heart Circ. Physiol.* 312, H711–H720. doi: 10.1152/ajpheart.00724.2016

Ley, K., Laudanna, C., Cybulsky, M. I., and Nourshargh, S. (2007). Getting to the site of inflammation: the leukocyte adhesion cascade updated. *Nat. Rev. Immunol.* 7, 678–689. doi: 10.1038/nri2156

Li, C., Zhou, Y., Loberg, A., Tahara, S. M., Malik, P., and Kalra, V. K. (2016). Activated transcription factor 3 in association with histone deacetylase 6 negatively regulates MicroRNA 199a2 transcription by chromatin remodeling and reduces endothelin-1 expression. *Mol. Cell Biol.* 36, 2838–2854. doi: 10.1128/mcb.00345-16

Li, D., Wang, D., Wang, Y., Ling, W., Feng, X., and Xia, M. (2010). Adenosine monophosphate-activated protein kinase induces cholesterol efflux from macrophage-derived foam cells and alleviates atherosclerosis in apolipoprotein E-deficient mice. *J. Biol. Chem.* 285, 33499–33509. doi: 10.1074/jbc.M110.159772

Li, D., Xie, S., Ren, Y., Huo, L., Gao, J., Cui, D., et al. (2011). Microtubule-associated deacetylase HDAC6 promotes angiogenesis by regulating cell migration in an EB1-dependent manner. *Protein Cell* 2, 150–160. doi: 10.1007/s13238-011-1015-4

Li, F., Zhao, H., Li, G., Zhang, S., Wang, R., Tao, Z., et al. (2020). Intravenous antagomiR-494 lessens brain-infiltrating neutrophils by increasing HDAC2-mediated repression of multiple MMPs in experimental stroke. *Faseb J.* 34, 6934–6949. doi: 10.1096/fj.201903127R

Li, M., van Esch, B., Henricks, P. A. J., Folkerts, G., and Garssen, J. (2018a). The anti-inflammatory effects of short chain fatty acids on lipopolysaccharide- or tumor necrosis factor α-stimulated endothelial cells via activation of GPR41/43 and inhibition of HDACs. *Front. Pharmacol.* 9:533. doi: 10.3389/fphar.2018.00533

Li, Y., Li, L., Qian, Z., Lin, B., Chen, J., Luo, Y., et al. (2018b). Phosphatidylinositol 3-Kinase-DNA Methyltransferase 1-miR-1281-Histone Deacetylase 4 regulatory axis mediates platelet-derived growth factor-induced proliferation and migration of pulmonary artery smooth muscle cells. *J. Am. Heart Assoc.* 7:e007572. doi: 10.1161/jaha.117.007572

Li, Y., Zhang, K., and Mao, W. (2018c). Inhibition of miR-34a prevents endothelial cell apoptosis by directly targeting HDAC1 in the setting of atherosclerosis. *Mol. Med. Rep.* 17, 4645–4650. doi: 10.3892/mmr.2018.8411

Libby, P., Buring, J. E., Badimon, L., Hansson, G. K., Deanfield, J., Bittencourt, M. S., et al. (2019). Atherosclerosis. *Nat. Rev. Dis. Primers* 5:56. doi: 10.1038/s41572-019-0106-z

Lin, S., and Du, L. (2020). The therapeutic potential of BRD4 in cardiovascular disease. *Hypertens Res.* 86, 1006–1014. doi: 10.1038/s41440-020-0459-4

Liu, M. Y., and Khachigian, L. M. (2009). Histone deacetylase-1 is enriched at the platelet-derived growth factor-D promoter in response to interleukin-1beta and forms a cytokine-inducible gene-silencing complex with NF-kappab p65 and interferon regulatory factor-1. *J. Biol. Chem.* 284, 35101–35112. doi: 10.1074/jbc.M109.061903

Liu, T., Wan, Y., Xiao, Y., Xia, C., and Duan, G. (2020). Dual-target inhibitors BASED on HDACs: novel antitumor agents for cancer therapy. *J. Med. Chem.* 63, 8977–9002. doi: 10.1021/acs.jmedchem.0c00491

Luo, X. Y., Qu, S. L., Tang, Z. H., Zhang, Y., Liu, M. H., Peng, J., et al. (2014). SIRT1 in cardiovascular aging. *Clin. Chim. Acta* 437, 106–114. doi: 10.1016/j.cca.2014.07.019

Lyu, X., Hu, M., Peng, J., Zhang, X., and Sanders, Y. Y. (2019). HDAC inhibitors as antifibrotic drugs in cardiac and pulmonary fibrosis. *Ther. Adv. Chronic Dis.* 10:2040622319862697. doi: 10.1177/2040622319862697

Mahapatra, S., Firpo, M. T., and Bacanamwo, M. (2010). Inhibition of DNA methyltransferases and histone deacetylases induces bone marrow-derived multipotent adult progenitor cells to differentiate into endothelial cells. *Ethn. Dis.* 20, S1–S60.

Manea, S. A., Vlad, M. L., Fenyo, I. M., Lazar, A. G., Raicu, M., Muresian, H., et al. (2020). Pharmacological inhibition of histone deacetylase reduces NADPH oxidase expression, oxidative stress and the progression of atherosclerotic lesions in hypercholesterolemic apolipoprotein E-deficient mice; potential implications for human atherosclerosis. *Redox Biol.* 28:101338. doi: 10.1016/j.redox.2019.101338

Margariti, A., Zampetaki, A., Xiao, Q., Zhou, B., Karamariti, E., Martin, D., et al. (2010). Histone deacetylase 7 controls endothelial cell growth through modulation of beta-catenin. *Circ. Res.* 106, 1202–1211. doi: 10.1161/CIRCRESAHA.109.213165

Marks, P. A. (2010). The clinical development of histone deacetylase inhibitors as targeted anticancer drugs. *Expert Opin. Investig Drugs* 19, 1049–1066. doi: 10.1517/13543784.2010.510514

Martin, D., Li, Y., Yang, J., Wang, G., Margariti, A., Jiang, Z., et al. (2014). Unspliced X-box-binding protein 1 (XBP1) protects endothelial cells from oxidative stress through interaction with histone deacetylase 3. *J. Biol. Chem.* 289, 30625–30634. doi: 10.1074/jbc.M114.571984

Mastoraki, A., Schizas, D., Charalampakis, N., Naar, L., Ioannidi, M., Tsilimigras, D., et al. (2020). Contribution of histone deacetylases in prognosis and therapeutic management of cholangiocarcinoma. *Mol. Diagn. Ther.* 24, 175–184. doi: 10.1007/s40291-020-00454-x

Mathew, O. P., Ranganna, K., and Yatsu, F. M. (2010). Butyrate, an HDAC inhibitor, stimulates interplay between different posttranslational modifications of histone H3 and differently alters G1-specific cell cycle proteins in vascular smooth muscle cells. *Biomed. Pharmacother.* 64, 733–740. doi: 10.1016/j.biopha.2010.09.017

McLure, K. G., Gesner, E. M., Tsujikawa, L., Kharenko, O. A., Attwell, S., Campeau, E., et al. (2013). RVX-208, an inducer of ApoA-I in humans, is a BET bromodomain antagonist. *PLoS One* 8:e83190. doi: 10.1371/journal.pone.0083190

Meng, F., Han, M., Zheng, B., Wang, C., Zhang, R., Zhang, X. H., et al. (2009). All-trans retinoic acid increases KLF4 acetylation by inducing HDAC2 phosphorylation and its dissociation from KLF4 in vascular smooth muscle cells. *Biochem. Biophys. Res. Commun.* 387, 13–18. doi: 10.1016/j.bbrc.2009.05.112

Michaelis, M., Suhan, T., Michaelis, U. R., Beek, K., Rothweiler, F., Tausch, L., et al. (2006). Valproic acid induces extracellular signal-regulated kinase 1/2 activation and inhibits apoptosis in endothelial cells. *Cell Death Differ.* 13, 446–453. doi: 10.1038/sj.cdd.4401759

Mihaylova, M. M., and Shaw, R. J. (2013). Metabolic reprogramming by class I and II histone deacetylases. *Trends Endocrinol. Metab.* 24, 48–57. doi: 10.1016/j.tem.2012.09.003

Miller, S. J., Zaloga, G. P., Hoggatt, A. M., Labarrere, C., and Faulk, W. P. (2005). Short-chain fatty acids modulate gene expression for vascular endothelial cell adhesion molecules. *Nutrition* 21, 740–748. doi: 10.1016/j.nut.2004.11.011

Miyoshi, M., Usami, M., and Ohata, A. (2008). Short-chain fatty acids and trichostatin A alter tight junction permeability in human umbilical vein endothelial cells. *Nutrition* 24, 1189–1198. doi: 10.1016/j.nut.2008.06.012

Mizuno, S., Yasuo, M., Bogaard, H. J., Kraskauskas, D., Natarajan, R., and Voelkel, N. F. (2011). Inhibition of histone deacetylase causes emphysema. *Am. J. Physiol. Lung. Cell Mol. Physiol.* 300, L402–L413. doi: 10.1152/ajplung.00207.2010

Mottet, D., Bellahcène, A., Pirotte, S., Waltregny, D., Deroanne, C., Lamour, V., et al. (2007). Histone deacetylase 7 silencing alters endothelial cell migration, a key step in angiogenesis. *Circ. Res.* 101, 1237–1246. doi: 10.1161/circresaha.107.149377

Nicholls, S. J., Puri, R., Wolski, K., Ballantyne, C. M., Barter, P. J., Brewer, H. B., et al. (2016). Effect of the BET protein inhibitor, RVX-208, on progression of coronary atherosclerosis: results of the phase 2b, randomized, double-blind, multicenter, ASSURE Trial. *Am. J. Cardiovasc. Drugs* 16, 55–65. doi: 10.1007/s40256-015-0146-z

Nicholls, S. J., Ray, K. K., Johansson, J. O., Gordon, A., Sweeney, M., Halliday, C., et al. (2018). Selective BET protein inhibition with apabetalone and cardiovascular events: a pooled analysis of trials in patients with coronary artery disease. *Am. J. Cardiovasc. Drugs* 18, 109–115. doi: 10.1007/s40256-017-0250-3

Nishida, K., Harrison, D. G., Navas, J. P., Fisher, A. A., Dockery, S. P., Uematsu, M., et al. (1992). Molecular cloning and characterization of the constitutive bovine aortic endothelial cell nitric oxide synthase. *J. Clin. Invest.* 90, 2092–2096. doi: 10.1172/jci116092

Niu, N., Xu, S., Xu, Y., Little, P. J., and Jin, Z. G. (2019). Targeting mechanosensitive transcription factors in atherosclerosis. *Trends Pharmacol. Sci.* 40, 253–266. doi: 10.1016/j.tips.2019.02.004

Ogawa, H., Rafiee, P., Fisher, P. J., Johnson, N. A., Otterson, M. F., and Binion, D. G. (2003). Butyrate modulates gene and protein expression in human intestinal endothelial cells. *Biochem. Biophys. Res. Commun.* 309, 512–519. doi: 10.1016/j.bbrc.2003.08.026

Ohashi, A., Yasuda, H., Kamiya, T., Hara, H., and Adachi, T. (2017). CAPE increases the expression of SOD3 through epigenetics in human retinal endothelial cells. *J. Clin. Biochem. Nutr.* 61, 6–13. doi: 10.3164/jcbn.16-109

Okam, M. M., Esrick, E. B., Mandell, E., Campigotto, F., Neuberg, D. S., and Ebert, B. L. (2015). Phase 1/2 trial of vorinostat in patients with sickle cell disease who have not benefitted from hydroxyurea. *Blood* 125, 3668–3669. doi: 10.1182/blood-2015-03-635391

Okamoto, H., Fujioka, Y., Takahashi, A., Takahashi, T., Taniguchi, T., Ishikawa, Y., et al. (2006). Trichostatin, A., an inhibitor of histone deacetylase, inhibits smooth muscle cell proliferation via induction of p21(WAF1). *J. Atheroscler Thromb.* 13, 183–191. doi: 10.5551/jat.13.183

Orekhov, A. N. (2018). LDL and foam cell formation as the basis of atherogenesis. *Curr. Opin. Lipidol.* 29, 279–284. doi: 10.1097/mol.0000000000000525

Pan, Y., Yang, J., Wei, Y., Wang, H., Jiao, R., Moraga, A., et al. (2018). Histone deacetylase 7-derived peptides play a vital role in vascular repair and regeneration. *Adv. Sci.* 5:1800006. doi: 10.1002/advs.201800006

Pandey, D., Sikka, G., Bergman, Y., Kim, J. H., Ryoo, S., Romer, L., et al. (2014). Transcriptional regulation of endothelial arginase 2 by histone deacetylase 2. *Arterioscler Thromb. Vasc. Biol.* 34, 1556–1566. doi: 10.1161/ATVBAHA.114.303685

Pang, J., Yan, C., Natarajan, K., Cavet, M. E., Massett, M. P., Yin, G., et al. (2008). GIT1 mediates HDAC5 activation by angiotensin II in vascular smooth muscle cells. *Arterioscler Thromb. Vasc. Biol.* 28, 892–898. doi: 10.1161/atvbaha.107.161349

Park, D., Park, H., Kim, Y., Kim, H., and Jeoung, D. (2014). HDAC3 acts as a negative regulator of angiogenesis. *BMB Rep.* 47, 227–232. doi: 10.5483/bmbrep.2014.47.4.128

Parra, M., and Verdin, E. (2010). Regulatory signal transduction pathways for class IIa histone deacetylases. *Curr. Opin. Pharmacol.* 10, 454–460. doi: 10.1016/j.coph.2010.04.004

Peng, Y., Stewart, D., Li, W., Hawkins, M., Kulak, S., Ballermann, B., et al. (2007). Irradiation modulates association of NF-Y with histone-modifying cofactors PCAF and HDAC. *Oncogene* 26, 7576–7583. doi: 10.1038/sj.onc.1210565

Pepper, M. S., Montesano, R., Mandriota, S. J., Orci, L., and Vassalli, J. D. (1996). Angiogenesis: a paradigm for balanced extracellular proteolysis during cell migration and morphogenesis. *Enzyme Protein* 49, 138–162. doi: 10.1159/000468622

Pietruczuk, P., Jain, A., Simo-Cheyou, E. R., Anand-Srivastava, M. B., and Srivastava, A. K. (2019). Protein kinase B/AKT mediates insulin-like growth factor 1-induced phosphorylation and nuclear export of histone deacetylase 5 via NADPH oxidase 4 activation in vascular smooth muscle cells. *J. Cell Physiol.* 234, 17337–17350. doi: 10.1002/jcp.28353

Poston, R. N. (2019). Atherosclerosis: integration of its pathogenesis as a self-perpetuating propagating inflammation: a review. *Cardiovasc. Endocrinol. Metab.* 8, 51–61. doi: 10.1097/xce.0000000000000172

Prestel, M., Prell-Schicker, C., Webb, T., Malik, R., Lindner, B., Ziesch, N., et al. (2019). The atherosclerosis risk variant rs2107595 mediates allele-specific transcriptional regulation of HDAC9 via E2F3 and Rb1. *Stroke* 50, 2651–2660. doi: 10.1161/strokeaha.119.026112

Rabinovitch, M. (2012). Molecular pathogenesis of pulmonary arterial hypertension. *J. Clin. Invest.* 122, 4306–4313. doi: 10.1172/jci60658

Rafehi, H., Karagiannis, T. C., and El-Osta, A. (2017). Pharmacological histone deacetylation distinguishes transcriptional regulators. *Curr. Top. Med. Chem.* 17, 1611–1622. doi: 10.2174/1568026617666161104104341

Rajasingh, J., Thangavel, J., Siddiqui, M. R., Gomes, I., Gao, X. P., Kishore, R., et al. (2011). Improvement of cardiac function in mouse myocardial infarction after transplantation of epigenetically-modified bone marrow progenitor cells. *PLoS One* 6:e22550. doi: 10.1371/journal.pone.0022550

Rambaldi, A., Dellacasa, C. M., Finazzi, G., Carobbio, A., Ferrari, M. L., Guglielmelli, P., et al. (2010). A pilot study of the histone-deacetylase inhibitor givinostat in patients with JAK2V617F positive chronic myeloproliferative neoplasms. *Br. J. Haematol.* 150, 446–455. doi: 10.1111/j.1365-2141.2010.08266.x

Ray, K. K., Nicholls, S. J., Buhr, K. A., Ginsberg, H. N., Johansson, J. O., Kalantar-Zadeh, K., et al. (2020). Effect of apabetalone added to standard therapy on major adverse cardiovascular events in patients with recent acute coronary syndrome and type 2 diabetes: a randomized clinical trial. *Jama* 323, 1565–1573. doi: 10.1001/jama.2020.3308

Reynoso-Roldán, A., Roldán, M. L., Cancino-Diaz, J. C., Rodríguez-Martínez, S., and Cancino-Diaz, M. E. (2012). Vascular endothelial growth factor production is induced by histone deacetylase 1 and suppressed by von Hippel-Lindau protein in HaCaT cells. *Clin. Invest. Med.* 35, E340–E350. doi: 10.25011/cim.v35i6.19205

Ricard, N., Tu, L., Le Hiress, M., Huertas, A., Phan, C., Thuillet, R., et al. (2014). Increased pericyte coverage mediated by endothelial-derived fibroblast growth factor-2 and interleukin-6 is a source of smooth muscle-like cells in pulmonary hypertension. *Circulation* 129, 1586–1597. doi: 10.1161/circulationaha.113.007469

Rinkevich, Y., Lindau, P., Ueno, H., Longaker, M. T., and Weissman, I. L. (2011). Germ-layer and lineage-restricted stem/progenitors regenerate the mouse digit tip. *Nature* 476, 409–413. doi: 10.1038/nature10346

Ross, R. (1993). The pathogenesis of atherosclerosis: a perspective for the 1990s. *Nature* 362, 801–809. doi: 10.1038/362801a0

Rossig, L., Li, H., Fisslthaler, B., Urbich, C., Fleming, I., Forstermann, U., et al. (2002). Inhibitors of histone deacetylation downregulate the expression of endothelial nitric oxide synthase and compromise endothelial cell function in vasorelaxation and angiogenesis. *Circ. Res.* 91, 837–844. doi: 10.1161/01.res.0000037983.07158.b1

Rossig, L., Urbich, C., Bruhl, T., Dernbach, E., Heeschen, C., Chavakis, E., et al. (2005). Histone deacetylase activity is essential for the expression of HoxA9 and for endothelial commitment of progenitor cells. *J. Exp. Med.* 201, 1825–1835. doi: 10.1084/jem.20042097

Ryu, Y., Kee, H. J., Sun, S., Seok, Y. M., Choi, S. Y., Kim, G. R., et al. (2019). Class I histone deacetylase inhibitor MS-275 attenuates vasoconstriction and inflammation in angiotensin II-induced hypertension. *PLoS One* 14:e0213186. doi: 10.1371/journal.pone.0213186

Serlin, Y., Shelef, I., Knyazer, B., and Friedman, A. (2015). Anatomy and physiology of the blood-brain barrier. *Semin. Cell Dev. Biol.* 38, 2–6. doi: 10.1016/j.semcdb.2015.01.002

Shah, P. K. (1996). Pathophysiology of plaque rupture and the concept of plaque stabilization. *Cardiol. Clin.* 14, 17–29. doi: 10.1016/s0733-8651(05)70258-7

Shi, W., Wei, X., Wang, Z., Han, H., Fu, Y., Liu, J., et al. (2016). HDAC9 exacerbates endothelial injury in cerebral ischaemia/reperfusion injury. *J. Cell Mol. Med.* 20, 1139–1149. doi: 10.1111/jcmm.12803

Shirodkar, A. V., and Marsden, P. A. (2011). Epigenetics in cardiovascular disease. *Curr. Opin. Cardiol.* 26, 209–215. doi: 10.1097/HCO.0b013e328345986e

Shishikura, D., Kataoka, Y., Honda, S., Takata, K., Kim, S. W., Andrews, J., et al. (2019). The effect of bromodomain and extra-terminal inhibitor apabetalone on attenuated coronary atherosclerotic plaque: insights from the ASSURE Trial. *Am. J. Cardiovasc. Drugs* 19, 49–57. doi: 10.1007/s40256-018-0298-8

Shroff, N., Ander, B. P., Zhan, X., Stamova, B., Liu, D., Hull, H., et al. (2019). HDAC9 polymorphism alters blood gene expression in patients with large vessel atherosclerotic stroke. *Transl. Stroke Res.* 10, 19–25. doi: 10.1007/s12975-018-0619-x

Smith, Q., Macklin, B., Chan, X. Y., Jones, H., Trempel, M., Yoder, M. C., et al. (2018). Differential HDAC6 activity modulates ciliogenesis and subsequent mechanosensing of endothelial cells derived from pluripotent stem cells. *Cell Rep.* 24, 895.e6–908.e6. doi: 10.1016/j.celrep.2018.06.083

Spronk, H. M., Borissoff, J. I., and ten Cate, H. (2013). New insights into modulation of thrombin formation. *Curr. Atheroscler Rep.* 15:363. doi: 10.1007/s11883-013-0363-3

Stein, S., Schäfer, N., Breitenstein, A., Besler, C., Winnik, S., Lohmann, C., et al. (2010). SIRT1 reduces endothelial activation without affecting vascular function in ApoE-/- mice. *Aging* 2, 353–360. doi: 10.18632/aging.100162

Stocker, R., and Keaney, J. F. Jr. (2004). Role of oxidative modifications in atherosclerosis. *Physiol. Rev.* 84, 1381–1478. doi: 10.1152/physrev.00047.2003

Su, Y. T., Gao, C., Liu, Y., Guo, S., Wang, A., Wang, B., et al. (2013). Monoubiquitination of filamin B regulates vascular endothelial growth factor-mediated trafficking of histone deacetylase 7. *Mol. Cell Biol.* 33, 1546–1560. doi: 10.1128/mcb.01146-12

Sun, L., Wang, C., Yuan, Y., Guo, Z., He, Y., Ma, W., et al. (2020). Downregulation of HDAC1 suppresses media degeneration by inhibiting the migration and phenotypic switch of aortic vascular smooth muscle cells in aortic dissection. *J. Cell Physiol.* 235, 8747–8756. doi: 10.1002/jcp.29718

Tang, F. B., Dai, Y. L., Zhou, G. Y., Zhang, W. H., Wang, H. B., Li, Y. G., et al. (2018). Valproic acid treatment inhibits vasopermeability and improves survival

in rats with lethal scald injury. *J. Burn. Care Res.* 39, 209–217. doi: 10.1097/bcr.0000000000000568

Tedgui, A., and Mallat, Z. (2003). Apoptosis, a major determinant of atherothrombosis. *Arch. Mal. Coeur Vaiss* 96, 671–675.

Tesfamariam, B., and DeFelice, A. F. (2007). Endothelial injury in the initiation and progression of vascular disorders. *Vascul. Pharmacol.* 46, 229–237. doi: 10.1016/j.vph.2006.11.005

Thangjam, G. S., Dimitropoulou, C., Joshi, A. D., Barabutis, N., Shaw, M. C., Kovalenkov, Y., et al. (2014). Novel mechanism of attenuation of LPS-induced NF-kappaB activation by the heat shock protein 90 inhibitor, 17-N-allylamino-17-demethoxygeldanamycin, in human lung microvascular endothelial cells. *Am. J. Respir. Cell Mol. Biol.* 50, 942–952. doi: 10.1165/rcmb.2013-0214OC

Tian, K., Ogura, S., Little, P. J., Xu, S. W., and Sawamura, T. (2019). Targeting LOX-1 in atherosclerosis and vasculopathy: current knowledge and future perspectives. *Ann. N. Y. Acad. Sci.* 1443, 34–53. doi: 10.1111/nyas.13984

Tian, R., Li, R., Liu, Y., Liu, J., Pan, T., Zhang, R., et al. (2019). Metformin ameliorates endotoxemia-induced endothelial pro-inflammatory responses via AMPK-dependent mediation of HDAC5 and KLF2. *Biochim. Biophys. Acta Mol. Basis Dis.* 1865, 1701–1712. doi: 10.1016/j.bbadis.2019.04.009

To, M., Yamamura, S., Akashi, K., Charron, C. E., Haruki, K., Barnes, P. J., et al. (2012). Defect of adaptation to hypoxia in patients with COPD due to reduction of histone deacetylase 7. *Chest* 141, 1233–1242. doi: 10.1378/chest.11-1536

Tsou, P. S., Wren, J. D., Amin, M. A., Schiopu, E., Fox, D. A., Khanna, D., et al. (2016). Histone Deacetylase 5 Is overexpressed in scleroderma endothelial cells and impairs angiogenesis via repression of proangiogenic factors. *Arthritis Rheumatol.* 68, 2975–2985. doi: 10.1002/art.39828

Urbich, C., Rossig, L., Kaluza, D., Potente, M., Boeckel, J. N., Knau, A., et al. (2009). HDAC5 is a repressor of angiogenesis and determines the angiogenic gene expression pattern of endothelial cells. *Blood* 113, 5669–5679. doi: 10.1182/blood-2009-01-196485

Usui, T., Morita, T., Okada, M., and Yamawaki, H. (2014). Histone deacetylase 4 controls neointimal hyperplasia via stimulating proliferation and migration of vascular smooth muscle cells. *Hypertension* 63, 397–403. doi: 10.1161/hypertensionaha.113.01843

Vallée, A., Vallée, J. N., and Lecarpentier, Y. (2019). Metabolic reprogramming in atherosclerosis: opposed interplay between the canonical WNT/β-catenin pathway and PPARγ. *J. Mol. Cell Cardiol.* 133, 36–46. doi: 10.1016/j.yjmcc.2019.05.024

Van den Bossche, J., Neele, A. E., Hoeksema, M. A., de Heij, F., Boshuizen, M. C., van der Velden, S., et al. (2014). Inhibiting epigenetic enzymes to improve atherogenic macrophage functions. *Biochem. Biophys. Res. Commun.* 455, 396–402. doi: 10.1016/j.bbrc.2014.11.029

Vinh, A., Gaspari, T. A., Liu, H. B., Dousha, L. F., Widdop, R. E., and Dear, A. E. (2008). A novel histone deacetylase inhibitor reduces abdominal aortic aneurysm formation in angiotensin II-infused apolipoprotein E-deficient mice. *J. Vasc. Res.* 45, 143–152. doi: 10.1159/000110041

Vinolo, M. A., Rodrigues, H. G., Nachbar, R. T., and Curi, R. (2011). Regulation of inflammation by short chain fatty acids. *Nutrients* 3, 858–876. doi: 10.3390/nu3100858

Wang, D., Yang, Y., Lei, Y., Tzvetkov, N. T., Liu, X., Yeung, A. W. K., et al. (2019). Targeting foam cell formation in atherosclerosis: therapeutic potential of natural products. *Pharmacol. Rev.* 71, 596–670. doi: 10.1124/pr.118.017178

Wang, H., Fu, H., Zhu, R., Wu, X., Ji, X., Li, X., et al. (2020). BRD4 contributes to LPS-induced macrophage senescence and promotes progression of atherosclerosis-associated lipid uptake. *Aging* 12, 9240–9259. doi: 10.18632/aging.103200

Wang, J., Mahmud, S. A., Bitterman, P. B., Huo, Y., and Slungaard, A. (2007). Histone deacetylase inhibitors suppress TF-kappaB-dependent agonist-driven tissue factor expression in endothelial cells and monocytes. *J. Biol. Chem.* 282, 28408–28418. doi: 10.1074/jbc.M703586200

Wang, S., Li, X., Parra, M., Verdin, E., Bassel-Duby, R., and Olson, E. N. (2008). Control of endothelial cell proliferation and migration by VEGF signaling to histone deacetylase 7. *Proc. Natl. Acad. Sci. U.S.A.* 105, 7738–7743. doi: 10.1073/pnas.0802857105

Wang, W., Ha, C. H., Jhun, B. S., Wong, C., Jain, M. K., and Jin, Z. G. (2010). Fluid shear stress stimulates phosphorylation-dependent nuclear export of HDAC5 and mediates expression of KLF2 and eNOS. *Blood* 115, 2971–2979. doi: 10.1182/blood-2009-05-224824

Wang, Y. H., Yan, Z. Q., Qi, Y. X., Cheng, B. B., Wang, X. D., Zhao, D., et al. (2010). Normal shear stress and vascular smooth muscle cells modulate migration of endothelial cells through histone deacetylase 6 activation and tubulin acetylation. *Ann. Biomed. Eng.* 38, 729–737. doi: 10.1007/s10439-009-9896-6

Wang, X. B., Han, Y. D., Sabina, S., Cui, N. H., Zhang, S., Liu, Z. J., et al. (2016). HDAC9 Variant Rs2107595 modifies susceptibility to coronary artery disease and the severity of coronary atherosclerosis in a chinese han population. *PLoS One* 11:e0160449. doi: 10.1371/journal.pone.0160449

Wang, Z., Tsai, L. K., Munasinghe, J., Leng, Y., Fessler, E. B., Chibane, F., et al. (2012). Chronic valproate treatment enhances postischemic angiogenesis and promotes functional recovery in a rat model of ischemic stroke. *Stroke* 43, 2430–2436. doi: 10.1161/strokeaha.112.652545

Weinbaum, S., Tarbell, J. M., and Damiano, E. R. (2007). The structure and function of the endothelial glycocalyx layer. *Annu. Rev. Biomed. Eng.* 9, 121–167. doi: 10.1146/annurev.bioeng.9.060906.151959

Williams, R. J. (2001). Trichostatin, A., an inhibitor of histone deacetylase, inhibits hypoxia-induced angiogenesis. *Expert Opin. Investig Drugs* 10, 1571–1573. doi: 10.1517/13543784.10.8.1571

Won, K. J., Jung, S. H., Jung, S. H., Lee, K. P., Lee, H. M., Lee, D. Y., et al. (2014). DJ-1/park7 modulates vasorelaxation and blood pressure via epigenetic modification of endothelial nitric oxide synthase. *Cardiovasc. Res.* 101, 473–481. doi: 10.1093/cvr/cvt274

Wright, L. H., Herr, D. J., Brown, S. S., Kasiganesan, H., and Menick, D. R. (2018). Angiokine Wisp-1 is increased in myocardial infarction and regulates cardiac endothelial signaling. *JCI Insight* 3:e95824. doi: 10.1172/jci.insight.95824

Wu, H., Cheng, X. W., Hu, L., Takeshita, K., Hu, C., Du, Q., et al. (2016). Cathepsin S activity controls injury-related vascular repair in mice via the TLR2-mediated p38MAPK and PI3K-Akt/p-HDAC6 signaling pathway. *Arterioscler Thromb. Vasc. Biol.* 36, 1549–1557. doi: 10.1161/atvbaha.115.307110

Wu, J., Jiang, Z., Zhang, H., Liang, W., Huang, W., Zhang, H., et al. (2018). Sodium butyrate attenuates diabetes-induced aortic endothelial dysfunction via P300-mediated transcriptional activation of Nrf2. *Free Radic. Biol. Med.* 124, 454–465. doi: 10.1016/j.freeradbiomed.2018.06.034

Xiao, Q., Zeng, L., Zhang, Z., Margariti, A., Ali, Z. A., Channon, K. M., et al. (2006). Sca-1+ progenitors derived from embryonic stem cells differentiate into endothelial cells capable of vascular repair after arterial injury. *Arterioscler Thromb. Vasc. Biol.* 26, 2244–2251. doi: 10.1161/01.ATV.0000240251.50215.50

Xu, S., Kamato, D., Little, P. J., Nakagawa, S., Pelisek, J., and Jin, Z. G. (2019). Targeting epigenetics and non-coding RNAs in atherosclerosis: from mechanisms to therapeutics. *Pharmacol. Ther.* 196, 15–43. doi: 10.1016/j.pharmthera.2018.11.003

Xu, S., Pelisek, J., and Jin, Z. G. (2018). Atherosclerosis Is an Epigenetic Disease. *Trends Endocrinol. Metab.* 29, 739–742. doi: 10.1016/j.tem.2018.04.007

Xu, Y., Xu, S., Liu, P., Koroleva, M., Zhang, S., Si, S., et al. (2017). Suberanilohydroxamic acid as a pharmacological kruppel-like factor 2 activator that represses vascular inflammation and atherosclerosis. *J. Am. Heart Assoc.* 6:e007134. doi: 10.1161/jaha.117.007134

Yamanegi, K., Kawabe, M., Futani, H., Nishiura, H., Yamada, N., Kato-Kogoe, N., et al. (2015). Sodium valproate, a histone deacetylase inhibitor, modulates the vascular endothelial growth inhibitor-mediated cell death in human osteosarcoma and vascular endothelial cells. *Int. J. Oncol.* 46, 1994–2002. doi: 10.3892/ijo.2015.2924

Yan, Z. Q., Yao, Q. P., Zhang, M. L., Qi, Y. X., Guo, Z. Y., Shen, B. R., et al. (2009). Histone deacetylases modulate vascular smooth muscle cell migration induced by cyclic mechanical strain. *J. Biomech.* 42, 945–948. doi: 10.1016/j.jbiomech.2009.01.012

Yang, D., Xie, P., and Liu, Z. (2012). Ischemia/reperfusion-induced MKP-3 impairs endothelial NO formation via inactivation of ERK1/2 pathway. *PLoS One* 7:e42076. doi: 10.1371/journal.pone.0042076

Yang, L., Liu, N., Zhao, W., Li, X., Han, L., Zhang, Z., et al. (2019). Angiogenic function of astragaloside IV in rats with myocardial infarction occurs via the PKD1-HDAC5-VEGF pathway. *Exp. Ther. Med.* 17, 2511–2518. doi: 10.3892/etm.2019.7273

Yang, Q., Sun, M., Ramchandran, R., and Raj, J. U. (2015). IGF-1 signaling in neonatal hypoxia-induced pulmonary hypertension: role of epigenetic regulation. *Vascul. Pharmacol.* 73, 20–31. doi: 10.1016/j.vph.2015.04.005

Yanginlar, C., and Logie, C. (2018). HDAC11 is a regulator of diverse immune functions. *Biochim. Biophys. Acta Gene Regul. Mech.* 1861, 54–59. doi: 10.1016/j.bbagrm.2017.12.002

Yao, Q. P., Zhang, P., Qi, Y. X., Chen, S. G., Shen, B. R., Han, Y., et al. (2014). The role of SIRT6 in the differentiation of vascular smooth muscle cells in response to cyclic strain. *Int. J. Biochem. Cell Biol.* 49, 98–104. doi: 10.1016/j.biocel.2014.01.016

Ye, Y., Zhao, X., Lu, Y., Long, B., and Zhang, S. (2018). Varinostat alters gene expression profiles in aortic tissues from ApoE(-/-) Mice. *Hum. Gene Ther. Clin. Dev.* 29, 214–225. doi: 10.1089/humc.2018.141

Yoshida, T., Gan, Q., and Owens, G. K. (2008). Kruppel-like factor 4, Elk-1, and histone deacetylases cooperatively suppress smooth muscle cell differentiation markers in response to oxidized phospholipids. *Am. J. Physiol. Cell Physiol.* 295, C1175–C1182. doi: 10.1152/ajpcell.00288.2008

You, D., Wen, X., Gorczyca, L., Morris, A., Richardson, J. R., and Aleksunes, L. M. (2019). Increased MDR1 transporter expression in human brain endothelial cells through enhanced histone acetylation and activation of aryl hydrocarbon receptor signaling. *Mol. Neurobiol.* 56, 6986–7002. doi: 10.1007/s12035-019-1565-7

Yu, D., Chen, W., Ren, J., Zhang, T., Yang, K., Wu, G., et al. (2014). VEGF-PKD1-HDAC7 signaling promotes endothelial progenitor cell migration and tube formation. *Microvasc. Res.* 91, 66–72. doi: 10.1016/j.mvr.2013.10.006

Yu, J., Ma, M., Ma, Z., and Fu, J. (2016). HDAC6 inhibition prevents TNF-α-induced caspase 3 activation in lung endothelial cell and maintains cell-cell junctions. *Oncotarget* 7, 54714–54722. doi: 10.18632/oncotarget.10591

Zampetaki, A., Zeng, L., Margariti, A., Xiao, Q., Li, H., Zhang, Z., et al. (2010). Histone deacetylase 3 is critical in endothelial survival and atherosclerosis development in response to disturbed flow. *Circulation* 121, 132–142. doi: 10.1161/circulationaha.109.890491

Zelko, I. N., and Folz, R. J. (2015). Regulation of oxidative stress in pulmonary artery endothelium. modulation of extracellular superoxide dismutase and NOX4 expression using histone deacetylase class i inhibitors. *Am. J. Respir. Cell Mol. Biol.* 53, 513–524. doi: 10.1165/rcmb.2014-0260OC

Zeng, L., Zampetaki, A., Margariti, A., Pepe, A. E., Alam, S., Martin, D., et al. (2009). Sustained activation of XBP1 splicing leads to endothelial apoptosis and atherosclerosis development in response to disturbed flow. *Proc. Natl. Acad. Sci. U.S.A.* 106, 8326–8331. doi: 10.1073/pnas.0903197106

Zeng, L., Zhang, Y., Chien, S., Liu, X., and Shyy, J. Y. (2003). The role of p53 deacetylation in p21Waf1 regulation by laminar flow. *J. Biol. Chem.* 278, 24594–24599. doi: 10.1074/jbc.M301955200

Zhang, B., Dong, Y., Liu, M., Yang, L., and Zhao, Z. (2019). miR-149-5p inhibits vascular smooth muscle cells proliferation, invasion, and migration by targeting histone deacetylase 4 (HDAC4). *Med. Sci. Monit.* 25, 7581–7590. doi: 10.12659/msm.916522

Zhang, H. N., Dai, Y., Zhang, C. H., Omondi, A. M., Ghosh, A., Khanra, I., et al. (2020). Sirtuins family as a target in endothelial cell dysfunction: implications for vascular ageing. *Biogerontology* 21, 495–516. doi: 10.1007/s10522-020-09873-z

Zhang, L., Zhang, J., Jiang, Q., Zhang, L., and Song, W. (2018). Zinc binding groups for histone deacetylase inhibitors. *J. Enzyme Inhib. Med. Chem.* 33, 714–721. doi: 10.1080/14756366.2017.1417274

Zhang, M. X., Zhang, C., Shen, Y. H., Wang, J., Li, X. N., Chen, L., et al. (2008). Effect of 27nt small RNA on endothelial nitric-oxide synthase expression. *Mol. Biol. Cell* 19, 3997–4005. doi: 10.1091/mbc.e07-11-1186

Zhang, R., and Ge, J. (2017). Proteinase-activated receptor-2 modulates ve-cadherin expression to affect human vascular endothelial barrier function. *J. Cell Biochem.* 118, 4587–4593. doi: 10.1002/jcb.26123

Zhao, Q., Yu, Z., Zhang, F., Huang, L., Xing, C., Liu, N., et al. (2019). HDAC3 inhibition prevents oxygen glucose deprivation/reoxygenation-induced transendothelial permeability by elevating PPARgamma activity in vitro. *J. Neurochem.* 149, 298–310. doi: 10.1111/jnc.14619

Zheng, B., Han, M., Shu, Y. N., Li, Y. J., Miao, S. B., Zhang, X. H., et al. (2011). HDAC2 phosphorylation-dependent Klf5 deacetylation and RARα acetylation induced by RAR agonist switch the transcription regulatory programs of p21 in VSMCs. *Cell Res.* 21, 1487–1508. doi: 10.1038/cr.2011.34

Zheng, X., Wu, Z., Xu, K., Qiu, Y., Su, X., Zhang, Z., et al. (2019). Interfering histone deacetylase 4 inhibits the proliferation of vascular smooth muscle cells via regulating MEG3/miR-125a-5p/IRF1. *Cell Adh. Migr.* 13, 41–49. doi: 10.1080/19336918.2018.1506653

Zheng, X. X., Zhou, T., Wang, X. A., Tong, X. H., and Ding, J. W. (2015). Histone deacetylases and atherosclerosis. *Atherosclerosis* 240, 355–366. doi: 10.1016/j.atherosclerosis.2014.12.048

Zhou, B., Margariti, A., Zeng, L., Habi, O., Xiao, Q., Martin, D., et al. (2011a). Splicing of histone deacetylase 7 modulates smooth muscle cell proliferation and neointima formation through nuclear β-catenin translocation. *Arterioscler Thromb. Vasc. Biol.* 31, 2676–2684. doi: 10.1161/atvbaha.111.230888

Zhou, B., Margariti, A., Zeng, L., and Xu, Q. (2011b). Role of histone deacetylases in vascular cell homeostasis and arteriosclerosis. *Cardiovasc. Res.* 90, 413–420. doi: 10.1093/cvr/cvr003

Ziegler, T., Abdel Rahman, F., Jurisch, V., and Kupatt, C. (2019). Atherosclerosis and the capillary network; pathophysiology and potential therapeutic strategies. *Cells* 9:50. doi: 10.3390/cells9010050

Conflict of Interest: The authors declare that the research was conducted in the absence of any commercial or financial relationships that could be construed as a potential conflict of interest.

frontiers in Cardiovascular Medicine

ORIGINAL RESEARCH
published: 30 November 2020
doi: 10.3389/fcvm.2020.594325

The Regulatory Role of Histone Modification on Gene Expression in the Early Stage of Myocardial Infarction

Jinyu Wang[1,2,3†], *Bowen Lin*[2,3†], *Yanping Zhang*[4†], *Le Ni*[2,3†], *Lingjie Hu*[2,3], *Jian Yang*[2,3], *Liang Xu*[2,3], *Dan Shi*[2,3*] *and Yi-Han Chen*[1,2,3,5*]

[1] Department of Physiology, Shanxi Medical University, Taiyuan, China, [2] Department of Cardiology, Shanghai East Hospital, Tongji University School of Medicine, Shanghai, China, [3] Key Laboratory of Arrhythmias of the Ministry of Education of China, Shanghai East Hospital, Tongji University School of Medicine, Shanghai, China, [4] Department of Cardiology, Ruijin Hospital, Shanghai Jiaotong University School of Medicine, Shanghai, China, [5] Department of Pathology and Pathophysiology, Tongji University School of Medicine, Shanghai, China

Myocardial infarction (MI) is a fatal heart disease with high morbidity and mortality. Various studies have demonstrated that a series of relatively specific biological events occur within 24 h of MI. However, the roles of histone modifications in this pathological process are still poorly understood. To investigate the regulation of histone modifications on gene expression in early MI, we performed RNA sequencing (RNA-seq) and chromatin immunoprecipitation sequencing (ChIP-seq) on myocardial tissues 24 h after the onset of MI. The genome-wide profiles of five histone marks (H3K27ac, H3K9ac, H3K4me3, H3K9me3, and H3K27me3) were explored through ChIP-seq. RNA-seq identified 1,032 differentially expressed genes (DEGs) between the MI and sham groups. ChIP-seq analysis found that 195 upregulated DEGs were modified by change of at least one of the three active histone marks (H3K27ac, H3K9ac, and H3K4me3), and the biological processes and pathways analysis showed that these DEGs were significantly enriched in cardiomyocyte differentiation and development, inflammation, angiogenesis, and metabolism. In the transcriptional regulatory network, *Ets1*, *Etv1*, and *Etv2* were predicted to be involved in gene expression regulation. In addition, by integrating super-enhancers (SEs) with RNA-seq data, 76 DEGs were associated with H3K27ac-enriched SEs in the MI group, and the functions of these SE-associated DEGs were mainly related to angiogenesis. Our results suggest that histone modifications may play important roles in the regulation of gene expression in the early stage of MI, and the early angiogenesis response may be initiated by SEs.

Keywords: transcriptome, histone modification, epigenomics, transcription factors, super-enhancer

OPEN ACCESS

Edited by:
Zhihua Wang,
Wuhan University, China

Reviewed by:
Jan Haas,
Heidelberg University Hospital, Germany
Shanshan Li,
Hubei University, China
Maoxiang Qian,
Fudan University, China
Cecilia Winata,
International Institute of Molecular and Cell Biology in Warsaw (IIMCB), Poland

***Correspondence:**
Yi-Han Chen
yihanchen@tongji.edu.cn
Dan Shi
shidan@tongji.edu.cn

† These authors have contributed equally to this work

Specialty section:
This article was submitted to Cardiovascular Genetics and Systems Medicine, a section of the journal Frontiers in Cardiovascular Medicine

Received: *13 August 2020*
Accepted: *20 October 2020*
Published: *30 November 2020*

Citation:
Wang J, Lin B, Zhang Y, Ni L, Hu L, Yang J, Xu L, Shi D and Chen Y-H (2020) The Regulatory Role of Histone Modification on Gene Expression in the Early Stage of Myocardial Infarction. Front. Cardiovasc. Med. 7:594325. doi: 10.3389/fcvm.2020.594325

INTRODUCTION

Myocardial infarction (MI) is a leading cause of death all over the world, mainly caused by acute coronary artery occlusion, which leads to severe myocardial ischemia, and subsequent myocardium necrosis (1). A considerable number of biological events occur in the early stage of MI, such as inflammation, apoptosis, autophagy, and angiogenesis, leading

to ventricular remodeling (2–4). Studies have demonstrated that myocardial pathological changes are mostly reversible, and intervention is more effective during this period (5, 6). Thus, it is of great significance to explore the key molecular events and regulatory mechanisms in the early stage of MI.

Histone modification is a post-translational modification including methylation, acetylation, phosphorylation, ubiquitylation, and SUMOylation, etc. (7), among which the methylation and acetylation of H3K4, H3K9, and H3K27 were common histone marks. Generally, acetylation correlates with transcriptional activation, such as acetylation of histone H3 on lys9 and lys27 (H3K9ac and H3K27ac) (8). Unlike acetylation, the transcriptional activity of methylation modifications on lysine residues varies according to the degree and site of methylation. Tri-methylation of histone H3 on lys9 and lys27 (H3K9me3 and H3K27me3) represents transcriptional suppression, whereas tri-methylation on lys4 (H3K4me3) is associated with transcriptional activation (9, 10).

Super-enhancers (SEs) are characterized as clusters of enhancers, which are enriched with transcription factors, cofactors, and epigenetic modifications, and considered to contain high transcription activity (11). Some enhancer-associated histone modification marks such as H3K27ac can be used to identify SEs (12). Emerging evidences suggest that SEs play important roles in differentiation, development, and tumorigenesis (13–15).

Previous studies had uncovered gene expression changes at the transcription level after MI. The expression of inflammatory response-related genes were reported to be significantly upregulated after MI, which resulted from the activation of NF-κB and TNF signaling pathways (16, 17). However, little is known about the roles of histone modifications and SEs in the early stage of MI. Here, by combining transcriptome and ChIP-seq of key histone modifiers, we set to reveal epigenetic patterns of differentially expressed genes and their roles in the early stage of MI.

MATERIALS AND METHODS

Mouse MI Model

The animal experiments were approved by the Ethics Committee of Tongji University. The mouse model of MI was established by permanent ligation of the left anterior descending (LAD) coronary artery as described previously (18). Briefly, 8-week male C57BL/6 mice were subjected to LAD coronary artery ligation under anesthesia. Sham-operated mice of the same age underwent the same procedure without LAD occlusion. Twenty-four hours after operation, the infarct border zones were dissected, snap-frozen in liquid nitrogen, and stored at −80°C for subsequent experiments.

RNA Isolation

Myocardial tissues from the infarct border zones of MI and sham group were collected for RNA isolation. Five biological replicates were used for each group. Briefly, total RNA was extracted with 1 ml of RNAiso Plus reagent (Takara, 9108). After adding 200 μl of chloroform, the sample was mixed thoroughly and incubated at room temperature for 3 min, then centrifuged at 12,000 g for 15 min at 4°C. The supernatant was transferred to a new Eppendorf tube on ice, mixed with an equal volume of ice-cooled isopropanol, and then centrifuged at 12,000 g for 15 min at 4°C after placing on ice for 10 min. The supernatant was discarded, and the pellet was washed with 75% ice-cooled ethanol three times, and RNA was dissolved in DEPC water.

Chromatin Immunoprecipitation (ChIP) Assay

ChIP was carried out with the SimpleChIP® Plus Sonication Chromatin IP kit (Cell Signaling Technology, 56383) according to the manufacturer's protocol. In brief, three biological replicates of myocardial tissues for each group from the infarct border zones were cross-linked with 1% formaldehyde for 10 min, then terminated by adding glycine. After disaggregating the samples into suspensions using Dounce homogenizer, the chromatins were isolated and sonicated to 100–300 bp fragments. Immunoprecipitation (IP) was performed with antibodies against H3K9me3 (Abcam, ab8898), H3K9ac (Active Motif, 39137), H3K4me3 (Abcam, ab8580), H3K27me3 (Cell Signaling Technology, 9733S), and H3K27ac (Active Motif, 39133). Finally, the chromatins were eluted, and then cross-links were reversed. The immunoprecipitated DNA and DNA input were purified using spin columns.

RNA Sequencing (RNA-Seq) and Analysis

The concentration and quality of RNA were measured by Qubit 4 Fluorometer (Invitrogen™, Q33238). For each group, two biological replicates of isolated RNA above (1 μg total RNA) with RIN > 8 were used for mRNA library construction. RNA sequencing libraries were generated with KAPA mRNA Hyper Prep kits (Roche, KK8581). The libraries were sequenced on an Illumina NovaSeq 6000 platform using a 2* 150-bp sequencing kit for double-ended sequencing.

The raw data were first evaluated by FastQC (v0.11.3). Trimmomatic (v0.36) (19) was applied to remove adaptors, and information of clean reads in RNA-seq data was listed in **Supplementary Table 1**. Clean reads were then mapped to the mouse genome (mm10) using Hisat2 (20), and the mapping rates of clean reads are listed at **Supplementary Table 2**. The sequencing alignment data were evaluated by Qualimap (21), and the coverage of gene bodies is shown in **Supplementary Figure 1.** The counts of genes in each sample were calculated using HTSeq (v0.9.1) (22) and normalized to fragments per kilobase million (FPKM) for further visualization. The raw counts of genes were used to identify differentially expressed genes (DEGs) between sham and MI groups through DESeq2 R package (v1.36.0) (23) with a false discovery rate (FDR) P_{FDR} value < 0.05 and $|\text{Log}_2 \text{ (Fold change)}| \geq 1$. Gene Ontology (GO) and Kyoto Encyclopedia of Genes and Genomes (KEGG) pathway analyses were conducted by R package clusterProfiler (v3.12.0) (24).

ChIP Sequencing (ChIP-Seq) and Analysis

VAHTSTM Universal DNA Library Prep Kit for Illumina® V3 kit (Vazyme, ND607-02) was used to construct the ChIP-DNA library. Three biological replicates for MI group and two

biological replicates for sham group were used for ChIP-seq library construction. The libraries were sequenced on an Illumina NovaSeq 6000 platform. Clean ChIP-seq reads were mapped to the mouse genome (mm10) using bowtie2 (25). To identify the H3K4me3, H3K9me3, H3K9ac, H3K27me3, and H3K27ac peaks, peaks of enriched occupancy relative to a background input were called using MACS 1.4 (26). The peaks were then annotated by the R package ChIPseeker (27) (v1.22.1). Peaks of each histone modification were merged by bedtools (v2.29.2) (28); unique peaks for each group were identified by MAnorm (v1.2.0) (29) software and confirmed by Diffbind R package (v2.14.0) (30). Diffbind R package was used to do the clustering. Hypergeometric optimization of motif enrichment (HOMER) (31) was used to discover motifs of specific regions. The bam files were converted into bigwig files using bedtools (v2.29.2) (28), and then bigwig files were visualized through deeptools (v3.3.0) (32) to generate metagene plots.

Quantitative Real-Time Quantitative Polymerase Chain Reaction (qRT-PCR) and ChIP-qPCR

Total RNA was reversely transcribed into cDNA with the PrimeScript RT reagent kit (Takara, RR036Q, Japan). qRT-PCR assays were performed in five biological replicates. The reaction volume of real-time qPCR is 20 μl, containing 10 μl of SYBR Green Master Mix (ABI, 4309155, USA), 4 μl cDNA, and 1 μl forward and reverse primers, the primers are listed in **Supplementary Table 3**. The relative gene expression was calculated with the $2^{-\Delta\Delta Ct}$ method. ChIP-qPCR was performed with 20 μl of reaction volume, containing 10 μl of SYBR Green Master Mix, 1 μl of forward and reverse primers, 2 μl of DNA, and 6 μl of H_2O. ChIP DNA enrichment was calculated as % of input, and the primers are listed in **Supplementary Table 3**. All qPCR assays were performed in three biological replicates.

Identification of Typical and Super-Enhancers

Ranking of super-enhancer (ROSE) (11) was applied to call typical enhancers (TEs) and super-enhancers (SEs). In brief, H3K27ac peaks with the distance shorter than 12.5 kb were merged and ranked by the H3K27ac signal. The inflection point with the tangent line slope equals 1 was the dividing point of TEs and SEs. Enhancers above or below the point were defined as SEs and TEs, respectively. The genes that were closest to the enhancers were considered as enhancer-associated genes. For the expression of enhancer-associated genes, the Wilcoxon rank sum test was performed to test statistical significance between two groups.

RESULTS

Transcriptomic Analysis and Histone Modification Profiling

Adult C57/BL6 mice (8 weeks old) were subjected to ligation of left anterior descending (LAD) or sham surgery randomly. The mice were sacrificed 24 h after the surgery, and the left ventricular tissues in the infarct border zone and normal tissues in the corresponding position were dissected to examine the expression profile of MI and sham groups by RNA-seq. The quality of the clean reads and mapping rates of RNA-seq are shown in **Supplementary Tables 1, 2**, and **Supplementary Figure 1**. Differentially expressed genes (DEGs), 1,032, between the MI and sham groups were identified by RNA-seq with an absolute log-fold change over or equal to 1 (adjusted P-value < 0.05) (**Figure 1B**, **Supplementary Table 4**). Among them, 423 (40.99%) and 609 (59.01%) genes were upregulated and downregulated, respectively, in the MI group. DEGs, 428 (41.47%), in our RNA-seq data, were overlapped with the DEGs from cardiac organoid model of human myocardial infarction (GSE113871, **Supplementary Figure 2**). Moreover, the expression of representative cardiac remodeling-related genes (*Nppa* and *Nppb*) was significantly increased in the MI group (**Supplementary Figure 3A**), which demonstrated the credibility of our MI models. We further performed qRT-PCR to validate the mRNA expression of *Nppa*, *Nppb*, and *Myh7* in samples both 24 and 48 h after MI. The expression of *Nppa* and *Nppb* increased in 24 h after MI, and then decreased in 48 h after MI (**Supplementary Figure 3B**). The upregulated genes were enriched in the function of muscle structure development, angiogenesis, positive regulation of cell death, muscle cell development, and ribosomal large subunit biogenesis. In contrast, downregulated genes were enriched in the establishment of organelle localization, oocyte meiosis, positive regulation of potassium ion transmembrane transport, flavonoid glucuronidation, and mitotic cell cycle process (**Figure 1C**).

To profile epigenetic changes in the early stage of MI, we selected H3K27ac, H3K9ac, and H3K4me3 (three marks associated with active regulatory regions) and H3K9me3 and H3K27me3 (two marks associated with repressive regulatory regions) antibodies to perform ChIP-Seq (**Figure 1A**). Hierarchical clustering demonstrated that these histone marks were mainly divided into three clusters (**Figure 1D**). While H3K9me3 and H3K27me3 (two marks associated with repressive regulatory regions) formed two separate clusters, interestingly, all the marks associated with active regulatory regions (H3K27ac, H3K9ac, and H3K4me3) formed a big cluster, suggesting that the active regions might be modified by multiple active histone marks. We then quantified peaks of different histone marks in genomic regions, the number of which was similar between MI and sham groups (**Figure 1D**). The numbers of peaks of different histone marks and the statistical information of sequencing reads are shown in **Table 1** and **Supplementary Figure 4**. The distribution of genomic regions modified by H3K27ac, H3K27me3, H3K4me3, H3K9ac, and H3K9me3 was classified into six regions (promoter, exon, 3′ UTR, 5′ UTR, intron, and intergenic). The H3K4me3 and H3K9ac marks were mainly mapped to promoters; H3K27ac and H3K27me3 marks were mapped to promoters, intron, and intergenic regions, and H3K9me3 marks were mostly mapped to intergenic regions (**Figure 1E**), which were consistent with the reported distribution modes of these histone marks (33).

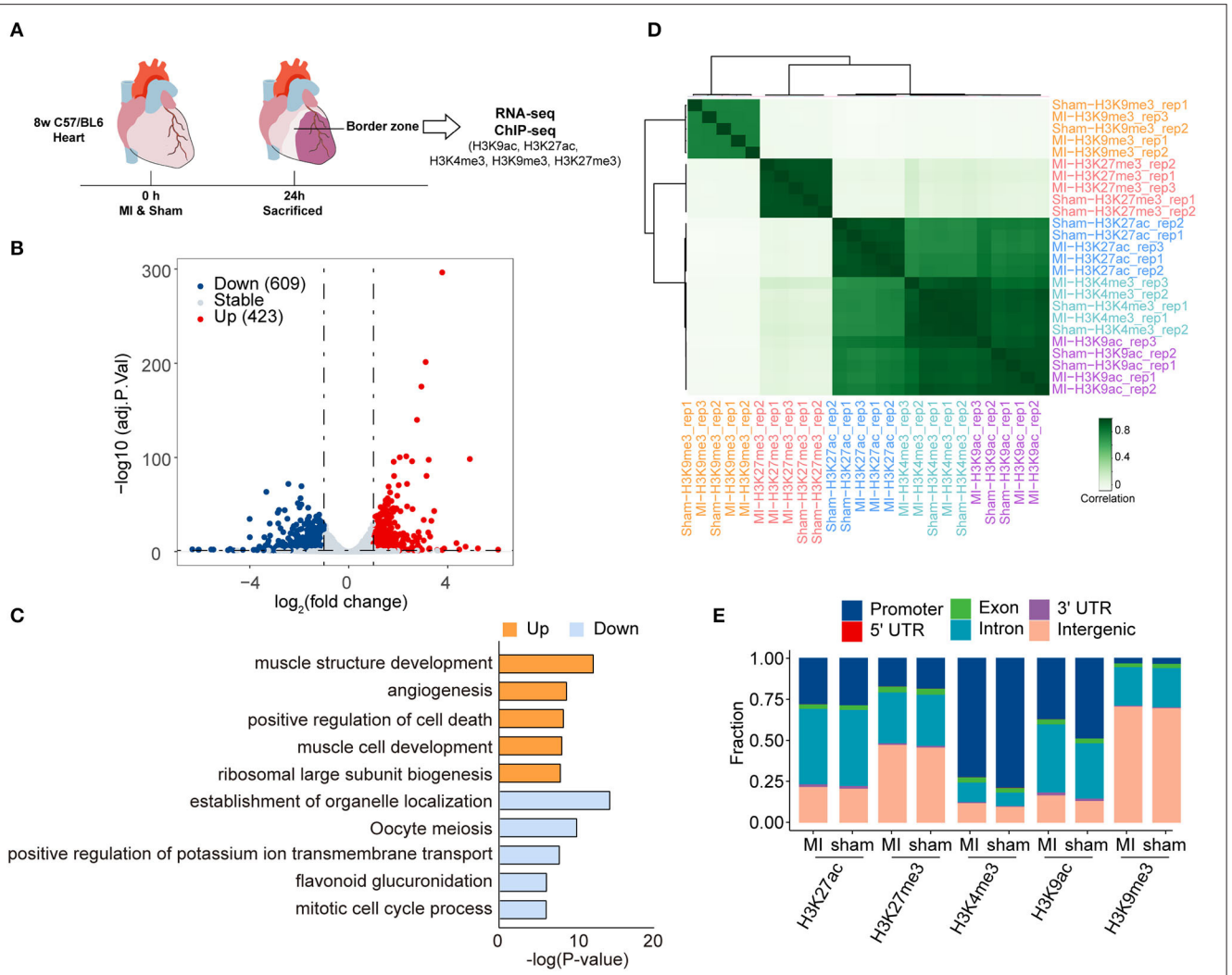

FIGURE 1 | Transcriptome analysis and histone modification profiling in the early stage of myocardial infraction (MI), **(A)** Schematic illustration of the present study. **(B)** Volcano plots showing the differentially expressed genes (DEGs) between sham and MI groups. Blue dots represent downregulated genes, and red dots represent upregulated genes. **(C)** Gene ontology (GO) analysis of the differentially expressed genes (DEGs) in RNA-seq. Orange bras represent the enrichment of upregulated genes; blue bars represent the enrichment of downregulated genes. **(D)** Hierarchical clustering of H3K9ac, H3K9me3, H3K27ac, H3K27me3, and H3K4me3 occupancy at genome wide in sham and MI group. Spearman correlation coefficient was used to calculate sample correlations. **(E)** The genomic distribution of different histone modification regions in sham and MI groups.

Epigenetic Profile Changes

To reveal the difference in histone modifications between MI and sham, we drew the average signals of histone marks relative to ±3 kb of the transcription start site (TSS) (**Figure 2A**). The average signals of active histone marks (H3K27ac, H3K4me3, and H3K9ac) were all higher in MI than those in the sham group. The signals of H3K9me3 in MI group were relatively lower than those in the sham group, while no apparent changes in H3K27me3 were observed between sham and MI. We identified 3,986 MI unique peaks for H3K27ac mark, 5,417 peaks for H3K27me3 mark, 1,910 peaks for H3K4me3 mark, 12,084 peaks for H3K9ac mark, and 937 peaks for H3K9me3 mark in the TSS ± 3 kb (**Figure 2B** and **Supplementary Tables 5–9**). We then performed gene ontology (GO) analysis to investigate the biological function of these MI unique peaks of each histone mark and discovered that the MI unique peaks of H3K27ac (2,778 mapped genes) were highly enriched in small GTPase-mediated signal transduction, H3K27me3 (3,325 mapped genes) in cell-substrate adhesion, H3K4me3 (1,500 mapped genes) in the process of inflammatory response, and H3K9ac (6,547 mapped genes) in small GTPase mediated signal transduction (**Figure 2C**).

Active Chromatin Regions Associated With the Upregulated Genes

Notably, there were few overlapped genes between downregulated genes in RNA-seq and unique peaks in repressive histone marks (**Supplementary Figure 5B**). Thus, we mainly

TABLE 1 | Information of the peaks called in different samples.

ID	Clean reads	Mapped reads	Mapped rate (%)	Number of peaks	Total length of peaks	Average length of peaks
MI24-input_rep1	59,329,700	57,982,915	97.73			
MI24-input_rep2	48,793,596	47,954,346	98.28			
MI24-input_rep3	73,326,196	72,145,644	98.39			
MI24-H3K27ac_rep1	55,638,462	52,016,398	93.49	46,521	153,946,563	3,309.18
MI24-H3K27ac_rep2	48,204,386	47,539,165	98.62	43,004	146,496,195	3,406.57
MI24-H3K27ac_rep3	58,656,804	57,536,459	98.09	50,192	156,520,708	3,118.44
MI24-H3K27me3_rep1	63,728,706	62,568,843	98.18	31,551	112,026,446	3,550.65
MI24-H3K27me3_rep2	51,994,578	51,282,252	98.63	26,864	106,249,613	3,955.09
MI24-H3K27me3_rep3	57,951,114	56,896,403	98.18	38,652	143,281,067	3,706.95
MI24-H3K4me3_rep1	61,403,310	60,193,664	98.03	17,023	41,311,218	2,426.79
MI24-H3K4me3_rep2	46,460,220	45,763,316	98.5	16,072	38,907,043	2,420.8
MI24-H3K4me3_rep3	65,778,746	64,318,457	97.78	20,150	50,138,955	2,488.29
MI24-H3K9ac_rep1	51,708,148	50,761,888	98.17	24,819	64,439,753	2,596.39
MI24-H3K9ac_rep2	37,375,860	35,981,740	96.27	32,902	78,887,608	2,397.65
MI24-H3K9ac_rep3	58,058,296	57,077,110	98.31	42,726	122,678,660	2,871.29
MI24-H3K9me3_rep1	58,645,664	57,437,563	97.94	19,934	36,535,935	1,832.85
MI24-H3K9me3_rep2	46,441,950	45,568,841	98.12	19,821	34,529,866	1,742.08
MI24-H3K9me3_rep3	58,184,316	56,671,523	97.4	23,662	41,583,430	1,757.39
Sham-input_rep1	65,704,850	64,574,726	98.28			
Sham-input_rep2	54,637,390	53,675,771	98.24			
Sham-H3K27ac_rep1	58,613,224	57,739,886	98.51	49,891	160,041,629	3,207.83
Sham-H3K27ac_rep2	51,299,442	50,545,340	98.53	44,392	125,831,890	2,834.56
Sham-H3K27me3_rep1	59,835,338	58,429,207	97.65	35,099	136,040,218	3,875.9
Sham-H3K27me3_rep2	51,733,232	50,734,780	98.07	36,054	113,291,599	3,142.28
Sham-H3K4me3_rep1	48,939,496	48,229,873	98.55	16,772	37,584,277	2,240.89
Sham-H3K4me3_rep2	58,911,408	57,462,187	97.54	17,218	42,505,603	2,468.67
Sham-H3K9ac_rep1	53,257,144	52,421,006	98.43	29,625	84,340,323	2,846.93
Sham-H3K9ac_rep2	56,017,696	55,059,793	98.29	26,963	74,877,575	2,777.05
Sham-H3K9me3_rep1	52,185,442	51,167,825	98.05	21,950	35,551,960	1,619.68
Sham-H3K9me3_rep2	52,790,998	51,756,294	98.04	22,301	37,809,809	1,695.43

study the regulation of histone modification on upregulated genes; we intersected the 423 activated genes in RNA-seq [Log2 (fold change) $\geq$ 1, adjusted *P*-value $<$ 0.05] with 7,226 open regions (the gain of active marks H3K9ac, H3K27ac, and H3K4me3 in the $\pm$2 kb from TSS). A total of 195 activated genes were enriched for at least one of H3K9ac (145/195), H3K27ac (79/195), or H3K4me3 (59/195) marks (**Figure 3A**, **Supplementary Figure 6**, and **Supplementary Table 10**). According to our pipeline, we further validated the 195 activated genes revealed by another method (Diffbind), which also identifies differential peaks. Of the genes, 42.05% (82/195) were shared by the two methods (**Supplementary Figure 5A** and **Supplementary Table 11**). We also checked the other 113 genes, which were not identified by Diffbind in genome browser. Most of the promoter regions of the 113 genes did have more active modifications in MI group than that in sham group. We then performed GO analysis to categorize the biological function of the 195 upregulated DEGs and found that they were mainly enriched in muscle cell-related processes (striated muscle cell development, muscle cell differentiation, muscle cell development), inflammatory response processes (leukocyte migration, negative regulation of response to external stimulus, myeloid leukocyte migration, leukocyte chemotaxis) and angiogenesis-related processes (regulation of vasculature development, positive regulation of vasculature development, and regulation of angiogenesis) (**Figure 3B**). KEGG analysis indicated that inflammatory-related signaling pathways, including TNF signaling pathway, IL-17 signaling pathway, and cytokine–cytokine receptor interaction; cell signal-related pathways (PI3K-Akt signaling pathway and MAPK signal pathway); ECM–receptor interaction and HIF-1 signaling pathways were activated in the process of MI (**Figure 3C**). The inflammatory response processes and pathways were revealed by enrichment analysis, and inflammatory response-related genes are shown in **Figure 3D**. Two typical genes (*Cxcl2* and *Cxcl3*) are shown in **Figures 3E,F**, with increasing H3K4me3, H3K9ac, and H3K27ac signals at the promoter or increasing H3K27ac signals at the enhancer region of *Cxcl2* and *Cxcl3* loci in MI group. ChIP-qPCR and RT-qPCR verified elevated H3K27ac modification in promoter

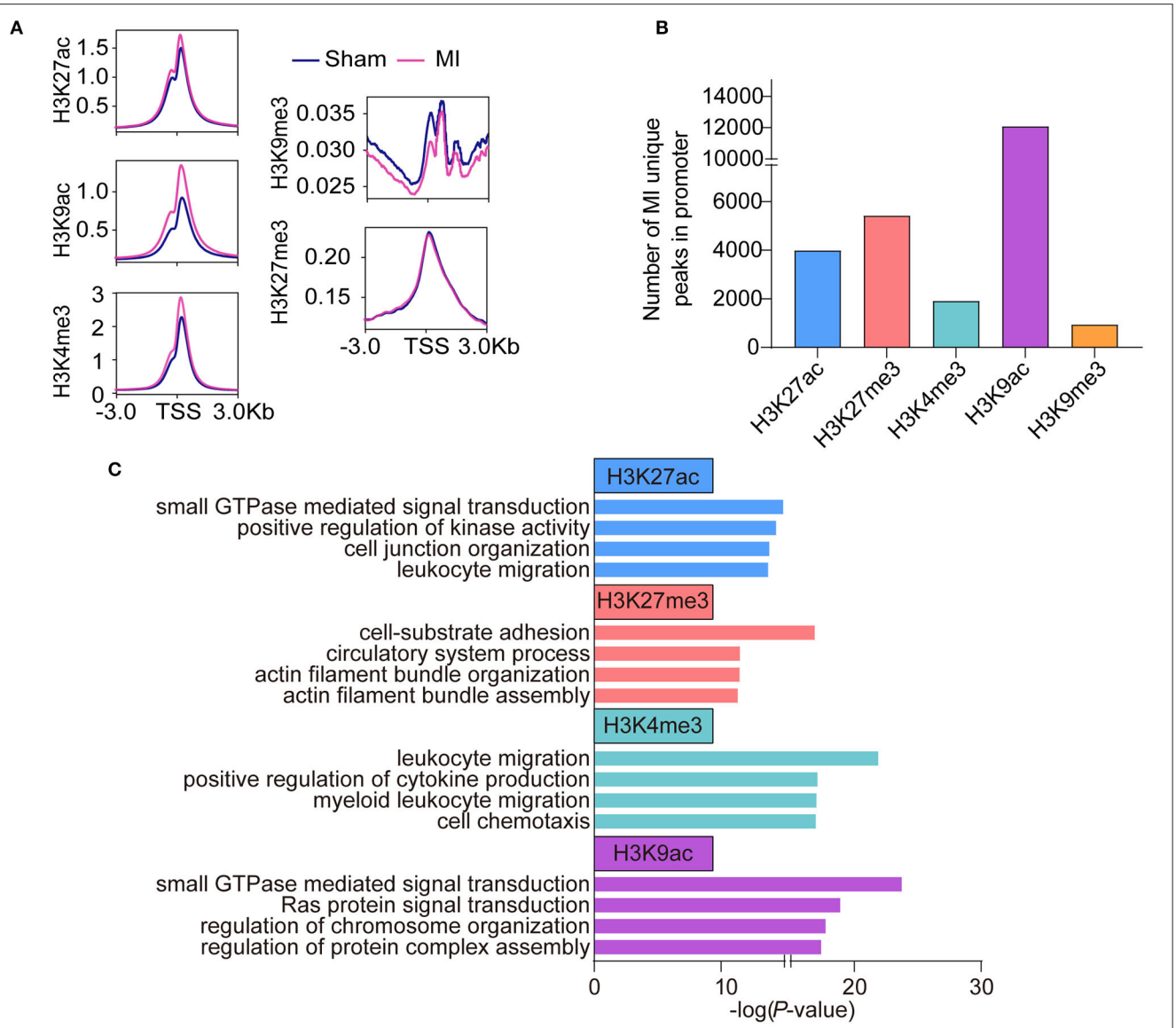

FIGURE 2 | Epigenetic profile change in the early stage of MI. **(A)** The average signals of each histone mark relative to ±3 kb of the transcription start site (TSS) between the sham and MI group. **(B)** The number of MI unique peaks in promoters of H3K9ac, H3K9me3, H3K27ac, H3K27me3, and H3K4me3 marks. **(C)** GO analysis of the MI unique peaks in promoters of H3K9ac, H3K27ac, H3K27me3, and, H3K4me3 marks.

regions and elevated expression of *Cxcl2* and *Cxcl3*, respectively (**Figures 3G,H**).

Moreover, to identify the transcription factors, which may regulate the upregulated genes in MI, we performed motif analysis at the promoter regions of unique peaks of three active marks (H3K27ac, H3K9ac, and H3K4me3) in the MI group. Hypergeometric optimization of motif enrichment (HOMER) was employed to identify top enriched motifs, which showed that motifs for transcription factors including ETS1 (*P*-value = 1e-15), ETV1 (*P*-value = 1e-14), and ETV2 (P-value = 1e-11) were significantly enriched in promoters of upregulated genes associated with active histone marks (**Figure 3I** and **Supplementary Table 12**).

Identification of MI-Specific SEs

The above data showed that the signal of H3K27ac was notably higher in the early stage of MI (**Figure 2A**). H3K27ac is also an active TE and SE marker; however, little is known about the function of SEs in the early stage of MI. We identified 20,337 TEs and 1,672 SEs in the sham group, and 21,444 TEs and 1,723 SEs in the MI group (**Figure 4A**), showing more enhancers activated in the MI group. Many SE-associated genes, such as *Per2*, *Adamts1*, *Ccl2*, *Pgf*, *Thbs1*, and *Tgfb2*, were known to be related to angiogenesis. Expression levels of SE-associated transcripts in MI were significantly higher than those of TE-associated transcripts (**Figure 4B**). SEs, 1,723, in the MI group were mapped to 1,565 SE-associated genes, and 76 SEs in the MI group were

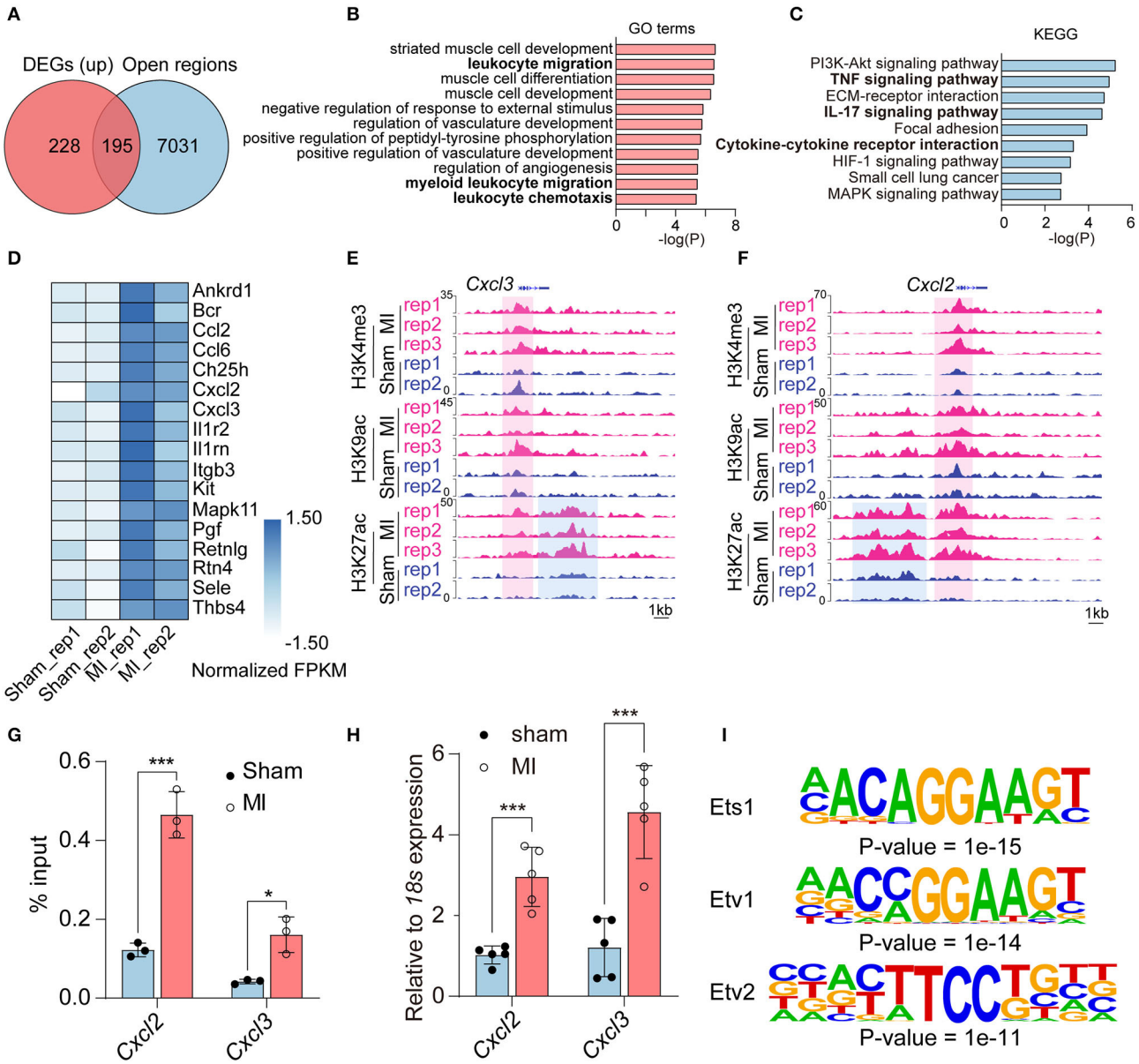

FIGURE 3 | The upregulated genes associated with gain of active histone marks. **(A)** Venn diagram showing upregulated DEGs associated with the open regions in the promoters (gain of H3K9ac, H3K27ac, and H3K4me3 marks in the ±2 kb from TSS). **(B)** GO analysis of the upregulated DEGs enriched in promoters (±2 kb from TSS) of H3K9ac, H3K27ac, and H3K4me3 marks. **(C)** Kyoto Encyclopedia of Genes and Genomes (KEGGs) pathway enrichment analysis of the upregulated DEGs enriched in promoters (±2 kb from TSS) of H3K9ac, H3K27ac, and H3K4me3 marks. **(D)** Heatmap showing the relative expression fragments per kilobase million (FPKM) of genes related to inflammatory response processes. **(E,F)** The increased active histone marks at promoters and enhancers of *Cxcl2* and *Cxcl3* in MI compared with the sham group. **(G)** ChIP-qPCR validation of the distribution of H3K27ac changes in *Cxcl2* and *Cxcl3*. **(H)** qPCR validation of the expression of *Cxcl2* and *Cxcl3*. **(I)** The transcription factors and binding motifs identified at promoter regions of upregulated DEGs enriched for H3K9ac, H3K27ac, and H3K4me3. $n = 3$; $^{*}P < 0.05$, $^{***}P < 0.001$.

in accordance with DEGs, which can be further categorized into 32 MI unique SEs and 44 common SEs (**Figure 4C**). We then performed GO analysis for the 76 SEs associated DEGs and found that about half of the differentially expressed SE-associated genes were enriched in the function of angiogenesis (**Figure 4D**), and the specific genes in the angiogenesis-related GO terms are listed in **Figure 4E**. In addition, SEs that were not connected with DEGs were mainly enriched in actin filament-based process (actin filament organization, muscle organ development, regulation of actin filament-based process, lamellipodium organization, and assembly) and cell migration (**Supplementary Figure 7**). Two representative MI SE-associated genes *Itgb2* and *Ccl2* are shown in **Figure 4F**, whose H3K27ac occupancy of some component enhancers in the MI group was higher than that

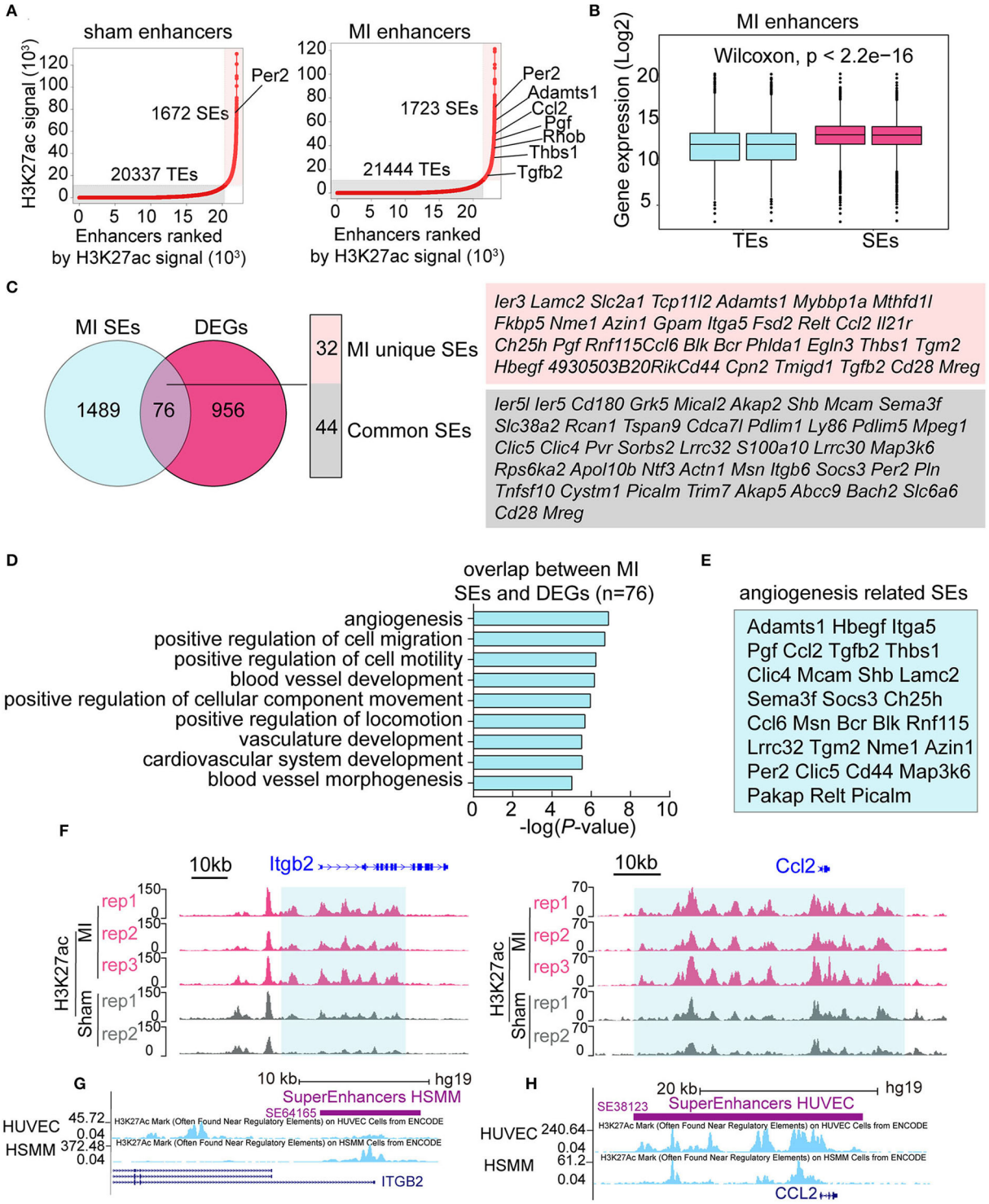

FIGURE 4 | Identification of MI specific super-enhancers (SEs). **(A)** Ranked plots of typical enhancers (TEs) and super enhancers (SEs) in the sham and MI group by increasing H3K27ac signal (normalized by the ratio to the highest H3K27ac reads of the enhancer). The axes values represent the ranks of enhancers by H3K27ac signal. Angiogenesis-related genes are marked out in the figures. **(B)** The expression (Log_2) of TE-associated genes vs. SE-associated genes in the MI group. *P*-value was determined by the Wilcoxon test. **(C)** Overlapping genes of DEGs and SE-associated genes in the MI group. The MI unique SE-associated genes and common SE-associated genes are listed. **(D)** GO analysis of the 76 overlapping genes between DEGs and SE-associated genes in the MI group. **(E)** The specific genes in the angiogenesis-related GO terms. **(F)** The H3K27ac occupancy of two representative angiogenesis-related genes *Itgb2* and *Ccl2* is shown. The red and gray peaks, respectively, mean MI and sham group. **(G,H)** *Itgb2*- and *Ccl2*-associated SEs on human umbilical vein endothelial cells (HUVECs) and human skeletal muscle myoblasts (HSMM) from ENCODE project.

in the sham group. *Itgb2- and Ccl2*-associated SEs can also be validated on the human umbilical vein endothelial cells (HUVEC) and human skeletal muscle myoblasts (HSMM) from ENCODE database (**Figures 4G,H**). Our analysis identified a set of SEs, which might be essential for the early response of MI and suggested that MI-induced global changes in SEs might coordinate with angiogenesis.

DISCUSSION

In this study, we correlated histone modifications to gene expression in the early stage of MI via integrative analysis of the transcriptome and ChIP-seq of histone marks. The biological processes of the upregulated DEGs modified by active marks (H3K9ac, H3K27ac, and H3K4me3) were enriched in cardiomyocyte differentiation and development, inflammation, and angiogenesis. Pathways implicated in the pathological processes of MI were activated, such as inflammation and metabolism-related pathways. Transcription factors, including ETS1, ETV1, and ETV2, may be involved in the transcriptional regulation of molecular events in the early stage of MI. Moreover, a set of SE-associated genes related to angiogenesis were also uncovered.

It is worth noting that inflammatory response was enriched in both function (GO) and pathway (KEGG) analysis, and H3K9ac, H3K27ac, and H3K4me3 regulated the expression of critical chemokines in the early stage of MI. After the occurrence of MI, chemokines were generated in injured myocardium, bound to the endothelial surface and extracellular matrix through glycosaminoglycans, and interacted with receptors on the surface of leukocytes to promote trafficking (34). CC and CXC, two main subtypes of chemokines, were significantly increased in infarcted tissue, which mediated leukocyte migration into the injured myocardium after MI (35, 36). Chemokines played a vital role in the inflammatory response and were associated with cardiac injury, repair, and remodeling following MI (36, 37). Our study showed that the expression of *Ccl2*, *Ccl6*, *Cxcl2*, *Cxcl3*, was upregulated and modified by H3K9ac, H3K27ac, and H3K4me3 marks. *Ccl2* and *Cxcl2* were two widely studied chemokines, which belong to the CC and CXC subtypes. *Ccl2* played an important role in recruiting and activating mononuclear cells, and inhibiting *Ccl2* reduced the infarct size and ameliorated the cardiac remolding after MI (38, 39). Meanwhile, *Cxcl2* mediated the recruitment of neutrophils in the inflammatory response and is involved in the occurrence and development of many cardiovascular diseases, including atherosclerosis, ischemic stroke, and myocardial infarction (40). Studies have demonstrated that highly expressed *Cxcl2* may exacerbate myocardial injury and inhibition of *Cxcl2* reduced neutrophil-mediated tissue injury and infarct size after MI (41–43). Our results revealed that these active histone marks increased at the promoter regions and may promote the expression of these key chemokines after MI. Moreover, biological processes related to cardiomyocyte differentiation and development were also enriched. Among them, *Csrp3*, *Pdlim5*, *Sorbs2*, *Rcan1*, and *Acta1*, which were related to cardiac hypertrophy and remodeling, were upregulated and modified by at least one active histone mark. Altogether, these results indicated that H3K9ac, H3K27ac, and H3K4me3 modifications might participate in cardiac remodeling by regulating the inflammatory response.

In order to get the transcription factors that coordinated the transcriptional regulatory network in the early stage of MI, we performed motif analysis and identified ETS1, ETV1, and ETV2. All three transcription factors were members of the ETS family. ETS1 was associated with fibrotic remodeling of the myocardium (44). ETV1 was involved in atrial remodeling and arrhythmia (45). ETV2 was reported to promote angiogenesis and improve myocardial repair after MI (46). These transcription factors may work with active histone modifications to regulate gene expression in the early stage of MI.

Super enhancers (SEs) were first identified as a large cluster of enhancers with the strong binding of transcription factors that drive the expression of cell identity genes (11). It has been reported that SEs mediate angiotensin II-induced vascular smooth muscle cell dysfunction (47), whereas their roles in MI were less known. In our study, we investigated the function of SEs in MI. We intersected SEs with DEGs and found that 76 DEGs may be regulated by SEs. These SEs can be further categorized into 32 MI unique SEs and 44 common SEs. We then performed GO analysis for the 76 DEGs and found that these genes were significantly enriched in angiogenesis. Angiogenesis after MI is considered to be an important factor leading to ventricular remodeling (48, 49), and neovascularization induced by angiogenic growth factors reduces the infarct size and improves ventricular remodeling (50, 51). Our results showed that SEs might mediate the transcription of angiogenesis-related genes at the border zone in the early stage of MI, consistent with the previous report that angiogenesis initiated in the border zone at the early stage post-MI (52). Moreover, some of these genes have been reported to be associated with angiogenesis in MI, such as *Pgf* and *Ccl2*. *Pgf* (placental growth factor) was reported to promote angiogenesis and myocardial repair post-MI (53, 54). *Ccl2* may be implicated in angiogenesis in ischemic myocardial tissue by attracting macrophages capable of producing angiogenic factors and by exerting direct pro-angiogenesis effects through endothelial cells (36, 55). Apart from SEs, which were associated with DEGs, SEs that were not connected with DEGs were significantly enriched in actin filament-based process and cell migration. These SE-associated genes may remain in a poised status in early MI and participate in the process of cardiac remodeling in the later stage of MI. A representative gene with broad and high levels of H3K27ac signal is *Itgb2*, which mediated the migration and recruitment of endothelial progenitor cells and angiogenesis in the infarcted myocardium (56). Taken together, the transcriptional regulation of angiogenesis-related genes by SEs in the early stage of MI may initiate vascular regeneration and promote repair of damaged myocardium post-MI, which may prevent pathological cardiac remodeling.

Our study also has limitations. We mainly focused on promoters and SEs, while other regulatory elements of gene expression in the early stage of MI were not investigated, which might lead to underestimation of the roles of histone

modifications in the early stage of MI. Besides, we only selected five histone marks to study the regulation of histone modification on gene expression in MI; the roles of other histone marks in MI were not investigated. Moreover, the results were based on a mouse model of MI, so further observation and validation in human samples are needed.

In summary, our study revealed the histone modification profile in the early stage of MI in mice and demonstrated that the modulation of histone modifications (H3K9ac, H3K27ac, and H3K4me3) might be involved in inflammation and angiogenesis by regulating promoters and SEs, and participating in the pathological processes of cardiac remodeling.

DATA AVAILABILITY STATEMENT

All the sequencing results have been uploaded and deposited in the NCBI Sequence Read Archive database (https://www.ncbi.nlm.nih.gov/bioproject/PRJNA657342) under accession No. SRP277594.

ETHICS STATEMENT

The animal study was reviewed and approved by Ethics Committee of Tongji University.

AUTHOR CONTRIBUTIONS

Y-HC and DS conceived and coordinated the study. YZ and JW constructed the MI models of mice and collected the samples. JW, YZ, LN, and LH constructed the library for RNA-seq and ChIP-seq and performed some experiments. BL made the bioinformatic analysis of RNA-seq and ChIP-seq and drew the figures. JW drafted the manuscript. JY and LX conducted and gave advice on the study. Y-HC, JY, DS, and BL reviewed and revised the manuscript. All authors have approved the final version of the manuscript.

FUNDING

This work was funded by the Grants from the National Key Research and Development Plan (2019YFA0801501 to Y-HC, 2018YFC1312504 to LX), the Programs of National Natural Science Foundation of China (81530017, 81930013, and 81770397 to Y-HC), the Key Disciplines Group Construction Project of Pudong Health Bureau of Shanghai (PWZxq2017-05), the Top-level Clinical Discipline Project of Shanghai Pudong District (PWYgf2018-02), the Research Unit of Origin and Regulation of Heart Rhythm, and the Chinese Academy of Medical Sciences (2019RU045). Y-HC was a Fellow at the Collaborative Innovation Center for Cardiovascular Disease Translational Medicine, Nanjing Medical University.

ACKNOWLEDGMENTS

We thank Dr. Feizhen Wu for comments on the data analyses and insightful scientific discussions.

SUPPLEMENTARY MATERIAL

The Supplementary Material for this article can be found online at: https://www.frontiersin.org/articles/10.3389/fcvm.2020.594325/full#supplementary-material

REFERENCES

1. Anderson JL, Morrow DA. Acute myocardial infarction. *N Engl J Med.* (2017) 376:2053–64. doi: 10.1056/NEJMra1606915
2. Kanamori H, Takemura G, Goto K, Maruyama R, Tsujimoto A, Ogino A, et al. The role of autophagy emerging in postinfarction cardiac remodelling. *Cardiovasc Res.* (2011) 91:330–9. doi: 10.1093/cvr/cvr073
3. Wang X, Guo Z, Ding Z, Mehta JL. Inflammation, autophagy, and apoptosis after myocardial infarction. *J Am Heart Assoc.* (2018) 7:e008024. doi: 10.1161/JAHA.117.008024
4. Xiang F, Shi Z, Guo X, Qiu Z, Chen X, Huang F, et al. Proteomic analysis of myocardial tissue from the border zone during early stage post-infarct remodelling in rats. *Eur J Heart Fail.* (2011) 13:254–63. doi: 10.1093/eurjhf/hfq196
5. Opie LH, Commerford PJ, Gersh BJ, Pfeffer MA. Controversies in ventricular remodelling. *Lancet.* (2006) 367:356–67. doi: 10.1016/S0140-6736(06)68074-4
6. Cohn JN, Ferrari R, Sharpe N. Cardiac remodeling–concepts and clinical implications: a consensus paper from an international forum on cardiac remodeling. Behalf of an international forum on cardiac remodeling. *J Am Coll Cardiol.* (2000) 35:569–82. doi: 10.1016/S0735-1097(99)00630-0
7. Bannister AJ, Kouzarides T. Regulation of chromatin by histone modifications. *Cell Res.* (2011) 21:381–95. doi: 10.1038/cr.2011.22
8. Shahbazian MD, Grunstein M. Functions of site-specific histone acetylation and deacetylation. *Annu Rev Biochem.* (2007) 76:75–100. doi: 10.1146/annurev.biochem.76.052705.162114
9. Black JC, Van Rechem C, Whetstine JR. Histone lysine methylation dynamics: establishment, regulation, biological impact. *Mol Cell.* (2012) 48:491–507. doi: 10.1016/j.molcel.2012.11.006
10. Kouzarides T. Chromatin modifications and their function. *Cell.* (2007) 128:693–705. doi: 10.1016/j.cell.2007.02.005
11. Whyte WA, Orlando DA, Hnisz D, Abraham BJ, Lin CY, Kagey MH, et al. Master transcription factors and mediator establish super-enhancers at key cell identity genes. *Cell.* (2013) 153:307–19. doi: 10.1016/j.cell.2013.03.035
12. Hnisz D, Abraham BJ, Lee TI, Lau A, Saint-Andre V, Sigova AA, et al. Super-enhancers in the control of cell identity and disease. *Cell.* (2013) 155:934–47. doi: 10.1016/j.cell.2013.09.053
13. Sun X, Ren Z, Cun Y, Zhao C, Huang X, Zhou J, et al. Hippo-YAP signaling controls lineage differentiation of mouse embryonic stem cells through modulating the formation of super-enhancers. *Nucleic Acids Res.* (2020) 48:7182–96. doi: 10.1093/nar/gkaa482
14. Wang X, Cairns MJ, Yan J. Super-enhancers in transcriptional regulation and genome organization. *Nucleic Acids Res.* (2019) 47:11481–96. doi: 10.1093/nar/gkz1038
15. Thandapani P. Super-enhancers in cancer. *Pharmacol Ther.* (2019) 199:129–38. doi: 10.1016/j.pharmthera.2019.02.014
16. Li Y, Wang C, Li T, Ma L, Fan F, Jin Y, et al. The whole transcriptome and proteome changes in the early stage of myocardial infarction. *Cell Death Discov.* (2019) 5:73. doi: 10.1038/s41420-019-0152-z
17. Zhao Q, Wu K, Li N, Li Z, Jin F. Identification of potentially relevant genes for myocardial infarction using RNA sequencing data analysis. *Exp Ther Med.* (2018) 15:1456–64. doi: 10.3892/etm.2017.5580

18. Li L, Weng Z, Yao C, Song Y, Ma T. Aquaporin-1 deficiency protects against myocardial infarction by reducing both edema and apoptosis in mice. *Sci Rep.* (2015) 5:13807. doi: 10.1038/srep13807
19. Bolger AM, Lohse M, Usadel B. Trimmomatic: a flexible trimmer for illumina sequence data. *Bioinformatics.* (2014) 30:2114–20. doi: 10.1093/bioinformatics/btu170
20. Kim D, Langmead B, Salzberg SL. HISAT: a fast spliced aligner with low memory requirements. *Nat Methods.* (2015) 12:357–60. doi: 10.1038/nmeth.3317
21. Garcia-Alcalde F, Okonechnikov K, Carbonell J, Cruz LM, Gotz S, Tarazona S, et al. Qualimap: evaluating next-generation sequencing alignment data. *Bioinformatics.* (2012) 28:2678–9. doi: 10.1093/bioinformatics/bts503
22. Anders S, Pyl PT, Huber W. HTSeq–a python framework to work with high-throughput sequencing data. *Bioinformatics.* (2015) 31:166–9. doi: 10.1093/bioinformatics/btu638
23. Love MI, Huber W, Anders S. Moderated estimation of fold change and dispersion for RNA-seq data with DESeq2. *Genome Biol.* (2014) 15:550. doi: 10.1186/s13059-014-0550-8
24. Yu G, Wang LG, Han Y, He QY. clusterProfiler: an R package for comparing biological themes among gene clusters. *Omics.* (2012) 16:284–7. doi: 10.1089/omi.2011.0118
25. Langmead B, Salzberg SL. Fast gapped-read alignment with bowtie 2. *Nat Methods.* (2012) 9:357–9. doi: 10.1038/nmeth.1923
26. Zhang Y, Liu T, Meyer CA, Eeckhoute J, Johnson DS, Bernstein BE, et al. Model-based analysis of ChIP-Seq (MACS). *Genome Biol.* (2008) 9:R137. doi: 10.1186/gb-2008-9-9-r137
27. Yu G, Wang LG, He QY. ChIPseeker: an R/Bioconductor package for ChIP peak annotation, comparison and visualization. *Bioinformatics.* (2015) 31:2382–3. doi: 10.1093/bioinformatics/btv145
28. Quinlan AR, Hall IM. BEDTools: a flexible suite of utilities for comparing genomic features. *Bioinformatics.* (2010) 26:841–2. doi: 10.1093/bioinformatics/btq033
29. Shao Z, Zhang Y, Yuan GC, Orkin SH, Waxman DJ. MAnorm: a robust model for quantitative comparison of ChIP-Seq data sets. *Genome Biol.* (2012) 13:R16. doi: 10.1186/gb-2012-13-3-r16
30. Ross-Innes CS, Stark R, Teschendorff AE, Holmes KA, Ali HR, Dunning MJ, et al. Differential oestrogen receptor binding is associated with clinical outcome in breast cancer. *Nature.* (2012) 481:389–93. doi: 10.1038/nature10730
31. Heinz S, Benner C, Spann N, Bertolino E, Lin YC, Laslo P, et al. Simple combinations of lineage-determining transcription factors prime cis-regulatory elements required for macrophage and B cell identities. *Mol Cell.* (2010) 38:576–89. doi: 10.1016/j.molcel.2010.05.004
32. Ramirez F, Ryan DP, Gruning B, Bhardwaj V, Kilpert F, Richter AS, et al. deepTools2: a next generation web server for deep-sequencing data analysis. *Nucleic Acids Res.* (2016) 44:W160–5. doi: 10.1093/nar/gkw257
33. Papait R, Cattaneo P, Kunderfranco P, Greco C, Carullo P, Guffanti A, et al. Genome-wide analysis of histone marks identifying an epigenetic signature of promoters and enhancers underlying cardiac hypertrophy. *Proc Natl Acad Sci USA.* (2013) 110:20164–9. doi: 10.1073/pnas.1315155110
34. Jung S, Littman DR. Chemokine receptors in lymphoid organ homeostasis. *Curr Opin Immunol.* (1999) 11:319–25. doi: 10.1016/S0952-7915(99)80051-X
35. Frangogiannis NG, Chemokines in ischemia and reperfusion. *Thromb Haemost.* (2007) 97:738–47. doi: 10.1160/TH07-01-0022
36. Chen B, Frangogiannis NG. Chemokines in myocardial infarction. *J Cardiovasc Transl Res.* (2020). doi: 10.1007/s12265-020-10006-7. [Epub ahead of print].
37. Cavalera M, Frangogiannis NG. Targeting the chemokines in cardiac repair. *Curr Pharm Des.* (2014) 20:1971–9. doi: 10.2174/13816128113199990449
38. Liehn EA, Piccinini AM, Koenen RR, Soehnlein O, Adage T, Fatu R, et al. A new monocyte chemotactic protein-1/chemokine CC motif ligand-2 competitor limiting neointima formation and myocardial ischemia/reperfusion injury in mice. *J Am Coll Cardiol.* (2010) 56:1847–57. doi: 10.1016/j.jacc.2010.04.066
39. Dewald O, Zymek P, Winkelmann K, Koerting A, Ren G, Abou-Khamis T, et al. CCL2/Monocyte chemoattractant protein-1 regulates inflammatory responses critical to healing myocardial infarcts. *Circ Res.* (2005) 96:881–9. doi: 10.1161/01.RES.0000163017.13772.3a
40. Guo LY, Yang F, Peng LJ, Li YB, Wang AP. CXCL2, a new critical factor and therapeutic target for cardiovascular diseases. *Clin Exp Hypertens.* (2020) 42:428–37. doi: 10.1080/10641963.2019.1693585
41. Liehn EA, Postea O, Curaj A, Marx N. Repair after myocardial infarction, between fantasy and reality: the role of chemokines. *J Am Coll Cardiol.* (2011) 58:2357–62. doi: 10.1016/j.jacc.2011.08.034
42. Montecucco F, Bauer I, Braunersreuther V, Bruzzone S, Akhmedov A, Luscher TF, et al. Inhibition of nicotinamide phosphoribosyltransferase reduces neutrophil-mediated injury in myocardial infarction. *Antioxid Redox Signal.* (2013) 18:630–41. doi: 10.1089/ars.2011.4487
43. Mylonas KJ, Turner NA, Bageghni SA, Kenyon CJ, White CI, McGregor K, et al. 11beta-HSD1 suppresses cardiac fibroblast CXCL2, CXCL5 neutrophil recruitment to the heart post MI. *J Endocrinol.* (2017) 233:315–27. doi: 10.1530/JOE-16-0501
44. Hao G, Han Z, Meng Z, Wei J, Gao D, Zhang H, et al. Ets-1 upregulation mediates angiotensin II-related cardiac fibrosis. *Int J Clin Exp Pathol.* (2015) 8:10216–27.
45. Rommel C, Rosner S, Lother A, Barg M, Schwaderer M, Gilsbach R, et al. The transcription factor ETV1 induces atrial remodeling and arrhythmia. *Circ Res.* (2018) 123:550–63. doi: 10.1161/CIRCRESAHA.118.313036
46. Lee S, Lee DH, Park BW, Kim R, Hoang AD, Woo SK, et al. *In vivo* transduction of ETV2 improves cardiac function and induces vascular regeneration following myocardial infarction. *Exp Mol Med.* (2019) 51:1–14. doi: 10.1038/s12276-019-0206-6
47. Das S, Senapati P, Chen Z, Reddy MA, Ganguly R, Lanting L, et al. Regulation of angiotensin II actions by enhancers and super-enhancers in vascular smooth muscle cells. *Nat Commun.* (2017) 8:1467. doi: 10.1038/s41467-017-01629-7
48. Saraste A, Koskenvuo JW, Saraste M, Parkka J, Toikka J, Naum A, et al. Coronary artery flow velocity profile measured by transthoracic doppler echocardiography predicts myocardial viability after acute myocardial infarction. *Heart.* (2007) 93:456–7. doi: 10.1136/hrt.2006.094995
49. Oostendorp M, Douma K, Wagenaar A, Slenter JM, Hackeng TM, van Zandvoort MA, et al. Molecular magnetic resonance imaging of myocardial angiogenesis after acute myocardial infarction. *Circulation.* (2010) 121:775–83. doi: 10.1161/CIRCULATIONAHA.109.889451
50. Yanagisawa-Miwa A, Uchida Y, Nakamura F, Tomaru T, Kido H, Kamijo T, et al. Salvage of infarcted myocardium by angiogenic action of basic fibroblast growth factor. *Science.* (1992) 257:1401–3. doi: 10.1126/science.1382313
51. Garbern JC, Minami E, Stayton PS, Murry CE. Delivery of basic fibroblast growth factor with a pH-responsive, injectable hydrogel to improve angiogenesis in infarcted myocardium. *Biomaterials.* (2011) 32:2407–16. doi: 10.1016/j.biomaterials.2010.11.075
52. Zhao W, Zhao T, Chen Y, Ahokas RA, Sun Y. Reactive oxygen species promote angiogenesis in the infarcted rat heart. *Int J Exp Pathol.* (2009) 90:621–9. doi: 10.1111/j.1365-2613.2009.00682.x
53. Iwama H, Uemura S, Naya N, Imagawa K, Takemoto Y, Asai O, et al. Cardiac expression of placental growth factor predicts the improvement of chronic phase left ventricular function in patients with acute myocardial infarction. *J Am Coll Cardiol.* (2006) 47:1559–67. doi: 10.1016/j.jacc.2005.11.064
54. Luttun A, Tjwa M, Moons L, Wu Y, Angelillo-Scherrer A, Liao F, et al. Revascularization of ischemic tissues by PlGF treatment, and inhibition of tumor angiogenesis, arthritis and atherosclerosis by anti-Flt1. *Nat Med.* (2002) 8:831–40. doi: 10.1038/nm731
55. Salcedo R, Ponce ML, Young HA, Wasserman K, Ward JM, Kleinman HK, et al. Human endothelial cells express CCR2 and respond to MCP-1: direct role of MCP-1 in angiogenesis and tumor progression. *Blood.* (2000) 96:34–40. doi: 10.1182/blood.V96.1.34.013a49_34_40
56. Wu Y, Ip JE, Huang J, Zhang L, Matsushita K, Liew CC, et al. Essential role of ICAM-1/CD18 in mediating EPC

recruitment, angiogenesis, and repair to the infarcted myocardium. *Circ Res.* (2006) 99:315–22. doi: 10.1161/01.RES.0000235986.35957.a3

Conflict of Interest: The authors declare that the research was conducted in the absence of any commercial or financial relationships that could be construed as a potential conflict of interest.

frontiers in Cardiovascular Medicine

REVIEW
published: 25 January 2021
doi: 10.3389/fcvm.2020.588347

Pivotal Role of TGF-β/Smad Signaling in Cardiac Fibrosis: Non-coding RNAs as Effectual Players

Somayeh Saadat[1], Mahdi Noureddini[1], Maryam Mahjoubin-Tehran[2], Sina Nazemi[3], Layla Shojaie[4], Michael Aschner[5], Behnaz Maleki[1], Mohammad Abbasi-kolli[6], Hasan Rajabi Moghadam[7], Behrang Alani[8]* and Hamed Mirzaei[9]**

[1] Physiology Research Centre, Kashan University of Medical Sciences, Kashan, Iran, [2] Department of Medical Biotechnology, Faculty of Medicine, Mashhad University of Medical Sciences, Mashhad, Iran, [3] Vascular and Thorax Surgery Research Center, Shiraz University of Medical Sciences, Shiraz, Iran, [4] Department of Medicine, Research Center for Liver Diseases, Keck School of Medicine, University of Southern California, Los Angeles, CA, United States, [5] Department of Molecular Pharmacology, Albert Einstein College of Medicine, Bronx, NY, United States, [6] Department of Medical Genetics, Faculty of Medical Sciences, Tarbiat Modares University, Tehran, Iran, [7] Department of Cardiology, Faculty of Medicine, Kashan University of Medical Sciences, Kashan, Iran, [8] Department of Applied Cell Sciences, Faculty of Medicine, Kashan University of Medical Sciences, Kashan, Iran, [9] Research Center for Biochemistry and Nutrition in Metabolic Diseases, Institute for Basic Sciences, Kashan University of Medical Sciences, Kashan, Iran

OPEN ACCESS

Edited by:
Suowen Xu,
University of Science and Technology of China, China

Reviewed by:
Osvaldo Contreras,
Victor Chang Cardiac Research Institute, Australia
Xiaohua Yan,
Nanchang University, China
Samir Jose Bolivar Gonzalez,
University of Atlántico, Colombia

***Correspondence:**
Hasan Rajabi Moghadam
hrmcardio@gmail.com
Behrang Alani
behranga@yahoo.com
Hamed Mirzaei
mirzaei-h@kaums.ac.ir;
h.mirzaei2002@gmail.com

Specialty section:
This article was submitted to Cardiovascular Genetics and Systems Medicine, a section of the journal Frontiers in Cardiovascular Medicine

Received: 28 July 2020
Accepted: 15 October 2020
Published: 25 January 2021

Citation:
Saadat S, Noureddini M, Mahjoubin-Tehran M, Nazemi S, Shojaie L, Aschner M, Maleki B, Abbasi-kolli M, Rajabi Moghadam H, Alani B and Mirzaei H (2021) Pivotal Role of TGF-β/Smad Signaling in Cardiac Fibrosis: Non-coding RNAs as Effectual Players. Front. Cardiovasc. Med. 7:588347. doi: 10.3389/fcvm.2020.588347

Unintended cardiac fibroblast proliferation in many pathophysiological heart conditions, known as cardiac fibrosis, results in pooling of extracellular matrix (ECM) proteins in the heart muscle. Transforming growth factor β (TGF-β) as a pivotal cytokine/growth factor stimulates fibroblasts and hastens ECM production in injured tissues. The TGF-β receptor is a heterodimeric receptor complex on the plasma membrane, made up from TGF-β type I, as well as type II receptors, giving rise to Smad2 and Smad3 transcription factors phosphorylation upon canonical signaling. Phosphorylated Smad2, Smad3, and cytoplasmic Smad4 intercommunicate to transfer the signal to the nucleus, culminating in provoked gene transcription. Additionally, TGF-β receptor complex activation starts up non-canonical signaling that lead to the mitogen-stimulated protein kinase cascade activation, inducing p38, JNK1/2 (c-Jun NH2-terminal kinase 1/2), and ERK1/2 (extracellular signal–regulated kinase 1/2) signaling. TGF-β not only activates fibroblasts and stimulates them to differentiate into myofibroblasts, which produce ECM proteins, but also promotes fibroblast proliferation. Non-coding RNAs (ncRNAs) are important regulators of numerous pathways along with cellular procedures. MicroRNAs and circular long ncRNAs, combined with long ncRNAs, are capable of affecting TGF-β/Smad signaling, leading to cardiac fibrosis. More comprehensive knowledge based on these processes may bring about new diagnostic and therapeutic approaches for different cardiac disorders.

Keywords: cardiac fibrosis, non-coding RNAs, Smad, TGF—transforming growth factor, microRNA

INTRODUCTION

Excessive aggregation of ECM, which is mainly produced by myofibroblasts, results in fibrosis (1). In addition, α-smooth muscle actin (α-SMA), a highly contractile protein, is expressed by myofibroblasts. ECM deposition is shown to be reversible, and improved cardiac function and coronary flow result in a minor collagen volume fraction regression (20% relative change and 1%

absolute change) (2), an important indicator of ECM content. Additionally, patients with heart failure (HF) are commonly treated with renin–angiotensin–aldosterone system modulators, which lessen cardiac fibrosis (3, 4). Cardiac fibrosis induces pathological processes, which lead to chamber dilatation, muscular hypertrophy, and apoptosis, eventually developing into congestive HF (5). Cardiac fibrosis pathogenesis is complex with no efficient treatment options (6).

Transforming growth factor β1 (TGF-β1) is the principal isoform of TGF-β in cardiac tissue, which can cause Smad2/Smad3 (its downstream mediator) phosphorylation, which in turn can stimulate cardiac fibrosis development. It has been shown in mice that cardiac fibrosis related to pressure overload can be diminished by specific deletion of TGF-β1 or Smad3 gene in the triggered cardiac fibroblasts (CFs) (7). Non-coding RNAs (ncRNAs) include small microRNAs (miRNAs or miRs; > ∼22 nucleotides) and long non-coding RNAs (lncRNAs; > ∼200 nucleotides), as well as circular RNAs (circRNAs; > ∼200 circular nucleotides) (1), all of which are involved in regulating several signaling pathways, including TGF-β and Smad, for the control of cytokine release, along with ECM production (8–10). Evidence corroborates the existence of cross-regulation between the two ncRNAs mediated fibrosis-stimulating pathways and its role in cardiac fibrosis pathophysiology. Recognizing mechanisms associated with such cross-regulation provides possibilities for the development of new therapeutic approaches to reverse cardiac fibrosis (10–12). The present review examines TGF-β, as well as Smad signaling, followed by their contribution in the cardiac fibrosis pathogenesis. In addition, evidence regarding TGF-β and Smad signaling involvement in vascular and cardiac remodeling across fibrotic events is detailed. Finally, ncRNAs (consisting of miRNAs, lncRNAs, and circRNAs) roles in TGF-β and Smad signaling in the heart are discussed. Specifically, the review will focus on the role of TGF-β/Smad signaling in ECM overproduction, cardiac fibrotic event, and myofibroblast alterations, which is the aim of this study. We point out the impacts of miRNAs and lncRNAs, as well as circular lncRNAs, on cardiac fibrosis *via* interaction with the signaling pathways of TGF-β/Smad.

PATHOGENESIS OF CARDIAC FIBROSIS

Cardiac fibrosis, namely, the accumulation of scar tissue in the heart, is a product of mismatch between production and degradation of ECM and is strongly associated with cardiac and endocrine disorders (13). Upon stimulation, circulation and myocardial fibrosis–promoting growth factors as well as cytokines levels will increase and initiate a fibrotic response (14). Attachment of the fibrotic-promoting growth factors and cytokines takes place in the corresponding receptors in fibroblasts, namely, cytokine receptors, integrins, syndecans, and CD44 (15), after which signaling pathways and transcriptional factors, such as Smad, mitogen-stimulated protein kinases (MAPKs), nuclear factor κB, and protein kinase B (also called AKT), are activated. These activations induce CFs to transform into myofibroblasts, capable of expressing the strongly contractile protein α-SMA and producing certain tissue inhibitor of metalloproteinases (TIMPs), as well as matrix metalloproteinases (MMPs) for the modulation of ECM homeostasis (14). Additionally, synthesis and release of fibrotic-promoting growth factors and cytokines in CFs are controlled by these transcriptional factors (16). The growth factors and cytokines secreted *via* CFs or other cells, such as cardiomyocytes, and endothelial cells affect CFs or cardiomyocytes and create a positive feedback with final enhancement of the fibrotic responses (16).

In addition to various cell types (such as inflammatory, epithelial, endothelial, and other cells) that contribute to fibrogenesis, three cellular signaling transduction pathways contribute significantly during fibrosis: MAPKs, TGF-β, and integrins. The first pathway, which includes c-Jun NH2-terminal kinase (JNK), p38 MAPK, and extracellular signal–modulated kinase in mammals, has mediating effects on signaling, initiated by extracellular stimulation, such as growth factors and cytokines, or stimulation within the cells (17). The second pathway contributes significantly to the regulation of cellular functions, such as proliferation, differentiation, apoptosis, and survival. Integrins include subunits of α and β, which surface receptors on every cell type with the exception of red blood cells (18). Alongside extracellular receptors, signals transducing pathways engaged in fibrogenesis are triggered by integrins working in coordination with integrin-associated kinases within the cells (18–21).

TGF-β/SMAD SIGNALING IN CARDIAC FIBROSIS

TGF-β can be described as a cytokine with multifunctionality, whose expression takes place by various kinds of cells (22). The superfamily of TGF-β included the TGF-β isoforms (TGF-β1, TGF-β2, and TGF-β3) and activins, as well as inhibins, growth-differentiating factors, bone morphogenetic proteins (BMPs), together with anti-müllerian hormones (AMH) as suborders (23, 24). TGF-β plays a role in different diseases such as cardiac abnormality, cardiac fibrosis, failure of the heart, and remodeling of chamber, as well as cardiac hypertrophy (22) (**Figure 1**). TGF-β isoforms function with activins toward stimulating signals within the cells through Smad2/3 transcribing factors (25). TGF-β ligand complex has seven different type I receptors (which are sometimes called activin-like kinase or ALK receptors) or five type II receptors (ActRIIA, ActRIIB, TGFBRII, BMPRII, and AMHRII) (26, 27).

It has been previously demonstrated that TGF-β-stimulated clone 22 (TSC-22) could facilitate TGF-β signaling by antagonizing Smad7 activity secondary to enhanced receptor stability. TSC-22 increases TGF-β-induced transcriptional responsiveness and phosphorylation of Smad2/3 (28). Furthermore, the stimulatory effect of TSC-22 is Smad7-dependent, and silencing the expression of Smad7 abolishes TSC-22's effect. TSC-22 can interact with TβRI (TGF-β type

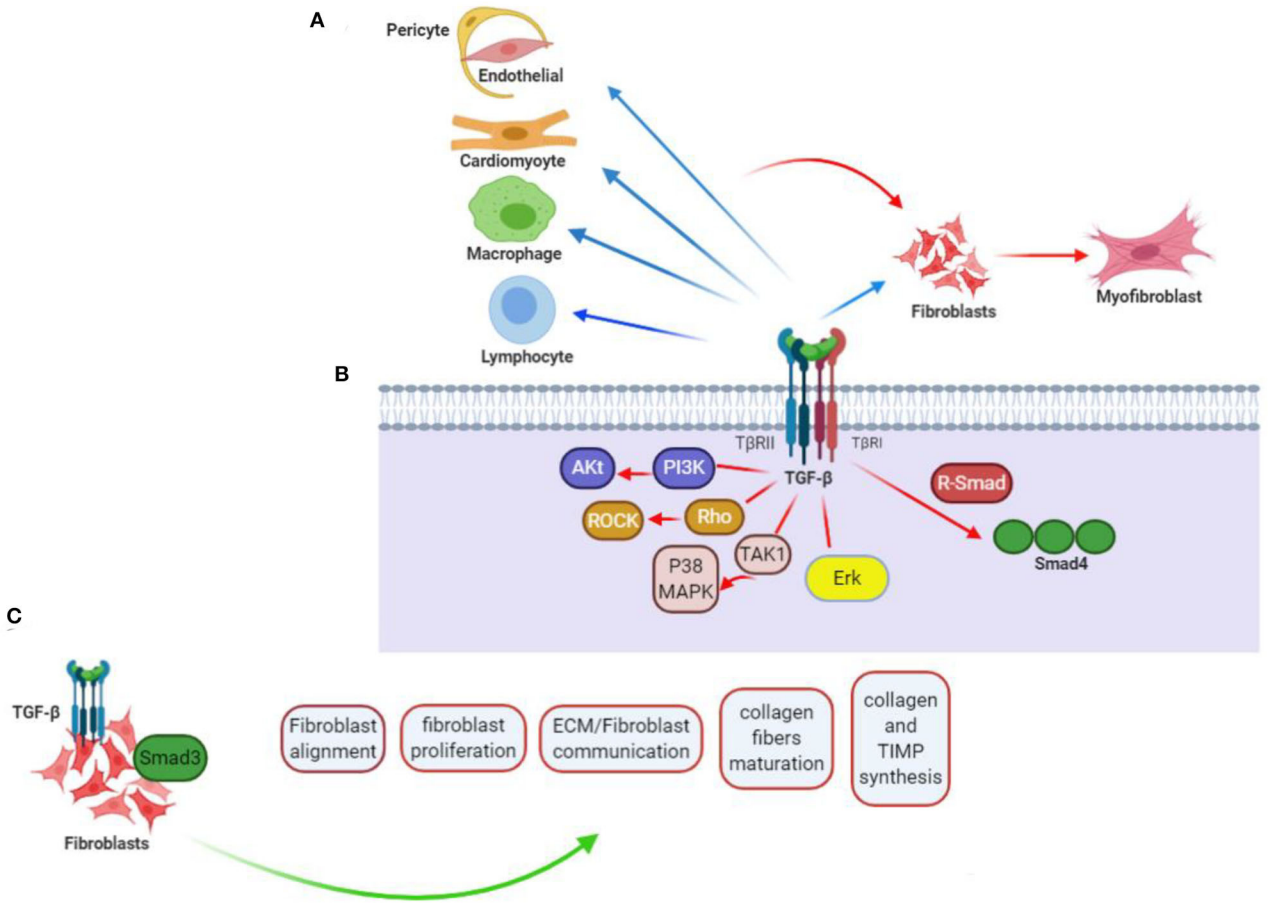

FIGURE 1 | TGF-β contribution to cardiac fibrotic events. **(A)** TGF-β affects phenotype along with operation in every cell somehow engaged in myocardial fibrotic event. Straightforward effects on conversing fibroblast (F) to myofibroblast (MF) and activating myofibroblast can be probably of more importance, but fibrogenesis caused by TGF-βs can further relate with its impacts on the phenotype of macrophage (Ma), differentiation and function of lymphocyte (L), and cardiomyocyte (CM) viability, as well as gene expression. Apart from that, TGF-β can encourage pericyte (P) to fibroblast transformation and endothelial-to-mesenchymal transdifferentiation, when induced by vascular cells to express fibrosis-associated genes. **(B)** TGF-βs regulate phenotypes of the cells through activation of Smad-related together with non-Smad signaling pathways. **(C)** TGF-β/Smad3 signaling effect on CFs. Current researches taking advantage of loss-of-function procedures associated with specific cells drew conclusion that activating Smad3 contributes significantly to the formation of organized myofibroblast arrays after myocardial infarction. Lack of Smad3 in fibroblasts deranges infarcted heart reparations, resulting in higher risks of late cardiac rupture and undesirable chamber dilation. The evidence points out the reparative operation of fibroblasts activated in the infarcted myocardium. Mediation of the Smad3 effects is being carried out by the integrin–ROS axis arousal. This figure was adapted from Frangogiannis (15).

I receptor) and Smad7 and prevent the Smad7/Smurfs and TβRI association and receptor degradation. TSC-22 also promotes cardiac myofibroblast differentiation by increasing fibrotic gene expression for α-SMA, fibronectin, plasminogen activator inhibitor 1 (PAI-1), and collagen I, consistent with TSC-22 upregulation and phospho-Smad2/3 in myocardial fibrotic hearts. Therefore, it has been suggested that TSC-22 could regulate TGF-β signaling through a positive-feedback mechanism and may lead to myocardial fibrosis (28).

Binding of type II receptor TGFBRII with TGF-β1 ligands leads to phosphorylation of the type I receptor ALK-5. Various ligands may bind to cell surface TGF-β receptors, which lead to activation of signaling effectors and the Sma- and Mad-related proteins (Smads), as well as interacting with deoxyribonucleic acid (29). TGF-β, myostatin, or activin activates both Smad2 and Smad3, whereas activation of Smad1, Smad5, and Smad8 is performed with BMPs, leading to interactions with Smad4, bringing forth modulating the target gene expression (24, 30, 31). It is noteworthy that TGF-β pathway activation will lead to upregulation of Smad6 and Smad7 expression as well, in turn deactivating the pathways (29). Several ncRNAs and their substrates play a role in the TGF-β signal transduction pathway regulation (21).

Smad2/3 activation affects various profibrotic gene expression, consisting of collagens [COL1A1, COL3A1, COL5A2, COL6A1, COL6A3, COL7A1, (32)], PAI-1 (33, 34), various proteoglycans (35–37), integrins (38), connective tissue growth factor (CTGF) (39), and MMPs (27, 40).

Considerable increase in the levels of TGF-β was observed in individuals experiencing ischemic cardiomyopathy (ICM)

and dilated cardiomyopathy (DCM), showing that TGF-β levels correlate with phosphorylated Smad2, along with collagen types I and III, triggering further myocardial fibrotic events in ICM and DCM secondary to activation of TGF-β (41). Fibulin 2 is an essential ECM protein for TGF-β/Smad signaling. Moreover, phosphorylation of Smad2 is achieved only in the presence of fibulin-2 (42). Peroxisome proliferator–activated receptor γ (PPARγ) activation was thought to moderate cardiac fibrosis. A study showed that TGF-β1 directly suppresses PPARγ expression by increasing binding of Smad2/3, Smad4, histone deacetylase 1 (HDAC1), and decreasing binding of HDAC3 to the PPARγ promoter in CFs (43). Another study has shown that reactive oxygen species (ROS) derived from NADPH oxidase 4 (Nox4) enhanced myocardial fibroblasts reaction against TGF-β1 through TGF-β Smad signaling pathways (44). Wnt/β-catenin pathway in inflammatory DCM has been shown to be activated by secretion of Wnt proteins in response to TGF-β signaling, mediated by Smad-independent TGF-β-activated kinase 1 (TAK1) (45, 46). Wnt inactivation or Wnt secretion hindrance impeded TGF-β-mediated CF transformation into pathogenic myofibroblasts, making Wnt protein secretion a neoteric downstream process of TGF-β-modulated cardiac fibrotic development (46). It has been demonstrated that CTGF, also known as CCN2, may play roles in the hypertension-induced myocardial fibrosis through regulation of TGF-β expression (22, 47).

ncRNAs IN CARDIAC FIBROSIS

ncRNAs are short RNAs that act as epigenetic regulators (48). The regulation of these molecules is related to modulation of several physiological properties such as apoptosis, cell proliferation, metabolism, and differentiation. Deregulation of these molecules shows associations with the onset and progress of various diseases, such as cardiovascular diseases, diabetes, cancer, and inflammatory disorders (49). According to existing evidence, ncRNAs can be categorized into two main groups: (i) short ncRNAs possessing fewer than 200 small nucleotides in their length (i.e., snoRNAs, siRNA, piwi-RNA, and miRNAs), (ii) lncRNAs possessing more than 200 nucleotides in their length including lncRNAs and circRNAs (16, 50). Cardiac fibrosis is a common feature in many types of heart diseases. ncRNA deregulation has been posited to be associated with cardiac fibrosis development and occurrence (49). **Table 1** summarizes the role of different ncRNAs contributing to cardiac fibrosis pathogenesis.

miRNAs

As mentioned previously, miRNAs can be defined as short ncRNAs with a length of 18 to 24 nucleotides (85, 86). miRNAs are capable of regulating the function of proteins by binding to target messenger RNA. This may result in the induction of mRNA degradation and/or suppression of protein translation. It has been shown that these molecules modulate myocardial fibrosis pathogenesis (**Table 1**) (87). Cardiac fibrosis is a complicated process involving the concerted interaction of multiple miRNAs. In this respect, different miRNAs are related to same pathologically fibrotic process. For instance, miR-24, miR-21, miR-34a, miR-29, and miR-433 contribute to fibrosis following infarction, and miR-26a, miR-21, and miR-125b are associated with pressure-overload fibrosis, which is caused by transverse aortic constriction (88–91). In addition, various miRNAs could be classified into antifibrotic (e.g., miR-15 family, miR-101a, miR-145, miR-378, miR-122, miR-142-3p) or profibrotic miRNAs (e.g., miR-29, miR-21, miR-34, miR-208, miR-155, miR-223) (88–91). miRNAs exert their regulatory effects on cardiac fibrosis, although affecting a sequence of cellular and molecular pathways, such as TGF-β/Smad system, MRTF/SRF axis RhoA/ROCK cascade, Wnt signaling, AngII/MAPK signaling, and the cationic channels that regulate calcium responses (92). Callis et al. evaluated miR-208a role in cardiac fibrosis induction. They indicated that miR-208a plays its role *via* targeting THRAP-1 and myostatin in myocardial hypertrophy (93). Furthermore, they showed miR-208a can induce cardiac fibrosis through increased endogen expression (93). Other study demonstrated that the upregulation of miR-208b is related to myocardial function enhancement and could inhibit type I collagen and alias α-SMA. In agreement, miR-208b exerts protection against post-infarction myocardial fibrosis by targeting GATA4 (94).

TGF-β1 can be associated with collagen secretion and activation in myocardial fibroblasts, which play a role in cardiac fibrosis development with other risk factors (95). Furin can modulate TGF-β activation by targeting AngII (96). Bearing that in mind, furin can exert its functions by TGF-β activation (97). Chen et al. showed that miR-24 downregulation is associated with cardiac infarction. Their findings confirmed that miR-24 exerts its effects by inhibiting TGF-β1 with having impact on furin. TGF-β1 and furin levels were elevated, indicating a critical role of miR-24 deregulation in myocardial fibrotic events following myocardial infarction (98).

Long Non-coding

Intra-action of the cell death and inflammation to myocardial fibrosis is crucial (99). Pyroptosis, namely, cell death triggered by inflammatory reactions, is described by apoptosis and necrosis (100). Nod-like receptor protein 3 (NLRP3) inflammasome expression in cardiac fibrosis is activated by inflammation; subsequently, it activates the cleaved caspase (101). Recent studies have corroborated the contribution of pyroptosis in myocardial fibrosis pathogenesis (102). Nonetheless, the initiating mechanisms for cardiac fibrosis and fibroblast-derived pyroptosis have yet to be determined. Thus, identification of the pathological mechanisms along with efficient treatment targets of myocardial fibrosis is essential. Growth arrest–specific 5 (GAS5), a lncRNA, whose encoding takes place by the GAS5 gene, has been introduced as a tumor suppressor in variety of cancer types (103). GAS5 contributes critically to cell apoptosis and pyroptosis (104). She et al. (105) identified lncRNA-GAS5 as the initiator of pyroptosis in CFs and cardiac fibrotic events. Upon lipopolysaccharide (LPS) stimulation, they detected ISO-induced CF pyroptosis and myocardial fibrosis. Proteins associated with pyroptosis include caspase 1, NLRP3, and DNMT1, higher in cardiac fibrotic tissues, with reduced

TABLE 1 | ncRNAs contributing to cardiac fibrosis.

Non-coding RNAs	Effect (s)	Expression in CF	Targets	Signaling pathway	Model	References
miRNA						
miR-21	Profibrosis	Upregulated	Spry1, PTEN CADM1	↑TGF-β1 →↓PTEN→ ↑MMP-2 CADM1/STAT3 pathway ↑cardiac fibrosis	Rat CFs	(51, 52)
miR-26a/b	Profibrosis	Upregulated	TRPC3	↑MiR-26a → ↓ TRPC3 → ↑CF	Dog fibroblasts model	(53)
			Col1a2/CTGF	miR-26b-5p→↓Col1a2/CTGF → ↑CF	Mouse CFs	(54)
miR-34	Profibrosis	Upregulated	VEGF, neurogenic locus notch homolog protein 1, vinculin, PPP1R10	Contributing to cardiomyocyte aging; inhibiting miR-34 and limiting cardiac fibrotic events	MI and TAC mice	(19, 55)
miR-132	Antifibrosis	Downregulated	Ras/Rap/SynGAP; methyl-CpG-binding protein 2	Akt/eNOS/Bcl-2 signaling pathway ↓Ras/Rap GTPase-activating protein ↓SynGAP;methyl-CpG-binding domain protein 2→↓CF	MI -CD1 mice	(56)
miR-133/miR-30	Antifibrosis	Downregulated	CTGF	Contributing to the progress of fibrosis *via* connective tissue growth factor targeting	Renin-2 tg rat	(57)
miR-133a	Antifibrosis	Downregulated	Collagen α-1(I) chain	Transgenic overexpression in cardiomyocytes inhibits fibrotic progress across overload of pressure and diabetic cardiomyopathy	TAC mice	(58)
miR-155	Profibrosis	Upregulated	Son of seven less gene (Sos1)	Macrophage-derived mir-155–comprising exosomes suppressing proliferation Of Fibroblasts and enhancing inflammation of fibroblasts across cardiac injury	mir-155–deficient mice	(59)
miR-199b	Antifibrosis	Downregulated	Dyrk1a calcineurin/NFAT target gene	Nuclear kinase Dyrk1a is targeted by miRNA-199b in an auto-amplification loop enhancing calcineurin/NFAT signaling inhibition→ ↓CF	mouse and human heart failure	(60)
miR-208	Profibrosis	Upregulated	Myosin-6, myosin-7	Inhibition results in decreased progress of fibrosis subject to cardiac stress	miR-208 mutant animals	(61)
miR-214	Antifibrosis	Downregulated	Sodium/calcium exchanger (1Ncx1)	Inhibition results in excessive progress of cardiac fibrosis following myocardial infarction	Ischemic cardiac tissue	(62)
miR-455	Antifibrosis	Downregulated	collagen I and III CTGF	miR-455 →↓ collagen I and III /CTGF ↓CF	Male diabetic mice	(63)
miRNA-155	Profibrosis	Upregulated	Ski SnoN	↓Antifibrotic Sloan–Kettering Institute proto-oncogene (Ski)/Ski-associated new gene, non–Alu-comprising (SnoN) signaling (negative TGF-β signaling regulating factors) →↑CF	Diabetic (db/db) mice	(13)
miR−223	Profibrosis	Upregulated	RASA1(RAS p21 protein activator 1)	siRASA1 enhanced MEK1/2, ERK1/2 and AKT phosphorylation →↑ collagen I, collagen III, and α-SMA→ ↑CF	CFs	(64)
miR-9	Antifibrosis	Downregulated	TGFBR2	Suppressing TGF-β receptor II→ ↓CF	High glucose/human CFs	(65)
Let-7i	Antifibrosis	Downregulated	IL-6 Mac-2	Let-7i →↓ interleukin-6/collagens →↓CF	AngII/mouse; NRCFs	(66)

(Continued)

TABLE 1 | Continued

Non-coding RNAs	Effect (s)	Expression in CF	Targets	Signaling pathway	Model	References
Let-7c	Antifibrosis	Downregulated	Activate Oct4 and Sox2	Improvement in cardiac function ↓apoptosis, ↓fibrosis, ↓number of discoidin domain receptor 2–positive fibroblasts	MI/mouse; NRCFs	(67)
lncRNAs						
lncRNA H19	Profibrosis	Upregulated	ERK1/2, Dual-specificity phosphatase 5 (DUSP5)	↑H19 →↓DUSP5 (negative regulation of prohypertrophic signaling by↓ ERK1/2) →↑α-SMA↑/cardiac fibroblast proliferation	Isolated rat cardiac fibroblasts	(68)
			miR-455 CTGF, collagen I, III, α-SMA	H19 and miR-455 modulated myocardial extracellular matrix accumulation	Male diabetic mice	(63)
lncRNA MIAT	Profibrosis	Upregulated	miRNAs-29, 21, 133, 30, and 24	MIAT↑ → miR-24↓ → Furin/TGF-β1↑ → cardiac fibrotic event↑	Anesthesia of healthy male C57BL/6 mice was carried out with Avertin (160 mg/kg, i.p. Sigma–Aldrich)	(69)
Malat1	Profibrosis	Upregulated	miR-145	↑MALAT1 →↓miRNA-145 (miR-145) →↑ TGF-β1→↑CF	MI mouse heart and AngII-treated CFs	(70)
			Mir-24 Mir-29 Mir-30 Mir-133	↑MALAT1 →↓ miR-24→↑ Furin and ↑TGF-β1→↑CF	Mouse model of MI	(69, 71)
Meg3	Profibrosis	Upregulated	p53 signaling MMP-2	Blockage of inducing Mmp-2 expression through TGF r-βI took place with Meg3 silencing by inhibiting P53 binding on the Mmp-2promoter	*In vivo In vitro*	(72)
lncRNA SRA1	Profibrosis	Upregulated	miR-148b	lncRNA SRA1 →↓ miR-148b→↑CF	Rat model	(73)
Wisper	Antifibrosis	Upregulated	Splicing of Plod2 mRNA by enabling nuclear localization of TIAR	Regulates cardiac fibrosis after injury ↓Pathological progress of cardiac fibrosis in response to MI while preventing unfavorable remodeling	Murine model of MI	(74)
AK081284	Profibrosis	Upregulated	TGF-β1	IL-17/AK081284/TGF-β1 signaling pathways mediate collagen production→↑CF induced by high glucose	Diabetic mouse Myocardial fibrosis model	(75)
lncRNA-NR024118 and Cdkn1c	Antifibrosis	Proregulated	↓cell cycle ↓ Cdkn1c	↑ AngII→ blocking AT1 receptor →↓NR024118 →↑CF	AngII/adult rat CFs	(75, 76)
lncRNA PFL (NONMMUT02255)	Profibrosis	Upregulated	let-7d Ptafr	lncRNA PFL →↓ let-7d→ Ptafr→↑CF	MI mice cardiac fibrosis in mice	(77, 78)
lncRNA-NONMMUT022554	Profibrosis	Upregulated	ECM–receptor PI3K-Akt	May affect ECM-receptor interactions and the phosphoinositid-3 kinase/protein kinase B (PI3K-Akt) signaling pathway →↑CF	MI/mouse	(79)
Mhrt	Antifibrosis	Downregulated	Brg1—chromatin remodeling	Binding of Mhrt to the helicase domain of Brg1, a domain which seems critical for tethering Brg1 to chromatin zed DNA targets	Pressure-overloaded hearts by trans aortic constriction	(80)
Circular RNAs						
CircActa2	Profibrosis	Upregulated	miR-548f-5p. NRG-1	NRG-1/circACTA2/miR-548f-5p Axis.	Animal model of cardiac remodeling and heart failure	(81, 82)

(Continued)

TABLE 1 | Continued

Non-coding RNAs	Effect (s)	Expression in CF	Targets	Signaling pathway	Model	References
circAmotl1	Antifibrosis	Downregulation	AKT1/PDK1	↓Dox/↑resistant fibrosis cardiac repair	Cardiac fibroblasts	(83)
circRNA_010567	Profibrosis	Upregulation	↓ miR-141 TGF-β1	CircRNA_010567 →↓miR-141 →↑TGF-β1 →↑Col I, Col III and α-SMA →↑CF	Mice myocardial fibrosis models	(84)

GAS5 expression. Furthermore, lncRNA GAS5 overexpression enhances and prevents CF pyroptosis and also decreases the expression of caspase 1 and NLRP3 in CF. Other research showed that treating with DNMT inhibitors, 5-aza-2-deoxycytidine, or downregulating DNMT1 caused an increase in expression of GAS5 by reversing promoter hypermethylation in CF. Notably, it has been shown that DNMT1 methylation of lncRNA GAS5 results in CF pyroptosis when NLRP3 axis is affected, suggesting a novel regulatory mechanism regarding CF pyroptosis subject to LPS stress (105).

RNA component of mitochondrial RNA processing endoribonuclease (RMRP) is known as a lncRNA (106). RMRP forms a distinct ribonucleoprotein complex by interaction with the telomerase reverse transcriptase catalytic subunit, which exhibits the activity of RNA-dependent RNA polymerase and makes double-stranded RNAs, which with getting processed can turn into small interfering RNA (siRNA) (106). Prior work has examined the contribution of RMRP to various cancers, such as in lung cancer, gastric cancer, and glioma (107–109). Additionally, Wang et al. (110) reported that the level of RMRP expression in nucleus pulposus tissues correlates with grade of disc degeneration. Another investigation gas demonstrated that overexpression of RMRP could induce nucleus pulposus cell growth and regulate the ECM expression with targeting miR-206. In a recent study, Greco et al. profiled 83-lncRNA expression in biopsies taken from left ventricle of patients suffering HF and corroborated remarkable upregulation of RMRP in these patients (111). Steinbusch et al. (112) found associations of RMRP with chondrocyte hypertrophy and determined chondrogenic differentiation, proposing the contribution of RMRP to the modulation of the dynamic balance of ECM degradation and synthesis. Zhang et al. (113) explored the biological role and mechanisms behind CF induction by the lncRNA, RNA component of RMRP. The findings showed that RMRP expression in an abdominal aortic banding–treated rat model was upregulated in the presence of myocardial fibrosis. Treatment with AngII enhanced RMRP expression in CFs, whereas RMRP knockdown by small-interfering RNA prevented CF proliferation and differentiation as well as collagen accumulation. Based on these findings, RMRP might regulate miR-613 negatively in CFs. Moreover, it was showed that miR-613 mediates the positive effect of RMRP on activation of CF. Based on the present study, RMRP increased CF activation with serving as a competing endogenous RNA for miR-613. Thus, RMRP may represent as a novel target to prevent or treat cardiac fibrosis (113).

circRNAs

miR-125b induces fibrotic process and upregulation in CFs, indicating numerous binding sites of miR-125b for circ_LAS1L, with inverse association of their expression in those with acute myocardial infarction (AMI) and CFs. RNA immunoprecipitation (RIP), pull-down, and dual-luciferase reporter gene assay supported direct binding of miR-125b bound to circ_LAS1L (114). Overexpressed Circ_LAS1L led to promotion of the downstream target gene secreted frizzled-associated protein 5 (SFRP5) expressions, while reducing α-SMA, collagen I, and collagen III expression; hindering CF proliferation and migration; and increasing apoptosis. Cotransfection with miR-125b mimics and circ_LAS1L overexpression vector did not show considerable changes. However, cotransfection of SFRP5 siRNA and circ_LAS1L overexpression vector resulted downregulation of SFRP5 expression and upregulation of collagen I, collagen III, and α-SMA, as well as enhancement in proliferation and migration of CFs. Accordingly, circ_LAS1L reduces miR-125b activities through its adsorption, consequently increasing SFRP5 and subsequent regulation of the CFs biological properties. Such results can be regarded as a significant experimental basis for regulating myocardial fibrosis following myocardial infarction. CircRNAs contribute critically to the cardiovascular diseases; however, little research has been done on their effect on the myocardial fibrosis. Sun et al. investigated that circ_LAS1L in those suffering AMI and CFs was downregulated and was capable of direct binding to miR-125b, consequently enhancing the downstream target gene secreted frizzled-related protein 5 (SFRP5) expression, finally repressing CF activating, proliferating, and migrating, along with inducing apoptosis. Thus, it is has been posited that the circ_LAS1L/miR-125b/SFRP5 pathway is capable of modulating the biological characteristics of CF and can contribute vitally to the process of cardiac fibrosis, therefore offering a significant theoretical basis to regulate cardiac fibrotic event following myocardial infarction (114).

Gu et al. (115) explored circRNA expression profile and identified circRNA contributions to myocardial fibrosis. Utilization of TGF-β1 aimed at establishing an *in vitro* cardiac fibrotic model in CFs. CircRNA sequencing unveiled that an overall number of 283 circRNAs was expressed abnormally in fibrotic CFs, of which 79 were experiencing upregulation and 204 receiving downregulation. Alterations in randomly selected circRNA expression could be verified with the use of real-time polymerase chain reaction. Establishment of a circRNA-based competing endogenous RNA network 1,755 nodes and 30,394 edges was followed by module analyses

performed with implementation of the plug-in MCODE. Kyoto Encyclopedia of Genes and Genomes pathway enrichment analyses targeted mRNAs, engaging in the top three enriched modules. It was found that these mRNAs were enriched in myocardial fibrosis–associated signaling pathways, namely, the AMPK signaling pathway, TGF-β signaling pathway, MAPK signaling pathway, and PI3K-Akt signaling pathway. The predicted ceRNAs and bioinformatics analysis unveiled the possible contribution of circRNAs in myocardial fibrotic event, providing novel knowledge on the mechanisms and searching for efficient preventive, as well as therapeutic targets for myocardial fibrosis (115).

Based on existing evidence, expression of abnormal circRNA takes place in the cardiac fibrotic process. During promotion of CF activated by TGF-β1 or AngII, marked suppression in circRNA circ_BMP2K and miR-455-3p expression has been observed, along with induction of SUMO1 expression (116). RIP, pull-down assay, and dual-luciferase reporter gene assay, demonstrating direct binding of miR-455-3p to circ_BMP2K and their induction of each other's expression. SUMO1 served as a target gene for miR-455-3p, and circ_BMP2K boosted the miR-455-3p inhibiting on the expression of the SUMO1. According to several studies, both circ_BMP2K and miR-455-3p suppressed expressing α-SMA and types I and III collagen, but SUMO1 increased their expression, and the regulatory impacts of circ_BMP2K and miR-455-3p were reversed by miR-455-3p inhibitors or SUMO1 overexpression. Circ_BMP2K and miR-455-3p reduced CF proliferation and migration, concomitantly inducing their apoptosis; however, SUMO1 effect was the opposite; circ_BMP2K and miR-455-3 upregulation on biological characteristics was reversed by miR-455-3p inhibitors or overexpression of SUMO1. Therefore, circ_BMP2K induces

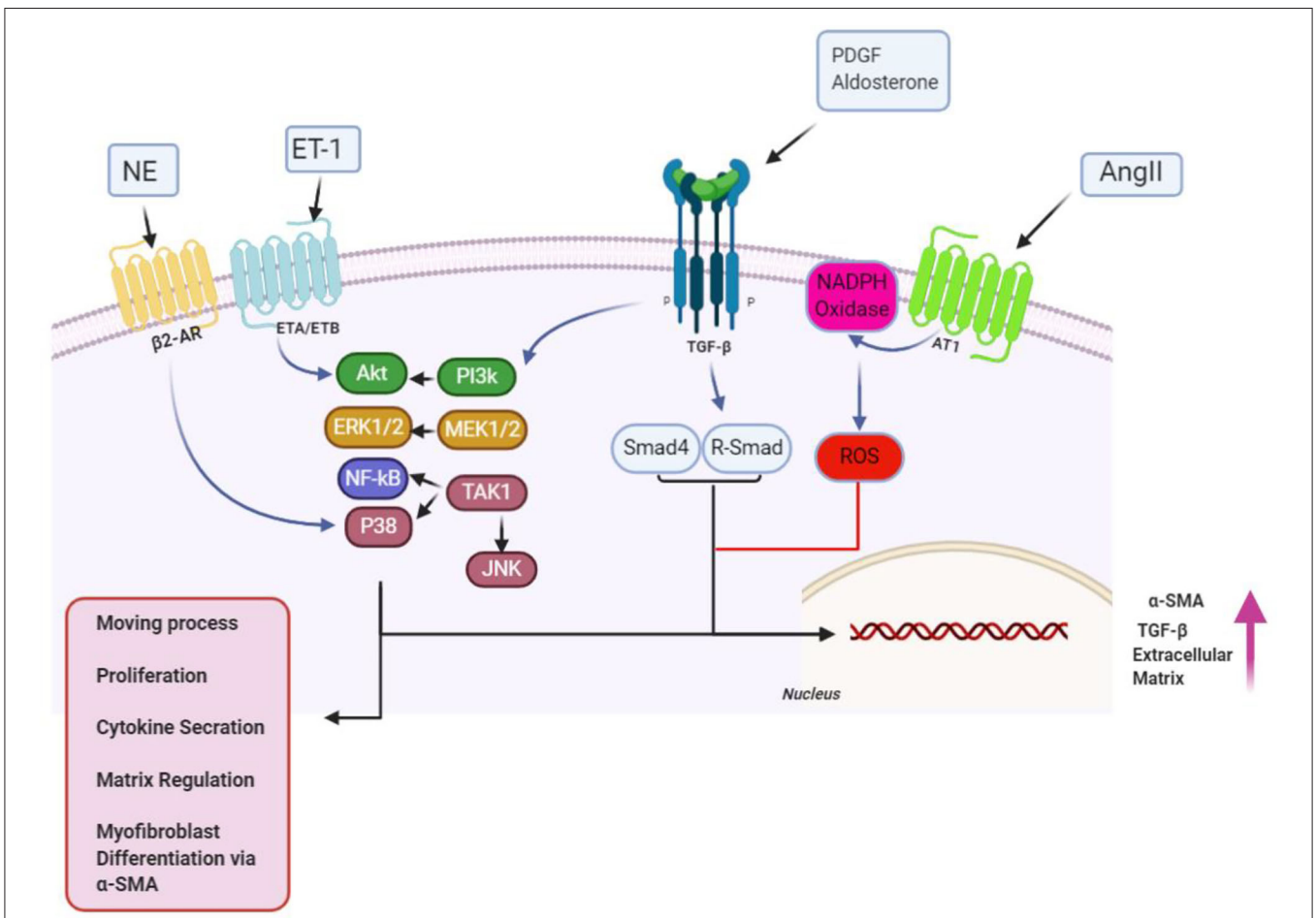

FIGURE 2 | Over the proliferation phase of infarct remedial, fibrogenic growth, as well as neurohumoral mediating factors, stimulates myofibroblast proliferating and migrating, along with activating. A broad scope of fibrogenic mediators, engaged in this phase of cardiac, has been considered in activation of myofibroblast. Neurohumoral mediating factors, including angiotensin II (AngII), aldosterone, and norepinephrine (NE), and growth factors [transforming growth factor (TGF-β), fibroblast growth factor, and platelet-derived growth factor (PDGFs)], together with special matrix proteins, including ED-A fibronectin and matricellular proteins, have cooperation in activating intracellular signaling pathways, which enhance conversion, as well as proliferation of myofibroblast, while modulating ECM protein expression, and of genes related to matrix metabolism. Design of the cartoon took place according to Servier Medical Art (https://smart.servier.com). AR1/4, adrenergicreceptor; ET1/4, endothelin; MMP1/4, matrix metalloproteinase; NF1/4, nuclear factor; ROS1/4, reactive oxygen species 1/4; SMA1/4, smooth muscle actin; TIMP1/4, tissue inhibitor of metalloproteinase. This figure was adapted from Humeres and Frangogiannis (119).

expression of miR-455-3p with subsequent downregulation of SUMO1 expression and ultimately prevents CF activation, growth, and migration (116).

THE RELATIONSHIP BETWEEN ncRNAs AND TGF-β/SMAD SIGNALING IN CARDIAC FIBROSIS

miRNA and TGF-β/Smad Signaling in Cardiac Fibrosis

Various ligands have the ability of binding to TGF-β receptors on the surfaces of cells, permitting regulatory messages transfer to the cells through activation of the signaling effectors, as well as the Sma- and Mad-associated proteins (Smads) and finally, showing interactions with deoxyribonucleic acid (29). Activation of Smad2 and Smad3 are carried out with TGF-β, myostatin, or activin, whereas Smad1, Smad5, and Smad8 are activated by BMPs; activating such proteins leads to interactions with Smad4, resulting in target gene expression modulation (117). Notably, the TGF-β pathway activation additionally leads to upregulation of Smad6 and Smad7 expression, which may end in the pathway deactivation (24, 29). Smad2 and Smad7 lessen fibrosis, but Smad3 results in the promotion of fibrosis (118) (**Figure 2**). Several miRNAs and their substrates contribute to regulating TGF-β signal transduction pathways (**Table 2**, **Figure 3**) (21).

miRNA-associated TGF-β pathways in cardiac fibrotic event exert their effects when they target the common ECM protein CTGF. Moreover, it was demonstrated that miR-101 inhibited interstitial fibrosis and then, by inhibition of a c-Fos/TGF-β1 axis, may promote myocardial infarction (136). Downregulation of miR-101 was evident in infarcted myocardium in mice and in angiotensin-cultured CFs. Interestingly, miR-101 overexpression inhibited proliferating and producing COL through suppression of its target c-Fos and the downstream protein TGF-β1 (136). Transfection of miR-101 mimic significantly suppressed the expression of TGF-β RI and p-Smad3, CF differentiation, and collagen content (137). According to He et al., miR-21 may reinforce the TGF-β1/Smad signaling pathway in atrial fibrosis stimulated by AF, through Smad7 downregulation (126). A reciprocal loop was ascertained between miR-21 and its target TGF receptor III, causing ECM remodeling and fibrotic process. Upregulation of cardiac miR-21 occurred in infarcted myocardium as a result of TGF-β1/Smad2/3 signaling pathway activation, whereas downregulation of its target gene (TGF receptor III) was evident. Nevertheless, lower expression of the TGF receptor III reinforced TGF-β1/Smad2/3 signaling pathway (126, 156).

Thum et al. (127) showed promotion of myocardial fibrosis by miR-21 by targeting extracellular modulated kinase inhibitor sprouty homolog 1 (Spry1) while activating MAPK signaling in cardiac fibroblasts. In a myocardial ischemia–reperfusion model, miR-21 was found to target Pten, subsequently leading to an increase in matrix metalloprotease 2 (Mmp2). Consistently, miR-21 antagonism leads to increased Pten in cardiac fibroblasts (157). miR-24 overexpression reduced secretion of the TGF-β and phosphorylation of the Smad2/3 in CFs (130). miR-24 showed protective features against myocardial fibrosis following myocardial infarction, which was dependent on the inhibitive effects on its target gene FURIN, suppressing the TGF-β signaling pathways (98, 130). Wang et al. (130) demonstrated interference of miR-24 with TGF signaling by targeting the pro-protein convertase, furin, and then downregulation of TGF level in cardiac fibroblasts with targeting CTGF. miR-18a and miR-19b downregulated the expression of the collagen (COL) 1A1 as well as COL3A1, reducing cardiac fibrosis in age-related cardiac failure triggered through activation of TGF-β (19, 124, 128). Functional examinations are consistent with prevention of HCF autophagy by miR-19a-3p/19b-3p with targeting TGF-β R II mRNA. Furthermore, autophagy development releases suppressive effects of miR-19a3p/19b-3p on Smad2 and Akt phosphorylation *via* TGF-βRII signaling (128).

In addition, many other miRNAs were also recognized to target collagens and TGF signaling to contribute to the fiwere also. For example, Let-7i and miR-26a reduce collagen deposition and impose their effects by targeting Col12 and Col11, correspondingly (66, 132, 158). miR-29b upregulation because of TGF/Smad3 inactivation downregulated profibrotic genes, such as ECM genes elastin (159), fibrillin 1 (Fbn1), collagen type I, 1 and 2 (Col11, Col12), and collagen type III, 1 (Col31) (160) and enhanced cardioprotective impacts of carvedilol vs. myocardial fibrosis triggered by AMI (79, 125). It was shown that insulin-like growth factor 1 and leukemia inhibitory factor, which are targeted by miR-29b, play roles in activating CF and proliferating ECM (20, 124).

Tao et al. investigated that miR-433 was related to cardiac fibrosis and is a potential target to mitigate cardiac fibrosis. Their study has found that cardiac fibrosis induces miR-433, subsequently decreasing the expression of AZIN1 and JNK1. Downregulated AZIN1 induces TGF-β1 pathway, whereas decreased JNK1 results in ERK and p38 kinase activation, causing Smad3 activation and eventually leading to cardiac fibrosis (123). In another study in that same year, Ooi et al. (161) suggested that AZIN1 expression reduction induces TGF-β/Smad3 signaling activation in CFs; (III) reduced JNK level would enhance ERK, P38 kinase, and Smad3 phosphorylation, and that is in turn associated with proliferation and differentiation of fibroblast into myofibroblasts.

miR-133a contribution to cardiac fibrosis and electrical repolarization in adult hearts with pressure overload can potentially indicate its regulatory impacts on Col11 A1, Serca2a, and calcineurin expression (58, 162). Based on existing evidence, miR-133a overexpression has prevented myocardial fibrotic event in both AngII-related hypertension and diabetes, even though the effector proteins were different in diabetes (fibronectin and COL4A1) and AngII-related hypertension (COL1A1) (21, 121, 162). Moreover, overexpression of the cardiac miR-133a inhibited ERK1/2 and Smad2 phosphorylation. Accordingly, it is posited that miR-133a may show efficacy in treating myocardial events triggered by diabetes (90, 121).

miR-15 family members are also regarded as having antifibrotic characteristics, through functions against TGF-β-mediated actions (163). miR-15 family members (miR-15a, miR-15b, miR-16, miR-195, miR-497, miR-322) can be observed in

TABLE 2 | ncRNAs and TGF-β/Smad signaling in cardiac fibrosis.

Non-coding RNAs	Effect(s)	Modulation	Targets Smads	Signaling pathway	Model	References
miRNA						
miR-25	Antifibrosis	Downregulated	COL1/COL3 Smad3	miR-25→↓ TGF-β1 →↓collagen I/III	Transaortic constricted mice	(120)
miR-133	Antifibrosis	Downregulated	EP300 COL4A1, FN1 Smad2	↑miR-133a→↓ phosphorylation of p-ERK1/2 and p- Smad2 →EP300/ ↓ TGF-β1/CTGFL/↓fibronectin/COL4A1→↓ cardiac fi/ COL4.	Streptozotocin-induced diabetic in mice	(121)
			Snai1 Gata4, Mef2c, and Tbx5 Mesp1	GMT/miR-133/ Snai1-induced aMHC-GFP→ ↑ cardiac reprogramming→↓CF	Mouse embryonic fibroblasts	(122)
miR-433	Profibrosis	Upregulated	TGF-β1, ERK, p38 kinase, and Smad3	Suppress AZIN1 and JNK1/ /TGF-β1, ERK, p38 kinase, and Smad3→↑ cardiac fibrosis.	MI/mice; NRCFs	(123)
miR-29b-3p miR-29c-3p	Antifibrosis	Upregulated	TGF-β2, Mmp2	miR-29b/miR29c →↑ MIF→ ↓ COL1A1, COL3A1/α-SMA,/ Smad3→↓ cardiac fibrosis.	(AngII)-infused mouse myocardium Mif-knockout (Mif-KO) mice	(124)
			mRNA 3′-UTR Col 1a1, Col 5a3, and Col 4a2 Smad3	↓TGF-β /Smad3→↓collagen I, III, fibronectin→↓CF	AngII-triggered cardiac fibrotic event in mice Mouse CFs	(125)
			Fibrillins and elastin	Altered the secretion of growth factors and cytokines, including MMP, IGF-1, LIF, and PTX-3 ↓ TGF-β→↓CFs	AngII (1.46 mg/kg/d, 14 d)-infused mouse myocardium	(20)
miR-21	Profibrosis	Upregulated	↓ Smad7	↑miR21→↑TGF-β1→↑myocardial fibrosis by inhibiting Smad7	Fibro TAC/mouse	(126)
			↓Smad2/3 ↓ TGF-β R III//p-Smad3	Activate sprouty homolog ↑1/ERK-MAP kinase ↑TGF-β1/Smad2/3 signaling pathway→↑CF	MI/mouse	(127)
			↑PTEN Spry1	Activate osteopontin/PTEN and ↓Smad7→↑CF	AngII/mousesis	(79)
miR-19a-3p/19b-3p	Antifibrosis	Upregulation	TGF-β R II	miR-19a-3p/19b-3p→↓ TGF-β→↓ phosphorylation of Smad2 and Akt →↓CF	Human Cardiac Fibroblasts (HCF)	(128)
miR-24	Antifibrosis	Upregulated	Furin–TGF-β pathway.	↓ TGF-β-p→↓ Smad2/3 →↓ Furin→↓ col-1/α-SMA→↓CF	Mouse model of MI	(129)
			Smad2/3	↓ TGF-β-p→↓ Smad2/3→↓CF	Mouse model of MI	(130)
			↓JP2(junctophilin-2)	miR-24 regulates excitation-contraction (E-C) coupling by targeting JP2	Aortic stenosis rat model	(131)
miR-26a	Profibrosis	Upregulated	Col1α2, Col1a1	Regulation of nuclear factor nuclear factor κB and progress of fibrosis	AngII/NRCFs	(129)
			CTGF/Smad1	BMP/Smad1 signaling	TAC/IkBa tg mouse	(132)
miR-15 family six miRs (miR-15a, miR-15b, miR-16, miR-195, miR-497, miR-322)	Antifibrosis	Upregulated	↓TGF-βR I	↓ TGF-β pathway ↓ Cardiac remodeling and fibrosis ↑cardiac function	Adult mice under ischemia–reperfusion (I/R) injuries	(133)
			p38, endoglin, Smad3/7	↓ECM remodeling in the overloaded heart ↓ TGF-β pathway	TAC/mouse	(134)
miR-1	Antifibrosis	Downregulated	↓Smad3	↓ TGF-β pathway→ ↓ Smad3→ ↓ CF	Mouse models of AngII-induced hypertension	(125)

(Continued)

TABLE 2 | Continued

Non-coding RNAs	Effect(s)	Modulation	Targets Smads	Signaling pathway	Model	References
miR-1	Antifibrosis	Downregulated	Fibullin	Activate ↑fibullin-2/MAPK→ ↓CF	AAB/rat	(135)
miR-101a	Antifibrosis	Downregulated	c-Fos Smad3	miR-101→↓c-Fos/TGF-β1 pathway → ↓p-Smad3 → ↓CF	Healthy male Sprague–Dawley rats (weight, 200–250 g) and C57BL/6 Mice	(136)
			TGF-βR1	↓TGF-βR I ↓ MAPK→ ↓CF	AngII, MI/rat MI, hypoxia/rat NRCFs and MI rat	(137)
miR-34a	Profibrosis	Upregulated	Smad4	↑TGF-β1/Smad4	MI, male C57BL/6 mice (12 weeks of age and a weight of 25–30 g)	
			Suppress PNUTS	Age-triggered expression of miR-34a→ ↓PNUTS→ inducing DNA damage responses along with telomere attrition→↑CF	Aging, MI/mice, human	(138)
miR-122	Antifibrosis	Downregulated	Smad4↓	↓TGF-β1→↓CF	AS (aortic stenosis patients)/human	(139, 140)
miR-378	Antifibrosis	Downregulated	↓Grb2/TGF /pSmad2/3, IGF1 receptor↓ Activate RTK Integrin β3↓ ↓cFos, ↓c-Jun and Ras	miR-378→ ↓TGF-β1–dependent paracrine mechanisms → ↓fibroblast migration and differentiation	AngII, TAC/mouse; NRCFs	(141)
miR-208a	Profibrosis	Upregulated	↑Smad3/4, ↑endoglin ↑β-MHC	↑miR-208a→ ↑TGF-β1 → ↑ endoglin/collagen I → ↑ CF	Aortacaval shunt/rat TAC mouse and RCFs	(142)
			↓Thrap1, myostatin ↑ Endoglin	Induced cardiac fibrosis and cardiac fiand card proliferation	TG mouse	(143)
miR-145	Antifibrosis	Upregulated	TGF-βR II	miR145 acts toward suppression of TGF-β-dependent extracellular matrix accumulation as well as fibrosis	Smooth muscle cells	(144)
			Smad2	Smad2 Alters macrophage sensitivity to TGF-β	AngII/mouse	(145)
miR-125b	Profibrosis	Upregulated	↓Apelin, p53	miR-125b→ Inhibition of p53→ induces fibroblast proliferation	TAC, AngII/mouse	(146)
miR-22	Profibrosis	Upregulated	Mimecan/osteoglycin (OGN)	miR-22→↓ OGN in age-associated cardiac alterations, including cardiac fibrosis	Aging/mouse; NRCFs	(147)
			Smad4 TGF-βR I in CFs	↑ TGF-β1→↑ complex (Smad2/3/4) →↑ CF	MI mice	(148, 149)
miR-142-3p	Antifibrosis	Downregulated	HMGB1 Smad3	miR-142-3p/HMGB1→↓ TGF-β1/Smad3→ ↓apoptosis and fibrosis	Mouse cardiomyocyte M6200 cells received treatment with H/R	
miR-433	Profibrosis	Upregulated	AZIN1 JNK1 Smad3	↓ AZIN1 → ↑ TGF-β1→↑ CF ↓JNK1 → ↑ MAPK kinase (ERK/P38) →↑ Smad3 →↑ CF	Neonatal rat CFs (8-week-old male C57BL/6 mice)	(123)
miR-499	Profibrosis	Upregulated	Acta1, Smads, Fos, Egr1, Egr2	↑ MAPK kinase (ERK/P38) /↑ TGF-β1 →↑CF	Neonatal rat cardiac fibroblasts. (NRCFs)	(143)
miR-10a	Profibrosis	Upregulated	↑Collagen I, collagen III, α-SMA, ↓ Smad7	TGF-β1/Smads ↑ Hydroxyproline →↑cardiac fibrosis and cardiac fibroblast proliferation	Atrial fibrillation (AF) rat	(8)

(Continued)

TABLE 2 | Continued

Non-coding RNAs	Effect(s)	Modulation	Targets Smads	Signaling pathway	Model	References
lncRNAs						
lncRNA, Crnde	Antifibrosis	Downregulated	Acta2 α-SMA Smad3	Smad3→↑ Crnde→ ↑rSBEs → ↓ Binding of Smad3 to the Acta2 / α-SMA gene promoter→↓CF ↑ Cardiac function	Mouse neonatal cardiac	(150)
GAS5	Antifibrosis	Downregulated	↓ miR-21/PTEN/MMP-2	GAS5→↓ miR-21 →↓TGF-β1/Smad2/3 →↓CF	ISO/rat; TGF-β1/NRCFs	(151)
5 lncRNAs(n379599, n379519, n384648, n380433, and n410105)	Profibrosis	Upregulated	↑P-Smad2/3 ↑Elastin, periostin, PAI-1, Snai1, Snai2, FBN1	TGF-β pathway →↑cardiac fibrosis	Ischemic cardiomyopathy	
			Col8A1,Col3A1 fibronection	TGF-β pathway (PAI-1, Snai1, Snai2,/p-Smad2/3) →↑cardiac fibrosis	ICM/human; mouse CFs	
lncRNAs CHRF	Profibrosis	Upregulated	miR-489	CHRF →regulate MyD88 and Smad3 by targeting miR-489→↑CF	AngII-treated myocytes Mouse model Human heart failure samples	(81, 152, 153)
Circular RNAs						
circ_000203	Profibrosis	Upregulated	MiR-26b-5p BMP/Smad1	CircRNA_000203→ ↓ miR-26b-5p(anti-fibrotic) →↑ Col1a2 /Col3a1/α-SMA CTGF→↑CF BMP/SMAD1 signaling	AngII/mouse CFs Diabetic mouse myocardium	(54, 84, 129, 154)
CircRNA_010567	Profibrosis	Upregulated	↓miR141 TGF-β/Smad pathway	CircRNA_010567→↓miR-141 →↑ TGF-β1 →↑Col I/ Col III/α-SMA. →↑CF	Diabetic mouse Myocardial fibrosis model	
circRNA–circNFIB	Antifibrosis	Upregulated	miR-433 TGF-β/Smad3	↑circNFIB →↓miR-433→↓CF	Mice post-MI cardiac fibroblasts	
circHIPK3	Pro fibrosis	Upregulated	miR-29b-3p Smad3	circHIPK3 → ↓miR-29b-3p →↑ TGF-β/Smad3→↑α-SMA, COL1A1, COL3A1 →↑CF	AngII-induced cardiac fibrosis	(155)

a variety of cardiac cell types, and with cardiac stress, they are expressed at higher levels (134, 163, 164). miR-15, in fibroblasts, targets some of TGF-β signaling cascade members, such as TGF-β1, p38, endoglin, Smad3, and Smad7, and as a result, leads to negative regulation of ECM production. Correspondingly, *in vivo* miR-15 suppression with LNA-based anti-miRs in mice resulted in higher levels of fibrosis following transverse aortic constriction (163). However, the miR-15 family inhibition in a mouse model of reperfusion injury led to smaller infarct sizes and lesser cardiac remodeling (134). **Table 2** lists various non-coding RNAs in the CF *via* activation/inhibition of Smad/TGF signaling pathway.

lncRNA and TGF-β/Smad Signaling in Cardiac Fibrosis

Several lncRNAs contribute to the TGF-β pathways affecting the ECM gene expression along with myofibroblast differentiation (165). According to Huang et al., regulation of lncRNAs expression took place in ICM dynamically, in which several lncRNAs further attend in the TGF-pathways provoking gene expression associated with accumulating collagen along with ECM protein encoding genes (e.g., COL14A1, COL16A1, COL12A1, COL8A1) and myofibroblast differentiation. Huang et al. reported altered lncRNA expression in ICM and demonstrated that CF-enriched lncRNAs such as n379599, n379519, n384648, n380433, and n410105 in mouse modulate the fimouse-associated gene expression by targeting TGF-β signaling (165). TGF-β expression targets PAI-1, Snai1, and Snai2 in CF, and several lncRNA overexpression indicated induction of these target gene expression by lncRNAs. It was also demonstrated that lncRNAs induced phosphorylated Smad2/3 and not Smad2/3 protein (165, 166).

Tao et al. recently studied the lncRNA growth arrest–specific 5 (GAS5) role and function in cardiac fibrosis and concluded that GAS5 *via* negative miR-21 regulation plays its suppressive role in cardiac fibrosis. Moreover, they demonstrated that the modulation of miR-21 regulated MMP-2 expression *via* a phosphatase as well as tensin homolog (PTEN) pathway in CFs

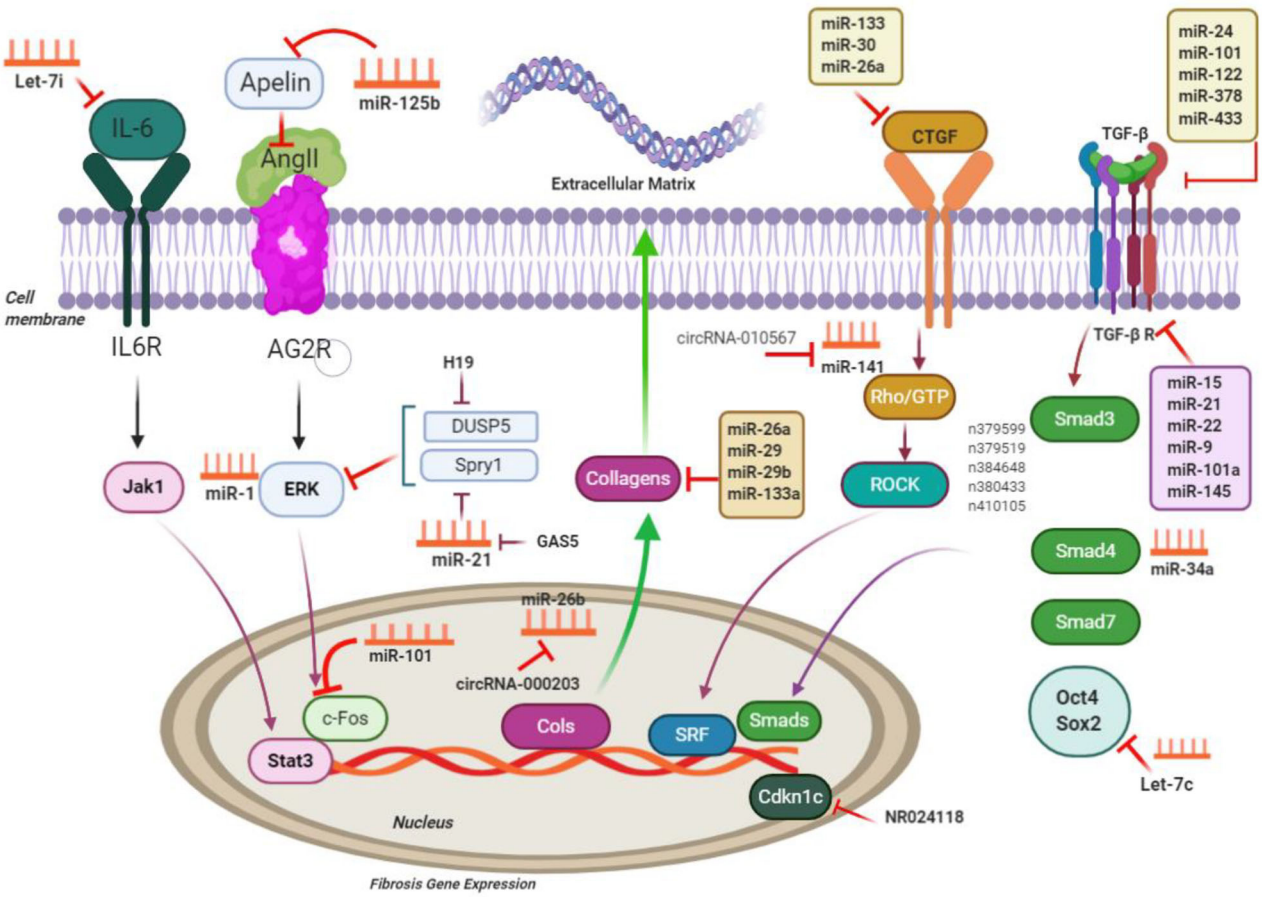

FIGURE 3 | ncRNAs engaged in the pathways of cardiac fibrosis; ncRNAs regulate processes related to cardiac fibrosis *via* targeting the main molecules mediating ECM gene transcription and performing TGF-β signaling; CTGF, connective tissue growth factor; Rho-GTP, Rho-GTPase-stimulating protein; ROCK, Rho related coiled-coil comprising protein kinase; SRF, serum response factor; MMP, matrix metalloproteinases; IL6, interleukin-6; Jak1, Janus kinase 1; Stat3, signal transducers and activators of transcription 3; c-Fos, FBJ murine osteosarcoma viral oncogene homolog; Spry1, sprouty homolog 1; ERK extracellular signal–regulated kinases; DUSP5, dual-specificity phosphatase 5. This figure was adapted from Chen et al. (49).

(151). miR-21 down regulation decreased secretion of TGF-β and phosphorylation of Smad2/3 in CFs (126).

lncRNAs and cardiac fibrosis CHRF (cardiac hypertrophy–related factor) upregulation was noted in myocytes treated with AngII and in the heart of a mouse model with transverse aortic constriction and human HF sample (152). CHRF knockdown increased miR-489 level but decreased Myd88 level in myocytes. CHRT overexpression reduced miR-489 level and upregulated Myd88 level and resulted in hypertrophic responses. Cardiac fibrosis was decreased in Myd88-knockout mice. CHRF regulates MyD88 and Smad3 by targeting miR-489. This study proposed CHRF as a role player in cardiac fibrosis by miR-489 and Myd88 adjustment (81, 152). lncRNA Crnde, by means of Smad3-Crnde negative feedback in diabetic cardiomyopathy, alleviates cardiac fibrosis. Crnde overexpression markedly prevents α-SMA promoter activity induced by TGF-β. Crnde stops Smad3 transcriptional activity *via* rSBEs (RNA SBEs) (49, 150, 165, 166).

circRNA and TGF-β/Smad Signaling in Cardiac Fibrosis

Zhou et al. (84) showed that circRNA-010567 boosts myocardial fibrosis through suppression of miR-141 suppression along with targeting TGF-β1 in a mice model with diabetes. In another recent article, it was shown that upregulation of CircRNA_000203 took place in diabetic mice cardiac muscle and in AngII-triggered fibroblasts in the animal's heart (54). CircRNA_000203 characterizes as a miR-26-5p sponge and interacts with miR-26-5p and fibrosis-related genes Col1a2, Col3a1, and α-SMA and CTGF in fibroblasts in mouse heart (54, 167).

Zhu et al. suggested that the circNFIB–miR-433 axis can potentially provide new therapeutic target to treat fibrotic diseases. circNFIB overexpression decreased pro-proliferative impacts stimulated by means of the miR-433 mimic, while inhibiting circNFIB led to contrary results. circNFIB was recognized as a miR-433 endogenous sponge. circNFIB

upregulation also lessened the activation of p38, ERK kinases, and the Smad3 signaling pathways were indicated through reduced ratios of p-p38/p38, p-ERK/ERK, and p-Smad3/Smad3 (168).

CircHIPK3 expression led to a significant increase in CFs and heart tissues following AngII treatments. CircHIPK3 silencing decreased CFs proliferating as well as migrating and the α-SMA expression level upregulation triggered by AngII *in vitro*. circHIPK3 served as a miR-29b-3p sponge, and circHIPK3 overexpression reversed miR-29b-3p–triggered inhibition of CF proliferation and migration, while altering miR-29b-3p targeting genes (α-SMA, COL1A1, COL3A1) expression levels *in vitro*. circHIPK3 silencing and miR-29b-3p overexpression conjointly exerted more severe effects on suppression of cardiac fibrotic event *in vivo* compared to either of them alone. In addition, the expression of circHIPK3 was also markedly increased after TGF-β1 treatment (155). Their data suggested that circHIPK3 functions as a miR-29b-3p sponge in the adjustment of CF proliferating, migrating, and promoting cardiac fibrotic event, introducing possible novel targets to be explored in preventing cardiac fibrosis triggered by AngII (155).

CONCLUSION

The uncompromising progress of fibrosis represents a pathological finding inherent to multiple cardiac diseases. Gaining insight into these fibrotic processes in terms of the functional characteristics and molecular profiling could make it possible to prevent and treat fibrotic lesions in the heart. An enlarging body of evidence addresses the cross-talk between the TGF-β and Smad signaling pathways and its contribution to cardiac fibrosis pathogenesis. Despite the fact that the TGF-β and Smad pathways have been extensively studied, their contributions to profibrotic pathways in cardiac diseases are yet to be known. ncRNAs have been identified as possible role players in strategies for mitigating CVDs, as discussed before. Current research on ncRNAs described herein focuses on the role of ncRNAs in regulating cell signaling pathways, particularly TGF-β and Smad signaling. The identified signaling pathways discussed herein, which have roles in the involvement of ncRNAs in cardiac fibrosis, may offer novel putative targets for therapeutic approaches for cardiac fibrosis. More studies are required to better understand the mechanisms by which the ncRNA network induces cardiac fibrotic events *via* TGF-β/Smad signaling. In addition, the potential clinical significance of the TGF-β/Smad-associated ncRNAs, including miRNAs implemented as therapeutic instruments and circRNAs employed as diagnostic/prognostic biomarkers for cardiac fibrotic cases, needs testing in additional animal models as well as clinical conditions.

AUTHOR CONTRIBUTIONS

HM involved in conception, design, statistical analysis, and drafting of the manuscript. LS, SN, MAs, MM-T, SS, BA, MN, BM, MAb, and HR contributed in data collection and manuscript drafting. All authors approved the final version for submission.

REFERENCES

1. Yousefi F, Shabaninejad Z, Vakili S, Derakhshan M, Movahedpour A, Dabiri H, et al. TGF-β and WNT signaling pathways in cardiac fibrosis: non-coding RNAs come into focus. *Cell Commun Signal.* (2020) 18:87. doi: 10.1186/s12964-020-00555-4
2. Schelbert EB, Fonarow GC, Bonow RO, Butler J, Gheorghiade M. Therapeutic targets in heart failure: refocusing on the myocardial interstitium. *J Am Coll Cardiol.* (2014) 63:2188–98. doi: 10.1016/j.jacc.2014.01.068
3. Zannad F, Alla F, Dousset B, Perez A, Pitt B. Limitation of excessive extracellular matrix turnover may contribute to survival benefit of spironolactone therapy in patients with congestive heart failure: insights from the randomized aldactone evaluation study (RALES). *Rales Invest Circ.* (2000) 102:2700–6. doi: 10.1161/01.CIR.102.22.2700
4. Izawa H, Murohara T, Nagata K, Isobe S, Asano H, Amano T, et al. Mineralocorticoid receptor antagonism ameliorates left ventricular diastolic dysfunction and myocardial fibrosis in mildly symptomatic patients with idiopathic dilated cardiomyopathy: a pilot study. *Circulation.* (2005) 112:2940–45. doi: 10.1161/CIRCULATIONAHA.105.571653
5. Travers JG, Kamal FA, Robbins J, Yutzey KE, Blaxall BC. Cardiac fibrosis: the fibroblast awakens. *Circ Res.* (2016) 118:1021–40. doi: 10.1161/CIRCRESAHA.115.306565
6. Dobaczewski, M., Gonzalez-Quesada, C., and Frangogiannis, N. G. (2010). The extracellular matrix as a modulator of the inflammatory and reparative response following myocardial infarction. *J Mol Cell Cardiol* 48, 504–511. doi: 10.1016/j.yjmcc.2009.07.015
7. Khalil H, Kanisicak O, Prasad V, Correll RN, Fu X, Schips T, et al. Fibroblast-specific TGF-β-Smad2/3 signaling underlies cardiac fibrosis. *J Clin Invest.* (2017) 127:3770–83. doi: 10.1172/JCI94753
8. Li P-F, He R-H, Shi S-B, Li R, Wang Q-T, Rao G-T., et al. Modulation of miR-10a-mediated TGF-β1/Smads signaling affects atrial fibrillation-induced cardiac fibrosis and cardiac fibroblast proliferation. *Biosci Rep.* (2019) 39:BSR20181931. doi: 10.1042/BSR20181931
9. Wang L, Jiang P, He Y, Hu H, Guo Y, Liu X, et al. A novel mechanism of Smads/miR-675/TGFβR1 axis modulating the proliferation and remodeling of mouse cardiac fibroblasts. *J Cell Physicol.* (2019) 234:20275–85. doi: 10.1002/jcp.28628
10. Wei Y, Wu Y, Feng K, Zhao Y, Tao R, Xu H, et al. Astragaloside IV inhibits cardiac fibrosis via miR-135a-TRPM7-TGF-β/Smads pathway. *J Ethnopharmacol.* (2020) 249:112404. doi: 10.1016/j.jep.2019.112404
11. Carthy JM, Garmaroudi FS, Luo Z, McManus BM. Wnt3a induces myofibroblast differentiation by upregulating TGF-β signaling through SMAD2 in a β-catenin-dependent manner. *PLoS ONE.* (2011) 6:e19809. doi: 10.1371/journal.pone.0019809
12. Tran BH, Yu Y, Chang L, Tan B. A novel liposomal s-propargyl-cysteine: a sustained release of hydrogen sulfide reducing myocardial fibrosis via TGF-β1/Smad Pathway. *Int J Nanomed.* (2019) 14:10061–77. doi: 10.2147/IJN.S216667
13. Weber KT, Brilla CG. Pathological hypertrophy and cardiac interstitium. Fibrosis and renin-angiotensin-aldosterone system. *Circulation.* (1991) 83:1849–65. doi: 10.1161/01.CIR.83.6.1849
14. Kong P, Christia P, Frangogiannis NG. The pathogenesis of cardiac fibrosis. *Cell Mol Life Sci.* (2014) 71:549–74. doi: 10.1007/s00018-013-1349-6
15. Frangogiannis NG. Cardiac fibrosis: cell biological mechanisms, molecular pathways and therapeutic opportunities. *Mol Aspects Med.* (2019) 65:70–99. doi: 10.1016/j.mam.2018.07.001
16. Ma Z-G, Yuan Y-P, Wu H-M, Zhang X, Tang Q-Z. Cardiac fibrosis: new insights into the pathogenesis. *Int J Biol Sci.* (2018) 14:1645. doi: 10.7150/ijbs.28103

17. Kim EK, Choi E-J. Compromised MAPK signaling in human diseases: an update. *Arch Toxicol.* (2015) 89:867–82. doi: 10.1007/s00204-015-1472-2
18. Beauvais S, Drevelle O, Jann J, Lauzon M-A, Foruzanmehr M, Grenier G, et al. Interactions between bone cells and biomaterials: an update. *Front Biosci (Sch Ed).* (2016) 8:227–63. doi: 10.2741/s460
19. van Almen GC, Verhesen W, van Leeuwen RE, van de Vrie M, Eurlings C, Schellings MW, et al. MicroRNA-18 and microRNA-19 regulate CTGF and TSP-1 expression in age-related heart failure. *Aging Cell.* (2011) 10:769–79. doi: 10.1111/j.1474-9726.2011.00714.x
20. Abonnenc M, Nabeebaccus AA, Mayr U, Barallobre-Barreiro J, Dong X, Cuello F, et al. Extracellular matrix secretion by cardiac fibroblasts: role of microRNA-29b and microRNA-30c. *Circ Res.* (2013) 113:1138–47. doi: 10.1161/CIRCRESAHA.113.302400
21. Yang C, Zheng SD, Wu HJ, Chen SJ. Regulatory mechanisms of the molecular pathways in fibrosis induced by microRNAs. *Chin Med J (Engl).* (2016) 129:2365–72. doi: 10.4103/0366-6999.190677
22. An Z, Yang G, Zheng H, Nie W, Liu G. Biomarkers in patients with myocardial fibrosis. *Open Life Sci.* (2017) 12:337–44. doi: 10.1515/biol-2017-0039
23. Bai J, Xi Q. Crosstalk between TGF-β signaling and epigenome. *Acta biochimica et biophysica Sinica.* (2018) 50:60–7. doi: 10.1093/abbs/gmx122
24. Hanna A, Frangogiannis NG. The role of the TGF-beta superfamily in myocardial infarction. *Front Cardiovasc Med.* (2019) 6:140. doi: 10.3389/fcvm.2019.00140
25. Hata A, Chen Y-G. TGF-β signaling from receptors to Smads. *Cold Spring Harb Perspect Biol.* (2016) 8:a022061. doi: 10.1101/cshperspect.a022061
26. Aykul S, Martinez-Hackert E. Transforming growth factor-β family ligands can function as antagonists by competing for type II receptor binding. *J Biol Chem.* (2016) 291:10792–804. doi: 10.1074/jbc.M115.713487
27. Walton KL, Johnson KE, Harrison CA. Targeting TGF-beta mediated SMAD signaling for the prevention of fibrosis. *Front Pharmacol.* (2017) 8:461. doi: 10.3389/fphar.2017.00461
28. Yan X, Zhang J, Pan L, Wang P, Xue H, Zhang L, et al. TSC-22 promotes transforming growth factor β-mediated cardiac myofibroblast differentiation by antagonizing Smad7 activity. *Mol Cell Biol.* (2011) 31:3700–9. doi: 10.1128/MCB.05448-11
29. MacDonald EM, Cohn RD. TGFβ signaling: its role in fibrosis formation and myopathies. *Curr Opin Rheumatol.* (2012) 24:628–34. doi: 10.1097/BOR.0b013e328358df34
30. Rebbapragada A, Benchabane H, Wrana J, Celeste A, Attisano L. Myostatin signals through a transforming growth factor β-like signaling pathway to block adipogenesis. *Mol Cell Biol.* (2003) 23:7230–42. doi: 10.1128/MCB.23.20.7230-7242.2003
31. Hudnall AM, Arthur JW, Lowery JW. Clinical relevance and mechanisms of antagonism between the BMP and activin/TGF-β signaling pathways. *J Am Osteopath Assoc.* (2016) 116:452. doi: 10.7556/jaoa.2016.089
32. Verrecchia F, Chu M-L, Mauviel A. Identification of novel TGF-β/Smad gene targets in dermal fibroblasts using a combined cDNA microarray/promoter transactivation approach. *J Biol Chem.* (2001) 276:17058–62. doi: 10.1074/jbc.M100754200
33. Dennler S, Itoh S, Vivien D, ten Dijke P, Huet S, Gauthier JM. Direct binding of Smad3 and Smad4 to critical TGFβ-inducible elements in the promoter of human plasminogen activator inhibitor-type 1 gene. *EMBO J.* (1998) 17:3091–100. doi: 10.1093/emboj/17.11.3091
34. Hua X, Liu X, Ansari DO, Lodish HF. Synergistic cooperation of TFE3 and smad proteins in TGF-β-induced transcription of the plasminogen activator inhibitor-1 gene. *Genes Dev.* (1998) 12:3084–95. doi: 10.1101/gad.12.19.3084
35. Schönherr E, Järveläinen H, Sandell L, Wight T. Effects of platelet-derived growth factor and transforming growth factor-beta 1 on the synthesis of a large versican-like chondroitin sulfate proteoglycan by arterial smooth muscle cells. *J Biol Chem.* (1991) 266:17640–7.
36. ROMARiS M, Bassols A, David G. Effect of transforming growth factor-β1 and basic fibroblast growth factor on the expression of cell surface proteoglycans in human lung fibroblasts. Enhanced glycanation and fibronectin-binding of CD44 proteoglycan, and down-regulation of glypican. *Biochem J.* (1995) 310:73–81. doi: 10.1042/bj3100073
37. Dadlani H, Ballinger ML, Osman N, Getachew R, Little PJ. Smad and p38 MAP kinase-mediated signaling of proteoglycan synthesis in vascular smooth muscle. *J Biol Chem.* (2008) 283:7844–52. doi: 10.1074/jbc.M703125200
38. Margadant C, Sonnenberg A. Integrin–TGF-β crosstalk in fibrosis, cancer and wound healing. *EMBO Rep.* (2010) 11:97–105. doi: 10.1038/embor.2009.276
39. Chen Y, Blom IE, Sa S, Goldschmeding R, Abraham DJ, Leask A. CTGF expression in mesangial cells: involvement of SMADs, MAP kinase, and PKC. *Kidney Int.* (2002) 62:1149–59. doi: 10.1111/j.1523-1755.2002.kid567.x
40. Yuan W, Varga J. Transforming growth factor-β repression of matrix metalloproteinase-1 in dermal fibroblasts involves Smad3. *J Biol Chem.* (2001) 276:38502–10. doi: 10.1074/jbc.M107081200
41. Khan S, Joyce J, Margulies KB, Tsuda T. Enhanced bioactive myocardial transforming growth factor-β in advanced human heart failure. *Circ J.* (2014) 78:2711–8. doi: 10.1253/circj.CJ-14-0511
42. Khan SA, Dong H, Joyce J, Sasaki T, Chu M-L, Tsuda T. Fibulin-2 is essential for angiotensin II-induced myocardial fibrosis mediated by transforming growth factor (TGF)-β. *Lab Invest.* (2016) 96:773. doi: 10.1038/labinvest.2016.52
43. Gong K, Chen Y-F, Li P, Lucas JA, Hage FG, Yang Q, et al. Transforming growth factor-β inhibits myocardial PPARγ expression in pressure overload-induced cardiac fibrosis and remodeling in mice. *J Hypertens.* (2011) 29:1810. doi: 10.1097/HJH.0b013e32834a4d03
44. Yu Q-G, Zhang Y. Transforming growth factor-β1 mediates NADPH oxidase 4: a significant contributor to the pathogenesis of myocardial fibrosis. *Int J Cardiol.* (2017) 227:53–4. doi: 10.1016/j.ijcard.2016.10.118
45. Kumawat K, Menzen MH, Slegtenhorst RM, Halayko AJ, Schmidt M, Gosens R. TGF-β-activated kinase 1 (TAK1) signaling regulates TGF-β-induced WNT-5A expression in airway smooth muscle cells via Sp1 and β-catenin. *PLoS ONE.* (2014) 9:e94801. doi: 10.1371/journal.pone.0094801
46. Blyszczuk P, Müller-Edenborn B, Valenta T, Osto E, Stellato M, Behnke S, et al. Transforming growth factor-β-dependent Wnt secretion controls myofibroblast formation and myocardial fibrosis progression in experimental autoimmune myocarditis. *Eur Heart J.* (2017) 38:1413–25. doi: 10.1093/eurheartj/ehw116
47. Zhang Y, Yan H, Guang G-c, Deng Z-r. Overexpressed connective tissue growth factor in cardiomyocytes attenuates left ventricular remodeling induced by angiotensin II perfusion. *Clin Exp Hyperten.* (2017) 39:168–74. doi: 10.1080/10641963.2016.1226893
48. Hashemian SM, Pourhanifeh MH, Fadaei S, Velayati AA, Mirzaei H, Hamblin MR. Non-coding RNAs and exosomes: their role in the pathogenesis of sepsis. *Mol Ther Nucleic Acids.* (2020) 21:51–74. doi: 10.1016/j.omtn.2020.05.012
49. Chen Z, Li C, Lin K, Cai H, Ruan W, Han J, et al. Non-coding RNAs in cardiac fibrosis: emerging biomarkers and therapeutic targets. *Cardiol J.* (2018) 25:732–41. doi: 10.5603/CJ.a2017.0153
50. Tao H, Yang J-J, Shi K-H. Non-coding RNAs as direct and indirect modulators of epigenetic mechanism regulation of cardiac fibrosis. *Expert Opin Ther Targets.* (2015) 19:707–16. doi: 10.1517/14728222.2014.1001740
51. Kumarswamy R, Volkmann I, Jazbutyte V, Dangwal S, Park D-H, Thum T. Transforming growth factor-β-induced endothelial-to-mesenchymal transition is partly mediated by microRNA-21. *Arterioscler Thromb Vasc Biol.* (2012) 32:361–9. doi: 10.1161/ATVBAHA.111.234286
52. Cao W, Shi P, Ge JJ. miR-21 enhances cardiac fibrotic remodeling and fibroblast proliferation via CADM1/STAT3 pathway. *BMC Cardiovasc Disord.* (2017) 17:88. doi: 10.1186/s12872-017-0520-7
53. Harada M, Luo X, Qi XY, Tadevosyan A, Maguy A, Ordog B, et al. Transient receptor potential canonical-3 channel-dependent fibroblast regulation in atrial fibrillation. *Circulation.* (2012) 126:2051–64. doi: 10.1161/CIRCULATIONAHA.112.121830
54. Tang CM, Zhang M, Huang L, Hu ZQ, Zhu JN, Xiao Z, et al. CircRNA_000203 enhances the expression of fibrosis-associated genes by derepressing targets of miR-26b-5p, Col1a2 and CTGF, in cardiac fibroblasts. *Sci Rep.* (2017) 7:40342. doi: 10.1038/srep40342
55. Bernardo BC, Gao X-M, Winbanks CE, Boey EJ, Tham YK, Kiriazis H, et al. Therapeutic inhibition of the miR-34 family attenuates pathological cardiac remodeling and improves heart function. *Proc Natl Acad Sci.* (2012) 109:17615–20. doi: 10.1073/pnas.1206432109

56. Katare R, Riu F, Mitchell K, Gubernator M, Campagnolo P, Cui Y, et al. Transplantation of human pericyte progenitor cells improves the repair of infarcted heart through activation of an angiogenic program involving micro-RNA-132. *Circ Res.* (2011) 109:894–906. doi: 10.1161/CIRCRESAHA.111.251546
57. Duisters RF, Tijsen AJ, Schroen B, Leenders JJ, Lentink V, et al. miR-133 and miR-30 regulate connective tissue growth factor: implications for a role of microRNAs in myocardial matrix remodeling. *Circ Res.* (2009) 104:170–8, 176p following 178. doi: 10.1161/CIRCRESAHA.108.182535
58. Matkovich SJ, Wang W, Tu Y, Eschenbacher WH, Dorn LE, Condorelli G, et al. MicroRNA-133a protects against myocardial fibrosis and modulates electrical repolarization without affecting hypertrophy in pressure-overloaded adult hearts. *Circ Res.* (2010) 106:166–75. doi: 10.1161/CIRCRESAHA.109.202176
59. Wang C, Zhang C, Liu L, Xi A, Chen B, Li Y, et al. Macrophage-derived mir-155-containing exosomes suppress fibroblast proliferation and promote fibroblast inflammation during cardiac injury. *Mol Ther.* (2017) 25:192–204. doi: 10.1016/j.ymthe.2016.09.001
60. da Costa Martins PA, Salic K, Gladka MM, Armand A-S, Leptidis S., El Azzouzi H, et al. MicroRNA-199b targets the nuclear kinase Dyrk1a in an auto-amplification loop promoting calcineurin/NFAT signalling. *Nat Cell Biol.* (2010) 12:1220. doi: 10.1038/ncb2126
61. van Rooij E, Sutherland LB, Qi X, Richardson JA, Hill J, Olson EN. Control of stress-dependent cardiac growth and gene expression by a microRNA. *Science.* (2007) 316:575–9. doi: 10.1126/science.1139089
62. Aurora AB, Mahmoud AI, Luo X, Johnson BA, Van Rooij E, Matsuzaki S, et al. (2012). MicroRNA-214 protects the mouse heart from ischemic injury by controlling Ca 2+ overload and cell death. *J Clin Invest.* 122:1222–32. doi: 10.1172/JCI59327
63. Huang ZW, Tian LH, Yang B, Guo RM. Long noncoding RNA H19 acts as a competing endogenous RNA to mediate CTGF expression by sponging miR-455 in cardiac fibrosis. *DNA Cell Biol.* (2017) 36:759–66. doi: 10.1089/dna.2017.3799
64. Liu X, Xu Y, Deng Y, Li H. MicroRNA-223 regulates cardiac fibrosis after myocardial infarction by targeting RASA1. *Cell Physiol Biochem.* (2018) 46:1439–54. doi: 10.1159/000489185
65. Li J, Dai Y, Su Z, Wei G. MicroRNA-9 inhibits high glucose-induced proliferation, differentiation and collagen accumulation of cardiac fibroblasts by down-regulation of TGFBR2. *Biosci Rep.* (2016) 36:e00417. doi: 10.1042/BSR20160346
66. Wang X, Wang H-X, Li Y-L, Zhang C-C, Zhou C-Y, Wang L, et al. MicroRNA Let-7i negatively regulates cardiac inflammation and fibrosis. *Hypertension.* (2015) 66:776–85. doi: 10.1161/HYPERTENSIONAHA.115.05548
67. Tolonen AM, Magga J, Szabo Z, Viitala P, Gao E, Moilanen AM, et al. Inhibition of Let-7 micro RNA attenuates myocardial remodeling and improves cardiac function postinfarction in mice. *Pharmacol Res Perspect.* (2014) 2:e00056. doi: 10.1002/prp2.56
68. Tao H, Cao W, Yang JJ, Shi KH, Zhou X, Liu LP, et al. Long noncoding RNA H19 controls DUSP5/ERK1/2 axis in cardiac fibroblast proliferation and fibrosis. *Cardiovasc Pathol.* (2016) 25:381–9. doi: 10.1016/j.carpath.2016.05.005
69. Qu X, Du Y, Shu Y, Gao M, Sun F, Luo S, et al. MIAT Is a pro-fibrotic long non-coding RNA governing cardiac fibrosis in post-infarct myocardium. *Sci Rep.* (2017) 7:42657. doi: 10.1038/srep42657
70. Huang S, Zhang L, Song J, Wang Z, Huang X, Guo Z, et al. Long noncoding RNA MALAT1 mediates cardiac fibrosis in experimental postinfarct myocardium mice model. *J Cell Physiol.* (2019) 234:2997–3006. doi: 10.1002/jcp.27117
71. Hobuss L, Bar C, Thum T. Long non-coding RNAs: at the heart of cardiac dysfunction? *Front Physiol.* (2019) 10:30. doi: 10.3389/fphys.2019.00030
72. Piccoli M-T, Gupta SK, Viereck J, Foinquinos A, Samolovac S, Kramer FL, et al. Inhibition of the cardiac fibroblast–enriched lncRNA Meg3 prevents cardiac fibrosis and diastolic dysfunction. *Circ Res.* (2017) 121:575–83. doi: 10.1161/CIRCRESAHA.117.310624
73. Guo M, Liu T, Zhang S, Yang L. RASSF1-AS1, an antisense lncRNA of RASSF1A, inhibits the translation of RASSF1A to exacerbate cardiac fibrosis in mice. *Cell Biol Int.* (2018) 43:1163–73. doi: 10.1002/cbin.11085
74. Micheletti R, Plaisance I, Abraham BJ, Sarre A, Ting C-C, Alexanian M, et al. The long noncoding RNA Wisper controls cardiac fibrosis and remodeling. *Sci Transl Med.* (2017) 9:eaai9118. doi: 10.1126/scitranslmed.aai9118
75. Zhang Y, Zhang YY, Li TT, Wang J, Jiang Y, Zhao Y, et al. Ablation of interleukin-17 alleviated cardiac interstitial fibrosis and improved cardiac function via inhibiting long non-coding RNA-AK081284 in diabetic mice. *J Mol Cell Cardiol.* (2018) 115:64–72. doi: 10.1016/j.yjmcc.2018.01.001
76. Kirabo A, Ryzhov S, Gupte M, Sengsayadeth S, Gumina RJ, Sawyer DB, et al. Neuregulin-1beta induces proliferation, survival and paracrine signaling in normal human cardiac ventricular fibroblasts. *J Mol Cell Cardiol.* (2017) 105:59–69. doi: 10.1016/j.yjmcc.2017.03.001
77. Leisegang MS. LET's sponge: how the lncRNA PFL promotes cardiac fibrosis. *Theranostics.* (2018) 8:874–7. doi: 10.7150/thno.23364
78. Liang H, Pan Z, Zhao X, Liu L, Sun J, Su X, et al. LncRNA PFL contributes to cardiac fibrosis by acting as a competing endogenous RNA of let-7d. *Theranostics.* (2018) 8:1180–94. doi: 10.7150/thno.20846
79. Zhu J-N, Chen R, Fu Y-H, Lin Q-X, Huang S, Guo L-L, et al. Smad3 inactivation and MiR-29b upregulation mediate the effect of carvedilol on attenuating the acute myocardium infarction-induced myocardial fibrosis in rat. *PLoS ONE.* (2013) 8:e75557. doi: 10.1371/journal.pone.0075557
80. Han P, Li W, Lin C-H, Yang J, Shang C, Nurnberg ST, et al. A long noncoding RNA protects the heart from pathological hypertrophy. *Nature.* (2014) 514:102. doi: 10.1038/nature13596
81. Wang K, Liu F, Zhou LY, Long B, Yuan SM, Wang Y, et al. The long noncoding RNA CHRF regulates cardiac hypertrophy by targeting miR-489. *Circ Res.* (2014) 114:1377–88. doi: 10.1161/CIRCRESAHA.114.302476
82. Sun Y, Yang Z, Zheng B, Zhang XH, Zhang ML, Zhao XS, et al. A novel regulatory mechanism of smooth muscle alpha-actin expression by NRG-1/circACTA2/miR-548f-5p axis. *Circ Res.* (2017) 121:628–35. doi: 10.1161/CIRCRESAHA.117.311441
83. Lin J-F, Chen P-C, Thomas I, Hwang S. Autophagy modulation by dysregulated micrornas in human bladder cancer. *Urological Sci.* (2019) 30:46. doi: 10.4103/UROS.UROS_97_18
84. Zhou B, Yu JW. A novel identified circular RNA, circRNA_010567, promotes myocardial fibrosis via suppressing miR-141 by targeting TGF-beta1. *Biochem Biophys Res Commun.* (2017) 487:769–75. doi: 10.1016/j.bbrc.2017.04.044
85. Pourhanifeh MH, Mahjoubin-Tehran M, Karimzadeh MR, Mirzaei HR, Razavi ZS, Sahebkar A, et al. Autophagy in cancers including brain tumors: role of MicroRNAs. *Cell Commun Signal.* (2020) 18:88. doi: 10.1186/s12964-020-00587-w
86. Pourhanifeh MH, Vosough M, Mahjoubin-Tehran M, Hashemipour M, Nejati M, Abbasi-Kolli M, et al. Autophagy-related microRNAs: possible regulatory roles and therapeutic potential in and gastrointestinal cancers. *Pharmacol Res.* (2020) 161:105133. doi: 10.1016/j.phrs.2020.105133
87. Thum T. Noncoding RNAs and myocardial fibrosis. *Nat Rev Cardiol.* (2014) 11:655–63. doi: 10.1038/nrcardio.2014.125
88. Latronico MV, Condorelli G. MicroRNAs and cardiac pathology. *Nat Rev Cardiol.* (2009) 6:418. doi: 10.1038/nrcardio.2009.56
89. Dong D-l, Yang B-f. Role of microRNAs in cardiac hypertrophy, myocardial fibrosis and heart failure. *Acta Pharmaceutica Sinica B.* (2011) 1:1–7. doi: 10.1016/j.apsb.2011.04.010
90. Wang J, Liew OW, Richards AM, Chen YT. Overview of MicroRNAs in cardiac hypertrophy, fibrosis, and apoptosis. *Int J Mol Sci.* (2016) 17:749. doi: 10.3390/ijms17050749
91. Colpaert RM, Calore M. microRNAs in cardiac diseases. *Cells.* (2019) 8:737. doi: 10.3390/cells8070737
92. Piccoli MT, Bar C, Thum T. Non-coding RNAs as modulators of the cardiac fibroblast phenotype. *J Mol Cell Cardiol.* (2016) 92:75–81. doi: 10.1016/j.yjmcc.2015.12.023
93. Callis TE, Pandya K, Seok HY, Tang RH, Tatsuguchi M, Huang ZP, et al. MicroRNA-208a is a regulator of cardiac hypertrophy and conduction in mice. *J Clin Invest.* (2009) 119:2772–86. doi: 10.1172/JCI36154
94. Zhou C, Cui Q, Su G, Guo X, Liu X, Zhang J. MicroRNA-208b alleviates post-infarction myocardial fibrosis in a rat model by inhibiting GATA4. *Med Sci Monit.* (2016) 22:1808–16. doi: 10.12659/MSM.896428

95. Meng XM, Tang PM, Li J, Lan HY. TGF-beta/Smad signaling in renal fibrosis. *Front Physiol.* (2015) 6:82. doi: 10.3389/fphys.2015.00082
96. Stawowy P, Margeta C, Kallisch H, Seidah NG, Chretien M, Fleck E, et al. Regulation of matrix metalloproteinase MT1-MMP/MMP-2 in cardiac fibroblasts by TGF-beta1 involves furin-convertase. *Cardiovasc Res.* (2004) 63:87–97. doi: 10.1016/j.cardiores.2004.03.010
97. Dogar AM, Towbin H, Hall J. Suppression of latent transforming growth factor (TGF)-beta1 restores growth inhibitory TGF-beta signaling through microRNAs. *J Biol Chem.* (2011) 286:16447–58. doi: 10.1074/jbc.M110.208652
98. Chen C, Ponnusamy M, Liu C, Gao J, Wang K, Li P. MicroRNA as a therapeutic target in cardiac remodeling. *Biomed Res Int.* (2017) 2017:1278436. doi: 10.1155/2017/1278436
99. Nakaya M, Watari K, Tajima M, Nakaya T, Matsuda S, Ohara H, et al. Cardiac myofibroblast engulfment of dead cells facilitates recovery after myocardial infarction. *J Clin Invest.* (2017) 127:383–401. doi: 10.1172/JCI83822
100. Del Re DP, Amgalan D. Fundamental mechanisms of regulated cell death and implications for heart disease. *Physicol Rev.* (2019) 99:1765–817. doi: 10.1152/physrev.00022.2018
101. Cáceres FT, Gaspari TA, Samuel CS, Pinar AA. Serelaxin inhibits the profibrotic TGF-β1/IL-1β axis by targeting TLR-4 and the NLRP3 inflammasome in cardiac myofibroblasts. *Faseb J.* (2019) 33:14717–33. doi: 10.1096/fj.201901079RR
102. Tschöpe C, Müller I, Xia Y, Savvatis K, Pappritz K, Pinkert S, et al. NOD2 (Nucleotide-Binding Oligomerization Domain 2) is a major pathogenic mediator of coxsackievirus B3-induced myocarditis. *Circ Heart Fail.* (2017) 10:e003870. doi: 10.1161/CIRCHEARTFAILURE.117.003870
103. Xu C, Zhang Y, Wang Q, Xu Z, Jiang J, Gao Y, et al. Long non-coding RNA GAS5 controls human embryonic stem cell self-renewal by maintaining NODAL signalling. *Nat Commun.* (2016) 7:13287. doi: 10.1038/ncomms13287
104. Wu N, Zhang X, Bao Y, Yu H, Jia D, Ma C. Down-regulation of GAS5 ameliorates myocardial ischaemia/reperfusion injury via the miR-335/ROCK1/AKT/GSK-3β axis. *J Cell Mol Med.* (2019) 23:8420–31. doi: 10.1111/jcmm.14724
105. She Q, Shi P, Xu SS, Xuan HY, Tao H, Shi KH. DNMT1 methylation of LncRNA GAS5 leads to cardiac fibroblast pyroptosis via affecting NLRP3 axis. *Inflamation.* (2020) 43:1065–76. doi: 10.1007/s10753-020-01191-3
106. Rosenbluh J, Nijhawan D, Chen Z, Wong KK, Masutomi K, Hahn WC. RMRP is a non-coding RNA essential for early murine development. *PLoS ONE.* (2011) 6:e26270. doi: 10.1371/journal.pone.0026270
107. Meng Q, Ren M, Li Y, Song X. LncRNA-RMRP acts as an oncogene in lung cancer. *PLoS ONE.* (2016) 11:e0164845. doi: 10.1371/journal.pone.0164845
108. Shao Y, Ye M, Li Q, Sun W, Ye G, Zhang X, et al. LncRNA-RMRP promotes carcinogenesis by acting as a miR-206 sponge and is used as a novel biomarker for gastric cancer. *Oncotarget.* (2016) 7:37812–24. doi: 10.18632/oncotarget.9336
109. Feng W, Li L, Xu X, Jiao Y, Du W. Up-regulation of the long non-coding RNA RMRP contributes to glioma progression and promotes glioma cell proliferation and invasion. *Arch Med Sci.* (2017) 13:1315–21. doi: 10.5114/aoms.2017.66747
110. Wang X, Peng L, Gong X, Zhang X, Sun R, Du J. LncRNA-RMRP promotes nucleus pulposus cell proliferation through regulating miR-206 expression. *J Cell Mol Med.* (2018) 22:5468–76. doi: 10.1111/jcmm.13817
111. Greco S, Zaccagnini G, Perfetti A, Fuschi P, Valaperta R, Voellenkle C, et al. Long noncoding RNA dysregulation in ischemic heart failure. *J Transl Med.* (2016) 14:183. doi: 10.1186/s12967-016-0926-5
112. Steinbusch MMF, Caron MMJ, Surtel DAM, Friedrich F, Lausch E, Pruijn GJM, et al. Expression of RMRP RNA is regulated in chondrocyte hypertrophy and determines chondrogenic differentiation. *Sci Rep.* (2017) 7:6440. doi: 10.1038/s41598-017-06809-5
113. Zhang SY, Huang SH, Gao SX, Wang YB, Jin P, Lu FJ. Upregulation of lncRNA RMRP promotes the activation of cardiac fibroblasts by regulating miR-613. *Mol Med Rep.* (2019) 20:3849–57. doi: 10.3892/mmr.2019.10634
114. Sun LY, Zhao JC, Ge XM, Zhang H, Wang CM, Bie ZD. Circ_LAS1L regulates cardiac fibroblast activation, growth, and migration through miR-125b/SFRP5 pathway. *Cell Biochem Funct.* (2020) 38:443–50. doi: 10.1002/cbf.3486
115. Gui X, Li Y, Zhang X, Su K, Cao W. Circ_LDLR promoted the development of papillary thyroid carcinoma via regulating miR-195-5p/LIPH axis. *Cancer Cell Int.* (2020) 20:241. doi: 10.1186/s12935-020-01327-3
116. Ma W, Zhao P, Zang L, Zhang K, Liao H, Hu Z. CircTP53 promotes the proliferation of thyroid cancer via targeting miR-1233-3p/MDM2 axis. *J Endocrinol Invest.* (2020). doi: 10.1007/s40618-020-01317-2. [Epub ahead of print].
117. Miyazawa K, Miyazono K. Regulation of TGF-β family signaling by inhibitory Smads. *Cold Spring Harb Perspect Biol.* (2017) 9:a022095. doi: 10.1101/cshperspect.a022095
118. Lan HY, Chung AC-K. TGF-β/Smad signaling in kidney disease. *Semin Nephrol.* (2012) 32:236–43. doi: 10.1016/j.semnephrol.2012.04.002
119. Humeres C, Frangogiannis NG. Fibroblasts in the infarcted, remodeling, and failing heart. *JACC Basic Transl Sci.* (2019) 4:449–67. doi: 10.1016/j.jacbts.2019.02.006
120. Divakaran V, Adrogue J, Ishiyama M, Entman ML, Haudek S, Sivasubramanian N, et al. Adaptive and maladptive effects of SMAD3 signaling in the adult heart after hemodynamic pressure overloading. *Circ Heart Fail.* (2009) 2:633–42. doi: 10.1161/CIRCHEARTFAILURE.108.823070
121. Chen S, Puthanveetil P, Feng B, Matkovich SJ, Dorn GW, II, Chakrabarti S. Cardiac miR-133a overexpression prevents early cardiac fibrosis in diabetes. *J Cell Mol Med.* (2014) 18:415–21. doi: 10.1111/jcmm.12218
122. Muraoka N, Yamakawa H, Miyamoto K, Sadahiro T, Umei T, Isomi M, et al. MiR-133 promotes cardiac reprogramming by directly repressing Snai1 and silencing fibroblast signatures. *EMBO J.* (2014) 33:1565–81. doi: 10.15252/embj.201387605
123. Tao L, Bei Y, Chen P, Lei Z, Fu S, Zhang H, et al. Crucial role of miR-433 in regulating cardiac fibrosis. *Theranostics.* (2016) 6:2068–83. doi: 10.7150/thno.15007
124. Liang JN, Zou X, Fang XH, Xu JD, Xiao Z, Zhu JN, et al. The Smad3-miR-29b/miR-29c axis mediates the protective effect of macrophage migration inhibitory factor against cardiac fibrosis. *Biochim Biophys Acta Mol Basis Dis.* (2019) 1865:2441–50. doi: 10.1016/j.bbadis.2019.06.004
125. Zhang Y, Huang XR, Wei LH, Chung AC, Yu CM, Lan HY. miR-29b as a therapeutic agent for angiotensin II-induced cardiac fibrosis by targeting TGF-beta/Smad3 signaling. *Mol Ther.* (2014) 22:974–85. doi: 10.1038/mt.2014.25
126. He X, Zhang K, Gao X, Li L, Tan H, Chen J, et al. Rapid atrial pacing induces myocardial fibrosis by down-regulating Smad7 via microRNA-21 in rabbit. *Heart Vessels.* (2016) 31:1696–708. doi: 10.1007/s00380-016-0808-z
127. Thum T, Gross C, Fiedler J, Fischer T, Kissler S, Bussen M, et al. MicroRNA-21 contributes to myocardial disease by stimulating MAP kinase signalling in fibroblasts. *Nature.* (2008) 456:980. doi: 10.1038/nature07511
128. Zou M, Wang F, Gao R, Wu J, Ou Y, Chen X, et al. Autophagy inhibition of hsa-miR-19a-3p/19b-3p by targeting TGF-beta R II during TGF-beta1-induced fibrogenesis in human cardiac fibroblasts. *Sci Rep.* (2016) 6:24747. doi: 10.1038/srep24747
129. Wang H, Cai J. The role of microRNAs in heart failure. *Biochim Biophys Acta Mol Basis Dis.* (2017) 1863:2019–30. doi: 10.1016/j.bbadis.2016.11.034
130. Wang J, Huang W, Xu R, Nie Y, Cao X, Meng J, et al. MicroRNA-24 regulates cardiac fibrosis after myocardial infarction. *J Cell Mol Med.* (2012) 16:2150–60. doi: 10.1111/j.1582-4934.2012.01523.x
131. Xu M, Wu HD, Li RC, Zhang HB, Wang M, Tao J, et al. Mir-24 regulates junctophilin-2 expression in cardiomyocytes. *Circ Res.* (2012) 111:837–41. doi: 10.1161/CIRCRESAHA.112.277418
132. Wei C, Kim IK, Kumar S, Jayasinghe S, Hong N, Castoldi G, et al. NF-κB mediated miR-26a regulation in cardiac fibrosis. *J Cell Physiol.* (2013) 228:1433–42. doi: 10.1002/jcp.24296
133. Porrello ER, Mahmoud AI, Simpson E, Johnson BA, Grinsfelder D, Canseco D, et al. Regulation of neonatal and adult mammalian heart regeneration by the miR-15 family. *Proc Natl Acad Sci USA.* (2013) 110:187–92. doi: 10.1073/pnas.1208863110
134. Hullinger TG, Montgomery RL, Seto AG, Dickinson BA, Semus HM, Lynch JM, et al. Inhibition of miR-15 protects against cardiac ischemic injury. *Circ Res.* (2012) 110:71–81. doi: 10.1161/CIRCRESAHA.111.244442

135. Karakikes I, Chaanine AH, Kang S, Mukete BN, Jeong D, Zhang S, et al. Therapeutic cardiac-targeted delivery of miR-1 reverses pressure overload-induced cardiac hypertrophy and attenuates pathological remodeling. *J Am Heart Assoc.* (2013) 2:e000078. doi: 10.1161/JAHA.113.000078
136. Pan Z, Sun X, Shan H, Wang N, Wang J, Ren J, et al. MicroRNA-101 inhibited postinfarct cardiac fibrosis and improved left ventricular compliance via the FBJ osteosarcoma oncogene/transforming growth factor-β1 pathway. *Circulation.* (2012) 126:840–50. doi: 10.1161/CIRCULATIONAHA.112.094524
137. Zhao X, Wang K, Liao Y, Zeng Q, Li Y, Hu F, et al. MicroRNA-101a inhibits cardiac fibrosis induced by hypoxia via targeting TGFbetaRI on cardiac fibroblasts. *Cell Physiol Biochem.* (2015) 35:213–26. doi: 10.1159/000369689
138. Boon RA, Iekushi K, Lechner S, Seeger T, Fischer A, Heydt S, et al. MicroRNA-34a regulates cardiac ageing and function. *Nature.* (2013) 495:107. doi: 10.1038/nature11919
139. Beaumont J, Lopez B, Hermida N, Schroen B, San José G, Heymans S, et al. microRNA-122 down-regulation may play a role in severe myocardial fibrosis in human aortic stenosis through TGF-β1 up-regulation. *Clin Sci.* (2014) 126:497–506. doi: 10.1042/CS20130538
140. Sun Y, Wang H, Li Y, Liu S, Chen J, Ying H. miR-24 and miR-122 negatively regulate the transforming growth factor-beta/smad signaling pathway in skeletal muscle fibrosis. *Mol Ther Nucleic Acids.* (2018) 11:528–37. doi: 10.1016/j.omtn.2018.04.005
141. Nagalingam RS, Sundaresan NR, Noor M, Gupta MP, Solaro RJ, Gupta M. Deficiency of cardiomyocyte-specific microRNA-378 contributes to the development of cardiac fibrosis involving a transforming growth factor beta (TGFbeta1)-dependent paracrine mechanism. *J Biol Chem.* (2014) 289:27199–214. doi: 10.1074/jbc.M114.580977
142. Tao H, Shi KH, Yang JJ, Huang C, Liu LP, Li J. Epigenetic regulation of cardiac fibrosis. *Cell Signal.* (2013) 25:1932–8. doi: 10.1016/j.cellsig.2013.03.024
143. Huang Y, Li J. MicroRNA208 family in cardiovascular diseases: therapeutic implication and potential biomarker. *J Physiol Biochem.* (2015) 71:479–86. doi: 10.1007/s13105-015-0409-9
144. Zhao N, Koenig SN, Trask AJ, Lin CH, Hans CP, Garg V, et al. MicroRNA miR145 regulates TGFBR2 expression and matrix synthesis in vascular smooth muscle cells. *Circ Res.* (2015) 116:23–34. doi: 10.1161/CIRCRESAHA.115.303970
145. Louafi F, Martinez-Nunez RT, Sanchez-Elsner T. MicroRNA-155 targets SMAD2 and modulates the response of macrophages to transforming growth factor-{beta}. *J Biol Chem.* (2010) 285:41328–36. doi: 10.1074/jbc.M110.146852
146. Nagpal V, Rai R, Place AT, Murphy SB, Verma SK, Ghosh AK, et al. MiR-125b Is Critical for fibroblast-to-myofibroblast transition and cardiac fibrosis. *Circulation.* (2016) 133:291–301. doi: 10.1161/CIRCULATIONAHA.115.018174
147. Jazbutyte V, Fiedler J, Kneitz S, Galuppo P, Just A, Holzmann A, et al. MicroRNA-22 increases senescence and activates cardiac fibroblasts in the aging heart. *Age.* (2013) 35:747–62. doi: 10.1007/s11357-012-9407-9
148. Hong Y, Cao H, Wang Q, Ye J, Sui L, Feng J, et al. MiR-22 may suppress fibrogenesis by targeting TGFbetaR I in cardiac fibroblasts. *Cell Physiol Biochem.* (2016) 40:1345–53. doi: 10.1159/000453187
149. Chen Z, Lu S, Xu M, Liu P, Ren R, Ma W. Role of miR-24, furin, and transforming growth factor-β1 signal pathway in fibrosis after cardiac infarction. *Med Sci Monit Int Med J Exp Clin Res.* (2017) 23:65. doi: 10.12659/MSM.898641
150. Zheng D, Zhang Y, Hu Y, Guan J, Xu L, Xiao W, et al. Long noncoding RNA Crnde attenuates cardiac fibrosis via Smad3-Crnde negative feedback in diabetic cardiomyopathy. *FEBS J.* (2019) 286:1645–55. doi: 10.1111/febs.14780
151. Tao H, Zhang JG, Qin RH, Dai C, Shi P, Yang JJ, et al. LncRNA GAS5 controls cardiac fibroblast activation and fibrosis by targeting miR-21 via PTEN/MMP-2 signaling pathway. *Toxicology.* (2017) 386:11–8. doi: 10.1016/j.tox.2017.05.007
152. Wu Q, Han L, Yan W, Ji X, Han R, Yang J, et al. miR-489 inhibits silica-induced pulmonary fibrosis by targeting MyD88 and Smad3 and is negatively regulated by lncRNA CHRF. *Sci Rep.* (2016) 6:30921. doi: 10.1038/srep30921
153. Chen L, Yan K-P, Liu X-C, Wang W, Li C, Li M, et al. Valsartan regulates TGF-β/Smads and TGF-β/p38 pathways through lncRNA CHRF to improve doxorubicin-induced heart failure. *Arch Pharm Res.* (2018) 41:101–9. doi: 10.1007/s12272-017-0980-4
154. Bayoumi AS, Aonuma T, Teoh JP, Tang YL, Kim IM. Circular noncoding RNAs as potential therapies and circulating biomarkers for cardiovascular diseases. *Acta Pharmacol Sin.* (2018) 39:1100–9. doi: 10.1038/aps.2017.196
155. Hurtado MD, Vella A. What is type 2 diabetes? *Medicine.* (2019) 47:10–5. doi: 10.1016/j.mpmed.2018.10.010
156. Liang H, Zhang C, Ban T, Liu Y, Mei L, Piao X, et al. A novel reciprocal loop between microRNA-21 and TGFβRIII is involved in cardiac fibrosis. *Int J Biochem Cell Biol.* (2012) 44:2152–60. doi: 10.1016/j.biocel.2012.08.019
157. Roy S, Khanna S, Hussain S-RA, Biswas S, Azad A, Rink C, et al. MicroRNA expression in response to murine myocardial infarction: miR-21 regulates fibroblast metalloprotease-2 via phosphatase and tensin homologue. *Cardiovasc Res.* (2009) 82:21–9. doi: 10.1093/cvr/cvp015
158. He W, Huang H, Xie Q, Wang Z, Fan Y, Kong B, et al. MiR-155 knockout in fibroblasts improves cardiac remodeling by targeting tumor protein p53-inducible nuclear protein 1. *J Cardiovasc Pharmacol Ther.* (2016) 21:423–35. doi: 10.1177/1074248415616188
159. Manzoni GM, Castelnuovo G, Proietti R. Assessment of psychosocial risk factors is missing in the 2010 ACCF/AHA guideline for assessment of cardiovascular risk in asymptomatic adults. *J Am Coll Cardiol.* (2011) 57:1569–70. doi: 10.1016/j.jacc.2010.12.015
160. Van Rooij E, Sutherland LB, Thatcher JE, DiMaio JM, Naseem RH, Marshall WS, et al. Dysregulation of microRNAs after myocardial infarction reveals a role of miR-29 in cardiac fibrosis. *Proc Natl Acad Sci.* (2008) 105:13027–32. doi: 10.1073/pnas.0805038105
161. Ooi JY, Bernardo BC, McMullen JR. Therapeutic potential of targeting microRNAs to regulate cardiac fibrosis: miR-433 a new fibrotic player. *Ann Transl Med.* (2016) 4:548. doi: 10.21037/atm.2016.12.01
162. Castoldi G, Di Gioia CR, Bombardi C, Catalucci D, Corradi B, Gualazzi MG, et al. MiR-133a regulates collagen 1A1: potential role of miR-133a in myocardial fibrosis in angiotensin II-dependent hypertension. *J Cell Physiol.* (2012) 227:850–6. doi: 10.1002/jcp.22939
163. Tijsen AJ, van der Made IM, van den Hoogenhof M, Wijnen WJ, van Deel ED, de Groot NE, et al. The microRNA-15 family inhibits the TGFbeta-pathway in the heart. *Cardiovasc Res.* (2014) 104:61–71. doi: 10.1093/cvr/cvu184
164. Van Rooij E, Sutherland LB, Liu N, Williams AH, McAnally J, Gerard RD, et al. A signature pattern of stress-responsive microRNAs that can evoke cardiac hypertrophy and heart failure. *Proc Natl Acad Sci.* (2006) 103:18255–60. doi: 10.1073/pnas.0608791103
165. Huang ZP, Ding Y, Chen J, Wu G, Kataoka M, Hu Y, et al. Long non-coding RNAs link extracellular matrix gene expression to ischemic cardiomyopathy. *Cardiovasc Res.* (2016) 112:543–54. doi: 10.1093/cvr/cvw201
166. Tang PM, Zhang YY, Lan HY. LncRNAs in TGF-beta-driven tissue fibrosis. *Noncoding RNA.* (2018) 4:26. doi: 10.3390/ncrna4040026
167. Wang X, Ding Z, Wu J, Wang S, Zou Y. Circular RNA in cardiovascular disease. *Noncoding RNA Invest.* (2017) 1:5. doi: 10.21037/ncri.2017.08.04
168. Zhu Y, Pan W, Yang T, Meng X, Jiang Z, Tao L, et al. Upregulation of circular RNA circNFIB attenuates cardiac fibrosis by sponging miR-433. *Front Genet.* (2019) 10:564. doi: 10.3389/fgene.2019.00564

Conflict of Interest: The authors declare that the research was conducted in the absence of any commercial or financial relationships that could be construed as a potential conflict of interest.

frontiers in Cardiovascular Medicine

ORIGINAL RESEARCH
published: 25 February 2021
doi: 10.3389/fcvm.2021.585691

EZH2 Dynamically Associates With Non-coding RNAs in Mouse Hearts After Acute Angiotensin II Treatment

Shun Wang[1†], Ningning Guo[1†], Shuangling Li[1†], Yuan He[2], Di Zheng[1], Lili Li[2] and Zhihua Wang[1,2]*

[1] Department of Cardiology, Renmin Hospital of Wuhan University, Wuhan, China, [2] Central Laboratory, Renmin Hospital of Wuhan University, Wuhan, China

OPEN ACCESS

Edited by:
George W. Booz,
University of Mississippi Medical Center School of Dentistry, United States

Reviewed by:
Anindita Das,
Virginia Commonwealth University, United States
Mohammadreza Hajjari,
Shahid Chamran University of Ahvaz, Iran

***Correspondence:**
Zhihua Wang
zhihuawang@whu.edu.cn

[†] These authors have contributed equally to this work

Specialty section:
This article was submitted to Cardiovascular Genetics and Systems Medicine, a section of the journal Frontiers in Cardiovascular Medicine

Received: 21 July 2020
Accepted: 01 February 2021
Published: 25 February 2021

Citation:
Wang S, Guo N, Li S, He Y, Zheng D, Li L and Wang Z (2021) EZH2 Dynamically Associates With Non-coding RNAs in Mouse Hearts After Acute Angiotensin II Treatment. Front. Cardiovasc. Med. 8:585691. doi: 10.3389/fcvm.2021.585691

Enhancer of zeste 2 (EZH2) governs gene reprogramming during cardiac hypertrophy through epigenetic remodeling, a process regulated by numerous non-coding RNAs (ncRNAs). However, the dynamic interaction between EZH2 and ncRNAs upon hypertrophic stimulation remains elusive. Here we performed an unbiased profiling for EZH2-associated ncRNAs in mouse hearts treated with Angiotensin II (AngII) at different time points (0, 4, and 24 h). The interactions between EZH2 and long ncRNAs (lncRNAs), Chaer, Mirt1, Hotair, and H19, were validated by PCR. RIP-seq analysis identified a total of 126 ncRNAs to be significantly associated with EZH2. These ncRNAs covers all five categories including intergenic, antisense, intron-related, promoter-related and both antisense and promoter-related. According to their changing patterns after AngII treatment, these ncRNAs were clustered into four groups, constantly enhanced, transiently enhanced, constantly suppressed and transiently suppressed. Structural prediction showed that EZH2 bound to hairpin motifs in ncRNAs including snoRNAs. Interaction strength prediction and RNA pull-down assay confirmed the direct interaction between EZH2 and Snora33. Interestingly, two antisense lncRNAs of Malat1, Gm20417, and Gm37376, displayed different binding patterns from their host gene after AngII treatment, suggesting a crucial role of this genomic locus in modulating EZH2 behavior. Our findings reveal the profile of EZH2-associated ncRNAs upon hypertrophic stimulation, and imply a dynamic regulation of EZH2 function in cardiac hypertrophy.

Keywords: epigenetics, EZH2, long non-coding RNAs, small nucleolar RNAs, RIP-Seq

INTRODUCTION

In mammalians, only 1–2% of the genome is responsible for protein coding though 70–90% is transcriptionally active (1, 2). The vast majority of human DNA are transcribed into non-coding RNAs (ncRNAs) including long non-coding RNAs (lncRNAs) (2, 3). LncRNAs differ from short ncRNAs simply in length with 200-nt as the separatrix. Although once considered as junk RNAs, ncRNAs have recently been recognized as crucial regulatory molecules involved in a series of cellular processes, such as chromatin remodeling, genomic stability, transcription, post-transcriptional modifications and signal transduction (4, 5). There is an increasing interest to explore the role of ncRNAs in numerous human diseases including cardiovascular diseases.

The function of ncRNAs largely depends on their subcellular location (6). A number of nucleus-localizing lncRNAs have been found directly interacting with epigenetic modifiers and modulate gene expression in *cis* or *trans* manners (6–10). Enhancer of zeste 2 (EZH2), a subunit of polycomb repressive complex 2 (PRC2) catalyzing tri-methylation of histone H3 at lysine 27 (H3K27me3) (11, 12), represents a major target of lncRNAs inside nucleus (13–18). Some lncRNAs function as a decoy by interacting with EZH2 to prevent PRC2 from binding with chromatin or to interfere with the allosteric activation of PRC2, without impeding its methylation catalytic activity (19, 20). Whereas, lncRNA-p21 has been proposed to disrupt the PRC2 complex and promote the binding of EZH2 with genes independent of the PRC2 complex, which triggers methylation of targeted genes (21, 22).

Cardiac hypertrophy is a common pathological process of many types of cardiovascular diseases (23). A number of lncRNAs, such as maternally expressed 3 (Meg3), myosin heavy-chain-associated RNA transcripts (Mhrt), cardiac hypertrophy-related factor (Chrf), Myocardial Infarction–Associated Transcript (Miat) have been reported to be involved in cardiac hypertrophy (24–27). We previously identified a heart-enriched lncRNA cardiac hypertrophy associated epigenetic regulator (Chaer), which transiently interacts with EZH2 at early phase of cardiac hypertrophy induced by transaortic constriction (TAC) surgery and prevents its targeting to the promoter region of hypertrophic genes (28), implicating a highly dynamic regulation of EZH2 by lncRNAs. However, the molecular mechanism for this dynamic process has yet been clarified.

In a previous study, we characterized the tissue-specificity of EZH2-associated lncRNAs using RNA immuno-precipitation coupled with sequencing (RIP-seq) (29). Here we performed an unbiased profiling for EZH2-binding ncRNAs in mouse hearts following Angiotensin II (AngII) treatment. Our findings reveal the landscape of EZH2-associated ncRNAs during early cardiac hypertrophy and provide novel insights into the dynamics of EZH2-mediated epigenetic remodeling.

MATERIALS AND METHODS

Animals

Male mice aged 10 weeks were housed in specific-pathogen-free (SPF) conditions with controlled temperature, humidity, and light and free access to food and water. Animal experiments were performed conforming to the 8th Edition of the Guide for the Care and Use of Laboratory Animals (Guide NRC, 2011) published by the US National Institutes of Health. Mice were randomly assigned to Sham, Angiotensin II (AngII) 4 h and AngII 24 h groups with two mice for each group. An osmotic minipump (Alzet, Cupertino, CA, USA) was implanted subcutaneously to deliver AngII (Sigma, St. Louis, MO) at a rate of 1 mg/kg/min as previously described (30). After infusion for 4 or 24 h, mice were sacrificed by dislocation of infra-cervical spine. Left ventricles were the quickly separated, washed in PBS and frozen in liquid nitrogen until use. Saline was infused instead of AngII for Sham groups.

Cell Culture and Plasmids

Mouse embryonic fibroblasts (MEFs) were maintained in DMEM supplemented with 10% fetal bovine serum, 2 mM L-glutamine, 100 U/mL penicillin and 100 μg/ml streptomycin. Gm20417 and Gm37376 were clone from mouse heart cDNA library into pcDNA3.1-CMV expression plasmid, and transfected into MEFs using Lipofectamine 2000 (Invitrogen, Thermo Fisher Scientific Inc.). Cells were harvested 24 h after transfection.

Western Blot

Frozen heart tissues or cells were homogenized in protein lysis buffer (50 mM HEPES [pH7.4], 150 mM NaCl, 1% Triton X-100, 1 mM EDTA, 1 mM EGTA, 1 mM glycerophosphate, 2.5 mM sodium pyrophosphate, 1 mM Na3VO4, 20 mM NaF, 1 mM phenylmethylsulfonyl fluoride, 1 mM DTT, 1 × complete protease inhibitor tablet [Roche, Swiss]). Total lysates were separated on 10 or 12% Bis-Tris gels and transferred onto PVDF membranes (Millipore). The blots were probed with antibodies for H3 (#12648), H3K27me3 (#9733), EZH2 (#5246), and GAPDH (#5174) from Cell Signaling Technologies, Inc. Protein signals were detected using HRP conjugated secondary antibodies and enhanced chemiluminescence (ECL) western blotting detection regents (Thermo Fisher Scientific, MA, USA).

RNA Immune-Precipitation

RNA immune-precipitation (RIP) was performed essentially as previously described (28, 29, 31). Left ventricles weighting ∼100 mg from each group were homogenized in 500 μl of polysome lysis buffer (10 mM HEPES-KOH [pH 7.0], 100 mM KCl, 5 mM $MgCl_2$, 25 mM EDTA, 0.5% IGEPAL, 2 mM dithiothreitol [DTT], 0.2 mg/mL Heparin, 50 U/mL RNase OUT [Life Technologies], 50 U/mL Superase IN [Ambion] and 1 × complete protease inhibitor tablet [Roche]). The suspension was centrifuged at 14,000 *g* at 4°C for 10 min to remove debris. Lysates were incubated with 500 ng normal IgG (Cell Signaling Technologies, MA, USA; #2729, 1:200) or anti-EZH2 (Cell Signaling Technologies; #5246, 1:200) at 4°C overnight on an inverse rotator. Protein A-sepharose beads (Life Technologies, 50 μl per tube) were first blocked in NT2 buffer (50 mM Tris-HCl (pH 7.5), 150 mM NaCl, 1 mM $MgCl_2$, and 0.05% IGEPAL) supplemented with 5% BSA, 0.02% sodium azide and 0.02 mg/mL heparin at 4°C for 1 h, and then added into the lysates followed by a 3-h incubation at 4°C on an inverse rotator. The beads were subsequently washed five times in NT2 buffer. RNAs were released by incubating in proteinase K buffer (50 mM Tris (pH 8.0), 100 mM NaCl, 10 mM EDTA, 1% SDS, and 1 U/mL proteinase K) for 30 min at 65°C, pelleted by adding an equal volume of isopropanol and centrifuged at 12,000 *g* at 4°C for 10 min. RNAs were washed once with 75% ethanol and stored at −80°C until use.

RNA Pull-Down Assay

To validate the direct interaction between EZH2 and Snora33, we employed the tagged RNA pull-down assay adjusted from a previous report (32). Snora33 was obtained using an T7 *in vitro* transcription kit (Merk Inc.), followed by biotin conjugation using the Biotinylation Kit (Thermo Fisher Scientific Inc.).

Biotinylated Snora33 was then incubated with MEF lysates in SA-RNP lysis buffer (20 mM Tris-HCl [pH7.5], 150 mM NaCl, 1.5 mM $MgCl_2$, 2 mM DTT, 50 U/ml RNase OUT [Invitrogen], 50 U/ml Superase IN [Ambion], 1× complete protease inhibitor tablet [Roche]) for 4 h at 4°C. Streptavidin sepharose beads were blocked with 500 ng/μl yeast tRNA and 1 mg/ml BSA in SA-RNP lysis buffer before added into cell lysates and incubated at 4°C for 2 h on a rotator. The beads were then pelleted and washed for 5 times with SA-RNP washing buffer (20 mM Tris-HCl [pH7.5], 300 mM NaCl, 5 mM $MgCl_2$, 2 mM DTT, 50 U/ml RNase OUT [Invitrogen], 50 U/ml Superase IN [Ambion], 1× complete protease inhibitor tablet [Roche]). After the last wash, RNA-bound proteins were eluted by addition of 5% RNase A (NEB) in low salt buffer (20 mM Tris-HCl [pH7.5], 30 mM NaCl, 5 mM MgCl2, 2 mM DTT, 1× complete protease inhibitor tablet [Roche]) for 30 min at 4°C. The eluted proteins, together with the flow-through and input samples, were then boiled in 4× LDS sample buffer (Life Technologies) and used for immunoblot analysis.

RNA Sequencing

Two independent RIP products from each group were mixed before reverse transcription into cDNA sequencing library using KAPA Stranded RNA-Seq Library Preparation Kit. The libraries were subjected to quality validation using the Agilent Bioanalyzer 2100, and sequenced using Illumina NextSeq 500 in DNA Link USA Inc. The reads were mapped to mouse genome (mm10) using TopHat2 (28), and visualized on the UCSC browser (http://genome.ucsc.edu). LncRNAs were picked out according to NONCODE database (33). Screening criteria was set as reads >1.0; ratio of anti-EZH2 group relative to normal IgG group >2 in at least one tissue.

Real-Time PCR

Briefly, 1 μg RNA was reverse-transcribed into first-strand cDNA using the Superscript III first-strand synthesis kit (Life Technologies, NY, USA) with random primers. Real-time PCR was performed using the CFX96 Real-Time PCR Detection System (Bio-Rad, CA, USA) using the iQ SYBR Green Supermix (Bio-Rad). Values were normalized to IgG controls. Primers are listed below.

Chaer: F-5′-TCCAATGAGGGAAGCGAAGC-3′, R-5′-GTCCGATGCCAGTTCCAGTT-3′;

Hotair: F-5′-CTTTCAAGGCCTGTCTCCTG-3′, R-5′-CAACATTCTAGCTGCACGGA-3′;

H19: F-5′-AGACTAGGCCAGGTCTCCAG-3′, R-5′-TAGAGGCTTGGCTCCAGGAT-3′;

Mirt1: F-5′-TGGGAGGCTGAGGCTAAGAT-3′, R-5′-ACCTACCCCTACTGCTGGAG-3′.

In Silicon RNA Secondary Structure Prediction

RNA secondary structure was predicted by RNAfold WebServer (http://rna.tbi.univie.ac.at/cgi-bin/RNAfold.cgi) based on minimum free energy (MFE) and partition function. The interaction strength between EZH2 and ncRNAs were predicted by an online program using random RNA sequences as (http://s.tartaglialab.com/page/catrapid_group) (34).

Statistics

Data were presented as mean ± SEM for repeated analyses. Statistical analysis was performed by one-way ANOVA and Turkey HSD *post hoc* test using GraphPad Prism. Comparisons between two groups were analyzed by student's *t*-test. $P < 0.05$ was considered statistically significant. EZH2 RIP data were presented as mean ± s.d. from two independent RIP products.

RESULTS

Validation of the RIP Method

Though not reaching statistical significance, AngII administration upregulated the protein expression of EZH2 after 4 h but reduced it after 24 h (**Figures 1A,B**). This pattern was inconsistent with the changes of global H3K27me3 (**Figures 1A,C**), suggesting a regulation of EZH2 activity by other factors. To explore the EZH2-associated ncRNAs, we then performed native RIP analysis followed by sequencing. After pull-down using anti-EZH2 or normal IgG antibodies, we firstly validated the RIP procedure with known EZH2-binding lncRNAs, including cardiac hypertrophy associated epigenetics regulator (Chaer), HOX transcript antisense RNA (Hotair), myocardial infarction-associated transcript 1 (Mirt1), and H19 (28, 35–37) using real-time PCR. The results showed that Chaer-EZH2 interaction was quickly enhanced after AngII treatment, whereas Hotair-EZH2 interaction was repressed (**Figures 1D,E**), which is consistent with our previous findings in cardiomyocyte hypertrophy induced by phenylephrine (28). In addition, Mirt1 and H19 were also detected in the EZH2 interactome with the former being enhanced while the latter being suppressed after AngII treatment (**Figures 1F,G**). These data verify the success of our RIP procedure, as well as the pro-hypertrophic effect of AngII treatment.

Identification of EZH2-Associated ncRNAs

In the RIP-seq analysis, we identified a total of 126 ncRNAs associated with EZH2 in all groups with no 0 reads in any group and over 2-fold enrichment in anti-EZH2 relative to normal IgG (**Figure 2A**). Separately, there were 76 ncRNAs in the Sham group, 66 in the 4-h AngII group and 63 in the 24-h AngII group. Among these EZH2-associated ncRNAs, 25 (20%) were shared by all three groups (**Figure 2A** and **Table 1**). From their genomic locations, these ncRNAs covered all five categories, including intergenic, antisense, intron-related, promoter-related and both antisense- and promoter-related (**Figures 2B,C**), suggesting a vast functional diversity of EZH2 in both local and global epigenetic regulations. Clustering analysis showed that EZH2-associated lncRNAs from AngII 4 h and AngII 24 h groups were clustered together, apart from that from the Sham group (**Figure 2D**), suggesting a quick response of EZH2-mediated epigenetic reprogramming to AngII stimulation whereby lncRNAs are functionally involved.

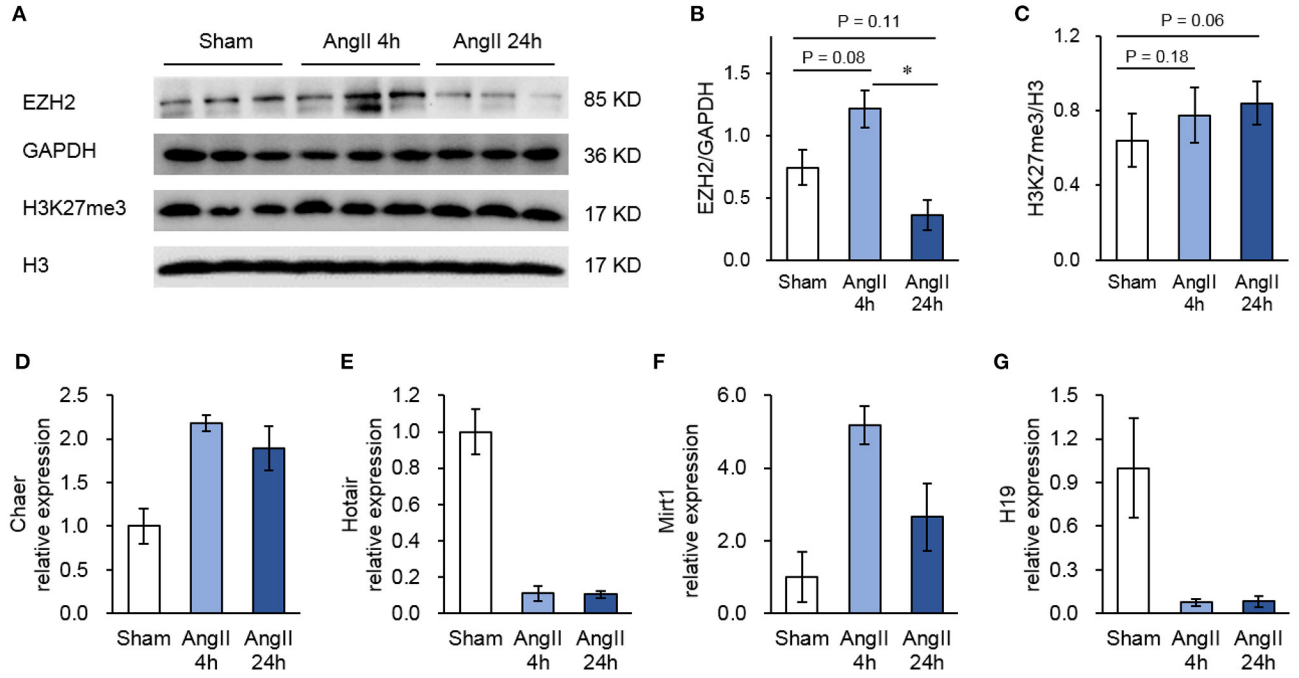

FIGURE 1 | Validation of the RIP method to pull-down Ezh2-binding lncRNAs. **(A)** Representative immunoblots showing the expression of EZH2, GAPDH, H3K27me3, and H3 in mouse hearts treated with Angiotensin II (AngII) at 0 (Sham), 4 and 24 h. **(B,C)** Analyzed results of EZH2 expression in relative to GAPDH **(B)** and H3K27me3 expression in relative to H3 **(C)**. Data are mean ± SEM; $^*P < 0.05$ vs. sham; $n = 3$. **(D–G)** Relative expression of known EZH2-binding lncRNAs including Chaer **(D)**, Hotair **(E)**, Mirt1 **(F),** and H19 **(G)** in mouse hearts treated with Angiotensin II (AngII) at 0 (Sham), 4 and 24 h. Data are mean ± SD from two independent experiments.

Dynamic Association Between EZH2 and ncRNAs During AngII Stimulation

We further analyzed the impact of AngII on EZH2-ncRNA interaction. A total of 93 EZH2-associated ncRNAs were altered >1.5-folds in all three comparisons. According to their alteration pattern following AngII treatment, these ncRNAs were classified into four groups; i.e., constantly enhanced (**Figure 3A**), transiently enhanced (**Figure 3B**), constantly suppressed (**Figure 3C**) and transiently suppressed (**Figure 3D**). Several known EZH2-interacting lncRNAs appeared in the list (37–40); e.g., growth arrest specific 5 (Gas5) was dissociated from EZH2 while maternally expressed 3 (Meg3) was recruited after AngII administration (**Figures 3A,C**). These results suggest that the interaction between EZh2 and ncRNAs is a highly dynamic process and may contribute to the epigenetic remodeling during early cardiac hypertrophy.

Structural Characteristics of EZH2-Associated ncRNAs

It has been reported that EZH2 tends to bind RNA motifs with tandem tetra-loop hairpins (28). We then analyzed the secondary structure of candidate ncRNAs using RNAfold (25). In Gm15832, a constantly enhanced EZH2-associated lncRNA during AngII treatment, we identified a potential 60-mer motif (100–159 nt) with a similar structure as that from Chaer or Hotair (28) (**Figure 4A**). Interestingly, EZH2 bound to a number of small nucleolar RNAs (snoRNAs) containing the H/ACA box, including Snora7a, Snora31, Snora33, Snora47, and Snora68 (**Figure 4B**), suggesting a role of EZH2 in rRNA processing (41, 42). Moreover, snoRNAs containing the C/D box, like Snord15a and Snord104, were also detected in the EZH2 interactome (**Figure 4B**). A number of uncharacterized ncRNAs (e.g., Gm23639) displayed the typical structural feature as snoRNAs (**Figure 4B**).

To validate the interactions, we performed an online prediction for the interaction strength using catRAPID algorithm (34). The results showed that Snora33 had the highest interaction strength (97%) with EZH2 protein among others (**Figure 5A**). RNA pull-down assay showed that the biotin-tagged Snora33 could strikingly pull down EZH2 compared with the EGFP control, along with a decrease of endogenous EZH2 in the flow-through sample (**Figure 5B**). These data further validate the validity of the EZH2-binding ncRNAs.

Malat1 Genomic Locus Is Involved in AngII-Induced Epigenetic Reprogramming

We previously identified two antisense lncRNAs, Gm20417, and Gm37376, at the gene locus of Malat1 displaying high tissue specificity (29). Here we found that all of these three lncRNAs significantly associated with EZH2; however, whereas Malat1-EZH2 interaction was transiently enhanced after AngII treatment, Gm20417-EZH2 interaction was transiently

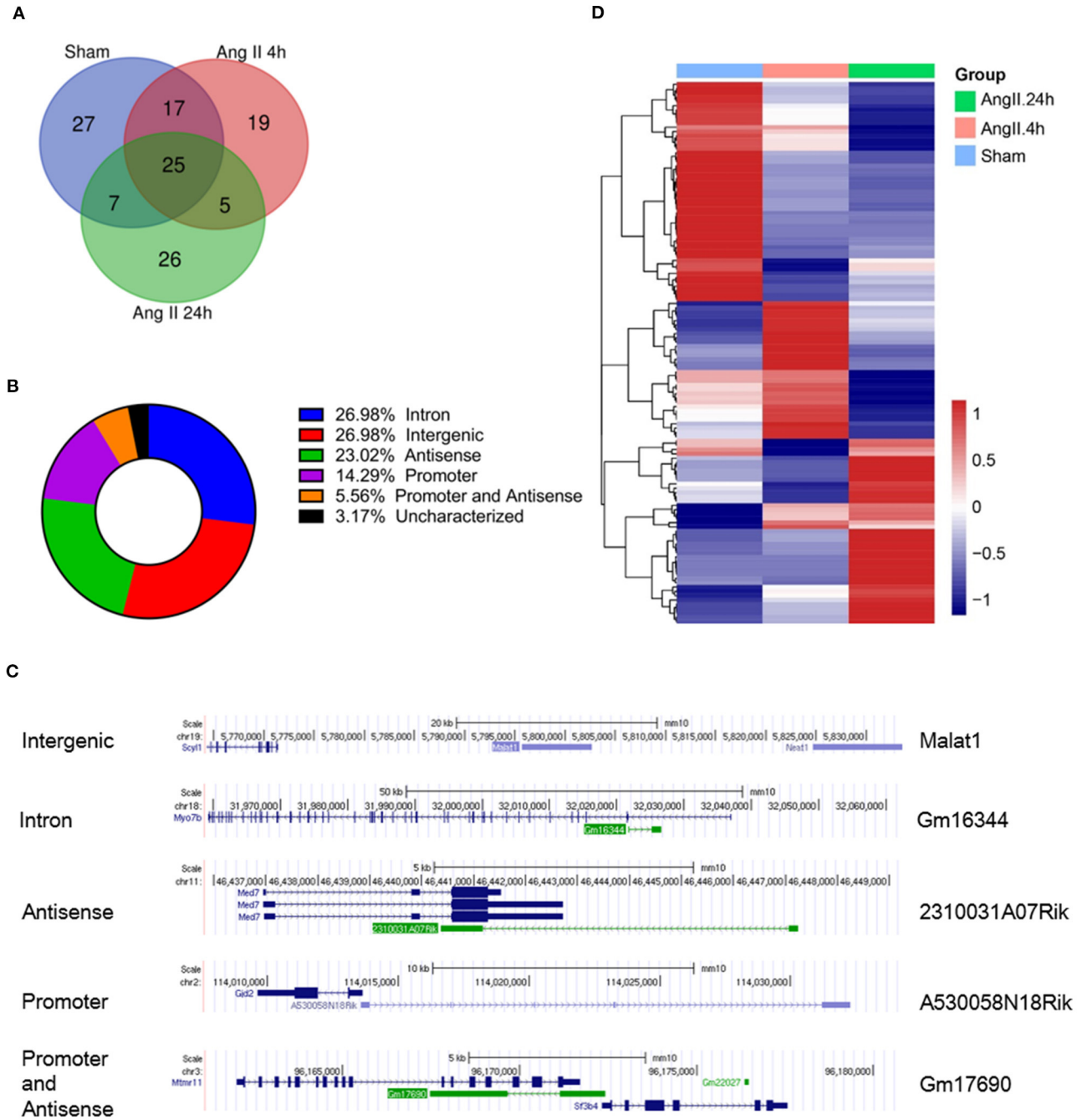

FIGURE 2 | Profiles of EZH2-binding ncRNAs in mouse hearts treated with AngII at different time points. **(A)** Venn diagram showing the number of overlapped ncRNAs from three groups as indicated. **(B)** Pie chart showing the distribution of ncRNA categories according to their genomic features. **(C)** Representative ncRNA for each category. **(D)** Heat map showing hierarchical clustering of changed EZH2-associated ncRNAs after AngII treatment at different time points. Up-regulated and down-regulated genes are colored in blue and yellow, respectively.

suppressed and Gm37376-EZH2 interaction was constantly enhanced (**Figures 6A–D**), suggesting a complex regulation of EZH2 function in AngII-induced cardiac hypertrophy. We then cloned Gm20417 and Gm37376, and expressed them in MEFs. Western blot analysis showed that Gm37376 and Gm20417 did not significantly alter the global level of H3K27me3 (**Figure 6E**), suggesting a regional regulation rather than regulating the global activity of EZH2 by these ncRNAs. These data also implicate that the Malat1 gene is a crucial locus to modify EZH2 function under stress.

TABLE 1 | Shared EZH2-associated lncRNAs in all groups.

Gene name	Tracking ID	Ratio to IgG			Category
		Sham	AngII 4 h	AngII 24 h	
Gas5	XLOC_001290	916.469	20.043	6.252	Intergenic
2410002F23Rik	XLOC_033560	78.164	835.468	1,041.137	Intergenic
Gm29055	XLOC_000696	17.072	7.540	8.856	Intron
Gm28268	XLOC_040459	12.568	3.984	2.580	Intergenic
Gm3052	XLOC_001918	10.709	2.320	4.242	Intergenic
Gm17131	XLOC_028763	9.803	4.295	2.793	Antisense
Gm9917	XLOC_039729	9.625	6.481	18.211	Promoter and antisense
Gm17132	XLOC_028762	9.357	9.789	6.614	Antisense
Gm37954	XLOC_002666	9.327	4.182	10.852	Intron
Gm26905	XLOC_036601	9.043	7.215	8.242	Antisense
Gm21897	XLOC_013754	7.216	4.441	3.814	Intergenic
Gm13722	XLOC_020816	5.984	4.678	2.653	Intergenic
Gm16793	XLOC_037281	5.346	2.848	16.772	Promoter
Gm37515	XLOC_023239	4.846	7.710	10.978	Intergenic
Gm20417	XLOC_017336	4.806	3.038	4.549	Antisense
C030037D09Rik	XLOC_005812	3.961	3.766	2.246	Promoter
Gm37376	XLOC_017337	3.838	5.611	10.619	Antisense
Gm37086	XLOC_001530	3.393	5.279	4.102	Intergenic
Gm26869	XLOC_021846	2.920	2.364	3.833	Antisense
Gm16344	XLOC_016557	2.904	5.573	3.629	Antisense
Bvht	XLOC_016764	2.851	2.056	2.034	Intergenic
Malat1	XLOC_017847	2.767	3.784	3.065	Intergenic
5330426P16Rik	XLOC_014583	2.758	2.656	3.264	Uncharaterized
Gm15662	XLOC_003933	2.046	3.031	2.679	Antisense
Gm17690	XLOC_024078	2.004	9.052	2.132	Promoter and antisense

DISCUSSION

Accumulating evidence highlights the crucial role of ncRNAs in cardiac hypertrophy. In this study, we found that EZH2 serves as a major target for not only lncRNAs but also snoRNAs. In addition to validating known EZH2-binding ncRNAs (e.g., Gas5, Meg3, and Malat1), our findings reveal a large panel of novel ncRNAs involved in the dynamic regulation of the EZH2 function during AngII-induced cardiac hypertrophy.

The dynamic interaction between EZH2 and ncRNAs suggests a complex role of EZH2 in the pathogenesis of cardiac hypertrophy. A huge change was observed as early as 4 h after AngII treatment. This is consistent with our previous report that Chaer-EZH2 interaction was transiently enhanced at the early phase of cardiac hypertrophy and that overall H3K27me3 was quickly diminished upon hypertrophic stimulation (28). The shift in binding property might rely on certain post-translation modifications of the EZH2 protein, since it can be modified by phosphorylation or glycosylation (43, 44). However, we did not detect changes of known EZH2 phosphorylation at T345 and T487 at the early phase of cardiac hypertrophy, though they were indeed sensitive to mTOR (mechanistic target of rapamycin) inhibition (Data not shown), implicating that other modifications or intrinsic EZH2 gene heterogeneity might underlie its dynamic interaction with ncRNAs. Further investigation is required to address this question in more details.

The EZH2-associated ncRNAs display diverse genomic features including intergenic, antisense, intron-related, promoter-related and both antisense- and promoter-related, suggesting diverse epigenetic regulations both *in cis* or *in trans*. EZH2 has been reported to undergo specificity and dynamics regulations in the context of heart development, whereby EZH2 is responsible for catalyzing H3K27me3 at the bivalent promoters of developmental genes (45–47). In Ezh2-deficient adult hearts, fetal genes are upregulated, giving rise to cardiac hypertrophy (48, 49). Regulatory RNAs are essential for PRC2 chromatin occupancy and function (50). Our previous study revealed that lncRNA Chaer transiently interacted with EZH2 at the early phase of cardiac hypertrophy. This interaction interfered with the binding of PRC2 to the promoters of pathological genes, thus allowing their activation by transcription factors (28). Here we found more ncRNAs displaying similar changing pattern during early hypertrophy, such as Gm24044, 2900076A07Rik, and Snora33 (**Figure 2B**). This mechanism is different from

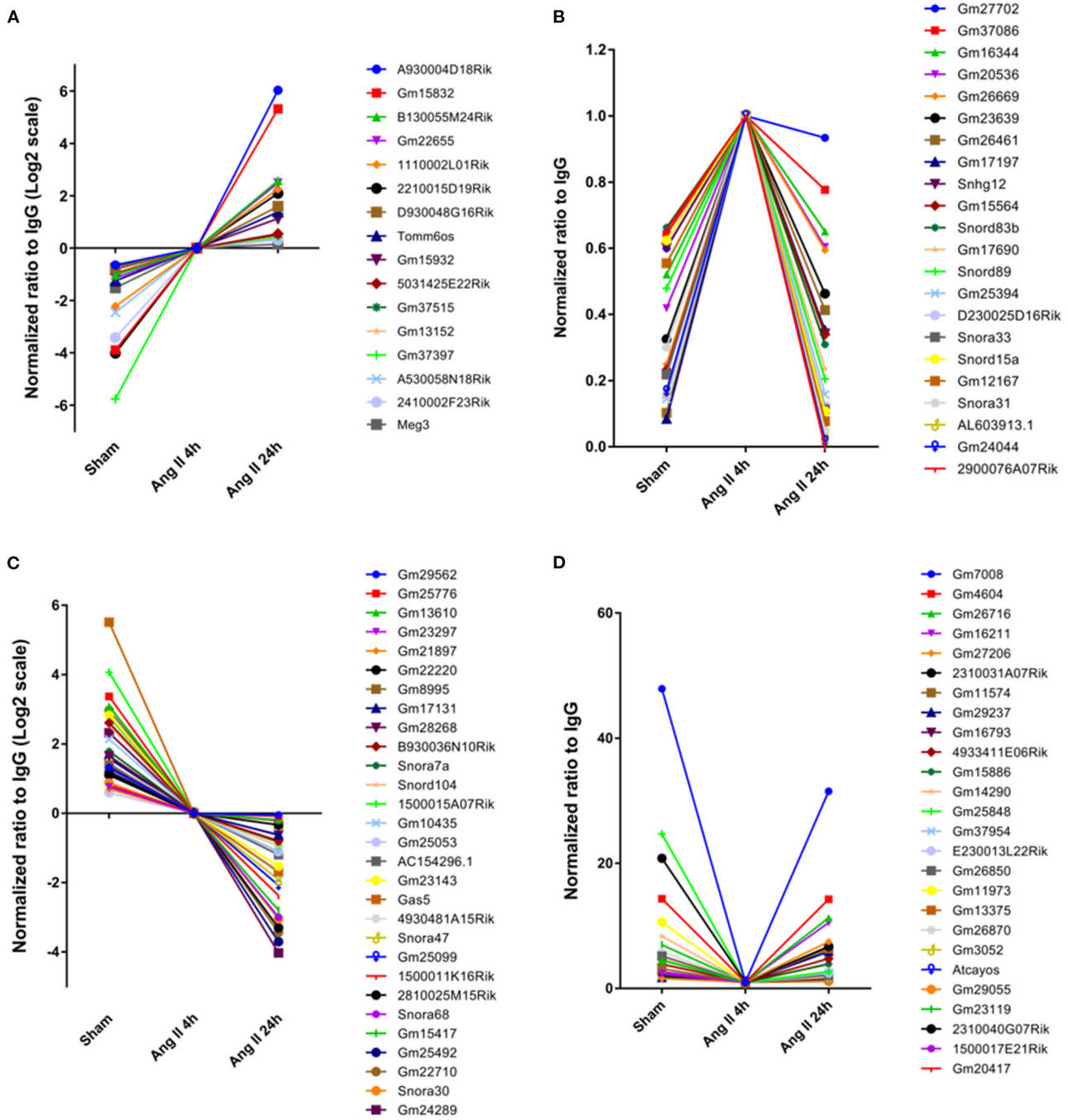

FIGURE 3 | Stratification of EZH2-associated ncRNAs according to their changing pattern after AngII treatment. **(A)** Constantly enhanced EZH2-binding ncRNAs in both AngII 4 and 24 h groups. **(B)** Transiently enhanced EZH2-binding ncRNAs after 4 h of AngII treatment but attenuated after 24 h of AngII treatment. **(C)** Constantly suppressed EZH2-binding ncRNAs in both AngII 4 and 24 h groups. **(D)** Transiently suppressed EZH2-binding ncRNAs after 4 h of AngII treatment but reversed after 24 h of AngII treatment. Data were normalized to the AngII 4 h group.

previously reported scaffold or guide ncRNAs like Hotair and Gtl2 (8, 37). Whether they also function like Chaer but not other ncRNAs needs further functional investigation. Along with the upregulated ncRNAs, the interaction between EZH2 and a number of ncRNAs, such as Gm7008 and Gm4604, was transiently suppressed upon AngII stimulus. These data suggest that ncRNAs compete for the access to the EZH2 binding site.

EZH2 does not contain a typical RNA-binding motif such as RRM (RNA recognition motif). Previous studies reveal

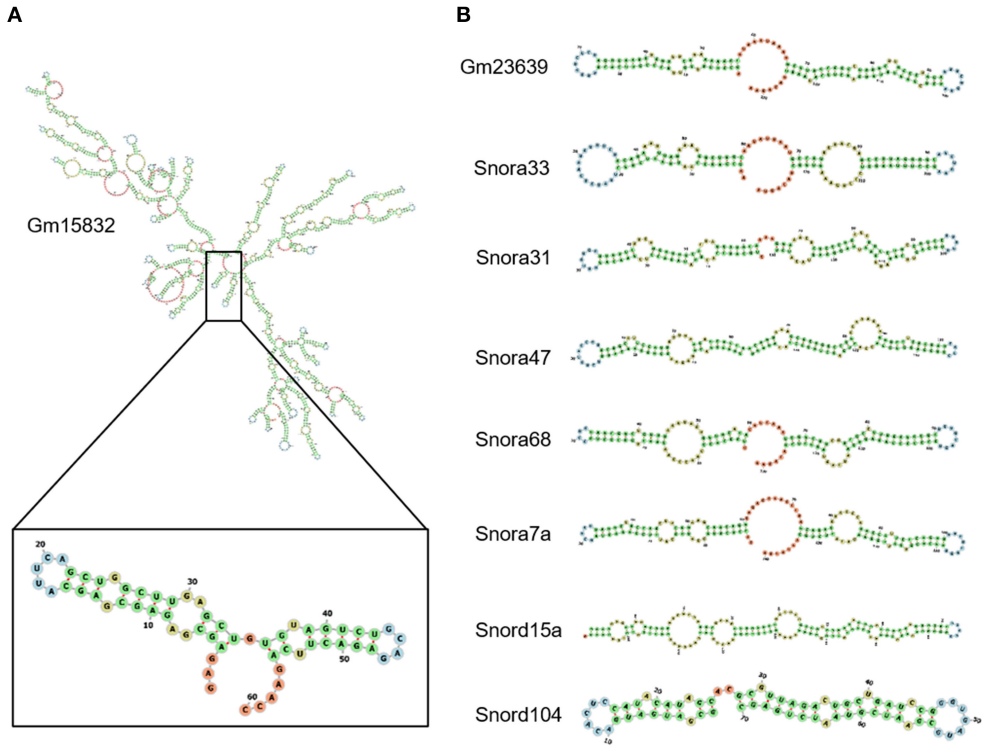

FIGURE 4 | Structural characteristics of EZH2-associated ncRNAs. Predicted secondary structure of lncRNA Gm15832 **(A)**, Snora family ncRNAs and Snord family ncRNAs **(B)** using RNAfolder.

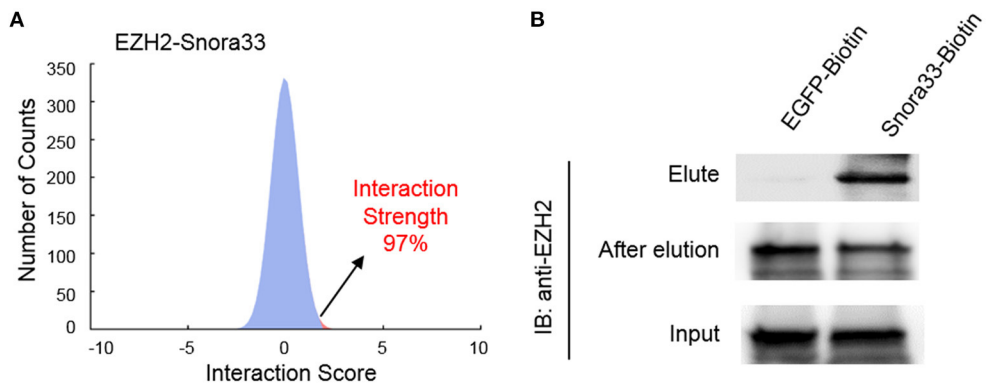

FIGURE 5 | Validation of the interaction between EZH2 and Snora33. **(A)** Predicted interaction strength between EZH2 and Snora33 using catRAPID. Among a thousand of random RNA sequences, Snora33 ranked 97% propensity to interact with EZH2. **(B)** RNA pull-down analysis to confirm the direct interaction between Snora33 and EZH2. Biotin was conjugated to the 3′ of Snora33 RNA *in vitro*, followed by streptavidin pull-down assay. Immunoblotting was performed with anti-EZH2 antibody using the elute, flow-through and input samples.

that the residues 342–368 in full-length EZH2 constitute a RNA-binding domain (51). Long et al. (52) found that the N-terminal helix of EZH2 is the major RNA-binding site and has a preferential binding of G-quadruplex RNA. The structural characteristics of EZH2-binding RNA have not been fully elucidated so far. Our previously study has shown that Chaer is capable of binding EZH2 through a tandem tetra-loop motif, which shared with several other EZH2-binding ncRNAs (28). Among the dynamic EZH2- binding ncRNA after AngII treatment, we identified Gm15832 that has a similar motif recognized by EZH2 (**Figure 4A**). An interesting finding is that EZH2 bind a series of snoRNAs with a typical tandem stem-loop structure, which can be classified into C/D-box (SNORD) and H/ACA-box (SNORA)

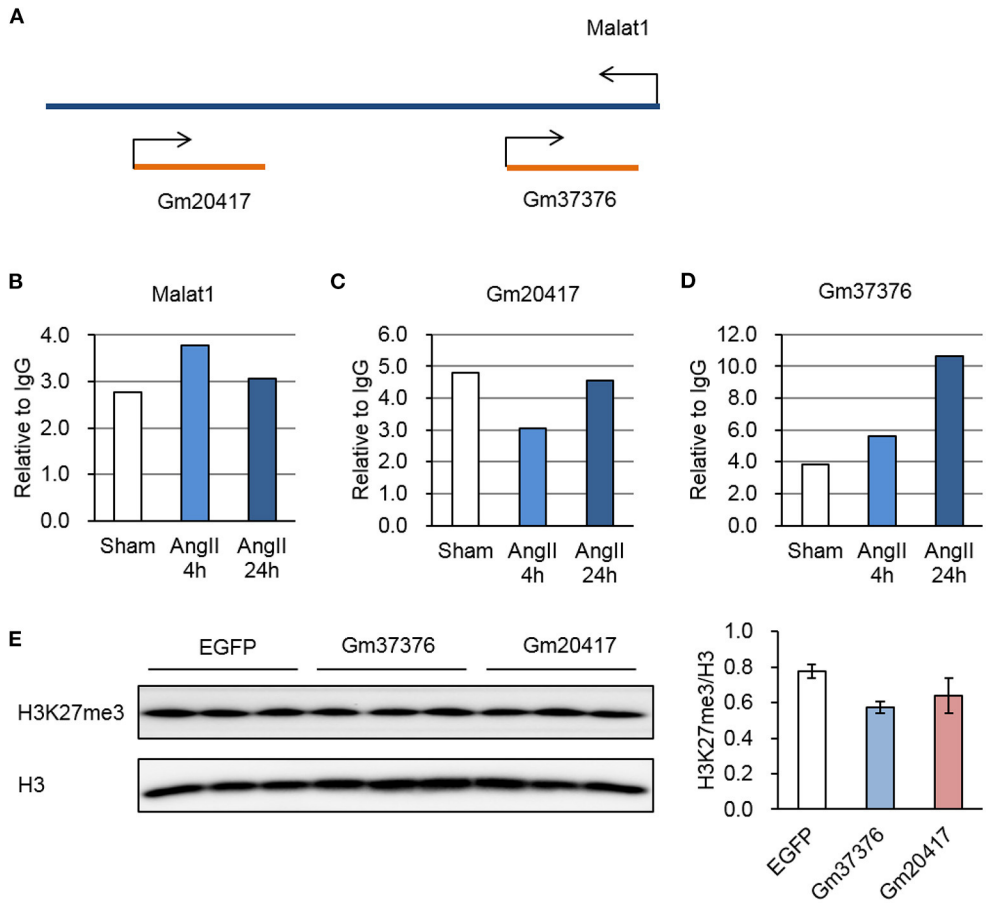

FIGURE 6 | Dynamic interaction between EZH2 and Malat1 locus-derived lncRNAs during AngII treatment. **(A)** Schematic diagram of the Malat1 genomic structure together with two antisense lncRNAs, Gm20417, and Gm37376. **(B–D)** Relative reads of Malat1 **(B)**, Gm20417 **(C)** and Gm37376 **(D)** normalized to corresponding IgG groups. **(E)** Impact of Gm37376 and Gm20417 on H3K27me3 in MEFs. Cells were collected 24 h after transfection, and the lysates were immunoblotted with anti-H3K27me3 and anti-H3 antibodies. Data are mean ± SEM; $n = 3$.

subfamilies (**Figures 4B,C**). Considering that snoRNAs mediate the rRNA acetylation and tRNA methylation modification (42), our findings indicate a potential role of EZH2 in mediating rRNA or tRNA maturation, as well as ribosome assembly inside nucleolus.

Although EZH2 has once been thought to promiscuously bind RNAs (53, 54), cumulating evidence including ours indicates that EZH2-binding ncRNAs possess specific structural commonness (28, 37). As found in RepA, Hotair and Chaer, a conserved tandem tetra-loop hairpin motif is responsible for the direct interaction between ncRNAs and EZH2 (28, 55). In this study, we screened the secondary structure for most of the identified ncRNAs. However, similar motif did not exist in all EZH2-associated ncRNAs except for Gm15832 (**Figure 3A**). Interestingly, EZH2-binding snoRNAs showed similar structural features (**Figure 3B**), suggesting divergent interaction patterns between EZH2 and ncRNAs possibly derived from different binding sites on the surface of EZH2 protein.

Compared with mRNAs, ncRNAs are less conserved among species (56). Similarly, most of the ncRNAs revealed in this study could not find their counterpart human homologs, but this does not exclude the possibility for certain structurally conserved counterparts to carry out the same function. One conserved lncRNA Malat1 was consistently detected in both the current and our previous reports (29). The role of Malat1 in cardiac hypertrophy is still under debate (57). The fact that three lncRNAs at this genomic locus could all bind to EZH2 and display diverse changing pattern after AngII treatment might add another layer to the Malat1-mediated epigenetic regulation. Moreover, novel function of EZH2 independent of forming PRC2 complex and subsequent H3K27me3 modification has been unveiled (58). It would be interesting to explore whether non-epigenetic function of EZH2 can be also modified by ncRNAs.

Taken together, our study provides direct evidence for the complex role of EZH2 during early cardiac hypertrophy, and unveils a novel access to modify EZH2 function through ncRNAs.

DATA AVAILABILITY STATEMENT

The RIP-seq data can be accessed in the GEO Database with accession number GSE167007.

ETHICS STATEMENT

The animal study was reviewed and approved by Ethical Committee of Renmin Hospital of Wuhan University.

AUTHOR CONTRIBUTIONS

ZW designed and supervised the study. SW, NG, and SL performed the experiments and analyzed the data with input from YH, DZ, and LL. SL and ZW drafted the manuscript. All authors contributed to the article and approved the submitted version.

FUNDING

This work was supported by National Natural Science Foundation of China (No. 81722007 and No. 82070231) and National Health Commission of China (No. 2017ZX10304402001-008).

ACKNOWLEDGMENTS

We would like to thank Jon Choi, Gun Eui Lee, and Anna Sheydina from DNA Link USA Inc. for helping with the RNA-seq and data analysis, and Shuxun Ren and Yibin Wang from University of California at Los Angeles, USA for their experimental assistance and insightful comments.

REFERENCES

1. Dhanoa JK, Sethi RS, Verma R, Arora JS, Mukhopadhyay CS. Long non-coding RNA: its evolutionary relics and biological implications in mammals: a review. *J Anim Sci Technol.* (2018) 60:25. doi: 10.1186/s40781-018-0183-7
2. Djebali S, Davis CA, Merkel A, Dobin A, Lassmann T, Mortazavi A, et al. Landscape of transcription in human cells. *Nature.* (2012) 489:101–8. doi: 10.1038/nature11233
3. Rotini A, Martinez-Sarra E, Pozzo E, Sampaolesi M. Interactions between microRNAs and long non-coding RNAs in cardiac development and repair. *Pharmacol Res.* (2018) 127:58–66. doi: 10.1016/j.phrs.2017.05.029
4. Anastasiadou E, Jacob LS, Slack FJ. Non-coding RNA networks in cancer. *Nat Rev Cancer.* (2018) 18:5–18. doi: 10.1038/nrc.2017.99
5. Matsui M, Corey DR. Non-coding RNAs as drug targets. *Nat Rev Drug Discov.* (2017) 16:167–79. doi: 10.1038/nrd.2016.117
6. Devaux Y, Zangrando J, Schroen B, Creemers EE, Pedrazzini T, Chang CP, et al. Long noncoding RNAs in cardiac development and ageing. *Nat Rev Cardiol.* (2015) 12:415–25. doi: 10.1038/nrcardio.2015.55
7. Laugesen A, Hojfeldt JW, Helin K. Molecular mechanisms directing PRC2 recruitment and H3K27 methylation. *Mol Cell.* (2019) 74:8–18. doi: 10.1016/j.molcel.2019.03.011
8. Tsai MC, Manor O, Wan Y, Mosammaparast N, Wang JK, Lan F, et al. Long noncoding RNA as modular scaffold of histone modification complexes. *Science.* (2010) 329:689–93. doi: 10.1126/science.1192002
9. Li Y, Ren Y, Wang Y, Tan Y, Wang Q, Cai J, et al. A compound AC1Q3QWB selectively disrupts HOTAIR-mediated recruitment of PRC2 and enhances cancer therapy of DZNep. *Theranostics.* (2019) 9:4608–23. doi: 10.7150/thno.35188
10. Khalil AM, Guttman M, Huarte M, Garber M, Raj A, Rivea Morales D, et al. Many human large intergenic noncoding RNAs associate with chromatin-modifying complexes and affect gene expression. *Proc Natl Acad Sci USA.* (2009) 106:11667–72. doi: 10.1073/pnas.0904715106
11. Yu JR, Lee CH, Oksuz O, Stafford JM, Reinberg D. PRC2 is high maintenance. *Genes Dev.* (2019) 33:903–35. doi: 10.1101/gad.325050.119
12. Li H, Liefke R, Jiang J, Kurland JV, Tian W, Deng P, et al. Polycomb-like proteins link the PRC2 complex to CpG Islands. *Nature.* (2017) 549:287–91. doi: 10.1038/nature23881
13. Zylicz JJ, Bousard A, Zumer K, Dossin F, Mohammad E, da Rocha ST, et al. The implication of early chromatin changes in X chromosome inactivation. *Cell.* (2019) 176:182–97. doi: 10.1016/j.cell.2018.11.041
14. Portoso M, Ragazzini R, Brencic Z, Moiani A, Michaud A, Vassilev I, et al. PRC2 is dispensable for HOTAIR-mediated transcriptional repression. *EMBO J.* (2017) 36:981–94. doi: 10.15252/embj.201695335
15. Sarma K, Cifuentes-Rojas C, Ergun A, Del Rosario A, Jeon Y, White F, et al. ATRX directs binding of PRC2 to Xist RNA and polycomb targets. *Cell.* (2014) 159:869–83. doi: 10.1016/j.cell.2014.10.019
16. Pintacuda G, Wei GF, Roustan C, Kirmizitas BA, Solcan N, Cerase A, et al. hnRNPK Recruits PCGF3/5-PRC1 to the Xist RNA B-repeat to establish polycomb-mediated chromosomal silencing. *Molecular Cell.* (2017) 68:955–69. doi: 10.1016/j.molcel.2017.11.013
17. Colognori D, Sunwoo H, Kriz AJ, Wang CY, Lee JT. Xist deletional analysis reveals an interdependency between Xist RNA and polycomb complexes for spreading along the inactive X. *Molecular Cell.* (2019) 74:101–17. doi: 10.1016/j.molcel.2019.01.015
18. Klattenhoff CA, Scheuermann JC, Surface LE, Bradley RK, Fields PA, Steinhauser ML, et al. Brave heart, a long noncoding RNA required for cardiovascular lineage commitment. *Cell.* (2013) 152:570–83. doi: 10.1016/j.cell.2013.01.003
19. Wang X, Paucek RD, Gooding AR, Brown ZZ, Ge EJ, Muir TW, et al. Molecular analysis of PRC2 recruitment to DNA in chromatin and its inhibition by RNA. *Nat Struct Mol Biol.* (2017) 24:1028–38. doi: 10.1038/nsmb.3487
20. Zhang Q, McKenzie NJ, Warneford-Thomson R, Gail EH, Flanigan SF, Owen BM, et al. RNA exploits an exposed regulatory site to inhibit the enzymatic activity of PRC2. *Nat Struct Mol Biol.* (2019) 26:237–47. doi: 10.1038/s41594-019-0197-y
21. Dimitrova N, Zamudio JR, Jong RM, Soukup D, Resnick R, Sarma K, et al. LincRNA-p21 activates p21 in cis to promote Polycomb target gene expression and to enforce the G1/S checkpoint. *Mol Cell.* (2014) 54:777–90. doi: 10.1016/j.molcel.2014.04.025
22. Luo J, Wang K, Yeh S, Sun Y, Liang L, Xiao Y, et al. LncRNA-p21 alters the antiandrogen enzalutamide-induced prostate cancer neuroendocrine differentiation via modulating the EZH2/STAT3 signaling. *Nat Commun.* (2019) 10:2571. doi: 10.1038/s41467-019-09784-9
23. Nakamura M, Sadoshima J. Mechanisms of physiological and pathological cardiac hypertrophy. *Nat Rev Cardiol.* (2018) 15:387–407. doi: 10.1038/s41569-018-0007-y
24. Piccoli MT, Gupta SK, Viereck J, Foinquinos A, Samolovac S, Kramer FL, et al. Inhibition of the cardiac fibroblast-enriched lncRNA Meg3 prevents cardiac fibrosis and diastolic dysfunction. *Circ Res.* (2017) 121:575–83. doi: 10.1161/CIRCRESAHA.117.310624
25. Han P, Li W, Lin CH, Yang J, Shang C, Nuernberg ST, et al. A long noncoding RNA protects the heart from pathological hypertrophy. *Nature.* (2014) 514:102–6. doi: 10.1038/nature13596
26. Wang K, Liu F, Zhou LY, Long B, Yuan SM, Wang Y, et al. The long noncoding RNA CHRF regulates cardiac hypertrophy by targeting miR-489. *Circ Res.* (2014) 114:1377–88. doi: 10.1161/CIRCRESAHA.114.302476

27. Zhu XH, Yuan YX, Rao SL, Wang P. LncRNA MIAT enhances cardiac hypertrophy partly through sponging miR-150. *Eur Rev Med Pharmaco.* (2016) 20:3653–60. Available online at: https://www.europeanreview.org/wp/wp-content/uploads/3653-3660-LncRNA-MIAT-enhances-cardiac-hypertrophy-partly-through-sponging-miR-150.pdf
28. Wang Z, Zhang XJ, Ji YX, Zhang P, Deng KQ, Gong J, et al. The long noncoding RNA Chaer defines an epigenetic checkpoint in cardiac hypertrophy. *Nat Med.* (2016) 22:1131–39. doi: 10.1038/nm.4179
29. Wang Y, Xie Y, Li L, He Y, Zheng D, Yu P, et al. EZH2 RIP-seq identifies tissue-specific long non-coding RNAs. *Curr Gene Ther.* (2018) 18:275–85. doi: 10.2174/1566523218666181008125010
30. Francois H, Athirakul K, Mao L, Rockman H, Coffman TM. Role for thromboxane receptors in angiotensin-II-induced hypertension. *Hypertension.* (2004) 43:364–9. doi: 10.1161/01.HYP.0000112225.27560.24
31. Baroni TE, Chittur SV, George AD, Tenenbaum SA. Advances in RIP-chip analysis : RNA-binding protein immunoprecipitation-microarray profiling. *Methods Mol Biol.* (2008) 419:93–108. doi: 10.1007/978-1-59745-033-1_6
32. Leppek K, Stoecklin G. An optimized streptavidin-binding RNA aptamer for purification of ribonucleoprotein complexes identifies novel ARE-binding proteins. *Nucleic Acids Res.* (2013) 42:e13. doi: 10.1093/nar/gkt956
33. Zhao Y, Li H, Fang S, Kang Y, Wu W, Hao Y, et al. NONCODE 2016: an informative and valuable data source of long non-coding RNAs. *Nucleic Acids Res.* (2016) 44:D203–8. doi: 10.1093/nar/gkv1252
34. Livi CM, Klus P, Ponti RD, Tartaglia GG. catRAPID signature: identification of ribonucleoproteins and RNA-binding regions. *Bioinformatics.* (2016) 32:773–75. doi: 10.1093/bioinformatics/btv629
35. Battistelli C, Cicchini C, Santangelo L, Tramontano A, Grassi L, Gonzalez FJ, et al. The Snail repressor recruits EZH2 to specific genomic sites through the enrollment of the lncRNA HOTAIR in epithelial-to-mesenchymal transition. *Oncogene.* (2017) 36:942–55. doi: 10.1038/onc.2016.260
36. Fazi B, Garbo S, Toschi N, Mangiola A, Lombari M, Sicari D, et al. The lncRNA H19 positively affects the tumorigenic properties of glioblastoma cells and contributes to NKD1 repression through the recruitment of EZH2 on its promoter. *Oncotarget.* (2018) 9:15512–25. doi: 10.18632/oncotarget.24496
37. Zhao J, Ohsumi TK, Kung JT, Ogawa Y, Grau DJ, Sarma K, et al. Genome-wide Identification of Polycomb-Associated RNAs by RIP-seq. *Mol Cell.* (2010) 40:939–53. doi: 10.1016/j.molcel.2010.12.011
38. Sun DY, Yu ZWW, Fang X, Liu MD, Pu YY, Shao Q, et al. LncRNA GAS5 inhibits microglial M2 polarization and exacerbates demyelination. *Embo Rep.* (2017) 18:1801–16. doi: 10.15252/embr.201643668
39. Zhang X, Hamblin MH, Yin KJ. The long noncoding RNA Malat1: its physiological and pathophysiological functions. *RNA Biol.* (2017) 14:1705–14. doi: 10.1080/15476286.2017.1358347
40. Hirata H, Hinoda Y, Shahryari V, Deng G, Nakajima K, Tabatabai ZL, et al. Long noncoding RNA MALAT1 promotes aggressive renal cell carcinoma through Ezh2 and interacts with miR-205. *Cancer Res.* (2015) 75:1322–31. doi: 10.1158/0008-5472.CAN-14-2931
41. Huang C, Shi J, Guo Y, Huang W, Huang S, Ming S, et al. A snoRNA modulates mRNA 3' end processing and regulates the expression of a subset of mRNAs. *Nucleic Acids Res.* (2017) 45:8647–60. doi: 10.1093/nar/gkx651
42. Bratkovic T, Bozic J, Rogelj B. Functional diversity of small nucleolar RNAs. *Nucleic Acids Res.* (2020) 48:1627–51. doi: 10.1093/nar/gkz1140
43. Anwar T, Arellano-Garcia C, Ropa J, Chen YC, Kim HS, Yoon E, et al. p38-mediated phosphorylation at T367 induces EZH2 cytoplasmic localization to promote breast cancer metastasis. *Nat Commun.* (2018) 9:2801. doi: 10.1038/s41467-018-05078-8
44. Lo PW, Shie JJ, Chen CH, Wu CY, Hsu TL, Wong CH. O-GlcNAcylation regulates the stability and enzymatic activity of the histone methyltransferase EZH2. *Proc Natl Acad Sci USA.* (2018) 115:7302–7. doi: 10.1073/pnas.1801850115
45. Vastenhouw NL, Schier AF. Bivalent histone modifications in early embryogenesis. *Curr Opin Cell Biol.* (2012) 24:374–86. doi: 10.1016/j.ceb.2012.03.009
46. Shan Y, Liang Z, Xing Q, Zhang T, Wang B, Tian S, et al. PRC2 specifies ectoderm lineages and maintains pluripotency in primed but not naive ESCs. *Nat Commun.* (2017) 8:672. doi: 10.1038/s41467-017-00668-4
47. Mas G, Blanco E, Ballare C, Sanso M, Spill YG, Hu D, et al. Promoter bivalency favors an open chromatin architecture in embryonic stem cells. *Nat Genet.* (2018) 50:1452–62. doi: 10.1038/s41588-018-0218-5
48. Delgado-Olguin P, Huang Y, Li X, Christodoulou D, Seidman CE, Seidman JG, et al. Epigenetic repression of cardiac progenitor gene expression by Ezh2 is required for postnatal cardiac homeostasis. *Nat Genet.* (2012) 44:343. doi: 10.1038/ng.1068
49. He AB, Ma Q, Cao JJ, von Gise A, Zhou PZ, Xie HF, et al. Polycomb repressive complex 2 regulates normal development of the mouse heart. *Circ Res.* (2012) 110:406. doi: 10.1161/CIRCRESAHA.111.252205
50. Long YC, Hwang T, Gooding AR, Goodrich KJ, Rinn JL, Cech TR. RNA is essential for PRC2 chromatin occupancy and function in human pluripotent stem cells. *Nature Genetics.* (2020) 52:931–8. doi: 10.1038/s41588-020-0662-x
51. Kaneko S, Li G, Son J, Xu CF, Margueron R, Neubert TA, et al. Phosphorylation of the PRC2 component Ezh2 is cell cycle-regulated and up-regulates its binding to ncRNA. *Genes Dev.* (2010) 24:2615–20. doi: 10.1101/gad.1983810
52. Long Y, Bolanos B, Gong L, Liu W, Goodrich KJ, Yang X, et al. Conserved RNA-binding specificity of polycomb repressive complex 2 is achieved by dispersed amino acid patches in EZH2. *Elife.* (2017) 6:e31558. doi: 10.7554/eLife.31558
53. Davidovich C, Wang XY, Cifuentes-Rojas C, Goodrich KJ, Gooding AR, Lee JT, et al. Toward a consensus on the binding specificity and promiscuity of PRC2 for RNA. *Mol Cell.* (2015) 57:552–8. doi: 10.1016/j.molcel.2014.12.017
54. Davidovich C, Zheng L, Goodrich KJ, Cech TR. Promiscuous RNA binding by Polycomb repressive complex 2. *Nat Struct Mol Biol.* (2013) 20:1250–7. doi: 10.1038/nsmb.2679
55. Zhao J, Sun BK, Erwin JA, Song JJ, Lee JT. Polycomb proteins targeted by a short repeat RNA to the mouse X chromosome. *Science.* (2008) 322:750–6. doi: 10.1126/science.1163045
56. Lee JH, Gao C, Peng G, Greer C, Ren S, Wang Y, et al. Analysis of transcriptome complexity through RNA sequencing in normal and failing murine hearts. *Circ Res.* (2011) 109:1332–41. doi: 10.1161/CIRCRESAHA.111.249433
57. Peters T, Hermans-Beijnsberger S, Beqqali A, Bitsch N, Nakagawa S, Prasanth KV, et al. Long non-coding RNA Malat-1 is dispensable during pressure overload-induced cardiac remodeling and failure in mice. *PLoS ONE.* (2016) 11:e0150236. doi: 10.1371/journal.pone.0150236
58. Koyen AE, Madden MZ, Park D, Minten EV, Kapoor-Vazirani P, Werner E, et al. EZH2 has a non-catalytic and PRC2-independent role in stabilizing DDB2 to promote nucleotide excision repair. *Oncogene.* (2020) 39:4798–813. doi: 10.1038/s41388-020-1332-2

Conflict of Interest: The authors declare that the research was conducted in the absence of any commercial or financial relationships that could be construed as a potential conflict of interest.

frontiers in Cardiovascular Medicine

ORIGINAL RESEARCH
published: 09 April 2021
doi: 10.3389/fcvm.2021.634774

Antiretroviral Drugs Regulate Epigenetic Modification of Cardiac Cells Through Modulation of H3K9 and H3K27 Acetylation

*Shiridhar Kashyap[1], Avni Mukker[1], Deepti Gupta[1], Prasun K. Datta[2], Jay Rappaport[2], Jeffrey M. Jacobson[3], Steven N. Ebert[1] and Manish K. Gupta[1]**

[1] Division of Metabolic and Cardiovascular Sciences, Burnett School of Biomedical Sciences, College of Medicine, University of Central Florida, Orlando, FL, United States, [2] Division of Pathology, Tulane National Primate Research Center, Covington, LA, United States, [3] Department of Medicine, Center for AIDS Research, Case Medical Center, Case Western Reserve University and University Hospital, Cleveland, OH, United States

OPEN ACCESS

Edited by:
Suowen Xu,
University of Science and Technology of China, China

Reviewed by:
Xupei Huang,
Florida Atlantic University, United States
Zhuoming Li,
Sun Yat-sen University, China

***Correspondence:**
Manish K. Gupta
manish.gupta@ucf.edu

Specialty section:
This article was submitted to Cardiovascular Genetics and Systems Medicine, a section of the journal Frontiers in Cardiovascular Medicine

Received: *28 November 2020*
Accepted: *08 March 2021*
Published: *09 April 2021*

Citation:
Kashyap S, Mukker A, Gupta D, Datta PK, Rappaport J, Jacobson JM, Ebert SN and Gupta MK (2021) Antiretroviral Drugs Regulate Epigenetic Modification of Cardiac Cells Through Modulation of H3K9 and H3K27 Acetylation. Front. Cardiovasc. Med. 8:634774. doi: 10.3389/fcvm.2021.634774

Antiretroviral therapy (ART) has significantly reduced the rate of mortality in HIV infected population, but people living with HIV (PLWH) show higher rates of cardiovascular disease (CVD). However, the effect of antiretroviral (ARV) drug treatment on cardiac cells is not clear. In this study, we explored the effect of ARV drugs in cardiomyocyte epigenetic remodeling. Primary cardiomyocytes were treated with a combination of four ARV drugs (ritonavir, abacavir, atazanavir, and lamivudine), and epigenetic changes were examined. Our data suggest that ARV drugs treatment significantly reduces acetylation at H3K9 and H3K27 and promotes methylation at H3K9 and H3K27, which are histone marks for gene expression activation and gene repression, respectively. Besides, ARV drugs treatment causes pathological changes in the cell through increased production of reactive oxygen species (ROS) and cellular hypertrophy. Further, the expression of chromatin remodeling enzymes was monitored in cardiomyocytes treated with ARV drugs using PCR array. The PCR array data indicated that the expression of epigenetic enzymes was differentially regulated in the ARV drugs treated cardiomyocytes. Consistent with the PCR array result, SIRT1, SUV39H1, and EZH2 protein expression was significantly upregulated in ARV drugs treated cardiomyocytes. Furthermore, gene expression analysis of the heart tissue from HIV+ patients showed that the expression of SIRT1, SUV39H1, and EZH2 was up-regulated in patients with a history of ART. Additionally, we found that expression of SIRT1 can protect cardiomyocytes in presence of ARV drugs through reduction of cellular ROS and cellular hypertrophy. Our results reveal that ARV drugs modulate the epigenetic histone markers involved in gene expression, and play a critical role in histone deacetylation at H3K9 and H3K27 during cellular stress. This study may lead to development of novel therapeutic strategies for the treatment of CVD in PLWH.

Keywords: antiretroviral therapy, cardiovascular disease, histone deacetylase, human immunodeficiency virus, methyltransferase, SIRT1, cellular hypertrophy, ROS

INTRODUCTION

Human immunodeficiency virus (HIV) has infected 38 million people globally, and 1.7 million new cases were diagnosed in 2019 (1). Although ART improves the life expectancy of people living with HIV (PLWH), it is also known to increase the risk for developing cardiovascular disease (CVD) (2–5). Recent studies have shown that cardiovascular risk is almost double in HIV patients compared to the healthy population, and claims more lives of HIV patients compared to any other disease (6–8). Many HIV patients began taking ARV drugs in the mid 1990's and are now reaching the age of 50, which suggests that the association of HIV infection and cardiovascular disease was established three decades ago (9, 10). It is estimated that by year 2030, 73% of HIV infected patients will show CVD by the age of 50 (11).

Due to application of ART, viral replication is inhibited and viral load becomes undetectable in the patient's serum. However, the limitation of ARV drugs is that patients have to commit to this treatment for their entire life to control viral reactivation. People receiving ART live longer, but often show symptoms of organ failure, neuronal dementia, kidney failure, and aging, (12–14). The first ART was the nucleoside reverse transcription inhibitor (NRTI) azidothymidine (AZT), which produced severe organ toxicity (15). Later, several less-toxic reverse transcriptase inhibitors, such as lamivudine, were developed (16). Due to partial effectiveness of the NRTI drugs, in 1995 FDA approved the use of another class of antiretroviral drug protease inhibitor in combination of NRTIs (17). In general, patients receive a combination of two or three drugs, such as nucleoside reverse transcriptase inhibitors (lamivudine and abacavir), along with protease inhibitors (ritonavir and atazanavir) (18). Although, in 2020 international antiviral society- USA panel suggest that regimens of three drugs including 2 nucleoside reverse transcriptase inhibitor and an integrase inhibitor can be useful to suppress the viral replication (19), some of the developing nations continuously using the old regime of first line NRTI-based cocktail along with protease inhibitors (20–22). Chronic administration of multiple drugs may lead to CVD and heart failure in HIV patients through cellular and molecular modification in cardiomyocytes, which leads to modulation of pathological gene expression (5, 23, 24). Concordant with the clinical data, it was also reported that combined ART causes cardiomyopathy and metabolic disorders in HIV mouse models (25).

Post translational modifications (PTMs) of histone protein are responsible for epigenetic changes, which regulate DNA conformation and chromatin packaging, leading to activation and/or suppression of associated gene expression (26, 27). Epigenetic changes in histones (acetylation and methylation) play a significant role in maintaining cellular homeostasis during environmental and oxidative stress (28, 29). ART is known to inhibit function of the endoplasmic reticulum and mitochondria, and induces oxidative stress (30), which may initiate modulation of epigenetic signatures and gene expression. These global epigenetic changes may impact transcriptional regulation of protective or detrimental gene expression in cardiomyocytes, leading to heart failure (31, 32). Acetylation of histone 3 at lysine 9 and 27 (H3K9ac and H3K27ac) promotes active gene transcription (33–35), whereas acetylation at H3K9 in the promoter of cardiac specific transcription factors induces expression of fatal genes that lead to cardiac hypertrophy (36). The epigenetic regulatory enzyme Sirtuin 1 (SIRT1) acts as a deacetylase at H3K9 marks of histone and regulates cellular oxidative stress through inactivation of fatal gene expression (37–39). Additionally, SIRT1 protects cells during stress through suppression of reactive oxygen species (ROS) production and reduction of cellular hypertrophy (37, 40).

This study was designed to explore the epigenetic relationship of ARV drugs with histone markers and their regulatory enzymes. We found that ARV drugs treatment led to decreased acetylation of histone 3 (at H3K9 and H3K27) and increased tri-methylation (at H3K9 and H3K27). Additionally, we found that ARV treatment modulates the expression of epigenetic enzymes specific to histone acetylation and methylation that may help to maintain cellular homeostasis during drug induced stress.

METHODOLOGY

Human Subject's Ethics Statement

Written informed consent was obtained from the participant individuals by National NeuroAIDS Tissue Consortium (NNTC) (New York), and partnering institute according to local IRB protocol. Human heart tissue from HIV positive patients and healthy donors were obtained from NNTC according to approved IRB protocol by University of Central Florida.

Cell Models and ARV Drugs Treatment

Animal studies were approved by the institutional IACUC. All experiments were performed with neonatal rat ventricular cardiomyocytes (NRVCs). Primary cardiomyocytes were isolated from the 1–2-day-old Harlan Sprague–Dawley rats (Jackson Laboratory, Bar Harbor, ME) as described previously (41). In brief, left ventricles were collected and digested with 0.05% trypsin at 4°C overnight, followed by collagen treatment for 40 min at 37°C. Cardiomyocytes were separated by pre-plating the digested cell suspension. Initially, NRVCs were grown in MEM (Gibco, Grand Island, NY) containing 10% fetal bovine serum (FBS) with 1X anti-anti (Gibco) for 24 h in 10 cm plates for protein isolation, and 2-well-chamber slides for immunostaining at a density of 1.5×10^6 and 1×10^5 cells, respectively. Total RNA was isolated from 1×10^5 cells grown in 6-well-plates. All experiments were performed in NRVCs grown for least 12 h in DMEM with 2% FBS. For western blot and microscopy, cells were treated with a combination of 5 μM each of the ARV drugs ritonavir, abacavir, atazanavir, and lamivudine for 4, 12, or 24 h (Selleck Chemicals Llc, Pittsburgh, PA). For adenovirus mediated overexpression, cells were incubated with adenovirus (1:1 pfu) in serum free DMEM for 2 h, then the cells were incubated in DMEM with 2% FBS for 48 h. The adenoviruses encoding green florescence protein (Ad-GFP), EZH2 (Ad-EZH2), and SIRT1(Ad-SIRT1) were obtained from Vector Biolabs (Malvern, PA).

PCR Array Profiling for Chromatin Modifying Enzymes

Total RNA was isolated from NRVCs treated with ARV drugs using the RNeasy miniprep kit (Qiagen, Germantown, MD) following the manufacturer instructions and quantified by Nanodrop 8000 (Thermo Scientific, Waltham, MA). Epigenetic modifying enzyme expression was assessed using the rat chromatin RT^2 Profiler PCR array (PARN-085Z, Qiagen). First-strand cDNA was generated from 500 ng total RNA using the RT^2 first-strand synthesis kit (Qiagen). Quantitative real-time PCR (qRT-PCR) reactions were prepared with RT^2 SYBR Green/ROX PCR master mix and run on the Step One-Plus PCR machine (Applied Biosciences, Foster City, CA) with the standard SYBR green PCR program. PCR data was analyzed using the web-based tool provided by manufacturer (https://dataanalysis2.qiagen.com/pcr). Differentially expressed chromatin modifying enzymes in ARV drugs-treated NRVCs were identified with a fold change >1.2. Statistical significance was determined by Student's *t*-test of the replicate $2^{-\Delta\Delta CT}$ values for each gene in the control vs. treatment groups. A $p < 0.05$ was considered significant. PCR array results were normalized using the housekeeping genes Actb, Ldha, Bm2, and Hrpt1. Expression of differentially expressed epigenetic chromatin modification enzymes was validated by qRT-PCR and western blot.

Expression Analysis by Real-Time PCR

RNA from cardiomyocytes was isolated using the RNeasy Mini kit (Qiagen). TRI reagent (Sigma, St. Louis, MO) was used for RNA isolation from clinical tissue samples and treated with RNase free DNAse (Qiagen) to remove DNA contamination. cDNA was synthesized with 500 ng RNA using a SuperScript III First-Strand Synthesis SuperMix reagent kit (ThermoFisher Scientific). Gene expression was analyzed by qRT-PCR using SYBR Green master mix (Applied Biosystems) using gene specific primers (**Table 1**). Data were normalized with GAPDH as internal control.

TABLE 1 | Primer set used for genes expression analysis.

Gene	Sequence (5′-3′) Forward	Sequence (5′-3′) Reverse
SIRT1 (Rat)	CTCCCAGATCCTCAAGCCAT	GCTCATGAATGCTGAGTTGCT
SUV39H1 (Rat)	GGGGTTGCTCTAGAATGTGGT	ATAAGGGGCCCCAAGTAGGA
EZH2 (Rat)	TCTCACCAGCTGCAAAGTGT	ACAAGTGACTCAACAACAAGTTCA
Suv39h1 (Human)	TGATGAGGGGCGGATTGAAC	CCGTAACCACGTACAGCCAT
Ezh2 (Human)	GGACTCAGAAGGCAGTGGAG	CTTCCGCCAACAAACTGGTC
SIRT1 (Human)	CCCTCAAAGTAAGACCAGTAGC	CACAGTCTCCAAGAAGCTCTAC
GAPDH (Human)	GTCTCCTCTGACTTCAACAGC	ACCACCCTGTTGCTGTAGCCAA

Protein Extraction and Western Blot Analysis

For western blotting, NRVCs were lysed with RIPA buffer (50 mM tris-HCl pH-8.0, 150 mM NaCl, 1% IGEPAL, 12 mM sodium deoxycholate, 1% SDS) and 1X mammalian protease inhibitor (Sigma). Cells were sonicated for 24 s with a setting for 2 s. on and 1 s. off at 35% amplitude (Q125 sonicator, QSonica, New Orleans, LA). Cell debris and unbroken cells were removed by centrifuged at 10,000 × g for 10 min at 4°C and supernatants were collected for western blotting. Protein concentration was measured using the BCA assay kit (ThermoFisher Scientific). Protein samples were prepared in 1X Laemmli buffer and resolved by SDS-PAGE (Bio-Rad, Hercules, CA). Resolved proteins were then transferred to PVDF membrane by electrophoresis. Membranes were blocked with LI-COR blocking buffer (LI-COR, Lincoln, NE) for 1 h at room temperature and incubated overnight at 4°C with primary antibody in blocking buffer (LI-COR). The membranes were then probed with secondary antibody (IRDye®680, red and 800, green, LI-COR) at room temperature for 2 h after washing twice with 1X PBST and once with 1X PBS. After incubation, the membranes were washed twice with 1X PBST and once with 1X PBS before scanning using a LI-COR-Odyssey scanner (LI-Cor). The following antibodies were used for western blotting: SIRT1, Histone, Suv39h1, H3K9me1, H3K9me2, H3K27me1, H3K9me2 (Cell Signaling, Danvers, MA), H3K9ac (MyBioSource, San Diego, CA), H3k27ac, H3K9me3, EZH2 (Abcam, Cambridge, MA), and GAPDH (Proteintech, Rosemont, IL).

Cell Viability Assay

Cellular viability was detected using CellTiter-Glo (Promega, Madison, WI). NRVCs were plated in a 96-well white plate at a density of 10,000 cells per well. The cells were then treated with ARV drugs (5 μM of Ritonavir, Abacavir, Atazanavir and Lamivudine, (Selleck Chemicals Llc, Pittsburgh, PA) for 24 h. Cellular viability was detected using the CellTiter-Glo luminescent cell viability assay (Promega). The plate was scanned with an EnVision luminometer (PerkinElmer, Waltham, MA) for a measurement time of 2 s.

Immunostaining

For immunocytochemistry, NRVCs plated in chamber slides were washed twice with 1X PBS and then fixed with 4% paraformaldehyde (PFA) for 10 min. After washing twice with 1X PBS, cells were permeabilized with 0.5% Triton X-100 for 10 min at room temperature. Cells were masked with 0.1 M glycine for 30 min at room temperature and then washed twice with 1X PBS. Blocking was performed at room temperature with blocking buffer (1% BSA, 0.1% Tween 20 in 1X PBS) for 1 h, then the slides were incubated with primary antibody in blocking buffer overnight at 4°C. After washing with 1X PBS, cells were probed with secondary antibody labeled with Alexa Fluor 488 and 490 (Thermo Fisher Scientific) in blocking buffer for 1 h at room temperature. For counter staining with a second primary antibody, cells were blocked for additional 30 min at room temperature before probing with antibody. Cells were mounted with VECTASHIELD HardSet

mounting medium with DAPI (Vector Laboratories, Burlingame, CA). Images were captured with a Zeiss 710 fluorescence microscope (Oberkochen, Germany). The following antibodies were used for immunocytochemistry H3K9ac (MyBioSource,), Actinin, H3K27ac, H3K9me3, H3K27me3, Ezh2 (Abcam), SIRT1 (Cell signaling).

ROS Measurement

Intracellular ROS level were detected in live cells by dihydroethidium (DHE) florescence probe (Life Technology) staining. NRVCs were plated in the 35 mm plate with DMEM having 2% FBS for the DHE staining. Cardiomyocytes were treated with cocktail of 5 μM each of the ARV drugs ritonavir, abacavir, atazanavir, and lamivudine or DMSO for 24 h and then live cells were incubated with DHE probe (5 uM) with cell culture media for 5 min. Then cells were washed with the culture media and further incubated in the cell culture media for the microscopy. DHE fluorescence intensity was measured using fluorescence microscope (BZ-X800, Keyence, Osaka, Japan).

Knockdown of SIRT1 and Ezh2

For knockdown of SIRT1, 1×10^6 rat primary cardiomyocytes were plated in 60 mm plates. siRNAs were transfected using Lipofectamine 2000 in optimum media (Gibco) for 3 h, then the media was replaced with DMEM having 2% FBS for 48 h. Sirt1 was knocked down in rat cardiomyocytes using siRNA (SASI-Rn 02; 00230695, 00230696, 00230697, Sigma), and control cells were transfected with universal negative siRNA (Sigma). When needed, cells were incubated with ARV drugs (5 μm of ritonavir, abacavir, atazanavir, and lamivudine) in DMEM having 2% FBS for different time points and cells were harvested for protein as described above. Similarly, knockdown of Ezh2 was performed using siRNA (s155284, Thermofisher).

SIRT1 Deacetylase Activity Assay

SIRT1 mediated deacetylase activity was measured using the SIRT1 activity assay kit (Abcam) according to the manufacturer instructions. Cell lysate was prepared in lysis buffer as described in the protocol. The reaction mixture was prepared by mixing SIRT1 assay buffer, fluoro-substrate peptide, and developer. The reaction was initiated by adding 15 μg protein lysate and incubated for 30 min in black transparent bottom 96-well-plates (Thermo Scientific). The fluorescent intensity was measured by spectrophotometer (Bio-Tak, Synergy 4, Winooski, VT) at 350 nm excitation and 450 nm emission, respectively.

Data Analysis and Statistical Procedures

All the experiments were performed three or more times. Statistical analyses were performed using Prism GraphPad 8.0. The results are presented as mean ± standard deviation. The unpaired student *t*-test was performed for statistical significance between the control and test groups. A $p < 0.05$ was considered to be significant.

RESULTS

ARV Drugs Suppress Histone Marks Responsible for Activation of Gene Expression

Earlier studies suggested that PTMs of histones can influence biological processes through activation or deactivation of cellular genes. Histone deacetylase regulates acetylation levels at H3K9 and H3K27, and plays a critical role in promoting chromatin inactivation marks (42–44). Another epigenetic regulating enzyme, histone methyltransferase regulates cellular gene deactivation by promoting tri-methylation of histones at H3K9 and H3K27 (45, 46). The effect of ARV drugs on the regulation of epigenetic histone marks is unclear. In this study, we tested the role of ARV drugs on the expression of epigenetic regulatory enzymes and its effect on cardiac epigenetic remodeling. To understand the effects of drugs on histone PTMs, NRVCs were treated with plasma levels of ARV drugs (5 μM of ritonavir, atazanavir, abacavir, and lamivudine) (47–50) for different duration (4, 12, and 24 h), and the level of histone acetylation and methylation was determined by western blotting. Western blot analysis showed that ARV drugs treatment significantly reduced acetylation at H3K9 and H3K27 (**Figures 1A,B**). To confirm ARV drugs mediated changes in histone PTMs, immunocytochemistry was performed using NRVCs and images were captured by confocal microscopy. Microscopy data showed that drug treatment significantly reduced acetylation of histone 3 at K9 (**Figures 1C,D**) and K27 (**Figures 1E,F**). We further tested the effects of individual drugs on histone protein acetylation. NRVCs were treated with individual ARV drugs for 12 h and the level of histone acetylation was detected by western blot. Western blot analysis showed that the protease inhibitors (ritonavir, atazanavir) and reverse transcriptase inhibitor lamivudine had a greater deacetylation effect compared to the reverse transcriptase inhibitor abacavir (**Figures 1G,H**) These results suggest that ARV drugs modulate PTMs of histone and cause significant reduction of active histone marks. Earlier studies reported that mono, di, and tri-methylation of histone plays a significant role in the regulation of chromatin mediated gene expression in heart (29, 31, 32). In this study, we tested the expression of histone methylation in cardiomyocytes after drug treatment. Western blot data indicated that drug treatment significantly increased tri-methylation at H3K9 and H3K27 histone marks (**Figures 2A,B**). Further immunocytochemistry was done in ARV treated cardiomyocytes with the H3K9me3 and H3K27me3 antibodies to evaluate status of histone 3 methylation. Microscopy data suggested that ARV drugs treatment significantly upregulate methylation of histone protein at H3K9 (**Figures 2C,D**) and H3K27 (**Figures 2E,F**). Additionally, we performed western blot analysis to determine the level of mono and dimethylation of histone in ARV drugs treated cells. Western blot analysis showed that ARV drugs treatment significantly increased the level of dimethylated histone (H3K9me2, H3K27me2) in drug treated cells but not the monomethylated form of histone (H3K9me1, H3K27me1) (**Supplementary Figures 1A,B**). To determine the effect of ARV drugs on cardiomyocytes remodeling and pathology, we treated

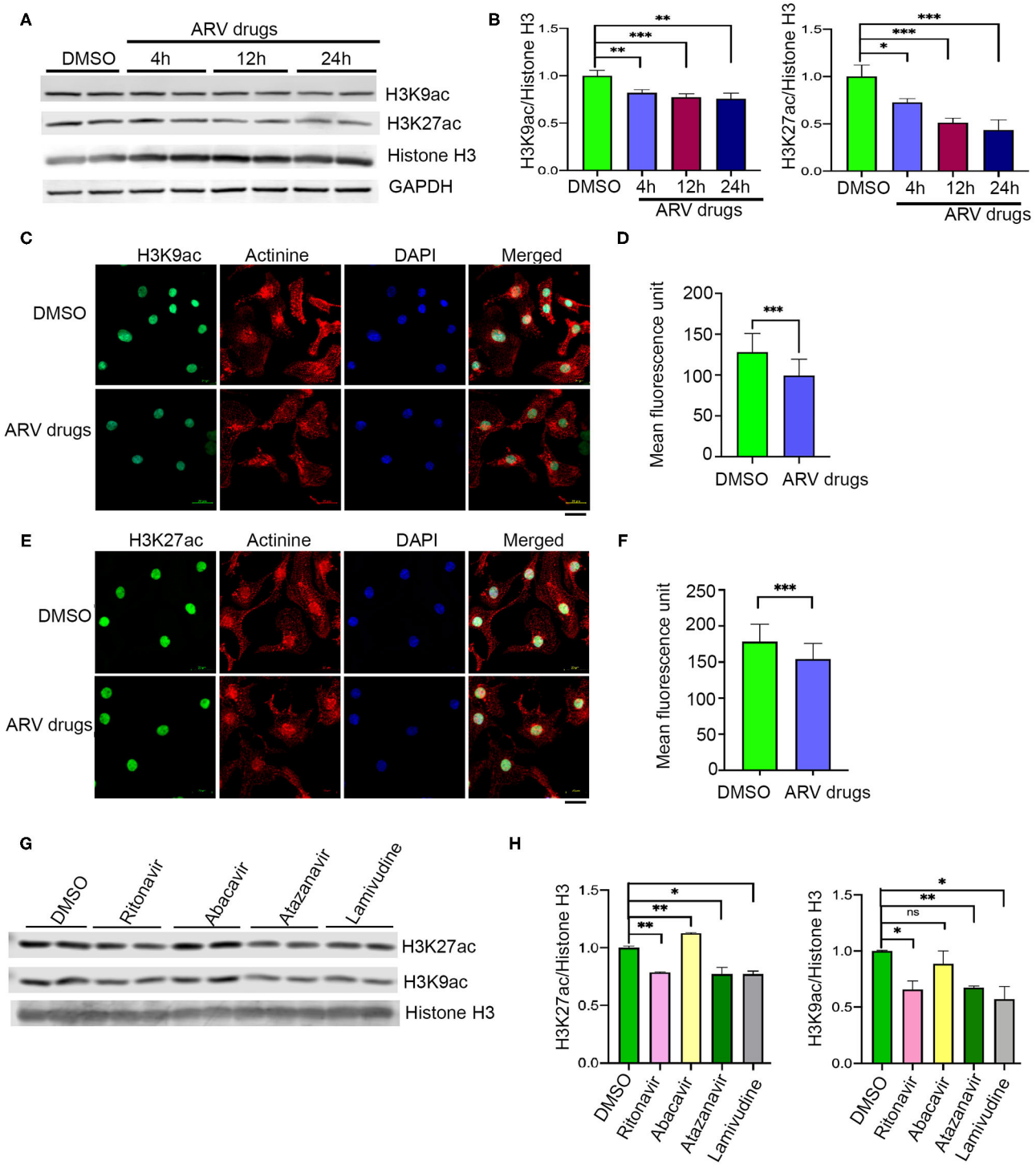

FIGURE 1 | ARV drugs treatment suppresses active histone marks. **(A,B)** Western blots show acetylation of histone at H3K9 and H3K27 and graphs show its quantification (***$p < 0.001$). NRVCs were treated with ARV drugs (5 μM of Ritonavir, Abacavir, Atazanavir and Lamivudine) for 4, 12, and 24 h and western blots were done with total protein lysate. **(C,D)** Representative images show immunofluorescence staining of NRVCs stained with H3K9ac (green), actinin (red), and nucleus stained with DAPI (blue). Cells were treated with ARV drugs for 12 h and fixed with 4% PFA. **(D)** Graph shows quantification of microscopic images ($n = 50$ cells); (*$p < 0.05$). **(E,F)** Representative images show immunofluorescence staining of NRVCs stained with H3K27ac (green), actinin (red), and nucleus stained with DAPI (blue). Cells were treated with ARV drugs for 12 h and fixed with 4% PFA. **(D)** Graph shows quantification of microscopic images ($n = 50$ cells); (*$p < 0.05$). **(G,H)** Western blot shows acetylation of NRVCs after drugs treatment. NRVCs were treated with individual ARV drug for 12 h and western blot was done with total protein lysate. Graphs show quantification of western blot (***$p < 0.001$; **$p < 0.01$, ns, not significant).

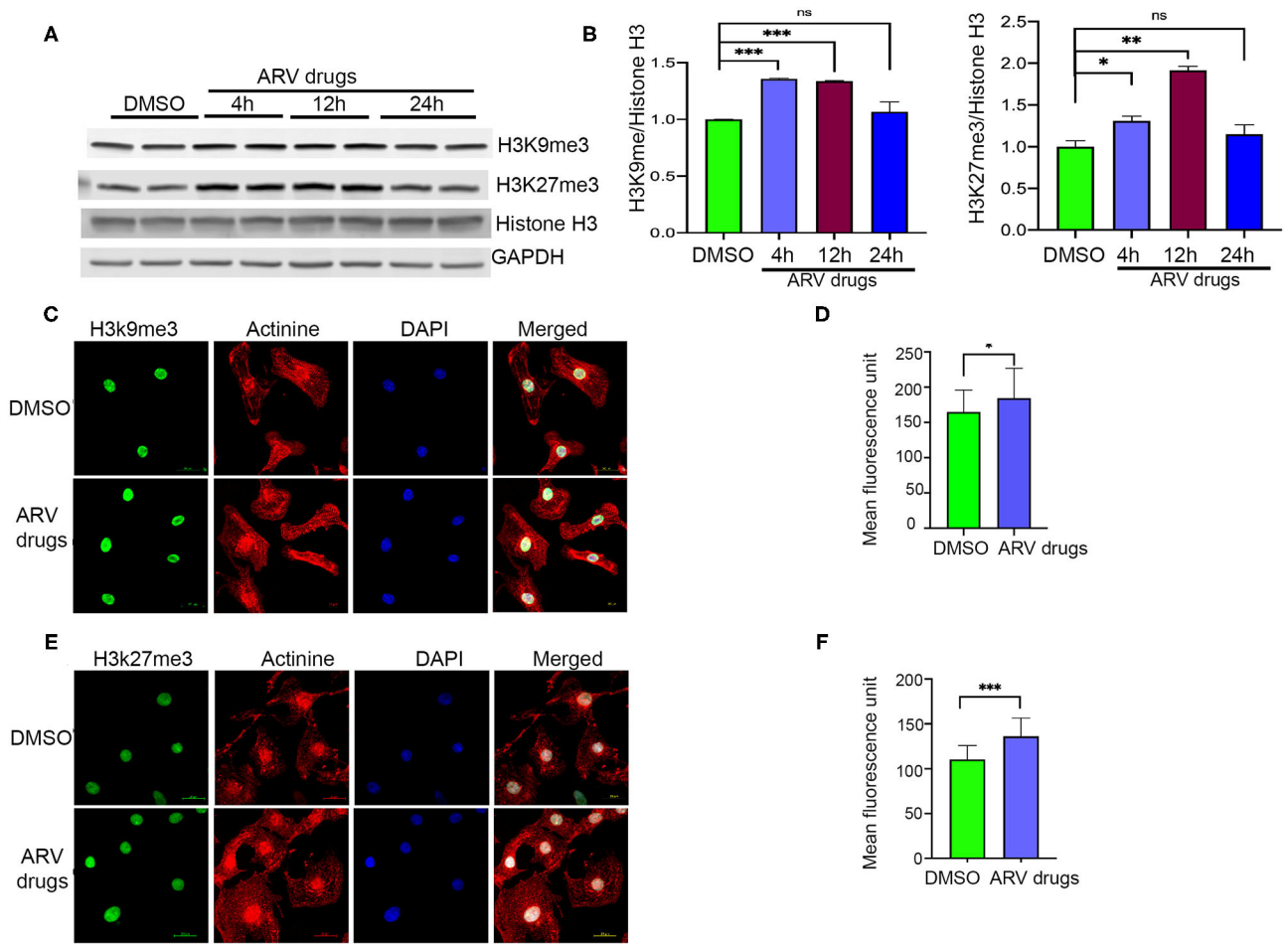

FIGURE 2 | ARV drugs treatment promotes repressive histone marks. **(A,B)** Western blot shows antiretroviral drug treatment increase the methylation of H3K27me3 and H3K9me3. NRVCs were treated with ARV drugs (5 μM of Ritonavir, Abacavir, Atazanavir and Lamivudine) for 4, 12, and 24 h and western blots were done with total protein lysate. Graph shows quantification of western blots (***$p < 0.001$; **$p < 0.01$, ns, not significant) **(C)** Representative images show immunofluorescence staining of NRVCs stained with H3K9me3 (green), actinin (red), and nucleus stained with DAPI (blue). Cells were treated with ARV drugs for 12 h and fixed with 4% PFA. **(D)** Graph shows quantification of microscopic images ($n = 50$ cells); (*$p < 0.05$). **(E)** Representative images show immunofluorescence staining of NRVCs stained with H3K27me3 (green), actinin (red), and nucleus stained with DAPI (blue). Cells were treated with ARV drugs for 12 h and fixed with 4% PFA. **(F)** Graph shows quantification of microscopic images ($n = 50$ cells); (***$p < 0.001$).

the NRVCs with combination drugs for 24 h and cellular hypertrophy and ROS level were determined. Our microscopy data show that ARV drugs treatment significantly increases the cardiomyocytes cell size (**Supplementary Figures 2A–C**), which is an indicator of cellular hypertrophy. Additionally, we found that ARV drugs treatment significantly increases the cellular ROS level (**Supplementary Figures 2D–F**). The increased ROS production is known to cause cardiomyocytes remodeling and pathological changes during stress condition.

Chromatin Modifying Enzymes Play a Critical Role in Epigenetic Modification of Histone During ARV Drugs Treatment

To understand the correlation of ARV drugs and epigenetic changes, we measured the expression of chromatin remodeling enzymes in NRVCs after ARV drugs treatment. NRVCs were treated with ARV drugs for 4, 12, and 24 h, and the expression of chromatin remodeling enzymes was assessed by RT^2 PCR array profiling. Analysis of the PCR array data showed that out of 84 genes, 50 epigenetic modifying chromatin enzymes were differentially regulated in NRVCs after drug treatment (**Table 2**). PCR array data analysis represented in clustergrams, scattered plots, and bar graphs (**Figures 3A–C**) showed that drug treatment differentially regulated the expression of chromatin modifying enzymes in cardiomyocytes. In our western blot data at **Figures 1**, **2**, we found that ARV drugs modify the acetylation as well as methylation of histone 3. Interestingly, in PCR array result we found that the histone deacetylase enzyme SIRT1 (Fold Change (FC) = 1.95; $p = 0.02$) and the methyl transferase enzyme SUV39H1 (FC = 1.36; $p = 0.01$) and Ezh2 (FC = 1.3; $p = 0.02$) were significantly modulated in ARV drug-treated cells compared to control cells (**Figures 3A–C**). PCR array results for

TABLE 2 | PCR array analysis of differentially expressed epigenetic chromatin modifying enzymes on ARV drugs treatment.

		Gene symbol	Fold regulation	*p*-value
1		Actb	1.56	1.026
2		Ash2l	1.93	0.013
3		Aurkc	1.75	0.031
4		Crebbp	1.47	0.043
5		Cxxc1	1.33	0.026
6		Dot1l	2.90	0.025
7		Ehmt2	2.60	0.044
8		Hdac10	2.00	0.041
9		Hdac11	2.14	0.020
10		Hdac3	1.43	0.019
11	ART 4 h	Hdac4	1.84	0.001
12		Hdac5	2.58	0.047
13		Hdac6	1.66	0.040
14		Hdac7	1.90	0.022
15		Hdac8	1.82	0.013
16		Med24	1.44	0.026
17		Ncor1	1.33	0.036
18		Prmt2	2.25	0.011
19		Prmt6	4.86	0.020
20		Rps6ka5	1.28	0.004
21		Sirt1	1.95	0.026
22		Setd6	1.30	0.046
23		Smyd1	1.50	0.004
24		Crebbp	1.36	0.026
25		Ep300	1.30	0.019
26	ART 12 h	Ezh2	1.28	0.022
27		Mta2	1.31	0.036
28		Ncor1	1.43	0.011
29		Smyd1	1.64	0.027
30		Suv420h1	1.35	0.041
31		Atf2	1.42	0.032
32		Cdk2	1.34	0.041
33		Edf1	1.52	0.016
34		Ep300	1.70	0.011
35		Ezh2	1.30	0.021
36		Fbxo11	1.44	0.027
37		Ing3	1.29	0.034
38		Med24	1.68	0.030
39		Mta2	1.45	0.027
40	ART 24 h	Ncoa6	1.46	0.006
41		Ncor1	1.45	0.048
42		Nek6	1.66	0.019
43		Nsd1	1.68	0.046
44		Prmt1	1.36	0.001
45		Rps6ka5	1.64	0.029
46		Setd6	1.51	0.027
47		Smyd1	1.8	0.005
48		Suv39h1	1.36	0.016
49		Suv420h1	1.87	0.024
50		Ube2b	1.42	0.046

SIRT1, EZH2, and SUV39H1 were validated with qRT-PCR in NRVCs treated with ARV drugs for 4, 12, and 24 h. Expression analysis confirmed that ARV drugs treatment upregulated the expression of SIRT1, SUV39H1, and EZH2 at 12 h post treatment (**Figure 4A**). We also examined the expression of SIRT1, EZH2, and SUV39H1 at the protein level in NRVCs treated with ARV drugs for 4, 12, and 24 h. Western blot analysis showed that the expression of these epigenetic regulating enzymes was significantly upregulated in drug treated cells (**Figures 4B,C**). Additionally, we validated our *in vitro* expression data in clinical samples obtained from HIV-1-infected patients treated with ART (**Table 3**). Total RNA was isolated from heart tissue and the expression of SIRT1, EZH2, and SUV39H1 was measured by qRT-PCR using gene specific primers (**Table 1**). We used healthy donor human heart tissue for comparison (**Table 3**). Expression analysis shows that similar to our *in vitro* results, the expression of SIRT1, EZH2, and SUV39H1 was significantly upregulated in HIV+ patients compared to healthy donor samples (**Figures 5A–C**).

SIRT1 Activity Is Critical for ARV Drugs Mediated Deacetylation of Histone in Cardiomyocytes

In our experiments, we found that ARV drugs treatment reduces acetylation of the histone 3 protein at H3K9 and H3K27 (**Figures 1A,B**). Additionally, our data showed that ARV drugs treatment induces the expression of SIRT1 at the transcriptional as well as translational level (**Figures 3C**, **4A,B**). To explore the role of SIRT1 in ARV drugs mediated changes in histone PTMs, we knocked down SIRT1 expression in NRVCs using siRNA for 48 h and then treated with ARV drugs for 12 h. Expression of H3K9 acetylation was measured by western blotting using total protein lysate. Western blot showed that siRNAs significantly reduced the expression of SIRT1 protein in NRVCs (**Figures 6A,B**). Interestingly, the acetylation of histone protein at H3K9 was significantly increased in SIRT1 knockdown cells after ART treatment (**Figures 6A,B**). Concomitantly, we found that overexpression of SIRT1 significantly reduced H3K9 acetylation in both drug treated and untreated cardiomyocytes, which suggests that SIRT1 is a critical regulator of ARV drugs-mediated histone acetylation at H3K9 (**Figures 6C,D**).

We also assessed the effect of ARV drugs on SIRT1 mediated deacetylase activity in NRVCs. Cells were treated with ARV drugs for 4–24 h, and then deacetylase activity was monitored using whole protein lysate. Deacetylase activity showed that enzyme activity significantly increased after drug treatment (**Figure 6E**). We also evaluated the effects of drug treatment on cellular viability using NRVCs. Cells were treated with ARV drugs for 24 h and viability was measured using CellTiter-Glo. The viability assay further suggests that drug treatment or knockdown of SIRT1 significantly decreases cellular viability (**Figure 6F**). Additionally, we found that SIRT1 over expression significantly improves the cellular viability during ARV mediated cellular stress (**Figure 6G**). Further, we found that SIRT1 expression significantly reduced cellular hypertrophy and ROS production in cardiomyocytes treated with the ARV drugs (**Figures 6H–K**).

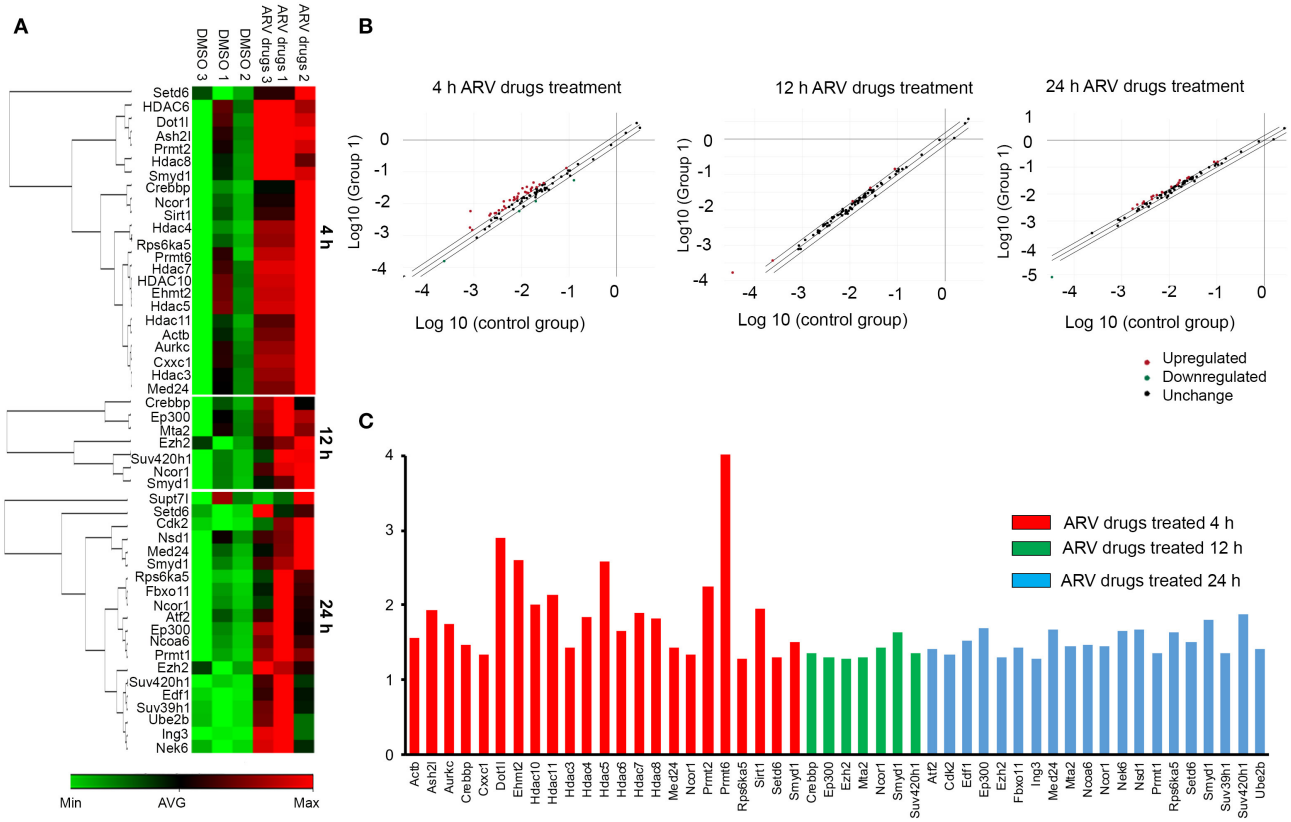

FIGURE 3 | ARV drugs treatment modulates expression of epigenetic regulating enzyme. NRVCs were treated with ARV drugs (5 μM of Ritonavir, Abacavir, Atazanavir, and Lamivudine) for 4, 12, and 24 h and expression of epigenetic enzyme was measured by RT^2 PCR array profiling. **(A)** Clustergram showing differentially expressed genes ($p < 0.05$, Fold Change >1.2) obtained on RT^2 PCR array profiling, green represent minimum and red represent maximum magnitude of expression. **(B)** Scatter Plot representing normalized expression of genes between 4, 12, and 24 h ARV drugs treated vs. control group. Central diagonal line represents no change, whereas, outer diagonal lines indicate the fold regulation threshold (>1.2). Genes with data points beyond the outer lines in the upper left and lower right corners are up-regulated or down-regulated, respectively. **(C)** Graphical representation of differentially expressed chromatin modifying enzymes against expression regulation on drug treatment at 4 h (red), 12 h (green), and 24 h (blue).

Our study suggests that SIRT1 plays a critical role during drug induced cellular toxicity and protects cardiomyocytes from oxidative stress.

Ezh2 Plays an Important Role in Maintaining the Repressive Histone Marks in Cardiomyocytes

In our study, we found that ARV drugs treatment significantly upregulates the di and trimethylated form of histone (H3K27me2, H3K27me3) along with histone methyl transferase enzyme Ezh2 (**Figures 2–4**). Further, to elucidate the role of methyl transferase during ARV drugs treatment we knockdown the expression of Ezh2 using siRNA. Western blots show that siRNA treatment significantly reduces the expression of Ezh2 in cardiomyocytes (**Supplementary Figures 3A,B**). Furthermore, we found that level of H3K27me3 level was significantly reduced in the Ezh2 knockdown cells (**Supplementary Figure 3C**). Additionally, we checked the cell size of the Ezh2 knockdown cells by microscopy. Microscopy images suggest that Ezh2 knockdown significantly increases the cell size in both DMSO treated as well as in ARV drug treated cells (**Supplementary Figures 3D,E**) which suggest that Ezh2 plays significant role in regulation of histone methylation and cardiomyocytes function.

DISCUSSION

Earlier studies suggested that HIV induced cardiomyopathy is one of the leading causes of death in HIV+ patients (51). Based on limited data available worldwide of HIV patients on ART, diastolic dysfunction, and heart failure remain the major causes of comorbidity in the HIV+ population (52). Although application of ART improves the survival of HIV+ patients, the effect of ART on cardiac function is still controversial. In addition, it is not clear how ART and HIV induce cellular and molecular changes in cardiomyocytes, which lead to heart failure (51, 52).

Epigenetic markers control gene-specific expression in cells, which regulates the cellular transcriptome and maintenance of cellular function (32). Distribution patterns of epigenetic markers

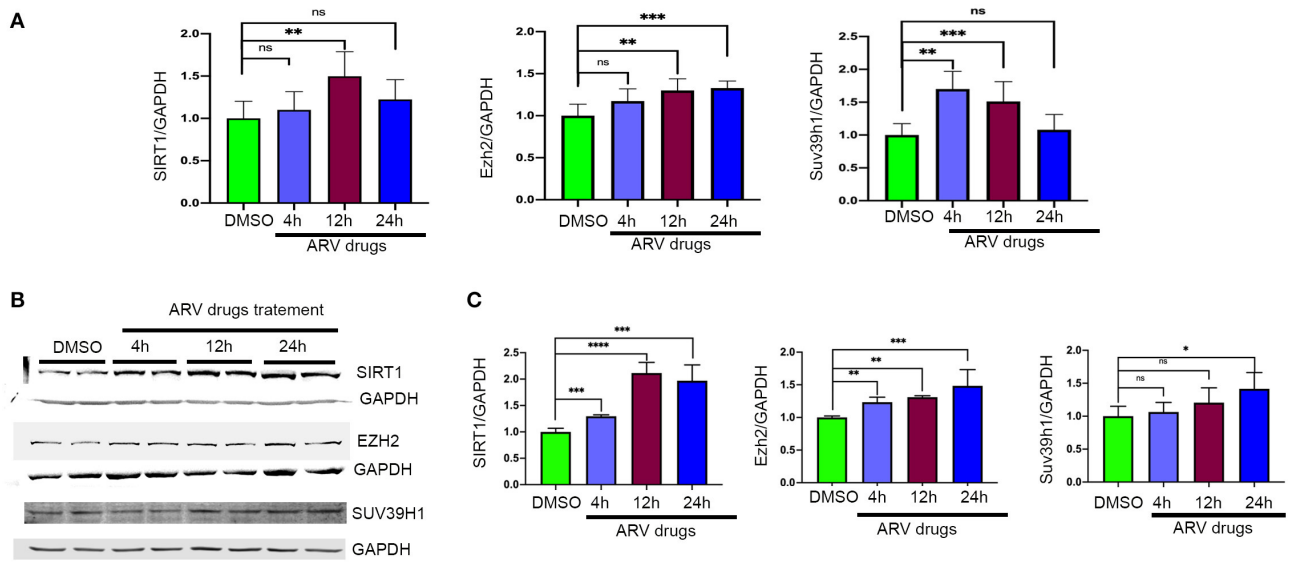

FIGURE 4 | Expression of epigenetic chromatin enzymes affected by ARV drugs treatment. **(A)** Graphs showing mRNA expression of Sirt1, Ezh2, and Suv39h1 in NRVCs treated with drugs. Cells were treated with ARV drugs (5 μM of Ritonavir, Abacavir, Atazanavir and Lamivudine) for different time point (4, 12, and 24 h) and expression was checked by qRT-PCR. **(B,C)** Western blots showing protein expression of SIRT1, SUV39H1, and EZH2 enzymes and graph show quantification. NRVCs were treated with ARV drugs (5 μM of Ritonavir, Abacavir, Atazanavir, and Lamivudine) for 4, 12, and 24 h and expression was checked in total protein lysate by western blot with respective antibody (*$p < 0.05$, **$p < 0.01$, ***$p < 0.001$, ****$p < 0.0001$, ns, not significant).

TABLE 3 | Patient's information.

Patients No	HIV status	Age	Race	Risk	ART	Viral load copies/ml	CD4
1	–	50–60	H	na	–	na	na
2	–	50–60	B	na	–	na	na
3	–	50–60	B	na	–	na	na
4	–	50–60	H	na	–	na	na
5	–	40–50	W	na	–	na	na
6	–	60–70	H	na	–	na	na
7	–	60–70	B	na	–	na	na
8	–	30–40	H	na	–	na	na
9	+	60–70	B	ivdu	+	30	137
10	+	60–70	H	sex	+	undetect (<20)	1808
11	+	70–80	W	unknown	+	undetect (<20)	472
12	+	70–80	B	ivdu	+	380	158
13	+	50–60	B	sex	+	undetect (<50)	42
14	+	60–70	B	sex	+	undetect (<20)	55
15	+	NA	NA	na	+	NA	NA
16	+	NA	NA	na	+	NA	NA

over the genome helps to determine cell types, and these markers remain mostly stable in mature cells (53). Changes in distribution patterns of epigenetics marks by upstream stress stimuli leads to gene expression modulation and development of disease phenotypes (28, 29, 54). This study explored the molecular mechanism of ARV drugs mediated epigenetic modification of histones along with its epigenetic regulating enzymes. We found that ARV drugs treatment in cardiomyocytes destabilized the active histone marks (H3K9ac and H3K27ac), while promoting the histone repressive marks (H3K9me2, H3K27me2, H3K9me3, and H3K27me3). Similar to our current findings, earlier studies also reported similar epigenetic modifications in mice hearts after pressure overload-induced cardiac hypertrophy, as well as in failing human hearts (31, 32, 55, 56). Those epigenetic modifications of active and repressive histone marks led to changes in pathological gene expression and caused cardiomyocytes remodeling as well as progression of heart failure (57, 58). In our study, we found that cardiomyocytes treated

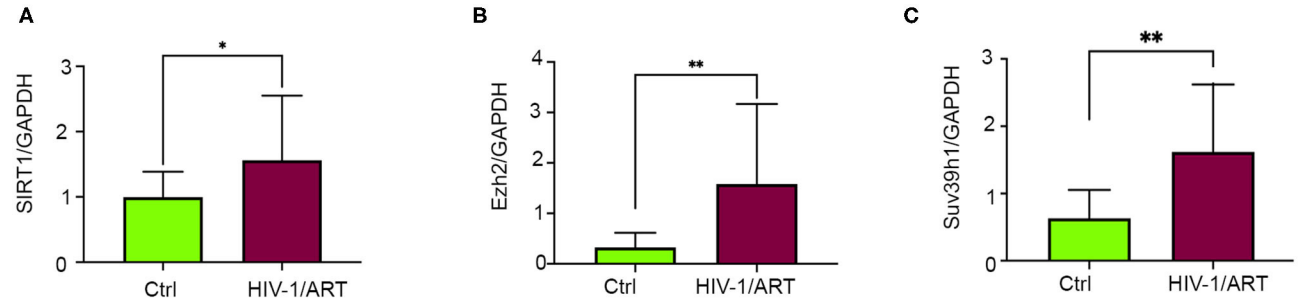

FIGURE 5 | Expression of epigenetic regulating enzymes dysregulated in HIV + patients have history of ART treatment. **(A–C)** Graphs show expression of SIRT1, SUV39H1, and EZH2 enzymes in human cardiac tissue. Total RNA was isolated from the frozen heart tissue and expression was checked by qRT-PCR (*$p < 0.05$, **$p < 0.01$).

with the ARV drugs leads to production of ROS and cellular hypertrophy which could be one of the mechanisam of ARV drugs medicated induction of cellular toxicity. Studies in clinical samples showed that loss of active gene expression associated with structure and functional changes of heart which may led to progressive heart failure in patients (31, 32). Similarly, we found significant alteration of epigenetic regulatory enzymes in tissue collected from the hearts of HIV patients undergoing ART. This suggests that ART could be one cause of pathological changes in the hearts of PLWH.

During adverse conditions, histone epigenetics dynamically change to regulate DNA template function and fulfill cellular demand. These histone PTMs are regulated by specific epigenetic chromatin enzymes, whose activities are required to make changes at active histone or repressive histone marks. In this study, we found that the expression of the epigenetic enzymes SIRT1, EZH2, and SUV39H1 was upregulated in ARV drugs-treated cardiomyocytes, as well as in heart tissue from HIV+ patients on ART. SIRT1 is an NAD dependent histone deacetylase and promotes transcriptional inactivation by deacetylation of histone marks such as H3K9ac (38, 59). We found that SIRT1 expression and activity increased in cardiomyocytes after ARV drugs treatment. Earlier studies suggested that SIRT1 expression increases during mild oxidative stress as a compensatory mechanisam and gives protection to cells through reduction of ROS production (60). Some studies also suggested that SIRT1 has a cardiac protective role in stress conditions and regulates cellular stress and cell death by allowing deacetylation of H3K9 (37–39, 61). Moreover, SIRT1 protects the heart by regulation of histone acetylation and methylation at H3K9 during ischemic and hypertrophic conditions (39). SIRT1 mediated deacetylation at H3K9 allows the modulation of physiological and pathological gene-specific expression through stress response pathways (62). Similarly, another study showed that SIRT1 agonism can protect cells by inhibition of inflammatory cytokine production, and reduces cellular oxidative stress by modulation of forkhead box O1 (Foxo1) (38). Additionally, SIRT1 can attenuate apoptosis in cardiomyocytes by preventing induction of caspase-3, as well as inhibition of autophagy by deacetylating major autophagy regulatory factors such as Atg5, Atg7, and Atg8 (63, 64). In our study we found that increased expression of SIRT1 can reduces ROS level of ARV drugs treated cells and improve cellular viability as well. Since, SIRT1 plays a cardioprotective role in response to oxidative stress in the cardiomyocytes, this may explain why upregulation of SIRT1 provides protection to cells during ART induced oxidative stress.

Moreover, ARV drugs treated cardiomyocytes or heart tissue from ART treated patients showed upregulation of the H3K9 and H3K27 methyl-transferase enzymes, EZH2 and SUV39H1, respectively. EZH2 is an enzymatic subunit of polycomb repressive complex 2, and is the only known H3K27 methyltransferase (65). A previous study suggested that it is essential to maintain EZH2 expression levels in cardiomyocytes to regulate cellular homeostasis and physiological gene expression. It is also reported that a hypertrophic response can promote EZH2 expression levels in the heart (66). In our current study, we found that Ezh2 protein required to maintain the cellular repressive histone marks (H3K27me3) and knockdown of Ezh2 causes cellular hypertrophy. The molecular mechanism driving EZH2 interaction in cardiomyocytes is not clear, however, TAC induced cardiac hypertrophic responses in mice showed that EZH2 interacts with the primary microRNA-208b to regulate the expression of antisense β-MHC and α-MHC (67, 68). Ezh1 and Ezh2 expression changes during heart development and regulates cellular gene expression by turn on and turn off mechanisam on responsive gene through switching from mono to di and trimethylation of histone (67, 69, 70). In this study, we found that another epigenetic chromatin enzyme, SUV39H1, was upregulated due to drug treatment. SUV39H1 is known to differentially regulated, and its increased expression is reported to be associated with the development of cardiac hypertrophy (71). The molecular mechanism of SUV39h1-mediated regulation of cardiomyocyte pathology in hypertrophic conditions is not clear; however, a previous study showed that kindlin-2 can interact with SUV39H1 and recruit the complex to the GATA4 gene promoter to suppress GATA4 transcription by bi- and trimethylation at H3K9 (72). Interestingly, some studies suggest that SIRT1 and SUV39H1 regulates each other expression and function through deacetylation and methylation, respectively, depending on the cellular stress condition (38, 40).

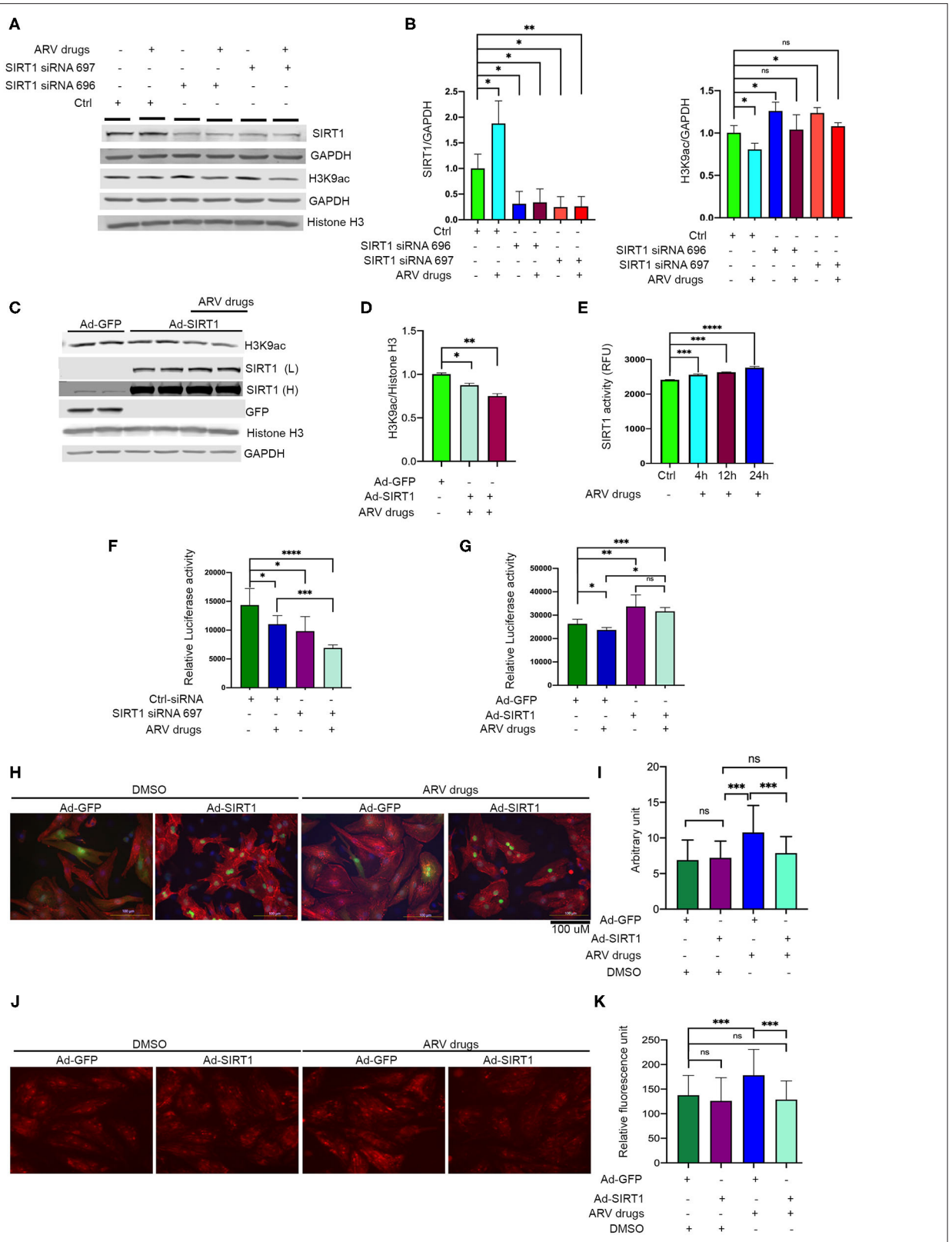

FIGURE 6 | Expression of SIRT1 is critical in ARV drugs mediated modulation of cellular acetylation. **(A,B)** Western blots show that knockdown of SIRT1 upregulate acetylation of histone at H3K9. NRVCs were treated with SIRT1 siRNA for 48 h and followed by ARV drugs treatment (5 μM of Ritonavir, Abacavir, Atazanavir, and

(Continued)

FIGURE 6 | Lamivudine) for 12 h. Graph shows quantification of western blot. (***$p < 0.001$; **$p < 0.01$, *$p < 0.05$, ns, not significant). **(C,D)** Western blots show that over expression of SIRT1 can significantly decreases the H3K9ac in rat cardiomyocytes. SIRT1 and GFP protein were over expressed in the cardiomyocytes for 48 h by adenoviral transduction and treated with the ARV drugs for another 24 h. Graph shows the quantification of H3K9ac (*$p < 0.05$). **(E)** Drug treatment upregulates the SIRT1 enzyme activity. NRVCs were treated with ARV drugs for 4–24 h and enzyme activity was determined in total protein lysate. (***$p < 0.001$; ****p < 0.0001, ns, not significant). **(F)** ARV drugs treatment reduces cellular viability in SIRT1 knockdown cells. NRVCs were treated with SIRT1 siRNA and ARV drugs and viability was measure by CellTiter-Glo (**$p < 0.01$; *$p < 0.05$, ns, not significant). **(G)** Graph shows that overexpression of SIRT1 improves cellular viability during ARV mediated cellular stress. NRVCs were transfected with adenovirus for 48 h and then treated with ARV drugs for another 24 h. Cellular viability was determined by the CellTiter-Glo (***$p < 0.001$; **$p < 0.01$, *$p < 0.05$, ns, not significant). **(H,I)** Representative microscopy images show that ARV drugs treatment induces cellular hypertrophy and SIRT1 over expression significantly reduces the cellular hypertrophy in ARV drugs treated cells (*$p < 0.05$). NRVCs were transfected with adenovirus for 48 h and then treated with ARV drugs for another 24 h. Drug treated cells were fixed with 4% PFA and stained with actinin antibody (red) and DAPI for nucleus. Cell size was determined by Image J software (National Institute of Health, USA). Graph shows the measurement of cell size (***$p < 0.001$, ns, not significant). **(J,K)** Representative images show that ARV drugs treatment induces cellular ROS level and SIRT1 over expression significantly reduces the ROS level of drug treated cells. Graph shows the quantification of ROS. NRVCs were transfected with adenovirus for 48 h and then treated with ARV drugs for another 24 h. ROS level of the cells were determined by DHE staining. Live imaging was done under fluorescence microscope (***$p < 0.001$, ns, not significant).

These data support that ARV drugs treatment of cardiomyocytes dysregulates the expression of epigenetic chromatin modifying enzymes and their downstream targets in histones, which triggers repression histone marks, as reported in cardiac tissue of heart failure patients.

CONCLUSION

Taken together, our data shows that combined ARV drugs treatment induces cardiotoxicity, which may lead to the development of cardiac dysfunction in HIV patients. ARV drugs-mediated cellular stress causes aberration of PTM at histones, which suppresses active histone marks and promotes inactivation of histone marks through the modulation of the expression and activity of chromatin modifying enzymes. Additionally, we found that SIRT1 plays a critical role in the regulation of acetylation levels at histone proteins, and may give protection to cardiomyocytes and the heart during ARV drugs-mediated stress.

DATA AVAILABILITY STATEMENT

The original contributions presented in the study are included in the article/**Supplementary Material**, further inquiries can be directed to the corresponding author/s.

ETHICS STATEMENT

All experiments were performed in accordance with relevant guidelines and regulations, and this study was reviewed and approved by the University of Central Florida Institutional review board (IRB). All patient samples were obtained under informed consent and approved by local IRB. Written informed consent for cardiac tissues was obtained and is maintained by the members of the National NeuroAIDS Tissue Consortium (NNTC) under local IRB approved protocol. De-identified samples were provided by the NNTC for this study. The patients/participants provided their written informed consent to participate in this study. The animal study was reviewed and approved by IACUC.

AUTHOR CONTRIBUTIONS

SK, MG, PD, JR, and JJ design the experiments. SK, AM, DG, and MG perform the experiments. SK and MG analyze the data. PD, JR, JJ, SE, and MG participate analysis of data and critical evaluation of manuscript. All authors contributed to the article and approved the submitted version.

FUNDING

This work was supported by grant 1R01HL141045-01A1.

ACKNOWLEDGMENTS

The authors thank the NNTC for providing clinical samples for this study.

SUPPLEMENTARY MATERIAL

The Supplementary Material for this article can be found online at: https://www.frontiersin.org/articles/10.3389/fcvm.2021.634774/full#supplementary-material

Supplementary Figure 1 | ARV drug treatment causes upregulation of dimethylated histone in cardiomyocytes. **(A)** Western blot data show that ARV drugs treatment significantly upregulates dimethylated histone (H2K9me2 and H3K27 me2), but monomethylated form of histone did not change (H2K9me1 and H3K27 me1). NRVCs were treated with ARV drugs (5 μM of Ritonavir, Abacavir, Atazanavir, and Lamivudine) for 4–24 h and western blot was performed with total protein lysate using antibodies specific to mono and dimethylation of histone. **(B)** Graph shows quantification of western blots (**$p < 0.01$; *$p < 0.05$).

Supplementary Figure 2 | ARV drugs treatment induces cellular hypertrophy and ROS production in cardiomyocytes. **(A–C)** Representative images show that ARV drug treatment increases the cell size in cardiomyocytes. Graph shows the quantification of cell size. NRVCs were treated with ARV drugs (5 μM of Ritonavir, Abacavir, Atazanavir, and Lamivudine) for 24 h and cells were fixed with 4% PFA. Fixed cells were stained with actinin antibody (red) and DAPI for the nucleus (blue). **(D–F)** Representative images and graph show that ARV drug treatment induces ROS production in cardiomyocytes. Cells were treated with ARV drugs (5 μM of Ritonavir, Abacavir, Atazanavir, and Lamivudine) for 24 h and stained with DHE. Live cell imaging was done with the help of fluorescence microscopy. Graph shows the quantification of DHE staining.

Supplementary Figure 3 | Ezh2 is critical to maintain the histone repressive marks of histone. **(A–C)** western blots show the expression of Ezh2 and H3K27m3 in cardiomyocytes treated with Ezh2 siRNA. NRVCs were treated with Ezh2 siRNA for 48 h and then treated with ARV drugs for another 12 h (5 μM of

Ritonavir, Abacavir, Atazanavir, and Lamivudine). Western blot was performed with total protein lysate. Graph shows the quantification of western blots. **(D,E)** Representative microscopy images show that knockdown of Ezh2 induces cellular hypertrophy. NRVCs were transfected with siRNAs for 48 h and then treated with ARV drugs for another 24 h. Drug treated cells were fixed with 4% PFA and stained with actinin antibody (red), Ezh2 antibody (green) and DAPI for nucleus. Cell size was determined by Image J software. Graph shows the measurement of cell size (***$p < 0.001$, **$p < 0.01$, *$p < 0.05$).

REFERENCES

1. (UNAIDS), J.U.N.P.o.H.A. *Fact Sheet: World AIDS Day 2019—Global HIV Statistics*. Geneva (2019).
2. Triant VA, Lee H, Hadigan C, Grinspoon SK. Increased acute myocardial infarction rates and cardiovascular risk factors among patients with human immunodeficiency virus disease. *J Clin Endocrinol Metab.* (2007) 92:2506–12. doi: 10.1210/jc.2006-2190
3. Currier JS, Lundgren JD, Carr A, Klein D, Sabin CA, Sax PE, et al. Epidemiological evidence for cardiovascular disease in HIV-infected patients and relationship to highly active antiretroviral therapy. *Circulation.* (2008) 118:e29–35. doi: 10.1161/CIRCULATIONAHA.107.189624
4. Francisci D, Giannini S, Baldelli F, Leone M, Belfiori B, Guglielmini G, et al. HIV type 1 infection, and not short-term HAART, induces endothelial dysfunction. *AIDS.* (2009) 23:589–96. doi: 10.1097/QAD.0b013e328325a87c
5. Hsue PY, Waters DD. HIV infection and coronary heart disease: mechanisms and management. *Nat Rev Cardiol.* (2019) 16:745–59. doi: 10.1038/s41569-019-0219-9
6. Law MG, Friis-Moller N, El-Sadr WM, Weber R, Reiss P, D'Arminio Monforte A, et al. The use of the Framingham equation to predict myocardial infarctions in HIV-infected patients: comparison with observed events in the D:A:D study. *HIV Med.* (2006) 7:218–30. doi: 10.1111/j.1468-1293.2006.00362.x
7. Greene M, Justice AC, Lampiris HW, Valcour V. Management of human immunodeficiency virus infection in advanced age. *JAMA.* (2013) 309:1397–405. doi: 10.1001/jama.2013.2963
8. Remick J, Georgiopoulou V, Marti C, Ofotokun I, Kalogeropoulos A, Lewis W, et al. Heart failure in patients with human immunodeficiency virus infection: epidemiology, pathophysiology, treatment, future research. *Circulation.* (2014) 129:1781–9. doi: 10.1161/CIRCULATIONAHA.113.004574
9. Hecht SR, Berger M, Van Tosh A, Croxson S. Unsuspected cardiac abnormalities in the acquired immune deficiency syndrome. an echocardiographic study. *Chest.* (1989) 96:805–8. doi: 10.1378/chest.96.4.805
10. Himelman RB, Chung WS, Chernoff DN, Schiller NB, Hollander H. Cardiac manifestations of human immunodeficiency virus infection: a two-dimensional echocardiographic study. *J Am Coll Cardiol.* (1989) 13:1030–6. doi: 10.1016/0735-1097(89)90256-8
11. Smit M, Brinkman K, Geerlings S, Smit C, Thyagarajan K, Sighem A, et al. Future challenges for clinical care of an ageing population infected with HIV: a modelling study. *Lancet Infect Dis.* (2015) 15:810–8. doi: 10.1016/S1473-3099(15)00056-0
12. Deeks SG. Immune dysfunction, inflammation, and accelerated aging in patients on antiretroviral therapy. *Top HIV Med.* (2009) 17:118–23.
13. Achhra AC, Nugent M, Mocroft A, Ryom L, Wyatt CM. Chronic kidney disease and antiretroviral therapy in HIV-positive individuals: recent developments. *Curr HIV/AIDS Rep.* (2016) 13:149–57. doi: 10.1007/s11904-016-0315-y
14. Gannon PJ, Akay-Espinoza C, Yee AC, Briand LA, Erickson MA, Gelman BB, et al. HIV protease inhibitors alter amyloid precursor protein processing via beta-site amyloid precursor protein cleaving Enzyme-1 translational up-regulation. *Am J Pathol.* (2017) 187:91–109. doi: 10.1016/j.ajpath.2016.09.006
15. McKee EE, Bentley AT, Hatch M, Gingerich J, Susan-Resiga D. Phosphorylation of thymidine and AZT in heart mitochondria: elucidation of a novel mechanism of AZT cardiotoxicity. *Cardiovasc Toxicol.* (2004) 4:155–67. doi: 10.1385/CT:4:2:155
16. Torres SM, Divi RL, Walker DM, McCash CL, Carter MM, Campen MJ, et al. In utero exposure of female CD-1 mice to AZT and/or 3TC: II. persistence of functional alterations in cardiac tissue. *Cardiovasc Toxicol.* (2010) 10:87–99. doi: 10.1007/s12012-010-9065-z
17. Kitchen VS, Skinner C, Ariyoshi K, Lane EA, Duncan IB, Burckhardt J, et al. Safety and activity of saquinavir in HIV infection. *Lancet.* (1995) 345:952–5. doi: 10.1016/S0140-6736(95)90699-1
18. Pirmohamed M, Back DJ. The pharmacogenomics of HIV therapy. *Pharmacogenom J.* (2001) 1:243–53. doi: 10.1038/sj.tpj.6500069
19. Saag MS, Gandhi RT, Hoy JF, Landovitz RJ, Thompson MA, Sax PE, et al. Antiretroviral drugs for treatment and prevention of HIV infection in adults: 2020 recommendations of the international antiviral society-USA panel. *JAMA.* (2020) 324:1651–69. doi: 10.1001/jama.2020.17025
20. Reyskens KM, Essop MF. HIV protease inhibitors and onset of cardiovascular diseases: a central role for oxidative stress and dysregulation of the ubiquitin-proteasome system. *Biochim Biophys Acta.* (2014) 1842:256–68. doi: 10.1016/j.bbadis.2013.11.019
21. Stockdale AJ, Saunders MJ, Boyd MA, Bonnett LJ, Johnston V, Wandeler G, et al. Effectiveness of protease Inhibitor/Nucleos(t)ide reverse transcriptase inhibitor-based second-line antiretroviral therapy for the treatment of human immunodeficiency virus Type 1 infection in Sub-Saharan Africa: a systematic review and meta-analysis. *Clin Infect Dis.* (2018) 66:1846–57. doi: 10.1093/cid/cix1108
22. Iwuji CC, Churchill D, Bremner S, Perry N, To Y, Lambert D, et al. A phase IV randomised, open-label pilot study to evaluate switching from protease-inhibitor based regimen to Bictegravir/Emtricitabine/Tenofovir Alafenamide single tablet regimen in Integrase inhibitor-naive, virologically suppressed HIV-1 infected adults harbouring drug resistance mutations (PIBIK study): study protocol for a randomised trial. *BMC Infect Dis.* (2020) 20:524. doi: 10.1186/s12879-020-05240-y
23. Alvi RM, Neilan AM, Tariq N, Awadalla M, Afshar M, Banerji D, et al. Protease inhibitors and cardiovascular outcomes in patients with HIV and heart failure. *J Am Coll Cardiol.* (2018) 72:518–30. doi: 10.1016/j.jacc.2018.04.083
24. Titanji B, Gavegnano C, Hsue P, Schinazi R, Marconi VC. Targeting inflammation to reduce atherosclerotic cardiovascular risk in people with HIV infection. *J Am Heart Assoc.* (2020) 9:e014873. doi: 10.1161/JAHA.119.014873
25. Lewis W, Haase CP, Raidel SM, Russ RB, Sutliff RL, Hoit BD, et al. Combined antiretroviral therapy causes cardiomyopathy and elevates plasma lactate in transgenic AIDS mice. *Lab Invest.* (2001) 81:1527–36. doi: 10.1038/labinvest.3780366
26. Strahl BD, Allis CD. The language of covalent histone modifications. *Nature.* (2000) 403:41–5. doi: 10.1038/47412
27. Tessarz P, Kouzarides T. Histone core modifications regulating nucleosome structure and dynamics. *Nat Rev Mol Cell Biol.* (2014) 15:703–8. doi: 10.1038/nrm3890
28. Niu Y, DesMarais TL, Tong Z, Yao Y, Costa M. Oxidative stress alters global histone modification and DNA methylation. *Free Radic Biol Med.* (2015) 82:22–8. doi: 10.1016/j.freeradbiomed.2015.01.028
29. Fabrizio P, Garvis S, Palladino F. Histone methylation and memory of environmental stress. *Cells.* (2019) 8:339. doi: 10.3390/cells8040339
30. Banerjee A, Abdelmegeed MA, Jang S, Song BJ. Zidovudine (AZT) and hepatic lipid accumulation: implication of inflammation, oxidative and endoplasmic reticulum stress mediators. *PLoS ONE.* (2013) 8:e76850. doi: 10.1371/journal.pone.0076850
31. Papait R, Cattaneo P, Kunderfranco P, Greco C, Carullo P, Guffanti A, et al. Genome-wide analysis of histone marks identifying an epigenetic signature of promoters and enhancers underlying cardiac hypertrophy. *Proc Natl Acad Sci USA.* (2013) 110:20164–9. doi: 10.1073/pnas.1315155110
32. Gilsbach R, Schwaderer M, Preissl S, Gruning BA, Kranzhofer D, Schneider P, et al. Distinct epigenetic programs regulate cardiac myocyte development and disease in the human heart *in vivo*. *Nat Commun.* (2018) 9:391. doi: 10.1038/s41467-017-02762-z
33. Roth SY, Denu JM, Allis CD. Histone acetyltransferases. *Annu Rev Biochem.* (2001) 70:81–120. doi: 10.1146/annurev.biochem.70.1.81
34. Tie F, Banerjee R, Stratton CA, Prasad-Sinha J, Stepanik V, Zlobin A, et al. CBP-mediated acetylation of histone H3 lysine 27 antagonizes Drosophila Polycomb silencing. *Development.* (2009) 136:3131–41. doi: 10.1242/dev.037127

35. Gates LA, Shi J, Rohira AD, Feng Q, Zhu B, Bedford MT, et al. Acetylation on histone H3 lysine 9 mediates a switch from transcription initiation to elongation. *J Biol Chem.* (2017) 292:14456–72. doi: 10.1074/jbc.M117.802074
36. Li S, Peng B, Luo X, Sun H, Peng C. Anacardic acid attenuates pressure-overload cardiac hypertrophy through inhibiting histone acetylases. *J Cell Mol Med.* (2019) 23:2744–52. doi: 10.1111/jcmm.14181
37. Alcendor RR, Gao S, Zhai P, Zablocki D, Holle E, Yu X, et al. Sirt1 regulates aging and resistance to oxidative stress in the heart. *Circ Res.* (2007) 100:1512–21. doi: 10.1161/01.RES.0000267723.65696.4a
38. Vaquero A, Scher M, Erdjument-Bromage H, Tempst P, Serrano L, Reinberg D. SIRT1 regulates the histone methyl-transferase SUV39H1 during heterochromatin formation. *Nature.* (2007) 450:440–4. doi: 10.1038/nature06268
39. Tong C, Morrison A, Mattison S, Qian S, Bryniarski M, Rankin B, et al. Impaired SIRT1 nucleocytoplasmic shuttling in the senescent heart during ischemic stress. *FASEB J.* (2013) 27:4332–42. doi: 10.1096/fj.12-216473
40. Yang G, Weng X, Zhao Y, Zhang X, Hu Y, Dai X, et al. The histone H3K9 methyltransferase SUV39H links SIRT1 repression to myocardial infarction. *Nat Commun.* (2017) 8:14941. doi: 10.1038/ncomms14941
41. Haq S, Choukroun G, Kang ZB, Ranu H, Matsui T, Rosenzweig A, et al. Glycogen synthase kinase-3beta is a negative regulator of cardiomyocyte hypertrophy. *J Cell Biol.* (2000) 151:117–30. doi: 10.1083/jcb.151.1.117
42. Barski A, Cuddapah S, Cui K, Roh TY, Schones DE, Wang Z, et al. High-resolution profiling of histone methylations in the human genome. *Cell.* (2007) 129:823–37. doi: 10.1016/j.cell.2007.05.009
43. Ernst J, Kheradpour P, Mikkelsen TS, Shoresh N, Ward LD, Epstein CB, et al. Mapping and analysis of chromatin state dynamics in nine human cell types. *Nature.* (2011) 473:43–9. doi: 10.1038/nature09906
44. Nguyen AT, Zhang Y. The diverse functions of Dot1 and H3K79 methylation. *Genes Dev.* (2011) 25:1345–58. doi: 10.1101/gad.2057811
45. Stewart MD, Li J, Wong J. Relationship between histone H3 lysine 9 methylation, transcription repression, and heterochromatin protein 1 recruitment. *Mol Cell Biol.* (2005) 25:2525–38. doi: 10.1128/MCB.25.7.2525-2538.2005
46. Lee TI, Jenner RG, Boyer LA, Guenther MG, Levine SS, Kumar RM, et al. Control of developmental regulators by Polycomb in human embryonic stem cells. *Cell.* (2006) 125:301–13. doi: 10.1016/j.cell.2006.02.043
47. Danner SA, Carr A, Leonard JM, Lehman LM, Gudiol F, Gonzales J, et al. A short-term study of the safety, pharmacokinetics, and efficacy of ritonavir, an inhibitor of HIV-1 protease. European-Australian Collaborative Ritonavir Study Group. *N Engl J Med.* (1995) 333:1528–33. doi: 10.1056/NEJM199512073332303
48. Minzi O, Mugoyela V, Gustafsson L. Correlation between lamivudine plasma concentrations and patient self-reported adherence to antiretroviral treatment in experienced HIV patients. *Ther Clin Risk Manag.* (2011) 7:441–6. doi: 10.2147/TCRM.S23625
49. Estevez JA, Molto J, Tuneu L, Cedeno S, Antonijoan RM, Mangues MA, et al. Ritonavir boosting dose reduction from 100 to 50 mg does not change the atazanavir steady-state exposure in healthy volunteers. *J Antimicrob Chemother.* (2012) 67:2013–9. doi: 10.1093/jac/dks152
50. Vourvahis M, Davis J, Langdon G, Layton G, Fang J, Choo HW, et al. Pharmacokinetic interactions between lersivirine and zidovudine, tenofovir disoproxil fumarate/emtricitabine and abacavir/lamivudine. *Antivir Ther.* (2013) 18:745–54. doi: 10.3851/IMP2566
51. Freiberg MS, Chang CH, Skanderson M, Patterson OV, DuVall SL, Brandt CA, et al. Association between HIV infection and the risk of heart failure with reduced ejection fraction and preserved ejection fraction in the antiretroviral therapy era: results from the veterans aging cohort study. *JAMA Cardiol.* (2017) 2:536–46. doi: 10.1001/jamacardio.2017.0264
52. Schuster I, Thoni GJ, Ederhy S, Walther G, Nottin S, Vinet A, et al. Subclinical cardiac abnormalities in human immunodeficiency virus-infected men receiving antiretroviral therapy. *Am J Cardiol.* (2008) 101:1213–7. doi: 10.1016/j.amjcard.2007.11.073
53. Bannister AJ, Kouzarides T. Regulation of chromatin by histone modifications. *Cell Res.* (2011) 21:381–95. doi: 10.1038/cr.2011.22
54. Suganuma T, Workman JL. Signals and combinatorial functions of histone modifications. *Annu Rev Biochem.* (2011) 80:473–99. doi: 10.1146/annurev-biochem-061809-175347
55. Angrisano T, Schiattarella GG, Keller S, Pironti G, Florio E, Magliulo F, et al. Epigenetic switch at atp2a2 and myh7 gene promoters in pressure overload-induced heart failure. *PLoS ONE.* (2014) 9:e106024. doi: 10.1371/journal.pone.0106024
56. Ito E, Miyagawa S, Fukushima S, Yoshikawa Y, Saito S, Saito T, et al. histone modification is correlated with reverse left ventricular remodeling in nonischemic dilated cardiomyopathy. *Ann Thorac Surg.* (2017) 104:1531–9. doi: 10.1016/j.athoracsur.2017.04.046
57. Portela A, Esteller M. Epigenetic modifications and human disease. *Nat Biotechnol.* (2010) 28:1057–68. doi: 10.1038/nbt.1685
58. Rosa-Garrido M, Chapski DJ, Vondriska TM. Epigenomes in cardiovascular disease. *Circ Res.* (2018) 122:1586–607. doi: 10.1161/CIRCRESAHA.118.311597
59. Imai S, Armstrong CM, Kaeberlein M, Guarente L. Transcriptional silencing and longevity protein Sir2 is an NAD-dependent histone deacetylase. *Nature.* (2000) 403:795–800. doi: 10.1038/35001622
60. Kietzmann T, Petry A, Shvetsova A, Gerhold JM, Gorlach A. The epigenetic landscape related to reactive oxygen species formation in the cardiovascular system. *Br J Pharmacol.* (2017) 174:1533–54. doi: 10.1111/bph.13792
61. Pillarisetti S. A review of Sirt1 and Sirt1 modulators in cardiovascular and metabolic diseases. *Recent Pat Cardiovasc Drug Discov.* (2008) 3:156–64. doi: 10.2174/157489008786263989
62. Vaquero A, Scher M, Lee D, Erdjument-Bromage H, Tempst P, Reinberg D. Human SirT1 interacts with histone H1 and promotes formation of facultative heterochromatin. *Mol Cell.* (2004) 16:93–105. doi: 10.1016/j.molcel.2004.08.031
63. Alcendor RR, Kirshenbaum LA, Imai S, Vatner SF, Sadoshima J. Silent information regulator 2alpha, a longevity factor and class III histone deacetylase, is an essential endogenous apoptosis inhibitor in cardiac myocytes. *Circ Res.* (2004) 95:971–80. doi: 10.1161/01.RES.0000147557.75257.ff
64. Lee IH, Cao L, Mostoslavsky R, Lombard DB, Liu J, Bruns NE, et al. A role for the NAD-dependent deacetylase Sirt1 in the regulation of autophagy. *Proc Natl Acad Sci USA.* (2008) 105:3374–9. doi: 10.1073/pnas.0712145105
65. Wilkinson FH, Park K, Atchison ML. Polycomb recruitment to DNA *in vivo* by the YY1 REPO domain. *Proc Natl Acad Sci USA.* (2006) 103:19296–301. doi: 10.1073/pnas.0603564103
66. Wang Z, Zhang XJ, Ji YX, Zhang P, Deng KQ, Gong J, et al. The long noncoding RNA Chaer defines an epigenetic checkpoint in cardiac hypertrophy. *Nat Med.* (2016) 22:1131–9. doi: 10.1038/nm.4179
67. Delgado-Olguin P, Huang Y, Li X, Christodoulou D, Seidman CE, Seidman JG, et al. Epigenetic repression of cardiac progenitor gene expression by Ezh2 is required for postnatal cardiac homeostasis. *Nat Genet.* (2012) 44:343–7. doi: 10.1038/ng.1068
68. Mathiyalagan P, Keating ST, Du XJ, El-Osta A. Interplay of chromatin modifications and non-coding RNAs in the heart. *Epigenetics.* (2014) 9:101–12. doi: 10.4161/epi.26405
69. Kook H, Seo SB, Jain R. EZ Switch From EZH2 to EZH1: Histone methylation opens a window of cardiac regeneration. *Circ Res.* (2017) 121:91–4. doi: 10.1161/CIRCRESAHA.117.311351
70. Liu CF, Tang WHW. Epigenetics in cardiac hypertrophy and heart failure. *JACC Basic Transl Sci.* (2019) 4:976–93. doi: 10.1016/j.jacbts.2019.05.011
71. Yang T, Gu H, Chen X, Fu S, Wang C, Xu H, et al. Cardiac hypertrophy and dysfunction induced by overexpression of miR-214 *in vivo*. *J Surg Res.* (2014) 192:317–25. doi: 10.1016/j.jss.2014.06.044
72. Qi L, Chi X, Zhang X, Feng X, Chu W, Zhang S, et al. Kindlin-2 suppresses transcription factor GATA4 through interaction with SUV39H1 to attenuate hypertrophy. *Cell Death Dis.* (2019) 10:890. doi: 10.1038/s41419-019-2121-0

Conflict of Interest: The authors declare that the research was conducted in the absence of any commercial or financial relationships that could be construed as a potential conflict of interest.

frontiers in Cell and Developmental Biology

REVIEW
published: 28 June 2021
doi: 10.3389/fcell.2021.699374

Roles and Mechanisms of DNA Methylation in Vascular Aging and Related Diseases

Hui Xu[1,2], *Shuang Li*[1,2] *and You-Shuo Liu*[1,2]*

[1] *Department of Geriatrics, The Second Xiangya Hospital, Central South University, Changsha, China,* [2] *Institute of Aging and Age-Related Disease Research, Central South University, Changsha, China*

Vascular aging is a pivotal risk factor promoting vascular dysfunction, the development and progression of vascular aging-related diseases. The structure and function of endothelial cells (ECs), vascular smooth muscle cells (VSMCs), fibroblasts, and macrophages are disrupted during the aging process, causing vascular cell senescence as well as vascular dysfunction. DNA methylation, an epigenetic mechanism, involves the alteration of gene transcription without changing the DNA sequence. It is a dynamically reversible process modulated by methyltransferases and demethyltransferases. Emerging evidence reveals that DNA methylation is implicated in the vascular aging process and plays a central role in regulating vascular aging-related diseases. In this review, we seek to clarify the mechanisms of DNA methylation in modulating ECs, VSMCs, fibroblasts, and macrophages functions and primarily focus on the connection between DNA methylation and vascular aging-related diseases. Therefore, we represent many vascular aging-related genes which are modulated by DNA methylation. Besides, we concentrate on the potential clinical application of DNA methylation to serve as a reliable diagnostic tool and DNA methylation-based therapeutic drugs for vascular aging-related diseases.

Keywords: DNA methylation, aging, vascular diseases, endothelial cells, vascular smooth muscle cells

OPEN ACCESS

Edited by:
Suowen Xu,
University of Science and Technology of China, China

Reviewed by:
Anna Lewinska,
University of Rzeszów, Poland
Goro Katsuumi,
Niigata University, Japan

***Correspondence:**
You-Shuo Liu
liuyoushuo@csu.edu.cn

Specialty section:
This article was submitted to Epigenomics and Epigenetics, a section of the journal Frontiers in Cell and Developmental Biology

Received: *23 April 2021*
Accepted: *07 June 2021*
Published: *28 June 2021*

Citation:
Xu H, Li S and Liu Y-S (2021) Roles and Mechanisms of DNA Methylation in Vascular Aging and Related Diseases. Front. Cell Dev. Biol. 9:699374. doi: 10.3389/fcell.2021.699374

INTRODUCTION

Vascular aging is characterized by gradual changes in the vasculature structure and function (Laina et al., 2018; Ding et al., 2020). With aging, the structure and mechanical properties of vascular wall alter, i.e., lumen dilation, wall thickening, decreased arterial compliance, and increased arterial stiffness (North and Sinclair, 2012). The anatomical structure of vascular includes intima, media, and adventitia. Significant changes occur in the intima and media in the vascular aging progression (Lakatta and Levy, 2003a). Vascular intima primarily comprises endothelial cells (ECs), media is composed of vascular smooth muscle cells (VSMCs), and vascular adventitia is primarily

Abbreviations: ECs, endothelial cells; VSMCs, vascular smooth muscle cells; CVD, cardiovascular disease; AD, Alzheimer's disease; 4mC, N^4-methylcytosine; 5mC, N^5-methylcytosine; 6mA, N^6-methyladenine; DNMTs, DNA methyltransferases; TETs, 10–11 translocations; 5hmC, 5-hydroxymethylcytosine; 5fC, 5-formylcytosine; 5caC, 5-carboxylcytosine; TDG, thymine DNA glycosylase; BER, base excision repair; ox-LDL, oxidized low-density lipoprotein; ROS, reactive oxygen species; LDL, low-density lipoprotein; eNOS, endothelial nitric oxide synthase; IL-1α, interleukin-1α; 5Aza, 5-aza-2′-deoxycytidine; RAAS, rennin–angiotensin–aldosterone system; HF, heart failure; AMI, acute myocardial infarction; CHD, coronary heart disease; CKD, chronic kidney disease; EGCG, epigallocatechin-3-*O*-gallate.

composed of fibroblasts. Vascular cell senescence triggers cell morphological and functional changes, hence, ECs dysfunction, phenotypic transition of VSMCs, macrophage polarization, and fibroblast differentiation to myofibroblast (Chi et al., 2019). Age is an independent risk factor for vascular disorders (Morgan et al., 2018). To date, the aging population is significantly increasing, and research estimated that by 2040, 22% of people will be over the age of 65 (Heidenreich et al., 2011). Several lines of studies indicated that vascular aging enhanced the incidence and mortality of atherosclerosis (Mahmood et al., 2014), Alzheimer's disease (AD) (Lakatta and Levy, 2003b), stroke (Lakatta and Levy, 2003a), etc. Vascular aging-related diseases are the leading causes of death among the elderly. Thus, there is an urgent need to identify reliable and efficient diagnosis and treatment for vascular aging-related diseases.

DNA methylation is an epigenetic mechanism involving multiple biological processes such as aging, metabolism, and autoimmune (Jones, 2012). Scholars believe that epigenetics is based on alterations in gene expression levels and does not involve DNA sequence changes (Brunet and Berger, 2014). DNA methylation is a dynamically reversible process regulated by methyltransferases and demethyltransferases and it regulates gene expression by recruiting proteins implicated in gene repression or inhibiting the binding of transcription factors to DNA (Moore et al., 2013). DNA methylation is tightly associated with vascular aging and related disorders. Although studies on the link between DNA methylation and vascular disease have got much attention, the underlying mechanisms and roles of DNA methylation in vascular aging are still not well elucidated.

Since the prevalence and mortality of vascular disorders are closely related to vascular aging, the diagnosis and treatment of vascular aging and related diseases have received significant research attention. Therefore, this review summarizes the current research and recent advances on DNA methylation in vascular aging, revealing the involvement of DNA methylation in ECs, VSMCs, fibroblasts, and macrophages functions. We review the physiological and pathological processes involving DNA methylation in vascular aging-related diseases and represent many vascular disease-related genes that are regulated by DNA methylation. Additionally, we concentrate primarily on the clinical prospect of DNA methylation as an early diagnostic tool and potential DNA methylation-based therapies for vascular aging-related diseases.

DNA METHYLATION

DNA methylation is a modification of DNA. In 1942, Waddington first proposed the concept of "epigenotype," which was used to explain the complex progression process between genotype and phenotype (Waddington, 2012). To date, it is generally accepted that epigenetics primarily focuses on regulating gene expression, including DNA methylation, histone modification, non-coding RNA modification, chromatin remodeling, gene imprinting, etc. Here, we majorly focus on DNA methylation and its vital role in vascular aging-related diseases, including cardiovascular disease (CVD), cerebrovascular disease, and kidney diseases. DNA methylation regulates gene expression by recruiting proteins involved in gene repression or inhibiting the binding of transcription factors to DNA (Moore et al., 2013). DNA methylation is a dynamically reversible process modulated by methyltransferases and demethyltransferases (Chen and Riggs, 2011). There exist three forms of DNA methylation, including N^4-methylcytosine (4mC), N^5-methylcytosine (5mC), and N^6-methyladenine (6mA) (Ratel et al., 2006) (**Figure 1**).

N^5-Methylcytosine (5mC)

N^4-methylcytosine (4mC) modification principally exists in the DNA of bacteria, hence, a subject ignored by this review (Ehrlich et al., 1985, 1987). DNA methylation mainly occurs on the CpG dinucleotide in vertebrates. In mammals, global DNA methylation is a dynamic process, thus there exist DNA methylation and demethylation. 5mC is generated by DNA methyltransferases (DNMTs) through transfer a methyl group from *S*-adenyl methionine to the fifth carbon atom of the cytosine (Moore et al., 2013; Lyko, 2018). The DNMTs family includes DNMT1, DNMT2, DNMT3a, DNMT3b, and DNMT3L (Lyko, 2018). The patterns of 5mC are categorized into two major groups, including maintenance methylation and *de novo* methylation. DNMT1 is implicated in the DNA methylation through copy 5mC from parental DNA strand onto the newly synthesized daughter strand during DNA replication, thus, DNMT1 is known as maintenance DNMT (Mortusewicz et al., 2005; Nelissen et al., 2011). The *de novo* DNMTs included DNMT3a and DNMT3b can generate methylation in unmethylated DNA (Law and Jacobsen, 2010; Moore et al., 2013). Generally, DNA methylation inhibits gene expression through two different mechanisms. One is on the basis of intervene the binding of transcription factors included E2F or CREB by DNA methylation to represses gene transcription. On the other hand, DNMTs interact with methyl-CpG binding domain proteins to suppress transcription through establish a repressive chromatin environment (Bogdanović and Veenstra, 2009). DNA hypermethylation is strongly associated with the development of vascular aging-related disorders. Besides, DNA demethylation refers to two different pathways, including active demethylation and passive demethylation. Active DNA demethylation involves the ten-eleven translocations (TETs) induced methylated base oxidation and the activation induced deaminase induced methylated or a nearby base deamination, respectively (Bochtler et al., 2017). Activation induced deaminase deaminates cytosine to uracil. Additionally, several sources of evidence confirmed that 5mC can be converted into 5-hydroxymethylcytosine (5hmC), 5-formylcytosine (5fC), and 5-carboxylcytosine (5caC) under the activation of TETs (Rasmussen and Helin, 2016; Wu and Zhang, 2017). The level of TETs is tightly associated with DNA methylation. A high generation of TETs significantly alleviated the level of 5mC while a lack of TETs induced DNA hypermethylation. TET-thymine DNA glycosylase (TDG)-base excision repair (BER) mechanism is involved in regulating active DNA demethylation (Weber et al., 2016). Additionally, passive DNA demethylation occurs in DNA replication via the dilution

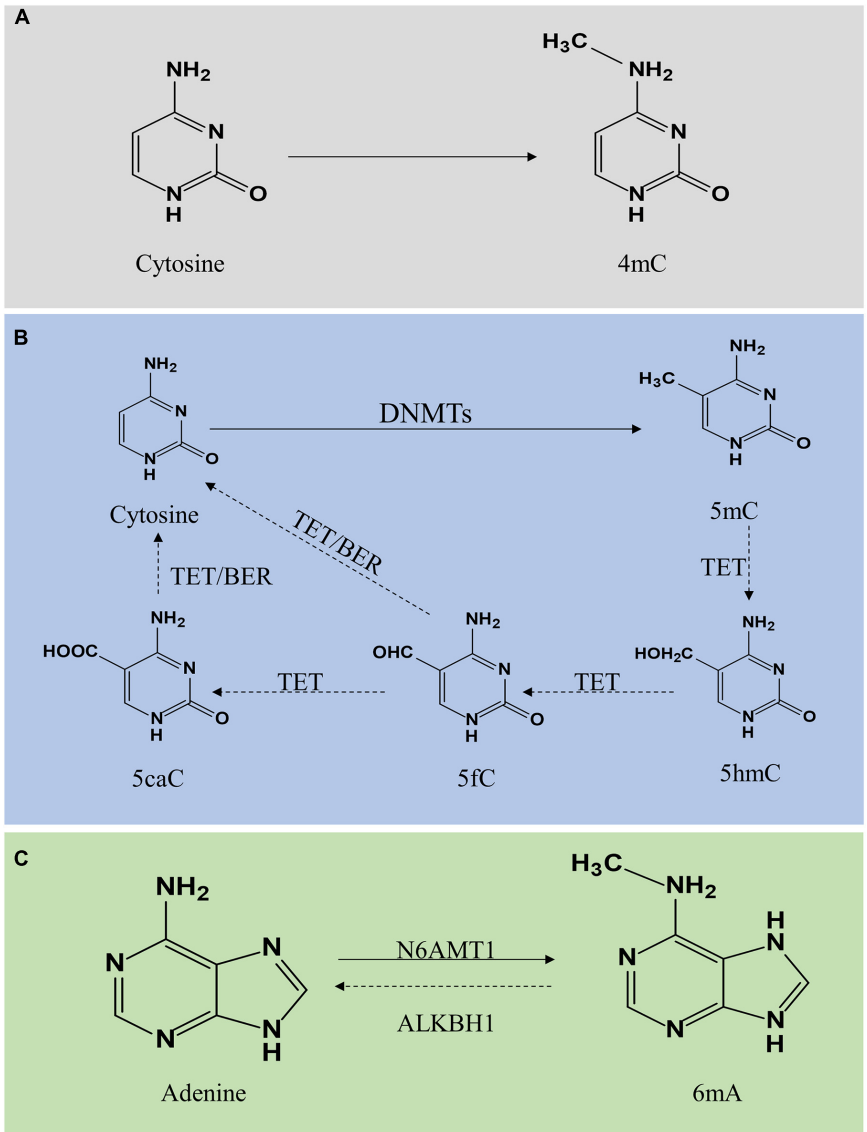

FIGURE 1 | Molecular mechanism of DNA methylation and demethylation. DNA methylation is divided into 4mC, 5mC, and 6mA. Panel **(A)** shows 4mC, a type of DNA methylation in prokaryotes. Panel **(B)** shows 5mC. A cytosine base can be methylated by DNMT1, DNMT3a, and DNMT3b to form 5mC, while TETs catalyze the oxidation of 5mC to 5hmC, 5fC, and 5caC. 5fC and 5caC are modulated by TDG/BER pathway. Panel **(C)** shows 6mA. Adenine is catalyzed by N6AMT1 to form 6 mA. In contrast, ALKBH1 mediates N^6-demethyladenine. 4mC, N^4-methylcytosine; 5mC, N^5-methylcytosine; 6mA, N^6-methyladenine; DNMTs, DNA methyltransferases; TETs, 10–11 translocations; 5hmC, 5-hydroxymethylcytosine; 5fC, 5-formylcytosine; 5caC, 5-carboxylcytosine; BER, base excision repair.

of methylation marks (Ooi and Bestor, 2008). DNMT1 is implicated in the process of maintenance methylation, inhibiting the expression or activation of DNMT1 reduces the level of DNA methylation.

N^6-Methyladenine (6mA)

DNA N^6-methyladenine (6mA) was previously considered the most prevalent form of DNA methylation in prokaryotes (Xiao et al., 2018). Surprisingly, recent reports suggested that 6mA also exists in eukaryotes, including *Caenorhabditis elegans* (Greer et al., 2015), *Drosophila* (Zhang G. et al., 2015), and *Chlamydomonas* (Fu et al., 2015). In *C. elegans*, 6mA is mediated by DAMT-1 and NMAD-1 (Greer et al., 2015). In *Drosophila*, DMAD is implicated in the regulation of 6mA demethylation (Zhang G. et al., 2015). In addition, a study revealed that 6mA was extensively present in the human genome and enriched in the coding region, modulating gene transcription activation (Xiao et al., 2018). Furthermore, human genome 6mA modification is modulated by the methyltransferase N6AMT1 while N^6-demethyladenine is mediated by ALKBH1. Several studies indicated that 6mA was involved in human diseases with controversy, thus, further exploration and in-depth studies on the roles of 6mA in the field of mammalian biomedicine are necessary to address the controversy.

THE ROLE AND MECHANISM OF DNA METHYLATION IN VASCULAR AGING

Aging is a decline of the biological system, accompanied by a decrease in function. Cell senescence is a permanent state of cell cycle arrest (Khor and Wong, 2020), causing tissue dysfunction and closely associated with aging-related diseases (Bitar, 2019). Accumulating evidence suggested that DNA methylation plays a significant role in regulating ECs, VSMCs, fibroblasts, and macrophages functions, and is implicated in the process of vascular aging and related disorders. Recent studies have identified a series of genes regulated through DNA methylation in the initiation and development of vascular aging (**Table 1**). This section primarily focuses on the mechanisms and roles of DNA methylation in the functions of ECs and VSMCs (**Figure 2**).

DNA Methylation and ECs Functions

Vascular endothelium is mainly composed of ECs, a barrier between blood and tissues. Endothelial dysfunction is caused by a variety of stimuli such as oxidized low-density lipoprotein (ox-LDL), hypoxia, shear stress, or inflammatory factors (Ni et al., 2020). DNA methylation modulates gene expression and mediates ECs biology in the development of its aging.

TABLE 1 | DNA methylation in vascular aging.

Vascular cells	Genes	Methylation status	Functions	References
ECs	*KLF2*	Hyper	Pro-inflammation	Kumar et al., 2013
	KLF4	Hyper	Pro-inflammation	Jiang et al., 2014
	SMAD7	Hyper	Pro-inflammation	Wei et al., 2018
	HoxA5	Hyper	Pro-inflammation	Dunn et al., 2014
	p66shc	Hypo	Pro-coagulant	Kim et al., 2012
	CTGF	Hypo	Pro-inflammation	Zhang et al., 2017
	ANXA5, BAX, CASP3, LOX-1	Hypo	Pro-apoptosis	Mitra et al., 2011
	BCL2, cIAP-1	Hyper	Anti- apoptosis	Mitra et al., 2011
	cyclin A	Hyper	Pro-proliferation	Zhang et al., 2017
	hTERT	Hypo	Pro-senescence	Zhang D. et al., 2015
VSMCs	*MFN2*	Hyper	Pro-proliferation	Xu L. et al., 2019
	PTEN	Hyper	Pro-proliferation	Ma et al., 2018
	ER-α	Hyper	Pro-proliferation	Min et al., 2016
	PDGF	Hypo	Pro-proliferation	Zhang et al., 2012
	HIF-1α	Hypo	Pro-migration	Wu et al., 2019
	MYOCD, SRF, MYH11	Hyper	Pro-differentiation	Liu et al., 2013
Fibroblasts	*RASSF1A*	Hyper	Fibrosis	Tao et al., 2014a
	RASAL1	Hyper	Fibrosis	Bechtel et al., 2010
	BMP-7	Hyper	Fibrosis	Xu et al., 2015a
	COL1A1	Hypo	Fibrosis	Pan et al., 2013
Macrophages	*PPARγ1*	Hyper	Pro-inflammation	Yang et al., 2014
	PSTPIP2	Hyper	Pro-inflammation	Luz et al., 2018
	LXRα	Hyper	Pro-inflammation	Cao et al., 2014

EC, endothelial cells; VSMC, vascular smooth muscle cells.

ECs Functions

Endothelial cells play a crucial role in maintaining vascular homeostasis (Gori, 2018). ECs regulate vasoconstriction and relaxation (Krüger-Genge et al., 2019), involved in physiological processes, including blood coagulation, angiogenesis, and metabolism. Besides, ECs cooperate with VSMCs in modulating blood flow to tissues (Michiels, 2003). ECs aging are characterized by endothelial dysfunction (Jia et al., 2019). Aging causes changes in vascular EC-mediated vasoconstriction and dilation, integrity destruction, increased permeability, destroying the blood–brain barrier, and impaired angiogenesis (Papapetropoulos et al., 1997). Furthermore, ECs senescence stimulates mitochondrial dysfunction and reactive oxygen species (ROS) accumulation, which further aggravates vascular senescence (Ungvari et al., 2008).

DNA Methylation and ECs

Generally, DNA methylation is altered in ECs during aging and upon exposure to stimuli such as shear stress, hypoxia, or ox-LDL. DNA hypermethylation and hypomethylation can result in inhibition and stimulation of gene transcription in ECs in response to injury (Levy et al., 2017). Quite a number of evidence highlighted that DNA methylation is involved in mediating the biological processes of ECs, including inflammation, proliferation, senescence, and apoptosis.

Endothelial cells inflammation is tightly linked with vascular disorders. DNMTs promote ECs inflammation by regulating the methylation level of pertinent gene promoter regions. Under the stimulation of low-density lipoprotein (LDL), *KLF2* promoter region was hypermethylated, arousing a down-expression of KLF2 in ECs and causing ECs inflammation and thrombogenesis (Kumar et al., 2013). In addition, the methylation level of relevant genes includes *KLF4* (Jiang et al., 2014), *SMAD7* (Wei et al., 2018), *HoxA5* (Dunn et al., 2014), and *CTGF* (Zhang et al., 2017) are participating in ECs inflammation and aging-related vascular diseases.

Endothelial cells proliferation and differentiation are modulated by DNA methylation. *In vivo*, DNMTs promote the hypermethylation of cell cycle regulator cyclin A, stimulating the proliferation and inflammation of ECs. Besides, endothelial nitric oxide synthase (eNOS) expression in ECs senescence declines, leading to a down-expression of NO and impairing vasodilation (Cau et al., 2012). The generation of eNOS can be regulated by DNA methylation (Chan et al., 2004). Moreover, inhibiting DNA methylation in the *eNOS* promoter region induces the differentiation of human embryonic liver cells into ECs (Lagarkova et al., 2008). In addition, ROS accumulated in aging ECs causes alternation in DNA methylation by changing DNMTs activity and DNA damage (O'Hagan et al., 2011; Tabaei and Tabaee, 2019).

Endothelial cells senescence and apoptosis arouse endothelial dysfunction. Under the condition of ox-LDL,

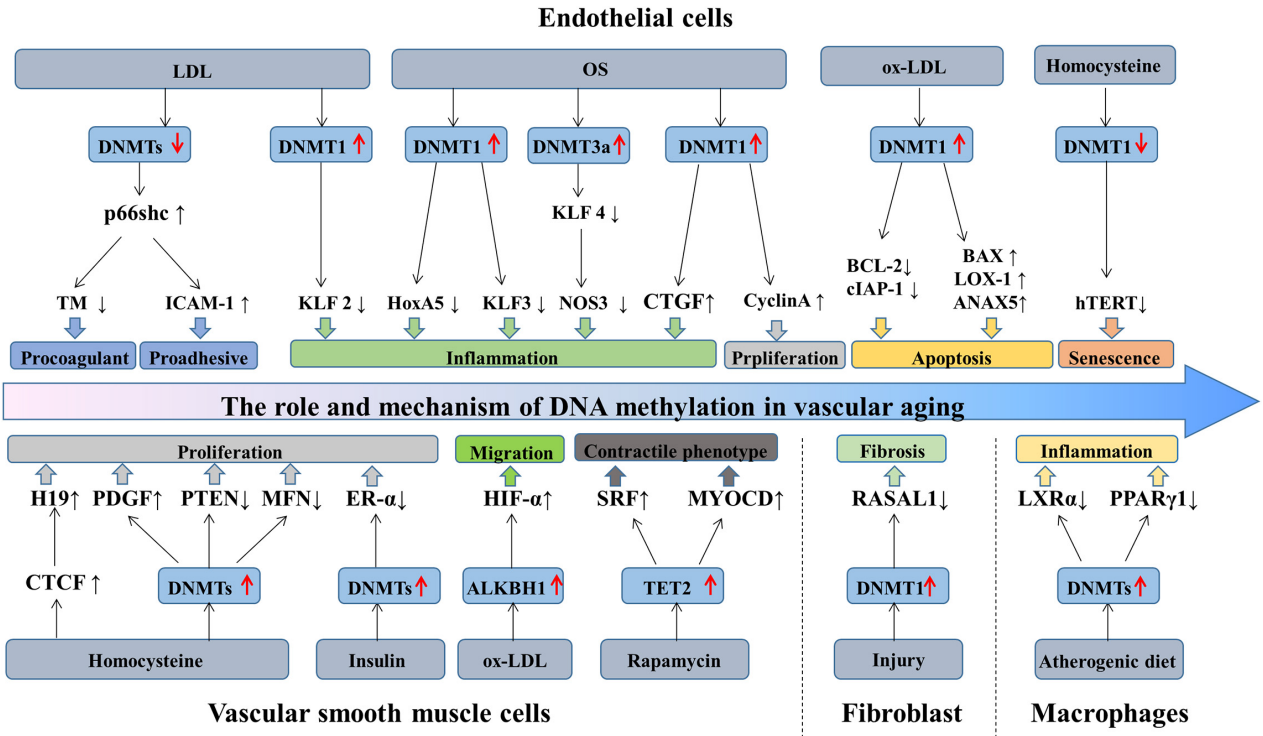

FIGURE 2 | The role and mechanism of DNA methylation in vascular aging. During aging, the structure and function of vascular cells change, causing ECs dysfunction, VSMCs proliferation and migration, fibroblasts differentiation, and macrophages inflammation. LDL stimulates p66shc expression by downregulating the activity of DNMTs and mediating the expression of ICAM-1 and TM, eventually exacerbating ECs dysfunction. Besides, LDL inhibits KLF2 expression via increasing DNMT1 activity, causing ECs inflammation. OS-treated ECs promotes DNMT1 activity and inhibits the generation of HoxA5 and KLF3. OS regulates KLF4, CTGF, and cyclinA methylation patterns by promoting DNMTs activity, causing ECs inflammation and proliferation. Ox-LDL triggers ECs apoptosis through the hypermethylation of cIAP-1 and BCL2 and the hypomethylation of BAX, LOX-1, and ANXA5. Homocysteine promotes ECs senescence by reducing hTERT expression via DNA methylation. Additionally, homocysteine increases CTGF and PDGF expression and decreases PTEN and MFN expression, mediating VSMCs proliferation. Insulin promotes VSMCs proliferation via ER-α hypermethylation. Ox-LDL promotes VSMCs migration by increasing HIF-1α generation through ALKBH1. TET2 overexpression promotes VSMCs differentiation by the upregulation of SRF and MYOCD expression. Besides, in response to injury, fibroblast activation through DNMT1 upregulation and *RASAL1* hypermethylation. Furthermore, the hypermethylation of *LXRα* and *PPARγ1* induces macrophages inflammation. DNMTs, DNA methyltransferases; TET, 10—11 translocations; LDL, low-density lipoprotein; OS, oscillatory shear stress; ECs, endothelial cells; VSMCs, vascular smooth muscle cells.

the proapoptosis-related genes such as *LOX-1*, *ANXA5*, *BAX*, and *CASP3* are activated due to the hypomethylation of its promoter region. In contrast, the anti-apoptotic *BCL2* and *cIAP-1* genes are down-regulated by the DNA hypermethylation, eventually resulting in ECs apoptosis (Mitra et al., 2011). Besides, homocysteine promotes ECs senescence through DNA hypomethylation of *hTERT* (Zhang D. et al., 2015).

DNA Methylation and VSMCs Functions

Vascular smooth muscle cells, the primary cells of vascular media, mediating blood flow and pressure via vascular contraction and relaxation. Environmental stresses such as oxidative stress, aging, or inflammation stimulate VSMCs contractile state switching into a proliferative and migratory synthetic phenotype, causing cell inflammation, proliferation, and migration. To date, multiple publications supported that DNA methylation plays a role in regulating VSMCs gene expression and VSMCs proliferation, migration, senescence, and apoptosis in response to vascular disorders.

VSMCs Functions

Vascular smooth muscle cells are implicated in maintaining the structural integrity and physiological function of blood vessels, regulating blood pressure and controlling vascular contraction and relaxation (Frismantiene et al., 2018; Chi et al., 2019). Besides, VSMCs and extracellular matrix are the primary regulators of arterial contraction tension and vascular tension (Wang G. et al., 2015; Chi et al., 2019). With aging, VSMCs suffer from mechanical stimulation, chronic inflammation, calcification, epigenetic events, etc. (Lacolley et al., 2018). VSMCs switch into synthetic phenotype, leading to hypertrophy of the vascular wall and collagen deposition, which is pertinent to vascular aging-related diseases.

DNA Methylation and VSMCs

DNA methylation is implicated in the modulation of VSMCs proliferation, migration, differentiation, and calcification. The proliferation of VSMCs is one of the primary features of vascular aging-related diseases, and DNA methylation is associated with

the regulation of gene transcription controlling cell proliferation. A large amount of evidence revealed that DNMTs inhibited gene expression by promoting DNA methylation and regulating the proliferation of VSMCs. DNA hypermethylation of *MFN2* (Xu L. et al., 2019), *PTEN* (Ma et al., 2018), and *ER*-α (Min et al., 2016) causes the corresponding low expression of MFN2, PTEN, and ER-α and promotes the proliferation of VSMCs. On the contrary, DNA demethylation of *PDGF* increases PDGF mRNA and protein expression and promotes the proliferation and migration of VSMCs (Zhang et al., 2012). Additionally, the hypomethylation of *HIF-1*α causes VSMCs proliferation and migration as well (Wu et al., 2019).

Vascular smooth muscle cells have apparent plasticity. TET2, a key enzyme in the DNA demethylation pathway, participates in regulating the differentiation of SMCs. A study demonstrated that in the case of vascular injury and vascular disorders, the expression of TET2 was downregulated, whereas the *MYOCD*, *SRF*, and *MYH11* were hypermethylated, resulting in SMCs differentiation (Liu et al., 2013).

The phenotypic modulation of SMCs triggers vascular disorders, including vascular calcification and atherosclerosis. Accumulating evidence reported that the contraction and synthetic phenotypes of VSMCs were mediated by DNA methylation. Furthermore, extracellular matrix mediates the phenotypic transition of SMCs via DNA methylation (Liu R. et al., 2015). Conversely, the DNMTs inhibitor 5-aza-2′-deoxycytidine (5Aza) reduces the DNA methylation level of the *ALP* in VSMCs and promotes the expression and activity of alkaline phosphatase, inducing vascular calcification (Azechi et al., 2014).

DNA Methylation and Vascular Fibroblasts Functions

The vascular adventitia is primarily composed of fibroblasts. Fibroblasts are thought to exhibit a broad range of physiological functions. Fibroblasts increase vasa vasorum-associated neointima formation and macrophage recruitment by enhancing the expression of vascular endothelial growth factors (Li X. D. et al., 2020). Besides, fibroblasts are involved in vascular remodeling, inflammation, and neointimal formation in vascular disorders (An et al., 2015). Moreover, fibroblasts play a role in providing a supporting framework of the vessel wall through generating and secreting fibrillar collagens, the main components of the adventitial extracellular matrix (Stenmark et al., 2013). Additionally, in response to injury, fibroblasts generate accumulative extracellular matrix, ultimately lead to organ dysfunction, such as liver cirrhosis and chronic renal failure (Thannickal et al., 2014).

It has been identified that aging is a risk factor for fibrosis. DNA methylation is involved in modulating fibroblasts activity. RASSF1A, a regulatory tumor inhibitor, is downregulated by DNMT3a in cardiac fibrosis and fibroblasts activation. Mechanistically, *RASSF1A* hypermethylation promoted cardiac fibrosis through the activation of the Ras/ERK signal pathway (Tao et al., 2014a). Besides, the hypermethylation of *RASAL1* induced by DNMT1 is consistently linked with fibroblast activation and kidney fibrosis (Bechtel et al., 2010). Aberrant hypermethylation of several genes includes *RASSF1A, RASAL1, BMP7,* and *COL1A1* are tightly correlated with fibroblast activation.

DNA Methylation and Vascular Macrophages Functions

Monocytes/macrophages, essential components of the immune system, are heterogeneous and exhibit a vital role in modulating inflammatory responses and vascular functions (Shapouri-Moghaddam et al., 2018). Accumulating studies revealed that monocytes and macrophages exert indispensable roles in the onset and development of chronic inflammatory disorders such as atherosclerosis, diabetes, and cancer. Commonly, macrophages exist in two distinct subpopulations includes classically activated or M1 macrophages and alternatively activated or M2 macrophages. M1 macrophages secrete numerous pro-inflammatory cytokines, such as interleukin-1α (IL-1α), IL-1β, IL-6, IL-12, and cyclooxygenase-2 whereas M2 macrophages generate anti-inflammatory cytokines such as IL-10 and transforming growth factor-β (Shapouri-Moghaddam et al., 2018). Macrophages interact with major histocompatibility complex molecules to present antigen. Moreover, macrophages are implicated in possessing the phagocytosis of pathogens, debris, and dead cells.

Increasing evidence indicated that DNA methylation functions as a significant regulator of monocyte-macrophage phenotypes and functions (Shapouri-Moghaddam et al., 2018). A study compared genome-wide DNA methylation among monocytes and macrophages and found that differential DNA methylation was presented in monocyte to macrophage differentiation, majorly restricted to very short regions (Dekkers et al., 2019). In addition, the loss of DNA methylation was pronounced during monocytes to dendritic cells differentiation and modulated by TET2 (Klug et al., 2013). Furthermore, macrophages polarization and inflammation are regulated by DNMT3b. The expression of DNMT3b was significantly lower in M2 macrophages compared with M1 macrophages. Notably, DNMT3b knockdown causes macrophage polarization to M2 phenotype and inhibits inflammation, whereas DNMT3b overexpression promotes to M1 phenotype and aggravates inflammation. Mechanistically, DNMT3b is implicated in silencing the promoter of *PPAR-γ1* (Yang et al., 2014). Besides, TET2 suppresses the expression of IL-6 in mouse macrophages (Hoeksema and de Winther, 2016).

DNA METHYLATION IN VASCULAR AGING-RELATED CVD

Cardiovascular disease is the leading cause of death among the elderly. By 2050, the global population aging above 60 years will approximate 2.1 billion (Wyss-Coray, 2016). Therefore, the incidence and mortality of CVD will have a gradual increase. Vascular aging is a major trigger of many vascular disorders, while vascular cell senescence shows significant effect on the progression of CVD. Increasing evidence revealed the role of epigenetic mechanisms in vascular aging-related

diseases. It's well-known that abnormal DNA methylation and DNMTs expression are tightly associated with vascular diseases (Hiltunen et al., 2002). In this part, we mainly focus on the roles and mechanisms of DNA methylation in aging-related atherosclerosis, hypertension, and other vascular disorders. Besides, we discuss the connection between clonal hematopoiesis and CVD.

Atherosclerosis

Atherosclerosis is a vascular disorder with complicated processes comprising ECs dysfunction, VSMCs proliferation and migration, macrophages inflammation, and collagen matrix accumulation. Age is a fundamental risk factor for atherosclerosis (Uryga and Bennett, 2016). DNA methylation plays a vital role in the initiation and progression of atherosclerosis. Besides, DNMTs act as regulators of vascular structure and functions (**Table 2**).

Endothelial cells senescence are accompanied by ECs dysfunction, decreased angiogenesis, and damaged eNOS activity, responsible for atherosclerosis progression (Colpani and Spinetti, 2019). Additionally, VSMCs are an important part of the fibrous cap and stromal cells of the artery (Chi et al., 2019). Accumulating evidence demonstrated that collagen secretion decreased in the aging of VSMCs, forming unstable fibrous caps (Gardner et al., 2015). VSMCs senescence enhances plaque vulnerability by secreting matrix metalloproteinases degrading the matrix and releases numerous pro-inflammatory cytokines promoting plaque inflammation and impairing the stability of plaques (Wang J. et al., 2015; Grootaert et al., 2018). Besides, Macrophages are defined as key modulators in atherosclerosis with aging and chronic inflammation (Moore and Tabas, 2011). Activated macrophages and foam cells trigger a cascade of inflammatory responses and induce atherosclerotic plaque formation. Notably, macrophages proliferation is the predominant mechanism in atherosclerotic plaques (Xu H. et al., 2019).

Numerous lines of evidence supported that atherosclerosis is manifested by global DNA hypomethylation and regional DNA hypermethylation. The level of DNA methylation in atherosclerotic arteries in rabbit models is lower compared to normal arteries (Laukkanen et al., 1999). Scholars confirmed that aberrant DNA methylation in atherosclerosis influence the transcription of key regulatory genes, inducing the pro-atherosclerotic cell phenotype (Castillo-Díaz et al., 2010). Gene hypermethylation including *ER*-α (Post et al., 1999; Huang et al., 2007), *DDAH2* (Niu et al., 2014), and *Foxp3* (Zhu et al., 2019) are tightly associated with the occurrence and development of atherosclerosis. Additionally, ROS accumulates in the aging of VSMCs and ECs (Chi et al., 2019; Tabaei and Tabaee, 2019), inducing DNA methylation changes via the altered activity of DNMTs and DNA damage, which modulates the formation and development of atherosclerotic plaques.

TABLE 2 | DNA methylation in vascular aging-related atherosclerosis.

Genes	Methylation Status	Sample source	References
KLF2	Hyper	ECs	Kumar et al., 2013
KLF4	Hyper	ECs	Jiang et al., 2014
HoxA5, KLF3	Hyper	ECs	Dunn et al., 2014, 2015
p66shc	Hypo	ECs	Kim et al., 2012
BAX, LOX-1, CASP3	Hypo	ECs	Mitra et al., 2011
cIAP-1, BCL2	Hyper	HUVEC	Mitra et al., 2011
HIF1α	Hypo	VSMCs	Wu et al., 2019
MYOCD, SRF, MYH11	Hyper	VSMCs	Liu et al., 2013
p53, PTEN, MFN2	Hyper	VSMCs	Ma et al., 2017
PDGF	Hypo	VSMCs	Ma et al., 2017
CTCF	Hypo	HUVSMCs	Li et al., 2009
PPARγ1	Hyper	Macrophages	Yang et al., 2014
PSTPIP2	Hyper	Macrophages	Luz et al., 2018
LXRα	Hyper	Macrophages	Cao et al., 2014
ABCA1, TIMP1, ACAT1	Hyper	Peripheral blood	Ma et al., 2016
SMAD7	Hyper	Peripheral blood	Wei et al., 2018
DDAH2	Hyper	Peripheral blood	Niu et al., 2014
IL-6	Hypo	Peripheral blood	Yang Q. et al., 2016
LDLR	Hypo	Peripheral blood	Guay et al., 2013
eNOS	Hyper	Artery	Chan et al., 2004
ERβ	Hyper	Artery	Kim et al., 2007
15-LO	Hypo	Artery	Liu et al., 2004
ERα	Hyper	Atherosclerotic plaque	Post et al., 1999
MAP4K4, ZEB1, FYN	Hyper	Atherosclerotic plaque	Yamada et al., 2014
Foxp3	Hyper	Atherosclerotic plaque	Zhu et al., 2019
HECA, EBF1, NOD2	Hypo	Atherosclerotic plaque	Yamada et al., 2014
MMP9	Hyper	Macrophages	Fisslthaler et al., 2019
APOE	Hyper	Human	Zhang et al., 2019

EC, endothelial cells; VSMC, vascular smooth muscle cells; HUVSMCs, human umbilical vein smooth muscle cells.

Hypertension

Hypertension, defined as average systolic blood pressure ≥140 mm Hg and/or average diastolic blood pressure ≥90 mm Hg, is the leading cause of CVD worldwide (Mills et al., 2020). Aging triggers a functional decline of various organ systems in the body. Vascular aging is significantly linked to hypertension prevalence and mortality among the elderly (Cheng et al., 2017; Donato et al., 2018). Besides, hypertension is an important risk factor for other vascular aging-related diseases, such as dementia, and cognitive decline (Cortes-Canteli and Iadecola, 2020; Fuchs and Whelton, 2020). Emerging documents demonstrated that DNA methylation exhibits a significant impact on hypertension development through modulating gene expression and vascular cell functions (**Table 3**).

It has been recognized that endothelial dysfunction contributed to the initiation and progression of hypertension.

TABLE 3 | DNA methylation in vascular aging-related hypertension.

Genes	Methylation Status	Functions	References
sACE, *ACE-1*	Hyper	RAAS	Rivière et al., 2011
ACE-2	Hyper	RAAS	Fan et al., 2017
Atgr1α	Hypo	RAAS	Pei et al., 2015
Atgr1β	Hypo	RAAS	Bogdarina et al., 2007
AGT	Hypo	RAAS	Wang et al., 2014
AGTR1	Hypo	RAAS	Fan et al., 2015
SULF1, *PRCP*	Hyper	Inflammation	Wang et al., 2013
IL-6	Hypo	Inflammation	Mao S. Q. et al., 2017
IFN-γ	Hypo	Inflammation	Bao et al., 2018
TLR2	Hypo	Chronic inflammation	Mao S. et al., 2017
EHMT2	Hypo	Chronic inflammation	Boström et al., 2016
ADD1	Hypo	Ionic balance	Zhang et al., 2013
NKCC1	Hypo	*Ionic balance*	Cho et al., 2011
SCNN1B	Hyper/hypo	Ionic balance	Zhong et al., 2016
MTHFD1	Hyper	Hyperhomocysteinemia	Xu M. et al., 2019
CBS	Hyper	Hyperhomocysteinemia	Wang et al., 2019
SHMT1	Hyper	Hyperhomocysteinemia	Xu G. et al., 2019
ERα	Hyper	Vasodilation	Dasgupta et al., 2012
11βHSD2(HSD11B2)	Hyper	Aldosterone	Alikhani-Koopaei et al., 2004

RAAS, renin–angiotensin–aldosterone system.

ECs release endothelin-1, prostacyclin, NO, and other vasoactive substances regulating vasoconstriction and relaxation (Sandoo et al., 2010). The dysfunction of aging ECs creates an imbalance between vasoconstriction and relaxation, leading to an increase in blood pressure (Jia et al., 2019). In addition, VSMCs mediate arterial compliance and total peripheral resistance (Chi et al., 2019). VSMCs senescence stimulates hypertension by the accumulation of oxidative stress and inflammation. Besides, vascular macrophages trigger endothelial dysfunction by increasing the expression of ROS and inflammatory cytokines, leading to vascular oxidative stress and blood pressure elevation (Justin Rucker and Crowley, 2017). The senescence of vascular cells promotes arterial stiffness, causing hypertension (Qiu et al., 2010; Chi et al., 2019).

DNA methylation is involved in hypertension (Gao et al., 2018; Guo et al., 2020; Amenyah et al., 2021). Kazmi et al. investigated the relationship between hypertension and DNA methylation in European men and discovered that 7 CpG sites were related to diastolic blood pressure (Kazmi et al., 2020). In addition, a study surveyed the association between blood pressure and DNA methylation among Europeans, Hispanics, and African Americans and identified 14 relevant CpG sites (Richard et al., 2017). Moreover, DNA methylation of the natriuretic peptide-A gene was decreased in patients diagnosed with hypertension among the Chinese community (Li J. et al., 2020). As we all know, the renin–angiotensin–aldosterone system (RAAS) is vital to the occurrence and progression of hypertension (Drummond et al., 2019). For instance, *AT1aR* promoter region hypomethylation in hypertensive rats upregulates the expression of AT1aR, critical to the development of hypertension (Pei et al., 2015). Administration of angiotensin receptor antagonists hinders the progression of hypertension in the early stages (Bogdarina et al., 2007). Besides, the level of 6mA is decreased in hypertensive mice and rat models, causing phenotypic transformation and migration of VSMCs (Guo et al., 2020).

DNA Methylation and Other Vascular Aging-Related CVD

Heart failure (HF) is a clinical syndrome caused by impairment of the systolic and diastolic functions. With the aging population, the incidence and mortality of HF are gradually increasing. In developed countries, the prevalence of HF among the elderly aged above 65 is approximately 11.8% (Groenewegen et al., 2020). Aging induces cardiovascular senescence and myocardial fibrosis (Horn and Trafford, 2016), leading to cardiac dysfunction and promoting HF progression (Triposkiadis et al., 2020). Notably, cardiovascular senescence, atherosclerosis (Triposkiadis et al., 2019), hypertension (Fuchs and Whelton, 2020), and ischemic cardiomyopathy (Napoli et al., 2020) are critical risk factors for HF (Li H. et al., 2020). DNA hypermethylation regulates cardiometabolism by destroying nuclear respiratory factor 1 dependent oxidative metabolism (Pepin et al., 2019). Additionally, in HF patients, the expression of DNMT3a and DNMT3b were upregulated, inhibiting the mRNA levels of several oxidative metabolism genes (Pepin et al., 2019). DNMT3b knockout can induce cardiac contractile insufficiency, ventricular wall thinning, and accelerating the deterioration of contractile function during HF (Vujic et al., 2015). Moreover, aberrant DNA methylation in dilated cardiomyopathies patients is associated with significant *ADORA2A* and *LY75* mRNA expression changes, but not in *HOXB13* and *ERBB3* (Haas et al., 2013).

Acute myocardial infarction (AMI) primarily occurs based on atherosclerotic stenosis of the coronary arteries. It is attributed to certain triggers of plaque rupture, including platelets gathering on the surface of the ruptured plaque, forming a thrombus that suddenly blocks the lumen of the coronary artery, leading to myocardial ischemic necrosis. The hypermethylation of the *ABO* gene is seemingly linked with an increased risk of AMI in Pakistani (Yousuf et al., 2020). Besides, the hypomethylation of *ZBTB12* gene and *LINE-1* gene are early biomarkers of MI in peripheral blood white cells (Guarrera et al., 2015). Besides, the methylation of *ZFHX3* and *SMARCA4* are independently and significantly related to MI (Nakatochi et al., 2017).

Coronary heart disease (CHD) is a heart condition caused by atherosclerotic lesions in the coronary arteries, causing ischemia, hypoxia or necrosis of the myocardium. DNA methylation is connected with the risk of future CHD. *ATP2B2, GUCA1B, CASR,* and *HPCAL1* are genes regulating calcium modulation (Agha et al., 2019). DNA methylation and hydroxymethylation among the elderly CHD patients were significantly upgraded. Report supported that a lower methylation level in the *SOAT1* gene might enhance the risk of CHD (Abuzhalihan et al., 2019).

Cardiac fibrosis is defined as the accumulation of extracellular matrix proteins in the cardiac interstitium (Tao et al., 2014b). Several studies indicated that DNA methylation is related to the onset and development of tissue fibrosis. Increased *RASAL1* and *RASSF1A* promoter methylation is involved in cardiac fibrosis (Tao et al., 2014a; Xu et al., 2015b). Besides, transforming growth factor-beta 1 can induce *COL1A1* demethylation and collagen type I expression by suppressing the generation and activity of DNMT1 and DNMT3a (Pan et al., 2013).

Clonal Hematopoiesis and CVD

Human aging is linked with an increased frequency of somatic mutations in hematopoietic system. This clonal hematopoiesis is associated with CVD (Evans et al., 2020). Age-related clonal hematopoiesis is major occurred in DNMT3a and TET2 and is associated with CVD (Jaiswal et al., 2014). TET2, highly expressed in murine macrophage differentiation, inhibits inflammatory gene expression in macrophages, reducing macrophages inflammation. In contrast, TET2-deficient macrophages affect phenotype of macrophages to promote chronic inflammation in vasculature, resulting in the progression of CVD (Cull et al., 2017). Studies in LDL receptor-deficient mice with TET2-deficient cells induce an increase in atherosclerotic plaque size. Besides, TET2-deficient macrophages enhance the secretion of interleukin-1β (IL-1β), regulated by inflammasome NLRP3 (Fuster et al., 2017). Additionally, DNMT3a is implicated in regulating inflammatory pathways and macrophage functions. Accumulating evidence revealed that hematopoietic DNMT3a mutation can promote HF through exacerbating inflammatory responses. HF Patients with monocytes carrying DNMT3a mutations show an increasing expression of inflammation genes, including IL-1B, IL-6, IL-8, NLRP3, CCL3, and CCL4, which may be contributing to exacerbating HF (Abplanalp et al., 2021). In addition, mice with mutations in TET2 or DNMT3a following an infusion of angiotensin II diminished cardiac function, increased fibrosis and inflammation (Sano et al., 2018). IL-1β was upregulated in TET2-deficient cells, while CXCL1 and CXCL2 were upregulated in DNMT3a-deficient cells. Research between clonal hematopoiesis and CVD is very much in its infancy. To date, only atherosclerosis and HF have been evaluated with clonal hematopoiesis in TET2 or DNMT3a mutation. Further studies should examine the role of clonal hematopoiesis in CVD beyond atherosclerosis and HF (Evans et al., 2020).

DNA METHYLATION AND VASCULAR AGING-RELATED CEREBROVASCULAR DISEASES

Cerebrovascular diseases are a group of diseases causing damage to brain tissue due to blood circulation disorder in the brain. Arterial stiffness and vascular aging trigger cerebrovascular dysfunction and blood–brain barrier contraction. Subsequently, a series of cerebrovascular diseases occur (Toth et al., 2017; Thorin-Trescases et al., 2018; Kalaria and Hase, 2019). Besides, small blood vessel diseases are common in the aging process, manifested as brain and parenchymal microcirculation changes (De Silva and Faraci, 2020), decreasing cerebral blood flow and damaging the blood–brain barrier, eventually lead to an aging-related functional decline of the brain (Iadecola et al., 2019). DNA methylation regulates various cerebrovascular diseases, such as stroke, dementia, and AD (**Table 4**).

Stroke

Stroke is a leading cause of death and disability globally. Endothelial dysfunction and macrophages polarization contribute to stroke (Blum et al., 2012). Besides, the vascular stiffness of the elderly population increases with aging. Studies indicated that carotid artery stiffness is a crucial factor in the onset and development of stroke (Mattace-Raso et al., 2006; van Sloten et al., 2015). Pulse wave velocity is used to analyze age-related changes in vascular structure and function as well as to evaluate the endothelial function and vascular stiffness (Stoner et al., 2012). In a cohort study based on a Chinese community population, assessing vascular aging might help stroke risk assessment (Yang et al., 2019). DNA methylation changes with age and is linked to stroke during aging (Soriano-Tárraga et al., 2014). In contrast with healthy subjects, the methylation level of the *TP53* promoter region increased among stroke patients (Wei et al., 2019). Besides, the methylation of *MTRNR2L8* is a potential therapeutic target for stroke (Shen et al., 2019).

Dementia and AD

Dementia is a decline in intelligence that severely disrupts daily life (Iadecola et al., 2019). The aging population is crucial to age-related cognitive abilities and important public health challenges (Deak et al., 2016). Research estimated that by 2050, 115 million people will be globally diagnosed with dementia (Prince et al., 2013). Endothelial dysfunction and damage might cause neurovascular dysfunction, resulting in microvascular thrombosis and destruction of the blood–brain

TABLE 4 | DNA methylation in vascular aging-related cerebrovascular diseases.

Diseases	Genes	Methylation status	References
Stroke	*CBS*	Hyper	Wang et al., 2019
	TM	Hyper	Yang Z. et al., 2016
	ApoE	Hyper	Zhang et al., 2019
	ABCG1	Hyper	Qin et al., 2019
	CDKN2B	Hyper	Zhou et al., 2017
	PPM1A	Aberrant	Gallego-Fabrega et al., 2016a
	TRAF3	Hypo	Gallego-Fabrega et al., 2016b
	LINE-1	Hypo	Baccarelli et al., 2010
	MTRNR2L8	Hypo	Shen et al., 2019
AD	*ApoE*	Hyper	Rajan et al., 2015
	ANK1	Hyper	Lunnon et al., 2014
	RHBDF2	Hyper	De Jager et al., 2014
	ABCA7	Hyper	Yamazaki et al., 2017
	RPL13,CDH23	Hyper	Prasad and Jho, 2019
	ANKRD30B	Hyper	Hua et al., 2019

AD, Alzheimer's disease.

barrier (Yamazaki et al., 2016). AD is the most prevalent cause of dementia, while age is an independent risk factor for AD (Delaye et al., 1975), and it has been proved that the progression of AD is tightly related to the alteration of DNA methylation (Qazi et al., 2018; Huo et al., 2019). Although AD is a neurodegenerative disease, it is also attributed to cerebrovascular aging (Iturria-Medina et al., 2016), and most AD patients suffer from Aβ amyloid angiopathy (Love and Miners, 2016). Studies suggest that genes including *ANK1* (Lunnon et al., 2014), *RHBDF2* (De Jager et al., 2014), *ABCA7* (Yamazaki et al., 2017), *RPL13*, and *CDH23* were hypermethylated in AD (Prasad and Jho, 2019). Among them, *ANK1*, *ABCA7*, and *RHBDF2* hypermethylation were associated with the formation of Aβ plaques. Higher DNA methylation levels in the promoter region of *APOE* promote the odds of dementia and AD (Karlsson et al., 2018). Besides, *ANKRD30B* is hypermethylated among AD patients, further implying that DNA methylation regulates the progression of AD (Semick et al., 2019).

DNA METHYLATION AND VASCULAR AGING-RELATED KIDNEY DISEASES

Chronic kidney disease (CKD) refers to abnormalities in chronic kidney structure or function caused by various reasons for more than 3 months (Ingrosso and Perna, 2020). CKD is characterized by the development of renal fibrosis subsequent renal failure. Macrophage polarization and fibroblasts differentiate into myofibroblasts are central processes of renal fibrosis (Tang et al., 2019). CKD and renal fibrosis affect approximately 10% of the world's population and half of the adults aged over 70 (Humphreys, 2018). DNA methylation changes in the renal cortex of patients with CKD (Chu et al., 2017). Besides, a study found that a low DNA methylation in patients with CKD (Zinellu et al., 2017). DNA methylation of genes is linked with CKD and renal fibrosis, including *PTPN6, CEBPB, EBF1, Klotho* (Chu et al., 2017; Yin et al., 2017), *SMAD7* (Yang et al., 2020), *sFRP5* (Yu et al., 2017), and *RASAL1*. Notably, DNA methylation inhibits erythropoietin expression, causing anemia, a prevalent complication of CKD (Yin and Blanchard, 2000).

DNA METHYLATION AS A DIAGNOSTIC TOOL AND THERAPEUTIC TARGET IN VASCULAR AGING-RELATED DISEASES

Aging is an inevitable process and significantly associated with many vascular aging-related disorders. Vascular aging is the structural and functional changes of the vasculature, including vascular cells senescence, inflammation, oxidative stress, and calcification (Ding et al., 2020). With aging, there is a gradual increase in the prevalence and mortality of vascular aging-related diseases. A high percentage of vascular aging-related diseases progress to functional failure because no available drugs can reverse vascular aging progression. Therefore, there is an urgent need to discover tools and methods for the early diagnosis and treatment of vascular aging-related diseases. Improving vascular cell senescence might ameliorate vascular aging and related diseases, providing novel ideas for clinical research as well as new prevention and treatment for vascular aging-related diseases.

DNA Methylation as a Diagnostic Tool in Vascular Aging-Related Diseases

The evidence mentioned above reveals that aberrant DNA methylation modification exists in aging-related vascular diseases and might be a potential biomarker for the diagnosis and prognosis of vascular aging-related diseases (Liu and Tang, 2019). Gene at DNA methylation status based on monocyte/macrophage might work as a diagnostic biomarker for clinical application (Bakshi et al., 2019). Notably, hyperhomocysteine is associated with CVD, potentially influencing DNA methylation modification, suggesting that DNA methylation is a biomarker for the increased risk of CVD (Kim et al., 2010). For example, *BRCA1* and *CRISP2* specific site methylation changes are associated with atherosclerosis, indicating that differentially methylated regions of *BRCA1* and *CRISP2* emerge as biomarkers for CVD (Istas et al., 2017). Moreover, the DNA methylation levels of *LINE-1* in the blood of 742 elderly men and discovered that *LINE-1* hypomethylation is linked to elevated serum vascular cell adhesion molecule-1, related to atherosclerosis progression and high cardiovascular risk (Baccarelli et al., 2010). Additionally, Additionally, DNMT3a expression can be used as novel diagnostic biomarkers for cerebrovascular aging-related diseases (Martínez-Iglesias et al., 2020). Besides, the methylation status of *LINE-1* and *MTRNR2L8* act as epigenetic biomarkers in stroke patients (Baccarelli et al., 2010; Shen et al., 2019). Specific gene methylation of diseases, combined with changes in DNMTs and TETs levels, are diagnostic and prognostic biomarkers providing broad clinical prospects. Further studies should concentrate on the clinical application of DNA methylation as a potential biomarker of vascular aging-related diseases.

DNA Methylation-Based Therapies in Vascular Aging-Related Diseases

DNA methylation is a dynamically reversible process, providing potential therapeutic targets for delaying or enhancing vascular aging-related diseases. Several agents targeting epigenetic modulators are currently undergoing preclinical or clinical evaluation to treat cancers and might have potential applications in treating cardiovascular events (Gorabi et al., 2020). Drugs that inhibit DNMTs have identified to be promising treatment strategies for many vascular disorders. There are many natural and synthetic compounds able to suppress DNMT activity (**Table 5**).

Nutrition and dietary compounds are identified to regulate DNA methylation. Nutrients implicated in one-carbon metabolism, including folates (vitamin B9), vitamins B6 and B12, choline, and methionine, are involved in DNA methylation for their essential role in the generation of *S*-adenyl methionine, the methyl group donor for DNA methylation (Park et al., 2012). Folic acid and folate drugs are used as therapeutics. For instance, folic acid or vitamins B6 and B12

TABLE 5 | DNA methylation-based drugs for vascular aging-related diseases.

Compounds	Nutrients/ drugs	Functions	References
Natural	Folic acid	*S*-adenyl methionine generation	Park et al., 2012
	vitamins B6 and B12	*S*-adenyl methionine generation	Park et al., 2012
	Vitamin C	TET2 activator	DiTroia et al., 2019
	Methionine	Increase DNA methylation	Waterland, 2006
	Catechin, epicatechin	DNMTs inhibitor	Nagai et al., 2004
	EGCG	DNMTs inhibitor	Wong et al., 2011
	Resveratrol	DNMTs inhibitor	Aldawsari et al., 2016
	Quercetin	DNMTs inhibitor	Liu C. M. et al., 2015
Synthetic	Azacytidine	DNMTs inhibitor	Strand et al., 2020
	Decitabine	DNMTs inhibitor	Zhuang et al., 2017
	RG108	DNMTs inhibitor	Stenzig et al., 2018
	Hydralazine	DNMTs inhibitor	Kao et al., 2011
	GLP-1 agonists	DNMTs inhibitor and TET2 activator	Scisciola et al., 2020
	SGLT2 inhibitors	Not available	Marumo et al., 2015

EGCG, epigallocatechin-3-O-gallate; decitabine, 5-Aza-2′-deoxycytidine; TET, 10–11 translocations; DNMT, DNA methyltransferases.

deficiencies can increase homocysteine levels, induce endothelial dysfunction, and aggravate atherosclerosis. On the contrary, dietary supplementation with folic acid can improve DNA methylation status, decrease inflammatory molecule levels, benefit atherosclerosis and reduce the risk of stroke (Wang et al., 2007; Hou and Zhao, 2021). Additionally, diet nutrition with folate and vitamin B6 has been recognized to improve memory and daily activities in AD patients (Chan et al., 2008). In addition, supplement methionine can increase DNA methylation (Waterland, 2006). Furthermore, vitamin C, as an antioxidant, can regulate the activity of TET and is involved in TET-mediated DNA methylation (DiTroia et al., 2019). Previous studies demonstrated that polyphenols [catechin, epicatechin, epigallocatechin-3-*O*-gallate (EGCG), and resveratrol] and bioflavonoids (quercetin, fisetin, and myricetin) inhibit DNA methylation by repressing DNMTs (Chistiakov et al., 2017). Catechin and epicatechin serve as DNMTs inhibitors through inhibiting human liver catechol-*O*-methyltransferase-mediated *O*-methylation of catechol estrogens (Nagai et al., 2004). EGCG is a major green tea polyphenol and can inhibit the activity of DNMTs such as DNMT1, DNMT3a, and DNMT3b (Wong et al., 2011). Besides, resveratrol has been recognized as DNMTs inhibitors to inhibit DNMTs expression (Aldawsari et al., 2016). Quercetin can protect against nickel-induced liver injury by suppressing DNMTs activity and decreasing the DNA methylation level of the NF-E2 related factor 2 (Liu C. M. et al., 2015). The ability of dietary nutrition offers promising therapies for vascular aging-related diseases by modulating DNMTs activities and DNA methylation.

DNA methyltransferases inhibitors are divided into two classes included nucleoside analogs inhibitors and non-nucleoside analogs inhibitors (Nicorescu et al., 2019). Nucleoside analogs inhibitors can incorporate into DNA during cell cycle and sequester DNMTs by regulating their proteasomal degradation. 5-azacytosine (azacytidine) and 5-Aza-2′-deoxycytidine (5Aza, decitabine), DNA hypomethylation agents, may beneficial in CVD, cerebrovascular disease, and kidney diseases. Azacytidine serves as a DNMT1 inhibitor, upregulated the expression of PTEN, reduced inflammatory factors secretion, and inhibited platelet-derived growth factor stimulated SMCs de-differentiation (Strand et al., 2020). Besides, silencing DNMTs in ECs by 5Aza or *siRNA*, decreased the level of DNA methylation and attenuated ECs inflammation. Administration of 5Aza in mouse atherosclerosis models decreases the formation of atherosclerotic lesions and promotes the prognosis of atherosclerosis (Dunn et al., 2014). Administering 5Aza combined with specific task training helps recover chronic stroke [144]. Decitabine can ameliorate atherosclerotic lesion, inhibit DNMT1 activity, and downregulate global DNA methylation level (Zhuang et al., 2017). Non-nucleoside analogs such as RG108 and hydralazine are developed to overcome the non-specificity and cytotoxicity of the nucleoside inhibitors (Nicorescu et al., 2019). RG108 can inhibit DNMT1 activity by binding to its active site. Stenzig et al. (2018) indicated that RG108 significantly attenuated global DNA methylation in cardiomyocytes and is associated with decreased cardiac hypertrophy. Hydralazine, an anti-hypertensive drug, can repress DNMT1 and DNMT3a mRNA expression and activity by suppressing Erk signaling pathway (Deng et al., 2003). Hydralazine-mediated the promoter region of *SERCA2a* demethylation can improve cardiac function (Kao et al., 2011).

Diabetes is characterized by hyperglycemia and act as a significantly risk factor of cardiovascular and kidney disorders. Numerous lines of evidence supported that diabetes is linked with DNA methylation (Salameh et al., 2020). Therefore, DNA methylation-based therapies can benefit diabetes and reduce diabetes-related vascular complications. Cells treated with high glucose exhibited lower DNA methylation levels of *NF-κB* and *SOD2*, while co-treatment with GLP-1 agonists reversed these effects by decreasing DNMT1 and DNMT3a mRNA and protein levels and increasing TET2 mRNA and protein levels (Scisciola et al., 2020). Additionally, it has been reported that *SGLT2* gene is hypomethylated in kidney proximal tubules, which suggest that SGLT2 inhibitors may be a DNA methylation modulators (Marumo et al., 2015).

Therefore, a better understanding of the mechanisms and roles of DNA methylation in the physiological and pathological process of vascular aging-related diseases might lead to the identification of promising biomarkers and therapeutic drugs. Much work is needed to validate the potential application of DNA methylation in vascular disorders.

PERSPECTIVES AND CONCLUSION

With the increase in the aging population, there is an urgent need to identify reliable and effective diagnostic tools and

therapies for early diagnosis and treatment of vascular aging. Endothelial dysfunction, VSMCs proliferation and migration, macrophages polarization, and aberrant DNA methylation are implicated in the development and progression of vascular inflammation and vascular aging-related diseases. Notably, DNA methylation is involved in regulating the expression of genes in these mechanisms. In this review, we summarize the cellular and functional alterations in the vascular system during the aging process and concentrated on the roles and mechanisms of DNA methylation in vascular aging-related CVD, cerebrovascular diseases, and kidney diseases. DNA methylation plays a vital role in vascular aging progression and might be a potential biomarker for diagnosis and therapeutic target in treating vascular aging-related diseases. DNA methylation promotes a better understanding of the underlying mechanisms of vascular aging and related diseases and ultimately facilitates the development of effective interventions for vascular aging-related disorders. Regarding the future clinical prospect of DNA methylation, numerous biological explorations should be conducted to clarify the feasibility of DNA methylation in the diagnosis, treatment, and prognosis of vascular aging-related diseases.

AUTHOR CONTRIBUTIONS

HX collected the literature and wrote the manuscript. SL drew the figures and supervised the manuscript. Y-SL conceived the idea and had been involved in manuscript conception and drafting. All authors read and approved the final manuscript.

FUNDING

This work was supported by the National Natural Science Foundation of China (Nos. 82071593, 81770833, and 81974223) and National Key R&D (or Research and Development) Program of China (Grant 2020YFC 2009000).

REFERENCES

Abplanalp, W. T., Cremer, S., John, D., Hoffmann, J., Schuhmacher, B., Merten, M., et al. (2021). Clonal hematopoiesis-driver DNMT3A mutations alter immune cells in heart failure. *Circ. Res.* 128, 216–228. doi: 10.1161/circresaha.120.317104

Abuzhalihan, J., Wang, Y. T., Ma, Y. T., Fu, Z. Y., Yang, Y. N., Ma, X., et al. (2019). SOAT1 methylation is associated with coronary heart disease. *Lipids Health Dis.* 18:192.

Agha, G., Mendelson, M. M., Ward-Caviness, C. K., Joehanes, R., Huan, T., Gondalia, R., et al. (2019). Blood Leukocyte DNA methylation predicts risk of future myocardial infarction and coronary heart disease. *Circulation* 140, 645–657. doi: 10.1161/CIRCULATIONAHA.118.039357

Aldawsari, F. S., Aguayo-Ortiz, R., Kapilashrami, K., Yoo, J., Luo, M., Medina-Franco, J. L., et al. (2016). Resveratrol-salicylate derivatives as selective DNMT3 inhibitors and anticancer agents. *J. Enzyme Inhib. Med. Chem.* 31, 695–703. doi: 10.3109/14756366.2015.1058256

Alikhani-Koopaei, R., Fouladkou, F., Frey, F. J., and Frey, B. M. (2004). Epigenetic regulation of 11 beta-hydroxysteroid dehydrogenase type 2 expression. *J. Clin. Invest.* 114, 1146–1157. doi: 10.1172/jci21647

Amenyah, S. D., Ward, M., McMahon, A., Deane, J., McNulty, H., Hughes, C., et al. (2021). DNA methylation of hypertension-related genes and effect of riboflavin supplementation in adults stratified by genotype for the MTHFR C677T polymorphism. *Int. J. Cardiol.* 322, 233–239. doi: 10.1016/j.ijcard.2020.09.011

An, S. J., Liu, P., Shao, T. M., Wang, Z. J., Lu, H. G., Jiao, Z., et al. (2015). Characterization and functions of vascular adventitial fibroblast subpopulations. *Cell Physiol. Biochem.* 35, 1137–1150. doi: 10.1159/000373939

Azechi, T., Sato, F., Sudo, R., and Wachi, H. (2014). 5-aza-2'-Deoxycytidine, a DNA methyltransferase inhibitor, facilitates the inorganic phosphorus-induced mineralization of vascular smooth muscle cells. *J. Atheroscler. Thromb.* 21, 463–476. doi: 10.5551/jat.20818

Baccarelli, A., Tarantini, L., Wright, R. O., Bollati, V., Litonjua, A. A., Zanobetti, A., et al. (2010). Repetitive element DNA methylation and circulating endothelial and inflammation markers in the VA normative aging study. *Epigenetics* 5, 222–228. doi: 10.4161/epi.5.3.11377

Bakshi, C., Vijayvergiya, R., and Dhawan, V. (2019). Aberrant DNA methylation of M1-macrophage genes in coronary artery disease. *Sci. Rep.* 9:1429.

Bao, X. J., Mao, S. Q., Gu, T. L., Zheng, S. Y., Zhao, J. S., and Zhang, L. N. (2018). Hypomethylation of the interferon γ gene as a potential Risk factor for essential hypertension: a case-control study. *Tohoku J. Exp. Med.* 244, 283–290. doi: 10.1620/tjem.244.283

Bechtel, W., McGoohan, S., Zeisberg, E. M., Müller, G. A., Kalbacher, H., Salant, D. J., et al. (2010). Methylation determines fibroblast activation and fibrogenesis in the kidney. *Nat. Med.* 16, 544–550. doi: 10.1038/nm.2135

Bitar, M. S. (2019). Diabetes impairs angiogenesis and induces endothelial cell senescence by Up-regulating thrombospondin-CD47-dependent signaling. *Int. J. Mol. Sci.* 20:673. doi: 10.3390/ijms20030673

Blum, A., Vaispapir, V., Keinan-Boker, L., Soboh, S., Yehuda, H., and Tamir, S. (2012). Endothelial dysfunction and procoagulant activity in acute ischemic stroke. *J. Vasc. Interv. Neurol.* 5, 33–39.

Bochtler, M., Kolano, A., and Xu, G. L. (2017). DNA demethylation pathways: additional players and regulators. *Bioessays* 39, 1–13. doi: 10.1002/bies.201600178

Bogdanović, O., and Veenstra, G. J. (2009). DNA methylation and methyl-CpG binding proteins: developmental requirements and function. *Chromosoma* 118, 549–565. doi: 10.1007/s00412-009-0221-9

Bogdarina, I., Welham, S., King, P. J., Burns, S. P., and Clark, A. J. (2007). Epigenetic modification of the renin-angiotensin system in the fetal programming of hypertension. *Circ. Res.* 100, 520–526. doi: 10.1161/01.res.0000258855.60637.58

Boström, A. E., Mwinyi, J., Voisin, S., Wu, W., Schultes, B., Zhang, K., et al. (2016). Longitudinal genome-wide methylation study of Roux-en-Y gastric bypass patients reveals novel CpG sites associated with essential hypertension. *BMC Med. Genom.* 9:20. doi: 10.1186/s12920-016-0180-y

Brunet, A., and Berger, S. L. (2014). Epigenetics of aging and aging-related disease. *J. Gerontol. A Biol. Sci. Med. Sci.* 69, S17–S20. doi: 10.1093/gerona/glu042

Cao, Q., Wang, X., Jia, L., Mondal, A. K., Diallo, A., Hawkins, G. A., et al. (2014). Inhibiting DNA Methylation by 5-Aza-2'-deoxycytidine ameliorates atherosclerosis through suppressing macrophage inflammation. *Endocrinology* 155, 4925–4938. doi: 10.1210/en.2014-1595

Castillo-Díaz, S. A., Garay-Sevilla, M. E., Hernández-González, M. A., Solís-Martínez, M. O., and Zaina, S. (2010). Extensive demethylation of normally hypermethylated CpG islands occurs in human atherosclerotic arteries. *Int. J. Mol. Med.* 26, 691–700. doi: 10.3892/ijmm-00000515

Cau, S. B., Carneiro, F. S., and Tostes, R. C. (2012). Differential modulation of nitric oxide synthases in aging: therapeutic opportunities. *Front. Physiol.* 3:218. doi: 10.3389/fphys.2012.00218

Chan, A., Paskavitz, J., Remington, R., Rasmussen, S., and Shea, T. B. (2008). Efficacy of a vitamin/nutriceutical formulation for early-stage Alzheimer's disease: a 1-year, open-label pilot study with an 16-month caregiver extension. *Am. J. Alzheimers Dis.* 23, 571–585. doi: 10.1177/1533317508325093

Chan, Y., Fish, J. E., D'Abreo, C., Lin, S., Robb, G. B., Teichert, A. M., et al. (2004). The cell-specific expression of endothelial nitric-oxide synthase: a role

for DNA methylation. *J. Biol. Chem.* 279, 35087–35100. doi: 10.1074/jbc.M405063200

Chen, Z. X., and Riggs, A. D. (2011). DNA methylation and demethylation in mammals. *J. Biol. Chem.* 286, 18347–18353. doi: 10.1074/jbc.r110.205286

Cheng, H. M., Park, S., Huang, Q., Hoshide, S., Wang, J. G., Kario, K., et al. (2017). Vascular aging and hypertension: implications for the clinical application of central blood pressure. *Int. J. Cardiol.* 230, 209–213. doi: 10.1016/j.ijcard.2016.12.170

Chi, C., Li, D. J., Jiang, Y. J., Tong, J., Fu, H., Wu, Y. H., et al. (2019). Vascular smooth muscle cell senescence and age-related diseases: state of the art. *Biochim. Biophys. Acta Mol. Basis Dis.* 1865, 1810–1821. doi: 10.1016/j.bbadis.2018.08.015

Chistiakov, D. A., Orekhov, A. N., and Bobryshev, Y. V. (2017). Treatment of cardiovascular pathology with epigenetically active agents: focus on natural and synthetic inhibitors of DNA methylation and histone deacetylation. *Int. J. Cardiol.* 227, 66–82. doi: 10.1016/j.ijcard.2016.11.204

Cho, H. M., Lee, H. A., Kim, H. Y., Han, H. S., and Kim, I. K. (2011). Expression of Na+-K+ -2Cl- cotransporter 1 is epigenetically regulated during postnatal development of hypertension. *Am. J. Hypertens.* 24, 1286–1293. doi: 10.1038/ajh.2011.136

Chu, A. Y., Tin, A., Schlosser, P., Ko, Y. A., Qiu, C., Yao, C., et al. (2017). Epigenome-wide association studies identify DNA methylation associated with kidney function. *Nat. Commun.* 8:1286. doi: 10.1038/s41467-017-01297-7

Colpani, O., and Spinetti, G. (2019). MicroRNAs orchestrating senescence of endothelial and vascular smooth muscle cells. *Vasc. Biol.* 1, H75–H81. doi: 10.1530/VB-19-0017

Cortes-Canteli, M., and Iadecola, C. (2020). Alzheimer's disease and vascular aging: JACC focus seminar. *J. Am. Coll. Cardiol.* 75, 942–951. doi: 10.1016/j.jacc.2019.10.062

Cull, A. H., Snetsinger, B., Buckstein, R., Wells, R. A., and Rauh, M. J. (2017). Tet2 restrains inflammatory gene expression in macrophages. *Exp. Hematol.* 55, 56–70.e13. doi: 10.1016/j.exphem.2017.08.001

Dasgupta, C., Chen, M., Zhang, H., Yang, S., and Zhang, L. (2012). Chronic hypoxia during gestation causes epigenetic repression of the estrogen receptor-α gene in ovine uterine arteries via heightened promoter methylation. *Hypertension* 60, 697–704. doi: 10.1161/hypertensionaha.112.198242

De Jager, P. L., Srivastava, G., Lunnon, K., Burgess, J., Schalkwyk, L. C., Yu, L., et al. (2014). Alzheimer's disease: early alterations in brain DNA methylation at ANK1, BIN1, RHBDF2 and other loci. *Nat. Neurosci.* 17, 1156–1163. doi: 10.1038/nn.3786

De Silva, T. M., and Faraci, F. M. (2020). Contributions of aging to cerebral small vessel disease. *Annu. Rev. Physiol.* 82, 275–295. doi: 10.1146/annurev-physiol-021119-034338

Deak, F., Freeman, W. M., Ungvari, Z., Csiszar, A., and Sonntag, W. E. (2016). Recent developments in understanding brain aging: implications for Alzheimer's disease and vascular cognitive impairment. *J. Gerontol. A Biol. Sci. Med. Sci.* 71, 13–20. doi: 10.1093/gerona/glv206

Dekkers, K. F., Neele, A. E., Jukema, J. W., Heijmans, B. T., and de Winther, M. P. J. (2019). Human monocyte-to-macrophage differentiation involves highly localized gain and loss of DNA methylation at transcription factor binding sites. *Epigenetics Chromatin* 12:34.

Delaye, J., Pourchaire, J., and Gonin, A. (1975). [Hemodynamic effects of the intravenous form of acebutolol]. *Nouv. Presse Med.* 46(Suppl.), 3239–3243.

Deng, C., Lu, Q., Zhang, Z., Rao, T., Attwood, J., Yung, R., et al. (2003). Hydralazine may induce autoimmunity by inhibiting extracellular signal-regulated kinase pathway signaling. *Arthritis Rheum.* 48, 746–756. doi: 10.1002/art.10833

Ding, Q., Shao, C., Rose, P., and Zhu, Y. Z. (2020). Epigenetics and vascular senescence-potential new therapeutic targets? *Front. Pharmacol.* 11:535395. doi: 10.3389/fphar.2020.535395

DiTroia, S. P., Percharde, M., Guerquin, M. J., Wall, E., Collignon, E., Ebata, K. T., et al. (2019). Maternal vitamin C regulates reprogramming of DNA methylation and germline development. *Nature* 573, 271–275. doi: 10.1038/s41586-019-1536-1

Donato, A. J., Machin, D. R., and Lesniewski, L. A. (2018). Mechanisms of dysfunction in the aging vasculature and role in age-related disease. *Circ. Res.* 123, 825–848 doi: 10.1161/circresaha.118.312563

Drummond, G. R., Vinh, A., Guzik, T. J., and Sobey, C. G. (2019). Immune mechanisms of hypertension. *Nat. Rev. Immunol.* 19, 517–532. doi: 10.1038/s41577-019-0160-5

Dunn, J., Qiu, H., Kim, S., Jjingo, D., Hoffman, R., Kim, C. W., et al. (2014). Flow-dependent epigenetic DNA methylation regulates endothelial gene expression and atherosclerosis. *J. Clin. Invest.* 124, 3187–3199. doi: 10.1172/jci74792

Dunn, J., Thabet, S., and Jo, H. (2015). Flow-dependent epigenetic DNA methylation in endothelial gene expression and atherosclerosis. *Arterioscler. Thromb. Vasc. Biol.* 35, 1562–1569. doi: 10.1161/atvbaha.115.305042

Ehrlich, M., Gama-Sosa, M. A., Carreira, L. H., Ljungdahl, L. G., Kuo, K. C., and Gehrke, C. W. (1985). DNA methylation in thermophilic bacteria: N4-methylcytosine, 5-methylcytosine, and N6-methyladenine. *Nucleic Acids Res.* 13, 1399–1412. doi: 10.1093/nar/13.4.1399

Ehrlich, M., Wilson, G. G., Kuo, K. C., and Gehrke, C. W. (1987). N4-methylcytosine as a minor base in bacterial DNA. *J. Bacteriol.* 169, 939–943. doi: 10.1128/jb.169.3.939-943.1987

Evans, M. A., Sano, S., and Walsh, K. (2020). Cardiovascular disease, aging, and clonal hematopoiesis. *Annu. Rev. Pathol.* 15, 419–438. doi: 10.1146/annurev-pathmechdis-012419-032544

Fan, R., Mao, S. Q., Gu, T. L., Zhong, F. D., Gong, M. L., Hao, L. M., et al. (2017). Preliminary analysis of the association between methylation of the ACE2 promoter and essential hypertension. *Mol. Med. Rep.* 15, 3905–3911. doi: 10.3892/mmr.2017.6460

Fan, R., Mao, S., Zhong, F., Gong, M., Yin, F., Hao, L., et al. (2015). Association of AGTR1 promoter methylation levels with essential hypertension risk: a matched case-control study. *Cytogenet. Genome Res.* 147, 95–102. doi: 10.1159/000442366

Fisslthaler, B., Zippel, N., Abdel Malik, R., Delgado Lagos, F., Zukunft, S., Thoele, J., et al. (2019). Myeloid-specific deletion of the AMPKα2 subunit alters monocyte protein expression and atherogenesis. *Int. J. Mol. Sci.* 20:3005. doi: 10.3390/ijms20123005

Frismantiene, A., Philippova, M., Erne, P., and Resink, T. J. (2018). Smooth muscle cell-driven vascular diseases and molecular mechanisms of VSMC plasticity. *Cell. Signal.* 52, 48–64. doi: 10.1016/j.cellsig.2018.08.019

Fu, Y., Luo, G. Z., Chen, K., Deng, X., Yu, M., Han, D., et al. (2015). N6-methyldeoxyadenosine marks active transcription start sites in Chlamydomonas. *Cell* 161, 879–892. doi: 10.1016/j.cell.2015.04.010

Fuchs, F. D., and Whelton, P. K. (2020). High blood pressure and cardiovascular disease. *Hypertension* 75, 285–292.

Fuster, J. J., MacLauchlan, S., Zuriaga, M. A., Polackal, M. N., Ostriker, A. C., Chakraborty, R., et al. (2017). Clonal hematopoiesis associated with TET2 deficiency accelerates atherosclerosis development in mice. *Science* 355, 842–847. doi: 10.1126/science.aag1381

Gallego-Fabrega, C., Carrera, C., Reny, J. L., Fontana, P., Slowik, A., Pera, J., et al. (2016a). PPM1A methylation is associated with vascular recurrence in aspirin-treated patients. *Stroke* 47, 1926–1929. doi: 10.1161/strokeaha.116.013340

Gallego-Fabrega, C., Carrera, C., Reny, J. L., Fontana, P., Slowik, A., Pera, J., et al. (2016b). TRAF3 epigenetic regulation is associated with vascular recurrence in patients with ischemic stroke. *Stroke* 47, 1180–1186. doi: 10.1161/strokeaha.115.012237

Gao, X., Colicino, E., Shen, J., Just, A. C., Nwanaji-Enwerem, J. C., Wang, C., et al. (2018). Accelerated DNA methylation age and the use of antihypertensive medication among older adults. *Aging* 10, 3210–3228. doi: 10.18632/aging.101626

Gardner, S. E., Humphry, M., Bennett, M. R., and Clarke, M. C. (2015). Senescent vascular smooth muscle cells drive inflammation through an interleukin-1α-dependent senescence-associated secretory phenotype. *Arterioscler. Thromb. Vasc. Biol.* 35, 1963–1974. doi: 10.1161/atvbaha.115.305896

Gorabi, A. M., Penson, P. E., Banach, M., Motallebnezhad, M., Jamialahmadi, T., and Sahebkar, A. (2020). Epigenetic control of atherosclerosis via DNA methylation: a new therapeutic target? *Life Sci.* 253:117682. doi: 10.1016/j.lfs.2020.117682

Gori, T. (2018). Endothelial function: a short guide for the interventional cardiologist. *Int. J. Mol. Sci.* 19:3838. doi: 10.3390/ijms19123838

Greer, E. L., Blanco, M. A., Gu, L., Sendinc, E., Liu, J., Aristizábal-Corrales, D., et al. (2015). DNA methylation on N6-Adenine in C. elegans. *Cell* 161, 868–878. doi: 10.1016/j.cell.2015.04.005

Groenewegen, A., Rutten, F. H., Mosterd, A., and Hoes, A. W. (2020). Epidemiology of heart failure. *Eur. J. Heart Fail.* 22, 1342–1356.

Grootaert, M. O. J., Moulis, M., Roth, L., Martinet, W., Vindis, C., Bennett, M. R., et al. (2018). Vascular smooth muscle cell death, autophagy and senescence in atherosclerosis. *Cardiovasc. Res.* 114, 622–634. doi: 10.1093/cvr/cvy007

Guarrera, S., Fiorito, G., Onland-Moret, N. C., Russo, A., Agnoli, C., Allione, A., et al. (2015). Gene-specific DNA methylation profiles and LINE-1 hypomethylation are associated with myocardial infarction risk. *Clin. Epigenet.* 7:133.

Guay, S. P., Brisson, D., Lamarche, B., Marceau, P., Vohl, M. C., Gaudet, D., et al. (2013). DNA methylation variations at CETP and LPL gene promoter loci: new molecular biomarkers associated with blood lipid profile variability. *Atherosclerosis* 228, 413–420. doi: 10.1016/j.atherosclerosis.2013.03.033

Guo, Y., Pei, Y., Li, K., Cui, W., and Zhang, D. (2020). DNA N(6)-methyladenine modification in hypertension. *Aging* 12, 6276–6291. doi: 10.18632/aging.103023

Haas, J., Frese, K. S., Park, Y. J., Keller, A., Vogel, B., Lindroth, A. M., et al. (2013). Alterations in cardiac DNA methylation in human dilated cardiomyopathy. *EMBO Mol. Med.* 5, 413–429.

Heidenreich, P. A., Trogdon, J. G., Khavjou, O. A., Butler, J., Dracup, K., Ezekowitz, M. D., et al. (2011). Forecasting the future of cardiovascular disease in the United States: a policy statement from the American Heart Association. *Circulation* 123, 933–944. doi: 10.1161/cir.0b013e31820a55f5

Hiltunen, M. O., Turunen, M. P., Häkkinen, T. P., Rutanen, J., Hedman, M., Mäkinen, K., et al. (2002). DNA hypomethylation and methyltransferase expression in atherosclerotic lesions. *Vasc. Med.* 7, 5–11. doi: 10.1191/1358863x02vm418oa

Hoeksema, M. A., and de Winther, M. P. (2016). Epigenetic regulation of monocyte and macrophage function. *Antioxid. Redox. Signal.* 25, 758–774. doi: 10.1089/ars.2016.6695

Horn, M. A., and Trafford, A. W. (2016). Aging and the cardiac collagen matrix: novel mediators of fibrotic remodelling. *J. Mol. Cell Cardiol.* 93, 175–185. doi: 10.1016/j.yjmcc.2015.11.005

Hou, H., and Zhao, H. (2021). Epigenetic factors in atherosclerosis: DNA methylation, folic acid metabolism, and intestinal microbiota. *Clin. Chim. Acta* 512, 7–11. doi: 10.1016/j.cca.2020.11.013

Hua, X., Chen, L. M., Zhu, Q., Hu, W., Lin, C., Long, Z. Q., et al. (2019). Efficacy of controlled-release oxycodone for reducing pain due to oral mucositis in nasopharyngeal carcinoma patients treated with concurrent chemoradiotherapy: a prospective clinical trial. *Support Care Cancer* 27, 3759–3767. doi: 10.1007/s00520-019-4643-5

Huang, Y., Peng, K., Su, J., Huang, Y., Xu, Y., and Wang, S. (2007). Different effects of homocysteine and oxidized low density lipoprotein on methylation status in the promoter region of the estrogen receptor alpha gene. *Acta Biochim. Biophys. Sin.* 39, 19–26.

Humphreys, B. D. (2018). Mechanisms of renal fibrosis. *Annu. Rev. Physiol.* 80, 309–326.

Huo, Z., Zhu, Y., Yu, L., Yang, J., De Jager, P., Bennett, D. A., et al. (2019). DNA methylation variability in Alzheimer's disease. *Neurobiol. Aging* 76, 35–44.

Iadecola, C., Duering, M., Hachinski, V., Joutel, A., Pendlebury, S. T., Schneider, J. A., et al. (2019). Vascular cognitive impairment and dementia: JACC scientific expert panel. *J. Am. Coll. Cardiol.* 73, 3326–3344.

Ingrosso, D., and Perna, A. F. (2020). DNA methylation dysfunction in chronic kidney disease. *Genes* 11:811. doi: 10.3390/genes11070811

Istas, G., Declerck, K., Pudenz, M., Szic, K. S. V., Lendinez-Tortajada, V., Leon-Latre, M., et al. (2017). Identification of differentially methylated BRCA1 and CRISP2 DNA regions as blood surrogate markers for cardiovascular disease. *Sci. Rep.* 7:5120.

Iturria-Medina, Y., Sotero, R. C., Toussaint, P. J., Mateos-Pérez, J. M., and Evans, A. C. (2016). Early role of vascular dysregulation on late-onset Alzheimer's disease based on multifactorial data-driven analysis. *Nat. Commun.* 7:11934.

Jaiswal, S., Fontanillas, P., Flannick, J., Manning, A., Grauman, P. V., Mar, B. G., et al. (2014). Age-related Clonal hematopoiesis associated with adverse outcomes. *N. Engl. J. Med.* 371, 2488–2498.

Jia, G., Aroor, A. R., Jia, C., and Sowers, J. R. (2019). Endothelial cell senescence in aging-related vascular dysfunction. *Biochim. Biophys. Acta Mol. Basis Dis.* 1865, 1802–1809. doi: 10.1016/j.bbadis.2018.08.008

Jiang, Y. Z., Jiménez, J. M., Ou, K., McCormick, M. E., Zhang, L. D., and Davies, P. F. (2014). Hemodynamic disturbed flow induces differential DNA methylation of endothelial Kruppel-Like Factor 4 promoter in vitro and in vivo. *Circ. Res.* 115, 32–43. doi: 10.1161/circresaha.115.303883

Jones, P. A. (2012). Functions of DNA methylation: islands, start sites, gene bodies and beyond. *Nat. Rev. Genet.* 13, 484–492. doi: 10.1038/nrg3230

Justin Rucker, A., and Crowley, S. D. (2017). The role of macrophages in hypertension and its complications. *Pflugers Arch.* 469, 419–430. doi: 10.1007/s00424-017-1950-x

Kalaria, R. N., and Hase, Y. (2019). Neurovascular ageing and age-related diseases. *Subcell. Biochem.* 91, 477–499. doi: 10.1007/978-981-13-3681-2_17

Kao, Y. H., Cheng, C. C., Chen, Y. C., Chung, C. C., Lee, T. I., Chen, S. A., et al. (2011). Hydralazine-induced promoter demethylation enhances sarcoplasmic reticulum Ca2+ -ATPase and calcium homeostasis in cardiac myocytes. *Lab. Invest.* 91, 1291–1297. doi: 10.1038/labinvest.2011.92

Karlsson, I. K., Ploner, A., Wang, Y., Gatz, M., Pedersen, N. L., and Hägg, S. (2018). Apolipoprotein E DNA methylation and late-life disease. *Int. J. Epidemiol.* 47, 899–907. doi: 10.1093/ije/dyy025

Kazmi, N., Elliott, H. R., Burrows, K., Tillin, T., Hughes, A. D., Chaturvedi, N., et al. (2020). Associations between high blood pressure and DNA methylation. *PLoS One* 15:e0227728. doi: 10.1371/journal.pone.0227728

Khor, E. S., and Wong, P. F. (2020). The roles of MTOR and miRNAs in endothelial cell senescence. *Biogerontology* 21, 517–530. doi: 10.1007/s10522-020-09876-w

Kim, J., Kim, J. Y., Song, K. S., Lee, Y. H., Seo, J. S., Jelinek, J., et al. (2007). Epigenetic changes in estrogen receptor beta gene in atherosclerotic cardiovascular tissues and in-vitro vascular senescence. *Biochim. Biophys. Acta* 1772, 72–80. doi: 10.1016/j.bbadis.2006.10.004

Kim, M., Long, T. I., Arakawa, K., Wang, R., Yu, M. C., and Laird, P. W. (2010). DNA methylation as a biomarker for cardiovascular disease risk. *PLoS One* 5:e9692. doi: 10.1371/journal.pone.0009692

Kim, Y. R., Kim, C. S., Naqvi, A., Kumar, A., Kumar, S., Hoffman, T. A., et al. (2012). Epigenetic upregulation of p66shc mediates low-density lipoprotein cholesterol-induced endothelial cell dysfunction. *Am. J. Physiol. Heart Circ. Physiol.* 303, H189–H196.

Klug, M., Schmidhofer, S., Gebhard, C., Andreesen, R., and Rehli, M. (2013). 5-Hydroxymethylcytosine is an essential intermediate of active DNA demethylation processes in primary human monocytes. *Genome Biol.* 14:R46.

Krüger-Genge, A., Blocki, A., Franke, R. P., and Jung, F. (2019). Vascular endothelial cell biology: an update. *Int. J. Mol. Sci.* 20:4411. doi: 10.3390/ijms20184411

Kumar, A., Kumar, S., Vikram, A., Hoffman, T. A., Naqvi, A., Lewarchik, C. M., et al. (2013). Histone and DNA methylation-mediated epigenetic downregulation of endothelial Kruppel-like factor 2 by low-density lipoprotein cholesterol. *Arterioscler. Thromb. Vasc. Biol.* 33, 1936–1942. doi: 10.1161/atvbaha.113.301765

Lacolley, P., Regnault, V., and Avolio, A. P. (2018). Smooth muscle cell and arterial aging: basic and clinical aspects. *Cardiovasc. Res.* 114, 513–528. doi: 10.1093/cvr/cvy009

Lagarkova, M. A., Volchkov, P. Y., Philonenko, E. S., and Kiselev, S. L. (2008). Efficient differentiation of hESCs into endothelial cells in vitro is secured by epigenetic changes. *Cell Cycle* 7, 2929–2935. doi: 10.4161/cc.7.18.6700

Laina, A., Stellos, K., and Stamatelopoulos, K. (2018). Vascular ageing: underlying mechanisms and clinical implications. *Exp. Gerontol.* 109, 16–30. doi: 10.1016/j.exger.2017.06.007

Lakatta, E. G., and Levy, D. (2003a). Arterial and cardiac aging: major shareholders in cardiovascular disease enterprises: Part I: aging arteries: a "set up" for vascular disease. *Circulation* 107, 139–146. doi: 10.1161/01.cir.0000048892.83521.58

Lakatta, E. G., and Levy, D. (2003b). Arterial and cardiac aging: major shareholders in cardiovascular disease enterprises: Part II: the aging heart in health: links to heart disease. *Circulation* 107, 346–354. doi: 10.1161/01.cir.0000048893.62841.f7

Laukkanen, M. O., Mannermaa, S., Hiltunen, M. O., Aittomäki, S., Airenne, K., Jänne, J., et al. (1999). Local hypomethylation in atherosclerosis found in rabbit ec-sod gene. *Arterioscler. Thromb. Vasc. Biol.* 19, 2171–2178.

Law, J. A., and Jacobsen, S. E. (2010). Establishing, maintaining and modifying DNA methylation patterns in plants and animals. *Nat. Rev. Genet.* 11, 204–220. doi: 10.1038/nrg2719

Levy, E., Spahis, S., Bigras, J. L., Delvin, E., and Borys, J. M. (2017). The epigenetic machinery in vascular dysfunction and hypertension. *Curr. Hypertens Rep.* 19:52.

Li, H., Hastings, M. H., Rhee, J., Trager, L. E., Roh, J. D., and Rosenzweig, A. (2020). Targeting age-related pathways in heart failure. *Circ. Res.* 126, 533–551. doi: 10.1161/circresaha.119.315889

Li, J., Zhu, J., Ren, L., Ma, S., Shen, B., Yu, J., et al. (2020). Association between NPPA promoter methylation and hypertension: results from Gusu cohort and replication in an independent sample. *Clin. Epigenet.* 12:133.

Li, L., Xie, J., Zhang, M., and Wang, S. (2009). Homocysteine harasses the imprinting expression of IGF2 and H19 by demethylation of differentially methylated region between IGF2/H19 genes. *Acta Biochim. Biophys. Sin.* 41, 464–471. doi: 10.1093/abbs/gmp033

Li, X. D., Hong, M. N., Chen, J., Lu, Y. Y., Ye, M. Q., Ma, Y., et al. (2020). Adventitial fibroblast-derived vascular endothelial growth factor promotes vasa vasorum-associated neointima formation and macrophage recruitment. *Cardiovasc. Res.* 116, 708–720. doi: 10.1093/cvr/cvz159

Liu, C. F., and Tang, W. H. W. (2019). Epigenetics in cardiac hypertrophy and heart failure. *JACC Basic Transl. Sci.* 4, 976–993.

Liu, C. M., Ma, J. Q., Xie, W. R., Liu, S. S., Feng, Z. J., Zheng, G. H., et al. (2015). Quercetin protects mouse liver against nickel-induced DNA methylation and inflammation associated with the Nrf2/HO-1 and p38/STAT1/NF-κB pathway. *Food Chem. Toxicol.* 82, 19–26. doi: 10.1016/j.fct.2015.05.001

Liu, C., Xu, D., Sjöberg, J., Forsell, P., Björkholm, M., and Claesson, H. E. (2004). Transcriptional regulation of 15-lipoxygenase expression by promoter methylation. *Exp. Cell Res.* 297, 61–67. doi: 10.1016/j.yexcr.2004.02.014

Liu, R., Jin, Y., Tang, W. H., Qin, L., Zhang, X., Tellides, G., et al. (2013). Ten-eleven translocation-2 (TET2) is a master regulator of smooth muscle cell plasticity. *Circulation* 128, 2047–2057. doi: 10.1161/circulationaha.113.002887

Liu, R., Leslie, K. L., and Martin, K. A. (2015). Epigenetic regulation of smooth muscle cell plasticity. *Biochim. Biophys. Acta* 1849, 448–453. doi: 10.1016/j.bbagrm.2014.06.004

Love, S., and Miners, J. S. (2016). Cerebrovascular disease in ageing and Alzheimer's disease. *Acta Neuropathol.* 131, 645–658.

Lunnon, K., Smith, R., Hannon, E., De Jager, P. L., Srivastava, G., Volta, M., et al. (2014). Methylomic profiling implicates cortical deregulation of ANK1 in Alzheimer's disease. *Nat. Neurosci.* 17, 1164–1170. doi: 10.1038/nn.3782

Luz, I., Soukri, M., and Lail, M. (2018). Transformation of single MOF nanocrystals into single nanostructured catalysts within mesoporous supports: a platform for pioneer fluidized-nanoreactor hydrogen carriers. *Chem. Commun.* 54, 8462–8465. doi: 10.1039/c8cc04562c

Lyko, F. (2018). The DNA methyltransferase family: a versatile toolkit for epigenetic regulation. *Nat. Rev. Genet.* 19, 81–92. doi: 10.1038/nrg.2017.80

Ma, S. C., Cao, J. C., Zhang, H. P., Jiao, Y., Zhang, H., He, Y. Y., et al. (2017). Aberrant promoter methylation of multiple genes in VSMC proliferation induced by Hcy. *Mol. Med. Rep.* 16, 7775–7783. doi: 10.3892/mmr.2017.7521

Ma, S. C., Zhang, H. P., Jiao, Y., Wang, Y. H., Zhang, H., Yang, X. L., et al. (2018). Homocysteine-induced proliferation of vascular smooth muscle cells occurs via PTEN hypermethylation and is mitigated by resveratrol. *Mol. Med. Rep.* 17, 5312–5319.

Ma, S. C., Zhang, H. P., Kong, F. Q., Zhang, H., Yang, C., He, Y. Y., et al. (2016). Integration of gene expression and DNA methylation profiles provides a molecular subtype for risk assessment in atherosclerosis. *Mol. Med. Rep.* 13, 4791–4799. doi: 10.3892/mmr.2016.5120

Mahmood, S. S., Levy, D., Vasan, R. S., and Wang, T. J. (2014). The framingham heart study and the epidemiology of cardiovascular disease: a historical perspective. *Lancet* 383, 999–1008. doi: 10.1016/s0140-6736(13)61752-3

Martínez-Iglesias, O., Carrera, I., Carril, J. C., Fernández-Novoa, L., Cacabelos, N., and Cacabelos, R. (2020). DNA methylation in neurodegenerative and cerebrovascular disorders. *Int. J. Mol. Sci.* 21:2220. doi: 10.3390/ijms21062220

Mao, S. Q., Sun, J. H., Gu, T. L., Zhu, F. B., Yin, F. Y., and Zhang, L. N. (2017). Hypomethylation of interleukin-6 (IL-6) gene increases the risk of essential hypertension: a matched case-control study. *J. Hum. Hypertens.* 31, 530–536. doi: 10.1038/jhh.2017.7

Mao, S., Gu, T., Zhong, F., Fan, R., Zhu, F., Ren, P., et al. (2017). Hypomethylation of the Toll-like receptor-2 gene increases the risk of essential hypertension. *Mol. Med. Rep.* 16, 964–970. doi: 10.3892/mmr.2017.6653

Marumo, T., Yagi, S., Kawarazaki, W., Nishimoto, M., Ayuzawa, N., Watanabe, A., et al. (2015). Diabetes induces aberrant DNA Methylation in the proximal tubules of the kidney. *J. Am. Soc. Nephrol.* 26, 2388–2397. doi: 10.1681/asn.2014070665

Mattace-Raso, F. U., van der Cammen, T. J., Hofman, A., van Popele, N. M., Bos, M. L., Schalekamp, M. A., et al. (2006). Arterial stiffness and risk of coronary heart disease and stroke: the rotterdam study. *Circulation* 113, 657–663. doi: 10.1161/circulationaha.105.555235

Michiels, C. (2003). Endothelial cell functions. *J. Cell. Physiol.* 196, 430–443.

Mills, K. T., Stefanescu, A., and He, J. (2020). The global epidemiology of hypertension. *Nat. Rev. Nephrol.* 16, 223–237.

Min, J., Weitian, Z., Peng, C., Yan, P., Bo, Z., Yan, W., et al. (2016). Correlation between insulin-induced estrogen receptor methylation and atherosclerosis. *Cardiovasc. Diabetol.* 15:156.

Mitra, S., Khaidakov, M., Lu, J., Ayyadevara, S., Szwedo, J., Wang, X. W., et al. (2011). Prior exposure to oxidized low-density lipoprotein limits apoptosis in subsequent generations of endothelial cells by altering promoter methylation. *Am. J. Physiol. Heart Circ. Physiol.* 301, H506–H513.

Moore, K. J., and Tabas, I. (2011). Macrophages in the pathogenesis of atherosclerosis. *Cell* 145, 341–355. doi: 10.1016/j.cell.2011.04.005

Moore, L. D., Le, T., and Fan, G. (2013). DNA methylation and its basic function. *Neuropsychopharmacology* 38, 23–38. doi: 10.1038/npp.2012.112

Morgan, R. G., Donato, A. J., and Walker, A. E. (2018). Telomere uncapping and vascular aging. *Am. J. Physiol. Heart Circ. Physiol.* 315, H1–H5.

Mortusewicz, O., Schermelleh, L., Walter, J., Cardoso, M. C., and Leonhardt, H. (2005). Recruitment of DNA methyltransferase I to DNA repair sites. *Proc. Natl. Acad. Sci. U. S. A.* 102, 8905–8909.

Nagai, M., Conney, A. H., and Zhu, B. T. (2004). Strong inhibitory effects of common tea catechins and bioflavonoids on the O-methylation of catechol estrogens catalyzed by human liver cytosolic catechol-O-methyltransferase. *Drug Metab. Dispos.* 32, 497–504. doi: 10.1124/dmd.32.5.497

Nakatochi, M., Ichihara, S., Yamamoto, K., Naruse, K., Yokota, S., Asano, H., et al. (2017). Epigenome-wide association of myocardial infarction with DNA methylation sites at loci related to cardiovascular disease. *Clin. Epigenet.* 9:54.

Napoli, C., Benincasa, G., Donatelli, F., and Ambrosio, G. (2020). Precision medicine in distinct heart failure phenotypes: focus on clinical epigenetics. *Am. Heart J.* 224, 113–128. doi: 10.1016/j.ahj.2020.03.007

Nelissen, E. C., van Montfoort, A. P., Dumoulin, J. C., and Evers, J. L. (2011). Epigenetics and the placenta. *Hum. Reprod. Update* 17, 397–417.

Ni, Y. Q., Zhan, J. K., and Liu, Y. S. (2020). Roles and mechanisms of MFG-E8 in vascular aging-related diseases. *Ageing Res. Rev.* 64:101176. doi: 10.1016/j.arr.2020.101176

Nicorescu, I., Dallinga, G. M., de Winther, M. P. J., Stroes, E. S. G., and Bahjat, M. (2019). Potential epigenetic therapeutics for atherosclerosis treatment. *Atherosclerosis* 281, 189–197. doi: 10.1016/j.atherosclerosis.2018.10.006

Niu, P. P., Cao, Y., Gong, T., Guo, J. H., Zhang, B. K., and Jia, S. J. (2014). Hypermethylation of DDAH2 promoter contributes to the dysfunction of endothelial progenitor cells in coronary artery disease patients. *J. Transl. Med.* 12:170. doi: 10.1186/1479-5876-12-170

North, B. J., and Sinclair, D. A. (2012). The intersection between aging and cardiovascular disease. *Circ. Res.* 110, 1097–1108. doi: 10.1161/circresaha.111.246876

O'Hagan, H. M., Wang, W., Sen, S., Destefano Shields, C., Lee, S. S., Zhang, Y. W., et al. (2011). Oxidative damage targets complexes containing DNA methyltransferases, SIRT1, and polycomb members to promoter CpG Islands. *Cancer Cell* 20, 606–619. doi: 10.1016/j.ccr.2011.09.012

Ooi, S. K., and Bestor, T. H. (2008). The colorful history of active DNA demethylation. *Cell* 133, 1145–1148. doi: 10.1016/j.cell.2008.06.009

Pan, X., Chen, Z., Huang, R., Yao, Y., and Ma, G. (2013). Transforming growth factor β1 induces the expression of collagen type I by DNA methylation in cardiac fibroblasts. *PLoS One* 8:e60335. doi: 10.1371/journal.pone.0060335

Papapetropoulos, A., García-Cardeña, G., Madri, J. A., and Sessa, W. C. (1997). Nitric oxide production contributes to the angiogenic properties of vascular endothelial growth factor in human endothelial cells. *J. Clin. Invest.* 100, 3131–3139. doi: 10.1172/jci119868

Park, L. K., Friso, S., and Choi, S. W. (2012). Nutritional influences on epigenetics and age-related disease. *Proc. Nutr. Soc.* 71, 75–83. doi: 10.1017/s0029665111003302

Pei, F., Wang, X., Yue, R., Chen, C., Huang, J., Huang, J., et al. (2015). Differential expression and DNA methylation of angiotensin type 1A receptors in vascular tissues during genetic hypertension development. *Mol. Cell. Biochem.* 402, 1–8. doi: 10.1007/s11010-014-2295-9

Pepin, M. E., Drakos, S., Ha, C. M., Tristani-Firouzi, M., Selzman, C. H., Fang, J. C., et al. (2019). DNA methylation reprograms cardiac metabolic gene expression in end-stage human heart failure. *Am. J. Physiol. Heart Circ. Physiol.* 317, H674–H684.

Post, W. S., Goldschmidt-Clermont, P. J., Wilhide, C. C., Heldman, A. W., Sussman, M. S., Ouyang, P., et al. (1999). Methylation of the estrogen receptor gene is associated with aging and atherosclerosis in the cardiovascular system. *Cardiovasc. Res.* 43, 985–991. doi: 10.1016/s0008-6363(99)00153-4

Prasad, R., and Jho, E. H. (2019). A concise review of human brain methylome during aging and neurodegenerative diseases. *BMB Rep.* 52, 577–588. doi: 10.5483/bmbrep.2019.52.10.215

Prince, M., Bryce, R., Albanese, E., Wimo, A., Ribeiro, W., and Ferri, C. P. (2013). The global prevalence of dementia: a systematic review and metaanalysis. *Alzheimers Dement.* 9, 63–75.e62.

Qazi, T. J., Quan, Z., Mir, A., and Qing, H. (2018). Epigenetics in Alzheimer's disease: perspective of DNA Methylation. *Mol. Neurobiol.* 55, 1026–1044. doi: 10.1007/s12035-016-0357-6

Qin, X., Li, J., Wu, T., Wu, Y., Tang, X., Gao, P., et al. (2019). Overall and sex-specific associations between methylation of the ABCG1 and APOE genes and ischemic stroke or other atherosclerosis-related traits in a sibling study of Chinese population. *Clin. Epigenet.* 11:189.

Qiu, H., Zhu, Y., Sun, Z., Trzeciakowski, J. P., Gansner, M., Depre, C., et al. (2010). Short communication: vascular smooth muscle cell stiffness as a mechanism for increased aortic stiffness with aging. *Circ. Res.* 107, 615–619. doi: 10.1161/circresaha.110.221846

Rajan, R., Raj, N. A., Madeswaran, S., and Babu, D. R. (2015). Dielectric studies on struvite urinary crystals, a gateway to the new treatment modality for urolithiasis. *Spectrochim. Acta A Mol. Biomol. Spectrosc.* 148, 266–270. doi: 10.1016/j.saa.2015.03.136

Rasmussen, K. D., and Helin, K. (2016). Role of TET enzymes in DNA methylation, development, and cancer. *Genes Dev.* 30, 733–750. doi: 10.1101/gad.276568.115

Ratel, D., Ravanat, J. L., Berger, F., and Wion, D. (2006). N6-methyladenine: the other methylated base of DNA. *Bioessays* 28, 309–315. doi: 10.1002/bies.20342

Richard, M. A., Huan, T., Ligthart, S., Gondalia, R., Jhun, M. A., Brody, J. A., et al. (2017). DNA Methylation analysis identifies loci for blood pressure regulation. *Am. J. Hum. Genet.* 101, 888–902. doi: 10.1016/j.ajhg.2017.09.028

Rivière, G., Lienhard, D., Andrieu, T., Vieau, D., Frey, B. M., and Frey, F. J. (2011). Epigenetic regulation of somatic angiotensin-converting enzyme by DNA methylation and histone acetylation. *Epigenetics* 6, 478–489. doi: 10.4161/epi.6.4.14961

Salameh, Y., Bejaoui, Y., and El Hajj, N. (2020). DNA methylation biomarkers in aging and age-related diseases. *Front. Genet.* 11:171.

Sandoo, A., van Zanten, J. J., Metsios, G. S., Carroll, D., and Kitas, G. D. (2010). The endothelium and its role in regulating vascular tone. *Open Cardiovasc. Med. J.* 4, 302–312. doi: 10.2174/1874192401004010302

Sano, S., Oshima, K., Wang, Y., Katanasaka, Y., Sano, M., and Walsh, K. (2018). CRISPR-mediated gene editing to assess the roles of Tet2 and Dnmt3a in clonal hematopoiesis and Cardiovascular disease. *Circ. Res.* 123, 335–341. doi: 10.1161/circresaha.118.313225

Scisciola, L., Rizzo, M. R., Cataldo, V., Fontanella, R. A., Balestrieri, M. L., D'Onofrio, N., et al. (2020). Incretin drugs effect on epigenetic machinery: new potential therapeutic implications in preventing vascular diabetic complications. *FASEB J.* 34, 16489–16503. doi: 10.1096/fj.202000860rr

Semick, S. A., Bharadwaj, R. A., Collado-Torres, L., Tao, R., Shin, J. H., Deep-Soboslay, A., et al. (2019). Integrated DNA methylation and gene expression profiling across multiple brain regions implicate novel genes in Alzheimer's disease. *Acta Neuropathol.* 137, 557–569. doi: 10.1007/s00401-019-01966-5

Shapouri-Moghaddam, A., Mohammadian, S., Vazini, H., Taghadosi, M., Esmaeili, S. A., Mardani, F., et al. (2018). Macrophage plasticity, polarization, and function in health and disease. *J. Cell. Physiol.* 233, 6425–6440. doi: 10.1002/jcp.26429

Shen, Y., Peng, C., Bai, Q., Ding, Y., Yi, X., Du, H., et al. (2019). Epigenome-wide association study indicates Hypomethylation of MTRNR2L8 in large-artery atherosclerosis stroke. *Stroke* 50, 1330–1338. doi: 10.1161/strokeaha.118.023436

Soriano-Tárraga, C., Jiménez-Conde, J., Giralt-Steinhauer, E., Mola, M., Ois, A., Rodríguez-Campello, A., et al. (2014). Global DNA methylation of ischemic stroke subtypes. *PLoS One* 9:e96543. doi: 10.1371/journal.pone.0096543

Stenmark, K. R., Yeager, M. E., El Kasmi, K. C., Nozik-Grayck, E., Gerasimovskaya, E. V., Li, M., et al. (2013). The adventitia: essential regulator of vascular wall structure and function. *Annu. Rev. Physiol.* 75, 23–47. doi: 10.1146/annurev-physiol-030212-183802

Stenzig, J., Schneeberger, Y., Löser, A., Peters, B. S., Schaefer, A., Zhao, R. R., et al. (2018). Pharmacological inhibition of DNA methylation attenuates pressure overload-induced cardiac hypertrophy in rats. *J. Mol. Cell Cardiol.* 120, 53–63. doi: 10.1016/j.yjmcc.2018.05.012

Stoner, L., Young, J. M., and Fryer, S. (2012). Assessments of arterial stiffness and endothelial function using pulse wave analysis. *Int. J. Vasc. Med.* 2012:903107.

Strand, K. A., Lu, S., Mutryn, M. F., Li, L., Zhou, Q., Enyart, B. T., et al. (2020). High throughput screen identifies the DNMT1 (DNA Methyltransferase-1) Inhibitor, 5-Azacytidine, as a potent inducer of PTEN (Phosphatase and Tensin Homolog): central role for PTEN in 5-Azacytidine protection against pathological vascular remodeling. *Arterioscler. Thromb. Vasc. Biol.* 40, 1854–1869. doi: 10.1161/atvbaha.120.314458

Tabaei, S., and Tabaee, S. S. (2019). DNA methylation abnormalities in atherosclerosis. *Artif. Cells Nanomed. Biotechnol.* 47, 2031–2041. doi: 10.1080/21691401.2019.1617724

Tang, P. M., Nikolic-Paterson, D. J., and Lan, H. Y. (2019). Macrophages: versatile players in renal inflammation and fibrosis. *Nat. Rev. Nephrol.* 15, 144–158. doi: 10.1038/s41581-019-0110-2

Tao, H., Yang, J. J., Chen, Z. W., Xu, S. S., Zhou, X., Zhan, H. Y., et al. (2014a). DNMT3A silencing RASSF1A promotes cardiac fibrosis through upregulation of ERK1/2. *Toxicology* 323, 42–50. doi: 10.1016/j.tox.2014.06.006

Tao, H., Yang, J. J., Shi, K. H., Deng, Z. Y., and Li, J. (2014b). DNA methylation in cardiac fibrosis: new advances and perspectives. *Toxicology* 323, 125–129. doi: 10.1016/j.tox.2014.07.002

Thannickal, V. J., Zhou, Y., Gaggar, A., and Duncan, S. R. (2014). Fibrosis: ultimate and proximate causes. *J. Clin. Invest.* 124, 4673–4677. doi: 10.1172/jci74368

Thorin-Trescases, N., de Montgolfier, O., Pinçon, A., Raignault, A., Caland, L., Labbé, P., et al. (2018). Impact of pulse pressure on cerebrovascular events leading to age-related cognitive decline. *Am. J. Physiol. Heart Circ. Physiol.* 314, H1214–H1224. doi: 10.1152/ajpheart.00637.2017

Toth, P., Tarantini, S., Csiszar, A., and Ungvari, Z. (2017). Functional vascular contributions to cognitive impairment and dementia: mechanisms and consequences of cerebral autoregulatory dysfunction, endothelial impairment, and neurovascular uncoupling in aging. *Am. J. Physiol. Heart Circ. Physiol.* 312, H1–H20. doi: 10.1152/ajpheart.00581.2016

Triposkiadis, F., Xanthopoulos, A., and Butler, J. (2019). Cardiovascular aging and heart failure: JACC review topic of the week. *J. Am. Coll. Cardiol.* 74, 804–813. doi: 10.1016/j.jacc.2019.06.053

Triposkiadis, F., Xanthopoulos, A., Parissis, J., Butler, J., and Farmakis, D. (2020). Pathogenesis of chronic heart failure: cardiovascular aging, risk factors, comorbidities, and disease modifiers. *Heart Fail Rev.* doi: 10.1007/s10741-020-09987-z Online ahead of print.

Ungvari, Z., Labinskyy, N., Gupte, S., Chander, P. N., Edwards, J. G., and Csiszar, A. (2008). Dysregulation of mitochondrial biogenesis in vascular endothelial and smooth muscle cells of aged rats. *Am. J. Physiol. Heart Circ. Physiol.* 294, H2121–H2128. doi: 10.1152/ajpheart.00012.2008

Uryga, A. K., and Bennett, M. R. (2016). Ageing induced vascular smooth muscle cell senescence in atherosclerosis. *J. Physiol.* 594, 2115–2124. doi: 10.1113/jp270923

van Sloten, T. T., Sedaghat, S., Laurent, S., London, G. M., Pannier, B., Ikram, M. A., et al. (2015). Carotid stiffness is associated with incident stroke: a systematic review and individual participant data meta-analysis. *J. Am. Coll. Cardiol.* 66, 2116–2125. doi: 10.1016/j.jacc.2015.08.888

Vujic, A., Robinson, E. L., Ito, M., Haider, S., Ackers-Johnson, M., See, K., et al. (2015). Experimental heart failure modelled by the cardiomyocyte-specific loss of an epigenome modifier. DNMT3B. *J. Mol. Cell Cardiol.* 82, 174–183. doi: 10.1016/j.yjmcc.2015.03.007

Waddington, C. H. (2012). The epigenotype. 1942. *Int. J. Epidemiol.* 41, 10–13. doi: 10.1093/ije/dyr184

Wang, C., Xu, G., Wen, Q., Peng, X., Chen, H., Zhang, J., et al. (2019). CBS promoter hypermethylation increases the risk of hypertension and stroke. *Clinics* 74:e630.

Wang, F., Demura, M., Cheng, Y., Zhu, A., Karashima, S., Yoneda, T., et al. (2014). Dynamic CCAAT/enhancer binding protein-associated changes of DNA methylation in the angiotensinogen gene. *Hypertension* 63, 281–288. doi: 10.1161/hypertensionaha.113.02303

Wang, G., Jacquet, L., Karamariti, E., and Xu, Q. (2015). Origin and differentiation of vascular smooth muscle cells. *J. Physiol.* 593, 3013–3030. doi: 10.1113/jp270033

Wang, J., Uryga, A. K., Reinhold, J., Figg, N., Baker, L., Finigan, A., et al. (2015). Vascular smooth muscle cell senescence promotes atherosclerosis and features of plaque vulnerability. *Circulation* 132, 1909–1919. doi: 10.1161/circulationaha.115.016457

Wang, X., Falkner, B., Zhu, H., Shi, H., Su, S., Xu, X., et al. (2013). A genome-wide methylation study on essential hypertension in young African American males. *PLoS One* 8:e53938. doi: 10.1371/journal.pone.0053938

Wang, X., Qin, X., Demirtas, H., Li, J., Mao, G., Huo, Y., et al. (2007). Efficacy of folic acid supplementation in stroke prevention: a meta-analysis. *Lancet* 369, 1876–1882. doi: 10.1016/s0140-6736(07)60854-x

Waterland, R. A. (2006). Assessing the effects of high methionine intake on DNA methylation. *J. Nutr.* 136, 1706s–1710s. doi: 10.1093/jn/136.6.1706S

Weber, A. R., Krawczyk, C., Robertson, A. B., Kuśnierczyk, A., Vågbø, C. B., Schuermann, D., et al. (2016). Biochemical reconstitution of TET1-TDG-BER-dependent active DNA demethylation reveals a highly coordinated mechanism. *Nat. Commun.* 7:10806. doi: 10.1038/ncomms10806

Wei, L., Zhao, S., Wang, G., Zhang, S., Luo, W., Qin, Z., et al. (2018). SMAD7 methylation as a novel marker in atherosclerosis. *Biochem. Biophys. Res. Commun.* 496, 700–705. doi: 10.1016/j.bbrc.2018.01.121

Wei, Y., Sun, Z., Wang, Y., Xie, Z., Xu, S., Xu, Y., et al. (2019). Methylation in the TP53 promoter is associated with ischemic stroke. *Mol. Med. Rep.* 20, 1404–1410. doi: 10.3892/mmr.2019.10348

Wong, C. P., Nguyen, L. P., Noh, S. K., Bray, T. M., Bruno, R. S., and Ho, E. (2011). Induction of regulatory T cells by green tea polyphenol EGCG. *Immunol. Lett.* 139, 7–13. doi: 10.1016/j.imlet.2011.04.009

Wu, L., Pei, Y., Zhu, Y., Jiang, M., Wang, C., Cui, W., et al. (2019). Association of N(6)-methyladenine DNA with plaque progression in atherosclerosis via myocardial infarction-associated transcripts. *Cell Death Dis.* 10:909. doi: 10.1038/s41419-019-2152-6

Wu, X., and Zhang, Y. (2017). TET-mediated active DNA demethylation: mechanism, function and beyond. *Nat. Rev. Genet.* 18, 517–534. doi: 10.1038/nrg.2017.33

Wyss-Coray, T. (2016). Ageing, neurodegeneration and brain rejuvenation. *Nature* 539, 180–186. doi: 10.1038/nature20411

Xiao, C. L., Zhu, S., He, M., Chen, D., Zhang, Q., Chen, Y., et al. (2018). N(6)-Methyladenine DNA modification in the human genome. *Mol. Cell.* 71, 306–318.e307. doi: 10.1016/j.molcel.2018.06.015

Xu, G., Wang, C., Ying, X., Kong, F., Ji, H., Zhao, J., et al. (2019). Serine hydroxymethyltransferase 1 promoter hypermethylation increases the risk of essential hypertension. *J. Clin. Lab. Anal.* 33:e22712. doi: 10.1002/jcla.22712

Xu, H., Jiang, J., Chen, W., Li, W., and Chen, Z. (2019). Vascular macrophages in atherosclerosis. *J. Immunol. Res.* 2019:4354786.

Xu, L., Hao, H., Hao, Y., Wei, G., Li, G., Ma, P., et al. (2019). Aberrant MFN2 transcription facilitates homocysteine-induced VSMCs proliferation via the increased binding of c-Myc to DNMT1 in atherosclerosis. *J. Cell Mol. Med.* 23, 4611–4626. doi: 10.1111/jcmm.14341

Xu, M., Li, J., Chen, X., Han, L., Li, L., and Liu, Y. (2019). MTHFD1 promoter hypermethylation increases the risk of hypertension. *Clin. Exp. Hypertens.* 41, 422–427. doi: 10.1080/10641963.2018.1501057

Xu, X., Friehs, I., Zhong, Hu, T., Melnychenko, I., Tampe, B., et al. (2015a). Endocardial fibroelastosis is caused by aberrant endothelial to mesenchymal transition. *Circ. Res.* 116, 857–866. doi: 10.1161/circresaha.116.305629

Xu, X., Tan, X., Tampe, B., Nyamsuren, G., Liu, X., Maier, L. S., et al. (2015b). Epigenetic balance of aberrant Rasal1 promoter methylation and hydroxymethylation regulates cardiac fibrosis. *Cardiovasc. Res.* 105, 279–291. doi: 10.1093/cvr/cvv015

Yamada, Y., Nishida, T., Horibe, H., Oguri, M., Kato, K., and Sawabe, M. (2014). Identification of hypo- and hypermethylated genes related to atherosclerosis by a genome-wide analysis of DNA methylation. *Int. J. Mol. Med.* 33, 1355–1363. doi: 10.3892/ijmm.2014.1692

Yamazaki, K., Yoshino, Y., Mori, T., Yoshida, T., Ozaki, Y., Sao, T., et al. (2017). Gene expression and methylation analysis of ABCA7 in patients with Alzheimer's disease. *J. Alzheimers Dis.* 57, 171–181. doi: 10.3233/jad-161195

Yamazaki, Y., Baker, D. J., Tachibana, M., Liu, C. C., van Deursen, J. M., Brott, T. G., et al. (2016). Vascular cell senescence contributes to blood-brain barrier breakdown. *Stroke* 47, 1068–1077. doi: 10.1161/strokeaha.115.010835

Yang, Q., Chen, H. Y., Wang, J. N., Han, H. Q., Jiang, L., Wu, W. F., et al. (2020). Alcohol promotes renal fibrosis by activating Nox2/4-mediated DNA methylation of Smad7. *Clin. Sci.* 134, 103–122. doi: 10.1042/cs20191047

Yang, Q., Zhao, Y., Zhang, Z., and Chen, J. (2016). Association of interleukin-6 methylation in leukocyte DNA with serum level and the risk of ischemic heart disease. *Scand. J. Clin. Lab. Invest.* 76, 291–295. doi: 10.3109/00365513.2016.1149616

Yang, X., Wang, X., Liu, D., Yu, L., Xue, B., and Shi, H. (2014). Epigenetic regulation of macrophage polarization by DNA methyltransferase 3b. *Mol. Endocrinol.* 28, 565–574. doi: 10.1210/me.2013-1293

Yang, Y., Wang, A., Yuan, X., Zhao, Q., Liu, X., Chen, S., et al. (2019). Association between healthy vascular aging and the risk of the first stroke in a community-based Chinese cohort. *Aging* 11, 5807–5816. doi: 10.18632/aging.102170

Yang, Z., Wang, L., Zhang, W., Wang, X., and Zhou, S. (2016). Plasma homocysteine involved in methylation and expression of thrombomodulin in cerebral infarction. *Biochem. Biophys. Res. Commun.* 473, 1218–1222. doi: 10.1016/j.bbrc.2016.04.042

Yin, H., and Blanchard, K. L. (2000). DNA methylation represses the expression of the human erythropoietin gene by two different mechanisms. *Blood* 95, 111–119. doi: 10.1182/blood.v95.1.111.001k20_111_119

Yin, S., Zhang, Q., Yang, J., Lin, W., Li, Y., Chen, F., et al. (2017). TGFβ-incurred epigenetic aberrations of miRNA and DNA methyltransferase suppress Klotho and potentiate renal fibrosis. *Biochim. Biophys. Acta Mol. Cell Res.* 1864, 1207–1216. doi: 10.1016/j.bbamcr.2017.03.002

Yousuf, F. A., Kazmi, K., Iqbal, J., Ahmed, N., and Iqbal, M. P. (2020). Higher DNA methylation of ABO gene promoter is associated with acute myocardial infarction in a hospital-based population in Karachi. *Pak. J. Med. Sci.* 36, 505–510.

Yu, Y., Guan, X., Nie, L., Liu, Y., He, T., Xiong, J., et al. (2017). DNA hypermethylation of sFRP5 contributes to indoxyl sulfate-induced renal fibrosis. *J. Mol. Med.* 95, 601–613. doi: 10.1007/s00109-017-1538-0

Zhang, D., Chen, Y., Xie, X., Liu, J., Wang, Q., Kong, W., et al. (2012). Homocysteine activates vascular smooth muscle cells by DNA demethylation of platelet-derived growth factor in endothelial cells. *J. Mol. Cell Cardiol.* 53, 487–496. doi: 10.1016/j.yjmcc.2012.07.010

Zhang, D., Sun, X., Liu, J., Xie, X., Cui, W., and Zhu, Y. (2015). Homocysteine accelerates senescence of endothelial cells via DNA hypomethylation of human telomerase reverse transcriptase. *Arterioscler. Thromb. Vasc. Biol.* 35, 71–78. doi: 10.1161/atvbaha.114.303899

Zhang, G., Huang, H., Liu, D., Cheng, Y., Liu, X., Zhang, W., et al. (2015). N6-methyladenine DNA modification in Drosophila. *Cell* 161, 893–906.

Zhang, H., Zhao, X., Wang, C., Du, R., Wang, X., Fu, J., et al. (2019). A preliminary study of the association between apolipoprotein E promoter methylation and atherosclerotic cerebral infarction. *J. Stroke Cerebrovasc. Dis.* 28, 1056–1061. doi: 10.1016/j.jstrokecerebrovasdis.2018.12.027

Zhang, L. N., Liu, P. P., Wang, L., Yuan, F., Xu, L., Xin, Y., et al. (2013). Lower ADD1 gene promoter DNA methylation increases the risk of essential hypertension. *PLoS One* 8:e63455. doi: 10.1371/journal.pone.0063455

Zhang, Y. P., Huang, Y. T., Huang, T. S., Pang, W., Zhu, J. J., Liu, Y. F., et al. (2017). The mammalian target of rapamycin and DNA methyltransferase 1 axis mediates vascular endothelial dysfunction in response to disturbed flow. *Sci. Rep.* 7:14996.

Zhong, Q., Liu, C., Fan, R., Duan, S., Xu, X., Zhao, J., et al. (2016). Association of SCNN1B promoter methylation with essential hypertension. *Mol. Med. Rep.* 14, 5422–5428. doi: 10.3892/mmr.2016.5905

Zhou, S., Cai, B., Zhang, Z., Zhang, Y., Wang, L., Liu, K., et al. (2017). CDKN2B Methylation and Aortic Arch calcification in patients with ischemic stroke. *J. Atheroscler. Thromb.* 24, 609–620. doi: 10.5551/jat.36897

Zhu, L., Jia, L., Liu, Z., Zhang, Y., Wang, J., Yuan, Z., et al. (2019). Elevated Methylation of FOXP3 (Forkhead Box P3)-TSDR (Regulatory T-Cell-Specific Demethylated Region) is associated with increased risk for adverse outcomes in patients with acute coronary syndrome. *Hypertension* 74, 581–589. doi: 10.1161/hypertensionaha.119.12852

Zhuang, J., Luan, P., Li, H., Wang, K., Zhang, P., Xu, Y., et al. (2017). The Yin-Yang dynamics of DNA Methylation is the key regulator for smooth muscle cell phenotype switch and vascular remodeling. *Arterioscler. Thromb. Vasc. Biol.* 37, 84–97. doi: 10.1161/atvbaha.116.307923

Zinellu, A., Sotgia, S., Sotgiu, E., Assaretti, S., Baralla, A., and Mangoni, A. A. (2017). Cholesterol lowering treatment restores blood global DNA methylation in chronic kidney disease (CKD) patients. *Nutr. Metab. Cardiovasc. Dis.* 27, 822–829. doi: 10.1016/j.numecd.2017.06.011

Conflict of Interest: The authors declare that the research was conducted in the absence of any commercial or financial relationships that could be construed as a potential conflict of interest.

frontiers in Genetics

ORIGINAL RESEARCH
published: 14 July 2021
doi: 10.3389/fgene.2021.671552

The Co-occurrence of Chronic Hepatitis B and Fibrosis Is Associated With a Decrease in Hepatic Global DNA Methylation Levels in Patients With Non-alcoholic Fatty Liver Disease

FangYuan Li[1], Qian Ou[1], ZhiWei Lai[1], LiuZhen Pu[1], XingYi Chen[1], LiRong Wang[1], LiuQiao Sun[1], XiaoPing Liang[1], YaoYao Wang[1], Hang Xu[1], Jun Wei[2], Feng Wu[2], HuiLian Zhu[3] and LiJun Wang[1]**

[1] Department of Nutrition, School of Medicine, Jinan University, Guangzhou, China, [2] Department of Science and Technology, Guangzhou Customs, Guangzhou, China, [3] Department of Nutrition, School of Public Health, Sun Yat-sen University, Guangzhou, China

OPEN ACCESS

Edited by:
Suowen Xu,
University of Science and Technology of China, China

Reviewed by:
Apiwat Mutirangura,
Chulalongkorn University, Thailand
Simonetta Friso,
University of Verona, Italy

***Correspondence:**
LiJun Wang
tswanglj5@jnu.edu.cn
HuiLian Zhu
zhuhl@mail.sysu.edu.cn

Specialty section:
This article was submitted to Epigenomics and Epigenetics, a section of the journal Frontiers in Genetics

Received: 24 February 2021
Accepted: 01 June 2021
Published: 14 July 2021

Citation:
Li FY, Ou Q, Lai ZW, Pu LZ, Chen XY, Wang LR, Sun LQ, Liang XP, Wang YY, Xu H, Wei J, Wu F, Zhu HL and Wang LJ (2021) The Co-occurrence of Chronic Hepatitis B and Fibrosis Is Associated With a Decrease in Hepatic Global DNA Methylation Levels in Patients With Non-alcoholic Fatty Liver Disease. Front. Genet. 12:671552. doi: 10.3389/fgene.2021.671552

Global DNA hypomethylation has been reported in patients with chronic hepatitis B (CHB) and non-alcoholic fatty-liver disease (NAFLD). However, the global DNA methylation profile of patients with concurrent NAFLD and CHB (NAFLD + CHB) is still unclear. We aimed to detect the hepatic global DNA methylation levels of NAFLD + CHB patients and assess the associated risk factors. Liver biopsies were collected from 55 NAFLD patients with or without CHB. The histological characteristics of the biopsy were then assessed. Hepatic global DNA methylation levels were quantified by fluorometric method. The hepatic global DNA methylation levels in NAFLD + CHB group were significantly lower than that in NAFLD group. Participants with fibrosis showed lower levels of hepatic global DNA methylation than those without fibrosis. Participants with both CHB and fibrosis had lower levels of hepatic global DNA methylation than those without either CHB or fibrosis. The co-occurrence of CHB and fibrosis was significantly associated with a reduction in global DNA methylation levels compared to the absence of both CHB and fibrosis. Our study suggests that patients with NAFLD + CHB exhibited lower levels of global DNA methylation than patients who had NAFLD alone. The co-occurrence of CHB and liver fibrosis in NAFLD patients was associated with a decrease in global DNA methylation levels.

Keywords: global DNA methylation, chronic hepatitis B, fibrosis, non-alcoholic fatty-liver disease, inflammation

Abbreviations: ALT, alanine aminotransferase; APOA, apolipoprotein A; APOB, apolipoprotein B; AST, aspartate aminotransferase; BMI, Body mass index; CHB, chronic hepatitis B; CIN, chromosomal instability; CpG, cytosine-phosphate-guanine; DBP, diastolic blood pressure; DM, diabetes mellitus; *DNMTs*, DNA methyltransferases; HBsAg, hepatitis B virus surface antigen; HBV, hepatitis B virus; HBx, HBV X protein; HCC, hepatocellular carcinoma; HDL, high-density lipoprotein; LDL, low-density lipoprotein; MET, metabolic equivalent; NAFLD, non-alcoholic fatty liver disease; NAFLD + CHB, patients with concurrent NAFLD and CHB; NAS, NAFLD activity score; NASH, non-alcoholic steatohepatitis; NASH-B, steatohepatitis borderline; SAM, S-adenosylmethionine; SS, simple steatosis; SBP, systolic Blood Pressure; TC, total cholesterol; TG, triglyceride.

INTRODUCTION

Non-alcoholic fatty-liver disease (NAFLD) is poised to become a predominant cause of chronic liver disease worldwide (Loomba and Sanyal, 2013). If obesity and diabetes mellitus (DM) stabilize in the future, it is predicted that there will be a modest growth in total NAFLD cases (0–30%) between 2016 and 2030, with the highest growth expected to be seen in China, due to the effects of urbanization (Estes et al., 2018). Chronic hepatitis B (CHB) is a disease caused by hepatitis B virus (HBV) infection and affects more than 257 million individuals worldwide. The rising prevalence of obesity and metabolic syndrome has resulted in an increase in the number of patients with concurrent NAFLD and CHB (NAFLD + CHB).

Both CHB and NAFLD are leading causes of liver-related morbidity and mortality. NAFLD comprises a spectrum of liver diseases that includes simple steatosis, non-alcoholic steatohepatitis, fibrosis, and cirrhosis, and ultimately develops into hepatocellular carcinoma (HCC) (Younossi et al., 2015). CHB contributes substantially to the global disease burden owing to its high prevalence and probability of progression to cirrhosis and HCC (Shen et al., 2012; Lok et al., 2017). Positive hepatitis B core antibody (anti-HBc) have been associated with cirrhosis and possibly HCC in Chinese patients with NAFLD (Chan et al., 2020). In a follow-up study, patients with NAFLD + CHB were found to have a 7.3-fold increased risk of HCC compared to patients with CHB alone (Chan et al., 2017). These studies highlight the challenge of preventing and treating NAFLD + CHB. However, the underlying mechanisms of this compound disease remain unclear.

DNA methylation is the best-known and most studied epigenetic modification, and it refers to heritable changes in gene expression associated with modifications of DNA that are not due to any alteration in the DNA sequence. DNA methylation plays a key role in transcriptional regulation by silencing genes through hypermethylation or activating genes through hypomethylation (Shen et al., 2012; Murphy et al., 2013; Zhang et al., 2013; Zeybel et al., 2016). In addition to gene-specific DNA methylation, the loss of global DNA methylation in sequences that are normally methylated, such as the repetitive sequences *LINE-1* and satellite-2 and inter-spread cytosine-phosphate-guanine (CpG) islands, can lead to chromosomal abnormalities, chromosomal instability, chromosome fragility, and ultimately the development of disease (Amir et al., 2012; Nishida et al., 2013; Patchsung et al., 2018).

DNA methylation accounts for the impacts of environmental factors on liver disease. Marked decrease in the global DNA methylation level was detected in the livers of NAFLD and HCC mice model fed with high fat diet and methyl donor deficient diet (choline, methionine, folic acid, and vitamin B12 deficiency) (Tryndyak et al., 2011; Wang et al., 2014). Similar change also occurs in chemically induced NAFLD and HCC (Chen et al., 2004; Tao et al., 2005; Komatsu et al., 2012). In addition, HBV X protein (HBx) encoding by HBV X gene induces global hypomethylation of satellite-2 repeating sequences (Park et al., 2007). HBx is required for the virus infection and has been shown to induce demethylation of distal regulatory regions to facilitate HCC tumorigenesis (Lee et al., 2014).

Global DNA hypomethylation has also been implicated in HBV exposed HCC patients (Zhang et al., 2013). Furthermore, reduced global DNA methylation of *LINE-1* in white blood cells has been associated with a twofold higher risk of HCC in hepatitis B surface antigen (HBsAg) carriers (Wu et al., 2012). These studies indicate that HBV exposure contributes to a decrease in global DNA methylation and a subsequent increase in the risk of developing HCC. Findings from our laboratory and others have shown that the NAFLD and HCC patients have lower levels of global DNA methylation than corresponding controls (Wu et al., 2012; Nishida et al., 2013; Wang et al., 2014; Lai et al., 2020). However, whether the co-occurrence of CHB with NAFLD further aggravates global DNA hypomethylation in NAFLD patients has not been evaluated.

The histological progression of liver diseases is associated with a decrease in global DNA methylation levels, especially in the case of fibrosis. Studies of animal liver fibrosis models induced by a methionine-choline-deficient diet have reported that the global DNA methylation level in the liver is reduced in these animals (Tryndyak et al., 2011; Page et al., 2016). Mouse models with early stage liver fibrosis also display hypomethylation (Komatsu et al., 2012). In advanced biliary atresia patients, DNA hypomethylation in blood was observed with severe fibrosis compared with mild fibrosis (Udomsinprasert et al., 2016). However, it is not clear whether the superposition of fibrosis on CHB is associated with the decrease in levels of global DNA methylation in NAFLD patients.

Given this uncertainty, we analyzed liver biopsies from NAFLD patients to test whether the co-occurrence of CHB with NAFLD aggravates global DNA hypomethylation, and whether the presence of concurrent CHB and liver fibrosis in NAFLD patients is also associated with a decrease in global DNA methylation levels.

MATERIALS AND METHODS

Human Subjects

The Medical Ethics Committee of the School of Public Health, Sun Yat-sen University (SYSU) approved the study protocol [Project identification code: (2012) No. 17]. Our study protocol conformed to the ethical guidelines of the 1975 Declaration of Helsinki. All subjects signed written informed consent forms prior to the study, which were then collected prior to the day of surgery.

Study Design

Fifty-five NAFLD patients were recruited from the 157th Hospital in Zhangzhou city, Fujian province in China between June 2012 and June 2013. A percutaneous liver biopsy was obtained using a disposable Menghini needle or an 18-gauge BARD Max-Core Disposable Biopsy Instrument.

Non-alcoholic fatty-liver disease diagnosis was based on the histological evidence for hepatic steatosis via percutaneous liver biopsy (more than 5% of steatosis in the proportion). CHB was defined as having medical records with a positive HBsAg for longer than 6 months. Participants who met the following criteria

were excluded from analysis: alcohol consumption (>20 g per day for males, >10 g per day for females); use of antiviral therapy in the 6 months prior to the study period; diagnosis of other viral hepatitis conditions, malignancy, autoimmune liver diseases, or severe hepatic injury or cirrhosis; vitamin use; weight change of more than 2 kg in a single year; and presence of a drug-induced or parental nutrition-induced fatty liver.

Demographic, Anthropometric, and Biochemical Evaluation

A face-to-face questionnaire was used to assess all participants before performing the liver biopsy. We collected the following information using the questionnaire: socio-demographic characteristics (e.g., age, sex, education level, occupation); lifestyle habits (e.g., alcohol, tobacco, and tea consumption); physical activities; and history of chronic diseases and medication (Chen et al., 2015). Physical activities were expressed as their metabolic equivalents.

When measuring the body weight, height, neck, and waist/hip circumferences, the participants were barefoot and wore light clothing. Body mass index (BMI) was calculated using the formula of weight in kilograms divided by height in meters squared. Systolic and diastolic blood pressure measurements were performed on the right arms of the participants after they had been sitting for at least 10 min.

Fasting serum samples were isolated and stored at −80°C until further analysis. Serum alanine aminotransferase, alanine transaminase, total cholesterol, triglyceride, low-density lipoprotein, high-density lipoprotein, apolipoprotein A, apolipoprotein B, fasting blood glucose, and uric acid concentrations were obtained from patients' records.

Histopathological Assessment

Liver samples were stained using both the hematoxylin and eosin and Masson's trichrome methods. The histological assessment was performed by microscopic examination in accordance with the non-alcoholic steatohepatitis Clinical Research Network Scoring System (Kleiner et al., 2005). Two experienced pathologists, who were blind to the participants' information, conducted the assessments. The severity of steatosis was graded from 0 to 3 based on the proportion of steatosis: grades 0 (<5%), 1 (5–33%), 2 (33–66%), and 3 (≥66%). The steatosis grade was defined as either mild (grade 1) or moderate (grades 2 and 3) based on the above assessments. Based on the number of inflammatory foci observed per field of view at a magnification of 200×, inflammation was classified as grades 0 (none), 1 (<2 foci/field), 2 (2–4 foci/field), and 3 (≥4 foci/field). The inflammation grade was defined as either mild (grades 0 and 1) or moderate (grades 2 and 3) based on the above assessments. Fibrotic severity was graded from 0 to 4 in accordance with the Brunt classification system: grades 0 (none), 1 (peri-sinusoidal or peri-cellular), 2 (fibrosis in both the peri-sinusoidal sinus and portal vein), 3 (bridging fibrosis without obvious cirrhosis), and 4 (cirrhosis). The total NAFLD activity score (NAS) was calculated as the sum of grades for steatosis, hepatocellular ballooning, and lobular inflammation. The obtained score was then categorized as simple steatosis (SS) (<3), steatohepatitis borderline (NASH-B) (3–4), and non-alcoholic steatohepatitis (NASH) (≥5).

DNA Methylation Analysis

Genomic DNA was isolated from liver tissue using a TIANamp Genomic DNA Kit (TIANGEN, Beijing, China). The extracted DNA was quantified using a NanoDrop® ND-1000 UV-Vis spectrophotometer (Thermo Scientific, Loughborough, United Kingdom). The global DNA methylation levels in liver tissues were determined using the MethylFlash Methylated DNA Quantification Kit (catalog No. P-103596, fluorometric; EpiGentek Group Inc., New York, NY, United States)

TABLE 1 | Anthropometric and biochemical characteristics of the study population based on the chronic hepatitis B status.

	NAFLD (*n* = 37)	NAFLD + CHB (*n* = 18)	*P*	P_{1*}
Anthropometric characteristic				
Age, years	34.30 ± 10.84	35.78 ± 9.65	0.625	–
Male, n (%)	30.00 (81.10)	14.00 (77.8)	0.779	–
BMI, kg/m^2	28.20 ± 3.33	27.35 ± 2.60	0.350	–
Weight, kg	80.86 ± 13.14	76.08 ± 8.18	0.164	0.192
Height, cm	170.00 (166.50, 175.0)	167.50 (162.25, 170.25)	0.102	0.283
Waist circumference, cm	96.63 ± 7.90	94.41 ± 5.52	0.292	0.572
Hip circumference, cm	103.43 ± 6.70	101.07 ± 5.76	0.205	0.423
Waist/hip ratio	0.93 ± 0.48	0.94 ± 0.05	0.942	0.888
Neck circumference, cm	40.01 ± 2.98	40.31 ± 2.70	0.719	0.167
Biochemical characteristic				
SBP, mmHg	126.12 ± 11.90	123.67 ± 15.91	0.524	0.209
DBP, mmHg	83.35 (73.00, 90.25)	86.50 (69.00, 90.25)	0.713	0.654
ALT, U/L	67.80 (33.20, 100.50)	44.75 (25.28, 76.60)	0.274	0.898
AST, U/L	31.90 (25.00, 47.35)	24.95 (19.95, 32.55)	0.136	0.893
ALT/AST	0.51 (0.41, 0.72)	0.65 (0.48, 0.70)	0.216	0.554
TG, mmol/L	1.81 (1.31, 2.65)	1.64 (1.02, 2.21)	0.524	0.630
TC, mmol/L	5.05 (4.51, 5.76)	4.88 (4.48, 5.52)	0.760	0.602
HDL, mmol/L	1.20 (1.05, 1.30)	1.15 (0.97, 1.36)	0.740	0.596
LDL, mmol/L	2.98 (2.52, 3.44)	2.82 (2.56, 3.47)	0.865	0.838
APOA, g/L	1.44 (1.26, 1.56)	1.36 (1.29, 1.54)	0.879	0.786
APOB, g/L	1.03 (0.86, 1.14)	1.06 (0.92, 1.28)	0.490	0.873
Uric acid, μM	418.61 ± 108.93	361.88 ± 105.75	0.073	0.104
Glucose, mmol/L	5.05 (4.73, 5.98)	5.08 (4.73, 6.34)	0.993	0.539

*Data are expressed as means ± standard deviation (SD) or median (interquartile range) based on the variable distribution. *P_1: P value was adjusted for age, sex, and body mass index. ALT, alanine aminotransferase; APOA, apolipoprotein A; APOB, apolipoprotein B; AST, aspartate aminotransferase; BMI, Body mass index; CHB, chronic hepatitis B; DBP, diastolic blood pressure; HDL, high-density lipoprotein; LDL, low-density lipoprotein; NAFLD, non-alcoholic fatty liver disease; NAFLD + CHB, concurrent non-alcoholic fatty liver disease and chronic hepatitis B; SBP, systolic Blood Pressure; TC, total cholesterol; TG, triglyceride.*

according to the manufacturer's instructions. Each sample was run in duplicate.

Statistical Analysis

EpiData was used for data input and Statistical Package for Social Sciences (SPSS) v23.0 was used for data analysis. Non-normal variables were presented as medians (interquartile range) and compared using the Mann–Whitney *U* test. Quantitative data were presented as means ± standard deviation (SD) if they were normally distributed. A *t*-test was used to compare the means of anthropometric characteristics, biological characteristics, and hepatic DNA methylation levels, based on the CHB status and histological grade of the study population. A one-way analysis of variance was used to compare the levels of hepatic DNA methylation between groups that were stratified by CHB status and histological characteristics. A chi-square test was used to analyze the distribution of liver histological grades between the NAFLD and NAFLD + CHB groups. The relationships between global DNA methylation level and anthropometric characteristics, biological characteristics, and hepatic histological characteristics were analyzed using univariate and multivariate linear regression. $P < 0.05$ was set as the significance threshold.

RESULTS

Baseline Characteristics of the Participants

The anthropometric and biochemical characteristics of the participants, classified based on the presence or absence of CHB, are shown in **Table 1**. After adjusting for age, sex, and BMI, none of the items were found to be significantly different between the NAFLD and NAFLD + CHB groups.

TABLE 2 | Liver pathology of the study population based on the disease status, n (%).

Factor	NAFLD (*n* = 37)	NAFLD + CHB (*n* = 18)	*P**
Steatosis grade			**0.016**
1 (mild)	16 (43.2)	14 (77.8)	
2–3 (moderate)	21 (56.8)	4 (22.2)	
Inflammation grade			0.196
0–1 (mild)	27 (73.0)	10 (55.6)	
2–3 (moderate)	10 (27.0)	8 (44.4)	
Fibrosis grade			0.141
0	18 (48.6)	5 (27.8)	
1–3	19 (51.4)	13 (72.2)	
NAFLD progression			0.282
SS	11 (29.7)	8 (44.4)	
NASH-B	26 (70.3)	10 (55.6)	

**P values in bold indicate a significant difference. CHB, chronic hepatitis B; NAFLD, non-alcoholic fatty liver disease; NAFLD + CHB, concurrent non-alcoholic fatty liver disease and chronic hepatitis B. NAFLD progression based on the NAFLD activity score (NAS), graded as simple steatosis (SS) and steatohepatitis borderline (NASH-B).*

Table 2 shows a comparison of histological assessments between the NAFLD and NAFLD + CHB groups. Fewer patients in the NAFLD + CHB group had moderate steatosis than in the NAFLD group (steatosis grade 2–3). There were no differences in terms of inflammation, fibrosis grade, and NAFLD progression between the two groups. However, after adjusting for anthropometric and biological characteristics, the logistic regression analysis revealed that fibrosis was a risk factor for NAFLD with CHB (OR = 9.723, $P = 0.037$).

Hepatic Global DNA Methylation Levels Based on CHB Status and Histological Characteristics

Compared to NAFLD subjects, the global DNA methylation levels in the livers of NAFLD + CHB patients were significantly reduced, by 34.85% (NAFLD vs. NAFLD + CHB: 4.85 vs. 3.16%, $P = 0.017$). After adjusting for age, sex, and BMI, the difference remained significant ($P = 0.004$) (**Figure 1**). The differences in global DNA methylation levels for each

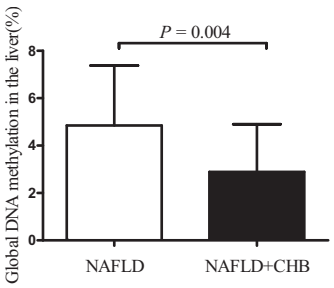

FIGURE 1 | Hepatic global DNA methylation levels based on chronic hepatitis B status. Data are expressed as means with standard deviation (SD). CHB, chronic hepatitis B; NAFLD, non-alcoholic fatty liver disease; NAFLD + CHB, concurrent non-alcoholic fatty liver disease and chronic hepatitis B. *P*-value was adjusted for age, sex, and body mass index.

TABLE 3 | Global DNA methylation levels for each histological grade across the study population.

Factor	Global DNA methylation (%)	*P**
Steatosis grade		0.155
1 (mild)	3.85 ± 2.16	
2-3 (moderate)	4.83 ± 2.91	
Inflammation grade		0.111
0-1 (mild)	4.68 ± 2.72	
2-3 (moderate)	3.51 ± 2.03	
Fibrosis grade		**0.026**
0	5.19 ± 2.59	
1-3	3.65 ± 2.36	
NAFLD progression[#]		0.943
SS	4.33 ± 2.17	
NASH-B	4.28 ± 2.76	

*Data are expressed as means ± standard deviation (SD). *P-values in bold indicate a significant difference. [#]NAFLD progression based on the NAFLD activity score (NAS), graded as simple steatosis (SS) and steatohepatitis borderline (NASH-B).*

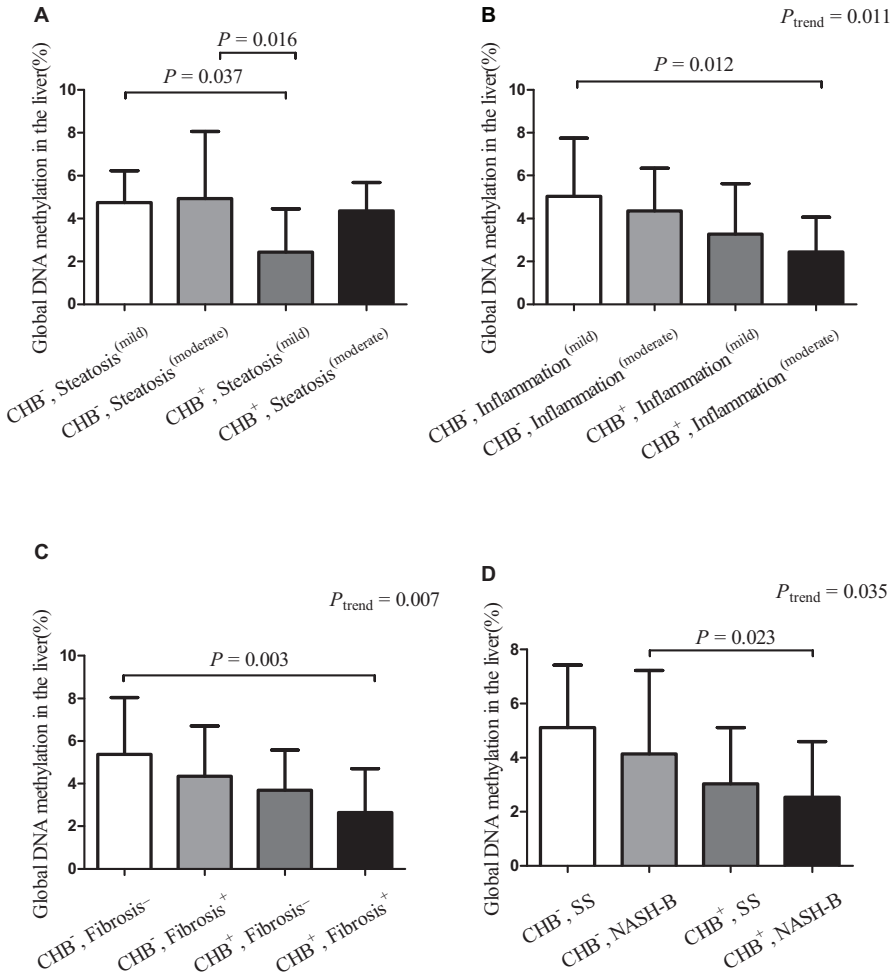

FIGURE 2 | Hepatic global DNA methylation levels in groups stratified by chronic hepatitis B status and histological characteristics*. Data are expressed as means with standard deviation (SD). *Hepatic global DNA methylation levels in groups, which were stratified by chronic hepatitis B status and steatosis grade **(A)**, inflammation grade **(B)**, the presence or absence of fibrosis **(C)**, NAFLD activity score **(D)**. CHB^{-}, non-alcoholic fatty liver disease without chronic hepatitis B; CHB^{+}, concurrent non-alcoholic fatty liver disease and chronic hepatitis B; $Fibrosis^{-}$, without fibrosis; $Fibrosis^{+}$, concurrent with fibrosis; $Inflammation^{(mild)}$, mild inflammation (grades 0 and 1); $Inflammation^{(moderate)}$, moderate inflammation (grades 2 and 3); NASH-B, steatohepatitis borderline; SS, simple steatosis; $Steatosis^{(mild)}$, mild steatosis (grade 1); $Steatosis^{(moderate)}$, moderate steatosis (grades 2 and 3).

histological grade are shown in **Table 3**. Participants with fibrosis had significantly lower levels of global DNA methylation than those without fibrosis (P = 0.026). With respect to steatosis grade, inflammation grade, and NAFLD progression, the global DNA methylation levels were not significantly different between the groups.

Hepatic Global DNA Methylation Levels in the NAFLD and NAFLD+CHB Groups as Stratified by Histological Severity

We further compared the differences in global DNA methylation levels between the NAFLD + CHB and NAFLD groups, which were stratified by histological grade (**Figure 2**). This revealed that the presence of CHB significantly decreased the global DNA methylation levels in subjects with mild steatosis (with both CHB and mild steatosis vs. without CHB and with mild steatosis: 2.82 vs. 4.75%, P = 0.037) (**Figure 2A**). Compared to patients without CHB and with mild inflammation, those with both CHB and concomitant moderate inflammation had lower levels of global DNA methylation (without CHB and with mild inflammation vs. with both CHB and moderate inflammation: 5.03 vs. 2.45%, P = 0.012) (**Figure 2B**). Compared to those without CHB and fibrosis, those with both CHB and fibrosis had lower levels of global DNA methylation (without CHB or fibrosis vs. with both CHB and fibrosis: 5.38 vs. 2.64%, P = 0.003) (**Figure 2C**). The presence of CHB significantly decreased the global DNA methylation levels in subjects with borderline steatohepatitis (with both CHB and borderline steatohepatitis vs. without CHB and with borderline steatohepatitis: 2.72 vs. 4.88%, P = 0.023) (**Figure 2D**). The global DNA methylation levels showed a decreasing trend in

TABLE 4 | Multivariable analysis of global DNA methylation and histological variables in patients after adjusting for anthropometric and biochemical variables.

Variable	Multivariable analysis	
	Global DNA methylation	***P****
CHB and Steatosis		
CHB^-, $Steatosis^{(mild)}$	Reference	–
CHB^-, $Steatosis^{(moderate)}$	−0.01 (−1.81, 1.75)	0.974
CHB^+, $Steatosis^{(mild)}$	−0.56 (−5.14, −1.39)	**0.001**
CHB^+, $Steatosis^{(moderate)}$	0.08 (−2.08, 3.61)	0.589
CHB and Inflammation		
CHB^-, $Inflammation^{(mild)}$	Reference	–
CHB^-, $Inflammation^{(moderate)}$	−0.00 (−2.09, 2.07)	0.992
CHB^+, $Inflammation^{(mild)}$	−0.27 (−3.63, 0.12)	0.066
CHB^+, $Inflammation^{(moderate)}$	−0.38 (−4.88, −0.53)	**0.016**
CHB and Fibrosis		
CHB^-, $Fibrosis^-$	Reference	–
CHB^-, $Fibrosis^+$	−0.29 (−3.41, 0.29)	0.094
CHB^+, $Fibrosis^-$	−0.21 (−4.53, 0.86)	0.175
CHB^+, $Fibrosis^+$	−0.55 (−5.15, −1.40)	**0.001**
CHB and NAFLD progression		
CHB^-, SS	Reference	–
CHB^-, NASH-B	0.02 (−1.91, 2.15)	0.907
CHB^+, SS	−0.28 (−4.40, 0.46)	0.108
CHB^+, NASH-B	−0.32 (−4.54, 0.31)	0.085

*Data are expressed as beta (95% CI). *P-values in bold indicate a significant difference. CHB^-, non-alcoholic fatty liver disease without chronic hepatitis B; CHB^+, concurrent non-alcoholic fatty liver disease and chronic hepatitis B; $Fibrosis^-$, without fibrosis; $Fibrosis^+$, concurrent with fibrosis; $Inflammation^{(mild)}$, mild inflammation (grades 0 and 1); $Inflammation^{(moderate)}$, moderate inflammation (grades 2 and 3); NASH-B, steatohepatitis borderline; SS, simple steatosis; $Steatosis^{(mild)}$, mild steatosis (grade 1); $Steatosis^{(moderate)}$, moderate steatosis (grades 2 and 3).*

the presence of co-occurrent CHB and inflammation progression (P_{trend} = 0.011), co-occurrent CHB and presence of fibrosis (P_{trend} = 0.007), and co-occurrent CHB and NAFLD progression (P_{trend} = 0.035).

The Correlation of Global DNA Methylation Levels With Anthropometric, Biochemical, and Histological Characteristics

Upon conducting univariate regression analysis, we found that BMI was negatively correlated with global genomic methylation levels, although anthropometric and biochemical characteristics did not share this association (**Supplementary Table 1**). **Table 4** shows the results of the multivariate analysis after adjusting for anthropometric and biochemical characteristics. In subjects with mild steatosis, the presence of CHB was negatively associated with global DNA methylation levels when compared to the absence of CHB (reference). The presence of CHB and moderate inflammation was negatively associated with global DNA methylation levels when compared to the group that had no CHB but had mild inflammation (reference). The presence of both CHB and fibrosis was negatively associated with global DNA methylation levels when compared to the absence of both CHB and fibrosis (reference).

DISCUSSION

This is the first study to report that patients with concurrent NAFLD and CHB show significantly lower levels of hepatic global DNA methylation than patients with NAFLD alone. The presence of both CHB and fibrosis was associated with decreased hepatic global DNA methylation levels, compared to those of patients who had neither of these conditions.

DNA methylation is one kind of epigenetic modifications that connect environment and disease. Feeding a methyl donor deficient diet caused loss of global DNA methylation in the livers of rodents and induced hepatic fibrosis and HCC (Tryndyak et al., 2011). DNA hypomethylation was also found in the livers of rodents with fatty liver induce by high fat diet and alcohol (Lu et al., 2000; Wang et al., 2014). On the contrary, methyl donor supplementation could restore the global DNA methylation level and reversed liver injury (Medici et al., 2013). In addition to diet, global DNA hypomethylation can be induced by many carcinogenic chemicals in the cells or livers such as arsenic, chromium (Takiguchi et al., 2003; Chen et al., 2004). Hepatitis infection is another risk factor to induce DNA hypomethylation. *In vivo* studies on human hepatocyte chimeric mouse models have shown that the levels of *LINE-1* methylation in long-term HBV- and HCV-infected mice are lower than those in uninfected control mice (Okamoto et al., 2014). Another *in vivo* study demonstrated that the HBV X protein induces global hypomethylation of satellite-2 repeating sequences (Park et al., 2007). Furthermore, global DNA hypomethylation has been implicated in HBV-exposed HCC patients (Zhang et al., 2013). Similarly, as we observed that the levels of global DNA methylation in NAFLD + CHB patients were lower than those in NAFLD patients.

However, the mechanisms for the decrease in global DNA methylation levels upon the co-occurrence of CHB is not very clear. DNA methylation is a process that transforms 5′-cytosine into 5′-methylcytosine with the adding methyl group from the universal methyl donor-S-adenosylmethionine (SAM). This reaction is catalyzed by a family of enzymes known as DNA methyltransferases (DNMTs). Several possibilities that may contribute to the development of DNA hypomethylation have been proposed. One underlying mechanism is the reduction of methylation capacity because of intracellular depletion of SAM. SAM is an essential and critical methyl donor for cellular transmethylation reactions including DNA, RNA, and histone methylation (Ouyang et al., 2020). Diet low in source of methyl donors, high in fat can lead to global DNA hypomethylation in the livers by impairing synthesis of SAM, which could be reversed by methyl donor supplementation (Medici et al., 2013; Wang et al., 2014; Bakir et al., 2019). However, the change of one-carbon metabolism in HBV is still unclear. The other mechanism is the changes in DNMTs expression and/or activity. HBV-induced aberrant global DNA hypomethylation is associated with the reduced expression

of genes *DNMT1* and *DNMT3b* (Park et al., 2007; Huang et al., 2010). Aside from regulating the transcription of *DNMT* genes, HBV also affects the capacity of these genes to bind their corresponding regulatory elements. A study using chromatin immunoprecipitation assays showed that HBV partially or completely abrogates *DNMT3a* binding to target gene promoters, contaminant with a decreased DNA methylation in regulatory elements (Zheng et al., 2009). Therefore, the global DNA hypomethylation of NAFLD patients with CHB may be associated with downregulated expression and activity of DNMTs. The DNA integrity is another critical factor that affects the normal status of DNA methylation (Pogribny and Beland, 2009). Diminished methylation capacity of DNA methyltransferases, leading to DNA hypomethylation can be induced by the presence of unrepaired lesions in DNA, such as 8-oxoguanine and 5-hydroxymethylcytosine (Pogribny and Beland, 2009). It has been reported that diet-induced NAFLD is associated with revisable 5-hydroxymethylcytosine change in the liver (Lyall et al., 2020). While the effect of HBV on genome integrity has not been reported yet.

Our study found that the presence of both CHB and fibrosis in NAFLD patients significantly reduced global DNA methylation levels compared to those in the absence of both conditions. After adjusting for anthropometric and biochemical characteristics, the presence of CHB and fibrosis was negatively associated with global DNA methylation levels in the liver. Hepatic global DNA methylation level is reduced in animal liver fibrosis models induced by a methionine-choline-deficient diet and intraperitoneal injection of CCl_4 (Tryndyak et al., 2011; Komatsu et al., 2012; Page et al., 2016). In addition, DNA hypomethylation has been observed in the blood of advanced biliary atresia patients with severe fibrosis, compared to those with mild fibrosis (Udomsinprasert et al., 2016). The above data from our study and others indicated that DNA hypomethylation may be involved in the pathological progress of liver diseases. While there is no consensus on how DNA hypomethylation promotes the development of disease. Generally, molecular mechanisms of global hypomethylation on adverse outcome may be attributed to the dysregulation of chromosomal abnormalities, and genomic instability. First, global DNA hypomethylation may lead to chromosomal abnormalities. Demethylation of repetitive sequences located at centromeric, pericentromeric, and subtelomeric chromosomal regions may cause the induction of chromosomal abnormalities (Pogribny and Beland, 2009). It has been reported that DNA hypomethylation in HCCs is clearly associated with the amount of chromosomal alterations (Nishida et al., 2013). Second, global DNA hypomethylation may promote chromosomal instability (CIN), which has been proved to be mediated by DNA damage. The increase of DNA strand breaks precedes DNA hypomethylation (James et al., 2003), and DNA damage is a precursor of mutation (Patchsung et al., 2018) and can lead to related pathological findings. In addition, global DNA hypomethylation can also lead to chromosome fragility, which in turn leads to CIN in HCC (Nishida et al., 2013). For example, global DNA hypomethylation promotes early liver tumor formation by leading to aneuploidy, chromosome translocation and copy number changes in HCC mouse models, human hepatoma cell lines (Yamada et al., 2005; Tryndyak et al., 2011; Komatsu et al., 2012; Udomsinprasert et al., 2016).

There are several limitations to the present study. First, the number of subjects was relatively small, leading to lack of power to determine the statistical differences in global DNA methylation levels between different groups. Second, the data were obtained from cross-sectional analyses, and we therefore could not detect the causal relationship between global DNA methylation and HBV infection or pathological changes. Third, this is an association study, so we cannot sum up the causes, mechanisms and consequences by itself. Whether or not there is an association between changes in DNA-methylation and gene expression remains unclear and should be investigated in following studies.

Despite the limitations of this study, we have assessed the level of global DNA methylation in patients who are affected by both NAFLD and CHB, which are rarely involved in previous studies. We also evaluated the association between global DNA hypomethylation and liver pathology. As the overexpression of oncogenes caused by DNA hypomethylation may play an important role in tumorigenesis (Good et al., 2018), global DNA methylation could be used to characterize the epigenetic characteristics of these patients. Our data also provide a theoretical basis for further investigations into the epigenetics of chronic liver disease.

In conclusion, our study shows that patients with concurrent NAFLD and CHB exhibited lower levels of global DNA methylation than patients with NAFLD alone. The co-occurrence of CHB and liver fibrosis in NAFLD patients was associated with a decrease in global DNA methylation levels. Our findings provide new insights into the epigenetic events underpinning NAFLD + CHB and may provide the basis for new research into specific epigenetic modifications mediated by virus.

DATA AVAILABILITY STATEMENT

The raw data supporting the conclusions of this article will be made available by the authors, without undue reservation.

ETHICS STATEMENT

The studies involving human participants were reviewed and approved by the Medical Ethics Committee of the School of Public Health, Sun Yat-sen University (SYSU) approved the study protocol (Project identification code: [2012] No. 17). The patients/participants provided their written informed consent to participate in this study. Written informed consent was obtained from the individual(s) for the publication of any potentially identifiable images or data included in this article.

AUTHOR CONTRIBUTIONS

FYL and LJW designed the research study, analyzed the data, and wrote the manuscript. QO, ZWL, LZP, XYC, LRW, LQS, XPL,

YYW, HX, JW, and FW performed the research and collected liver biopsy and other biological samples. HLZ was acting as the submission's guarantor and revised the manuscript. All authors approved the final version of the article, including the authorship list.

FUNDING

This work was supported in part by the National Natural Science Foundation of China (Grant Number: 81803212) and Natural Science Foundation of Guangdong Province (Grant Number: 2018030310464).

SUPPLEMENTARY MATERIAL

The Supplementary Material for this article can be found online at: https://www.frontiersin.org/articles/10.3389/fgene.2021.671552/full#supplementary-material

Supplementary Table 1 | Univariate analysis of global DNA methylation and anthropometric, biochemical characteristics and histological variables in patients.

REFERENCES

Amir, F. G., Alpana Waghmare, E., and Jaenisch, R. (2012). Chromosomal instability and tumors promoted by DNA hypomethylation. *Science* 300, 455–455. doi: 10.1126/science.1083557

Bakir, M., Salama, M., Refaat, R., Ali, M., Khalifa, E., and Kamel, M. (2019). Evaluating the therapeutic potential of one-carbon donors in nonalcoholic fatty liver disease. *Eur. J. Pharmacol.* 847, 72–82. doi: 10.1016/j.ejphar.2019.01.039

Chan, A. W., Wong, G. L., Chan, H. Y., Tong, J. H., Yu, Y. H., Choi, P. C., et al. (2017). Concurrent fatty liver increases risk of hepatocellular carcinoma among patients with chronic hepatitis B. *J. Gastroenterol. Hepatol.* 32, 667–676. doi: 10.1111/jgh.13536

Chan, T. T., Chan, W. K., Wong, G. L., Chan, A. W., Nik Mustapha, N. R., Chan, S. L., et al. (2020). Positive hepatitis B core antibody is associated with cirrhosis and hepatocellular carcinoma in nonalcoholic fatty liver disease. *Am. J. Gastroenterol.* 115, 867–875. doi: 10.14309/ajg.0000000000000588

Chen, H., Li, S., Liu, J., Diwan, B., Barrett, J., and Waalkes, M. (2004). Chronic inorganic arsenic exposure induces hepatic global and individual gene hypomethylation: implications for arsenic hepatocarcinogenesis. *Carcinogenesis* 25, 1779–1786. doi: 10.1093/carcin/bgh161

Chen, Y. M., Liu, Y., Liu, Y. H., Wang, X., Guan, K., and Zhu, H. L. (2015). Higher serum concentrations of betaine rather than choline is associated with better profiles of DXA-derived body fat and fat distribution in Chinese adults. *Int. J. Obes.* 39, 465–471. doi: 10.1038/ijo.2014.158

Estes, C., Anstee, Q. M., Arias-Loste, M. T., Bantel, H., Bellentani, S., Caballeria, J., et al. (2018). Modeling NAFLD disease burden in China, France, Germany, Italy, Japan, Spain, United Kingdom, and United States for the period 2016-2030. *J. Hepatol.* 69, 896–904. doi: 10.1016/j.jhep.2018.05.036

Good, C. R., Panjarian, S., Kelly, A. D., Madzo, J., Patel, B., Jelinek, J., et al. (2018). TET1-mediated hypomethylation activates oncogenic signaling in triple-negative breast cancer. *Cancer Res.* 78, 4126–4137. doi: 10.1158/0008-5472.can-17-2082

Huang, J., Wang, Y., Guo, Y., and Sun, S. (2010). Down-regulated microRNA-152 induces aberrant DNA methylation in hepatitis B virus-related hepatocellular carcinoma by targeting DNA methyltransferase 1. *Hepatology* 52, 60–70. doi: 10.1002/hep.23660

James, S., Pogribny, I., Pogribna, M., Miller, B., Jernigan, S., and Melnyk, S. (2003). Mechanisms of DNA damage, DNA hypomethylation, and tumor progression in the folate/methyl-deficient rat model of hepatocarcinogenesis. *J. Nutr.* 133, 3740S–3747S.

Kleiner, D. E., Brunt, E. M., Van Natta, M., Behling, C., Contos, M. J., Cummings, O. W., et al. (2005). Design and validation of a histological scoring system for nonalcoholic fatty liver disease. *Hepatology* 41, 1313–1321. doi: 10.1002/hep.20701

Komatsu, Y., Waku, T., Iwasaki, N., Ono, W., Yamaguchi, C., and Yanagisawa, J. (2012). Global analysis of DNA methylation in early-stage liver fibrosis. *BMC Med. Genomics* 5:5.

Lai, Z., Chen, J., Ding, C., Wong, K., Chen, X., Pu, L., et al. (2020). Association of hepatic global DNA methylation and serum one-carbon metabolites with histological severity in patients with NAFLD. *Obesity* 28, 197–205. doi: 10.1002/oby.22667

Lee, S., Lee, Y., Bae, J., Choi, J., Tayama, C., Hata, K., et al. (2014). HBx induces hypomethylation of distal intragenic CpG islands required for active expression of developmental regulators. *Proc. Natl. Acad. Sci. U.S.A.* 111, 9555–9560. doi: 10.1073/pnas.1400604111

Lok, A. S., Zoulim, F., Dusheiko, G., and Ghany, M. G. (2017). Hepatitis B cure: from discovery to regulatory approval. *Hepatology* 66, 1296–1313. doi: 10.1002/hep.29323

Loomba, R., and Sanyal, A. J. (2013). The global NAFLD epidemic. *Nat. Rev. Gastroenterol. Hepatol.* 10, 686–690. doi: 10.1038/nrgastro.2013.171

Lu, S., Huang, Z., Yang, H., Mato, J., Avila, M., and Tsukamoto, H. (2000). Changes in methionine adenosyltransferase and S-adenosylmethionine homeostasis in alcoholic rat liver. *Am. J. Physiol. Gastrointest. Liver Physiol.* 279, G178–G185.

Lyall, M. J., Thomson, J. P., Cartier, J., Ottaviano, R., Kendall, T. J., Meehan, R. R., et al. (2020). Non-alcoholic fatty liver disease (NAFLD) is associated with dynamic changes in DNA hydroxymethylation. *Epigenetics* 15, 61–71. doi: 10.1080/15592294.2019.1649527

Medici, V., Shibata, N., Kharbanda, K., LaSalle, J., Woods, R., Liu, S., et al. (2013). Wilson's disease: changes in methionine metabolism and inflammation affect global DNA methylation in early liver disease. *Hepatology* 57, 555–565. doi: 10.1002/hep.26047

Murphy, S. K., Yang, H., Moylan, C. A., Pang, H., Dellinger, A., Abdelmalek, M. F., et al. (2013). Relationship between methylome and transcriptome in patients with nonalcoholic fatty liver disease. *Gastroenterology* 145, 1076–1087. doi: 10.1053/j.gastro.2013.07.047

Nishida, N., Kudo, M., Nishimura, T., Arizumi, T., Takita, M., Kitai, S., et al. (2013). Unique association between global DNA hypomethylation and chromosomal alterations in human hepatocellular carcinoma. *PLoS One* 8:e72312. doi: 10.1371/journal.pone.0072312

Okamoto, Y., Shinjo, K., Shimizu, Y., Sano, T., Yamao, K., Gao, W., et al. (2014). Hepatitis virus infection affects DNA methylation in mice with humanized livers. *Gastroenterology* 146, 562–572. doi: 10.1053/j.gastro.2013.10.056

Ouyang, Y., Wu, Q., Li, J., Sun, S., and Sun, S. (2020). S-adenosylmethionine: a metabolite critical to the regulation of autophagy. *Cell Prolif.* 53:e12891.

Page, A., Paoli, P., Moran Salvador, E., White, S., French, J., and Mann, J. (2016). Hepatic stellate cell transdifferentiation involves genome-wide remodeling of the DNA methylation landscape. *J. Hepatol.* 64, 661–673. doi: 10.1016/j.jhep.2015.11.024

Park, I. Y., Sohn, B. H., Yu, E., Suh, D. J., Chung, Y. H., Lee, J. H., et al. (2007). Aberrant epigenetic modifications in hepatocarcinogenesis induced by hepatitis B virus X protein. *Gastroenterology* 132, 1476–1494. doi: 10.1053/j.gastro.2007.01.034

Patchsung, M., Settayanon, S., Pongpanich, M., Mutirangura, D., Jintarith, P., and Mutirangura, A. (2018). Alu siRNA to increase Alu element methylation and prevent DNA damage. *Epigenomics* 10, 175–185. doi: 10.2217/epi-2017-0096

Pogribny, I., and Beland, F. (2009). DNA hypomethylation in the origin and pathogenesis of human diseases. *Cell. Mol. Life Sci.* 66, 2249–2261. doi: 10.1007/s00018-009-0015-5

Shen, J., Wang, S., Zhang, Y. J., Kappil, M., Wu, H. C., Kibriya, M. G., et al. (2012). Genome-wide DNA methylation profiles in hepatocellular carcinoma. *Hepatology* 55, 1799–1808. doi: 10.1002/hep.25569

Takiguchi, M., Achanzar, W., Qu, W., Li, G., and Waalkes, M. (2003). Effects of cadmium on DNA-(Cytosine-5) methyltransferase activity

and DNA methylation status during cadmium-induced cellular transformation. *Exp. Cell Res.* 286, 355–365. doi: 10.1016/s0014-4827(03)00062-4

Tao, L., Wang, W., Li, L., Kramer, P., and Pereira, M. (2005). DNA hypomethylation induced by drinking water disinfection by-products in mouse and rat kidney. *Toxicol. Sci.* 87, 344–352. doi: 10.1093/toxsci/kfi257

Tryndyak, V. P., Han, T., Muskhelishvili, L., Fuscoe, J. C., Ross, S. A., Beland, F. A., et al. (2011). Coupling global methylation and gene expression profiles reveal key pathophysiological events in liver injury induced by a methyl-deficient diet. *Mol. Nutr. Food Res.* 55, 411–418. doi: 10.1002/mnfr.201000300

Udomsinprasert, W., Kitkumthorn, N., Mutirangura, A., Chongsrisawat, V., Poovorawan, Y., and Honsawek, S. (2016). Global methylation, oxidative stress, and relative telomere length in biliary atresia patients. *Sci. Rep.* 6:26969.

Wang, L. J., Zhang, H. W., Zhou, J. Y., Liu, Y., Yang, Y., Chen, X. L., et al. (2014). Betaine attenuates hepatic steatosis by reducing methylation of the MTTP promoter and elevating genomic methylation in mice fed a high-fat diet. *J. Nutr. Biochem.* 25, 329–336. doi: 10.1016/j.jnutbio.2013.11.007

Wu, H. C., Wang, Q., Yang, H. I., Tsai, W. Y., Chen, C. J., and Santella, R. M. (2012). Global DNA methylation levels in white blood cells as a biomarker for hepatocellular carcinoma risk: a nested case-control study. *Carcinogenesis* 33, 1340–1345. doi: 10.1093/carcin/bgs160

Yamada, Y., Jackson-Grusby, L., Linhart, H., Meissner, A., Eden, A., Lin, H., et al. (2005). Opposing effects of DNA hypomethylation on intestinal and liver carcinogenesis. *Proc. Natl. Acad. Sci. U.S.A.* 102, 13580–13585. doi: 10.1073/pnas.0506612102

Younossi, Z. M., Otgonsuren, M., Henry, L., Venkatesan, C., Mishra, A., Erario, M., et al. (2015). Association of nonalcoholic fatty liver disease (NAFLD) with hepatocellular carcinoma (HCC) in the United States from 2004 to 2009. *Hepatology* 62, 1723–1730. doi: 10.1002/hep.28123

Zeybel, M., Vatansever, S., Hardy, T., Sari, A. A., Cakalagaoglu, F., Avci, A., et al. (2016). DNA methylation profiling identifies novel markers of progression in hepatitis B-related chronic liver disease. *Clin. Epigenet.* 8, 48.

Zhang, C., Fan, L., Fan, T., Wu, D., Gao, L., Ling, Y., et al. (2013). Decreased PADI4 mRNA association with global hypomethylation in hepatocellular carcinoma during HBV exposure. *Cell Biochem. Biophys.* 65, 187–195. doi: 10.1007/s12013-012-9417-3

Zheng, D. L., Zhang, L., Cheng, N., Xu, X., Deng, Q., Teng, X. M., et al. (2009). Epigenetic modification induced by hepatitis B virus X protein via interaction with de novo DNA methyltransferase DNMT3A. *J. Hepatol.* 50, 377–387. doi: 10.1016/j.jhep.2008.10.019

Conflict of Interest: The authors declare that the research was conducted in the absence of any commercial or financial relationships that could be construed as a potential conflict of interest.

frontiers in Cell and Developmental Biology

ORIGINAL RESEARCH
published: 21 July 2021
doi: 10.3389/fcell.2021.702579

Changes in N6-Methyladenosine Modification Modulate Diabetic Cardiomyopathy by Reducing Myocardial Fibrosis and Myocyte Hypertrophy

Wenhao Ju[1,2,3†], Kai Liu[2,3,4†], Shengrong Ouyang[2,3], Zhuo Liu[2,3], Feng He[2,3] and Jianxin Wu[1,2,3,5]*

[1] Graduate School, Peking Union Medical College, Beijing, China, [2] Department of Biochemistry and Immunology, Capital Institute of Pediatrics, Beijing, China, [3] Beijing Municipal Key Laboratory of Child Development and Nutriomics, Beijing, China, [4] Department of Biochemistry & Immunology, Capital Institute of Pediatrics-Peking University Teaching Hospital, Beijing, China, [5] Beijing Tongren Hospital, Capital Medical University, Beijing, China

OPEN ACCESS

Edited by:
Zhihua Wang,
Chinese Academy of Medical Sciences and Peking Union Medical College, China

Reviewed by:
Haojian Zhang,
Wuhan University, China
Ang Guo,
North Dakota State University, United States

***Correspondence:**
Jianxin Wu
cipbiolab@163.com

[†] These authors have contributed equally to this work

Specialty section:
This article was submitted to Epigenomics and Epigenetics, a section of the journal Frontiers in Cell and Developmental Biology

Received: 29 April 2021
Accepted: 21 June 2021
Published: 21 July 2021

Citation:
Ju W, Liu K, Ouyang S, Liu Z, He F and Wu J (2021) Changes in N6-Methyladenosine Modification Modulate Diabetic Cardiomyopathy by Reducing Myocardial Fibrosis and Myocyte Hypertrophy. Front. Cell Dev. Biol. 9:702579. doi: 10.3389/fcell.2021.702579

In this study, we aimed to systematically profile global RNA N6-methyladenosine (m^6A) modification patterns in a mouse model of diabetic cardiomyopathy (DCM). Patterns of m^6A in DCM and normal hearts were analyzed via m^6A-specific methylated RNA immunoprecipitation followed by high-throughput sequencing (MeRIP-seq) and RNA sequencing (RNA-seq). m^6A-related mRNAs were validated by quantitative real-time PCR analysis of input and m^6A immunoprecipitated RNA samples from DCM and normal hearts. A total of 973 new m^6A peaks were detected in DCM samples and 984 differentially methylated sites were selected for further study, including 295 hypermethylated and 689 hypomethylated m^6A sites (fold change (FC) > 1.5, $P < 0.05$). Gene ontology (GO) and Kyoto Encyclopedia of Genes and Genomes (KEGG) Pathway analyses indicated that unique m^6A-modified transcripts in DCM were closely linked to cardiac fibrosis, myocardial hypertrophy, and myocardial energy metabolism. Total m^6A levels were higher in DCM, while levels of the fat mass and obesity-associated (FTO) protein were downregulated. Overexpression of FTO in DCM model mice improved cardiac function by reducing myocardial fibrosis and myocyte hypertrophy. Overall, m^6A modification patterns were altered in DCM, and modification of epitranscriptomic processes, such as m^6A, is a potentially interesting therapeutic approach.

Keywords: diabetic cardiomyopathy, m^6A, myocardial fibrosis, FTO, myocyte hypertrophy

INTRODUCTION

There are more than 450 million patients with diabetes worldwide, and by 2045 this number is predicted to increase to 693 million (Cho et al., 2018). Cardiovascular disease accounts for 50.3% of total deaths of patients with diabetes (Einarson et al., 2018). Diabetes not only increases the risk of heart failure, but also increases the mortality rate from heart failure by 2.5 times (Tan et al., 2020). Diabetic cardiomyopathy (DCM) is a metabolic cardiovascular disease

resulting in decreased myocardial glucose consumption, modestly increased ketone metabolism, and significantly increased utilization of fatty acids (Ritchie and Abel, 2020; Tan et al., 2020). The main features of DCM are myocardial hypertrophy, cardiac fibrosis, coronary microvascular dysfunction, left ventricular enlargement, and weakened ventricular wall motion (Ritchie and Abel, 2020); however, the causal relationships among these complications are not clear. To date, therapies for DCM are limited and cannot prevent the eventual development of the disease. Therefore, additional treatment options are needed.

Although multiple aspects of epigenetic regulation, from DNA modification to protein modification, have been extensively studied in DCM, the role of RNA modification in the regulation of gene expression is just beginning to be elucidated (Gluckman et al., 2009; Zhang et al., 2018). The most pervasive internal mRNA modification is m^{6}A methylation, which affects RNA metabolism throughout its life cycle (Nachtergaele and He, 2018). The m^{6}A methyltransferase complex consists of at least three components, METTL3, METTL14, and WTAP, and m^{6}A is catalyzed by a core writer complex, comprising the catalytic enzyme, METTL3, and is its allosteric activator, METTL14 (Wang P. et al., 2016; Wang X. et al., 2016). WTAP, a mammalian splicing factor, is an indispensable component of the m^{6}A methyltransferase complex; it does not have methyltransferase activity, but can interact with METTL3 and METTL14 to influence cellular m^{6}A deposition (Liu et al., 2014). In addition to this core complex, a writer complex, comprising VIRMA, RBM15 or RBM15B, and ZC3H3 subunits, has been identified (Patil et al., 2016; Wen et al., 2018; Yue et al., 2018). The m^{6}A modification is dynamic and can be demethylated by FTO and ALKBH5 (Jia et al., 2011; Zheng et al., 2013; Mauer et al., 2017; Wei et al., 2018). FTO was the first m^{6}A demethylase to be discovered (Jia et al., 2011) and it can demethylate internal m^{6}A, cap m^{6}Am, and tRNA m^{1}A (Wei et al., 2018), whereas ALKBH5 specifically demethylates m^{6}A by affecting RNA metabolism and mRNA export (Zheng et al., 2013). In addition, RNA-binding proteins that bind to m^{6}A modification sites are regarded as m^{6}A readers, which regulate the functions of m^{6}A-modified RNAs through various mechanisms. YTH domain-containing proteins bind to RNA in an m^{6}A-dependent manner (Li et al., 2014; Zhu et al., 2014). YTHDC1 is predominantly expressed in the nucleus, where it regulates mRNA splicing (Roundtree and He, 2016). YTHDC2 expresses in nuclear and cytosolic and promotes translation (Wojtas et al., 2017). The family of cytosolic YTHDF proteins includes YTHDF1, YTHDF2, and YTHDF3 (Du et al., 2016; Shi et al., 2017; Patil et al., 2018). YTHDF1 can facilitate the translation of m^{6}A-modified mRNAs alongside translation initiation factors, YTHDF2 can cause degradation of m^{6}A-containing RNAs, and YTHDF3 can facilitate both translation and degradation functions (Du et al., 2016; Shi et al., 2017; Patil et al., 2018). Besides the YTH domain-containing proteins, HNRNPA2B1, HNRNPC, HNRNPG, and IGF2BP1-3 have also been reported to preferentially bind to m^{6}A-modified mRNAs (Alarcon et al., 2015a; Liu et al., 2015, 2017; Edupuganti et al., 2017; Huang et al., 2018).

The development of methods for analysis of genome-wide m^{6}A topology has allowed extensive study of m^{6}A-dependent regulation of RNA fate and function (Wang X. et al., 2014; Wang Y. et al., 2014; Alarcon et al., 2015b; Wang X. et al., 2015). Two independent studies reported m^{6}A RNA methylomes in mammalian genomes for the first time using an m^{6}A-specific methylated RNA immunoprecipitation approach, followed by high-throughput sequencing (MeRIP-seq) (Dominissini et al., 2012; Meyer et al., 2012). Emerging evidence indicates that m^{6}A modification is associated with normal biological processes and with the initiation and progression of different types of heart disease (Dorn et al., 2019; Kmietczyk et al., 2019; Mathiyalagan et al., 2019; Mo et al., 2019; Song et al., 2019; Berulava et al., 2020; Gao et al., 2020; Kruger et al., 2020; Lin et al., 2020).

Dysregulation of m^{6}A is associated with cardiac homeostasis and diseases, such as cardiac hypertrophy, cardiac remodeling, myocardial infarction, and heart failure (Dorn et al., 2019; Mathiyalagan et al., 2019; Mo et al., 2019; Song et al., 2019; Berulava et al., 2020; Gao et al., 2020; Lin et al., 2020); however, the transcriptome-wide distribution of m^{6}A in DCM remains largely unknown. In this study, we report the m^{6}A-methylation profiles of heart tissue samples from a db/db mice which is a well-established DCM model for diabetic complications and normal control mice (db/ +), and demonstrate highly diverse m^{6}A-modified patterns in the two groups. We show that abnormal m^{6}A RNA modifications in DCM likely modulate cardiac fibrosis, myocardial hypertrophy, and myocardial energy metabolism. Our results provide evidence that m^{6}A modification is closely associated with DCM pathogenesis, and will facilitate further investigations of the potential targeting of m^{6}A modification in DCM therapy.

MATERIALS AND METHODS

Animals

This study was approved by the Ethics Committee of the Capital Institute of Pediatrics with the permit number: DWLL2019003. All procedures performed in the study complied with the relevant ethical standards. Leptin receptor-deficient (db/db) mice and control mice (db/ +) were purchased from Shanghai Model Organisms Center, which genetic background is C57BL/6J. All mice were used for experiments at 8–12 weeks old and were housed in constant 24 degrees cages with a 12 h alternating light/dark cycle and free access to water and food. To construct a diabetic heart disease model (DCM), mice were continuously fed to 24 weeks of age, then euthanized, hearts collected in 1.5 ml RNase-free centrifuge tubes, immediately immersed in liquid nitrogen to prevent RNA degradation, and finally stored at −80°C. Five pairs of db/db and db/ + heart samples were selected for RNA sequencing, and the remaining samples were saved for validation.

Echocardiographic Assessment

Echocardiographic evaluation was blinded and conducted using a Vevo 2100 imaging system to the mouse at 24 weeks age, with two-dimensional guided M-mode image used to

determine left ventricle size at papillary muscle level in the parasternal views (short axis and long axis), and calculate ejection fractions (EF) and fractional shortening (FS) by using standard equations (EF = (EDV-ES) × 100%/EDV; FS = (LVEDD-LVESD)/LVEDD × 100%). All measurements were averages from at least three beats.

Western Blotting and Antibodies

Western blotting assays were conducted using standard protocols. In brief, mouse heart tissues were ground in a mortar and pestle under liquid nitrogen, then tissue lysate prepared using RIPA lysis buffer (Beyotime Biotechnology), supplemented with protease inhibitor. Blots were screened using specific antibodies: FTO (ab92821, 1:1,000, Abcam), GAPDH (5174, 1:10,000, CST), and m^{6}A (ab208577, 1:500, Abcam).

Histological Analysis

Mouse hearts were fixed in 4% paraformaldehyde for 12 h. After dehydration in 5% sucrose, samples were embedded in paraffin and hematoxylin and eosin (HE) staining performed on 5 μm thick sections.

In addition, frozen heart tissue samples were cut into 7 μm sections, incubated with wheat germ agglutinin (1:100) in the dark for 1 h, and then washed three times with PBS. DAPI (1:1000) was used to stain cell nuclei (10 min), followed by three washes with PBS. Water-soluble anti-fade mounting medium was dripped onto samples, which were then covered with glass cover slips and observed by confocal microscopy (Leica SP8). The cross-sectional areas of cardiomyocytes were calculated using Image-Pro Plus 6.0 software. To assess cardiac fibrosis, heart sections were stained using the standard Masson's trichrome method.

Overexpression of FTO

Empty adeno-associated virus (AAV-EV) and adeno-associated virus expressing FTO (AAV-FTO) under the control of a heart-specific *cTNT* promoter with an EGFP tag were constructed by Hanbio Biotechnology Ltd (Shanghai, China). The virus titer was approximately 1×10^{12} V.g/ml. At 16 weeks, db/db mice were injected with AAV-EV and AAV-FTO virus, respectively, via a tail vein (120 μ l per mouse).

m^{6}A Dot Blot Assay

TRIzol (Invitrogen) was used to extract total RNA from mouse hearts. For mRNA denaturation, samples were heated at 95°C for 5 min, then immediately chilled on ice. Next, RNA samples were spotted on a positively charged nylon membrane (GE Healthcare) and cross-linked using an 80-degree hybridizer. Uncrosslinked RNA was eluted with PBS containing 0.01% Tween 20 for 5 min, then membranes incubated with anti-m^{6}A antibody (1: 500 in PBS containing 0.01% Tween 20) at 4°C for 12 h after blocking with 5% skim milk (in PBS containing 0.01% Tween 20) for 1 h. Then, membranes were incubated with horseradish peroxidase-conjugated anti-rabbit IgG secondary antibody, gently agitated at room temperature for 1 h, and washed four times with PBS for 10 min, followed by development with chemiluminescence. Methylene blue staining was used to confirm that duplicate dots contained the same amount of total RNA.

MeRIP-Seq

After five 24-week-old mice in each group were euthanized, total RNA samples were harvested from heart tissue specimens and quantified using a NanoDrop ND-1000 (Thermo Fisher Scientific, MA, United States). Then, complete mRNA was obtained by purification using Arraystar Seq-Star^{TM} ploy(A) mRNA Isolation Kit, and broken into fragments of approximately 100 nucleotides by incubation in fragmentation buffer [10 mM Zn^{2+} and 10 mM Tris–HCl (pH7.0)] at 94°C for 5–7 min. RNA fragments containing m^{6}A methylation sites were enriched by immunoprecipitation using anti-m^{6}A antibody (Synaptic Systems, 202003). A KAPA Stranded mRNA-seq Kit (Illumina) was used to construct sequencing libraries of post-enrichment m^{6}A mRNA and input mRNA, which were then subjected to 150 bp paired-end sequencing on the Illumina NovaSeq 6000 platform.

FastQC (v0.11.7) was used for quality inspection of raw sequence data, and original sequence filtered using Trimmomatic (V0.32). Filtered high-quality data were compared with the reference genome (HISAT2 v2.1.0) in the Ensembl database, and exomePeak (v2.13.2) used to identify peaks in each sample and differentially methylated peaks in compared samples. Peaks were annotated according to Ensembl database annotation information, peaks in different regions [5' untranslated region (5'UTR), coding sequences (CDS), and 3' untranslated region (3'UTR)] of each transcript counted in every sample, and the resulting data used for motif analysis with MEME-ChIP software.

mRNA-Seq

After five 24-week-old mice in each group were euthanized, total RNA samples were harvested from heart tissue specimen. RNA concentrations were determined using a NanoDrop ND-1000, and total RNA samples enriched using oligo dT (rRNA removal) and then selected using a KAPA Stranded RNA-Seq Library Prep Kit (Illumina) for library construction. Constructed libraries were quality assessed using an Agilent 2100 Bioanalyzer, and quantified by qPCR. Mixed libraries containing different samples were sequenced using the Illumina NovaSeq 6000 sequencer. Solexa pipeline version 1.8 (Off-Line Base Caller software, version 1.8)

TABLE 1 | The gene-specific qPCR primers used were as follows.

Gene	Forward and reverse primer
MEF2A	F:5′ ACACCCTTAATGAATTGATGAC 3′
	R:5′ CAACATACAGCTTTGGCTTATA 3′
KLF15	F:5′ CATCCTCCAACTTGAACCTGC 3′
	R:5′ GAGGTGGCTGCTCTTGGTGT 3′
BCL2L2	F:5′ GGTCCTAAGAGCTGCCATCC 3′
	R:5′ TCAGCCACTAGAGCCCGTGT 3′
CD36	F:5′ CTTTAGGAGAAGAAATGGTGGT 3′
	R:5′ AATCTTTTGAAATATGCTGTGACT 3′
SLC25A33	F:5′ GAAACAGCGAAGGCCATAGAA 3′
	R:5′ AGCCCAGTAAGCACAAAGGAG 3′

software was used for image processing and base identification. FastQC (v0.11.7) software was applied to evaluate sequencing read quality after adapter removal, Hisat2 (v2.1.0) software for comparison with the reference genome, and StringTie (v1.3.3) software to estimate transcript abundance, with reference to official database annotation information. The Ballgown package in R software was applied to calculate fragments per kilobase of transcript per million mapped reads at the gene and transcript levels, and screen out genes differentially expressed between samples or groups.

MeRIP-qPCR Validation

Five genes with differentially methylated sites according to MeRIP-seq were tested by reverse transcription (RT) qPCR. After total RNA samples were harvested from heart tissue specimen, total RNA were carried out mRNA-specific enrichment and fragmentation through Arraystar Seq-Star TM poly(A) mRNA Isolation Kit (AS-MB-006-01/02). Then the interrupted mRNA fragments were enriched by m^{6}A antibody [Affinity purified anti-m^{6}A rabbit polyclonal antibody (Synaptic Systems, 202003)] and IgG antibody [Dynabeads^{TM} M-280 Sheep Anti-Rabbit IgG (Invitrogen, 11203D)]. Next, we eluted the RNA bound by m^{6}A antibody and IgG antibody, and reverse transcribed into cDNA with random primers. RT-qPCR was performed on the input control and m^{6}A-IP-enriched samples using gene-specific primers (**Table 1**).

Statistical Analysis

All data are from three or more independent experiments and are presented as mean ± standard deviation. Statistical analyses were conducted GraphPad Prism 5.0 software. Comparisons of DCM and normal control (NC) samples were conducted using the paired Student's *t*-test. Differences among three or more groups were assessed by one-way analysis of variance (ANOVA). Differences with $P < 0.05$ were defined as statistically significant.

RESULTS

Cardiac Dysfunction and Myocardial Fibrosis in DCM Are Linked to Changes in Global m^{6}A Levels

Leptin receptor deficient db/db mice are mature animal models of type 2 diabetes mellitus and diabetic cardiomyopathy (DCM). Cardiac hypertrophy and fibrosis are pervasive characteristics in DCM, and are usually present in mice with DCM at the age of 24 weeks (Tan et al., 2020). In our study, db/db mice manifested obvious cardiac hypertrophy, with significantly enlarged hearts, compared with db/ + mice (**Figures 1A,B**), and also had evidently elevated heart weight to tibia length ratios ($n = 5$, $P < 0.001$; **Figure 1C**). Further, db/db mice had clearly increased interstitial fibrosis ($n = 5$, $P < 0.001$; **Figures 1D,E**), as well as markedly elevated cardiomyocyte cross-sectional area ($n = 5$, $P < 0.0001$; **Figures 1F,G**).

To provide further evidence that cardiac function was maladjusted, we performed serial echocardiography in NC and DCM group mice at 24 weeks old. The db/db mice manifested decreased cardiac function at 24 weeks old, and significantly reduced left ventricle ejection fraction (LVEF) and left ventricle fractional shortening (LVFS) compared with NC mice ($n = 5$, $P < 0.0001$; **Figures 1H,I,L**). Furthermore, mice with DCM showed a significantly decreased E to A wave ratio (E/A) compared with the NC group ($n = 5$, $P < 0.0001$; **Figures 1J,K**), indicating that the diastolic function of the heart was abnormal in DCM mice. Blood glucose (BG), triglyceride (TG), and total cholesterol (TC) were also significantly increased in db/db (DCM) mice at 16 weeks compared with db/ + mice (**Supplementary Figure 1**), indicating that db/db mice had abnormal blood glucose and lipid metabolism. Overall, these data demonstrate that we successfully constructed a mouse model of DCM.

Next, to assess global m^{6}A levels in db/db and db/ + mouse hearts, we performed dot blot analysis on heart samples from both groups and found relatively higher total m^{6}A levels in db/db mice than the db/ + mice (**Figures 1M,N**; $P < 0.05$). Therefore, we conducted transcriptome-wide MeRIP-seq and RNA-Seq to generate an m^{6}A-methylation map of DCM.

Transcriptome-Wide MeRIP-Seq Demonstrates Differential m^{6}A Modification Patterns in DCM Compared With NC Mouse Hearts

Diabetic cardiomyopathy hearts had unique m^{6}A modification patterns that differed from those of NC heart samples. We identified 4968 m^{6}A peaks, representing 3,704 gene transcripts, in the DCM group by model-based analysis using exomePeak (v2.13.2) (**Figure 2A**). In the NC group, 5297 m^{6}A peaks were identified, corresponding to 3,863 gene transcripts (**Figure 2A**). We detected 3995 unique m^{6}A peaks and 3230 m^{6}A peaks associated with transcripts in both groups. The DCM heart had 973 new peaks, and 1302 new peaks were absent relative to the NC group. This finding indicates that global m^{6}A modification patterns in the DCM group differed from those in the NC group (474 vs. 633; **Figure 2B**).

Analysis of m^{6}A peak distribution showed that approximately 69.47% of modified genes had an individual m^{6}A-modified peak, and the majority of genes had one to three m^{6}A modification sites (**Figure 2C**). m^{6}A methylation was further mapped using MEME-ChIP software which identified the top consensus motif in m^{6}A peaks as GGACU (**Figure 2D**), which is similar to the previously identified RRACH motif (where R = G or A; A = m^{6}A, and H = U, A, or C) (Dominissini et al., 2012; Meyer et al., 2012).

Within genes, m^{6}A peaks were predominantly distributed in coding sequences (CDS) following the 3' untranslated region (3'UTR) and in the immediate vicinity of the stop codon (**Figure 2E**). Total and unique m^{6}A peaks were analyzed in DCM and NC whole transcriptome data and divided into 5' UTR, transcription start site region (TSS), CDS, stop codon, and 3'UTR regions, based on their locations in RNA transcripts. The major regions of m^{6}A peak enrichment were in CDS, 3'UTR, and

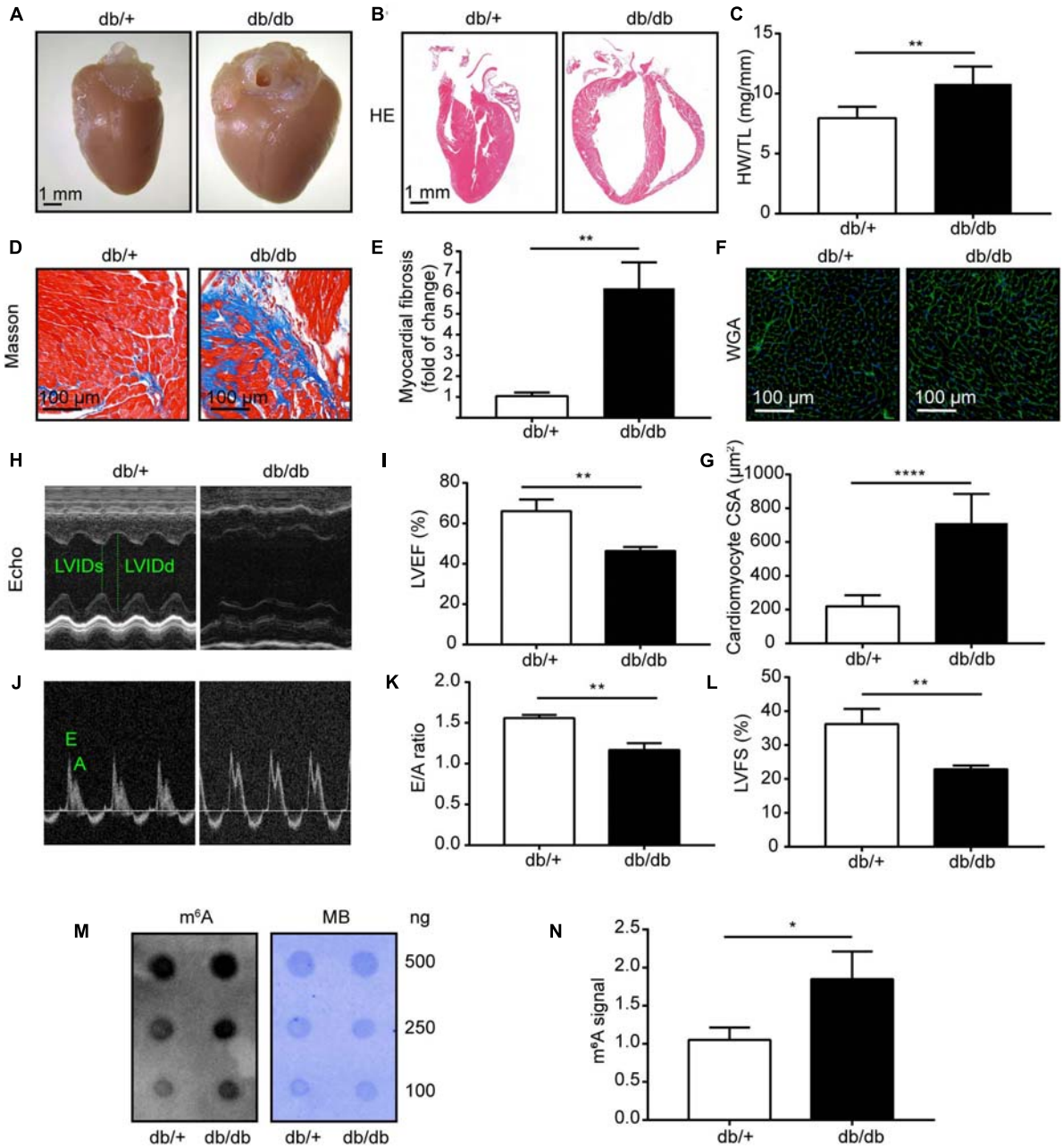

FIGURE 1 | Heart morphology and function were significantly changed in db/db (DCM) mice compared with those in normal control (NC) mice. **(A)** Representative images of hearts from DCM and NC mice. **(B)** Gross morphology of mouse hearts stained with hematoxylin and eosin (HE); scale bar, 1 mm. **(C)** Ratio of heart weight to tibia length. **(D,E)** Representative images of Masson trichrome stained (Masson) hearts and quantitative analysis of interstitial fibrosis; scale bar, 100 μm. **(F,G)** Representative images of wheat germ agglutinin staining (WGA) and quantitative analysis of cardiomyocyte cross-sectional area; scale bar, 100 μm. **(H)** Representative M-mode echocardiography images; left ventricular internal diameter in systole (LVIDs) and left ventricular internal diameter in diastole (LVIDd) are labeled. **(I)** LVEF, left ventricular ejection fraction. **(J,K)** Representative Doppler echocardiography images and E/A ratio. **(L)** LVFS, left ventricular fractional shortening. **(M)** Representative dot blot showing m^{6}A levels in hearts from DCM and NC mice; MB, methylene blue staining. **(N)** Quantification of m^{6}A levels in hearts from DCM and NC mice. DCM, diabetic cardiomyopathy group; NC, normal control group; $n = 5$. Data are presented as mean ± SEM; differences between two groups were analyzed using the Student's *t*-test; $^{****}P < 0.0001$, $^{**}P < 0.01$, $^{*}P < 0.05$ vs. NC.

stop codon vicinity regions (**Figure 2F**), consistent with previous m^{6}A-seq results (Meyer et al., 2012). DCM-unique m^{6}A peaks distributions showed a different pattern from NC-unique peaks, with a relative increase in the m^{6}A residues in CDS regions and a relative decrease in 3' UTR (35.57 vs. 34.14%; 37.71 vs. 40.5%, **Figure 2F**).

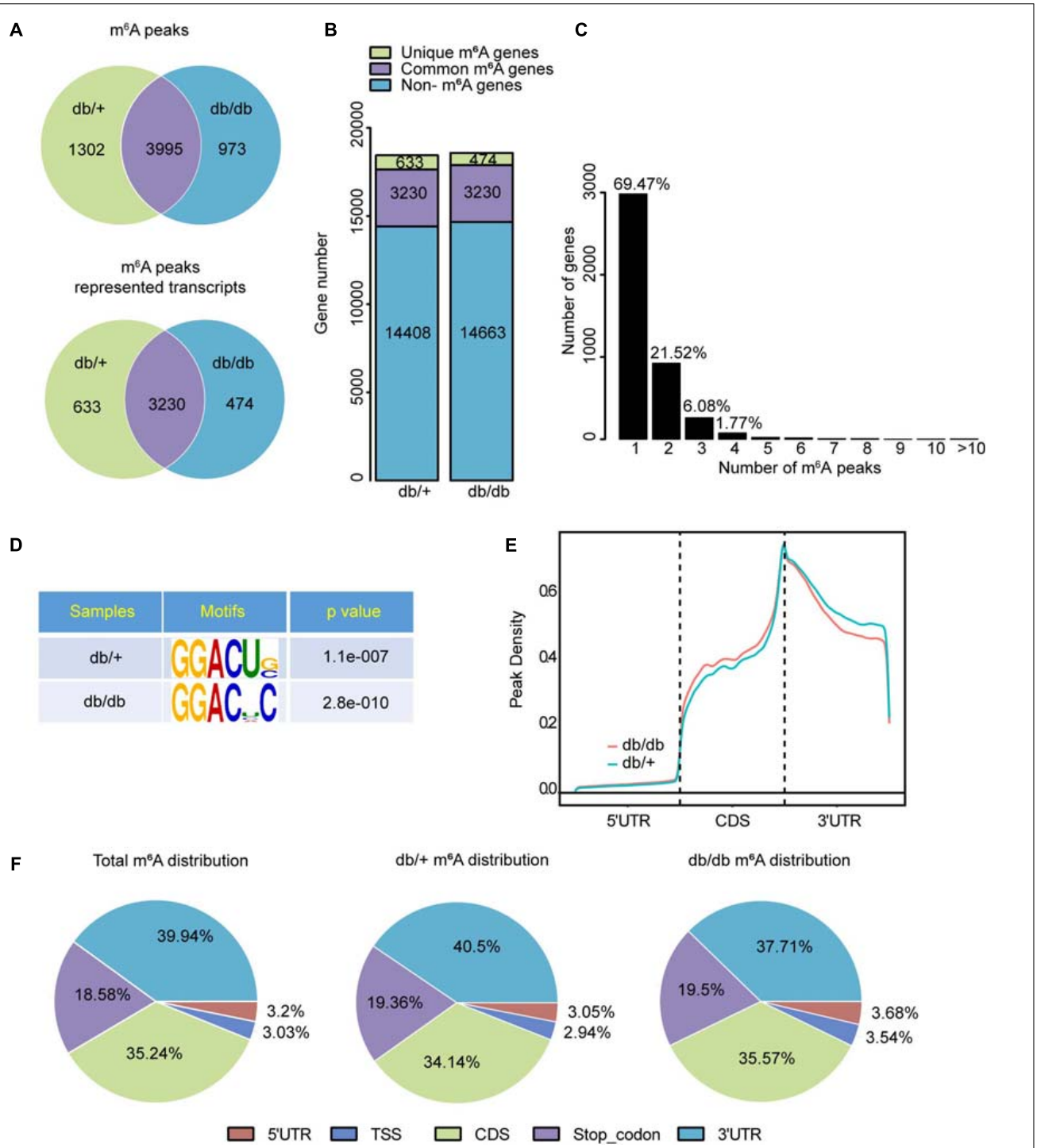

FIGURE 2 | Transcriptome-wide m^{6}A-seq and analysis of m^{6}A peaks. **(A)** Overlap of m^{6}A peaks in db/ + and db/db samples. Identification of m^{6}A peaks using exomePeak; numbers of DCM-unique, control-unique, and common m^{6}A peaks are shown as Venn diagram of m^{6}A peaks representing transcripts in the two groups. **(B)** Summary of m^{6}A-modified genes identified in m^{6}A-seq. **(C)** Distribution of m^{6}A-modified peaks per numbers gene. **(D)** Top m^{6}A motifs enriched from all identified m^{6}A peaks in the two groups. **(E)** Density curve showing the accumulation of differentially methylated m^{6}A peaks in transcripts for the two groups; each transcript is divided into three regions: 5′UTR, CDS, and 3′UTR. **(F)** Proportion of m^{6}A peaks distributed in the indicated regions in the NC and DCM samples; loss of existing m^{6}A peaks (NC-unique peaks) or appearance of new m^{6}A peaks (DCM-unique peaks) in the DCM group.

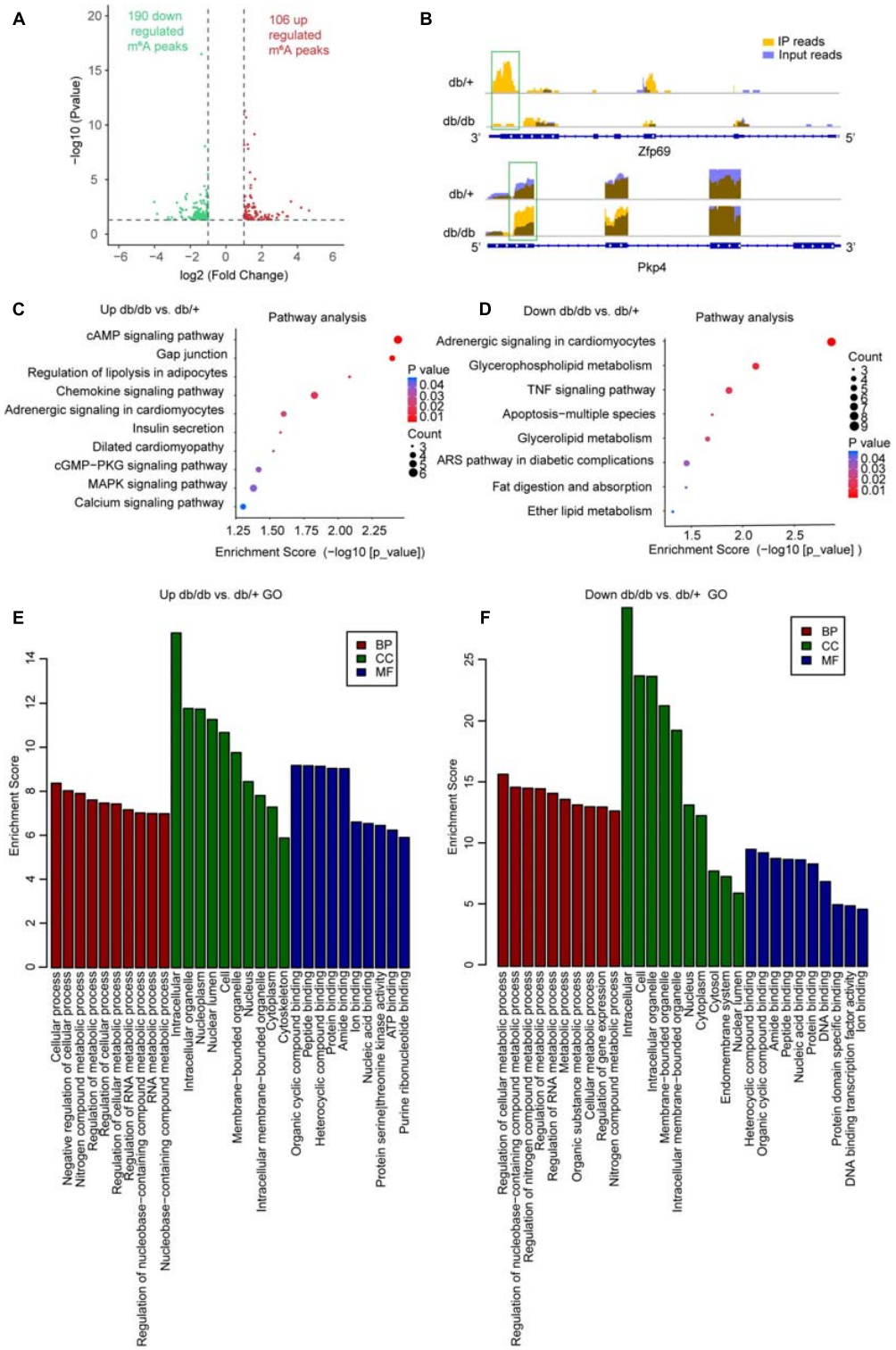

FIGURE 3 | Global m^{6}A modification changes in DCM hearts compared with control heart tissue. **(A)** Identification of 106 hyper-methylated and 190 hypo-methylated m^{6}A peaks that were significantly increased or decreased (fold-change > 2, $P < 0.05$) in abundance, respectively, in the DCM compared with NC samples. **(B)** m^{6}A abundance in *Zfp69* and *Pkp4* mRNA transcripts in the NC and DCM samples, as detected by m^{6}A-seq; m^{6}A peaks in green rectangles showed significantly increased or decreased abundance (fold-change > 2, $P < 0.05$) in the DCM compared with NC samples. **(C–F)** Gene ontology enrichment and pathway analyses of differentially altered m^{6}A mRNA in DCM compared with NC groups; top 10 significantly enriched pathways for upregulated **(C)** and downregulated **(D)** genes; major gene ontology terms significantly enriched for up-methylated **(E)** and down-methylated **(F)** genes. ARS pathway involved in diabetic complications: AGE-RAGE signaling.

Pathways Enriched for Transcripts Differentially m^{6}A Methylated in DCM Are Closely Linked to Cardiac Fibrosis, Myocardial Hypertrophy, and Myocardial Energy Metabolism

Next, we identified differentially methylated transcripts and analyzed them using Gene Ontology (GO), Kyoto Encyclopedia of Genes and Genomes (KEGG) Pathway, and protein interaction network analyses.

We compared the abundance of m^{6}A peaks between NC and DCM samples and found among the 3995 m^{6}A peaks detected in both samples, 984 differentially methylated sites were detected and selected for further study. Among them, 295 hypermethylated and 689 hypomethylated m^{6}A sites were found in the DCM group [fold change (FC) > 1.5, $P < 0.05$; **Figure 3A**]. Differentially methylated sites in both groups showed significantly altered intensity on analysis using Integrative Genomics Viewer (IGV) software. Representative m^{6}A-methylated mRNA peaks in the zinc finger domain transcription factor (*Zfp69*) and plakophilin-4 (*Pkp4*) genes are shown in **Figure 3B** as examples of sites with decreased and increased m^{6}A levels, respectively.

To determine the potential biological significance of changes in m^{6}A methylation associated with DCM, we conducted GO analysis of differentially methylated RNAs. The results revealed that, compared with db/ + mice, hypermethylated and hypomethylated RNAs in db/db mice were particularly associated with metabolism-related terms; for example, regulation of metabolic process, RNA metabolic process, organic substance metabolic process, cellular metabolic process, regulation of gene expression, nucleobase-containing compound, and nitrogen compound metabolic process, indicating that the differentially methylated RNAs were closely associated with metabolism (**Figures 3E,F**). Further, KEGG Pathway analysis of RNAs differentially methylated in DCM were mainly associated with cardiac fibrosis, myocardial hypertrophy, and myocardial energy metabolism; for example, the cAMP signaling pathway, dilated cardiomyopathy, and cGMP-PKG signaling pathway, which are strongly associated with myocardial hypertrophy (**Figures 3C,D**). The chemokine signaling pathway, adrenergic signaling in cardiomyocytes, TNF signaling pathway, and the advanced glycation end products (AGEs)- receptors for AGEs (RAGE) pathway (which is involved in diabetic complications) also appear to be important mechanisms associated with cardiac fibrosis (**Figures 3C,D**). Further, glycerophospholipid metabolism, apoptosis-multiple species, glycerolipid metabolism, fat digestion and absorption, ether lipid metabolism, and the calcium signaling pathway associated with myocardial energy metabolism were enriched among differentially methylated transcripts (**Figures 3C,D**). Overall, our data indicate that these differentially methylated RNAs may be involved in DCM pathogenesis.

Protein interaction network analysis of genes with differentially methylated transcripts was performed using Cytoscape software. BCL2L2, MEF2A, and VEGF-A were the most central proteins, and are particularly associated with the advanced glycation end products (AGEs)-RAGE pathway, which is involved in diabetic complications (**Supplementary Figure 2**). Therefore, these genes and the corresponding signaling pathways are likely of great importance in protein-protein interaction networks and molecular events underlying DCM.

In summary, transcripts with DCM-unique m^{6}A peaks were are closely related to cardiac fibrosis, myocardial hypertrophy, and myocardial energy metabolism, which are major pathological features of left ventricle remodeling in DCM.

Combined Analysis of MeRIP-seq and RNA-Seq Data Reveals That Unique m^{6}A-Modified Transcripts Were Highly Relevant to Left Ventricle Remodeling Pathological Features of DCM

RNA-Seq data showed that 127 mRNAs were significantly dysregulated in DCM samples compared with NCs, including 61 downregulated and 66 upregulated mRNAs (FC > 1.5, $P < 0.05$; **Figure 4A**). Hierarchical clustering analysis of RNA-Seq data showed that the trend in differential gene expression between the groups was consistent among individual samples within each group ($n = 5$ per group) (**Figure 4B**). Further, principal component analysis showed that samples from the DCM and NC groups clustered separately, with only small differences among samples within each group (**Supplementary Figure 3**). Interestingly, GO and KEGG pathway analyses showed that differentially expressed genes were mainly associated with cardiac fibrosis, myocardial hypertrophy, and myocardial energy metabolism (**Supplementary Figures 4A,B, 5A,B**), consistent with involvement in myocardial remodeling pathology (Ritchie and Abel, 2020).

Next, we performed combined analysis of MeRIP-seq and RNA-Seq data to identify target genes that were modified by m^{6}A. We detected 166 hypermethylated m^{6}A peaks within mRNA transcripts, 57 and 109 of which were significantly downregulated and upregulated, respectively (**Figure 4C**). Further, 308 hypomethylated m^{6}A peaks were detected in mRNA transcripts, with 158 and 150 clearly upregulated and downregulated, respectively (**Figure 4C**). The top three ranking genes showing the most distinct changes in m^{6}A and mRNA levels in DCM samples relative to NC in each quadrant of **Figure 4C** are presented in **Table 2**. Comparisons of the whole transcriptome of DCM versus NC, m^{6}A methylated genes were more upregulated than downregulated in DCM. This trends did not exist for non-m^{6}A methylated genes (**Figure 4D**).

Furthermore, combined analysis of MeRIP-seq and RNA-Seq data demonstrated that unique m^{6}A-modified transcripts were highly relevant to cardiac fibrosis, myocardial hypertrophy, and myocardial energy metabolism; therefore, we focused on genes critical for these processes, including *Mef2a*, *Klf15*, *Bcl2l2*, *Cd36*, and *Slc25a33* (**Figure 4C** and **Table 2**).

We used quantitative reverse-transcription PCR (RT-PCR) to validate the key genes *Mef2a*, *Klf15*, *Bcl2l2*, *Cd36*, and *Slc25a33*, which are associated with DCM pathophysiology and found that all of them were significantly enriched in immunoprecipitation

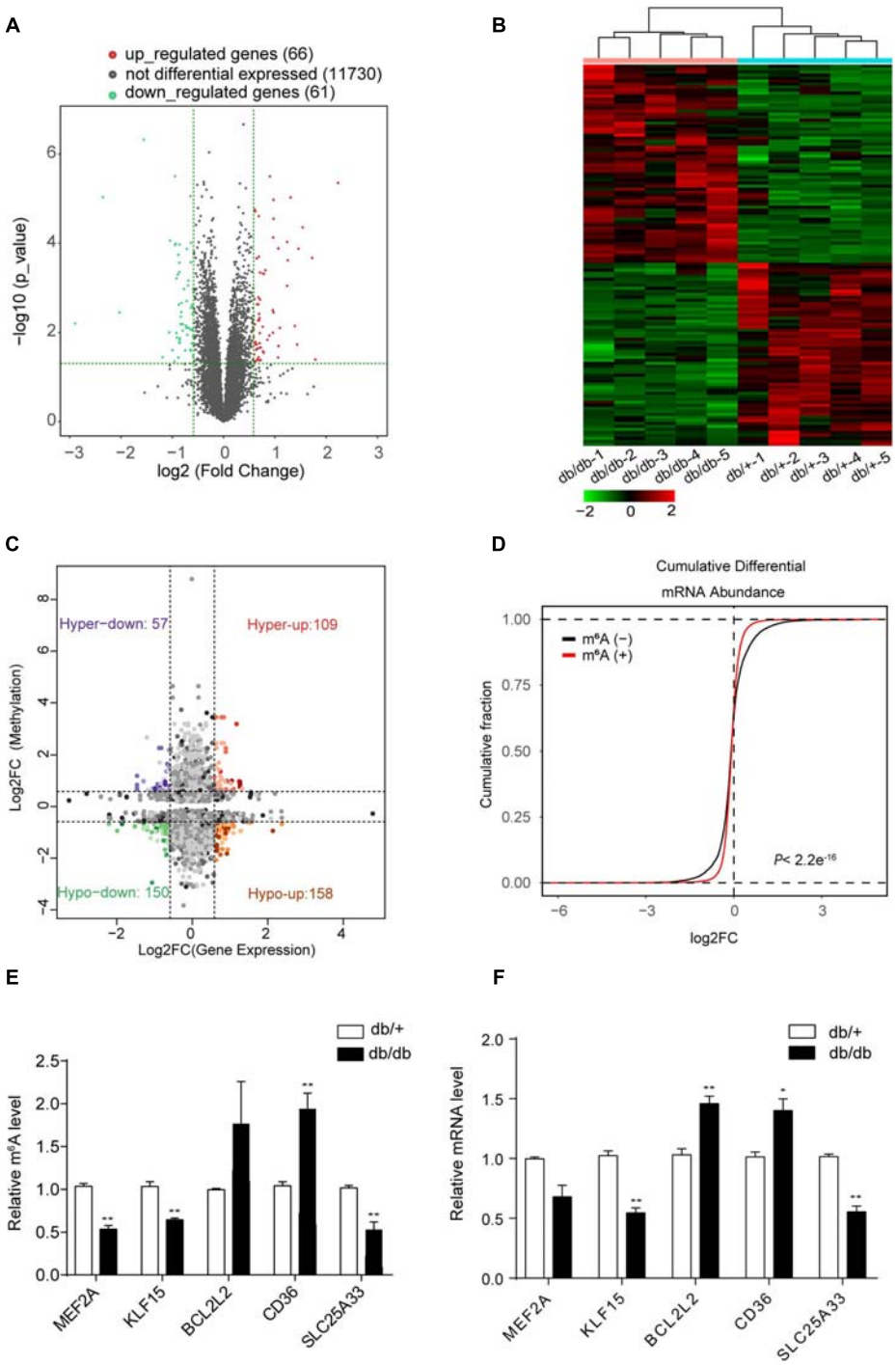

FIGURE 4 | Combined analysis of RNA-seq and MeRIP data comparing DCM and NC samples. **(A)** Volcano plots showing mRNAs significantly differentially expressed in comparisons between DCM and NC samples (fold-change > 1.5 and $P < 0.05$). **(B)** Cardiac clustering analysis of differentially expressed mRNAs ($P < 0.01$). **(C)** Four quadrant graph showing the distribution of transcripts with significant changes in m^{6}A-modification level and corresponding mRNA expression (fold-change > 1.2 and $P < 0.05$). **(D)** Cumulative distribution of mRNA expression changes between DCM and NC samples for m^{6}A-modified genes (red) and non-target genes (black). *P* values were calculated by two-sample Kolmogorov-Smirnov test. **(E)** MeRIP-qPCR validation of m^{6}A level changes in five representative hyper-methylated or hypo-methylated genes in NC and DCM group samples. **(F)** Relative mRNA levels of five representative genes were measured by real-time PCR in normal control and DCM group samples. Data are expressed as mean ± SD; data were analyzed using the Student's *t*-test. $^*P < 0.05$; $^{**}P < 0.01$ vs. NC group ($n = 3$ per group).

TABLE 2 | The ranking of the top 3 genes in each quadrant graph.

		m^{6}A level change					mRNA level change		
Pattern	**Chromosome**	**Peak region**	**Peak start**	**Peak end**	**Fold Change**	***P* value**	**Strand**	**Fold Change**	***P* value**
Hyper-up	chr6	cds	140623718	140633781	1.97794	1.31826E-09	+	1.880101649	0.021856265
Hyper-up	chrX	cds,utr5, TSS	20688477	20693415	1.69349	0.000144544	+	2.40714967	0.015432908
Hyper-up	chr17	utr5,cds, TSS	28438026	28441603	1.99308	0.000020893	–	2.070126156	0.0063377
Hyper-down	chr1	cds	131977633	131977962	1.94531	0.0147911	+	0.60843951	0.04150425
Hyper-down	chr7	cds	44516146	44517004	1.68646	0.00812831	–	0.550175197	0.000444612
Hyper-down	chr2	cds	181501928	181508184	1.63354	2.75423E-05	+	0.504849429	0.014587297
Hypo-up	chr8	utr3	66468623	66468863	0.34151	0.0281838	+	1.572498891	0.031693695
Hypo-up	chr10	utr3	88473835	88474016	0.441351	9.12011E-09	–	1.627484569	0.019479321
Hypo-up	chr9	utr3	113919351	113919682	0.665265	0.000501187	+	2.101866893	0.020272987
Hypo-down	chr17	cds	35852716	35852926	0.395021	0.0190546	+	0.625425926	0.009485677
Hypo-down	chr4	utr3	149744394	149744665	0.609205	0.0040738	–	0.523997734	0.00010282
Hypo-down	chr5	utr3	16374390	16374511	0.577143	0.000331131	+	0.651881805	0.016484324

(IP) pull-down samples (**Figure 4E**). Further, the mRNA levels of these genes were measured in db/ + and db/db hearts samples (**Figure 4F**), and the results showed that they all had similar mRNA expression tendencies consistent with their m^{6}A-methylation levels (**Figure 4F**).

In summary, these data suggest that differentially methylated RNAs affect cardiac fibrosis, myocardial hypertrophy, and myocardial energy metabolism, thereby affecting protein homeostasis in a transcription-independent manner.

FTO Is Downregulated in DCM, and Overexpression of FTO Improves Cardiac Function by Reducing Myocardial Fibrosis and Myocyte Hypertrophy

Based on the results of GO/KEGG analysis of unique genes and combined analysis of MeRIP-seq and RNA-Seq data in DCM and NC hearts, we suspected that the demethylase, FTO, may have an important role in DCM pathogenesis, which is closely related to energy metabolism regulation. Therefore, in the next experiment, we assessed the role of FTO in the mechanism underlying DCM. FTO was downregulated in db/db mice compared with db/ + group. The mRNA and protein expression levels of the FTO demethylase enzyme were measured in hearts from the db/db and db/ + groups to determine whether fibrosis is related to m^{6}A modification. FTO protein levels estimated by western blotting were significantly decreased in the db/db group compared with db/ + group ($P < 0.001$; $n = 6$/group; **Figures 5A,B**). *Fto* mRNA expression was also significantly decreased in db/db mice compared with db/ + controls ($P < 0.001$; $n = 6$/group; **Figure 5C**). In addition, immunostaining showed that FTO was predominantly expressed in cell nuclei, and that integrated optical density of FTO was decreased in db/db mice compared with the db/ + group ($P < 0.05$; $n = 6$/group; **Figures 5D,E**). We also detected expression of other important methyltransferases and demethylases, including Mettl3, Mettl14, and ALKBH5; however, no significant differences were detected (**Supplementary Figure 6**).

Overexpression of FTO significantly improved cardiac function by reducing myocardial fibrosis and myocyte hypertrophy in db/db mice. To determine whether overexpression of FTO protected hearts against DCM, adeno-associated virus vectors encoding FTO were injected into 16-week-old db/db or db/ + mice via a tail vein and FTO expression assessed 8 weeks later (**Supplementary Figure 7A**). Myocardial FTO expression was increased approximately 2.2-fold in db/db mouse hearts 8 weeks after injection of FTO-expressing adeno-associated virus (AAV-FTO) (**Supplementary Figures 7B,C**). Overexpression of FTO leaded to decrease total m^{6}A levels in db/db mice (**Supplementary Figures 7D,E**); $P < 0.05$). Eight weeks after adenovirus injection, reconstitution of FTO efficiently prevented myocardial fibrosis by reducing interstitial fibrosis in db/db mouse hearts (**Figures 6A,B**). Further, reconstitution of FTO efficiently reduced myocyte hypertrophy, as evidenced by decreased cardiomyocyte cross-sectional area in db/db mouse hearts (**Figures 6A,C**). Moreover, reconstitution of FTO significantly enhanced cardiac function in db/db mice by increasing LVEF and LVFS (**Figures 6D,E**). Furthermore, Doppler echocardiography indicated that FTO reconstitution also alleviated diastolic dysfunction in db/db mice by elevating the E/A ratio (**Figure 6F**). Overexpression of FTO decreased the mRNA levels of *Bcl2l2* and *Cd36* (**Figures 6G,H**). Taken together, these data indicate that reconstitution of FTO prevented myocardial fibrosis and myocyte hypertrophy, and overexpression of FTO improved cardiac systolic and diastolic function in db/db mice.

DISCUSSION

Diabetic cardiomyopathy is a specific type of cardiomyopathy caused by abnormal metabolism during diabetes. The main features of DCM are myocardial hypertrophy, cardiac fibrosis, coronary microvascular dysfunction, left ventricular enlargement, and weakened ventricular wall motion (Ritchie and Abel, 2020; Tan et al., 2020). In the early stage of DCM, echocardiography mainly indicates diastolic dysfunction, while

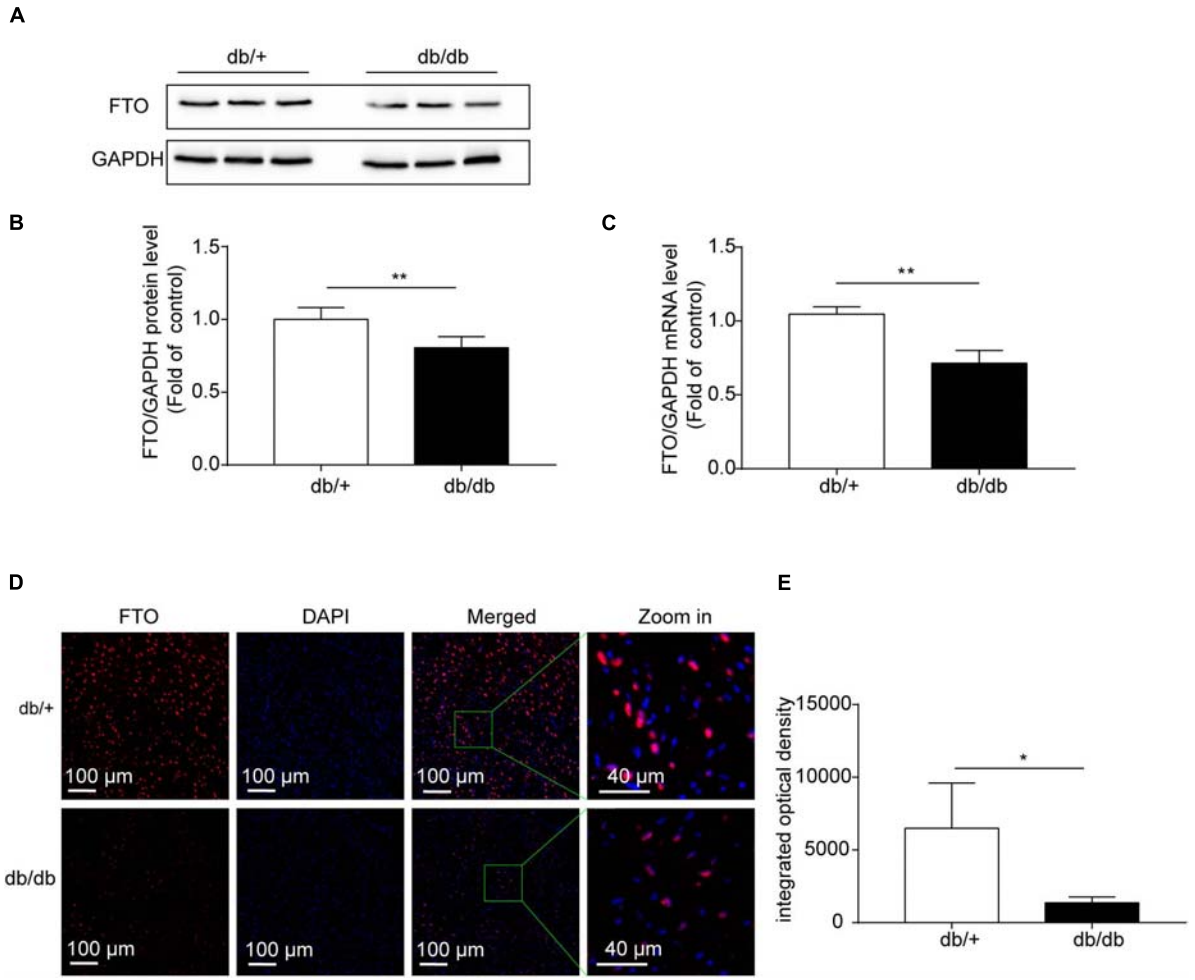

FIGURE 5 | Fat mass and obesity-associated (FTO) protein levels were significantly downregulated in diabetic cardiomyopathy. **(A,B)** Representative western blots and quantitative analysis of FTO/GAPDH protein expression in hearts from DCM and NC mice (n = 6 per group). **(C)** *Fto* mRNA levels in hearts from DCM and NC mice (n = 6 per group). **(D)** Confocal immunofluorescence using specific antibodies against FTO (red) in DCM hearts. Nuclei were stained with DAPI (blue), merged images show co-localization. Scale bar, 100 μm. **(E)** Quantification of FTO fluorescence intensity. Data are presented as mean ± SEM; differences between two groups were analyzed using the Student's t-test; $^*P < 0.05$ vs. NC, $^{**}P < 0.01$ vs. NC.

later stage disease is manifested as abnormal systolic function (Tan et al., 2020). Although multiple aspects of epigenetic regulation, from DNA to protein modification, have been extensively studied in DCM, the role of RNA modification in the regulation of gene expression is just beginning to be explored. Previous studies have demonstrated that m^{6}A dysregulation is associated with cardiac homeostasis and diseases, such as cardiac hypertrophy, cardiac remodeling, myocardial infarction, and heart failure (Dorn et al., 2019; Mathiyalagan et al., 2019; Mo et al., 2019; Song et al., 2019; Berulava et al., 2020; Gao et al., 2020; Lin et al., 2020); however, the transcriptome-wide distribution of m^{6}A in DCM remains largely unknown. Our study reveals that m^{6}A RNA methylation is altered in db/db mice, which exhibit unique m^{6}A modification patterns that differ from those in db/ + mice at the transcriptome-wide and gene-specific scales. GO and KEGG analyses revealed that genes with m^{6}A RNA methylation differences between db/db and db/ + mice were particularly associated with cardiac fibrosis, myocardial hypertrophy, and myocardial energy metabolism. FTO was downregulated in db/db mice compared with db/ + mice, and overexpression of FTO in db/db mice improved cardiac function and significantly reduced myocardial fibrosis and myocyte hypertrophy. FTO is a critical RNA-modifying enzyme that may control cardiomyocyte function by catalyzing the demethylation of m^{6}A on specific subsets of mRNAs; for example, *Mef2a*, *Klf15*, *Bcl2l2*, *Cd36*, and *Slc25a33*.

The m^{6}A modification patterns in db/db mice differed from those of db/ + mice at both the transcriptome-wide and gene-specific scales. We detected 4,968 m^{6}A peaks in DCM, consistent with the 3,208 and 3,922 peaks described in heart failure and myocardial hypertrophy, respectively (Mathiyalagan et al., 2019; Berulava et al., 2020). Together, these results indicate that m^{6}A is a ubiquitous post-transcriptional RNA modification in cardiovascular diseases. Furthermore,

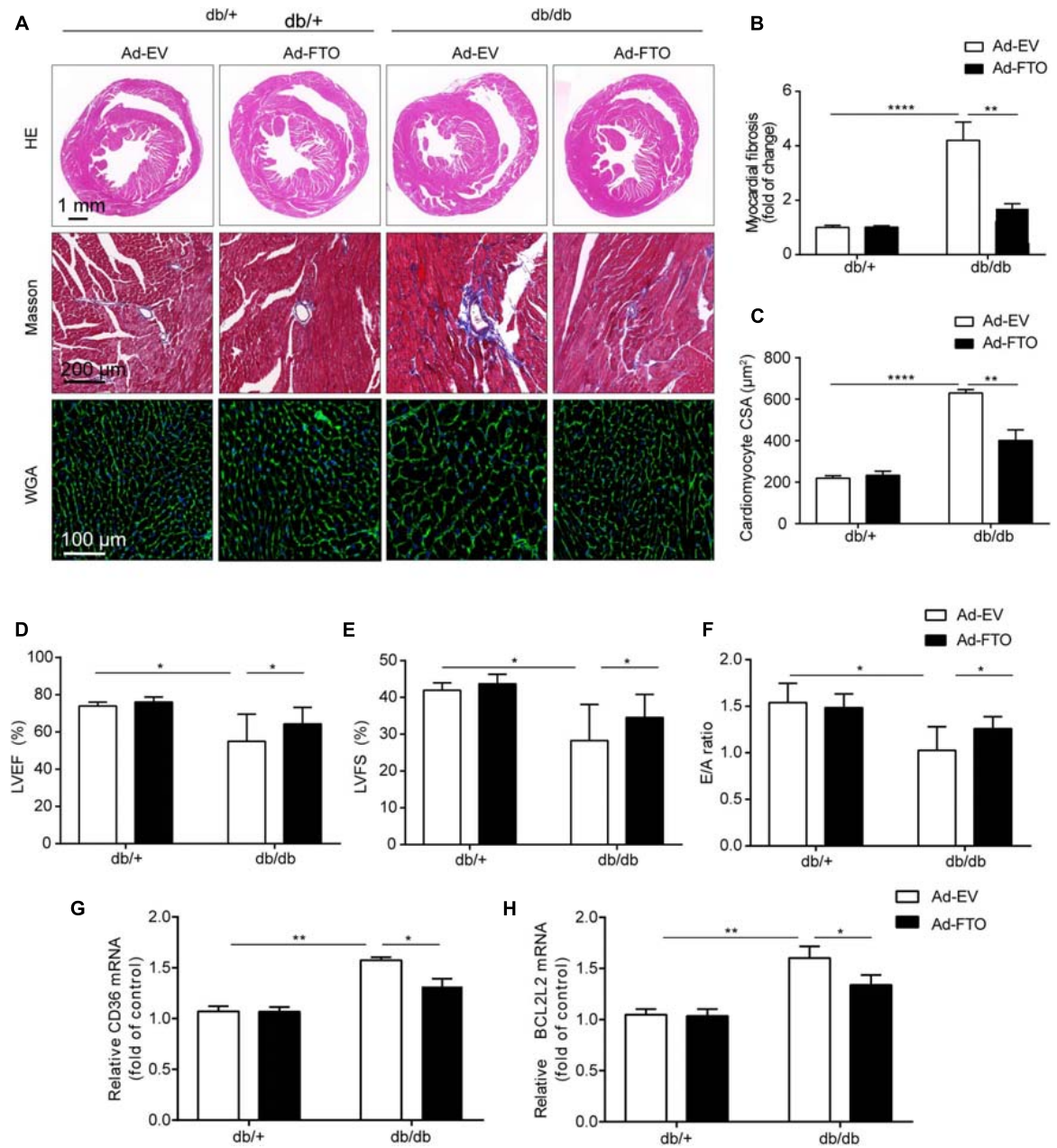

FIGURE 6 | Reconstitution of FTO alleviated cardiac hypertrophy and fibrosis in diabetic db/db mice. **(A)** The gross morphology of hearts stained with HE, Masson, and WGA. Scale bar, 2 mm **(B,C)** Quantitative analysis of interstitial fibrosis and cardiomyocyte cross-sectional area. Scale bar, 20 μm. Mice with reconstituted FTO showed significantly increased ejection fraction **(D)**, fractional shortening **(E)**, and E/A ratio **(F)**. Mice with reconstituted FTO showed reduced *Cd36* **(G)** and *Bcl2l2* **(H)** expression, as determined by qPCR. Data are expressed as mean ± SD and were analyzed using the Student's *t*-test. $^*P < 0.05$; $^{**}P < 0.01$, $^{****}P < 0.0001$ vs. NC group ($n = 3$ per group).

we investigated differentially methylated RNAs during DCM development and found that numbers were higher than those of genes with differential mRNA levels (296 vs. 127), indicating that the changes in m^{6}A RNA methylation far exceeded those in gene expression. Importantly, we found that, in DCM, m^{6}A was primarily present in the CDS and 3'UTR regions, which may influence mRNA stability, translation efficiency, and alternative splicing. Therefore, we speculate that the differential methylation of RNA in DCM may influence RNA at the post-transcription and translation levels, and particularly translation efficiency.

Gene Ontology and Kyoto Encyclopedia of Genes and Genomes analyses showed that transcripts with differential m^{6}A methylation in DCM were significantly enriched in processes and pathways associated with myocardial energy metabolism, such

as glycerophospholipid metabolism, glycerolipid metabolism, and regulation of cellular metabolic processes (**Figures 4C–F**). DCM is defined as a loss of flexibility in myocardial substrate metabolism, which leads to mitochondrial dysfunction, inflammation, and myocardial fibrosis (Peterson and Gropler, 2020). Cardiomyocyte ATP is mainly (60–90%) derived from fatty acid fat β oxidation under physiological conditions (Peterson and Gropler, 2020); however, in the diabetic state, fatty acid oxidation can produce numerous lipid intermediates, which accumulate in cardiomyocytes to cause lipotoxicity and ultimately lead to impaired heart function. Further, excessive fatty acid oxidation can cause accumulation of reactive oxygen species (ROS), leading to oxidative stress, which damages myocardial cells (Peterson and Gropler, 2020; Ritchie and Abel, 2020). We propose that m^{6}A methylation may be involved in the key pathogenic processes underlying DCM, including abnormal myocardial substrate metabolism. Furthermore, our RNA-Seq data demonstrate that abnormally up-regulated genes in the DCM samples were significantly enriched in biological processes involving lipid metabolism, cellular lipid metabolism, and fatty acid metabolism (**Supplementary Figure 3A**), consistent with myocardial energy metabolism pathology (Ritchie and Abel, 2020; Tan et al., 2020). Moreover, pathway analysis showed that unsaturated fatty acid biosynthesis, fatty acid elongation, butanoate metabolism, PPAR signaling pathway, and the HIF-1 signaling pathway were significantly altered among up-regulated genes (**Supplementary Figure 4B**). These results support that changes in m^{6}A RNA methylation mainly occur in transcripts coding for proteins involved in cardiac metabolic processes, with differences in gene expression also linked to metabolic regulation (Jia et al., 2018). In addition, combined analysis of MeRIP-seq and RNA-Seq data identified the target genes *Cd36* and *Slc5a33*, which were validated by MeRIP-qPCR (**Figures 4E,F**). CD36 deficiency rescues lipotoxic cardiomyopathy by preventing myocardial lipid accumulation in MHC-PPARα mice (Yang et al., 2007). In our study, *Cd36* m^{6}A-methylation and mRNA expression levels were upregulated, indicating that m^{6}A modification may influence mRNA stability or translation efficiency.

Our GO and KEGG analyses showed that transcripts differentially m^{6}A methylated in DCM were significantly enriched in processes and pathways associated with cardiac fibrosis and myocardial hypertrophy. The cAMP signaling, cGMP-PKG signaling, and dilated cardiomyopathy pathways are closely related to myocardial hypertrophy, while adrenergic signaling in cardiomyocytes, the TNF signaling pathway, the mitogen activated protein kinase (MAPK) signaling pathway, the AGEs-RAGE pathway, and chemokine signaling are strongly associated with cardiac fibrosis (**Figures 4C,D**). The main pathological changes in DCM include myocardial interstitial fibrosis, cardiomyocyte hypertrophy, cardiomyocyte apoptosis, and microvascular disease (Jia et al., 2018; Peterson and Gropler, 2020; Ritchie and Abel, 2020; Tan et al., 2020). In our study, GO analysis showed that metabolic processes involving nitrogen compounds were up-regulated while the cGMP-PKG signaling pathway was also increased, consistent with a previous study showing decreased NO signaling in endothelial cells and cardiomyocytes, leaded to cardiomyocyte hypertrophy by reducing the activity of soluble guanylate cyclase (sGC) and cyclic guanylate (cGMP) content, as well as cardiomyocyte loss of the protective effects of protein kinase G (PKG) in DCM (Park et al., 2018; Tan et al., 2020). Hence, our data suggest that m^{6}A methylation could be involved in the important pathogenic processes underlying myocardial hypertrophy in DCM. Furthermore, AGEs promote an imbalance of inflammatory gene expression by binding to specific cell surface receptors, thus increasing matrix protein expression through the MAPK pathway in vascular and heart tissues (Jia et al., 2018). Simultaneously, AGEs are involved in increasing ROS production and promoting myocardial inflammation and fibrosis (Wang Y. et al., 2020). Our KEGG analysis of transcripts differentially m^{6}A methylated in DCM showed that MAPK signaling was up-regulated, while the AGEs-RAGE pathway was down-regulated. Interestingly, enriched GO terms for genes differentially expressed in DCM based on RNA-seq data included extracellular matrix organization, myofibril assembly, and collagen-containing extracellular complex organization, indicating that m^{6}A methylation may contribute to important pathogenic processes underlying cardiac fibrosis in DCM. We also validated two target genes, *Mef2a* and *Klf15*, by MeRIP-qPCR (**Figures 4E,F**). KLF15 affects myocardial hypertrophy by inhibition of *MEF2* and *GATA4* transcription (Zhao et al., 2019), and can reduce myocardial fibrosis by down-regulating the expression of transforming growth factor-β (TGF-β), connective tissue growth factor, and myocardial protein-associated transcription factor-A in myocardial fibroblasts (Zhao et al., 2019). Further, knockout of the *MEF2A* gene improves cardiac dysfunction and collagen deposition in DCM, while inhibition of MEF2A can reduce extracellular matrix accumulation by regulating the Akt and TGF-β1/Smad signaling pathways (Chen et al., 2015). We found significant associations between differentially m^{6}A methylated transcripts and cardiac fibrosis, myocardial hypertrophy, and myocardial energy metabolism in DCM, suggesting that DCM may be regulated by epitranscriptomic processes, such as m^{6}A RNA methylation.

FTO is downregulated in DCM, and overexpression of FTO improves cardiac function by reducing myocardial fibrosis and myocyte hypertrophy. The *FTO* gene was discovered in 2007 in a genome-wide association study of type 2 diabetes (Frayling et al., 2007). Further, a population cohort study found that the role of FTO risk genes is related to energy intake (Haupt et al., 2009); however, the mechanisms by which FTO influences obesity and the specific pathways related to energy metabolism remain unclear. Animal experiments showed that this increase in energy metabolism does not involve physiological exercise, and may be caused by increased activity of the sympathetic nervous system (SNS) (Church et al., 2010). Further, the increased SNS activity may promote lipolysis of fat and muscle tissues and improve fat burning efficiency, thereby reducing the occurrence of obesity (Church et al., 2010). Our KEGG pathway analysis of differentially methylated RNAs showed that they were mainly associated with adrenergic signaling in cardiomyocytes (**Figure 4F**). In adipogenesis, FTO can also improve the binding

ability of C/EBPs with methylated or unmethylated DNA, thereby enhancing the transcription activity of the corresponding gene promoter, and stimulating preadipocyte differentiation (Wu et al., 2010). In summary, FTO plays an important role in energy metabolism.

Recent studies have shown that FTO expression is downregulated in failing mammalian hearts and hypoxic cardiomyocytes, thereby increasing m^{6}A levels in RNA and decreasing cardiomyocyte contractile function (Mathiyalagan et al., 2019). Simultaneously, overexpression of FTO in mouse reduces fibrosis and promotes angiogenesis (Mathiyalagan et al., 2019). In our study, overexpression of FTO also reduced myocardial fibrosis (**Figures 6A,B**). In addition, FTO knockout can lead to impaired cardiac function and promote heart failure (Berulava et al., 2020). In our study, overexpression of FTO improved heart function by increasing the LVEF and LVFS (**Figures 6D,E**). In summary, overexpression of FTO improves cardiac function by reducing myocardial fibrosis and myocyte hypertrophy.

This study has limitations. Firstly, no human heart samples were analyzed, therefore we will further seek human heart samples to further explore the association of m^{6}A with the DCM pathogenic process in the future. Second, although the target genes modified by m^{6}A were detected, the mechanism by which methylation readers regulate the target genes was not explored. In the future, we will investigate whether readers influence the stability, translation efficiency, or degradation of target genes. Third, although we purposely overexpressed FTO in the heart to improve cardiac function, future experiments will use conditional knockout mice and additional DCM models to study the exact mechanism by which FTO mediates DCM.

In conclusion, m^{6}A RNA methylation was altered in db/db mice, which had unique m^{6}A modification patterns that differed from those in db/ + mice at the transcriptome-wide and gene-specific scales. GO and KEGG analysis indicated that differentially methylated genes were particularly associated with cardiac fibrosis, myocardial hypertrophy, and myocardial energy metabolism. FTO is downregulated in db/db mice compared with db/ + mice, and overexpression of FTO in db/db mice improved cardiac function and significantly reduced myocardial fibrosis and myocyte hypertrophy. FTO is a critical RNA-modifying enzyme that may control cardiomyocyte function by catalyzing the demethylation of m^{6}A on specific subsets of mRNAs, including *Mef2a*, *Klf15*, *Bcl2l2*, *Cd36*, and *Slc25a33*.

DATA AVAILABILITY STATEMENT

The datasets presented in this study can be found in online repositories. The names of the repository/repositories and accession number(s) can be found below: GSE173384, https://www.ncbi.nlm.nih.gov/bioproject/?term=GSE173384.

ETHICS STATEMENT

The animal study was reviewed and approved by the Ethics Committee of the Capital Institute of Pediatrics.

AUTHOR CONTRIBUTIONS

WJ and JW designed the experiments and wrote the manuscript. WJ, KL, and FH carried out the experiments. SO analyzed the data. JW and ZL supervised this project. All authors gave final approval for publication, and no conflict of interest exits in the submission of this manuscript.

FUNDING

This work was supported by the National Key Research and Development Program of China (2018YFC1002503), CAMS Innovation Fund for Medical Sciences (CIFMS) (2016-I2M-1-008), and the Special Fund of the Pediatric Medical Coordinated Development Center of Beijing Hospitals Authority (No. XTZD20180402).

SUPPLEMENTARY MATERIAL

The Supplementary Material for this article can be found online at: https://www.frontiersin.org/articles/10.3389/fcell.2021.702579/full#supplementary-material

REFERENCES

Alarcon, C. R., Goodarzi, H., Lee, H., Liu, X., Tavazoie, S., and Tavazoie, S. F. (2015a). HNRNPA2B1 Is a Mediator of m(6)A-Dependent Nuclear RNA Processing Events. *Cell* 162, 1299–1308. doi: 10.1016/j.cell.2015.08.011

Alarcon, C. R., Lee, H., Goodarzi, H., Halberg, N., and Tavazoie, S. F. (2015b). N6-methyladenosine marks primary microRNAs for processing. *Nature* 519, 482–485. doi: 10.1038/nature14281

Berulava, T., Buchholz, E., Elerdashvili, V., Pena, T., Islam, M. R., Lbik, D., et al. (2020). Changes in m6A RNA methylation contribute to heart failure progression by modulating translation. *Eur. J. Heart Fail.* 22, 54–66. doi: 10.1002/ejhf.1672

Chen, X., Liu, G., Zhang, W., Zhang, J., Yan, Y., Dong, W., et al. (2015). Inhibition of MEF2A prevents hyperglycemia-induced extracellular matrix accumulation by blocking Akt and TGF-beta1/Smad activation in cardiac fibroblasts. *Int. J. Biochem. Cell Biol.* 69, 52–61. doi: 10.1016/j.biocel.2015.10.012

Cho, N. H., Shaw, J. E., Karuranga, S., Huang, Y., Fernandes, J. D., Ohlrogge, A. W., et al. (2018). IDF Diabetes Atlas: global estimates of diabetes prevalence for 2017 and projections for 2045. *Diabetes Res. Clin. Pract.* 138, 271–281. doi: 10.1016/j.diabres.2018.02.023

Church, C., Moir, L., McMurray, F., Girard, C., Banks, G. T., Teboul, L., et al. (2010). Overexpression of Fto leads to increased food intake and results in obesity. *Nat. Genet.* 42, 1086–1092. doi: 10.1038/ng.713

Dominissini, D., Moshitch-Moshkovitz, S., Schwartz, S., Salmon-Divon, M., Ungar, L., Osenberg, S., et al. (2012). Topology of the human and mouse m6A RNA methylomes revealed by m6A-seq. *Nature* 485, 201–206. doi: 10.1038/nature11112

Dorn, L. E., Lasman, L., Chen, J., Xu, X., Hund, T. J., Medvedovic, M., et al. (2019). The N(6)-Methyladenosine mRNA Methylase METTL3 Controls

Cardiac Homeostasis and Hypertrophy. *Circulation* 139, 533–545. doi: 10.1161/circulationaha.118.036146

Du, H., Zhao, Y., He, J., Zhang, Y., Xi, H., Liu, M., et al. (2016). YTHDF2 destabilizes m(6)A-containing RNA through direct recruitment of the CCR4-NOT deadenylase complex. *Nat. Commun.* 7:12626.

Edupuganti, R. R., Geiger, S., Lindeboom, R. G. H., Shi, H., Hsu, P. J., Lu, Z., et al. (2017). N(6)-methyladenosine (m(6)A) recruits and repels proteins to regulate mRNA homeostasis. *Nat. Struct. Mol. Biol.* 24, 870–878. doi: 10.1038/nsmb.3462

Einarson, T. R., Acs, A., Ludwig, C., and Panton, U. H. (2018). Prevalence of cardiovascular disease in type 2 diabetes: a systematic literature review of scientific evidence from across the world in 2007-2017. *Cardiovasc. Diabetol.* 17:83.

Frayling, T. M., Timpson, N. J., Weedon, M. N., Zeggini, E., Freathy, R. M., Lindgren, C. M., et al. (2007). A common variant in the FTO gene is associated with body mass index and predisposes to childhood and adult obesity. *Science* 316, 889–894.

Gao, X. Q., Zhang, Y. H., Liu, F., Ponnusamy, M., Zhao, X. M., Zhou, L. Y., et al. (2020). The piRNA CHAPIR regulates cardiac hypertrophy by controlling METTL3-dependent N(6)-methyladenosine methylation of Parp10 mRNA. *Nat. Cell Biol.* 22, 1319–1331. doi: 10.1038/s41556-020-0576-y

Gluckman, P. D., Hanson, M. A., Buklijas, T., Low, F. M., and Beedle, A. S. (2009). Epigenetic mechanisms that underpin metabolic and cardiovascular diseases. *Nat Rev. Endocrinol.* 5, 401–408. doi: 10.1038/nrendo.2009.102

Haupt, A., Thamer, C., Staiger, H., Tschritter, O., Kirchhoff, K., Machicao, F., et al. (2009). Variation in the FTO gene influences food intake but not energy expenditure. *Exp. Clin. Endocrinol. Diabetes* 117, 194–197. doi: 10.1055/s-0028-1087176

Huang, H., Weng, H., Sun, W., Qin, X., Shi, H., Wu, H., et al. (2018). Recognition of RNA N(6)-methyladenosine by IGF2BP proteins enhances mRNA stability and translation. *Nat. Cell Biol.* 20, 285–295. doi: 10.1038/s41556-018-0045-z

Jia, G., Fu, Y., Zhao, X., Dai, Q., Zheng, G., Yang, Y., et al. (2011). N6-methyladenosine in nuclear RNA is a major substrate of the obesity-associated FTO. *Nat. Chem. Biol.* 7, 885–887. doi: 10.1038/nchembio.687

Jia, G., Whaley-Connell, A., and Sowers, J. R. (2018). Diabetic cardiomyopathy: a hyperglycaemia- and insulin-resistance-induced heart disease. *Diabetologia* 61, 21–28. doi: 10.1007/s00125-017-4390-4

Kmietczyk, V., Riechert, E., Kalinski, L., Boileau, E., Malovrh, E., Malone, B., et al. (2019). m(6)A-mRNA methylation regulates cardiac gene expression and cellular growth. *Life Sci. Alliance* 2:e201800233. doi: 10.26508/lsa.201800233

Kruger, N., Biwer, L. A., Good, M. E., Ruddiman, C. A., Wolpe, A. G., DeLalio, L. J., et al. (2020). Loss of Endothelial FTO Antagonizes Obesity-Induced Metabolic and Vascular Dysfunction. *Circ. Res.* 126, 232–242. doi: 10.1161/circresaha.119.315531

Li, F., Zhao, D., Wu, J., and Shi, Y. (2014). Structure of the YTH domain of human YTHDF2 in complex with an m(6)A mononucleotide reveals an aromatic cage for m(6)A recognition. *Cell Res.* 24, 1490–1492. doi: 10.1038/cr.2014.153

Lin, J., Zhu, Q., Huang, J., Cai, R., and Kuang, Y. (2020). Hypoxia Promotes Vascular Smooth Muscle Cell (VSMC) Differentiation of Adipose-Derived Stem Cell (ADSC) by Regulating Mettl3 and Paracrine Factors. *Stem Cells Int.* 2020:2830565.

Liu, J., Yue, Y., Han, D., Wang, X., Fu, Y., Zhang, L., et al. (2014). A METTL3-METTL14 complex mediates mammalian nuclear RNA N6-adenosine methylation. *Nat. Chem. Biol.* 10, 93–95. doi: 10.1038/nchembio.1432

Liu, N., Dai, Q., Zheng, G., He, C., Parisien, M., and Pan, T. (2015). N(6)-methyladenosine-dependent RNA structural switches regulate RNA-protein interactions. *Nature* 518, 560–564. doi: 10.1038/nature14234

Liu, N., Zhou, K. I., Parisien, M., Dai, Q., Diatchenko, L., and Pan, T. (2017). N6-methyladenosine alters RNA structure to regulate binding of a low-complexity protein. *Nucleic Acids Res.* 45, 6051–6063. doi: 10.1093/nar/gkx141

Mathiyalagan, P., Adamiak, M., Mayourian, J., Sassi, Y., Liang, Y., Agarwal, N., et al. (2019). FTO-Dependent N(6)-Methyladenosine Regulates Cardiac Function During Remodeling and Repair. *Circulation* 139, 518–532. doi: 10.1161/circulationaha.118.033794

Mauer, J., Luo, X., Blanjoie, A., Jiao, X., Grozhik, A. V., Patil, D. P., et al. (2017). Reversible methylation of m(6)Am in the 5' cap controls mRNA stability. *Nature* 541, 371–375. doi: 10.1038/nature21022

Meyer, K. D., Saletore, Y., Zumbo, P., Elemento, O., Mason, C. E., and Jaffrey, S. R. (2012). Comprehensive analysis of mRNA methylation reveals enrichment in 3'. UTRs and near stop codons. *Cell* 149, 1635–1646. doi: 10.1016/j.cell.2012.05.003

Mo, X. B., Lei, S. F., Zhang, Y. H., and Zhang, H. (2019). Examination of the associations between m(6)A-associated single-nucleotide polymorphisms and blood pressure. *Hypertens. Res.* 42, 1582–1589. doi: 10.1038/s41440-019-0277-8

Nachtergaele, S., and He, C. (2018). Chemical Modifications in the Life of an mRNA Transcript. *Annu. Rev. Genet.* 52, 349–372. doi: 10.1146/annurev-genet-120417-031522

Park, M., Sandner, P., and Krieg, T. (2018). cGMP at the centre of attention: emerging strategies for activating the cardioprotective PKG pathway. *Basic Res. Cardiol.* 113:24.

Patil, D. P., Chen, C. K., Pickering, B. F., Chow, A., Jackson, C., Guttman, M., et al. (2016). m(6)A RNA methylation promotes XIST-mediated transcriptional repression. *Nature* 537, 369–373. doi: 10.1038/nature19342

Patil, D. P., Pickering, B. F., and Jaffrey, S. R. (2018). Reading m(6)A in the Transcriptome: m(6)A-Binding Proteins. *Trends Cell Biol.* 28, 113–127. doi: 10.1016/j.tcb.2017.10.001

Peterson, L. R., and Gropler, R. J. (2020). Metabolic and Molecular Imaging of the Diabetic Cardiomyopathy. *Circ. Res.* 126, 1628–1645. doi: 10.1161/circresaha.120.315899

Ritchie, R. H., and Abel, E. D. (2020). Basic Mechanisms of Diabetic Heart Disease. *Circ. Res.* 126, 1501–1525. doi: 10.1161/circresaha.120.315913

Roundtree, I. A., and He, C. (2016). Nuclear m(6)A Reader YTHDC1 Regulates mRNA Splicing. *Trends Genet.* 32, 320–321. doi: 10.1016/j.tig.2016.03.006

Shi, H., Wang, X., Lu, Z., Zhao, B. S., Ma, H., Hsu, P. J., et al. (2017). YTHDF3 facilitates translation and decay of N(6)-methyladenosine-modified RNA. *Cell Res.* 27, 315–328. doi: 10.1038/cr.2017.15

Song, H., Feng, X., Zhang, H., Luo, Y., Huang, J., Lin, M., et al. (2019). METTL3 and ALKBH5 oppositely regulate m(6)A modification of TFEB mRNA, which dictates the fate of hypoxia/reoxygenation-treated cardiomyocytes. *Autophagy* 15, 1419–1437. doi: 10.1080/15548627.2019.1586246

Tan, Y., Zhang, Z., Zheng, C., Wintergerst, K. A., Keller, B. B., and Cai, L. (2020). Mechanisms of diabetic cardiomyopathy and potential therapeutic strategies: preclinical and clinical evidence. *Nat. Rev. Cardiol.* 17, 585–607. doi: 10.1038/s41569-020-0339-2

Wang, P., Doxtader, K. A., and Nam, Y. (2016). Structural Basis for Cooperative Function of Mettl3 and Mettl14 Methyltransferases. *Mol. Cell* 63, 306–317. doi: 10.1016/j.molcel.2016.05.041

Wang, X., Feng, J., Xue, Y., Guan, Z., Zhang, D., Liu, Z., et al. (2016). Structural basis of N(6)-adenosine methylation by the METTL3-METTL14 complex. *Nature* 534, 575–578. doi: 10.1038/nature18298

Wang, X., Lu, Z., Gomez, A., Hon, G. C., Yue, Y., Han, D., et al. (2014). N6-methyladenosine-dependent regulation of messenger RNA stability. *Nature* 505, 117–120. doi: 10.1038/nature12730

Wang, X., Zhao, B. S., Roundtree, I. A., Lu, Z., Han, D., Ma, H., et al. (2015). N(6)-methyladenosine Modulates Messenger RNA Translation Efficiency. *Cell* 161, 1388–1399. doi: 10.1016/j.cell.2015.05.014

Wang, Y., Li, Y., Toth, J. I., Petroski, M. D., Zhang, Z., and Zhao, J. C. (2014). N6-methyladenosine modification destabilizes developmental regulators in embryonic stem cells. *Nat. Cell Biol.* 16, 191–198. doi: 10.1038/ncb2902

Wang, Y., Luo, W., Han, J., Khan, Z. A., Fang, Q., Jin, Y., et al. (2020). MD2 activation by direct AGE interaction drives inflammatory diabetic cardiomyopathy. *Nat. Commun.* 11:2148.

Wei, J., Liu, F., Lu, Z., Fei, Q., Ai, Y., He, P. C., et al. (2018). Differential m(6)A, m(6)Am, and m(1)A Demethylation Mediated by FTO in the Cell Nucleus and Cytoplasm. *Mol. Cell* 71, 973.e–985.e.

Wen, J., Lv, R., Ma, H., Shen, H., He, C., Wang, J., et al. (2018). Zc3h13 Regulates Nuclear RNA m(6)A Methylation and Mouse Embryonic Stem Cell Self-Renewal. *Mol. Cell* 69, 1028.e–1038.e.

Wojtas, M. N., Pandey, R. R., Mendel, M., Homolka, D., Sachidanandam, R., and Pillai, R. S. (2017). Regulation of m(6)A Transcripts by the 3'– > 5' RNA Helicase YTHDC2 Is Essential for a Successful Meiotic Program in the Mammalian Germline. *Mol. Cell* 68, 374.e–387.e.

Wu, Q., Saunders, R. A., Szkudlarek-Mikho, M., Serna Ide, L., and Chin, K. V. (2010). The obesity-associated Fto gene is a transcriptional coactivator. *Biochem. Biophys. Res. Commun.* 401, 390–395. doi: 10.1016/j.bbrc.2010.09.064

Yang, J., Sambandam, N., Han, X., Gross, R. W., Courtois, M., Kovacs, A., et al. (2007). CD36 deficiency rescues lipotoxic cardiomyopathy. *Circ. Res.* 100, 1208–1217. doi: 10.1161/01.res.0000264104.25265.b6

Yue, Y., Liu, J., Cui, X., Cao, J., Luo, G., Zhang, Z., et al. (2018). VIRMA mediates preferential m(6)A mRNA methylation in 3'UTR and near stop codon and associates with alternative polyadenylation. *Cell Discov.* 4:10.

Zhang, W., Song, M., Qu, J., and Liu, G. H. (2018). Epigenetic Modifications in Cardiovascular Aging and Diseases. *Circ. Res.* 123, 773–786. doi: 10.1161/circresaha.118.312497

Zhao, Y., Song, W., Wang, L., Rane, M. J., Han, F., and Cai, L. (2019). Multiple roles of KLF15 in the heart: underlying mechanisms and therapeutic implications. *J. Mol. Cell Cardiol.* 129, 193–196. doi: 10.1016/j.yjmcc.2019.01.024

Zheng, G., Dahl, J. A., Niu, Y., Fedorcsak, P., Huang, C. M., Li, C. J., et al. (2013). ALKBH5 is a mammalian RNA demethylase that impacts RNA metabolism and mouse fertility. *Mol. Cell* 49, 18–29. doi: 10.1016/j.molcel.2012.10.015

Zhu, T., Roundtree, I. A., Wang, P., Wang, X., Wang, L., Sun, C., et al. (2014). Crystal structure of the YTH domain of YTHDF2 reveals mechanism for recognition of N6-methyladenosine. *Cell Res.* 24, 1493–1496. doi: 10.1038/cr.2014.152

Conflict of Interest: The authors declare that the research was conducted in the absence of any commercial or financial relationships that could be construed as a potential conflict of interest.

frontiers in Cell and Developmental Biology

REVIEW
published: 19 August 2021
doi: 10.3389/fcell.2021.685775

Oxidative Stress-Induced Ferroptosis in Cardiovascular Diseases and Epigenetic Mechanisms

Jiamin Li[1†], Yunxiang Zhou[2†], Hui Wang[3], Jianyao Lou[4], Cameron Lenahan[5,6], Shiqi Gao[7], Xiaoyu Wang[7], Yongchuan Deng[2], Han Chen[1*] and Anwen Shao[7*]*

[1] Department of Cardiology, Zhejiang Provincial Key Lab of Cardiovascular Disease Diagnosis and Treatment, Second Affiliated Hospital, Zhejiang University School of Medicine, Hangzhou, China, [2] Department of Surgical Oncology, The Second Affiliated Hospital, School of Medicine, Zhejiang University, Hangzhou, China, [3] Department of Medical Oncology, The Second Affiliated Hospital, School of Medicine, Zhejiang University, Hangzhou, China, [4] Department of General Surgery, The Second Affiliated Hospital, School of Medicine, Zhejiang University, Hangzhou, China, [5] Burrell College of Osteopathic Medicine, Las Cruces, NM, United States, [6] Center for Neuroscience Research, School of Medicine, Loma Linda University, Loma Linda, CA, United States, [7] Department of Neurosurgery, The Second Affiliated Hospital, School of Medicine, Zhejiang University, Hangzhou, China

OPEN ACCESS

Edited by:
Christoph D. Rau,
University of North Carolina at Chapel Hill, United States

Reviewed by:
Douglas J. Chapski,
University of California, Los Angeles, United States
Mingyi Zhao,
Central South University, China

***Correspondence:**
Yongchuan Deng
dyc001@zju.edu.cn
Han Chen
chenhanzju@zju.edu.cn
Anwen Shao
shaoanwen@zju.edu.cn

[†] These authors have contributed equally to this work

Specialty section:
This article was submitted to Epigenomics and Epigenetics, a section of the journal Frontiers in Cell and Developmental Biology

Received: 25 March 2021
Accepted: 04 August 2021
Published: 19 August 2021

Citation:
Li J, Zhou Y, Wang H, Lou J, Lenahan C, Gao S, Wang X, Deng Y, Chen H and Shao A (2021) Oxidative Stress-Induced Ferroptosis in Cardiovascular Diseases and Epigenetic Mechanisms. Front. Cell Dev. Biol. 9:685775. doi: 10.3389/fcell.2021.685775

The recently discovered ferroptosis is a new kind of iron-regulated cell death that differs from apoptosis and necrosis. Ferroptosis can be induced by an oxidative stress response, a crucial pathological process implicated in cardiovascular diseases (CVDs). Accordingly, mounting evidence shows that oxidative stress-induced ferroptosis plays a pivotal role in angio-cardiopathy. To date, the inhibitors and activators of ferroptosis, as well as the many involved signaling pathways, have been widely explored. Among which, epigenetic regulators, molecules that modify the package of DNA without altering the genome, emerge as a highly targeted, effective option to modify the signaling pathway of ferroptosis and oxidative stress, representing a novel and promising therapeutic potential target for CVDs. In this review, we will briefly summarize the mechanisms of ferroptosis, as well as the role that ferroptosis plays in various CVDs. We will also expound the epigenetic regulators of oxidative stress-induced ferroptosis, and the promise that these molecules hold for treating the intractable CVDs.

Keywords: iron, ferroptosis, oxidative stress, epigenetic regulators, cardiovascular diseases

INTRODUCTION

Cardiovascular diseases (CVDs), including heart conditions and vascular disorders, are the leading cause of mortality around the world, and comprise approximately one-third of annual deaths [World Health Organization (WHO), 2017]. Moreover, CVDs carry an enormous economic burden to every country, especially China and India [The Institute for Health Metrics and Evaluation (IHME), 2018]. The most prevalent CVDs include hypertension, coronary heart disease, atrial fibrillation, and valvular heart disease, but most CVDs develop into heart failure at the advanced or terminal stages. In 2017, update of the guidelines for the management of heart failure released by ACC/AHA/HFSA (American College of Cardiology Foundation/American Heart Association/Heart Failure Society of America), angiotensin receptor–neprilysin inhibitors (ARNI) (sacubitril/valsartan) and sinoatrial node modulators (ivabradine) were classified as the therapy for stage C heart failure in the evidence of level B-R, but require further high-quality

randomized clinical trials to be conducted (Dixon et al., 2012; Yancy et al., 2017). The current treatment of CVDs is unsatisfactory, and the underlying mechanisms are not fully understood. As such, it is imperative that new mechanisms and corresponding therapeutic targets are explored.

Ferroptosis was first introduced by Dixon et al. (2012), and was featured as an iron-dependent lipid peroxidation, a regulated cell death that is different from apoptosis and necrosis. Currently, ferroptosis was defined as a unique iron-dependent form of non-apoptotic cell death triggered by erastin, an oncogenic RAS-selective lethal small molecule, and inhibited by ferrostatin-1 in cancer cells or glutamate-induced cell death in organotypic rat brain slices (Dixon et al., 2012). Mitochondria are crucial in ferroptosis, tricarboxylic acid (TCA) cycle participates in cysteine-deprivation induced ferroptosis and that the electron transport chain (ETC) regulates the process (Gao et al., 2019). Mitochondria participate in metabolism, and are the main source of reactive oxygen species (ROS) (Tang D. et al., 2021). Oxidative stress occurs when the antioxidant defense systems, such as GSH, coenzyme Q10, and tetrahydrobiopterin (BH4), cannot find equilibrium of ROS (Dixon et al., 2012; Bersuker et al., 2019; Doll et al., 2019; Kraft et al., 2020; Soula et al., 2020). GSH, the major antioxidant in mammalian cells, is tightly tuned intracellularly and extracellularly for homeostasis (Gao et al., 2018), and is also the key component in ferroptosis. Ferroptosis has been found in many diseases, such as cancer, CVD, neurological disease, and ischemia/reperfusion injuries in kidney, liver, lung, and skeletal muscle (Stamenkovic et al., 2019). Ferroptosis may be a potential mechanism underlying CVDs as many studies pointed out that ferroptosis have been implicated in CVDs (Birnbaum et al., 1996; Shiomi et al., 2004; Dabkowski et al., 2008; Fang et al., 2019).

The biological processes are regulated by genetics and epigenetics. Epigenetics is known as the unchanged nucleotide sequence of the gene that is modulated by several environmental factors while genetics irreversibly change the gene code via mutation (Borrelli et al., 2008). Epigenetics act on DNA or chromatin by DNA methylation, histone modifications, chromatin remodeling and noncoding RNAs (Prasher et al., 2020; Wu et al., 2020). Based on epidemiological studies, alteration of lifestyle and environment can reduce the risk of developing CVDs (Wang et al., 2013). It has been suggested that ferroptosis can be regulated by epigenetic, transcriptional, and post-translational mechanisms (Chen et al., 2020). Accumulating evidence indicates that a series of epigenetic regulators are involved in the processes of ferroptosis. In the present review, we will elaborate on the mechanism of ferroptosis, the roles of ferroptosis in CVDs, as well as the roles of epigenetic regulators in oxidative stress-induced ferroptosis, and we will offer an option for the therapeutic application of ferroptosis in CVDs.

MECHANISM OF FERROPTOSIS

Cell death is frequently required to maintain the normal functions of the body/system, either under physiological conditions or pathophysiological circumstances. Two major classifications of cell death are apoptosis and necrosis. Other patterns of "non-classical" cell death, such as autophagy, pyroptosis, and necroptosis, reportedly also have important roles in cell survival and body function (Dixon et al., 2012).

Dolma et al. (2003) found a novel compound that can kill tumor cells without damaging isogenic normal cell counterparts. They named it "erastin," and it induces nonapoptotic cell death in a RAS^{V12}- and small T(ST)-dependent manner (Dolma et al., 2003). Furthermore, Yang and Stockwell (2008) found that two small molecules, RSL (ras-selective-lethal compound) 3 and RSL5, were lethal to tumors with oncogenic RAS, similar to the function of erastin. RSL3- or RSL5-induced cell death is considered iron-dependent as it could be inhibited by either iron chelation or decreased iron uptake, with increased levels of ROS (Yang and Stockwell, 2008). Ferroptotic cells cannot be restrained by inhibitors of necrosis, apoptosis, or autophagy and exhibit morphological changes in mitochondria, such as decreased size, increased membrane density, and reduction or disappearance of cristae (Xie et al., 2016). In 2012, the team of Dixon SJ conducted further research to support and extend this newly discovered form of regulated cell death. They proposed the concept of ferroptosis for the first time, and defined it as the regulatory cell death induced by the accumulation of lipid peroxides and ROS, which can be inhibited by lipid peroxide inhibitors and iron chelators (Dixon et al., 2012). Outer mitochondrial membrane (OMM) rupture was observed in immortalized fibroblasts and glutathione peroxidase 4 (GPX4)-inactivated kidney tissue (Angeli et al., 2014).

Iron is an important essential microelement in the human body, and plays a key role in maintaining homeostasis of the internal environment, and ensuring the normal physiological functions of cells. Iron in the human body is mostly distributed in the hemoglobin of red blood cells and the myoglobin of muscles, but a small amount exists in enzymes, such as cytochrome oxidase, peroxidase, and catalase. There are two types of iron ions: ferrous and ferric. Ferric ions bind to transferrin, and are transported into the cell, entering via the transferrin receptor 1 (TFR1) on the cell membrane (Gao M. et al., 2015). Ferrous ions reduced to ferric ions in the cell, and are then transported and released into the cytoplasmic iron pool. Ferrous ion can react with oxygen, and generates ROS, such as hydroxyl radical (•OH) and hydrogen peroxide (H_2O_2), in a process known as the Fenton reaction. Iron overload leads to an increase of ROS, which cause harm to DNA, protein, and lipids. The Haber–Weiss reaction provides •OH from the substrates of H_2O_2 and superoxide ($\bullet O_2^-$): (1) $Fe^{3+}+\bullet O_2^- \rightarrow Fe^{2+}+O_2$; (2) $Fe^{2+}+H_2O_2 \rightarrow Fe^{3+}+OH^-+\bullet OH$ (Fenton reaction); (3) $\bullet O2^-+H_2O_2 \rightarrow \bullet OH+OH^-+O_2$ (Gao M. et al., 2015). Cellular iron overload can impair mitochondrial oxidative phosphorylation and produce a large amount of ROS, even exceeding the scavenging ability of the body's antioxidant system [e.g., glutathione (GSH) and GPX4], thereby oxidizing cell membranes, as well as the unsaturated fatty acids on cell and organelle membranes, forming lipid peroxides, destroying cell structure and function, and causing cell damage or death (Dixon et al., 2012; Ooko et al., 2015; Hassan et al., 2016).

It is widely accepted that ferroptosis is regulated by the cystine/glutamate antiporter system (system Xc^-) and GPX)

(Dixon et al., 2012). System Xc^- is an amino acid antiporter, which mainly includes SLC7A11 (solute carrier family 7 member 11) and SLC3A2 (solute carrier family 3 member 2), which causes the exchange of cysteine and glutamate into and out of the cell, respectively, at a 1:1 ratio (Lewerenz et al., 2013). Glutathione is an important antioxidant and free radical scavenger in vivo, and can be categorized as either reduced (GSH) or oxidized (GSSG). GPx4 converts GSH to GSSG, GSH/GSSG constitutes an antioxidant system and provides reducing equivalents to eliminate oxidative species (Xie et al., 2016; Yang W. S. et al., 2014). The synthesis of GSH depends on the cysteine, which is made by cystine, and glutamate-cysteine ligase (GCL). As a member of the glutathione peroxidase family, GPX4 inhibits ferroptosis by decreasing the level of lipid peroxides (Liang et al., 2009). While erastin and RSL-3 are both inducers of ferroptosis, erastin depends on VDAC2/VDAC3 or downregulation of GSH. However, RSL-3 does not require the above-mentioned molecules. Lipid oxidation is observed in both erastin and RSL3-induced cell death. Further investigation verified that GPX4 is the target of RSL-3 through a binding site (Yang W. S. et al., 2014). Many inducers (e.g., erastin, RSL3, RSL5, buthioninesulfoximine, acetaminophen, fin, lanperisone, sulfasalazine, sorafenib, and artesunate) and inhibitors (e.g., ferrostatin, liproxstatin-1, and zileuton) of ferroptosis have been identified, but the specific mechanisms and pathways are diverse (Xie et al., 2016). In summary, ferroptosis is a complex process, and more pathways will be discussed in the following sections (**Figure 1**).

ROLES OF FERROPTOSIS IN CVDs

The Pathophysiologic Mechanisms of CVDs

The heart is one of the most important organs, and is responsible for pumping blood throughout the body, providing energy and oxygen to nourish tissues and organs, and removing metabolites, such as carbon dioxide. There are complex regulatory mechanisms involved in maintaining normal cardiac function.

Inflammation is an important molecular trigger in CVD. Considerable evidence has shown the close relationship between inflammation and atherosclerosis (Ross, 1999; Libby and Ridker, 2006; Wong et al., 2012), and some anti-inflammatory drugs, such as statins, work to prevent cardiovascular events (Shepherd et al., 1995; Ridker et al., 2001, 2005).

Endothelial dysfunction arises when endothelial cells (EC) are injured, or if there is an imbalance between vasoconstriction

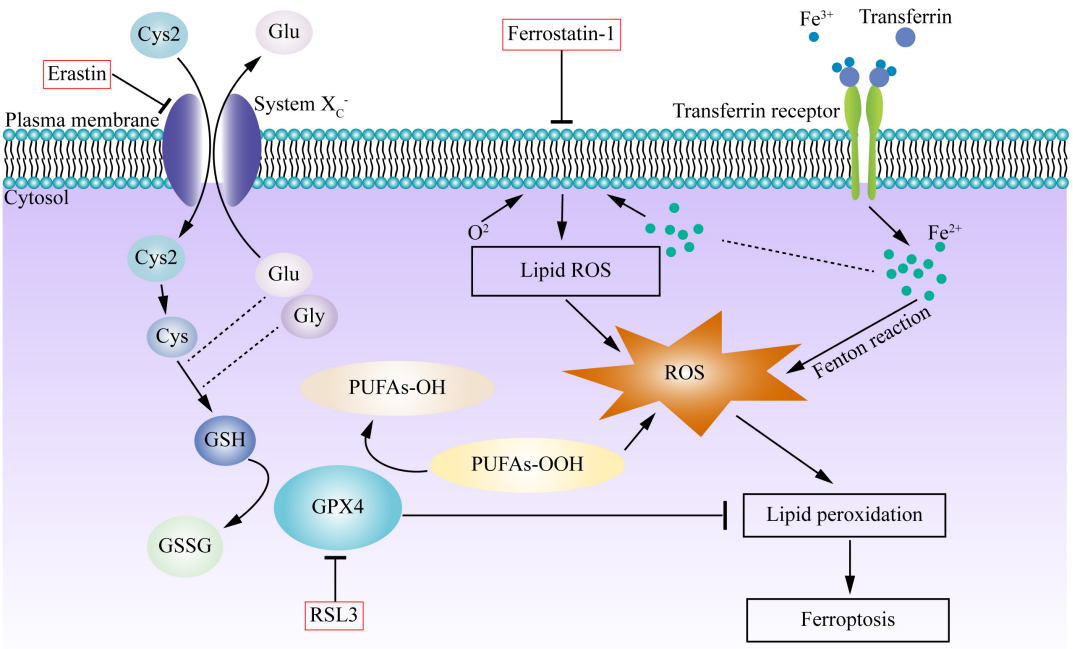

FIGURE 1 | Graphic mechanisms of ferroptosis. Dysregulation of intracellular iron metabolism or glutathione peroxidation pathways leads to accumulation of lipid ROS and eventually causes ferroptosis. Various inducers and inhibitors are shown in the red box. Arrows indicate promotion; blunt-ended lines indicate inhibition. Excessive free irons are the foundation for ferroptosis execution. Circulated Fe^{3+} was combined with transferrin, and then entered into cells by transferrin receptor. Iron in Fe^{3+} form was deoxidized into iron in Fe^{2+}, the latter generated ROS by Fenton reaction. System Xc- is an antiporter that imports cystine and exports glutamate, providing cysteine for glutathione synthesis, can be inhibited by erastin. GPX4 is a redox enzyme which reduces reactive aldehydes (PUFAs-OOH) to their alcohol form (PUFAs-OH), reduces ROS accumulation, plays important roles in the regulation of ferroptosis. RSL3 directly inhibit GPX4, which inhibits lipid peroxidation and prevent cell death, triggering the accumulation of ROS and boost ferroptosis. Ferrostatin-1 reduced the production of lipid ROS and attenuated ferroptosis. Cys, cysteine; Cys2, cystine; Glu, glutamate; Gly, glycine; GSH, glutathione; GSSH, glutathione disulfide; GPX4, glutathione peroxidase 4; PUFA, polyunsaturated fatty acid.

and vasodilation (Chatzizisis et al., 2007). The gathering of low-density lipoprotein (LDL) in the subendothelial layer is thought to be the initial event of atherogenesis (Russell et al., 1989; Williams and Tabas, 1995; Tabas et al., 2007). Oxidative-LDLs (Ox-LDLs) induce proinflammatory expression and formation of foam cells, which lead to endothelial dysfunction (Berliner et al., 2009; Golia et al., 2014), including the release of proinflammatory cytokines, such as interleukin (IL), interferon-γ (IFN-γ), and tumor necrosis factor (TNF; Ait-Oufella et al., 2006; Moriya, 2019). Many autoimmune diseases (e.g., system lupus erythematosus, psoriasis, and rheumatoid arthritis), are found to correlate with increased cardiovascular risk (Kiss et al., 2006; Hak et al., 2009; Vena et al., 2010; Dougados et al., 2014). When anti-inflammatory therapy is applied to systemic lupus erythematosus patients, the mortality of CVD is lower. The mortality is also lower when anti-inflammatory therapy is given to patients with psoriasis (Leonardi et al., 2012; Papp et al., 2012) and rheumatoid arthritis (Liuzzo et al., 1999; Pasceri and Yeh, 1999). Moreover, inflammatory responses, including the monocyte-macrophages, neutrophils, T-cell subsets, and oxidative stress, also contribute to the initiation and development of heart failure (Tanai and Frantz, 2016).

Substrate metabolism is essential for normal cellular physiological function, carbohydrates (e.g., glucose and lactate), and fatty acids are the general cellular energy substrates (Ussher et al., 2016). The production of ATP in the heart is derived mainly from mitochondrial oxidative phosphorylation (OXPHOS), the others come from glycolysis (Bertero and Maack, 2018). When the cardiac supply cannot satisfy the demand, the heart will shift from one substrate to another. The glucose metabolism produces much more phosphates, but less ATP than lipids, which means that glucose metabolism expends less oxygen compared to fatty acid oxidation (FAO) when synthesizing equivalent ATP (Nagoshi et al., 2011). As is shown in the Randle cycle, the lipid metabolism correlates with glucose metabolism in a competitive manner (Randle et al., 1963; Randle, 1998; Sugden, 2007).

Mechanistically, calcium overload regulates the cardiomyocytes, especially in ischemia/reperfusion. When the blood supply decreases, anaerobic metabolism will be upregulated, but cellular pH and ATP production will decline. Accordingly, the Na^+/H^+ exchanger (NHE) excretes hydrogen ions in exchange for sodium ions (Pike et al., 1993; Sanada et al., 2011). Ca^{2+} efflux deficiency, and constriction of the reuptake by the endoplasmic reticulum (ER) due to the lack of ATP, will result in calcium overload. Subsequently, the mitochondrial permeability transition (MPT) pore will open, and the mitochondrial membrane potential will change, further weaken the production of energy. After the blood supply is re-established, a cascade of events will be triggered to aggravate the injury.

Many kinds of cell death were found to be engaged in CVDs. Kuwana et al. (2002) provide compelling evidence that the permeabilization of the OMM is involved in apoptosis. When Ca^{2+} gets access into the mitochondria, and opens the mitochondrial permeability transition pore (mPTP), water flows into the mitochondria, causing it to swell and undergo necrosis (Baines et al., 2005). Matsui et al. (2007) reported that autophagy was mediated by AMP-activated protein kinase (AMPK)-dependent pathway in the heart during ischemia/reperfusion injury. Kanamori et al. (2011) verified that autophagy can protect cardiomyocytes from death when suffering from ischemia.

Ohara et al. (1993) first pictured the hallmark of oxidative stress in CVDs in a hypercholesterolemia model. The redox crosstalk contributes to many diseases, such as atherosclerosis. Endothelial dysfunction initiates the process of atherosclerosis. Oxidized LDL (oxLDL) leads to the release bioactive phospholipids that can activate ECs and promote the pathogenesis of atherosclerosis (Hansson et al., 2006). Judkins et al. (2010) discovered the elevated expression of NOX2, an isoform of NADPH oxidase, in ECs and macrophages of lipoprotein deficient ApoE-/- mice, which leads to the formation of atherosclerotic lesions and increased aortic superoxide production. Two studies led by Nishida et al. (2000, 2002) indicate that activation of G-protein coupled receptors (GPCR) can generate ROS. Experiments on neonatal rat ventricular myocytes verified the function of ROS in activating hypertrophic growth signaling via G-proteins (Dai et al., 2011). In hypertension, ROS elevate the concentration of intracellular Ca^{2+} as a second messenger, causing vasoconstriction (Brito et al., 2015). The NOX signaling pathway is important in vascular processes, and lack of NO (nitric oxide), but increased oxidative stress, can be observed in hypertension (Touyz, 2004). Dudley et al. (2005) found increased oxidative stress and $O^{2\cdot-}$ production relating to NADPH oxidase in an atrial fibrillation model. Aforementioned articles show evidence suggesting the function of oxidative stress in various kinds of CVDs, but further research on the mechanisms of oxidative stress may produce some unexpected breakthroughs.

Oxidative Stress-Induced Ferroptosis and CVDs

Cardiomyocytes account for approximately 75% of the heart's volume, and are rich in mitochondria. They are the main source of cardiac energy metabolism, and are the main site for the production of reactive oxidative species (ROS). Different kinds of cell death, including apoptosis, necrosis, pyroptosis, and ferroptosis, have been shown to be involved in the pathophysiologic process of various CVDs. Studies that describe the roles of ferroptosis in CVDs are listed in **Table 1**.

With the development of international research on ferroptosis, various types of iron death inducers and inhibitors were invented, but the specific mechanisms remain unknown. Myocardium iron overload is detected in mice I/R model, and the treatment of ferroptosis inhibitors can greatly improve cardiac function after I/R (Bulluck et al., 2016; Fang et al., 2019). Proteomic studies found that the down-regulation of myocardial GPX4 expression was detected in the early-stage (1 day) and mid-term (1 week) of myocardial infarction in mice, and inhibition of GPX4 expression or function in an *in vitro* model can significantly increase ferroptosis of myocardial cells (Park et al., 2019). Park et al. (2019) revealed that ROS and GPX4 is downregulated in the progression of MI regarding the involvement of the glutathione metabolic pathway. Li et al. found that severe

TABLE 1 | Existing studies suggesting the roles of ferroptosis in cardiovascular diseases.

References	Year	Models	Findings	Pathways
Li et al., 2020	2020	DM model were injected with streptozotocin in the tail vein	Inhibited ferroptosis could alleviate diabetes myocardial IRI	ATF4-CHOP pathway
				ERS pathway
		I/R model was made by ligation of LAD		
Chen et al., 2019	2019	Aortic banding (AB) group and sham-operated (SO) group	Increased TLR4 and NOX4 in HF; activated autophagy and increased ferroptosis	TLR4/NADPH oxidase 4 pathway
		TLR4-siRNAs group and NOX4-siRNAs group		
Feng et al., 2019	2019	Sham hearts, excised hearts in perfusion with KH buffer+LIP-1, or KH buffer+vehicle	Decreased infarct size, increased mitochondrial function	VDAC1
				GPX4
			Lip-1 protected heart from I/R injury	
Li et al., 2019	2019	Non-transplant-related myocardial IRI with vehicle or Fer-1. WT, TLR4-, CD14-, and Trif-deficient hearts	Inhibited ferroptosis and targeted the TLR4/Trif/type I IFN pathway improved IRI and inflammation after heart transplant	TLR4/Trif/type I IFN pathway
Song et al., 2021	2021	AMI models with infusion of PBS or exosomes	Decreased AMI mice myocardial injury through inhibiting ferroptosis	miR-23a-3p
				DMT1
Tang L. J. et al., 2021	2021	Rat model of myocardial ischemia or IRI	Ferroptosis mainly occurred in the phase of myocardial reperfusion but not ischemia	ACSL4, iron, malondialdehyde, and GPX4
Wang J. Y. et al., 2020	2020	A TAC mice model to establish Chronic Heart Failure	MiR-351 can decreased the level of MLK3	The JNK/p53 signaling pathway
Wang C. Y. et al., 2020	2020	Cecal ligation and puncture (CLP) operation. Control (ctrl), CLP, CLP + Dex, and CLP + Dex + YOH groups	Decreased sepsis-induced myocardial ferroptosis	HO-1, iron
				GPX4
Tadokoro et al., 2020	2020	Doxorubicin-induced cardiomyopathy (DIC) model in GPx4 Tg mice and GPx4 hetKO mice	Decreased GPX4 and increased ferroptosis in mitochondria	GPX4
Nemade et al., 2018	2018	Purified human iCell cardiomyocytes which are derived from hiPSCs treated with/without etoposide	The inhibitor of ferroptosis and apoptosis attenuated the heart injury caused by ETP	p53-mediated ferroptosis pathway
Park et al., 2019	2019	Myocardial infarction mouse model	Downregulation of GPX4 in MI advanced ferroptosis in cardiomyocytes	Glutathione, ROS, and GPX4

DM, diabetes mellitus; LAD, left anterior descending branch; I/R, ischemia/reperfusion; IRI, ischemia reperfusion injury; AB, aortic banding; SO, sham-operated; AMI, acute myocardial infarction; CLP, Cecal ligation and puncture; DIC, Doxorubicin-induced cardiomyopathy; HF, heart failure; Dex, Dexmedetomidine.

myocardial damage is observed in DM rat with I/R and cell in high-glucose reoxygenation. Ferrostatin-1, the inhibitor of ferroptosis, reduces the endoplasmic reticulum stress (ERS) and myocardial injury in diabetes mellitus (DM) rats with I/R, whereas erastin shows the opposite effect (Li et al., 2020). Ferroptosis is thought to contribute in the progression of heart failure. Chen et al. (2019) found that toll-like receptor 4 (TLR4) and NADPH oxidase 4 (NOX4) were up-regulated and differentially expressed genes (DEGs) in myocardium resulting from heart failure. The HF rats with knock-down of TLR4 and NOX4 by lentivirus siRNA were detected with attenuated autophagy and ferroptosis, improved heart function, and decreased death of myocytes. Friedmann Angeli et al. (2014) showed that liprostatin-1 suppresses ferroptosis in human cells. Feng et al. (2019) provided evidence suggesting that Lip-1 reduced the size of MI and preserved the mitochondrial function via the I/R model reperfused with Lip-1, further study suggested that Lip-1 treatment reduced VDAC1 level and oligomerization, increased antioxidant GPX4 protein level and decreased mitochondrial ROS production. Tang et al. concluded that ferroptosis participates in the phase of reperfusion rather than ischemia (Tang L. J. et al., 2021). The addition of ferrostatin-1 leads to reduced size of MI, and it improved systolic function. It is proposed that ferroptosis and the TLR4/Trif/type I IFN signaling pathway initiate the inflammation which is involved in the adhesion of neutrophils and endothelium after cardiac transplantation (Li et al., 2019). Human umbilical cord blood (HUCB) mesenchymal stem cells (MSC)-derived exosomes inhibited ferroptosis, and exhibited cardioprotective effects on myocardial injury of acute myocardial injury mice, which may be related to the reduced divalent metal transporter 1 (DMT1) expression caused by miR-23a-3p (Song et al., 2021). Mixed lineage kinase 3 (MLK3) regulates oxidative stress through the JNK/p53 signaling pathway, inducing ferroptosis in the pathophysiologic process of myocardial fibrosis under pressure overload (Wang J. Y. et al., 2020).

Research conducted by Wang C. Y. et al. (2020) found that dexmedetomidine can promote sepsis-related myocardial

ferroptosis and heart injury, acting through the decline of Ho-1 overexpression, iron levels, and GPX4 activity. Doxorubicin (DOX) is a traditional anthracycline chemotherapeutic with dose-dependent cardiac toxicity. In a study conducted by Tadokoro et al., DOX induced ferroptosis via downregulation of GPX4 and lipid peroxidation in mitochondria (Tadokoro et al., 2020). The other anti-cancer drug, etoposide (ETP), also causes cardiotoxicity. Human pluripotent stem cell-derived cardiomyocytes (hPSC-CMs) treated with liproxstatin-1 had increased function after the addition of ETP. The activation of the p53-mediated ferroptosis pathway by ETP is the key toward ETP-induced cardiotoxicity (Nemade et al., 2018). In summary, ferroptosis can be a target for protection against many CVDs, such as autotaxin (ATX), ferritin H, rapamycin, apart from ferroptosis inhibitors, such as ferrostatin-1 and liproxstatin-1 (Baba et al., 2017; Bai et al., 2018; Fang et al., 2019, 2020).

EPIGENETIC REGULATORS OF FERROPTOSIS AND OXIDATIVE STRESS

Epigenetic Regulators of Ferroptosis

In 1942, Waddington CH first proposed the name "epigenotype" and used the term "epigenetics" as the branch of biology emphasizing the relation between genes and their products (Waddington, 2012). Owing to the technological advances and new discoveries, the definition of epigenetics has evolved. Nowadays the most common definition is "the study of mitotically and/or meiotically heritable changes in gene function that cannot be explained by changes in DNA sequence" (Bonasio et al., 2010). One hallmark of epigenetics is the fixed nucleotide sequence (Goldberg et al., 2007). It is a new direction for the therapy of some related diseases. Epigenetics is a bridge that links genotype and phenotype. Currently, the epigenetic process can be clarified into DNA methylation, histone modification (including methylation, acetylation, phosphorylation, ubiquitination, and SUMOylation) and RNA-based mechanism [including long non-coding RNAs (lncRNAs) and microRNAs (miRNAs)] (Prasher et al., 2020).

Several studies have investigated the effect of some epigenetic molecules in ferroptosis in recent years. In Jiang et al.'s study, lymphocyte-specific helicase (LSH), a DNA methylation modifier, can interact with WDR76 to inhibit ferroptosis at the transcriptional level. WDR76 induce lipid metabolic gene and ferroptosis related gene expression in DNA methylation and histone modification via LSH and chromatin modification, the process is affected by lipid ROS and iron concentration (Tao et al., 2017). LncRNAs are made up of over 200 nucleotides but the ability to code protein is relatively low. Abnormal expression of LncRNAs have been shown to be associated with tumorigenesis. For example, LncRNAs participate in the pathophysiology of non-small cell lung cancers (NSCLC) by regulating ferroptosis (Wu et al., 2020). LncRNA function analysis showed that the ferroptosis pathway is associated with SLC7A11 which was downregulated in XAV939-treated NCI-H1299 cells, giving a potential therapeutic target for NSCLC (Yu et al., 2019). Different LncRNAs play different roles in ferroptosis. P53RRA activates the p53 pathway and influences gene transcription to promote ferroptosis, whereas LINC0336 decreases iron concentration and lipid ROS by interacting with ELAV-like RNA binding protein 1 (ELAVL1) to inhibit ferroptosis (Mao et al., 2018; Wang M. et al., 2019). Deubiquitinase is encoded by BRCA1-associated protein (BAP1). Several studies have revealed that BAP1 can inhibit ubiquitinated histone 2A (H2Aub) occupancy on the SLC7A11 promoter (Zhang et al., 2018). Experiments confirm that the downregulated SLC7A11 leads to cystine starvation and GSH depletion to block ferroptosis (Fan et al., 2018). Monoubiquitination of histone H2B on lysine 120 (H2Bub1) promotes the expression of SLC7A11 and regulates many metabolic-related genes, but the p53-USP7-H2Bub1 axis regulates ferroptosis (Wang Y. F. et al., 2019). Selenium-induced selenome gene augmentation can inhibit ferroptosis and protect neuronal cells at the epigenetic level (Alim et al., 2019). Research shows low DNA methylation and elevated levels of H3K4me3 and H3K27ac upstream of GPX4, indicating that high levels of GPX4 may be related with epigenetic regulation (Zhang et al., 2020). Wang et al. reported that overexpression of KDM3B (a histone H3 lysine 9 demethylase) led to decreased histone H3 lysine 9 methylation, but increased the expression of SLC7A11 with the transcription factor, ATF4 (Wang Y. S. et al., 2020).

Epigenetic Regulators of Oxidative Stress Response

There are also some epigenetic factors that affect oxidative stress response, but have not yet been proven to be directly related to ferroptosis, owing to the close contact between ferroptosis and oxidative stress, a brief introduction is made here. Experimental studies exploring epigenetic regulators of the oxidative stress response are shown in **Table 2**.

Many studies regarding epigenetic regulation have been conducted in cancers, mental illnesses, and immune diseases in recent years. Epigenetic regulation also plays a strong part in CVDs. In a study conducted by Xiao et al. (2019), they found that S-adenosylhomocysteine (SAH) levels in plasma were positively correlated with oxidative stress, and were inversely correlated with flow-mediated dilation and methylation of p66shc promoter in CAD (coronary artery disease) patients and normal subjects. Further research indicates that inhibition of SAH hydrolase results in the increased level of SAH and oxidative stress by epigenetic regulation of p66shc expression, leading to the endothelium injury that may accelerate the progression of atherosclerosis (Xiao et al., 2019).

Nitric oxide is a fundamental molecule that can regulate vasodilatation and prevent vascular inflammation (Tsutsui et al., 2006). SIRT1, a class III histone deacetylase involved in the aging of mice fibroblasts, human ECs, and tumor cells (Ota et al., 2006), may be relevant to the production of ROS and oxidative stress (Hwang et al., 2013). Ota et al. conducted a series of studies on the effects of SIRT1 in ECs. The elevated level of NO strengthens the SIRT1 activity and delays endothelial senescence, but the accumulation of oxidative stress and decreased production of NO in aging will lead to SIRT1 inactivation (Ota et al., 2008). Cilostazol, a selective inhibitor of PDE3, protects ECs from

TABLE 2 | Experiments on the epigenetic regulators of oxidative stress response.

References	Year	Models	Findings	Pathways
Xiao et al., 2019	2019	Animals were conducted with apolipoprotein E-deficient (apoE$^{-/-}$) and heterozygous SAHH knockout (SAHH$^{+/-}$) mice	Inhibition of SAHH led to decrease SAH levels in plasma, increase oxidative stress and endothelial dysfunction	p66shc-mediated pathway
Ota et al., 2010	2010	HUVECs were pretreated with vehicle, atorvastatin, pravastatin, or pitavastatin diluted in EGM-2 medium for 1 day	Decreased oxidative stress-induced endothelial senescence	The Akt Pathway
Ota et al., 2008	2008	Proliferating HUVECs exposed for 24 h to the indicated concentrations of sirtinol (Calbiochem) or nicotinamide (NAM, Wako Chemical Industries) diluted in medium.	Decreased oxidative stress-induced premature senescence	SIRT1
Hu et al., 2019	2019	NRVFs and rat aortic smooth muscle cells were equilibrated in corresponding medium with 0.1% FBS for 24 h prior to incubation with DMSO, TMP195, or AI-1 for 48 h	HDAC5 inhibition stimulated cardiac NRF2 activity by triggering oxidative stress and HDAC5 catalytic activity reduced cardiomyocyte oxidative stress	NRF2
Costantino et al., 2018	2018	Diabetes was induced in 4-month-old male C57/B6 mice by a single high dose of streptozotocin. An equal volume of citrate buffer was administered in control animals	P66Shc upregulated and induced oxidative stress in the diabetic heart. In vivo gene silencing of p66Shc rescued diabetes-induced myocardial dysfunction	P66shc
Xu et al., 2017	2017	The specific HDAC3 inhibitor RGFP966 and pan-HDAC inhibitor valproic acid were subcutaneously injected into the mice every other day for 3 months	RGFP966 prevented diabetes-induced cardiac dysfunction, inhibited diabetes-induced oxidative stress and inflammation in the mouse	DUSP5-ERK1/2 pathway
Hussain et al., 2020	2020	Diabetes was induced by streptozotocin and control group	Decreased JunD mRNA and protein expression in STZ-induced diabetes	JunD

apoE$^{-/-}$, apolipoprotein E-deficient; SAH, S-adenosylhomocysteine; SAHH, SAH hydrolase; HUVECs, Human umbilical vein endothelial cells; STZ, streptozotocin.

ischemic damage by producing NO. Ota and his colleagues observed cells treated with H_2O_2 or Cilostazol, and evaluated the expression of senescence-associated beta-galactosidase assay (SA-betagal). They found that cilostazol increased phosphorylation of Akt at Ser473, as well as eNOS at Ser1177, but the phosphorylation increased SIRT1 expression in a dose-dependent manner (Ota et al., 2008). A similar experiment was conducted by Ota et al. to determine the mechanisms underlying the vascular protective effects of statins. Statins prevent the endothelium from aging by enhancing SIRT1 through the Akt pathway (Ota et al., 2010). Hu et al. found that HDAC5 catalytic activity inhibits cardiomyocyte oxidative stress via NRF2 stimulation. The selective class IIa HDAC inhibitors, TMP195 or TMP269, or shRNA-mediated knockdown of HDAC5 can lead to NRF2-mediated transcription (Hu et al., 2019).

In the diabetic heart, the expression of p66shc increases, but 3-week intensive glycemic control cannot reverse it. Further experiments, which silence the gene of p66shc *in vivo*, lead to the inhibition of ROS and promotion of cardiac function. Upregulation of miR-218 and miR-34a results in changes of the DNMT3b/SIRT1 axis in the diabetic heart, which may be a potential target to cure diabetic cardiomyopathy (Costantino et al., 2018). Another study, conducted by Hussain et al. (2020), found that JunD (a member of AP-1 transcript family) mRNA and protein are shown to have decreased expression in STZ-induced diabetes, which is relevant to oxidative stress, and is regulated by DNA hypermethylation, post-translational modification of histone markers, and translational inhibition by miRNA. Xu et al. treated diabetic mice with HDAC3 inhibitor, RGFP966, and found improved heart dysfunction, hypertrophy, fibrosis, and diminished oxidative stress. Furthermore, increased phosphorylated extracellular signal-regulated kinases (ERK) 1/2 and decreased dual specificity phosphatase 5 (DUSP5) were observed, but RGFP966 can reverse this. Elevated histone H3 acetylation plays an important role DUSP5 gene promoter in diabetic cardiomyopathy (Xu et al., 2017).

EPIGENETIC REGULATORS AS NOVEL THERAPEUTICS

Over the past two decades, mounting efforts have been made to uncover new ways for cardiac repair, such as drug development (e.g., diuretics and ARNI), cardiac devices [e.g., pacemakers and implantable cardiac defibrillators (ICD)], and operations [e.g., electrical defibrillations and transcatheter aortic valve replacement (TAVR)]. In addition, the prognosis of CVD is not satisfied, and further investigation exploring fundamental mechanisms of impaired cardiomyocytes is needed. Epigenetic regulators provide a potential kind of therapy to treat CVDs, which will lay the foundation for individualized medical care.

Iron metabolism homeostasis is strictly regulated by multiple genes, including divalent metal transport-1 (DMT1), TFR1, TFR2, ferroportin (FPN), hepcidin (HAMP), hemojuvelin (HJV), and Ferritin H (Duan et al., 2020). Moreover, epigenetic regulators, such as DNA methylation, histone acetylation, and microRNA participate in iron metabolism homeostasis.

The therapies of CVDs targeting epigenetics are relatively rare. As mentioned above, SIRT1 expression has positive effects in many diseases, including cancer, CVDs, chronic obstructive pulmonary disease (COPD), and type 2 diabetes (Satoh et al., 2011). Resveratrol, a SIRT1 activator, has been

suggested to improve heart function via vasodilation, antioxidant activity, and platelet aggregation (Baur and Sinclair, 2006). Resveratrol regulate the vasorelaxant activity through Ca^{2+}-activated K+ channels (Li et al., 2000) and NO signaling in the endothelium (Orallo et al., 2002). Das et al. suggested resveratrol upregulates both endothelial and inducible NO synthase (eNOS and iNOS) (Das et al., 2005). Cilostazol protects ECs from ischemic injury by increasing SIRT1-dependent eNOS phosphorylation, producing substantial NO, and the inhibition of SIRT1 leads to inactivation of cilostazol on premature senescence (Ota et al., 2008). Currently, cilostazol is a common clinical drug aiming at ameliorating damage from ischemic injury. A novel SIRT activator, 1,4-dihydropyridine derivatives (DHPs), shows enhanced mitochondrial activity involving PGC-1α (Mai et al., 2009).

Noncoding RNAs are reportedly a potential target for therapeutics in CVDs (Lucas et al., 2018). In acute myocardial infarction, several families of miRNAs kick in, miR-34 can promote telomere erosion, and can regulate the target gene PNUTS (Bernardo et al., 2012; Boon et al., 2013), miR-24 target sirtuin 1, and can regulate EC apoptosis (Fiedler et al., 2011). Inhibition of miR-25 promotes heart function pertaining to the calcium uptake pump, SERCA2a (sarco/ER Ca^{2+}-ATPase 2a) (Wahlquist et al., 2014). The related therapies include antisense oligonucleotides, siRNAs, antagomiRNAs, and antimiRNA application.

Yang K. C. et al. (2014) described the myocardial RNA sequence, suggested that the expression profiles of lncRNAs, but not mRNAs or miRNAs, can predict the different pathology of failing heart, indicating the important role of lncRNAs in CVDs. The lncRNA Mhrt (myosin heavy chain-associated RNA transcript) was found repressed under pathological stress condition such as pressure overload-induced hypertrophy and showed cardioprotective effects when restore the physiological concentration (Han et al., 2014). Piccoli et al. (2017) provided evidence suggesting that Inhibition of lncRNA Meg3, which is rich in cardiac fibroblasts, can prevent cardiac fibrosis and diastolic dysfunction. Mutations of the lncRNA H19 have been found related to coronary artery disease (Gao W. et al., 2015). The expression of H19 is highly reduced in atherosclerotic plaques or vascular injury, indicating the important role in cardiovascular system (Kim et al., 1994; Han et al., 1996). LncRNA therapeutics are also promising, in addition to inhibit lncRNA by antimiRs, the function of lncRNA can be blocked by shRNAs including siRNAs, modifed ASOs (antisense oligonucleotides), and gapmers (Lucas et al., 2018).

A growing number of experiments show evidence suggesting the involvement of epigenetics in cancer, CVDs, and metabolic diseases, which provides new ideas on the therapy of refractory diseases. Precision medicine and personalized therapy is the trend, as the development of medicine, genomics, and epigenetics will be the most important tools of the new generation of doctors.

CONCLUSION

Ferroptosis is a novel programmed cell death involving inhibition of enzyme GPX4 and lipid hydroperoxides, which was first widely studied in oncology. Oxidative stress-induced ferroptosis have been found to be extensively involved in the biogenesis and development of CVDs, and the inducers, the inhibitors, and the pathways of ferroptosis have been widely explored. Nowadays, the understanding of the role of epigenetics in ferroptosis have greatly increased. However, epigenetic mechanisms, such as lncRNAs, histone monoubiquitination, and DNA methylation are showed to engage in the ferroptosis process involved with CVDs.

Research on epigenetic drugs for CVDs has made great achievements, such as resveratrol, cilostazol, and miRNA family, which reveal the potential of epigenetic therapy for CVDs. However, the current epigenetic molecular mechanism of ferroptosis and the study of cardiac ferroptosis still need to be studied in depth. Thorough research in both basic research and clinical studies, are necessary to fully elucidate the relationship between ferroptosis and epigenetics in CVDs. Some biology approaches including total RNA-sequencing (RNA-seq), single cell RNA-seq, chromatin-immunoprecipitation-sequencing (ChIP-seq), and DNA methylation profiling can help us to further explore the epigenetic regulation with ferroptosis (Xu et al., 2018). And modern biotechnologies such as CRISPR/Cas9, Cre-loxp, proteomics, metabolism omics can comprehensively study the specific mechanisms of epigenetic regulation of ferroptosis for different genes and different stages of iron homeostasis. Hopefully, therapy against epigenetic targets will be promising for treating CVDs in the future.

AUTHOR CONTRIBUTIONS

YZ and JLi participated in the design of the review. JLi, YZ, HW, and JLo drafted the manuscript and made the original figures. HC, CL, and YD critically revised the texts and the figures. AS, HC, and YD supervised the research and led the discussion. All authors read and approved the final manuscript.

FUNDING

This work was funded by the National Natural Science Foundation of China (81701144).

REFERENCES

Ait-Oufella, H., Salomon, B. L., Potteaux, S., Robertson, A. K., Gourdy, P., Zoll, J., et al. (2006). Natural regulatory T cells control the development of atherosclerosis in mice. *Nat. Med.* 12, 178–180. doi: 10.1038/nm1343

Alim, I., Caulfield, J. T., Chen, Y. X., Swarup, V., Geschwind, D. H., Ivanova, E., et al. (2019). Selenium drives a transcriptional adaptive program to block

ferroptosis and treat stroke. *Cell* 177, 1262.e–1279.e. doi: 10.1016/j.cell.2019.03.032

Angeli, J. P. F., Schneider, M., Proneth, B., Tyurina, Y. Y., Tyurin, V. A., Hammond, V. J., et al. (2014). Inactivation of the ferroptosis regulator Gpx4 triggers acute renal failure in mice. *Nat Cell Biol* 16, 1180–1191. doi: 10.1038/ncb3064

Baba, Y., Higa, J. K., Shimada, B. K., Horiuchi, K. M., Suhara, T., Kobayashi, M., et al. (2017). Protective effects of the mechanistic target of rapamycin against excess iron and ferroptosis in cardiomyocytes. *Am. J. Physiol. Heart Circ. Physiol.* 314, H659–H668. doi: 10.1152/ajpheart.00452.2017

Bai, Y. T., Chang, R., Wang, H., Xiao, F. J., Ge, R. L., and Wang, L. S. (2018). ENPP2 protects cardiomyocytes from erastin-induced ferroptosis. *Biochem. Biophys. Res. Commun* 499, 44–51. doi: 10.1016/j.bbrc.2018.03.113

Baines, C. P., Kaiser, R. A., Purcell, N. H., Blair, N. S., Osinska, H., Hambleton, M. A., et al. (2005). Loss of cyclophilin D reveals a critical role for mitochondrial permeability transition in cell death. *Nature* 434, 658–662. doi: 10.1038/nature03434

Baur, J. A., and Sinclair, D. A. (2006). Therapeutic potential of resveratrol: the in vivo evidence. *Nat. Rev. Drug Discov.* 5, 493–506. doi: 10.1038/nrd2060

Berliner, J. A., Leitinger, N., and Tsimikas, S. (2009). The role of oxidized phospholipids in atherosclerosis. *J. Lipid Res.* 50(Suppl.), S207–S212. doi: 10.1194/jlr.R800074-JLR200

Bernardo, B. C., Gao, X. M., Winbanks, C. E., Boey, E. J., Tham, Y. K., Kiriazis, H., et al. (2012). Therapeutic inhibition of the miR-34 family attenuates pathological cardiac remodeling and improves heart function. *Proc. Natl. Acad. Sci. U.S.A.* 109, 17615–17620. doi: 10.1073/pnas.1206432109

Bersuker, K., Hendricks, J. M., Li, Z., Magtanong, L., Ford, B., Tang, P. H., et al. (2019). The CoQ oxidoreductase FSP1 acts parallel to GPX4 to inhibit ferroptosis. *Nature* 575, 688–692. doi: 10.1038/s41586-019-1705-2

Bertero, E., and Maack, C. (2018). Metabolic remodelling in heart failure. *Nat. Rev. Cardiol.* 15, 457–470. doi: 10.1038/s41569-018-0044-6

Birnbaum, Y., Hale, S. L., and Kloner, R. A. (1996). The effect of coenzyme Q10 on infarct size in a rabbit model of ischemia/reperfusion. *Cardiovasc. Res.* 32, 861–868.

Bonasio, R., Tu, S., and Reinberg, D. (2010). Molecular signals of epigenetic states. *Science* 330, 612–616. doi: 10.1126/science.1191078

Boon, R. A., Iekushi, K., Lechner, S., Seeger, T., Fischer, A., Heydt, S., et al. (2013). MicroRNA-34a regulates cardiac ageing and function. *Nature* 495, 107–110. doi: 10.1038/nature11919

Borrelli, E., Nestler, E. J., Allis, C. D., Murakami, K., Hayashidani, S., Ikeuchi, M., et al. (2008). Decoding the epigenetic language of neuronal plasticity. *Neuron* 60, 961–974. doi: 10.1016/j.neuron.2008.10.012

Brito, R., Castillo, G., Gonzalez, J., Valls, N., and Rodrigo, R. (2015). Oxidative stress in hypertension: mechanisms and therapeutic opportunities. *Exp. Clin. Endocrinol. Diabetes* 123, 325–335. doi: 10.1055/s-0035-1548765

Bulluck, H., Rosmini, S., Abdel-Gadir, A., White, S. K., Bhuva, A. N., Treibel, T. A., et al. (2016). Residual myocardial iron following intramyocardial hemorrhage during the convalescent phase of reperfused ST-segment-elevation myocardial infarction and adverse left ventricular remodeling. *Circ. Cardiovasc. Imaging* 9:e004940. doi: 10.1161/CIRCIMAGING.116.004940

Chatzizisis, Y. S., Coskun, A. U., Jonas, M., Edelman, E. R., Feldman, C. L., and Stone, P. H. (2007). Role of endothelial shear stress in the natural history of coronary atherosclerosis and vascular remodeling: molecular, cellular, and vascular behavior. *J. Am. Coll. Cardiol.* 49, 2379–2393. doi: 10.1016/j.jacc.2007.02.059

Chen, X., Li, J., Kang, R., Klionsky, D. J., and Tang, D. (2020). Ferroptosis: machinery and regulation. *Autophagy* 1–28. doi: 10.1080/15548627.2020.1810918

Chen, X. Q., Xu, S. D., Zhao, C. X., and Liu, B. (2019). Role of TLR4/NADPH oxidase 4 pathway in promoting cell death through autophagy and ferroptosis during heart failure. *Biochem. Biophys. Res. Commun.* 516, 37–43. doi: 10.1016/j.bbrc.2019.06.015

Costantino, S., Paneni, F., Mitchell, K., Mohammed, S. A., Hussain, S., Gkolfos, C., et al. (2018). Hyperglycaemia-induced epigenetic changes drive persistent cardiac dysfunction via the adaptor p66(Shc). *Int. J. Cardiol.* 268, 179–186. doi: 10.1016/j.ijcard.2018.04.082

Dabkowski, E. R., Williamson, C. L., and Hollander, J. M. (2008). Mitochondria-specific transgenic overexpression of phospholipid hydroperoxide glutathione peroxidase (GPx4) attenuates ischemia/reperfusion-associated cardiac dysfunction. *Free Radic. Biol. Med.* 45, 855–865. doi: 10.1016/j.freeradbiomed.2008.06.021

Dai, D. F., Johnson, S. C., Villarin, J. J., Chin, M. T., Nieves-Cintrón, M., Chen, T., et al. (2011). Mitochondrial oxidative stress mediates angiotensin II-induced cardiac hypertrophy and Galphaq overexpression-induced heart failure. *Circ. Res.* 108, 837–846. doi: 10.1161/CIRCRESAHA.110.232306

Das, S., Alagappan, V. K., Bagchi, D., Sharma, H. S., Maulik, N., and Das, D. K. (2005). Coordinated induction of iNOS-VEGF-KDR-eNOS after resveratrol consumption: a potential mechanism for resveratrol preconditioning of the heart. *Vascul. Pharmacol.* 42, 281–289. doi: 10.1016/j.vph.2005.02.013

Dixon, S. J., Lemberg, K. M., Lamprecht, M. R., Skouta, R., Zaitsev, E. M., Gleason, C. E., et al. (2012). Ferroptosis: an iron-dependent form of nonapoptotic cell death. *Cell* 149, 1060–1072. doi: 10.1016/j.cell.2012.03.042

Doll, S., Freitas, F. P., Shah, R., Aldrovandi, M., da Silva, M. C., Ingold, I., et al. (2019). FSP1 is a glutathione-independent ferroptosis suppressor. *Nature* 575, 693–698. doi: 10.1038/s41586-019-1707-0

Dolma, S., Lessnick, S. L., Hahn, W. C., and Stockwell, B. R. (2003). Identification of genotype-selective antitumor agents using synthetic lethal chemical screening in engineered human tumor cells. *Cancer Cell* 3, 285–296. doi: 10.1016/S1535-6108(03)00050-3

Dougados, M., Soubrier, M., Antunez, A., Balint, P., Balsa, A., Buch, M. H., et al. (2014). Prevalence of comorbidities in rheumatoid arthritis and evaluation of their monitoring: results of an international, cross-sectional study (COMORA). *Ann. Rheum. Dis.* 73, 62–68. doi: 10.1136/annrheumdis-2013-204223

Duan, L., Yin, X., Meng, H., Fang, X., Min, J., and Wang, F. (2020). [Progress on epigenetic regulation of iron homeostasis]. *Zhejiang Da Xue Xue Bao Yi Xue Ban* 49, 58–70.

Dudley, S. C., Hoch, N. E., McCann, L. A., Honeycutt, C., Diamandopoulos, L., Fukai, T., et al. (2005). Atrial fibrillation increases production of superoxide by the left atrium and left atrial appendage–role of the NADPH and xanthine oxidases. *Circulation* 112, 1266–1273. doi: 10.1161/Circulationaha.105.538108

Fan, L. H., Yin, S. T., Zhang, E. X., and Hu, H. (2018). Role of p62 in the regulation of cell death induction. *Apoptosis* 23, 187–193. doi: 10.1007/s10495-018-1445-z

Fang, X., Wang, H., Han, D., Xie, E., Yang, X., Wei, J., et al. (2019). Ferroptosis as a target for protection against cardiomyopathy. *Proc. Natl. Acad. Sci. U.S.A.* 116, 2672–2680. doi: 10.1073/pnas.1821022116

Fang, X. X., Cai, Z. X., Wang, H., Han, D., Cheng, Q., Zhang, P., et al. (2020). Loss of cardiac ferritin H facilitates cardiomyopathy via Slc7a11-mediated ferroptosis. *Circ. Res.* 127, 486–501. doi: 10.1161/Circresaha.120.316509

Feng, Y. S., Madungwe, N. B., Aliagan, A. D. I., Tombo, N., and Bopassa, J. G. (2019). Liproxstatin-1 protects the mouse myocardium against ischemia/reperfusion injury by decreasing VDAC1 levels and restoring GPX4 levels. *Biochem. Biophys. Res. Commun.* 520, 606–611. doi: 10.1016/j.bbrc.2019.10.006

Fiedler, J., Jazbutyte, V., Kirchmaier, B. C., Gupta, S. K., Lorenzen, J., Hartmann, D., et al. (2011). MicroRNA-24 regulates vascularity after myocardial infarction. *Circulation* 124, 720–730. doi: 10.1161/CIRCULATIONAHA.111.039008

Friedmann Angeli, J. P., Schneider, M., Proneth, B., Tyurina, Y. Y., Tyurin, V. A., Hammond, V. J., et al. (2014). Inactivation of the ferroptosis regulator Gpx4 triggers acute renal failure in mice. *Nat. Cell Biol.* 16, 1180–1191. doi: 10.1038/ncb3064

Gao, H., Bai, Y. S., Jia, Y. Y., Zhao, Y., Kang, R., Tang, D., et al. (2018). Ferroptosis is a lysosomal cell death process. *Biochem. Biophys. Res. Commun.* 503, 1550–1556. doi: 10.1016/j.bbrc.2018.07.078

Gao, M., Monian, P., Quadri, N., Ramasamy, R., and Jiang, X. (2015). Glutaminolysis and transferrin regulate ferroptosis. *Mol. Cell* 59, 298–308. doi: 10.1016/j.molcel.2015.06.011

Gao, M., Yi, J., Zhu, J., Minikes, A. M., Monian, P., Thompson, C. B., et al. (2019). Role of mitochondria in ferroptosis. *Mol. Cell* 73, 354.e3–363.e3. doi: 10.1016/j.molcel.2018.10.042

Gao, W., Zhu, M., Wang, H., Zhao, S., Zhao, D., Yang, Y., et al. (2015). Association of polymorphisms in long non-coding RNA H19 with coronary artery disease risk in a Chinese population. *Mutat. Res.* 772, 15–22. doi: 10.1016/j.mrfmmm.2014.12.009

Goldberg, A. D., Allis, C. D., and Bernstein, E. (2007). Epigenetics: a landscape takes shape. *Cell* 128, 635–638. doi: 10.1016/j.cell.2007.02.006

Golia, E., Limongelli, G., Natale, F., Fimiani, F., Maddaloni, V., Pariggiano, I., et al. (2014). Inflammation and cardiovascular disease: from pathogenesis to therapeutic target. *Curr. Atheroscler. Rep.* 16:435. doi: 10.1007/s11883-014-0435-z

Hak, A. E., Karlson, E. W., Feskanich, D., Stampfer, M. J., and Costenbader, K. H. (2009). Systemic lupus erythematosus and the risk of cardiovascular disease: results from the nurses' health study. *Arthritis Rheum.* 61, 1396–1402. doi: 10.1002/art.24537

Han, D. K., Khaing, Z. Z., Pollock, R. A., Haudenschild, C. C., and Liau, G. (1996). H19, a marker of developmental transition, is reexpressed in human atherosclerotic plaques and is regulated by the insulin family of growth factors in cultured rabbit smooth muscle cells. *J. Clin. Invest.* 97, 1276–1285. doi: 10.1172/JCI118543

Han, P., Li, W., Lin, C. H., Yang, J., Shang, C., Nuernberg, S. T., et al. (2014). A long noncoding RNA protects the heart from pathological hypertrophy. *Nature* 514, 102–106. doi: 10.1038/nature13596

Hansson, G. K., Robertson, A. K. L., and Soderberg-Naucler, C. (2006). Inflammation and atherosclerosis. *Annu. Rev. Pathol. Mech.* 1, 297–329. doi: 10.1146/annurev.pathol.1.110304.100100

Hassan, W., Noreen, H., Khalil, S. U., Hussain, A., Rehman, S., Sajjad, S., et al. (2016). Ethanolic extract of *Nigella sativa* protects Fe(II) induced lipid peroxidation in rat's brain, kidney and liver homogenates. *Pak. J. Pharm. Sci.* 29, 231–237.

Hu, T. J., Schreiter, F. C., Bagchi, R. A., Tatman, P. D., Hannink, M., and McKinsey, T. A. (2019). HDAC5 catalytic activity suppresses cardiomyocyte oxidative stress and NRF2 target gene expression. *J. Biol. Chem.* 294, 8640–8652. doi: 10.1074/jbc.RA118.007006

Hussain, S., Khan, A. W., Akhmedov, A., Suades, R., Costantino, S., Paneni, F., et al. (2020). Hyperglycemia induces myocardial dysfunction via epigenetic regulation of JunD. *Circ. Res.* 127, 1261–1273. doi: 10.1161/Circresaha.120.317132

Hwang, J. W., Yao, H. W., Caito, S., Sundar, I. K., and Rahman, I. (2013). Redox regulation of SIRT1 in inflammation and cellular senescence. *Free Radic. Biol. Med.* 61, 95–110. doi: 10.1016/j.freeradbiomed.2013.03.015

Judkins, C. P., Diep, H., Broughton, B. R. S., Mast, A. E., Hooker, E. U., Miller, A. A., et al. (2010). Direct evidence of a role for Nox2 in superoxide production, reduced nitric oxide bioavailability, and early atherosclerotic plaque formation in ApoE(-/-) mice. *Am. J. Physiol. Heart Circ. Physiol.* 298, H24–H32. doi: 10.1152/ajpheart.00799.2009

Kanamori, H., Takemura, G., Goto, K., Maruyama, R., Ono, K., Nagao, K., et al. (2011). Autophagy limits acute myocardial infarction induced by permanent coronary artery occlusion. *Am. J. Physiol. Heart Circ. Physiol.* 300, H2261–H2271. doi: 10.1152/ajpheart.01056.2010

Kim, D. K., Zhang, L., Dzau, V. J., and Pratt, R. E. (1994). H19, a developmentally regulated gene, is reexpressed in rat vascular smooth muscle cells after injury. *J. Clin. Invest.* 93, 355–360. doi: 10.1172/JCI116967

Kiss, E., Soltesz, P., Der, H., Kocsis, Z., Tarr, T., Bhattoa, H., et al. (2006). Reduced flow-mediated vasodilation as a marker for cardiovascular complications in lupus patients. *J. Autoimmun.* 27, 211–217. doi: 10.1016/j.jaut.2006.09.008

Kraft, V. A. N., Bezjian, C. T., Pfeiffer, S., Ringelstetter, L., Müller, C., Zandkarimi, F., et al. (2020). GTP cyclohydrolase 1/tetrahydrobiopterin counteract ferroptosis through lipid remodeling. *ACS Central Sci.* 6, 41–53. doi: 10.1021/acscentsci.9b01063

Kuwana, T., Mackey, M. R., Perkins, G., Ellisman, M. H., Latterich, M., Schneiter, R., et al. (2002). Bid, Bax, and lipids cooperate to form supramolecular openings in the outer mitochondrial membrane. *Cell* 111, 331–342. doi: 10.1016/s0092-8674(02)01036-x

Leonardi, C., Matheson, R., Zachariae, C., Cameron, G., Li, L., Edson-Heredia, E., et al. (2012). Anti-interleukin-17 monoclonal antibody ixekizumab in chronic plaque psoriasis. *N. Engl. J. Med.* 366, 1190–1199. doi: 10.1056/NEJMoa1109997

Lewerenz, J., Hewett, S. J., Huang, Y., Lambros, M., Gout, P. W., Kalivas, P. W., et al. (2013). The cystine/glutamate antiporter system x(c)(-) in health and disease: from molecular mechanisms to novel therapeutic opportunities. *Antioxid. Redox Signal.* 18, 522–555. doi: 10.1089/ars.2011.4391

Li, H. F., Chen, S. A., and Wu, S. N. (2000). Evidence for the stimulatory effect of resveratrol on Ca(2+)-activated K+ current in vascular endothelial cells. *Cardiovasc. Res.* 45, 1035–1045. doi: 10.1016/s0008-6363(99)00397-1

Li, W., Feng, G., Gauthier, J. M., Lokshina, I., Higashikubo, R., Evans, S., et al. (2019). Ferroptotic cell death and TLR4/Trif signaling initiate neutrophil recruitment after heart transplantation. *J. Clin. Invest.* 129, 2293–2304. doi: 10.1172/JCI126428

Li, W. Y., Li, W., Leng, Y., Xiong, Y., and Xia, Z. (2020). Ferroptosis is involved in diabetes myocardial ischemia/reperfusion injury through endoplasmic reticulum stress. *DNA Cell Biol.* 39, 210–225. doi: 10.1089/dna.2019.5097

Liang, H. Y., Yoo, S. E., Na, R., Walter, C. A., Richardson, A., and Ran, Q. (2009). Short form glutathione peroxidase 4 is the essential isoform required for survival and somatic mitochondrial functions. *J. Biol. Chem.* 284, 30836–30844. doi: 10.1074/jbc.M109.032839

Libby, P., and Ridker, P. M. (2006). Inflammation and atherothrombosis–from population biology and bench research to clinical practice. *J. Am. Coll. Cardiol.* 48, A33–A46. doi: 10.1016/j.jacc.2006.08.011

Liuzzo, G., Kopecky, S. L., Frye, R. L., O'Fallon, W. M., Maseri, A., Goronzy, J. J., et al. (1999). Perturbation of the T-cell repertoire in patients with unstable angina. *Circulation* 100, 2135–2139. doi: 10.1161/01.cir.100.21.2135

Lucas, T., Bonauer, A., and Dimmeler, S. (2018). RNA therapeutics in cardiovascular disease. *Circ. Res.* 123, 205–220. doi: 10.1161/CIRCRESAHA.117.311311

Mai, A., Valente, S., Meade, S., Carafa, V., Tardugno, M., Nebbioso, A., et al. (2009). Study of 1,4-dihydropyridine structural scaffold: discovery of novel sirtuin activators and inhibitors. *J. Med. Chem.* 52, 5496–5504. doi: 10.1021/jm9008289

Mao, C., Wang, X., Liu, Y. T., Wang, M., Yan, B., Jiang, Y., et al. (2018). A G3BP1-interacting lncRNA promotes ferroptosis and apoptosis in cancer via nuclear sequestration of p53. *Cancer Res.* 78, 3484–3496. doi: 10.1158/0008-5472.Can-17-3454

Matsui, Y., Takagi, H., Qu, X. P., Abdellatif, M., Sakoda, H., Asano, T., et al. (2007). Distinct roles of autophagy in the heart during ischemia and reperfusion–roles of AMP-activated protein kinase and Beclin 1 in mediating autophagy. *Circ. Res.* 100, 914–922. doi: 10.1161/01.Res.0000261924.76669.36

Moriya, J. (2019). Critical roles of inflammation in atherosclerosis. *J. Cardiol.* 73, 22–27. doi: 10.1016/j.jjcc.2018.05.010

Nagoshi, T., Yoshimura, M., Rosano, G. M., Lopaschuk, G. D., and Mochizuki, S. (2011). Optimization of cardiac metabolism in heart failure. *Curr. Pharm. Des.* 17, 3846–3853. doi: 10.2174/138161211798357773

Nemade, H., Chaudhari, U., Acharya, A., Hescheler, J., Hengstler, J. G., Papadopoulos, S., et al. (2018). Cell death mechanisms of the anti-cancer drug etoposide on human cardiomyocytes isolated from pluripotent stem cells. *Arch. Toxicol.* 92, 1507–1524. doi: 10.1007/s00204-018-2170-7

Nishida, M., Maruyama, Y., Tanaka, R., Kontani, K., Nagao, T., and Kurose, H. (2000). G alpha(i) and G alpha(o) are target proteins of reactive oxygen species. *Nature* 408, 492–495. doi: 10.1038/35044120

Nishida, M., Schey, K. L., Takagahara, S., Kontani, K., Katada, T., Urano, Y., et al. (2002). Activation mechanism of Gi and Go by reactive oxygen species. *J. Biol. Chem.* 277, 9036–9042. doi: 10.1074/jbc.M107392200

Ohara, Y., Peterson, T. E., and Harrison, D. G. (1993). hypercholesterolemia increases endothelial superoxide anion production. *J. Clin. Invest.* 91, 2546–2551. doi: 10.1172/Jci116491

Ooko, E., Saeed, M. E. M., Kadioglu, O., Sarvi, S., Colak, M., Elmasaoudi, K., et al. (2015). Artemisinin derivatives induce iron-dependent cell death (ferroptosis) in tumor cells. *Phytomedicine* 22, 1045–1054. doi: 10.1016/j.phymed.2015.08.002

Orallo, F., Alvarez, E., Camina, M., Leiro, J. M., Gómez, E., and Fernández, P. (2002). The possible implication of trans-resveratrol in the cardioprotective effects of long-term moderate wine consumption. *Mol. Pharmacol.* 61, 294–302. doi: 10.1124/mol.61.2.294

Ota, H., Eto, M., Kano, M. R., Kahyo, T., Setou, M., Ogawa, S., et al. (2010). Induction of endothelial nitric oxide synthase, SIRT1, and catalase by statins inhibits endothelial senescence through the Akt pathway. *Arterioscler. Thromb. Vasc. Biol.* 30, 2205–2211. doi: 10.1161/Atvbaha.110.210500

Ota, H., Eto, M., Kano, M. R., Ogawa, S., Iijima, K., Akishita, M., et al. (2008). Cilostazol inhibits oxidative stress-induced premature senescence via upregulation of Sirt1 in human endothelial cells. *Arterioscler. Thromb. Vasc. Biol.* 28, 1634–1639. doi: 10.1161/Atvbaha.108.164368

Ota, H., Tokunaga, E., Chang, K., Hikasa, M., Iijima, K., Eto, M., et al. (2006). Sirt1 inhibitor, sirtinol, induces senescence-like growth arrest with attenuated Ras-MAPK signaling in human cancer cells. *Oncogene* 25, 176–185. doi: 10.1038/sj.onc.1209049

Papp, K. A., Leonardi, C., Menter, A., Ortonne, J. P., Krueger, J. G., Kricorian, G., et al. (2012). Brodalumab, an anti-interleukin-17-receptor antibody for psoriasis. *N. Engl. J. Med.* 366, 1181–1189. doi: 10.1056/NEJMoa1109017

Park, T. J., Park, J. H., Lee, G. S., Lee, J.-Y., Shin, J. H., Kim, M. W., et al. (2019). Quantitative proteomic analyses reveal that GPX4 downregulation during myocardial infarction contributes to ferroptosis in cardiomyocytes. *Cell Death Dis.* 10:835. doi: 10.1038/s41419-019-2061-8

Pasceri, V., and Yeh, E. T. (1999). A tale of two diseases: atherosclerosis and rheumatoid arthritis. *Circulation* 100, 2124–2126. doi: 10.1161/01.cir.100.21.2124

Piccoli, M. T., Gupta, S. K., Viereck, J., Foinquinos, A., Samolovac, S., Kramer, F. L., et al. (2017). Inhibition of the cardiac fibroblast-enriched lncRNA Meg3 prevents cardiac fibrosis and diastolic dysfunction. *Circ. Res.* 121, 575–583. doi: 10.1161/CIRCRESAHA.117.310624

Pike, M. M., Luo, C. S., Clark, M. D., Kirk, K. A., Kitakaze, M., Madden, M. C., et al. (1993). NMR measurements of Na+ and cellular energy in ischemic rat heart: role of Na(+)-H+ exchange. *Am. J. Physiol.* 265(6 Pt 2), H2017–H2026. doi: 10.1152/ajpheart.1993.265.6.H2017

Prasher, D., Greenway, S. C., and Singh, R. B. (2020). The impact of epigenetics on cardiovascular disease. *Biochem. Cell Biol.* 98, 12–22. doi: 10.1139/bcb-2019-0045

Randle, P. J. (1998). Regulatory interactions between lipids and carbohydrates: the glucose fatty acid cycle after 35 years. *Diabetes Metab. Rev.* 14, 263–283. doi: 10.1002/(Sici)1099-0895(199812)14:4<263::Aid-Dmr233<3.0.Co;2-C

Randle, P. J., Garland, P. B., Hales, C. N., and Newsholme, E. A. (1963). The glucose fatty-acid cycle. Its role in insulin sensitivity and the metabolic disturbances of diabetes mellitus. *Lancet* 1, 785–789. doi: 10.1016/s0140-6736(63)91500-9

Ridker, P. M., Cannon, C. P., Morrow, D., Rifai, N., Rose, L. M., McCabe, C. H., et al. (2005). C-reactive protein levels and outcomes after statin therapy. *N. Engl. J. Med.* 352, 20–28. doi: 10.1056/NEJMoa042378

Ridker, P. M., Rifai, N., Clearfield, M., Downs, J. R., Weis, S. E., Miles, J. S., et al. (2001). Measurement of C-reactive protein for the targeting of statin therapy in the primary prevention of acute coronary events. *N. Engl. J. Med.* 344, 1959–1965. doi: 10.1056/NEJM200106283442601

Ross, R. (1999). Atherosclerosis–an inflammatory disease. *N. Engl. J. Med.* 340, 115–126. doi: 10.1056/NEJM199901143400207

Russell, P., Garland, D., and Epstein, D. L. (1989). Analysis of the proteins of calf and cow trabecular meshwork: development of a model system to study aging effects and glaucoma. *Exp. Eye Res.* 48, 251–260. doi: 10.1016/s0014-4835(89)80074-0

Sanada, S., Komuro, I., and Kitakaze, M. (2011). Pathophysiology of myocardial reperfusion injury: preconditioning, postconditioning, and translational aspects of protective measures. *Am. J. Physiol. Heart Circ. Physiol.* 301, H1723–H1741. doi: 10.1152/ajpheart.00553.2011

Satoh, A., Stein, L., and Imai, S. (2011). The role of mammalian sirtuins in the regulation of metabolism, aging, and longevity. *Handb. Exp. Pharmacol.* 206, 125–162. doi: 10.1007/978-3-642-21631-2_7

Shepherd, J., Cobbe, S. M., Ford, I., Isles, C. G., Lorimer, A. R., MacFarlane, P. W., et al. (1995). Prevention of coronary heart disease with pravastatin in men with hypercholesterolemia. West of Scotland coronary prevention study group. *N. Engl. J. Med.* 333, 1301–1307. doi: 10.1056/NEJM199511163332001

Shiomi, T., Tsutsui, H., Matsusaka, H., Murakami, K., Hayashidani, S., Ikeuchi, M., et al. (2004). Overexpression of glutathione peroxidase prevents left ventricular remodeling and failure after myocardial infarction in mice. *Circulation* 109, 544–549. doi: 10.1161/01.CIR.0000109701.77059.E9

Song, Y. F., Wang, B. C., Zhu, X. L., Hu, J., Sun, J., Xuan, J., et al. (2021). Human umbilical cord blood-derived MSCs exosome attenuate myocardial injury by inhibiting ferroptosis in acute myocardial infarction mice. *Cell Biol. Toxicol.* 37, 51–64. doi: 10.1007/s10565-020-09530-8

Soula, M., Weber, R. A., Zilka, O., Alwaseem, H., La, K., Yen, F., et al. (2020). Metabolic determinants of cancer cell sensitivity to canonical ferroptosis inducers. *Nat. Chem. Biol.* 16, 1351–1360. doi: 10.1038/s41589-020-0613-y

Stamenkovic, A., Pierce, G. N., and Ravandi, A. (2019). Phospholipid oxidation products in ferroptotic myocardial cell death. *Am. J. Physiol. Heart Circ. Physiol.* 317, H156–H163. doi: 10.1152/ajpheart.00076.2019

Sugden, M. C. (2007). In appreciation of Sir Philip Randle: the glucose-fatty acid cycle. *Br. J. Nutr.* 97, 809–813. doi: 10.1017/S0007114507659054

Tabas, I., Williams, K. J., and Boren, J. (2007). Subendothelial lipoprotein retention as the initiating process in atherosclerosis–update and therapeutic implications. *Circulation* 116, 1832–1844. doi: 10.1161/Circulationaha.106.676890

Tadokoro, T., Ikeda, M., Ide, T., Deguchi, H., Ikeda, S., Okabe, K., et al. (2020). Mitochondria-dependent ferroptosis plays a pivotal role in doxorubicin cardiotoxicity. *JCI Insight* 5:e132747. doi: 10.1172/jci.insight.132747

Tanai, E., and Frantz, S. (2016). Pathophysiology of heart failure. *Compr. Physiol.* 6, 187–214. doi: 10.1002/cphy.c140055

Tang, D., Chen, X., Kang, R., and Kroemer, G. (2021). Ferroptosis: molecular mechanisms and health implications. *Cell Res.* 31, 107–125. doi: 10.1038/s41422-020-00441-1

Tang, L. J., Luo, X. J., Tu, H., Chen, H., Xiong, X. M., Li, N. S., et al. (2021). Ferroptosis occurs in phase of reperfusion but not ischemia in rat heart following ischemia or ischemia/reperfusion. *Naunyn. Schmiedebergs Arch. Pharmacol.* 394, 401–410. doi: 10.1007/s00210-020-01932-z

Tao, Y. G., Liu, S., and Jiang, Y. Q. (2017). EGLN1/c-Myc induced lymphoid-specific helicase inhibits ferroptosis through lipid metabolic gene expression changes. *Cancer Res.* 77, 3293–3305. doi: 10.1158/1538-7445.Am2017-4317

The Institute for Health Metrics and Evaluation (IHME) (2018). *GBD Compare | Viz Hub*. Washington, DC: IHME.

Touyz, R. M. (2004). Reactive oxygen species, vascular oxidative stress, and redox signaling in hypertension: what is the clinical significance? *Hypertension* 44, 248–252. doi: 10.1161/01.HYP.0000138070.47616.9d

Tsutsui, M., Shimokawa, H., Morishita, T., Nakashima, Y., and Yanagihara, N. (2006). Development of genetically engineered mice lacking all three nitric oxide synthases. *J. Pharmacol. Sci.* 102, 147–154. doi: 10.1254/jphs.CPJ06015X

Ussher, J. R., Elmariah, S., Gerszten, R. E., and Dyck, J. R. (2016). The emerging role of metabolomics in the diagnosis and prognosis of cardiovascular disease. *J. Am. Coll. Cardiol.* 68, 2850–2870. doi: 10.1016/j.jacc.2016.09.972

Vena, G. A., Vestita, M., and Cassano, N. (2010). Psoriasis and cardiovascular disease. *Dermatol. Ther.* 23, 144–151. doi: 10.1111/j.1529-8019.2010.01308.x

Waddington, C. H. (2012). The epigenotype. 1942. *Int. J. Epidemiol.* 41, 10–13. doi: 10.1093/ije/dyr184

Wahlquist, C., Jeong, D., Rojas-Munoz, A., Kho, C., Lee, A., Mitsuyama, S., et al. (2014). Inhibition of miR-25 improves cardiac contractility in the failing heart. *Nature* 508, 531–535. doi: 10.1038/nature13073

Wang, C. Y., Yuan, W. L., Hu, A. M., Lin, J., Xia, Z., Yang, C. F., et al. (2020). Dexmedetomidine alleviated sepsis-induced myocardial ferroptosis and septic heart injury. *Mol. Med. Rep.* 22, 175–184. doi: 10.3892/mmr.2020.11114

Wang, D., He, Y. N., Li, Y. P., Luan, D., Zhai, F., Yang, X., et al. (2013). Joint association of dietary pattern and physical activity level with cardiovascular disease risk factors among Chinese Men: a cross-sectional study. *PloS One* 8:e66210. doi: 10.1371/journal.pone.0066210

Wang, J. Y., Deng, B., Liu, Q., Huang, Y., Chen, W., Li, J., et al. (2020). Pyroptosis and ferroptosis induced by mixed lineage kinase 3 (MLK3) signaling in cardiomyocytes are essential for myocardial fibrosis in response to pressure overload. *Cell Death Dis.* 11:574. doi: 10.1038/s41419-020-02777-3

Wang, M., Mao, C., Ouyang, L. L., Liu, Y., Lai, W., Liu, N., et al. (2019). Long noncoding RNA LINC00336 inhibits ferroptosis in lung cancer by functioning as a competing endogenous RNA. *Cell Death Differ.* 26, 2329–2343. doi: 10.1038/s41418-019-0304-y

Wang, Y. F., Yang, L., Zhang, X. J., Cui, W., Liu, Y., Sun, Q. R., et al. (2019). Epigenetic regulation of ferroptosis by H2B monoubiquitination and p53. *EMBO Rep.* 20:e47563. doi: 10.15252/embr.201847563

Wang, Y. S., Zhao, Y., Wang, H. H., Zhang, C., Wang, M., Yang, Y., et al. (2020). Histone demethylase KDM3B protects against ferroptosis by upregulating SLC7A11. *FEBS Open Bio* 10, 637–643. doi: 10.1002/2211-5463.12823

Williams, K. J., and Tabas, I. (1995). The response-to-retention hypothesis of early atherogenesis. *Arterioscler. Thromb. Vasc. Biol.* 15, 551–561. doi: 10.1161/01.atv.15.5.551

Wong, B. W., Meredith, A., Lin, D., and McManus, B. M. (2012). The biological role of inflammation in atherosclerosis. *Can. J. Cardiol.* 28, 631–641. doi: 10.1016/j.cjca.2012.06.023

World Health Organization (WHO) (2017). *Cardiovascular Diseases (CVDs)*. Available online at: https://www.who.int/en/news-room/fact-sheets/detail/cardiovascular-diseases-(cvds) (accessed June 11, 2021).

Wu, Y. Q., Zhang, S. W., Gong, X. X., Tam, S., Xiao, D., Liu, S., et al. (2020). The epigenetic regulators and metabolic changes in ferroptosis-associated cancer progression. *Mol. Cancer* 19:39. doi: 10.1186/s12943-020-01157-x

Xiao, Y. J., Xia, J. J., Cheng, J. Q., Huang, H., Zhou, Y., Yang, X., et al. (2019). Inhibition of S-adenosylhomocysteine hydrolase induces endothelial dysfunction via epigenetic regulation of p66shc-mediated oxidative stress pathway. *Circulation* 139, 2260–2277. doi: 10.1161/Circulationaha.118.036336

Xie, Y., Hou, W., Song, X., Yu, Y., Huang, J., Sun, X., et al. (2016). Ferroptosis: process and function. *Cell Death Differ.* 23, 369–379. doi: 10.1038/cdd.2015.158

Xu, S., Pelisek, J., and Jin, Z. G. (2018). Atherosclerosis is an epigenetic disease. *Trends Endocrinol. Metab.* 29, 739–742. doi: 10.1016/j.tem.2018.04.007

Xu, Z., Tong, Q., Zhang, Z. G., Wang, S., Zheng, Y., Liu, Q., et al. (2017). Inhibition of HDAC3 prevents diabetic cardiomyopathy in OVE26 mice via epigenetic regulation of DUSP5-ERK1/2 pathway. *Clin. Sci.* 131, 1841–1857. doi: 10.1042/Cs20170064

Yancy, C. W., Jessup, M., Bozkurt, B., Butler, J., Casey, D. E. Jr., Colvin, M. M., et al. (2017). 2017 ACC/AHA/HFSA focused update of the 2013 ACCF/AHA guideline for the management of heart failure: a report of the American College of Cardiology/American Heart Association task force on clinical practice guidelines and the heart failure society of America. *J. Card. Fail.* 23, 628–651. doi: 10.1016/j.cardfail.2017.04.014

Yang, K. C., Yamada, K. A., Patel, A. Y., Topkara, V. K., George, I., Cheema, F. H., et al. (2014). Deep RNA sequencing reveals dynamic regulation of myocardial noncoding RNAs in failing human heart and remodeling with mechanical circulatory support. *Circulation* 129, 1009–1021. doi: 10.1161/CIRCULATIONAHA.113.003863

Yang, W. S., SriRamaratnam, R., Welsch, M. E., Shimada, K., Skouta, R., Viswanathan, V. S., et al. (2014). Regulation of ferroptotic cancer cell death by GPX4. *Cell* 156, 317–331. doi: 10.1016/j.cell.2013.12.010

Yang, W. S., and Stockwell, B. R. (2008). Synthetic lethal screening identifies compounds activating iron-dependent, nonapoptotic cell death in oncogenic-RAS-harboring cancer cells. *Chem. Biol.* 15, 234–245. doi: 10.1016/j.chembiol.2008.02.010

Yu, H. X., Han, Z. F., Xu, Z. A., An, C., Xu, L., and Xin, H. (2019). RNA sequencing uncovers the key long non-coding RNAs and potential molecular mechanism contributing to XAV939-mediated inhibition of non-small cell lung cancer. *Oncol. Lett.* 17, 4994–5004. doi: 10.3892/ol.2019.10191

Zhang, X. F., Sui, S. Y., Wang, L. L., Li, H., Zhang, L., Xu, S., et al. (2020). Inhibition of tumor propellant glutathione peroxidase 4 induces ferroptosis in cancer cells and enhances anticancer effect of cisplatin. *J. Cell. Physiol.* 235, 3425–3437. doi: 10.1002/jcp.29232

Zhang, Y. L., Shi, J. J., Liu, X. G., Feng, L., Gong, Z., Koppula, P., et al. (2018). BAP1 links metabolic regulation of ferroptosis to tumour suppression. *Nat. Cell Biol.* 20, 1181–1192. doi: 10.1038/s41556-018-0178-0

Conflict of Interest: The authors declare that the research was conducted in the absence of any commercial or financial relationships that could be construed as a potential conflict of interest.

Publisher's Note: All claims expressed in this article are solely those of the authors and do not necessarily represent those of their affiliated organizations, or those of the publisher, the editors and the reviewers. Any product that may be evaluated in this article, or claim that may be made by its manufacturer, is not guaranteed or endorsed by the publisher.

frontiers in Cardiovascular Medicine

ORIGINAL RESEARCH
published: 28 September 2021
doi: 10.3389/fcvm.2021.728976

GRB10 rs1800504 Polymorphism Is Associated With the Risk of Coronary Heart Disease in Patients With Type 2 Diabetes Mellitus

Yang Yang[1†], Wentao Qiu[1,2†], Qian Meng[1†], Mouze Liu[3], Weijie Lin[1], Haikui Yang[1], Ruiqi Wang[1], Jiamei Dong[1], Ningning Yuan[1], Zhiling Zhou[1] and Fazhong He[1*]*

[1] Department of Pharmacy, Zhuhai People's Hospital (Zhuhai Hospital Affiliated With Jinan University), Zhuhai, China, [2] College of Pharmacy, Jinan University, Guangzhou, China, [3] Department of Pharmacy, The Second Xiangya Hospital, Central South University, Changsha, China

OPEN ACCESS

Edited by:
Suowen Xu,
University of Science and Technology of China, China

Reviewed by:
Chao-Qiang Lai,
Jean Mayer USDA Human Nutrition Research Center on Aging at Tufts University, United States
Miguel Cruz,
Mexican Social Security Institute (IMSS), Mexico
Daniel Petrovič,
University of Ljubljana, Slovenia

***Correspondence:**
Fazhong He
fazhong2006@ext.jnu.edu.cn
Zhiling Zhou
zhouzl@aliyun.com

[†]These authors share first authorship

Specialty section:
This article was submitted to Cardiovascular Genetics and Systems Medicine, a section of the journal Frontiers in Cardiovascular Medicine

Received: 23 June 2021
Accepted: 02 September 2021
Published: 28 September 2021

Citation:
Yang Y, Qiu W, Meng Q, Liu M, Lin W, Yang H, Wang R, Dong J, Yuan N, Zhou Z and He F (2021) GRB10 rs1800504 Polymorphism Is Associated With the Risk of Coronary Heart Disease in Patients With Type 2 Diabetes Mellitus. Front. Cardiovasc. Med. 8:728976. doi: 10.3389/fcvm.2021.728976

Diabetic vascular complications are one of the main causes of death and disability. Previous studies have reported that genetic variation is associated with diabetic vascular complications. In this study, we aimed to investigate the association between *GRB10* polymorphisms and susceptibility to type 2 diabetes mellitus (T2DM) vascular complications. Eight single nucleotide polymorphisms (SNPs) in the *GRB10* gene were genotyped by MassARRAY system and 934 patients with type 2 diabetes mellitus (T2DM) were included for investigation. We found that *GRB10* rs1800504 CC+CT genotypes were significantly associated with increased risk of coronary heart disease (CHD) compared with TT genotype (OR = 2.24; 95%CI: 1.36–3.70, $p = 0.002$). Consistently, levels of cholesterol (CHOL) (CC+CT vs. TT, 4.44 ± 1.25 vs. 4.10 ± 1.00 mmol/L; $p = 0.009$) and low density lipoprotein cholesterin (LDL-CH) (CC+CT vs. TT, 2.81 ± 1.07 vs. 2.53 ± 0.82 mmol/L; $p = 0.01$) in T2DM patients with TT genotype were significant lower than those of CC+CT genotypes. We further validated in MIHA cell that the total cholesterol (TC) level in *GRB10*-Mut was significantly reduced compared with *GRB10*-WT; $p = 0.0005$. Likewise, the reversed palmitic acid (PA) induced lipid droplet formation in *GRB10*-Mut was more effective than in *GRB10*-WT. These results suggest that rs1800504 of *GRB10* variant may be associated with the blood lipids and then may also related to the risk of CHD in patients with T2DM.

Keywords: type 2 diabetes mellitus, *GRB10*, genetic variation, vascular complications, lipid metabolism

INTRODUCTION

Diabetes is a metabolic disease that is characterized by hyperglycemia. This disease is caused by abnormal glucose, lipid, and protein metabolism. Ultimately, this leads to impaired insulin secretion, insulin resistance, or both. The common types of diabetes include type 1 diabetes mellitus (T1DM), type 2 diabetes mellitus (T2DM), and gestational diabetes. T2DM is caused by ineffective use of insulin by the body. T2DM patients are characterized by high blood sugar, relative lack of insulin, insulin resistance and so on (1). Statistical evidence shows that T2DM accounts for more than 95% of all diabetic cases in the Chinese population (2). Over time, T2DM is becoming an increasingly serious problem for global health. The International Diabetes Federation estimated

that there were 463 million adults aged 20–70 years with T2DM worldwide in 2019. By 2045, this number is predicted to increase to 700 million (3). T2DM patients often have various complications, including multi-organ damage caused by macrovascular and microvascular complications (4). Diabetic vascular complications significantly increase the disability and mortality rate of diabetic patients, seriously affect the quality of life and cause a huge national economic burden. In a systematic review of 4,549,481 patients with T2DM, the incidence of macrovascular complications was determined to be 32.2%, of which 21.2% of patients had coronary heart disease (CHD) (5). It is evident the CHD has become the main factor threatening the health and life of patients with T2DM. A previous study reported that the occurrence of T2DM vascular disease showed clear associations with both ethnicity and family history (5, 6). Furthermore, multiple studies have reported that gene polymorphisms are associated with diabetic vascular complications (7–9). Therefore, the identification of susceptibility genes related to T2DM vascular complications could provide a possible treatment strategy for the early prevention of this disease. These factors are of great significance with regards to prolonging the survival period of patients and improving their quality of life.

Growth factor receptor-binding protein 10 (GRB10) is an adaptor protein of the GRB7/GRB10/GRB14 protein family. GRB10 can interact with a variety of tyrosine kinase receptors and affect a variety of signal pathways (10). Furthermore, GRB10 has been confirmed to play an important role in regulating cell proliferation, apoptosis, and metabolism, as well as many signaling pathways (11–13). GRB10 is expressed at high levels in tissues that are involved in insulin action and glucose metabolism, including the muscles, pancreas and fat. The IGF/IGFR signaling pathway plays an important role in the regulation and conduction of diabetes mellitus and related complications. GRB10 can interact with IGFR to regulate the IGF/IGFR signaling pathway in a negative manner (14). In one study, the minor allele (MA) of *GRB10* rs4947710 was associated with a reduced risk of T2DM in white subjects from Italy. In another study, *GRB10* rs2237457 genetic variation was associated with T2DM in the Amish population (15, 16). These studies proved that *GRB10* gene polymorphism is closely related to susceptibility for T2DM. As we all know, vascular endothelial growth factor (VEGF) is an important regulator of angiogenesis and it is involved in the development and progression of many angiogenesis dependent diseases. According to previous reports, GRB10 could be involved in a positive feedback loop in VEGF signaling. VEGF could stimulate GRB10 expression, and GRB10 overexpression induced an increase in the amount and the tyrosine phosphorylation of VEGF-R2 (17, 18). Furthermore, *GRB10*, as a key downstream mediator of vascular smooth muscle cell (*VSMC*) miR-504 function, is closely related to vascular diseases under the conditions of diabetes mellitus (19). Collectively, this information indicates that *GRB10* may be a key gene involved in the regulation of diabetes mellitus and related vascular complications.

We previously found that GRB10 is highly expressed in cardioembolic stroke patients by using the Gene Expression Omnibus (GEO) database analysis. Furthermore, previous studies have confirmed that GRB10 is closely related to T2DM and vascular diseases (15, 16, 19). Nevertheless, no study has investigated the relationship between *GRB10* gene polymorphism and T2DM cardiovascular complications. In this study, we studied the influence of *GRB10* gene polymorphism on cardiovascular complications in patients with T2DM.

PATIENTS AND METHODS

Diagnostic Criteria

According to the Chinese Guidelines for the Prevention and Treatment of Type 2 Diabetes (2020 Edition), the diagnostic criteria for diabetes are typical diabetes symptoms plus random blood glucose $\geq$ 11.1 mmol/L; Or add fasting blood glucose $\geq$ 7.0mmol/L; Or add OGTT 2h blood sugar $\geq$ 11.1mmol/L; Or add HbA1C$\geq$6.5%. Typical diabetes symptoms include polydipsia, polyuria, polyphagia and unexplained weight loss. Excluding T1DM and special types of diabetes, the patients with T2DM were included in the study. At the early stage of disease, it is sometimes difficult to determine the type of diabetes. If the classification cannot be determined immediately, a temporary classification can be carried out to guide the treatment. Then, according to the patients' initial response to treatment and the clinical manifestations during follow-up, the patients were re-evaluated and classified (20).

Coronary atherosclerotic heart disease refers to heart disease caused by myocardial ischemia, hypoxia or necrosis due to stenosis or occlusion of lumen caused by coronary atherosclerosis, which is referred to as coronary heart disease (CHD) for short (21). The diagnostic criteria of patients with CHD in this study were implemented in accordance with Chinese Guidelines for Clinical Diagnosis and Treatment of Coronary Heart Disease (2010 Edition) (22).

According to the Guidelines for Primary Diagnosis and Treatment of Hypertension in China (2019 Edition), without using antihypertensive drugs, the blood pressure should be measured three times on different days, with systolic blood pressure (SBP) $\geq$140 mmHg and/or diastolic blood pressure (DBP) $\geq$90 mmHg. SBP $\geq$ 140 mmHg and DBP $<$ 90 mmHg are simple systolic hypertension. The patient has a history of hypertension, and is currently taking antihypertensive drugs. Although the blood pressure is lower than 140/90 mmHg, he or she is still diagnosed as hypertension (23).

Patients

This was a retrospective study involving patients with T2DM. The experimental design was approved by the ethics committee of the Institute of Clinical Pharmacology, Central South University and was registered at http://www.chictr.org.cn (Registration number: ChiCTR1800015661). Participants in this study were randomly enrolled from inpatients at the Second Xiangya Hospital of Central South University between December 2017 and December 2019. Our study included patients who were diagnosed with T2DM on admission and aged between 18 and 80 years. We collected clinical data for all participants, including gender, age, height, weight, body mass index (BMI),

waist circumference, hip circumference, waist-to-hip ratio, systolic blood pressure (SBP), diastolic blood pressure (DBP), cardiovascular history, cerebrovascular history, smoking history, drinking history, hypertension, hyperglycemia, family diabetes history, triglyceride (TG) level, cholesterol (CHOL) level, high density lipoprotein-cholesterol (HDL-CH) level, low density lipoprotein-cholesterol (LDL-CH) level, and fasting blood glucose level. We also recorded the levels of GLU-60, GLU-120, glycosylated hemoglobin (HbA1C), 25-hydroxyvitamin D, Cpst-0, Cpst-60, Cpst-120, along with the glomerular filtration rate (eGFR) and medication status (hypoglycemic drugs, lipid-lowering drugs, antihypertensive drugs). The clinical endpoint events included type 2 diabetes vascular complications, blood glucose, blood pressure, TG, CHOL, HDL-CH, and LDL-CH. We excluded patients whose discharge diagnosis was not T2DM and those from which the blood samples were not obtained. We also excluded patients who did not provide informed consent and those did not have a complete set of clinical data.

Candidate Genes and SNP Selection

We identified two gene chip datasets (GSE22255 and GSE58294) relating to cardioembolic stroke patients in the GEO database (**Supplementary Table 1**). We merged the two raw datasets and applied RMA standardization. Next, we used the R-Limma package to process differential gene analysis, $|\log_2 FC| > 1.5$ and $p < 0.05$ were considered to be statistically significant. Then, we used the ENCODE database to assess the potential function of SNPs within or near candidate genes. We included candidate SNPs with a minor allele frequency $\geq 5\%$ and a pairwise linkage disequilibrium (r^2) < 0.30 within the same and adjacent genes [1,000 Genomes phase 3 Han Chinese in Beijing (CHB)].

DNA Extraction and Mass Spectrometry Typing

Peripheral venous blood was collected from all patients who met the inclusion criteria. DNA was extracted from peripheral venous blood using the E.Z.N.A. SQ blood DNA Kit II (Omega Bio-Tek Company, USA). The extracted DNAs were then stored at −80°C wait for analysis. The Sequenom MassARRAY SNP system was used to screen the genotypes of all candidate SNPs (Bioyong Technologies Inc.). Information relating to the probe is shown in **Supplementary Table 2**. Finally, 5% of the participants were randomly selected for verification by Sanger sequencing.

Cell Culture and Cell Transfection

An immortalized hepatocyte cell line, MIHA, was cultured in Roswell Park Memorial Institute (RPMI) 1640 Medium supplemented with 10% fetal bovine serum (FBS). Cells were then cultured in a standard humidified incubator at 37°C in a 5% CO_2 atmosphere.

Plasmids containing an empty vector, and the *GRB10* mutation were subcloned into a lentivirus vector (pHBLV-CMV-MCS-3FLAG-EF1-ZsGreen-T2A-PURO) to construct the recombinant plasmid (Hanheng Biotechnology, Shanghai, China). The *GTB10*-Mut plasmid featured an rs1800504 mutation (allele C to T). The detailed information of the construction of *GRB10* mutant lentiviral vector is shown in the **Supplementary Files 2**. MIHA cells were transfected with Lentiviral vector using Polybrene (Hanheng Biotechnology,Shanghai, China) according to the manufacturer's instructions.When the expression of GRB10 reached its peak, the cell lines with stable expression were screened by Puromycin.

Western Blot and Real-Time Polymerase Chain Reaction (PCR)

The protocol used for western blotting was described in previous report (24). The membranes were first probed with GRB10 (#3702) and GAPDH (#5174S) primary antibodies purchased from Cell Signaling Technology (CST). Following incubation, membranes were probed with a horseradish peroxidase (HRP)-labeled anti-rabbit secondary antibody from CST (#2708) (diluted with 5% BSA to 1:1,000). Antibody binding was subsequently detected by an enhanced chemiluminescence detection kit (ECL) (Biosharp Biotechnology, BL520B).

Total RNA was extracted from MIHA cells using an RNA-Quick Purification Kit (ES Science). Complementary DNA (cDNA) was synthesized using ReverTra Ace reverse transcriptase (Novoprotein, E04710A) in accordance with the manufacturer's instructions. Real-time RT-PCR was performed with a SYBR qPCR SuperMix Plus Kit (Novoprotein, E096) on a 7300 plus/Bio-RAD iCycler in accordance with the manufacturer's instructions. The primer sequences were as follows: GRB10, forward, 5′-CGAAACTCACCCGTCCAG-3′; reverse, 5′-GGATTCACAGTGTCGGTTGG-3; β-actin: forward, 5′-CATGTACGTTGCTATCCAGGC-3′; reverse, 5′-CTCCTTA ATGTCACGCACGAT-3′. The gene expression levels for each amplicon were calculated by the ΔΔCT method and normalized against β-actin mRNA.

The Determination of Total Cholesterol and Oil Red Staining

According to the Trinder reaction principle, cholesterol makes 4-aminoantipyrine react with phenol (PAP) to produce a red quinoneimine pigment. Using this strategy, we used a TC kit operating standard (BB-47435) and a Microplate Reader to determine the absorbance of samples at a wavelength of 510 nm.

Oil red O can be used to stain lipids in cells. Positive staining changes the color of fat from orange to red. After 24 h, the cells were washed twice with phosphate buffered saline (PBS) and fixed with 4% paraformaldehyde at room temperature for 30 min. After removing the fixative, the cells were washed twice with distilled water and soaked in 60% isopropanol for 5 min. After discarding the isopropanol, we added freshly prepared ORO stain (ORO stain:distilled water; 3:2) for 10–20 min. The staining solution was then discarded, and the cells were washed with water twice. We then added Mayer hematoxylin staining solution to stain the nuclei for cycler 1–2 min, the staining solution was then washed away and replaced with water so that we could monitor the developing staining effect. Finally, we used distilled water to cover the cells and observed the cells with an EVOS microscope (Life Technologies/Thermo Fisher Scientific, US).

Statistical Analysis

SPSS Statistical software (version 22.0 for windows, Chicago, IL) was used for statistical analysis and GraphPad Prism version 5 software (GraphPad Prism Software Inc., La Jolla, CA) was used to create figures. Power and sample size calculations software (Version 3.0.43) was used to calculate the sample size required for the study. The *T*-test or the Mann–Whitney *U*-test were used for the statistical analysis of measurement data (mean ± standard deviation), as appropriate. The chi-squared or Fisher's exact test was used to determine whether the gene distribution conformed to the Hardy–Weinberg equilibrium. Logistic regression analysis was used to calculate the odds ratio (OR) and 95% confidence interval (CI) between the *GRB10* single-nucleotide polymorphisms (SNPs) and diabetic vascular complications after adjusting for age, BMI, gender, hypertension, smoking and drinking. Comparison of biochemical indicators variance between the *GRB10* genotype was performed with Univariate Analysis of Variance (ANOVA) after adjusting for potential confounders, such as age, BMI and gender. Linkage disequilibrium (LD) and haplotypes analyses were performed using SHEsis online software (http://analysis.bio-x.cn/myAnalysis.php). $p < 0.05$ (2-tailed) was considered to indicate statistical significance.

RESULTS

Patient Characteristics and Genotyping

We collected clinical data and matched DNA samples from 1,026 Chinese patients with an initial diagnosis of T2DM. Following final diagnosis, 70 cases were classified as non-T2DM, and 22 DNA samples were not genotyped. Finally, 934 patients were included in the study. According to our research scheme, eight candidate SNPs in *GRB10* were screened, including rs1800504, rs2237460, rs17133917, rs55834323, rs4947710, rs4245555, rs9791817, and rs9791887 (The SNP genotyping data has been uploaded to the DRYAD, https://datadryad.org/stash/share/pDGln0dQK5R8YEMJKAZLJEFs6xWtE7xOi8rD9frUSYA). In total, 919 patients were successfully genotyped with all SNPs (**Figure 1**). The detailed results related to the loci of these SNPs are shown in **Supplementary Table 3**. Analysis showed that rs9791887, rs9791817, and rs424555, were not consist with the Hardy-Weinberg Equilibrium. Next, we analyzed the SNP linkage disequilibrium of *GRB10*. Results showed that there was strong linkage among rs9791887-rs4245555, rs9791887-rs9791817, rs55834323-rs4947710, and rs4245555-rs9791817 (**Supplementary Figure 1**). The baseline clinical characteristics of participants with rs1800504 are shown in **Table 1**. There were significant differences in BMI; $p = 0.02$.

The Association Between *GRB10* rs1800504 Gene Polymorphism and Diabetic Coronary Heart Disease in Patients With T2DM

We analyzed the relationships between the eight candidate SNPs in *GRB10* and T2DM cardiovascular complications. We found that rs1800504 genetic variation was significantly related to the occurrence of CHD in T2DM patients; $p = 0.011$. However, there was no significant association with other cardiovascular

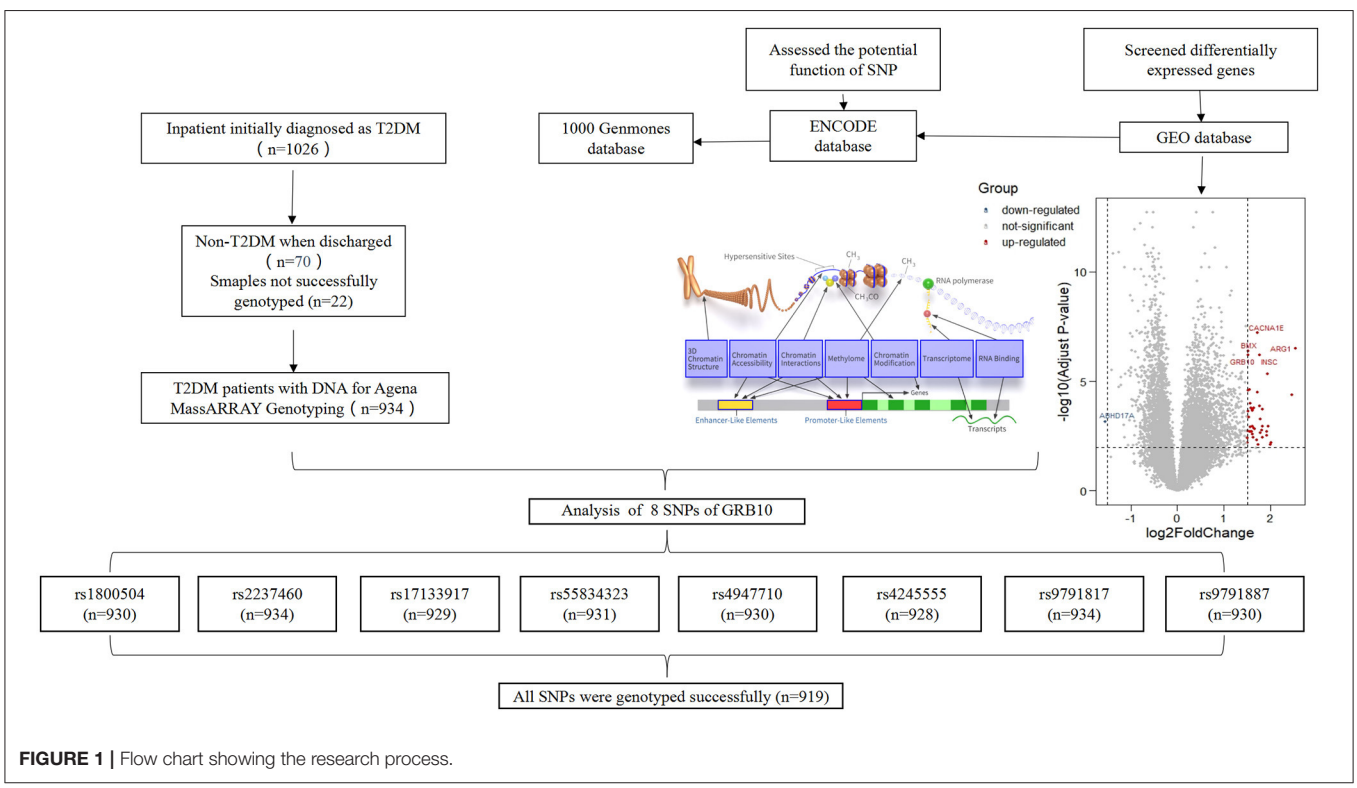

FIGURE 1 | Flow chart showing the research process.

TABLE 1 | Baseline characteristics of T2DM patients with rs1800504.

Variable	Coronary heart disease		Non-coronary heart disease		Total	
	CC+CT (*n* = 222)	TT (*n* = 26)	CC+CT (*n* = 542)	TT (*n* = 134)	CC+CT (*n* = 770)	TT (*n* = 160)
Age (year), mean (SD)	64.6 (9.51)	67.6 (8.25)	56.0 (11.3)	57.8 (10.3)	58.5 (11.5)	59.4 (10.6)
Male, *n* (%)	124 (55.9)	14 (53.8)	323 (59.6)	78 (58.2)	451 (58.6)	90 (56.3)
Smoking history, *n* (%)	72 (36.0)	10 (40.0)	189 (37.1)	40 (31.5)	264 (37.0)	50 (32.9)
Drinking history, *n* (%)	63 (31.7)	7 (29.2)	146 (28.7)	35 (27.3)	211 (29.6)	42 (27.6)
History of cardiovascular disease, *n* (%)	87 (39.7)	14 (56.0)	19 (3.6)	5 (3.8)	106 (14.0)	19 (12.1)
History of cerebrovascular disease, *n* (%)	34 (15.5)	1 (4.0)	37 (6.9)	6 (4.5)	73 (9.6)	7 (4.5)
BMI (kg/m^2), mean (SD)*	24.5 (3.24)	23.7 (3.30)	24.2 (4.30)	23.4 (3.67)	24.3 (4.01)	23.5 (3.60)
Waist-hip ratio, mean (SD)	0.95 (0.07)	0.95 (0.06)	0.96 (0.01)	0.95 (0.37)	0.95 (0.31)	0.93 (0.06)
Vitamin D deficiency rickets, *n* (%)	138 (62.2)	13 (50.0)	352 (64.9)	86 (64.2)	494 (64.2)	99 (61.9)
Fasting blood glucose (mmol/l), mean (SD)	7.36 (2.85)	8.32 (2.31)	7.70 (2.92)	7.52 (2.59)	7.61 (2.91)	7.65 (2.56)
GLU-60 (mmol/L), mean (SD)	11.9 (3.85)	11.2 (3.85)	12.1 (3.74)	10.9 (3.39)	12.0 (3.74)	10.9 (3.42)
GLU-120 (mmol/L), mean (SD)	12.3 (4.07)	13.0 (4.48)	12.3 (4.24)	12.4 (4.09)	12.3 (4.18)	12.5 (4.14)
Cpst-0 (pmol/L), mean (SD)	499.1 (471.2)	440.5 (247.1)	418.8 (322.5)	375.3 (221.1)	441.3 (370.8)	386.0 (225.8)
Cpst-60 (pmol/L), mean (SD)	819.8 (483.0)	772.4 (435.7)	714.0 (531.7)	603.9 (408.5)	748.7 (517.5)	634.9 (412.9)
Cpst-120 (pmol/L), mean (SD)	1,059.5 (840.0)	945.7 (552.2)	920.3 (681.9)	1,100.3 (903.5)	961.1 (733.4)	1,073.4 (852.9)
AST (IU/L), mean (SD)	23.5 (34.4)	19.7 (7.8)	21.6 (15.3)	21.4 (14.2)	22.1 (22.5)	21.1 (13.4)
ALT (IU/L), mean (SD)	23.6 (46.1)	17.0 (6.3)	22.8 (22.1)	22.1 (19.5)	23.0 (30.9)	21.3 (18.2)
CREA (μmol/l), mean (SD)	102.4 (101.2)	82.1 (44.4)	84.3 (77.8)	78.4 (55.7)	89.6 (85.4)	79.0 (53.9)
TBA (μmol/L), mean (SD)	5.5 (5.5)	8.1 (9.1)	5.47 (7.34)	6.15 (7.87)	5.47 (6.80)	6.47 (8.08)
eGFR (ml/min/1.73 m^2), mean (SD)	80.6 (32.7)	82.8 (40.5)	98.5 (34.2)	96.5 (32.3)	93.7 (34.6)	95.0 (33.3)
Medical treatment						
Insulin drugs, *n* (%)	186 (89.9)	21 (95.5)	403 (87.6)	97 (87.4)	594 (88.4)	118 (88.7)
Biguanides, *n* (%)	85 (38.3)	11 (42.3)	267 (49.3)	75 (56.0)	355 (46.1)	86 (53.8)
Insulin agonist, *n* (%)	9 (4.1)	2 (7.7)	34 (6.3)	11 (8.2)	43 (5.6)	13 (8.1)
DPP-4 inhibitor, *n* (%)	91 (41.0)	9 (34.6)	245 (45.2)	51 (38.1)	339 (44.0)	60 (37.5)
GLP-1 receptor agonist, *n* (%)	5 (2.3)	0 (0.0)	19 (3.5)	2 (1.5)	24 (3.1)	2 (1.3)
SGLT-2 inhibitor, *n* (%)	9 (4.1)	0 (0.0)	21 (3.9)	6 (4.5)	32 (4.2)	6 (3.8)
Lipid-lowering agents, *n* (%)	188 (84.7)	21 (80.8)	363 (67.0)	86 (64.2)	556 (72.2)	107 (66.9)
Glucosidase inhibitor, *n* (%)	119 (53.6)	18 (69.2)	305 (56.3)	79 (59.0)	428 (55.6)	97 (60.6)
Calcium Dobesilate, *n* (%)	108 (49.1)	13 (50.0)	253 (46.8)	55 (41.0)	366 (47.7)	68 (42.5)
β-receptor blocker, *n* (%)	81 (36.5)	12 (46.2)	64 (11.8)	13 (9.7)	145 (18.8)	25 (15.6)
Calcium antagonists, *n* (%)	109 (49.1)	11 (42.3)	178 (32.8)	43 (32.1)	290 (37.7)	54 (33.8)
ACEI/ARB, *n* (%)	116 (52.3)	17 (65.4)	198 (36.5)	48 (35.8)	317 (41.2)	65 (40.6)

*BMI, body mass index; GLU, glucose; Cpst, the secretion rate of C-peptide; AST, aspartate aminotransferase; ALT,alanine aminotransferase; CREA, creatinine; TBA, total bile acids; eGFR, glomerular filtration rate; ACEI, angiotensin-converting enzyme inhibitors; ARB, angiotensin receptor blockers; *p-value of any one of Coronary heart disease, Non-coronary heart disease and Total group is <0.05.*

complications (**Table 2**). In this study, 930 patients were successfully genotyped for rs1800504. In the recessive model, the CC+CT genotypes were associated with a significantly increased risk of CHD compared with the TT genotype (OR: 2.24; 95% CI: 1.36–3.70; $p = 0.002$; **Table 3**). Other SNPs had no significant effect on the CHD of T2DM patients (**Supplementary Table 4**).

The Relationship Between *GRB10* rs1800504 Gene Polymorphism and Blood Lipid Levels in T2DM Patients

Moreover, we analyzed the relationship between *GRB10* rs1800504 genetic variation and biochemical indicators. We found that rs1800504 variation was associated with plasma lipids level differences in T2DM patients. There were significant differences in the levels of CHOL and LDL-CH when compared between different rs1800504 genotypes. The levels of CHOL in the TT and CC+CT genotypes were 4.10 ± 1.00 mmol/L and 4.44 ± 1.25 mmol/L, respectively; $p = 0.009$. The levels of LDL-CH for the TT and CC+CT genotypes were 2.53 ± 0.82 mmol/L and 2.81 ± 1.07 mmol/L, respectively; $p = 0.01$ (**Figure 2** and **Table 4**). However, none of significant effect was observed as for *GRB10* rs1800504 mutation on blood glucose or blood pressure. Haplotype analysis also showed that the haplotypes of these SNPs did not have a significant impact on the relevant clinical endpoint events (**Supplementary Table 5**).

TABLE 2 | The association between *GRB10* rs1800504 genetic variation and the risk of vascular complications in T2DM patients.

Events	Genotype	Number of patients (%)	OR (95%CI)	*p*-value
Coronary heart disease*	TT	26 (16.3)	Ref.	/
	CT	146 (30.6)	2.35 (1.40–3.95)	**0.001**
	CC	76 (25.9)	2.07 (1.18–3.61)	**0.011**
Peripheral neuropathy	TT	101 (63.5)	Ref.	/
	CT	296 (64.5)	1.09 (0.73–1.63)	0.67
	CC	189 (64.5)	1.20 (0.78–1.84)	0.41
Retinopathy	TT	15 (9.4)	Ref.	/
	CT	56 (11.7)	1.06 (0.71–1.57)	0.79
	CC	37 (12.6)	1.20 (0.79–1.83)	0.40
Nephropathy	TT	66 (41.3)	Ref.	/
	CT	282 (47.3)	0.93 (0.62–1.39)	0.72
	CC	122 (41.9)	1.08 (0.70–1.67)	0.73
		33 (11.3)		
Cerebral infarction	TT	17 (10.6)	Ref.	/
	CT	62 (13.0)	1.04 (0.57–1.91)	0.90
	CC	33 (11.3)	1.03 (0.53–2.00)	0.92
Diabetic foot	TT	24 (15.0)	Ref.	/
	CT	79 (16.6)	1.06 (0.63–1.80)	0.82
	CC	49 (16.7)	1.22 (0.70–2.13)	0.49

$p < 0.05$, indicates a significant statistical difference. The bold values mean p value is less than 0.05.

TABLE 3 | The association between rs1800504 and the risk of CHD in T2DM patients.

Model	Genotype	Number of patients (%)		OR (95%CI)	*p*-value
		CHD ($n = 248$)	Non-CHD ($n = 680$)		
Additive model*	TT	26 (16.3)	134 (19.7)	Ref.	/
	CT	146 (30.6)	327 (48.1)	2.35 (1.40–3.95)	**0.001**
	CC	76 (25.9)	215 (31.6)	2.07 (1.18–3.61)	**0.011**
Dominant model	CC	76 (25.9)	215 (31.6)	Ref.	/
	CT+TT	172 (69.4)	461 (67.8)	1.06 (7.38–1.53)	0.74
Recessive model*	TT	26 (16.3)	134 (19.7)	Ref.	/
	CC+CT	222 (89.5)	542 (79.7)	2.24 (1.36–3.70)	**0.002**

*CHD, coronary heart disease. Ref., reference. *$p < 0.05$, indicates a significant statistical difference. The bold values mean p value is less than 0.05.*

The Role of *GRB10* rs1800504 Mutation in Liver Lipid Metabolism

To further determine the role of *GRB10* rs1800504 in liver lipid metabolism, we performed verification experiments *in vitro* with normal hepatocyte MIHA cells. We constructed a *GRB10* site-directed mutagenesis lentiviral vector and transfected the empty vector, *GRB10*-WT, and *GRB10*-Mut into MIHA cells (**Figure 3A**). We found that the expression of GRB10 in MIHA cells was significantly increased after transfection, and that the expression levels of cells transfected with *GRB10*-Mut were significantly higher than the levels of cells transfected with *GRB10*-WT (**Figures 3B,C**). Next, we measured the levels of TC in each group. Following the transfection of *GRB10*, the TC level in MIHA cells was significantly reduced, the levels of TC in the cells transfected with *GRB10*-Mut were 2–3 times lower than those in cells transfected with *GRB10*-WT (**Figure 3D**). Previous studies have shown that palmitic acid (PA) can significantly induce lipid accumulation in hepatocytes. We found that levels of the GRB10 protein were significantly decreased in MIHA cells that had been treated with PA (100 μM) (**Figure 3E**). After adding PA (100 μM) to MIHA cells transfected with *GRB10*-WT, *GRB10*-Mut, and the empty vector, we found that the overexpression of GRB10 reversed the formation of lipid droplets induced by PA, and we also discovered that the inhibitory effect of the *GRB10*-Mut vector had the most significant effect (**Figure 3F**).

DISCUSSION

For the first time, we found that *GRB10* gene polymorphism plays a role in the genetic susceptibility of T2DM-related CHD. Rs1800504 polymorphism of the *GRB10* gene was associated

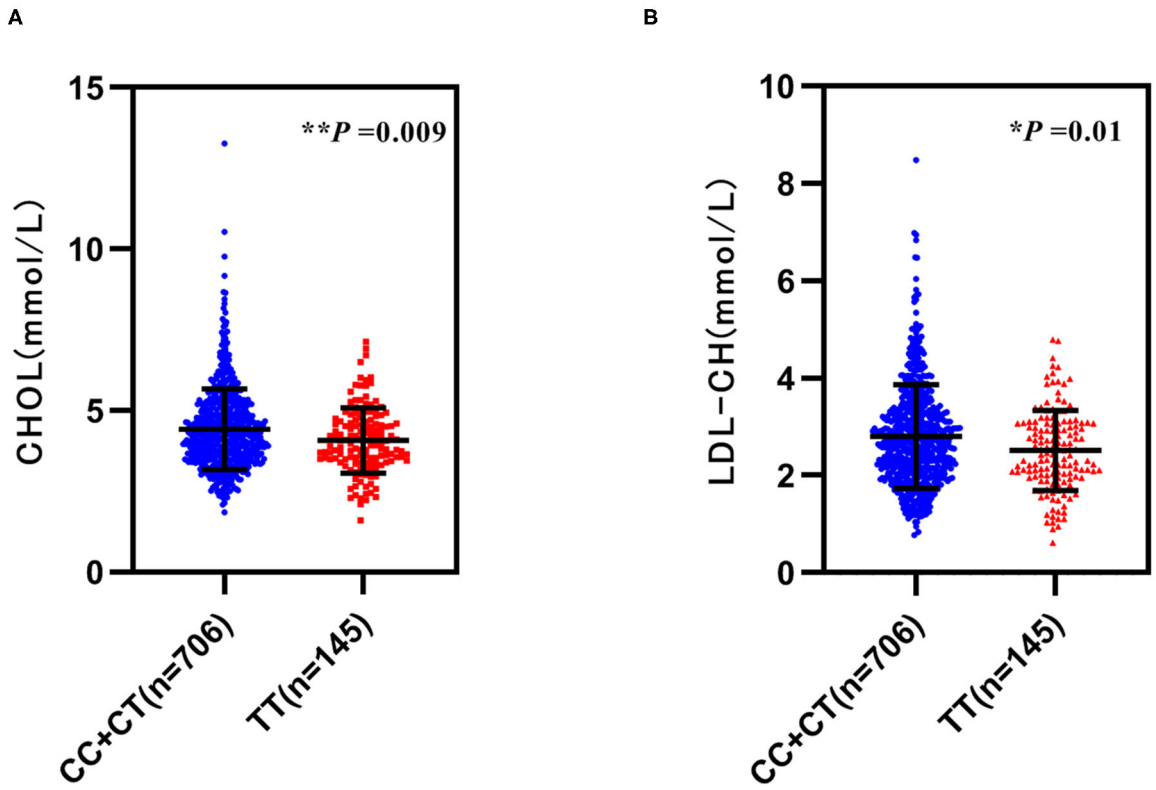

FIGURE 2 | The relationship between *GRB10* rs1800504 gene polymorphism and blood lipid levels inpatients with T2DM. **(A,B)** The levels of cholesterol (CHOL) and low-density lipoprotein (LDL-CH) in a recessive model of rs1800504. Significant differences between groups are indicated by $*p < 0.05$ and $**p < 0.01$.

TABLE 4 | Relationship between rs1800504 and blood lipids in T2DM patients.

Variable	Recessive model		*p*-value
	CC+CT (*n* = 706)	TT (*n* = 145)	
SBP (mmHg), mean (SD)	136.4 (19.8)	135.5 (20.3)	0.71
DBP (mmHg), mean (SD)	80.8 (12.6)	81.2 (13.9)	0.39
Glycated hemoglobin (%), mean (SD)	8.62 (1.99)	8.39 (2.06)	0.26
TG (mmol/L), mean (SD)	2.16 (2.34)	1.94 (1.93)	0.52
CHOL (mmol/L), mean (SD)*	4.44 (1.25)	4.10 (1.00)	**0.009**
HDL-CH (mmol/L), mean (SD)	1.03 (0.29)	1.03 (0.29)	0.57
LDL-CH (mmol/L), mean (SD)*	2.81 (1.07)	2.53 (0.82)	**0.01**

*SBP, systolic blood pressure; DBP, Diastolic blood pressure; TG, triglyceride; CHOL, cholesterol; HDL-CH, high density lipoprotein-cholesterol; LDL-CH, low density lipoprotein-cholesterol; *p < 0.05, indicates a significant difference; the bold values mean p value is less than 0.05.*

with the risk of CHD in T2DM patients. We also found that the genetic variation of rs1800504 was related to the levels of CHOL and LDL-CH. The levels of CHOL and LDL-CH in the mutated TT genotype were significantly lower than those in the CC+CT genotype. We found that the expression of GRB10 in MIHA cells transfected with *GRB10*-WT and *GRB10*-Mut were significantly different, thus indicating that mutation in the rs1800504 gene can affect the expression of GRB10. After the transfection of a GRB10 vectors, the levels of TC in MIHA cells were significantly reduced. The levels of TC in cells transfected with *GRB10*-Mut were 2–3 times lower than the levels in cells transfected with *GRB10*-WT. Using PA-induced lipid damage experiments, we found that *GRB10*-Mut was more effective than *GRB10*-WT in reversing the formation of lipid droplets induced by PA, thus confirming that rs1800504 genetic variation could result in different biological functions.

GRB10 is an adaptor protein that can interact with a variety of activated receptor protein tyrosine kinases, including the insulin receptor (IR), the insulin-like growth factor (IGF)-1 receptor, and the epidermal growth factor (EGF) receptor. A previous study showed that the overexpression of GRB10 in muscle cells and adipocytes inhibited insulin signaling, and that transgenic mice that overexpressed GRB10 showed impaired levels of glucose tolerance (25). It has also been reported that GRB10 is an important negative regulator of insulin/IGF-1 signaling in pancreatic β-cells, and it is also a potential target for improving β-cell function. As an inhibitor of insulin receptor signal transduction, GRB10 may become a candidate drug target for T2DM (26, 27). In one study, the minor allele (MA) of *GRB10* rs4947710 was associated with a reduced risk of T2DM in white subjects from Italy. In another SNP, *GRB10* rs2237457 was recently reported to be associated

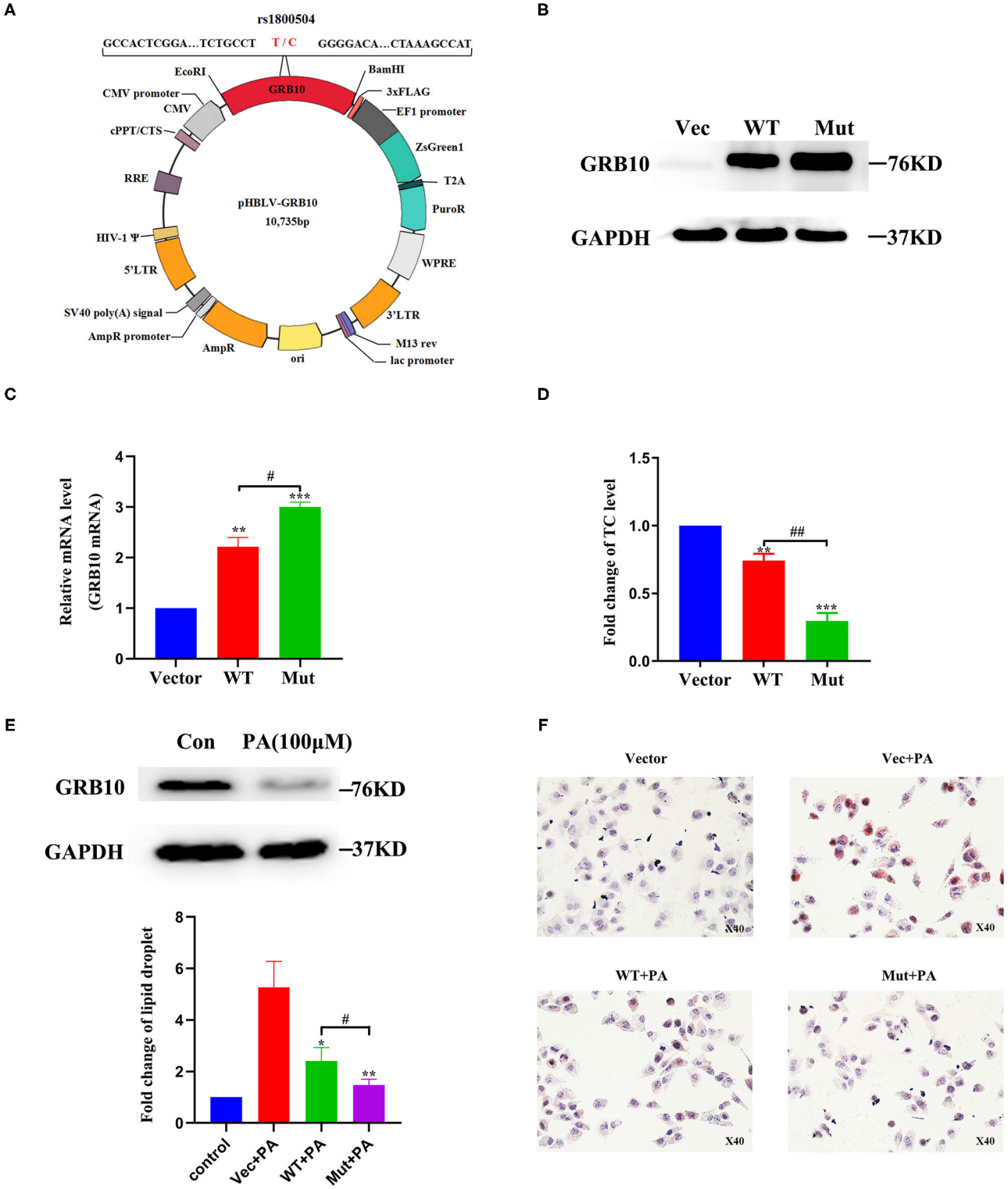

FIGURE 3 | The role of *GRB10* rs1800504 mutation in MIHA cells. **(A)** Diagram showing the constructed vectors pHBLV-rs1800504-C and pHBLV-rs1800504-T. **(B)** GRB10 protein expression in MIHA cells, as determined by western blotting after the transfection of *GRB10* rs1800504 lentivirus. **(C)** GRB10 mRNA expression in MIHA cells assayed by q-PCR after transfection. **(D)** The levels of TC in MIHA cells transfected with *GRB10*-vector, *GRB10*-WT, and *GRB10*-Mut. **(E)** GRB10 expression in MIHA cells after 48 h of treatment with PA (100 μM). **(F)** Lipid droplet formation in MIHA cells transfected with *GRB10*-vector, *GRB10*-WT and *GRB10*-Mut after treatment with PA (100 μM) for 48 h. $^{*}p < 0.05$, $^{**}p < 0.01$, and $^{***}p < 0.001$ represent significantly differences compared with *GRB10*-vector. $^{\#}p < 0.05$ and $^{\#\#}p < 0.01$ represent significant differences compared with the *GRB10*-WT ($n = 3$).

with T2DM in Amish subjects (15, 16). These results indicate that *GRB10* gene polymorphism may be closely related to susceptibility for diabetes. Previous analysis proved that *GRB10* is a key downstream mediator of VSMC miR-504 function. The upregulation of miR-504 in diabetes mellitus may be one of the mechanisms that enhances growth factor signals and VSMC dysfunction in vascular diseases. *GRB10* knockout can enhance the activation of ERK1/2 induced by PDGF, increase the expression of inflammatory genes (*CCL2* and *IL6*), and promote a pro-atherosclerotic phenotype in VSMC. The knockout of *GRB10* also enhanced VSMC migration while inhibiting EGR2 and contractile gene expression in a similar manner to miR-504 overexpression (19). These studies showed that *GRB10* is closely related to vascular diseases. Although *GRB10* is associated with both diabetes and vascular disease, the relationship between *GRB10* gene polymorphism and diabetic cardiovascular disease had not been studied previously. In this study, we genotyped 934 DNA samples from Chinese patients with T2DM, and found for the first time that *GRB10* rs1800504 genetic variation was associated with the occurrence of CHD in T2DM patients. Compared with the TT genotype, the CC+CT genotypes may be associated with a significant increase in CHD in T2DM patients (**Table 3**).

T2DM is often associated with hypercholesterolemia, dyslipidemia, hypertension, and obesity. Meanwile, these are also risk factors for cardiovascular events. The main cardiovascular event is atherosclerotic disease in patients with T2DM, while plasma lipids disorders are the basis of atherosclerosis (28–31). Therefore, the control of dyslipidemia has become critical goal for diabetic cardiovascular disease. In this study, we found that the levels of CHOL and LDL-CH in patients with the TT genotype of rs1800504 were significantly lower than those in patients with the CC+CT genotype (**Figure 2** and **Table 4**). Therefore, allele C may represent as a risk factor for the abnormal elevation of CHOL and LDL-CH, thereby increasing the risk of CHD in T2DM patients. In recent years, an increasing evidence has indicated that the target of rapamycin complex (mTORC) plays a key role in the regulation of fat metabolism (32, 33). Two recent studies have shown that mTOR directly phosphorylates GRB10, and that cold exposure can significantly induce the expression of GRB10 in adipose tissue. In addition, the fat-specific knockout of GRB10 was shown to inhibit lipolysis and thermogenic gene expression, reduce energy consumption, and aggravate diet-induced obesity and insulin resistance. Collectively, these studies revealed that GRB10 is an important regulator of adipose tissue metabolism and energy homeostasis (34, 35). The liver is the main organ and for human lipid metabolism. Therefore hepatocyte MIHA cells were used as a model for *in vitro* experiments. When MIHA cells were transfected with *GRB10*-WT, *GRB10*-Mut, and *GRB10*-Vector, we found that the expression of GRB10 increased in cells transfected with the WT and Mut vectors, and that the expression levels of GRB10 in cells transfected with the Mut vector were significantly higher than cells transfected with the WT (**Figures 3B,C**). Western blotting found that when MIHA cells were treated with PA (100 μM) for 48 h, the levels of GRB10 protein had clearly decreased (**Figure 3E**). This result indicated that GRB10 may be related to plasma lipids metabolism. Moreover, both the *GRB10*-Mut and *GRB10*-WT vectors could reduce the levels of totalcholesterol (TC) and reverse the formation of lipid droplets induced by PA in MIHA cells (**Figures 3D,F**). Consistent with previous studies, our results indicate that *GRB10* rs1800504 mutation is a protective factor and can inhibit the excessive accumulation of cellular lipids. However, our conclusions need to be verified by further experiments and the mechanism of GRB10 regulating plasma lipids remains to be studied. Collectively, our data indicated that the influence of the rs1800504 mutation should be considered carefully in the diagnosis and intervention of T2DM complications.

CONCLUSION

In conclusion, we report for the first time that *GRB10* rs1800504 genetic variation is closely related to the risk of CHD in T2DM patients. This mechanism may be achieved by regulating the levels of circulating blood lipids. Our *in vitro* experiments further confirmed that *GRB10* rs1800504 genetic variation is related to lipid metabolism in hepatocytes. However, our results need to be merited further study.

DATA AVAILABILITY STATEMENT

The datasets presented in this study can be found in online repositories. The names of the repository/repositories and accession number(s) can be found in the article.

ETHICS STATEMENT

The studies involving human participants were reviewed and approved by Institute of Clinical Pharmacology, Central South University. The patients/participants provided their written informed consent to participate in this study.

AUTHOR CONTRIBUTIONS

YY: analyzed data and wrote manuscript. WQ: performed cell experiment and reviewed manuscript. QM: contributed to data reduction. WL and ML: collected the clinical samples. HY, RW, JD, and NY: recorded the clinical patient information. All authors contributed to the article and approved the submitted version.

FUNDING

This study was supported by the Zhuhai People's Hospital (Zhuhai hospital affiliated with Jinan University) Cultivation project (No. 2009PY-09) and National Scientific Foundation of China (No. 81903715).

SUPPLEMENTARY MATERIAL

The Supplementary Material for this article can be found online at: https://www.frontiersin.org/articles/10.3389/fcvm.2021.728976/full#supplementary-material

REFERENCES

1. DeFronzo RA, Ferrannini E, Groop L, Henry RR, Herman WH, Holst JJ, et al. Type 2 diabetes mellitus. *Nat Rev Dis Primers.* (2015) 1:15019. doi: 10.1038/nrdp.2015.19
2. Weng J, Zhou Z, Guo L, Zhu D, Ji L, Luo X, et al. Incidence of type 1 diabetes in China, 2010-13: population based study. *BMJ.* (2018) 360:j5295. doi: 10.1136/bmj.j5295
3. Pouya S, Inga P, Paraskevi S, Belma M, Suvi K, Nigel U, et al. Global and regional diabetes prevalence estimates for 2019 and projections for 2030 and 2045: results from the International Diabetes Federation Diabetes Atlas, 9th edition. *Diabetes Res Clin Pract.* (2019) 157:107843. doi: 10.1016/j.diabres.2019.107843
4. Dal Canto E, Ceriello A, Rydén L, Ferrini M, Hansen TB, Schnell O, et al. Diabetes as a cardiovascular risk factor: an overview of global trends of macro and micro vascular complications. *Eur J Prev Cardiol.* (2019) 26(2_Suppl):25–32. doi: 10.1177/2047487319878371
5. Einarson TR, Acs A, Ludwig C, Panton UH. Prevalence of cardiovascular disease in type 2 diabetes: a systematic literature review of scientific evidence from across the world in 2007-2017. *Cardiovasc Diabetol.* (2018) 17:83. doi: 10.1186/s12933-018-0728-6
6. Liu C, Li Y, Guan T, Lai Y, Shen Y, Zeyaweiding A, et al. ACE2 polymorphisms associated with cardiovascular risk in Uygurs with type 2 diabetes mellitus. *Cardiovasc Diabetol.* (2018) 17:127. doi: 10.1186/s12933-018-0771-3
7. Hudson BI, Stickland MH, Futers TS, Grant PJ. Effects of novel polymorphisms in the RAGE gene on transcriptional regulation and their association with diabetic retinopathy. *Diabetes.* (2001) 50:1505–11. doi: 10.2337/diabetes.50.6.1505
8. Zhang HM, Chen LL, Wang L, Liao YF, Yi LL. Association of 1704G/T and G82S polymorphisms in the receptor for advanced glycation end products gene with diabetic retinopathy in Chinese population. *J Endocrinol Invest.* (2009) 32:258–62. doi: 10.1007/BF03346463
9. Osei-Hyiaman D, Hou LF, Mengbai F, Zhiyin R, Kano K. Coronary artery disease risk in Chinese type 2 diabetics: is there a role for paraxonase 1 gene (Q192R) polymorphism? *Eur J Endocrinol.* (2001) 144:639–44. doi: 10.1530/eje.0.1440639
10. Garcia-Palmero I, Pompas-Veganzones N, Villalobo E, Gioria S, Haiech J, Villalobo A. The adaptors Grb10 and Grb14 are calmodulin-binding proteins. *FEBS Lett.* (2017) 591:1176–86. doi: 10.1002/1873-3468.12623
11. Holt LJ, Siddle K. Grb10 and Grb14: enigmatic regulators of insulin action - and more? *Biochem J.* (2005) 388 (Pt 2):393. doi: 10.1042/BJ20050216
12. Heimo R. Grb10 exceeding the boundaries of a common signaling adapter. *Front Bioence.* (2004) 9:603–18. doi: 10.2741/1227
13. Kabir NN, Kazi JU. Grb10 is a dual regulator of receptor tyrosine kinase signaling. *Mol Biol Rep.* (2014) 41:1985. doi: 10.1007/s11033-014-3046-4
14. Wang L, Balas B, Christ-Roberts CY, Kim RY, Ramos FJ, Kikani CK, et al. Peripheral disruption of the Grb10 gene enhances insulin signaling and sensitivity *in vivo*. *Mol Cell Biol.* (2007) 27:6497–505. doi: 10.1128/MCB.00679-07
15. Di PR. Association of hGrb10 genetic variations with type 2 diabetes in Caucasian subjects. *Diabetes Care.* (2006) 29:1181. doi: 10.2337/dc05-2551
16. Paola RD, Wojcik J, Succurro E, Marucci A, Chandalia M, Padovano L, et al. GRB10 gene and type 2 diabetes in Whites. *J Intern Med.* (2010) 267:132–3. doi: 10.1111/j.1365-2796.2009.02089.x
17. Giorgetti-Peraldi S, Murdaca J, Mas JC, Van, Obberghen E. The adapter protein, Grb10, is a positive regulator of vascular endothelial growth factor signaling. *Oncogene.* (2001) 20:3959–68. doi: 10.1038/sj.onc.1204520
18. Murdaca J, Treins C, Monthouel-Kartmann MN, Pontier-Bres R, Kumar S, Obberghen EV, et al. Grb10 prevents Nedd4-mediated vascular endothelial growth factor receptor-2 degradation. *J Biol Chem.* (2004) 279:26754–61. doi: 10.1074/jbc.M311802200
19. Reddy MA, Das S, Zhuo C, Jin W, Wang M, Lanting L, et al. Regulation of vascular smooth muscle cell dysfunction under diabetic conditions by miR-504. *Arterioscler Thromb Vasc Biol.* (2016) 36:864–73. doi: 10.1161/ATVBAHA.115.306770
20. Chinese Diabetes Society. Guidelines for prevention and treatment of type 2 diabetes in China 2020. *Chin J Diabetes Mellitus.* (2021) 13:315–409. doi: 10.3760/cma.j.cn115791-20210221-00095
21. National Health and Family Planning Commission Expert Committee on Rational Drug Use. Chinese Pharmacists Association, Guidelines for rational drug use in coronary heart disease (2nd edition). *Chin J Front Med.* (2018) 10:7–136. doi: 10.3969/j.issn.1674-7372.2016.06.007
22. Yan HB. *Clinical Guidelines for Diagnosis and Treatment of Coronary Heart Disease*. China: People's Medical Publishing House (PMPH) (2010).
23. Hu DY, Zhang YQ, Sun NL. Guidelines for primary diagnosis and treatment of hypertension. *Chin J Gen Pract.* (2019) 18:13. doi: 10.3760/cma.j.issn.1671-7368.2019.04.002
24. Ma N, Wang Y-K, Xu S, Ni Q-Z, Zheng Q-W, Zhu B, et al. PPDPF alleviates hepatic steatosis through inhibition of mTOR signaling. *Nat Commun.* (2021) 12:3059. doi: 10.1038/s41467-021-23285-8
25. Li L, Li X, Zhu Y, Zhang M, Yin D, Lu J, et al. Growth receptor binding protein 10 inhibits glucose-stimulated insulin release from pancreatic beta-cells associated with suppression of the insulin/insulin-like growth factor-1 signalling pathway. *Clin Exp Pharmacol Physiol.* (2013) 40:841–7. doi: 10.1111/1440-1681.12160
26. Zhang J, Zhang N, Liu M, Li X, Zhou L, Huang W, et al. Disruption of growth factor receptor-binding protein 10 in the pancreas enhances β-cell proliferation and protects mice from streptozotocin-induced β-cell apoptosis. *Diabetes.* (2012) 61:3189–98. doi: 10.2337/db12-0249
27. Doiron B, Hu W, Norton L, DeFronzo RA. Lentivirus shRNA Grb10 targeting the pancreas induces apoptosis and improved glucose tolerance due to decreased plasma glucagon levels. *Diabetologia.* (2012) 55:719–28. doi: 10.1007/s00125-011-2414-z
28. Wei FJ, Cai CY, Shi WT. Correlation of hyperuricemia with dyslipidemia, insulin resistance, and hypertension in T2DM patients. *Chin J Diabetes.* (2013) 21:97–9.
29. Grams J, Garvey WT. Weight loss and the prevention and treatment of type 2 diabetes using lifestyle therapy, pharmacotherapy, and bariatric surgery: mechanisms of action. *Curr Obes Rep.* (2015) 4:287–302. doi: 10.1007/s13679-015-0155-x
30. Liu MM, Peng J, Guo YL, Wu NQ, Li JJ. Impact of diabetes on coronary severity and cardiovascular outcomes in patients with heterozygous familial hypercholesterolaemia. *Eur J Prev Cardiol.* (2021) doi: 10.1093/eurjpc/zwab042
31. Tomlinson B, Patil NG, Fok M, Lam C. Managing dyslipidemia in patients with type 2 diabetes. *Expert Opin Pharmacother.* (2021) 1–14. doi: 10.1080/14656566.2021.1912734
32. Luo X, Zheng E, Wei L, Zeng H, Chen Y. The fatty acid receptor CD36 promotes HCC progression through activating Src/PI3K/AKT axis-dependent aerobic glycolysis. *Cell Death Dis.* (2021) 12:328. doi: 10.1038/s41419-021-03596-w
33. Lim H, Lee H, Lim Y. Effect of vitamin D3 supplementation on hepatic lipid dysregulation associated with autophagy regulatory AMPK/Akt-mTOR signaling in type 2 diabetic mice. *Exp Biol Med.* (2021) 246:1535370220987524. doi: 10.1177/1535370220987524
34. Liu B, Liu F. Feedback regulation of mTORC1 by Grb10 in metabolism and beyond. *Cell Cycle.* (2014) 13:2643–4. doi: 10.4161/15384101.2014.954221
35. Liu M, Bai J, He S, Villarreal R, Hu D, Zhang C, et al. Grb10 promotes lipolysis and thermogenesis by phosphorylation-dependent feedback inhibition of mTORC1. *Cell Metab.* (2014) 19:967–80. doi: 10.1016/j.cmet.2014.03.018

Conflict of Interest: The authors declare that the research was conducted in the absence of any commercial or financial relationships that could be construed as a potential conflict of interest.

Publisher's Note: All claims expressed in this article are solely those of the authors and do not necessarily represent those of their affiliated organizations, or those of the publisher, the editors and the reviewers. Any product that may be evaluated in this article, or claim that may be made by its manufacturer, is not guaranteed or endorsed by the publisher.

frontiers in Cardiovascular Medicine

ORIGINAL RESEARCH
published: 14 October 2021
doi: 10.3389/fcvm.2021.720884

CYP17A1–ATP2B1 SNPs and Gene–Gene and Gene–Environment Interactions on Essential Hypertension

Bi-Liu Wei[1], *Rui-Xing Yin*[1,2,3]*, *Chun-Xiao Liu*[1], *Guo-Xiong Deng*[1], *Yao-Zong Guan*[1] and *Peng-Fei Zheng*[1]

[1] Department of Cardiology, Institute of Cardiovascular Diseases, The First Affiliated Hospital, Guangxi Medical University, Nanning, China, [2] Guangxi Key Laboratory Base of Precision Medicine in Cardio-Cerebrovascular Disease Control and Prevention, Nanning, China, [3] Guangxi Clinical Research Center for Cardio-Cerebrovascular Diseases, Nanning, China

OPEN ACCESS

Edited by:
Christoph D. Rau,
University of North Carolina at Chapel Hill, United States

Reviewed by:
Umamaheswaran Gurusamy,
University of California, San Francisco, United States
Milagros Romay,
Northwestern University, United States

***Correspondence:**
Rui-Xing Yin
yinruixing@163.com
orcid.org/0000-0001-7883-4310

Specialty section:
This article was submitted to Cardiovascular Genetics and Systems Medicine, a section of the journal Frontiers in Cardiovascular Medicine

Received: 05 June 2021
Accepted: 09 September 2021
Published: 14 October 2021

Citation:
Wei B-L, Yin R-X, Liu C-X, Deng G-X, Guan Y-Z and Zheng P-F (2021) CYP17A1–ATP2B1 SNPs and Gene–Gene and Gene–Environment Interactions on Essential Hypertension. Front. Cardiovasc. Med. 8:720884. doi: 10.3389/fcvm.2021.720884

Background: The association between the *CYP17A1* and *ATP2B1* SNPs and essential hypertension (referred to as hypertension) is far from being consistent. In addition to the heterogeneity of hypertension resulting in inconsistent results, gene–gene and gene–environment interactions may play a major role in the pathogenesis of hypertension rather than a single gene or environmental factor.

Methods: A case–control study consisting of 1,652 individuals (hypertension, 816; control, 836) was conducted in Maonan ethnic minority of China. Genotyping of the four SNPs was performed by the next-generation sequencing technology.

Results: The frequencies of minor alleles and genotypes of four SNPs were different between the two groups ($p < 0.001$). According to genetic dominance model analysis, three (rs1004467, rs11191548, and rs17249754) SNPs and two haplotypes (*CYP17A1* rs1004467G-rs11191548C and *ATP2B1* rs1401982G-rs17249754A) were negatively correlated, whereas rs1401982 SNP and the other two haplotypes (*CYP17A1* rs1004467A-rs11191548T and *ATP2B1* rs1401982A-rs17249754G) were positively associated with hypertension risk ($p \leq 0.002$ for all). Two best significant two-locus models were screened out by GMDR software involving SNP–environment (rs11191548 and BMI $\geq$ 24 kg/m^2) and haplotype–environment (*CYP17A1* rs1004467G-rs11191548C and BMI $\geq$ 24 kg/m^2) interactions ($p \leq 0.01$). The subjects carrying some genotypes increased the hypertension risk.

Conclusions: Our outcomes implied that the rs1004467, rs11191548, and rs17249754 SNPs and *CYP17A1* rs1004467G-rs11191548C and *ATP2B1* rs1401982G-rs17249754A haplotypes have protective effects, whereas the rs1401982 SNP and *CYP17A1* rs1004467A-rs11191548T and *ATP2B1* rs1401982A-rs17249754G haplotypes showed adverse effect on the prevalence of hypertension. Several SNP–environment interactions were also detected.

Keywords: *CYP17A1*, *ATP2B1*, single nucleotide polymorphisms, interactions, hypertension

INTRODUCTION

Essential hypertension (referred to as hypertension) is a regular multifactorial disease affecting about one-fourth of adults worldwide (1). Conversely, most of its potential mechanisms are still unknown. It is well-known that environmental factors, including excessive salt intake, tobacco use, physical inactivity, alcohol abuse, overweight, and obesity, increase blood pressure (BP) levels (2), but about half of population BP changes are determined by genetic factors (3, 4).

Genome-wide association studies (GWASs) can screen and analyze hypertension risk genes (5). For instance, two large GWASs (Global BPgen and CHARGE) have identified 14 risk loci that reached genome-wide significant closely related to BP in 2009, including ATPase, Ca^{2+} transporting, plasma membrane 1 gene (*ATP2B1*) and cytochrome P450, family 17, subfamily A, and polypeptide 1 gene (*CYP17A1*) (6, 7). The results about single-nucleotide polymorphism (SNP) of *ATP2B1* and *CYP17A1* were tested and verified soon afterwards in different ethnic groups (8–12). In particular, the reproductions about *ATP2B1* and *CYP17A1* were also conducted in Chinese Han population according to the GWASs (4, 13). However, the evidence that showed the relationship of *ATP2B1* and *CYP17A1* with the hypertension risk from Maonan being one of China's ethnic minorities was still rare.

The *CYP17A1* encodes the P450c17 protein, a member of the cytochrome P450 superfamily of enzymes speeding up plenty of chemical synthesis processes involving steroids, cholesterin, and other blood fats (14). Recently, some articles have reported that the *CYP17A1* is related to hypertension, and one reason for how this gene leads to hypertension may be that genetic factors can influence the distribution of fat in body, and then lipid metabolism disorders can cause BP elevating (15–19). Several hypertension susceptibility genes are also associated with lipid profile and fat distribution (17–19). For instance, Zhang et al. reported that two SNPs (rs11191548 and rs1004467) in the *CYP17A1* locus were correlated with hypercholesterolemia in Han Chinese (19). In addition, in 2012, a Japanese research also found that the *CYP17A1* rs1004467 SNP was associated with the reduction of two types of fat, including visceral and subcutaneous (17). However, Liu et al. had a different opinion regarding the relationship between the *CYP17A1* polymorphism and body mass index (BMI) (4).

ATP2B1 is attributed to the family of P-type primary ion transport ATPases (10). The associations of two SNPs (rs1401982, a common intronic variant, and rs17249754, a common intergenic variant with the strongest association of the SNPs) in the *ATP2B1* region with both BP and risk of hypertension susceptibility were previously found by GWASs (6, 7, 11) and replicated in the Japanese (8, 9), Korean (10), East Asian (12), and Chinese populations (13). Wang et al. reported that two loci (rs17249754 and rs1401982) were negatively associated with hypertension in a Chinese population (13). However, a Korean genome epidemiology study showed that *ATP2B1* rs17249754 polymorphism may be increased the incident hypertension, when sodium was excessively consumed (20). Tabara et al. also demonstrated that the rs1401982 minor allele may be at higher risk of hypertension in the Japanese (8). The underlying mechanism of *ATP2B1* affecting BP may be that the *ATP2B1* encodes plasma membrane calcium ATPase with an important function in intracellular calcium homeostasis (21, 22). Therefore, some studies have suggested that *ATP2B1* polymorphism may change arterial stiffness by affecting vascular reactivity (13, 23).

The above studies have shown significant association between the *CYP17A1–ATP2B1* SNPs and hypertension, but others also showed no association between them. The contradictory results may be related to the following factors (14): (1) ignoring the influence of environment–environment, environment–gene, and gene–gene interactions on BP parameters; (2) some variants found in GWASs may not be functional and have little effect on BP phenotype; (3) variation found in GWASs may have linkage disequilibrium (LD) with some functional variants rather than their own role; (4) the frequency of a high-risk genotype is not alike in different races. For example, in the International 1000 Genomes database (https://www.ncbi.nlm.nih.gov/variation/tools/1000genomes/), the frequency of rs1004467GG genotype in the Chinese Han population was 0.364, which was slightly higher than the genotype frequency of 0.322 in the Japanese population, but both were significantly higher than that (0.104) in the European population. These differences may be caused by evolutionary divergence, or it may be the result of negative selection of rs1004467 risk alleles in European populations. Therefore, we should continue (1) to evaluate the differences in genotypes and allele frequencies in other populations of different ancestry; (2) to screen larger cohorts with clinical BP abnormalities; and (3) to evaluate gene–gene (G × G) and gene–environment (G × E) interactions on BP and hypertension, which are very meaningful and necessary (14).

Maonan is one of the mountain ethnic groups with a small population in China (24). Its living environment, dietary structure, lifestyle, and genetic background are different from the local Han population (25–28). Our previous popular survey found that the prevalence of hypertension in this ethnic group was higher than that in the local Han population (49 vs. 31%, $p < 0.001$) (24). However, up to now, the reason for these differences in BP levels between the two ethnic groups and their risk factors has not been understood. Therefore, the purpose of this research was to test the association of *ATP2B1* (rs1401982 and rs17249754) and *CYP17A1* (rs1004467 and rs11191548) SNPs, and their haplotypes, G × G and G × E interactions, with hypertension in the Maonan population.

METHODS

SNP Selection

There were five steps for screening four SNPs of *CYP17A1* and *ATP2B1*: (1) SNPs belonging to tagging SNPs were detected by Haploview (Broad Institute or MIT and Harvard, Cambridge, MA, USA, version 4.2). (2) *CYP17A1* (rs1004467 and rs11191548) and *ATP2B1* (rs1401982 and rs17249754) SNPs were then chosen by SHEsis Main (http://analysis.bio-x.cn/myAnalysis.php). (3) The minor allele frequency (MAF) of the SNPs was more than 1%. (4) SNPs may be associated with

hypertension according to the previous investigations. (5) SNP-related information was acquired from NCBI dbSNP Build 132 (http://www.ncbi.nlm.nih.gov/SNP/).

Research Populations

A total of 1,652 Maonan subjects were randomly extracted from previously stratified random samples to conduct a cross-sectional study of hypertensive molecular epidemiology (29). The participants were aged 18–90 years with an average age of 56.6 ± 13.1 years in controls and 56.7 ± 12.3 years in hypertensives. The detailed description of the selection criteria for Maonan participants can be found in two previous studies (24, 30). Besides, all participants were also demonstrated to be Maonan ethnic group by Y chromosome and mitochondrial diversity studies (31). Subjects had complete data on BP and other laboratory parameters and no various related illnesses such as cardiovascular disease, secondary hypertension, and nephropathy. Calculating sample quantity was performed using quanto software (32). All participants had signed informed consent. All the research programs of this project have been approved by the Ethics Committee of the First Affiliated Hospital of Guangxi Medical University (No: Lunshen-2014-KY-Guoji-001; Mar. 7, 2014) (31).

Epidemiological Survey

International standardization methods were used for the epidemiological survey (24, 33). Trained health professionals collected data such as demographics, medical history, and lifestyle elements by standardized questionnaires. Alcohol and cigarette usage was designated into either one of two groups (yes or no) (34). BMI (kg/m^2) was calculated as weight/(height^2). Sitting BP was determined three times after taking a rest at least 5 min using a manual sphygmomanometer, and the average of three readings was used for BP analysis (24).

Serum Lipid Measurements

Serum cholesterol (TC), triglyceride (TG), high-density lipoprotein cholesterol (HDL-C), and low-density lipoprotein cholesterol (LDL-C) were tested by commercially available enzyme assays (31), and all the tests were carried out by an automatic analyzer in the Clinical Science Experiment Center of the First Affiliated Hospital, Guangxi Medical University (31, 35).

Genotyping

The genome DNA was isolated from venous blood white cells with phenol-chloroform (36). All DNA samples were saved at −80°C for the next analysis. Genotyping of the four SNPs was achieved by next-generation sequencing techniques [Sangon Biotech (Shanghai) Co; Ltd] (31). The sense and antisense primers used in this study are shown in **Supplementary Table 1**.

Diagnostic Criteria

Hypertension was defined as an average systolic blood pressure (SBP) ≥ 140 mmHg and/or diastolic blood pressure (DBP) ≥ 90 mmHg, or using drugs for treating high BP (37). Hyperlipidemia was diagnosed as an average TC > 5.17 mmol/L, and/or TG > 1.70 mmol/L (31, 38). Age subgroup was divided into two groups: <60 and ≥60 years (34, 35). A BMI < 24, 24–28, and > 28 kg/m^2 was defined as normal weight, overweight, and obesity, respectively (36).

Statistical Analyses

Statistical analyses of the data were realized by the SPSS 22.0 (31), which was the statistical software (SPSS Inc., Chicago, IL, USA). Differences in quantitative data of normal distribution, non-normally distributed data, and qualitative data between hypertension and control participants were analyzed by *t*-test, Wilcoxon–Mann–Whitney test, and chi-square test, respectively. The analyses of Hardy–Weinberg equilibrium (HWE), genotype and allele frequencies, pairwise LD, and haplotype frequencies were mainly performed by the SHEsis online genetics software (http://analysis.bio-x.cn/myAnalysis.php) (31, 39). Logistic regression analyses employed not only the association between SNPs and hypertension, but also the interactions of G × G and G × E on the risk of hypertension after adjustment of sex, age, cigarette smoking, drinking, BMI, and hyperlipidemia (35, 36). A p-value < 0.05 was considered statistically significant. The best G × G and G × E interaction combination was screened by Generalized multifactor dimensionality reduction (GMDR) (31, 40–42). Then, the best model with the maximation of cross-validation consistency was chosen (36, 43). Finally, the prediction accuracy of the recognition model was statistically tested by a sign test (providing empirical p-values) (31). G × G and G × E interactions of the best model were presented by hierarchical interaction graphs and interaction dendrograms of MDR (43). Besides, traditional

TABLE 1 | General characteristics of the study subjects.

Parameter	Control	Hypertension	$t(\chi^2)$	p
Number	836	816		
Age (years)	56.7 ± 13.1	56.7 ± 12.3	−0.01	0.99
Body mass index (kg/m^2)	22.9 ± 4.47	25.3 ± 4.14	−10.79	<0.001
Waist circumference (cm)	77.4 ± 9.6	83.3 ± 10.2	−11.96	<0.001
Systolic blood pressure (mmHg)	119 ± 11	151 ± 16	−46.34	<0.001
Diastolic blood pressure (mmHg)	74 ± 8	92 ± 10	−37.88	<0.001
Glucose (mmol/L)	6.06 ± 1.32	6.43 ± 1.46	−5.41	<0.001
Total cholesterol (mmol/L)	4.87 ± 0.88	5.18 ± 0.99	−6.74	<0.001
Triglyceride (mmol/L)	1.26 (0.93)	1.68 (1.18)	−10.55	<0.001
HDL-C (mmol/L)	1.30 ± 0.23	1.24 ± 0.31	4.45	<0.001
LDL-C (mmol/L)	3.08 ± 0.41	3.25 ± 0.55	−7.28	<0.001
Male/female	426/410	415/401	0.002	0.97
Smoking status [*n* (%)]				
Non-smoker	614 (73.4)	608 (74.5)		
Smoker	222 (26.6)	208 (25.5)	0.24	0.62
Alcohol consumption [*n* (%)]				
Non-drinker	659 (78.8)	633 (77.6)		
Drinker	177 (21.2)	183 (22.4)	0.38	0.54

Normal distribution quantitative data are presented as mean ± SD. Non-normal distribution data such as triglyceride are expressed as median (interquartile range). Qualitative variables are expressed as percentages (%). LDL-C, low-density lipoprotein cholesterol; HDL-C, high-density lipoprotein cholesterol.

statistical approaches were applied to test the outcomes from MDR analyses, and $p < 0.016$ was considered statistically significant after Bonferroni correction (0.05/3) (36, 43).

RESULTS

Demographic Characteristics

The demographic parameters of 1,652 subjects are shown in **Table 1**. Compared with the control group, hypertensive patients had higher BMI, SBP, DBP, blood glucose, TC, TG, and LDL-C, but lower HDL-C ($p < 0.001$). However, there was no difference in age, sex ratio, smoking, and drinking between the control and case groups ($p > 0.05$ for all).

Genotype and Allele Frequencies and Hypertension

As shown in **Table 2**, the minor allele and genotype distribution of the rs1004467, rs11191548, rs1401982, and rs17249754 SNPs was different between the patient and control groups ($p < 0.001$). **Figure 1** shows the genotype and allele frequencies of each SNP in control and hypertension groups. The genotype distribution was consistent with the HWE ($p > 0.05$ for all). Simultaneously, the rs1401982 SNP enhanced the risk of hypertension, whereas the rs1004467, rs11191548, and rs17249754 SNPs decreased the susceptibility of hypertension in the dominant model ($p \leq 0.002$ for all).

Haplotypes and the Risk of Hypertension

LD analysis showed that the four SNPs did not have statistical independence in the control or case group. However, the LD between the rs1004467 and rs11191548 ($D' = 0.950$) or between the rs1401982 and rs17249754 SNPs ($D' = 0.951$) was strong in both control and hypertension groups (**Supplementary Figure 1**; **Supplementary Table 2**). As shown in **Table 3**, the most common haplotypes were *CYP17A1* rs1004467A-rs11191548T and *ATP2B1* rs1401982A-rs17249754G (≥ 67% of the samples). The frequencies of *CYP17A1* rs1004467A-rs11191548T, *CYP17A1* rs1004467G-rs11191548C, *ATP2B1* rs1401982A-rs17249754G, and *ATP2B1* rs1401982G-rs17249754A haplotypes were significantly different between the control and case groups. Meanwhile, the haplotypes of *CYP17A1* rs1004467A-rs11191548T, *CYP17A1* rs1004467G-rs11191548C, and *ATP2B1* rs1401982G-rs17249754A had a protective effect for hypertension, whereas the haplotype of *ATP2B1* rs1401982A-rs17249754G revealed an increased susceptibility of disease ($p < 0.001$).

G × G and G × E Interaction on Hypertension

The GMDR model was utilized to analyze the interaction of G × G and G × E among SNPs, haplotypes, BMI, age, gender, alcohol, and/or cigarette usage on the risk of hypertension. **Table 4** summarizes the results of G × G and G × E interactions of the two and three loci models derived from GMDR analysis. A significant two-locus model revealed a potential SNP–environment interaction between the rs11191548 SNP and BMI ≥ 24 kg/m^2 ($p = 0.01$), with a cross-validation consistency (7/10) and a testing accuracy of 62.7%. Another significant two-locus model (*CYP17A1* rs1004467G-rs11191548C and BMI ≥ 24 kg/m^2, $p = 0.0004$) indicated a potential haplotype–environment interaction, with a cross-validation consistency (9/10) and a testing accuracy of 63.5%.

Entropy-based interaction dendrograms obtained from MDR analysis are shown in **Figure 2**, which exhibited the strongest antagonistic effect of the SNP–SNP interaction (rs1401982 and rs17249754), SNP–environment interaction (rs11191548 and BMI ≥ 24 kg/m^2), haplotype–haplotype interaction (*CYP17A1* rs1004467A-rs11191548T and *CYP17A1* rs1004467G-rs11191548C), and haplotype–environment interaction (*CYP17A1* rs1004467G-rs11191548C and age), respectively. In order to obtain the OR and 95% CI for the joint effects, we implemented an interaction study by logistic regression analyses (**Table 5**). When the SNP–environment interaction was analyzed, we found that the individuals with rs11191548 TC/CC genotypes and BMI ≥ 24 kg/m^2 raised the risk of hypertension (adjusted OR = 1.45, 95% CI = 1.08–1.94, $p = 0.014$) compared to the individuals with rs11191548 TT and BMI ≥ 24 kg/m^2.

DISCUSSION

In this cross-sectional study of hypertensive molecular epidemiology, the association of the *ATP2B1* and *CYP17A1* SNPs, and their haplotypes, G × G and G × E interactions, with hypertension in the Maonan population was observed for the first time. The main findings are as follows: (1) The genotype and allele frequencies of the *CYP17A1* rs1004467, *CYP17A1* rs11191548, *ATP2B1* rs1401982, and *ATP2B1* rs17249754 SNPs were significantly different between the control and hypertension groups. (2) The *ATP2B1* rs1401982 SNP enhanced the risk of hypertension, whereas the *CYP17A1* rs1004467, *CYP17A1* rs11191548, and *ATP2B1* rs17249754 SNPs decreased the prevalence of hypertension in the dominant models. (3) The frequencies of *CYP17A1* rs1004467A-rs11191548T, *CYP17A1* rs1004467G-rs11191548C, *ATP2B1* rs1401982A-rs17249754G, and *ATP2B1* rs1401982G-rs17249754A haplotypes were significantly different between the control and case groups. (4) The *CYP17A1* rs1004467A-rs11191548T, *CYP17A1* rs1004467G-rs11191548C, and *ATP2B1* rs1401982G-rs17249754A haplotypes had a protective effect for hypertension, whereas the *ATP2B1* rs1401982A-rs17249754G haplotype increased the risk of hypertension. (5) Several interactions including rs11191548-BMI ≥ 24 kg/m^2 (SNP–environment) and rs1004467G-rs11191548C-BMI ≥ 24 kg/m^2 (haplotype–environment) on the risk of hypertension were also observed. (6) The individuals with rs11191548 TC/CC genotypes and BMI ≥ 24 kg/m^2 raised the risk of hypertension.

In the past 10 years, according to the results of GWAS scans, both *ATP2B1* and *CYP17A1* have correlation with BP and/or hypertension (6, 7). However, the genetic association between the *ATP2B1* or *CYP17A1* and hypertension was conflicting. The most important reasons for the discrepant outcomes may be that hypertension is a complicated illness

TABLE 2 | Correlation between the *CYP17A1–ATP2B1* polymorphisms and hypertension.

SNP	Genotype	Control ($n = 836$)	Hypertension ($n = 816$)	χ^2	*p*	Adjusted OR (95% CI)	**p*
CYP17A1	AA	410 (49.0)	487 (59.7)	22.9	1.07E-005	1	–
rs1004467 A>G	AG+ GG	426 (51.0)	329 (40.3)			0.66 (0.54–0.81)	<0.001
	MAF	511 (30.6)	376 (23.0)	23.8	1.09E-006		
	P_{HWE}	0.26	0.47				
CYP17A1	TT	436 (52.1)	538 (65.9)	33.08	6.55E-008	1	–
rs11191548T>C	TC+ CC	400 (47.9)	278 (34.1)			0.57 (0.46–0.7)	<0.001
	MAF	461 (27.6)	314 (19.2)	31.93	1.64E-008		
	P_{HWE}	0.66	0.19				
ATP2B1	GG	91 (10.9)	47 (5.8)	22.42	1.36E-005	1	–
rs1401982 G>A	GA+ AA	745 (89.1)	769 (94.2)			1.83 (1.24–2.7)	0.002
	MAF	1142 (68.3)	1235 (75.7)	22.24	2.45E-006		
	P_{HWE}	0.26	0.81				
ATP2B1	GG	460 (55.0)	544 (66.7)	24.06	5.97E-006	1	
rs17249754 G>A	GA+ AA	376 (45.0)	272 (33.3)			0.68 (0.55–0.84)	<0.001
	MAF	425 (25.4)	302 (18.5)	23.0	1.65E-006		
	P_{HWE}	0.36	0.63				

*CYP17A1, cytochrome P450 17A1; ATP2B1, ATPase, Ca^{2+} transporting, plasma membrane 1; MAF, minor allele frequency; HWE, Hardy–Weinberg equilibrium. p is the probability of chi-square test; *p is the probability of logistic regression analyses. The symbol "–" means there is no data.*

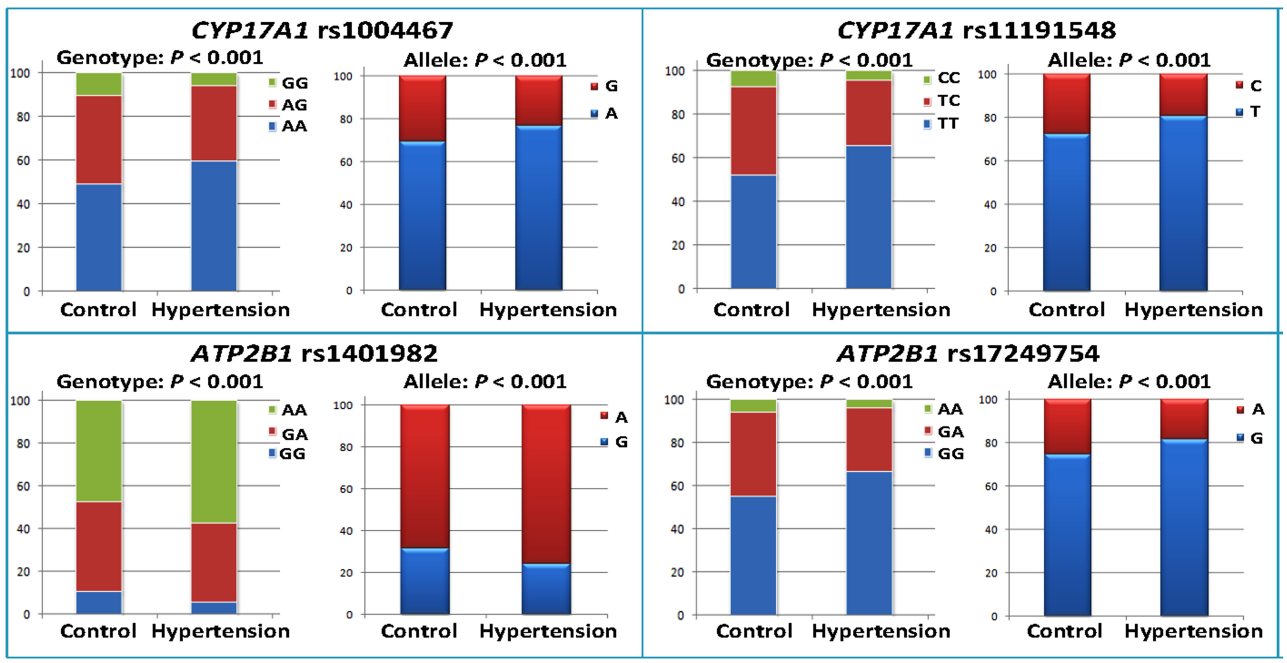

FIGURE 1 | Genotype and allele frequencies of the four *CYP17A1–ATP2B1* SNPs in the control and hypertension groups.

that is influenced by various environmental elements, small effect polygenes, and their interactions (44). The genotype and allele frequencies of the *CYP17A1–ATP2B1* SNPs are different in distinct races, ethnic groups, or populations according to the International 1,000 Genomes database (https://www.ncbi.nlm.nih.gov/variation/tools/1000genomes/). The *CYP17A1*

TABLE 3 | Association between the haplotypes and hypertension risk.

Haplotype	Hypertension Fre.	Control Fre.	χ^2	*p*	OR (95% CI)
rs1004467A-rs11191548C	12.56 (0.008)	15.61 (0.009)	–	–	–
rs1004467A-rs11191548T	1,243.44 (0.76)	1,145.39 (0.69)	24.16	9.04E-007	1.48 (1.26–1.72)
rs1004467G-rs11191548C	301.44 (0.19)	445.39 (0.27)	31.86	1.70E-008	0.62 (0.53–0.73)
rs1004467G-rs11191548T	74.56 (0.05)	65.61(0.04)	0.83	0.36	1.17 (0.83–1.64)
rs1401982 A-rs17249754A	9.61 (0.006)	16.16 (0.010)	–	–	–
rs1401982A-rs17249754G	1,225.39 (0.75)	1,125.84 (0.67)	22.96	1.68E-006	1.45 (1.25–1694)
rs1401982G-rs17249754A	292.39 (0.18)	408.84 (0.25)	21.67	3.28E-006	0.67 (0.57–0.79)
rs1401982G-rs17249754G	104.61 (0.06)	121.16 (0.07)	0.97	0.33	0.87 (0.67–1.15)

The haplotype is combined with CYP17A1 rs1004467-rs11191548 and ATP2B1 rs1401982-rs17249754. Control Fre., the frequency of haplotypes in control individuals; Hypertension Fre., the frequency of haplotypes in hypertension subjects. Rare Hap (frequency < 3%) has been ignored in control and case subjects.

TABLE 4 | GMDR analysis of SNPs, haplotypes, and environments showed different interactions.

Locus no.	Best combination	Training Bal. Acc	Testing Bal. Acc	Cross-validation consistency	χ^2	*p*	OR (95% CI)
SNP–SNP interaction							
2	Rs11191548, rs17249754	0.58	0.56	8/10	1.55	0.21	1.71 (0.69, 4.2)
3	Rs1004467, rs11191548, rs1401982	0.59	0.57	8/10	1.82	0.18	1.82 (0.74, 4.47)
SNP–environment interaction							
2	Rs11191548, BMI ≥ 24	0.64	0.63	7/10	6.07	0.01	3.26 (1.27, 8.38)
3	Rs11191548, BMI ≥ 24, gender	0.66	0.64	6/10	6.81	0.009	3.41 (1.35, 8.61)
Haplotype–haplotype interaction							
2	G-C, A-G	0.56	0.56	9/10	2.58	0.11	1.64 (0.88, 3.06)
3	A-T, G-T, A-G	0.56	0.56	10/10	3.11	0.08	1.72 (0.93, 3.21)
Haplotype–environment interaction							
2	G-C, BMI ≥ 24	0.64	0.63	9/10	12.75	0.0004	3.23 (1.69, 6.18)
3	Age, BMI ≥ 24, G-C	0.64	0.64	7/10	12.51	0.0004	3.12 (1.65, 5.9)

p, adjusting for gender, age, smoking, alcohol consumption, BMI, and hyperlipidemia. The haplotype is combined with CYP17A1 rs1004467-rs11191548 and ATP2B1 rs1401982-rs17249754.

rs1004467G allele frequency in Chinese Dai in Xishuangbanna, China (CDX), Han Chinese in Beijing, China (CHB), and Southern Han Chinese (CHS) was 28.49, 36.41, and 35.71%, respectively. The *CYP17A1* rs11191548C allele frequency in CDX, CHB, and CHS was 25.27, 29.61, and 28.10%, respectively. The *ATP2B1* rs1401982G allele frequency in CDX, CHB, and CHS was 27.96, 34.95, and 39.05%, respectively. The *ATP2B1* rs17249754A allele frequency in CDX, CHB, and CHS was 18.82, 32.04, and 36.67%, respectively. In the present study, we found that the MAF of these SNPs was lower than other Chinese, especially in the hypertension group, but it was higher in our study populations than in Europeans or Africans. These results might also be a reasonable explanation for the distinct prevalence of hypertension between Chinese and Europeans or Africans.

Maonan people not only like to eat beef, pork, and animal viscera, all of which are rich in saturated fatty acid, but also like sour marinated meat, snails, and sour pickles that contain a lot of salt (36). High-fat diet is an important element leading to obesity, dyslipidemia (45), atherosclerosis, and hypertension (46, 47). In particular, high-salt diet has a significant impact on hypertension (2, 4, 15). Therefore, the eating habits of Maonan residents may explain the differences in BMI, BP, TC, and TG values between the control and case groups.

There was no statistical significance in alcohol and cigarette consumption rates between control and hypertension groups in our research. The effects of drinking and smoking on hypertension have been reported by previous articles. The extent to which alcohol is associated with hypertension may be partly related to the amount of alcohol consumed (48–51). Low levels of alcohol use mean no different from or slightly lower BP (48–51), and high levels of alcohol consumption are a strong predictor of the high BP risk (48, 52). Smokers usually have higher BP than non-smokers (53, 54). However, the effects of alcohol and tobacco on the risk of hypertension in many

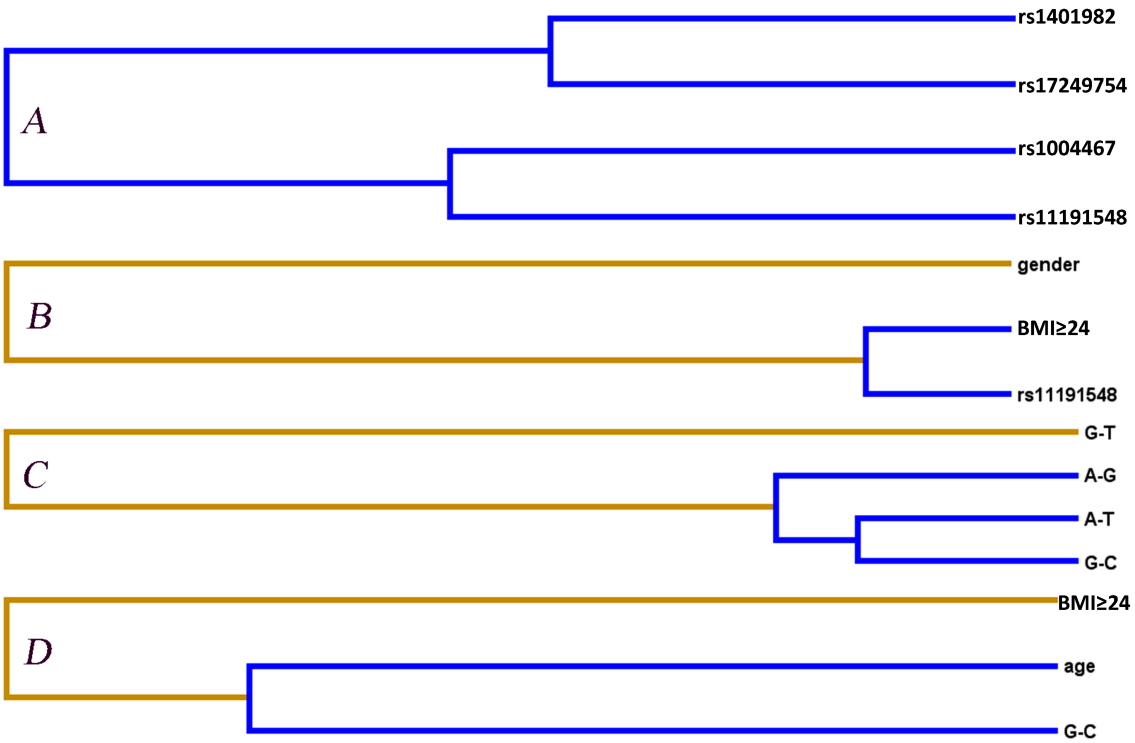

FIGURE 2 | Different types of interaction dendrogram for gene–gene **(A,C)** and gene–environment **(B,D)** on the hypertension risk. Orange color (synergy); blue color (strong antagonism interaction). The elements with stronger interaction are closer at the leaves of the tree.

studies were still inconsistent (48–51). We assume that these discrepancies could be due to numerous factors, including sample size, misclassification bias according to participants' self-reported questionnaires, ethnicities, age groups, and gender, warranting that further research should take into account the factors above (48–51, 55, 56). To address the possibility that many genetic variants associated with hypertension found by the GWASs might be the result of different environmental as well as direct genetic effects (57), our study used some examples, including eating habits and alcohol and cigarette consumption.

In the current study, minor allele and genotype frequencies of all four SNPs had a difference in control and case groups ($p < 0.001$). These results showed that *CYP17A1* and *ATP2B1* SNPs were correlated with hypertension and genetic factors might play a part in susceptibility to hypertension. Furthermore, according to genetic dominance model analysis, three SNPs (rs1004467, rs11191548, and rs17249754) and two haplotypes (*CYP17A1* rs1004467G-rs11191548C and *ATP2B1* rs1401982G-rs17249754A) were negatively correlated with hypertension risk, while the rs1401982 SNP and the other two haplotypes (*CYP17A1* rs1004467A-rs11191548T and *ATP2B1* rs1401982A-rs17249754G) were positively associated with hypertension risk ($p \leq 0.002$). Meanwhile, GMDR analysis showed no statistical difference between the interaction of *CYP17A1* and *ATP2B1* on hypertension. However, two best significant two-locus models were screened out involving SNP–environment (rs11191548 and BMI $\geq$ 24 kg/m^2) and haplotype–environment (*CYP17A1* rs1004467G-rs11191548C and BMI $\geq$ 24 kg/m^2) interactions ($p \leq 0.01$). The participants with the rs11191548 TT genotype and BMI $\geq$ 24 kg/m^2 had higher risk of hypertension than the individuals with the rs11191548 TC/CC genotypes and BMI $\geq$ 24 kg/m^2. G $\times$ E interaction on the development of hypertension was also observed in this cross-sectional study.

The prevalence of hypertension is increasing year by year, so new and more effective measures are urgently needed to prevent and treat hypertension. However, this depends on the discovery of mechanism of BP regulation. Although lifestyle intervention can successfully reduce BP in some patients, there are still a number of patients with hypertension who need new drugs to decrease BP. GWASs have confirmed that the *ATP2B1* encoding plasma membrane Ca^{2+} ATPase 1 (PMCA1) is strongly associated with BP and hypertension. Several studies have confirmed that PMCA1 plays a physiological role in regulating BP and resistance artery function. PMCA1 may be a potential target for the treatment of essential hypertension (58). At present, the specific mechanism of hypertension has not been fully clarified, and further studies are needed to explore this. This study may provide new information and ideas for the scientists in this field.

There are several potential limitations in our study. First, the number of controls and patients with hypertension was relatively small. Larger samples are necessary to confirm our findings in this study. Second, the general characteristics of the two study populations were different. The potential effects of these factors

TABLE 5 | Various types of interactions were analyzed by logistic regression analysis.

Variable 1	Variable 2	OR (95% CI)	*P*
SNP–SNP interaction			
Rs1401982	Rs17249754		
GG	No	1	–
GG	Yes	1.55 (0.24–10.27)	0.65
GA+AA	No	3.12 (0.49–19.88)	0.23
GA+AA	Yes	2.26 (0.35–14.49)	0.39
SNP–environment interaction			
Rs11191548	BMI ≥ 24		
TT	No	1	
TT	Yes	4.38 (3.31–5.79)	<0.001
TC+CC	No	1.03 (0.76–1.39)	0.87
TC+CC	Yes	1.45 (1.08–1.94)	0.014
Haplotype–haplotype interaction			
A-T	G-C		
Non-carriers	Non-carriers	1	
Non-carriers	Carriers	0.63 (0.44–0.91)	0.012
Carriers	Non-carriers	1.02 (0.73–1.42)	0.92
Carriers	Carriers	–	–
Haplotype–environment interaction			
G-C	Age ≥ 60		
Non-carriers	No	1	–
Non-carriers	Yes	1.61 (1.35–1.91)	<0.001
Carriers	No	0.78 (0.62–0.99)	0.041
Carriers	Yes	0.75 (0.58–0.96)	0.023

P, adjusting for gender, age, smoking, alcohol consumption, BMI, and hyperlipidemia. G-C and A-T are combined with CYP17A1 rs1004467-rs11191548. p < 0.016 was considered statistically significant after Bonferroni correction (0.05/3).

on BP and hypertension could not be completely eliminated even if the statistical analyses were adjusted. Third, a small number of patients with hypertension received some secondary prevention drugs. Some of these drugs may have a certain effect on BP and hypertension. Fourth, it is worth noting that the four SNPs tested in this study may have LD with some functional variants rather than their own role on BP and hypertension. Fifth, diet and physical activity have a significant impact on BP and hypertension. The statistical analysis of this study failed to adjust the effects of dietary nutrients and physical activity intensity on BP and hypertension. This is also the deficiency of this article. Finally, statistical significance is not entirely consistent with biological significance.

CONCLUSIONS

Our outcomes implied that the rs1004467, rs11191548, and rs17249754 SNPs and *CYP17A1* rs1004467G-rs11191548C and *ATP2B1* rs1401982G-rs17249754A haplotypes revealed protective effects on hypertension, whereas the rs1401982 SNP and *CYP17A1* rs1004467A-rs11191548T and *ATP2B1* rs1401982A-rs17249754G haplotypes showed adverse effect on the prevalence of hypertension. The rs11191548-BMI ≥ 24 kg/m^2 interaction on hypertension was also observed.

DATA AVAILABILITY STATEMENT

The data presented in the study are deposited in the **Supplementary Material**.

ETHICS STATEMENT

The studies involving human participants were reviewed and approved by the Ethics Committee of the First Affiliated Hospital of Guangxi Medical University (No. Lunshen-2014 KY-Guoji-001, Mar. 7, 2014). The patients/participants provided their written informed consent to participate in this study.

AUTHOR CONTRIBUTIONS

B-LW conceived the research, took part in design, performed genotyping and statistical analysis, and drafted the manuscripts. R-XY conceived the research, took part in the design, conducted the epidemiological investigation, collected the samples, and helped to draft the manuscript. C-XL collaborated

to the genotyping. G-XD, Y-ZG, and P-FZ conducted the epidemiological investigation and helped to collect the samples. All authors contributed to the article and approved the submitted version.

FUNDING

This work was supported by the National Natural Science Foundation of China (No. 81460169). There was no role of the funding body in the design of the study and collection, analysis, and interpretation of data and in writing the manuscript.

SUPPLEMENTARY MATERIAL

The Supplementary Material for this article can be found online at: https://www.frontiersin.org/articles/10.3389/fcvm.2021.720884/full#supplementary-material

REFERENCES

1. Wu Y, Huxley R, Li L, Anna V, Xie G, Yao C, et al. Prevalence, awareness, treatment, and control of hypertension in China: data from the China national nutrition and health survey 2002. *Circulation.* (2008) 118:2679–86. doi: 10.1161/CIRCULATIONAHA.108.788166
2. Whelton PK, He J, Appel LJ, Cutler JA, Havas S, Kotchen TA, et al. Primary prevention of hypertension: clinical and public health advisory from the national high blood pressure education program. *JAMA.* (2002) 288:1882–8. doi: 10.1001/jama.288.15.1882
3. Garcia EA, Newhouse S, Caulfield MJ, Munroe PB. Genes and hypertension. *Curr Pharm Des.* (2003) 9:1679–89. doi: 10.2174/1381612033454513
4. Liu C, Li H, Qi Q, Lu L, Gan W, Loos RJ, et al. Common variants in or near *FGF5*, *CYP17A1* and *MTHFR* genes are associated with blood pressure and hypertension in Chinese Hans. *J Hypertens.* (2011) 29:70–5. doi: 10.1097/HJH.0b013e32833f60ab
5. Manolio TA. Genomewide association studies and assessment of the risk of disease. *N Engl J Med.* (2010) 363:166–76. doi: 10.1056/NEJMra0905980
6. Levy D, Ehret GB, Rice K, Verwoert GC, Launer LJ, Dehghan A, et al. Genome-wide association study of blood pressure and hypertension. *Nat Genet.* (2009) 41:677–87. doi: 10.1038/ng.384
7. Newton-Cheh C, Johnson T, Gateva V, Tobin MD, Bochud M, Coin L, et al. Genome-wide association study identifies eight loci associated with blood pressure. *Nat Genet.* (2009) 41:666–76. doi: 10.1038/ng.361
8. Tabara Y, Kohara K, Kita Y, Hirawa N, Katsuya T, Ohkubo T, et al. Common variants in the *ATP2B1* gene are associated with susceptibility to hypertension: the Japanese millennium genome project. *Hypertension.* (2010) 56:973–80. doi: 10.1161/HYPERTENSIONAHA.110.153429
9. Takeuchi F, Isono M, Katsuya T, Yamamoto K, Yokota M, Sugiyama T, et al. Blood pressure and hypertension are associated with 7 loci in the Japanese population. *Circulation.* (2010) 121:2302–9. doi: 10.1161/CIRCULATIONAHA.109.904664
10. Hong KW, Jin HS, Lim JE, Kim S, Go MJ, Oh B. Recapitulation of two genomewide association studies on blood pressure and essential hypertension in the Korean population. *J Hum Genet.* (2010) 55:336–41. doi: 10.1038/jhg.2010.31
11. Kato N, Takeuchi F, Tabara Y, Kelly TN, Go MJ, Sim X, et al. Meta-analysis of genome-wide association studies identifies common variants associated with blood pressure variation in east Asians. *Nat Genet.* (2011) 43:531–8. doi: 10.1038/ng.834
12. Cho YS, Go MJ, Kim YJ, Heo JY, Oh JH, Ban HJ, et al. A large-scale genome-wide association study of Asian populations uncovers genetic factors influencing eight quantitative traits. *Nat Genet.* (2009) 41:527–34. doi: 10.1038/ng.357
13. Wang Y, Zhang Y, Li Y, Zhou X, Wang X, Gao P, et al. Common variants in the *ATP2B1* gene are associated with hypertension and arterial stiffness in Chinese population. *Mol Biol Rep.* (2013) 40:1867–73. doi: 10.1007/s11033-012-2242-3
14. Dai CF, Xie X, Ma YT, Yang YN, Li XM, Fu ZY, et al. The relationship between the polymorphisms of the *CYP17A1* gene and hypertension: a meta-analysis. *J Renin Angiotensin Aldosterone Syst.* (2015) 16:1314–20. doi: 10.1177/1470320315585683
15. Lin Y, Lai X, Chen B, Xu Y, Huang B, Chen Z, et al. Genetic variations in *CYP17A1*, *CACNB2* and *PLEKHA7* are associated with blood pressure and/or hypertension in She ethnic minority of China. *Atherosclerosis.* (2011) 219:709–14. doi: 10.1016/j.atherosclerosis.2011.09.006
16. Auchus RJ. The genetics, pathophysiology, and management of human deficiencies of P450c17. *Endocrinol Metab Clin North Am.* (2001) 30:101–19, vii. doi: 10.1016/S0889-8529(08)70021-5
17. Hotta K, Kitamoto A, Kitamoto T, Mizusawa S, Teranishi H, Matsuo T, et al. Genetic variations in the *CYP17A1* and *NT5C2* genes are associated with a reduction in visceral and subcutaneous fat areas in Japanese women. *J Hum Genet.* (2012) 57:46–51. doi: 10.1038/jhg.2011.127
18. Mitri J, Hamdy O. Diabetes medications and body weight. *Expert Opin Drug Saf.* (2009) 8:573–84. doi: 10.1517/14740330903081725
19. Zhang N, Chen H, Jia J, Ye X, Ding H, Zhan Y. The *CYP17A1* gene polymorphisms are associated with hypercholesterolemia in Han Chinese. *J Gene Med.* (2019) 21:e3102. doi: 10.1002/jgm.3102
20. Lee S, Kim SH, Shin C. Interaction according to urinary sodium excretion level on the association between *ATP2B1* rs17249754 and incident hypertension: the Korean genome epidemiology study. *Clin Exp Hypertens.* (2016) 38:352–8. doi: 10.3109/10641963.2015.1116544
21. Olson S, Wang MG, Carafoli E, Strehler EE, McBride OW. Localization of two genes encoding plasma membrane $Ca^{2(+)}$-transporting ATPases to human chromosomes 1q25-32 and 12q21-23. *Genomics.* (1991) 9:629–41. doi: 10.1016/0888-7543(91)90356-J
22. Kobayashi Y, Hirawa N, Tabara Y, Muraoka H, Fujita M, Miyazaki N, et al. Mice lacking hypertension candidate gene *ATP2B1* in vascular smooth muscle cells show significant blood pressure elevation. *Hypertension.* (2012) 59:854–60. doi: 10.1161/HYPERTENSIONAHA.110.165068
23. LeBoeuf A, Mac-Way F, Utescu MS, De Serres SA, Douville P, Desmeules S, et al. Impact of dialysate calcium concentration on the progression of aortic stiffness in patients on haemodialysis. *Nephrol Dial Transpl.* (2011) 26:3695–701. doi: 10.1093/ndt/gfr138
24. Zheng PF, Yin RX, Wei BL, Liu CX, Deng GX, Guan YZ. Associations of *PRKN-PACRG* SNPs and G × G and G × E interactions with the risk of hyperlipidaemia. *Sci Rep.* (2020) 10:13010. doi: 10.1038/s41598-020-68826-1
25. Ogata S, Shi L, Matsushita M, Yu L, Huang XQ, Shi L, et al. Polymorphisms of human leucocyte antigen genes in Maonan people in China. *Tissue Antig.* (2007) 69:154–60. doi: 10.1111/j.1399-0039.2006.00698.x
26. Deng Q, Xu L, Gong J, Zhou L, Li S, Deng X, et al. Genetic relationships among four minorities in Guangxi revealed by analysis of 15 STRs. *J Genet Genom.* (2007) 34:1072–9. doi: 10.1016/S1673-8527(07)60122-2
27. Meng JH, Yao J, Xing JX, Xuan JF, Wang BJ, Ding M. Investigation of control region sequences of mtDNA in a Chinese Maonan population. *Mitochondrial DNA A DNA Mapp Seq Anal.* (2017) 28:350–4. doi: 10.3109/19401736.2015.1122776
28. Li XM, Ouyang Y, Yang YC, Lin R, Xu HB, Xie ZY, et al. Distribution of food-borne parasitic diseases and dietary habits in human population in Guangxi. *Zhongguo Ji Sheng Chong Xue Yu Ji Sheng Chong Bing Za Zhi.* (2009) 27:151–5.
29. Guo T, Yin RX, Lin WX, Wang W, Huang F, Pan SL. Association of the variants and haplotypes in the *DOCK7*, *PCSK9* and *GALNT2* genes and the risk of hyperlipidaemia. *J Cell Mol Med.* (2016) 20:243–65. doi: 10.1111/jcmm.12713

30. Liu CX, Yin RX, Shi ZH, Deng GX, Zheng PF, Wei BL, et al. *EHBP1* SNPs, their haplotypes, and gene-environment interactive effects on serum lipid levels. *ACS Omega.* (2020) 5:7158–69. doi: 10.1021/acsomega.9b03522
31. Wei BL, Yin RX, Liu CX, Deng GX, Guan YZ, Zheng PF. The *MC4R* SNPs, their haplotypes and gene-environment interactions on the risk of obesity. *Mol Med.* (2020) 26:77. doi: 10.1186/s10020-020-00202-1
32. Wang ZP, Li HQ. Sample size requirements for association studies on gene-gene interaction in case-control study. *Zhonghua Liu Xing Bing Xue Za Zhi.* (2004) 25:623–6. doi: 10.3760/j.issn:0254-6450.2004.07.020
33. Zhang QH, Yin RX, Gao H, Huang F, Wu JZ, Pan SL, et al. Association of the *SPTLC3* rs364585 polymorphism and serum lipid profiles in two Chinese ethnic groups. *Lipids Health Dis.* (2017) 16:1. doi: 10.1186/s12944-016-0392-3
34. Li WJ, Yin RX, Cao XL, Chen WX, Huang F, Wu JZ. *DOCK7-ANGPTL3* SNPs and their haplotypes with serum lipid levels and the risk of coronary artery disease and ischemic stroke. *Lipids Health Dis.* (2018) 17:30. doi: 10.1186/s12944-018-0677-9
35. Aung LH, Yin RX, Wu DF, Wang W, Liu CW, Pan SL. Association of the variants in the *BUD13-ZNF259* genes and the risk of hyperlipidaemia. *J Cell Mol Med.* (2014) 18:1417–28. doi: 10.1111/jcmm.12291
36. Miao L, Yin RX, Pan SL, Yang S, Yang DZ, Lin WX. *BCL3-PVRL2-TOMM40* SNPs, gene-gene and gene-environment interactions on dyslipidemia. *Sci Rep.* (2018) 8:6189. doi: 10.1038/s41598-018-24432-w
37. Chalmers J, MacMahon S, Mancia G, Whitworth J, Beilin L, Hansson L, et al. 1999 world health organization-international society of hypertension guidelines for the management of hypertension. Guidelines sub-committee of the world health organization. *Clin Exp Hypertens.* (1999) 21:1009–60. doi: 10.3109/10641969909061028
38. Wu DF, Yin RX, Cao XL, Huang F, Wu JZ, Chen WX. *MADD-FOLH1* polymorphisms and their haplotypes with serum lipid levels and the risk of coronary heart disease and ischemic stroke in a Chinese Han population. *Nutrients.* (2016) 8:208. doi: 10.3390/nu8040208
39. Shi YY, He L. SHEsis, a powerful software platform for analyses of linkage disequilibrium, haplotype construction, and genetic association at polymorphism loci. *Cell Res.* (2005) 15:97–8. doi: 10.1038/sj.cr.7290272
40. Lou XY. UGMDR: a unified conceptual framework for detection of multifactor interactions underlying complex traits. *Heredity.* (2015) 114:255–61. doi: 10.1038/hdy.2014.94
41. Lou XY, Chen GB, Yan L, Ma JZ, Zhu J, Elston RC, et al. A generalized combinatorial approach for detecting gene-by-gene and gene-by-environment interactions with application to nicotine dependence. *Am J Hum Genet.* (2007) 80:1125–37. doi: 10.1086/518312
42. Xu HM, Xu LF, Hou TT, Luo LF, Chen GB, Sun XW, et al. GMDR: versatile software for detecting gene-gene and gene-environment interactions underlying complex traits. *Curr Genom.* (2016) 17:396–402. doi: 10.2174/1389202917666160513102612
43. Lin Z, Su Y, Zhang C, Xing M, Ding W, Liao L, et al. The interaction of *BDNF* and *NTRK2* gene increases the susceptibility of paranoid schizophrenia. *PLoS ONE.* (2013) 8:e74264. doi: 10.1371/journal.pone.0074264
44. Binder A. A review of the genetics of essential hypertension. *Curr Opin Cardiol.* (2007) 22:176–84. doi: 10.1097/HCO.0b013e3280d357f9
45. Lottenberg AM, Afonso Mda S, Lavrador MS, Machado RM, Nakandakare ER. The role of dietary fatty acids in the pathology of metabolic syndrome. *J Nutr Biochem.* (2012) 23:1027–40. doi: 10.1016/j.jnutbio.2012.03.004
46. Teixeira AA, Lira FS, Pimentel GD, Oliveira de Souza C, Batatinha H, Biondo LA, et al. Aerobic exercise modulates the free fatty acids and inflammatory response during obesity and cancer cachexia. *Crit Rev Eukaryot Gene Expr.* (2016) 26:187–98. doi: 10.1615/CritRevEukaryotGeneExpr.2016016490
47. Ruixing Y, Jinzhen W, Yaoheng H, Jing T, Hai W, Muyan L, et al. Associations of diet and lifestyle with hyperlipidemia for middle-aged and elderly persons among the Guangxi Bai Ku Yao and Han populations. *J Am Diet Assoc.* (2008) 108:970–6. doi: 10.1016/j.jada.2008.03.010 (accessed Sep 25, 2021).
48. Campbell NR, Ashley MJ, Carruthers SG, Lacourcière Y, McKay DW. Lifestyle modifications to prevent and control hypertension. 3. Recommendations on alcohol consumption. Canadian Hypertension Society, Canadian Coalition for High Blood Pressure Prevention and Control, Laboratory Centre for Disease Control at Health Canada, Heart and Stroke Foundation of Canada. *CMAJ.* (1999) 160(Suppl. 9):S13–20.
49. Reed D, McGee D, Yano K. Biological and social correlates of blood pressure among Japanese men in Hawaii. *Hypertension.* (1982) 4:406–14. doi: 10.1161/01.HYP.4.3.406
50. Bulpitt CJ, Shipley MJ, Semmence A. The contribution of a moderate intake of alcohol to the presence of hypertension. *J Hypertens.* (1987) 5:85–91. doi: 10.1097/00004872-198702000-00012
51. MacMahon SW, Blacket RB, Macdonald GJ, Hall W. Obesity, alcohol consumption and blood pressure in Australian men and women. The national heart foundation of Australia risk factor prevalence study. *J Hypertens.* (1984) 2:85–91. doi: 10.1097/00004872-198402000-00015
52. Stamler J, Caggiula AW, Grandits GA. Relation of body mass and alcohol, nutrient, fiber, and caffeine intakes to blood pressure in the special intervention and usual care groups in the multiple risk factor intervention trial. *Am J Clin Nutr.* (1997) 65(Suppl. 1):338s−65s. doi: 10.1093/ajcn/65.1.338S
53. Bae J, Yi YH, Kim YJ, Lee JG, Tak YJ, Lee SH, et al. Time to first cigarette and the risk of hypertension: a nationwide representative study in Korea. *Am J Hypertens.* (2019) 32:202–8. doi: 10.1093/ajh/hpy170
54. Hering D, Kucharska W, Kara T, Somers VK, Narkiewicz K. Smoking is associated with chronic sympathetic activation in hypertension. *Blood Press.* (2010) 19:152–5. doi: 10.3109/08037051.2010.484150
55. Kim SH, Lee JS. The association of smoking and hypertension according to cotinine-verified smoking status in 25,150 Korean adults. *Clin Exp Hypertens.* (2019) 41:401–8. doi: 10.1080/10641963.2018.1489548
56. Kim BJ, Seo DC, Kim BS, Kang JH. Relationship between cotinine-verified smoking status and incidence of hypertension in 74,743 Korean adults. *Circ J.* (2018) 82:1659–65. doi: 10.1253/circj.CJ-17-1188
57. Gage SH, Smith GD, Ware JJ, Flint J, Munafo MR. Correction: G = E: What GWAS can tell us about the environment. *PLoS Genet.* (2016) 12:e1006065. doi: 10.1371/journal.pgen.1006065
58. Little R, Cartwright EJ, Neyses L, Austin C. Plasma membrane calcium ATPases (PMCAs) as potential targets for the treatment of essential hypertension. *Pharmacol Ther.* (2016) 159:23–34. doi: 10.1016/j.pharmthera.2016.01.013

Conflict of Interest: The authors declare that the research was conducted in the absence of any commercial or financial relationships that could be construed as a potential conflict of interest.

Publisher's Note: All claims expressed in this article are solely those of the authors and do not necessarily represent those of their affiliated organizations, or those of the publisher, the editors and the reviewers. Any product that may be evaluated in this article, or claim that may be made by its manufacturer, is not guaranteed or endorsed by the publisher.

frontiers in Cardiovascular Medicine

ORIGINAL RESEARCH
published: 05 January 2022
doi: 10.3389/fcvm.2021.755321

Network-Based Approach and IVI Methodologies, a Combined Data Investigation Identified Probable Key Genes in Cardiovascular Disease and Chronic Kidney Disease

*Mohd Murshad Ahmed[1], Safia Tazyeen[1], Shafiul Haque[2], Ahmad Sulimani[3], Rafat Ali[4], Mohd Sajad[1], Aftab Alam[1], Shahnawaz Ali[5], Hala Abubaker Bagabir[6], Rania Abubaker Bagabir[7] and Romana Ishrat[1]**

[1] Centre for Interdisciplinary Research in Basic Sciences, Jamia Millia Islamia, New Delhi, India, [2] Research and Scientific Unit, College of Nursing and Allied Health Science, Jazan University, Jazan, Saudi Arabia, [3] Department of Medical Laboratory Technology, College of Applied Medical Sciences, Jazan University, Jazan, Saudi Arbia, [4] Department of Bioscience, Jamia Millia Islamia, New Delhi, India, [5] Centre for Stem Cell & Regenerative Medicine, KING' College London, Guy's Hospital, London, United Kingdom, [6] Department of Medical Physiology, Faculty of Medicine, King Abdulaziz University, Rabigh, Saudi Arabia, [7] Department of Hematology and Immunology, College of Medicine, Umm-Al-Qura University, Mecca, Saudi Arabia

OPEN ACCESS

Edited by:
Christoph D. Rau, University of North Carolina at Chapel Hill, United States

Reviewed by:
Mohd Amir, Jamia Millia Islamia, India
Shahzaib Ahamad, International Centre for Genetic Engineering and Biotechnology, India

***Correspondence:**
Romana Ishrat
rishrat@jmi.ac.in
orcid.org/0000-0001-9744-9047

Specialty section:
This article was submitted to Cardiovascular Genetics and Systems Medicine, a section of the journal Frontiers in Cardiovascular Medicine

Received: *08 August 2021*
Accepted: *17 November 2021*
Published: *05 January 2022*

Citation:
Ahmed MM, Tazyeen S, Haque S, Sulimani A, Ali R, Sajad M, Alam A, Ali S, Bagabir HA, Bagabir RA and Ishrat R (2022) Network-Based Approach and IVI Methodologies, a Combined Data Investigation Identified Probable Key Genes in Cardiovascular Disease and Chronic Kidney Disease. Front. Cardiovasc. Med. 8:755321. doi: 10.3389/fcvm.2021.755321

In fact, the risk of dying from CVD is significant when compared to the risk of developing end-stage renal disease (ESRD). Moreover, patients with severe CKD are often excluded from randomized controlled trials, making evidence-based therapy of comorbidities like CVD complicated. Thus, the goal of this study was to use an integrated bioinformatics approach to not only uncover Differentially Expressed Genes (DEGs), their associated functions, and pathways but also give a glimpse of how these two conditions are related at the molecular level. We started with GEO2R/R program (version 3.6.3, 64 bit) to get DEGs by comparing gene expression microarray data from CVD and CKD. Thereafter, the online STRING version 11.1 program was used to look for any correlations between all these common and/or overlapping DEGs, and the results were visualized using Cytoscape (version 3.8.0). Further, we used MCODE, a cytoscape plugin, and identified a total of 15 modules/clusters of the primary network. Interestingly, 10 of these modules contained our genes of interest (key genes). Out of these 10 modules that consist of 19 key genes (11 downregulated and 8 up-regulated), Module 1 (RPL13, RPLP0, RPS24, and RPS2) and module 5 (MYC, COX7B, and SOCS3) had the highest number of these genes. Then we used ClueGO to add a layer of GO terms with pathways to get a functionally ordered network. Finally, to identify the most influential nodes, we employed a novel technique called Integrated Value of Influence (IVI) by combining the network's most critical topological attributes. This method suggests that the nodes with many connections (calculated by hubness score) and high spreading potential (the spreader nodes are intended to have the most impact on the information flow in the network) are

the most influential or essential nodes in a network. Thus, based on IVI values, hubness score, and spreading score, top 20 nodes were extracted, in which RPS27A non-seed gene and RPS2, a seed gene, came out to be the important node in the network.

Keywords: CVD, CKD, PPIN network, IVI, hubness score, spreading score

INTRODUCTION

The risk of getting cardiovascular disease (CVD) in patients with chronic kidney disease (CKD) is more than without CKD as discussed by Jankowski et al. (1). Chronic kidney disease (CKD) is a systemic condition that affects almost 10% of the population. The prevalence of CKD has increased in recent decades due to aging which affects about one out of every 10 people (2). Multiple studies have confirmed that individuals with renal disease undergo rapid aging, which accelerates the onset of pathologies, such as CVD, which is strongly correlated with older age. Furthermore, patients with CKD are more prone to CVD and even death due to the progression of end-stage renal disease (ESRD) (3). CVD, along with chronic renal disease, remains the leading cause of morbidity and mortality in individuals, particularly in those involving a systemic inflammatory process, such as atherosclerosis (4). CKD is the 14th leading cause of mortality, with the death rate anticipated to increase to 14 per 100,000 people by 2030 (5). Despite the rising pervasiveness of CKD and its frequent combination with CVD, patients with severe CKD (eGFR 30 ml/min per 1.73 m2) were commonly omitted from key randomized controlled studies (6). Traditional CVD risk factors, such as hypertension, advanced age, diabetes, male sex, dyslipidemia, and smoking, are also prevalent in CKD. The number of people with end-stage renal disease (ESRD) is expected to rise by 50% in the next 20 years (7). In the current era, CKD is a severe health and economic burden. CKD-related mortality has increased by 82.3% in the last two decades. In addition, it has risen to third place among the world's top 25 major causes of death (8). Now, the molecular description of CKD onset and progression is lacking. Based on these findings, the researchers have described CKD as a worldwide epidemic (9). The present method for prioritizing disease-related genes is based on the "guilt-by-association" assumption, which states that physically and functionally related genes have similar phenotypic effects and are likely to be involved in the same biological pathways (10).

Network theory is a useful tool for deciphering the topological features and dynamics of complex systems and their functional modules. Many extant networks can be classified as scale-free, small world, random, or hierarchical networks. The hierarchical form of the network includes modules and sparsely dispersed hubs to manage the network which is of particular interest to biologists (11). Moreover, the identification of essential and critical protein(s) is crucial for understanding progression of the disease. Thus, the current paradigm for investigating CVD and CKD focuses on combining protein interactions, functions, and disease networks to identify important regulators of CVD and CKD among DEGs. Also, it is substantial to study network's topological characteristics, so that the essential key regulators, their function, and regulating mechanism could be forecasted (12). The topology of a network and its many centrality measures (metrics reflecting the impact of each node within a network) can be examined and evaluated to explore fundamental biological meanings and prominent regulatory molecules (13). A network could best be studied in relation to the spreader nodes as these are projected to have the biggest impact on the process of distribution of information throughout the network because they have strong connections with other nodes. So these influential nodes can commonly be identified by calculating the characteristics like hubness and spreading potential (14). Since the fundamental characteristics of a network and its centrality metrics are universal, it can be applied to any network domain, including biological networks (15). These network centralities can be used to further narrow down and validate the extracted influential nodes. In our present study, we have used the seed genes, gene ontology, and pathways in an integrating manner to give a glimpse of molecular relation between CVD and CKD that may further facilitate the identification and validation of novel biomarkers.

METHODOLOGY

Acquisition of mRNA Expression Data

The mRNA expression profile of CVD and CKD were downloaded from the publicly available databases of gene expression microarrays, stored in the repository bank Gene Expression Omnibus (GEO) NCBI [www.ncbi.nlm.nih.gov/geo/; (16)]. These were the mRNAs expression profiles series of CVD (GSE26887, GSE42955, GSE67492, GSE71226, GSE141512, GSE48060) and CKD (GSE15072, GSE23609, GSE43484, GSE62792, GSE66494) consisting of normal and treated samples. The selection of the datasets using inclusion and exclusion criteria were made using the following keywords in the NCBI : CVD, cardiac failure, cardiac arrest, chronic heart failure (CHF), etc., whereas, CKD, AKI, chronic kidney disease, renal failure AND human [Organism] (17). The details of all GSE series are given in **Table 1**. Patient samples from various sources were not differentiated during the data integration procedure to show a common and/or overlapped gene signature. The expression microarray is a method for studying gene expression on a genome-wide scale that is widely utilized. Batch effects can be decreased through proper experimental design, but they cannot be eradicated until the entire study is conducted in one batch. Before analyzing microarray data, a few algorithms are now available to correct for batch effects. We employed the Empirical Bayes method built-in function in LIMMA, in combination with the fit2 function. Meta-analyses based on microarray data integration require effective *in silico* methods. We may now use *in silico* tools to efficiently merge numerous microarray datasets while ignoring differing demographics, experimental designs,

TABLE 1 | Samples from the GSE series and their DEGs.

SERIES	Total sample	Normal	Disease	Up regulated	Down regulated	Fold change	Illness	Country	Year	Platform	Authors	Source
GSE48060	52	21	31	15	14	0.5	CVD	USA	2014	GPL-570	Xing Li	Peripheral blood
GSE67492	6	2	4	73	16	0.5	CVD	USA	2015	GPL-6244	James West	Right ventricular wall
GSE26887	24	5	19	58	95	0.5	CVD	Italy	2012	GPL-6244	Fabio Martelli	Left ventricular wall
GSE71226	6	3	3	97	82	1.5	CVD	China	2015	GPL-570	Bofan Meng	Peripheral blood
GSE42955	29	5	24	125	236	0.5	CVD	Spain	2013	GPL-6244	M. M. Molina	Heart
GSE141512	12	6	6	69	85	0.5	CVD	Russia	2019	GPL-17586	German Osmak	Blood
GSE66494	61	8	53	102	325	0.5	CKD	Japan	2015	GPL-6480	Satohiro Masada	Kidney
GSE43484	6	3	3	134	136	0.5	CKD	Sweden	2013	GPL-571	Elham Dadfar	Uremic monocyte
GSE15072	29	8	21	51	38	2	CKD	Italy	2009	GPL-96	Palo Pontrelli	PBMC
GSE62792	18	6	12	352	262	0.5	CKD	Sri Lanka	2018	GPL-10558	D. N. Magana	Blood
GSE23609	24	7	17	219	189	0.5	CKD	USA	2010	GPL-6454	Persis P. Wadia	Serum

The entire sample available in the GSE series is shown in column 2, and the fold change values are shown in column 7. In each GSE series, the total up and down regulated genes were recorded in 5 and 6 columns, respectively. For the GSE series, the platform GPL in column 11 indicates the number of probes and the type of data (Affymetrix data and oligo data).

and specimen sources with the advancements of ever-growing theories and bioinformatics tools (18).

Identification of CVD and CKD Associated DEGs

To further analyze the obtained data samples series, the GEO2R tool (http://www.ncbi.nlm.nih.gov/geo/geo2r/) was used. GEO2R is a web-based analytical tool with a built-in R program and GEO query for Linear Models for Microarray Data (Limma). The default settings were utilized to prepare the datasets (19). Differentially Expressed mRNAs were extracted applying criteria $p < 0.05$ and log fold-change |0.5–2| as the threshold values. Up and downregulated genes from meta-analysis were used as genes of interest in PPIN network. As a result, the Benjamini-Hochberg (BH) correction method was utilized to adjust the significant value of p obtained by the original hypothesis test during differential expression analysis. Finally, for DEGs screening, log Fold change was employed as the key index. *Log fold change* |0.5–2| was employed as a DEG screening condition in this study. The criteria [i.e., value of $p < 0.05$ and fold change 0.5–2] were selected in order to expand the total number of DEGs between healthy control and diseases samples. Since very few genes were differentially expressed with respect to this threshold, therefore it made the threshold more stringent and would lead to nearly no or very few DEGs. If the fold change is altered, the resulting DEGs will be changed as well, and vice versa. There is no standard value for fold change when it comes to selecting DEGs (20).

Network Construction of Protein-Protein Interactions (PPIN)

The network was built using the String online database and imported into Cytoscape v.3.80. It supports bipartite graph visualization of gene-gene linking/interaction/regulation (gene-disease associations) and also provides gene-centric views of the network data (21). The Probe Ids were mapped to their corresponding gene symbols to build the native network from DEGs. The gene regulatory network of CVD and CKD was built using the simple premise of one gene and one protein. A variety of features can be used to construct and filter the network. The network combines data from curated databases with knowledge gleaned from the literature (22). Because the networks might be based on a certain gene or condition, the PPIN networks are visualized using the Cytoscape program (23). To discover the significant modules and top-ranked genes in the PPIN network, the Cytoscape plugin Molecular Complex Detection (MCODE; version 2.0.0) and the igraph with Influential packages in R (version 3.6.3) were used. The network's topological properties were estimated using Network analyzer, a Cytoscape version 3.8.0. plug-in, while the eigenvalues were generated using CytoNCA, another Cytoscape plug-in for topological properties calculation. This could also be useful for double-checking Network Analyzer data (24).

Module/Cluster/Subnetwork Finding: Molecular COmplex DEtection Method

The MCODE method (A cytoscape plugin) was used to detect the modules/clusters/communities (Strongly interconnected regions) in the native network. In a PPI network, protein complexes and pathways are prevalent groupings (clusters) (25). To separate the dense regions according to provided parameters, the approach uses vertex weighting by local neighborhood density and outward traversal from a locally dense seed protein. The algorithm has the advantage of having a directed mode, which permits fine-tuning of clusters of interest without considering the remainder of the network and investigation of cluster interconnectivity, which is important in protein networks (26). The modules from the native network along with sub-modules from modules at each level of organization were identified until only motifs remained (i.e., 3 nodes with 3

edges). Vertex weighting, complex prediction, and possible post-processing to filter or add proteins in the generated complexes are the three stages of the MCODE algorithm (27). Intuitively, a network of interacting molecules can be represented as a graph with vertices representing molecules and edges representing chemical interactions. If the temporal pathway or cell signaling information is known, a directed graph with arcs reflecting chemical activity or information flow can be created. Otherwise, an undirected graph is employed. Graph theoretic methods can be used to aid in the analysis and solution of biological problems using this graph model of a biological system (28).

Gene Ontology, Pathway Analysis, and HE

Gene ontology words are a standardized set of terms separated into three categories: Molecular function, Biological Processes, and Protein Class (29). Thus, DEGs were collected and sent to ClueGO (a Cytoscape plug-in that facilitates biological interpretation and visualizes functionally grouped terms in the form of networks, tables, and charts) to enrich the given set of DEGs to possible GO terms for exploratory research. We used ClueGO to assess the function of hub genes and define the GO term. ClueGO employs kappa statistics to link the terms in the network. It creates a dynamical network structure by considering the gene lists of interest at the start. It also constructs a functionally ordered GO/pathway term network by combining GO terms and KEGG/BioCarta pathways (30). A number of adjustable limitation criteria allow for visualizations of various levels of specificity. ClueGO can also compare gene groups and highlight their functional differences. ClueGO also makes use of Cytoscape's flexible visualization framework and works in tandem with the GOlorize plug-in. Gene lists can be imported directly into ClueGO or produced interactively from gene network graphs shown in Cytoscape. ClueGO comes with a few gene identities and species by default, and it is simple to add more via a plug-in. ClueGO is an open-source Java application that uses different ontologies to extract non-redundant biological information for huge clusters of genes (31).

For gene annotation and gene list enrichment analysis, Metascapes leverages a variety of databases and technologies. Metascape uses lists of gene identifiers to extract rich annotations, find statistically enriched pathways, and build PPIN networks. Pathway or process enrichment analysis uses the standard accumulative hypergeometric statistical test to identify ontology words with significant input genes given a gene list (32). We give more arguably better ontology concepts, including ones from Broad's MSigDB, than other GO-based enrichment analysis tools. Modules were also subjected to MCODE to identify sub-modules and sub-sub-modules. All modules, sub-modules, and sub-sub-modules with clustering coefficients less than or equal to unity were examined. We discovered modules and sub-modules that were related to independent functions and followed the modularity laws, and the fact that their activities are non-linear (33). As a result, we needed to quantify their role as important genes at the systems biology level, which we did by utilizing HE analysis of biological networks (34).

Identification of the Most Influential Nodes Using IVI Methods

The IVI is a new method for detecting influential nodes. Hubness and spreading values combine to form the IVI algorithm. IVI captures all the network's topological dimensions. In domains ranging from transportation to biological systems, identifying critical individuals within a network is a persistent challenge. Identifying the most powerful nodes with the ability to have the most influence on the PPIN network (35), degree centrality (DC) and ClusterRank (CR), neighborhood connectivity (NC), local H index, betweenness centrality (BC), and collective influence (CI), respectively, and to synergize their effect for the unbiased identification of prominent nodes in the network (36). Influential is an R package that primarily focuses on identifying the most influential nodes in a network, as well as categorizing and rating top candidate characteristics (37).

RESULTS

Figure 1 depicts the workflow of the entire integrative network-based approach used in this study. Adobe Illustrator CS6 was used to create the flowchart.

Selection of DEGs

The GSE series of CVD denoted by X and the GSE series of CKD was denoted by Y. There are 6 GSE series of X (X_1, X_2, X_3, X_4, X_5, and X_6) and 5 GSE series of Y ($Y_1, \ldots\ldots Y_5$).

$$Xu = (X_1u_1,\ X_2u_2, \ldots X_6u_6) \tag{1}$$

where u stands for upregulation.

$$Xd = (X_1\ d_1,\ X_2d_2 \ldots X_6d_6) \tag{2}$$

d stands for downregulation.

$$Yu = (Y_1\ u_1, \ldots Y_5u_5) \tag{3}$$

$$Yd = (Y_1d_1, \ldots Y_5d_5) \tag{4}$$

To find DEGs, we combine equations, i.e., (1) with (3) and (2) with (4), as follows:

$$Xu \cap Yu = \{Xu\} \cap \{Yu\} \tag{5}$$

$$Xd \cap Yd = \{Xd\} \cap \{Yd\} \tag{6}$$

The intersection of (5) and (6) gives the Overlapped genes. Genes showing a value of $p \leq 0.05$ and *log fold change* $|0.5–2.0|$ were considered statistically significant and differentially expressed. The total upregulated genes in all 11 GSE series of CVD and CKD was $Xu \cap Yu = \{1295\}$, whereas total downregulated genes are $Xd \cap Yd = \{1478\}$. Total up and downregulated genes in CKD and CVD, separately, are 437 and 528, and 858 and 950 while the total upregulated genes in all 11 GSE series of CVD and CKD are 1,295, and downregulated genes are 1478 (**Table 2**). After comparison of CVD vs. CKD, we finally got 43 overlapped genes, including 24 upregulated genes in CVD and CKD, and 19 genes downregulated in both diseases (**Figure 2**).

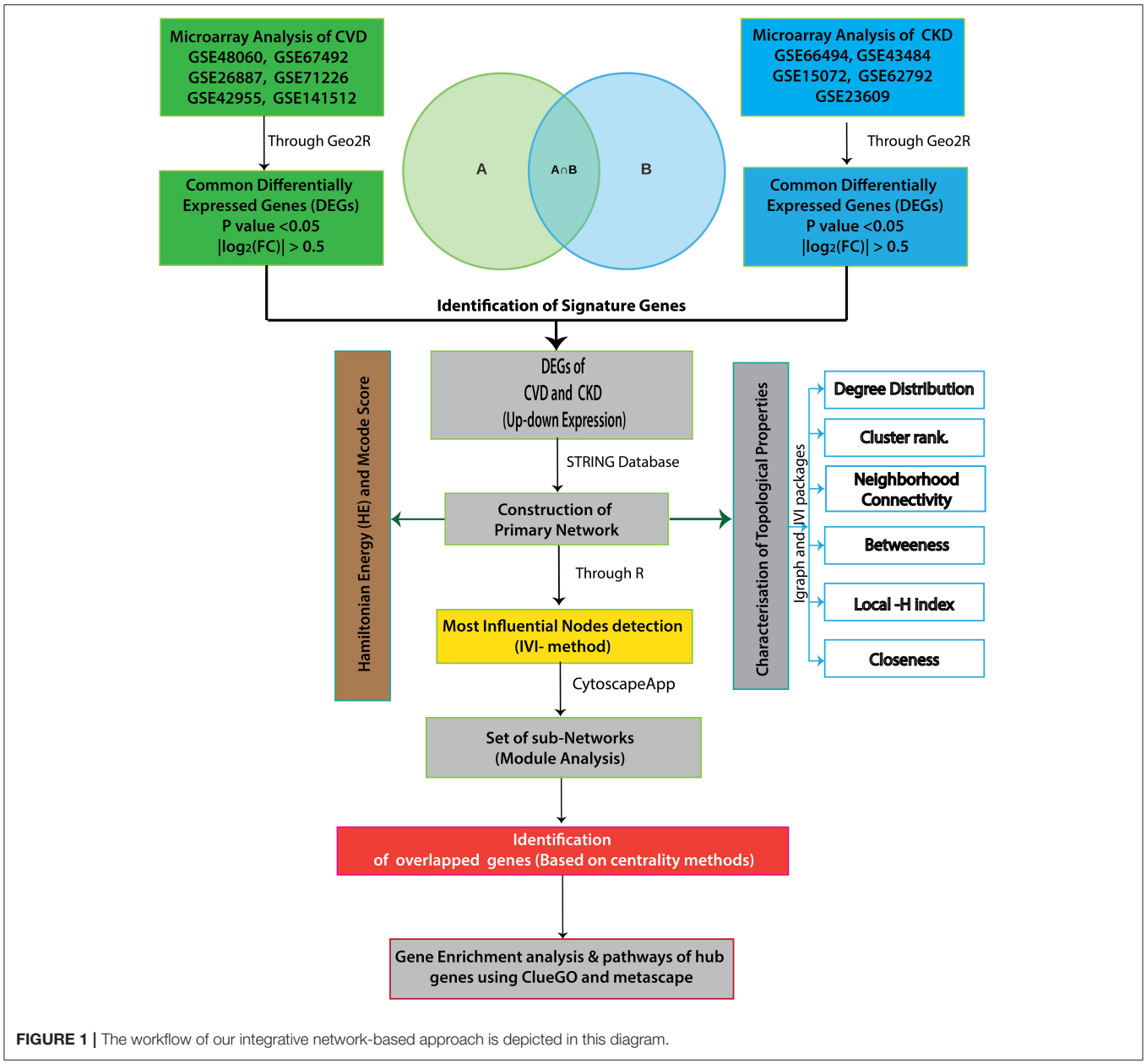

FIGURE 1 | The workflow of our integrative network-based approach is depicted in this diagram.

Gene Network Construction

Based on mRNA profiling and protein networks, to generate subnetwork biomarkers (interconnected genes whose aggregate expression levels are predictive of disease state), networks provide a rich source of biomarkers for illness classification. To construct a CVD and CKD interaction network and infer gene-disease correlations using network features (38), we started with a list of seed/key genes (43 DEGs) that are known to be associated to the disease, and each gene is represented by a single node in the interaction network. Next, we built a disease-specific gene-interaction network where the nodes are the genes and the edges are their connections (39) using selection of top ranked genes in the network via IVI -Value, Spreading score, Hubness score, ClusterRank, Collective influence, h-index, Local h-index degree centrality (D_C), betweenness centrality (B_C), and Neighborhood Connectivity (N_K) centrality metrics.

A network representation and analysis is a powerful tool for studying the complicated behavior of biological systems' physiology and pathology (40). Through cluster/module analysis, it was studied that the CVD and CKD network shows hierarchical scale free nature. The 19 key genes and their presence in various modules are traced following MCODE community finding algorithm. There are 15 modules (highly connected nodes) extracted from the native network. Ten out of 15 modules were

TABLE 2 | The up and downregulated genes are listed in a table with a count number column.

Sr. No.	Common genes in CVD and CKD	# Count	Gene symbol
1	UP regulation	19	NPR3, NFE2L1, TNFSF10, HMGB2, GABPB2, KDM5D, RSRP1, GPCPD1, ZNF83, THY1, COX7B, NPPB, PDZK1IP1, BCL6, IRAK3, GRN, SOCS3, CASP5, RPS24
2	Down regulation	24	BCL3, ZRANB2, NR1D2, C7, LYN, ANXA3, PER3, PTP4A3, RPLP0, HSPB1, ACTG1, RPL13, HCAR3, FCGR3A, MAP2K3, MYC, CIRBP, AHSA2, ATP1A1, NPIPB3, PNISR, RPS2, ENO1, CNN1

Up-regulated genes have red lettering, whereas downregulated genes have green text.

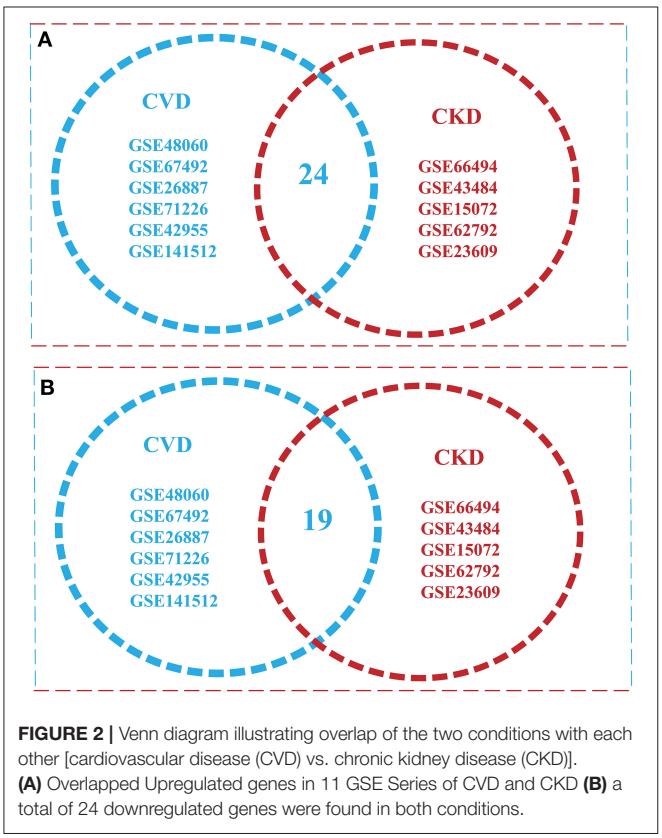

FIGURE 2 | Venn diagram illustrating overlap of the two conditions with each other [cardiovascular disease (CVD) vs. chronic kidney disease (CKD)]. **(A)** Overlapped Upregulated genes in 11 GSE Series of CVD and CKD **(B)** a total of 24 downregulated genes were found in both conditions.

found to be having our seed genes (**Figure 3**). These genes will be utilized to build a gene network and to investigate their biological importance.

Gene Enrichment Analysis and Pathways

The key genes are submitted to ClueGO a cytoscape plugin to find the Gene Ontology term. The default setting of ClueGO are network specificity (medium), organism (human), visuals styles (group), evidence of experiments, all experimental (EXP, IDA, IPI, IMP, IGI, and IEP), and value of $p < 0.05$ (41). ClueGO constructs a functionally ordered GO/pathway term network by combining Gene Ontology (GO) terms and KEGG/BioCarta pathways. It can evaluate and compare numerous lists of genes and visualize functionally grouped terms in a comprehensive way. ClueGO can be used in conjunction with the GOlorize plug-in to offer an intuitive depiction of the analysis results. ClueGO is enhanced with CluePedia, which allows for a thorough examination of pathways (42). WikiPathways is a collaborative, open-source tool for curating biological pathways. Metascape selects the most informative phrases from the GO clusters obtained using a heuristic method. It takes a sample of the 20 highest-scoring clusters, picks up to 10 best-scoring words (lowest p-values) inside each cluster, and then connects all term pairs with Kappa similarity >0.3 (**Figure 4**). Cytoscape is used to show the resulting network, with each node representing one enriched phrase. The cluster IDs or the p-values can be used to color the nodes. Edges connect phrases that are similar—the thicker the edge, the greater the resemblance (43). To maintain readability, only one label (corresponding to one term) is displayed per cluster (**Figure 4**).

Hamiltonian Energy

$$HE = E_c - \gamma N_c,$$

where E_c represents number of edges in a cluster, N_c for number of nodes, and the gamma constant $\gamma = 0.8$. The HE calculation for a network within the modules considers contributions from the organization of nodes and edges in a competitive manner, and this energy is used in organizing or re-organizing the network at various levels. This approach can also magnify the significant changes in the network organization when it goes down to various levels of organization, which capture the importance of hubs in the network and at the modular level. Therefore, HE formalism proves to be a useful technique for considering variations in the network organization (44). For hubs at each level of all potential modules in the network, the HE was determined (**Figure 2**). When the network's HE is plotted as a function of network modules, we discover that the energy distribution is highest in the native network and gradually decreases as the amount of organization grows. Because HE is based on node and edge competition for a set resolution parameter value (gamma symbol), a drop in HE reflects the dominance of interacting edges over the network size, implying rapid information processing (45).

Most Influential, Potential, and Sovereignty of the Nodes in a Network

Integrated Value of Influence (IVI) is a method for identifying the most influential nodes in a network that considers all topological aspects. The IVI formula combines the most important local (degree centrality and Cluster Rank), semi-local (neighborhood connectivity and local H-index), and global (betweenness centrality and collective influence) centrality measures in such a way that their effects are synergized and their biases are eliminated (46). The degree function from the igraph package can be used to calculate degree centrality, which is the most used local

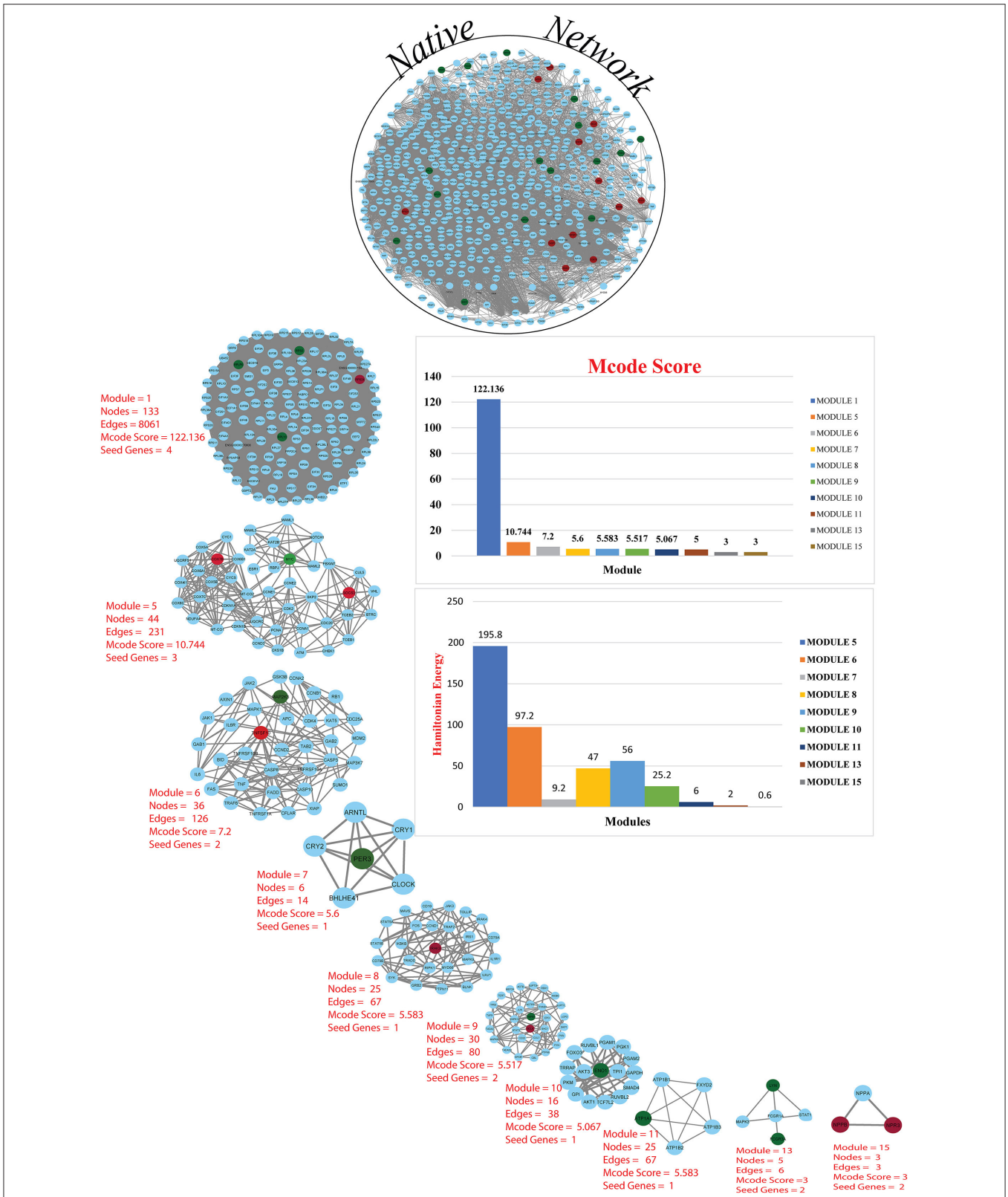

FIGURE 3 | Cardiovascular disease and CKD parental network (merge network) with 587 nodes and 13,887 edges, red and green colors for seed genes and blue for interaction partners (non-seed genes). Using the MCODE cytoscape plugin, the native network is broken down into subnetworks up to the motif level. Each module

(Continued)

FIGURE 3 | subnetwork from native network represents with MCODE score and seed genes (up-regulated red and downregulated green). The hierarchy of energy is depicted on the right side of the illustration by a Hamiltonian energy (HE) bar graph. As the number of nodes in the modules decreases, so does the amount of energy used. The HE was calculated for nodes at each level of all conceivable modules in the network. The HE of the CVD and CKD networks is given as a function of network levels. We determined that energy distribution is greatest in the core network and diminishes as the level of (modules) organization increases. Because HE is dependent on nodes and edges for a fixed resolution parameter value (gamma = 0.8), the drop in HE shows the dominance of interacting edges over the network size, indicating rapid information processing. The HE of a complex network is a measure of overall energy in the system, and its value fluctuates as the network structure changes.

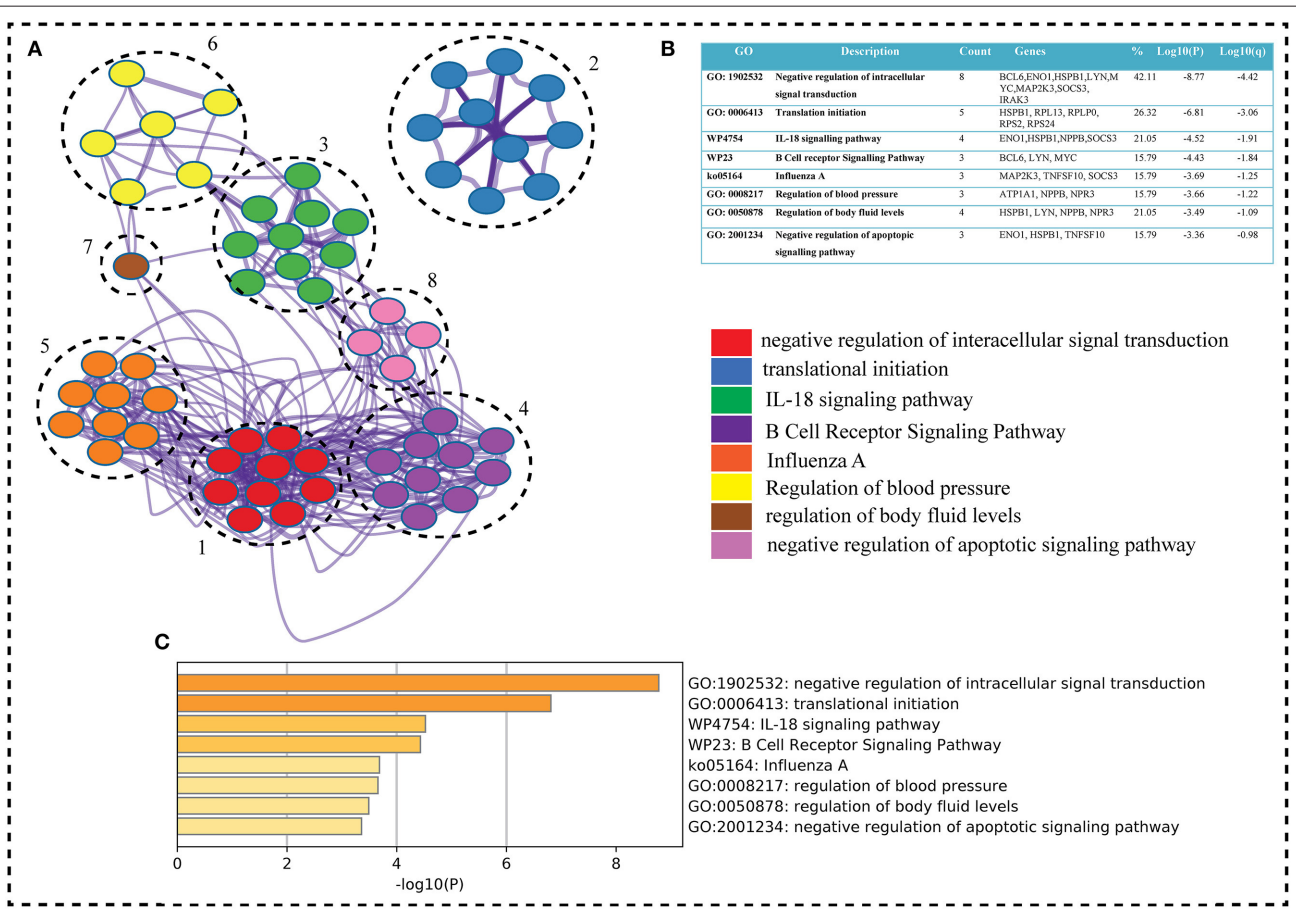

GO	Description	Count	Genes	%	Log10(P)	Log10(q)
GO: 1902532	Negative regulation of intracellular signal transduction	8	BCL6,ENO1,HSPB1,LYN,MYC,MAP2K3,SOCS3, IRAK3	42.11	-8.77	-4.42
GO: 0006413	Translation initiation	5	HSPB1, RPL13, RPLP0, RPS2, RPS24	26.32	-6.81	-3.06
WP4754	IL-18 signalling pathway	4	ENO1,HSPB1,NPPB,SOCS3	21.05	-4.52	-1.91
WP23	B Cell receptor Signalling Pathway	3	BCL6, LYN, MYC	15.79	-4.43	-1.84
ko05164	Influenza A	3	MAP2K3, TNFSF10, SOCS3	15.79	-3.69	-1.25
GO: 0008217	Regulation of blood pressure	3	ATP1A1, NPPB, NPR3	15.79	-3.66	-1.22
GO: 0050878	Regulation of body fluid levels	4	HSPB1, LYN, NPPB, NPR3	21.05	-3.49	-1.09
GO: 2001234	Negative regulation of apoptopic signalling pathway	3	ENO1, HSPB1, TNFSF10	15.79	-3.36	-0.98

FIGURE 4 | (A) Metascape, a web-based application, was used to enrich the gene ontology of our interest genes (seed genes). Metascape created an 8-cluster network for the go term (Biological Process), with color according on gene proportion. Each cluster has a large number of genes, including seed genes. Each cluster's node has a different GO term, but the main term is taken into account because of the seed genes (8 genes in first term and seed genes count decreases from top to bottom term whereas Log *P*-value increases). The GO keywords, gene counts, gene symbols, and lop *p*-value are shown in **(B)** table shows GO terms, genes count, genes symbols, and lop *p*-value. The term having seed genes count and log *p*-value higher were on top. In the GO term table w and k represents wiki and keg pathways, respectively. **(C)** Bar graph on the basis of *p*-value shows the GO term. As *P*-values decreases the go term goes top to bottom.

centrality measure. The degree centrality (DC) $DCi = \sum_{i \neq j} = A_{ij}$ is the simplest local centrality metric for a graph, where A represents the adjacency matrix of the associated network and Aij = 1 if nodes i and j are connected and Aij = 0, otherwise (47). Betweenness centrality, like degree centrality, is a widely used centrality metric. However, it only represents a node's global centrality. Another important centrality metric that reflects a node's semi-local centrality is neighborhood connectedness. For the first time, this centrality measure can be calculated in the R environment using the influential package. ClusterRank is another local centrality metric that removes the negative impacts of local clustering by intermediating between local and semi-local properties of a node. The H-index is a measure of how well a piece of the H-index is a semi-local centrality metric that was inspired by its use in analyzing the influence of researchers and is now available in the R environment for the first time via the influential package (48). Local H-index (LH-index) is a semi-local centrality measure and an upgraded variant of H-index centrality that applies the H-index to a node's second order neighbors and is now calculable in R using the influential package. The product of

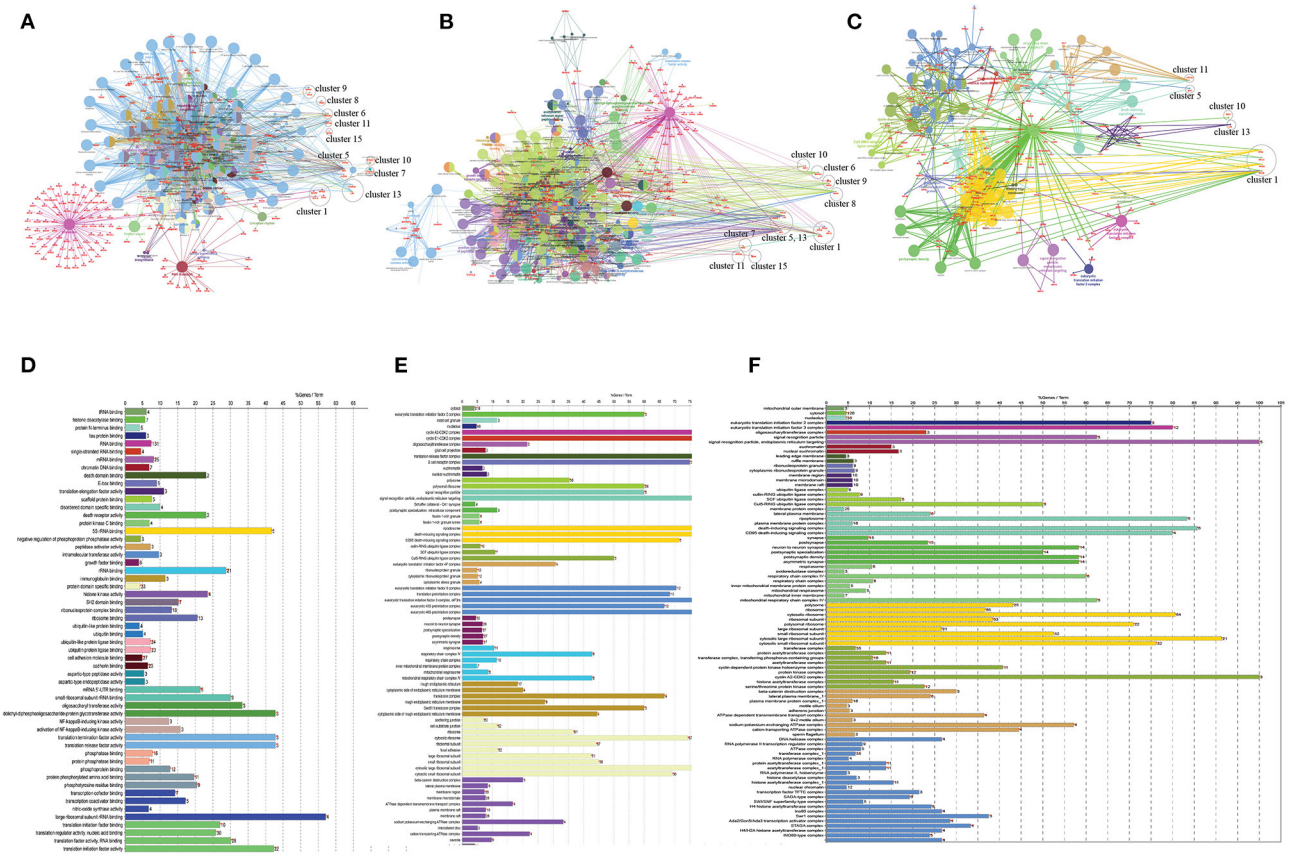

FIGURE 5 | (A) Gene ontology study of hub genes (CVD and CKD) using ClueGO, a cytoscape plugin, including KEGG pathways **(B)**, molecular function **(C)**, and cellular localization, and **(D–F)** their respective bar plots. In the case of KEGG pathways, the network encompasses all modules and their seed genes. The modules are labeled with a circle and are referred to as clusters. There are four seed genes in the first cluster. The different colors of nodes indicate which genes are involved in which functions. All clusters are included in the molecular function, whereas only five clusters are visible in cellular localization (cluster 1, 5, 10, 11, and cluster 13).

TABLE 3 | The gene tracing in a network where the primary network is broken down into subnetworks/clusters/modules is shown in this table.

Sr. No.	Module	Nodes	Edges	#Count	Gene of interest
1	Module 1	133	8061	4	RPL13, RPLP0, RPS2, RPS24
2	Module 5	44	231	3	MYC, COX7B, SOCS3
3	Module 6	36	126	2	MAP2K3, TNFSF10
4	Module 7	6	14	1	PER3
5	Module 8	25	67	1	IRAK3
6	Module 9	30	80	2	BCL6, HSPB1
7	Module 10	16	38	1	ENO1
8	Module 11	5	10	1	ATP1A1
9	Module 13	5	6	2	LYN, FCGR3A
10	Module 15	3	3	2	NPR3, NPPB

Ten modules out of fifteen have our gene of interest (seed genes). The table displays the number of nodes, edges, and genes in the specific module. Upregulation genes are shown in red, whereas downregulation genes are highlighted in green. There are a total of 19 genes that have been traced (11 downregulation and 8 up-regulation).

the reduced degree (degree – 1) of a node and the total reduced degree of all nodes at a distance d from the node is calculated as Collective Influence (CI). For the first time, this centrality metric is included in a R package. Two global centrality measures, betweenness centrality and collective influence, are among the most extensively used for identifying network influencers. Betweenness is the likelihood of a node in a network to be on the shortest path between nodes. Influencers of information flow inside a network are nodes with a high betweenness. Sometimes, we want to find the nodes that have the most potential for propagating information throughout the network, rather than the most influential nodes. ClusterRank, neighborhood connectedness, betweenness centrality, and collective impact all contribute to the spreading score, which is an integrative score made up of four separate centrality measurements. Also, one of the primary components of the IVI is the spreading score, which measures the spreading potential of each node within a network. In some circumstances, we wish to find out which nodes have the most sovereignty in their immediate surroundings. Hubness score is an integrative score comprised of two different centrality

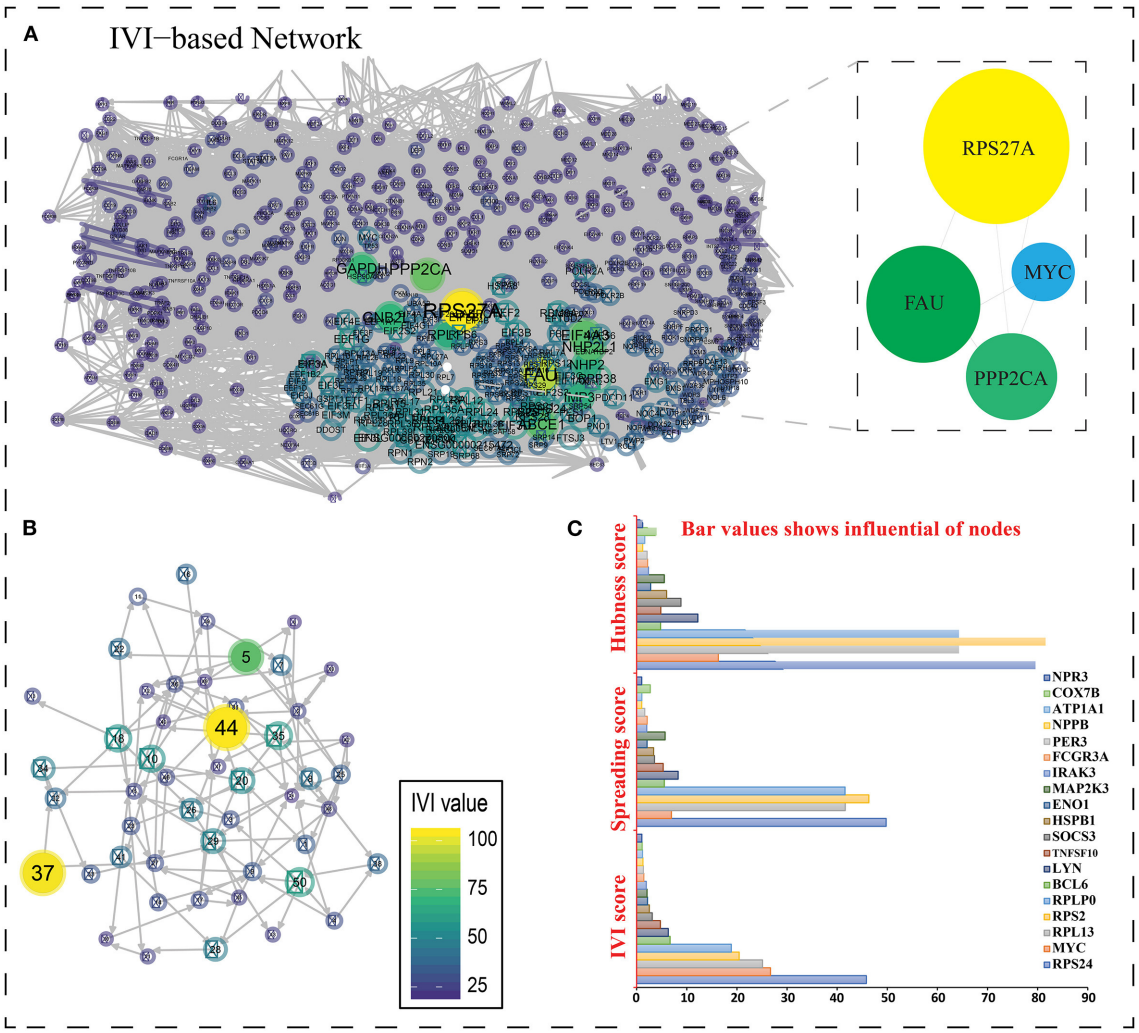

FIGURE 6 | (A) The most important nodes are shown in the network created with R and influential packages. Zooming closer on the nodes reveals their color and interaction. The nodes in the native network are mostly the same color, indicating that they have a score of <25. The values of nodes are represented using a color spectrum. If the nodes are yellow, it suggests they are larger in size and have values >75. **(B)** Higher values are represented by a larger IVI value representation with yellow color. **(C)** A bar graph depicting three scores (IVI-Score, Spreading Score, and Hubness Score) for 19 essential genes' hub nodes. RPS27A is the highest non-seed gene in all three scores, with a value of 100, whereas RPS24 is the top seed gene in two of them (IVI-Score and Spreading score), with values of 45.82538 and 49.77075, respectively. In hubness score 81.57813, RPS2 is the top seed gene. The most powerful node in the network is RPS27A (non-seed gene).

measures: degree centrality and local H-index (49). In addition, the Hubness score, which is one of the key components of the IVI, shows the power of each node in its surrounding environment (**Figure 5**).

DISCUSSION

The risk of CVD is increased with stages of CKD by promoting myocardial hypertrophy, coronary (CAD), atherosclerosis, and fluid overload. As the two most important organs of the body, the heart and kidneys work in close relation to each other. So, to unroll this methodical relationship at the molecular level, the present study was intervened. In this study, we have used integrated network-based approach and IVI methods to extracts the information (influential of nodes), hub genes, functions, and pathways. One of the limitations of this kind of study is that we have different cell and tissue types. Using p-adjustment is not the right choice under such circumstances as we did get no significant genes at 0.5 adjusted *P*-value for the GSE43484 and GSE67492. The current study is more like the meta-analysis of gene expression datasets using common microarray platforms which is quite widespread in many species. Apart from all the technicalities, the sharing of similar functions associated with transcripts of similar expression has persistently been used to annotate functions for humans in bioinformatics. Thus, using multiple datasets within functional premises governed by genes expressing in cell/tissue for a phenotype can be considered to involve similar pathways. This study retrieved 2,773 DEGs from

TABLE 4 | The top 20 nodes in the network were extract on the basis of IVI-score, spreading score, hubness score, CI score, and local HI score.

Sr. No.	Gene	IVI-value	Gene	Spreading score	Gene	Hubness score	CI	Gene	Local HI	Gene
1	RPS27A	100	RPS27A	100	RPS27A	100	1453138	EIF4G1	19288	RPS27A
2	FAU	86.54204	UBA52	66.35965	UBA52	83.6756	919132	FAU	17854	UBA52
3	PPP2CA	69.49985	EIF2S2	53.61083	RPS6	82.12102	910888	RPL10	17813	RPS6
4	EIF4A3	66.75017	EIF3M	53.49261	RPS2	81.57813	897390	RPL10A	17813	RPS2
5	ABCE1	65.97182	EIF3C	53.38627	RPS7	81.44018	866059	RPL10L	17792	RPS14
6	NHP2L1	64.97156	EIF3J	53.20541	RPS9	81.44018	862729	RPL11	17761	RPS7
7	GAPDH	61.76868	EIF2S1	53.19844	RPS14	81.30669	816804	RPL12	17692	RPS9
8	GNB2L1	60.52372	EIF3D	52.99297	RPS3	80.93769	806190	RPL13	17649	RPS3
9	IMP3	56.46971	EIF3K	52.99297	RPS18	80.63545	774473	RPL13A	17606	RPS11
10	NHP2	56.35967	EIF3B	52.53035	RPS11	80.50452	769952	RPL14	17606	RPS18
11	RPL11	55.67579	EIF5	52.38929	RPS27	80.35306	761514	RPL15	17606	RPS27
12	RPP38	51.82545	EIF3F	52.28384	RPS13	80.3332	751443	RPL17	17606	RPS13
13	EIF3D	46.9192	EIF3H	52.28384	RPS16	80.3332	681471	RPL18	17606	RPS15
14	RPS24	45.82538	EIF1AX	52.28095	RPS17	80.3332	674001	RPL18A	17606	RPS16
15	EEF1G	45.05756	PPP2CA	51.95736	RPS23	80.3332	646646	RPL19	17606	RPS17
16	BOP1	44.26816	RPS14	51.83609	RPS3A	80.3332	634176	RPL21	17606	RPS23
17	EIF3L	43.55821	RPS7	51.10068	RPS4X	80.3332	630175	RPL22	17598	RPS3A
18	RPL24	42.99506	RPS9	51.10068	RPS5	80.3332	624200	RPL22L1	17584	RPS4X
19	RPL14	42.20691	GNB2L1	50.96442	RPS8	80.3332	622336	RPL23	17548	RPS5
20	RPS28	41.40638	SEC61B	50.94699	RPS15	80.27672	621550	RPL23A	17548	RPS8

These 20 nodes/genes are the most important nodes in the network retrieved from IVI methods. Using versatile methods (IVI-methods), most influential network nodes can be detected.

11 GSE Series (6 CVD and 5 CKD) series with thousands of genes. The 2,873 genes were overlapped in both cases during the process of distinguishing between the significant genes. Finally, based on our filtering criterion, we got to 43 key (or seed) genes in both conditions (24 down and 19 up-regulated genes) represented by Venn diagram in **Figure 2**.

Our retrieved key genes might be of significance in understanding the pathological degree of CRS in a better way. The network was constructed from 43 seed genes (487 nodes and 12,027 edges) using String (a web tools) with an interaction score of 0.9, the network was then imported to Cytoscape (3.8.1) for further downstream analysis. Out of 43, only 19 seed genes (8 up and 11 downregulated genes) were retained by the native network.

To find the involvement of the DEG(s) at different levels in the constructed network, the native or primary network was further broken down to 15 subnetworks or modules using MCODE (MCODE parameters were used for network scoring and cluster finding, i.e., "Degree cutoff = 2," "node score cutoff = 0.2," "k-score = 2," and "max. depth = 100." Out of these 15 modules, 10 modules were found to have seed genes. Interestingly, Module 1 contains 4 downregulated (RPL13, RPLP0, RPS2) and one upregulated (RPS24) gene, module 5 contains one downregulated gene (MYC) and two (SOCS3, COX7B) upregulated genes, module 6 contains two genes, one (MAP2K3) downregulated and one (TNFSF10) up-regulated gene. Modules 7 and 8 consist of one downregulated (PER3) and one (IRAK3) up-regulated gene. Module 9 contains two genes, one BCL6 (upregulated) and one HSPB1 (downregulated). Module 10 contains one downregulated gene (ENO1). Module 11 contains the gene ATP1A1 (downregulated), and module 13 and 15 contain two genes each, namely, LYN, FCGR3A (downregulated) and NPR3, NPPB (up-regulated) as shown in **Table 3**. As the number of nodes and edges decreases, the MCODE score decreases as shown in **Figure 3**. A high MCODE score indicates that the nodes are well-connected (dense network). To further establish the stability and integrity of these modules, Hamiltonian energy was calculated using the formalism in the method section where low HE suggests less likely to remain stable under stress (say when seed genes are removed). Module 7 shows very low value of HE, while modules 8 and 9 bar indicate higher values than module 5 (see **Figure 3**). The decline of top to bottom indicates the hierarchy of nodes. Seed genes (19) were further studied for their functions (GO TERM) and pathways. These 19 genes were submitted to Metascape, an online database, to get an understanding of the biological processes, molecular functions, and pathways they represent. Gene ontology terms are a comprehensible input of terms organized into three categories: Molecular function, Biological Processes, and Protein Class. Thus, these extracted DEGs were submitted to ClueGO, a Cytoscape plug-in that facilitates the biological interpretation, functional differences, and visualizes functionally grouped terms in the form of networks, tables, and charts (**Figure 4**). It illustrates the clusters of 8 networks based on the color of the gene connections and the percentage of genes in each cluster. The seed gene count, *p*-value, and gene symbol, along with their GO-TERM are represented in the table.

Based on GO term enrichment, the highest represented a group of 8 genes (BCL6, ENO1, HSPB1, LYN, MYC, MAP2K3, SOCS3, and IRAK3) perform negative regulation of intracellular

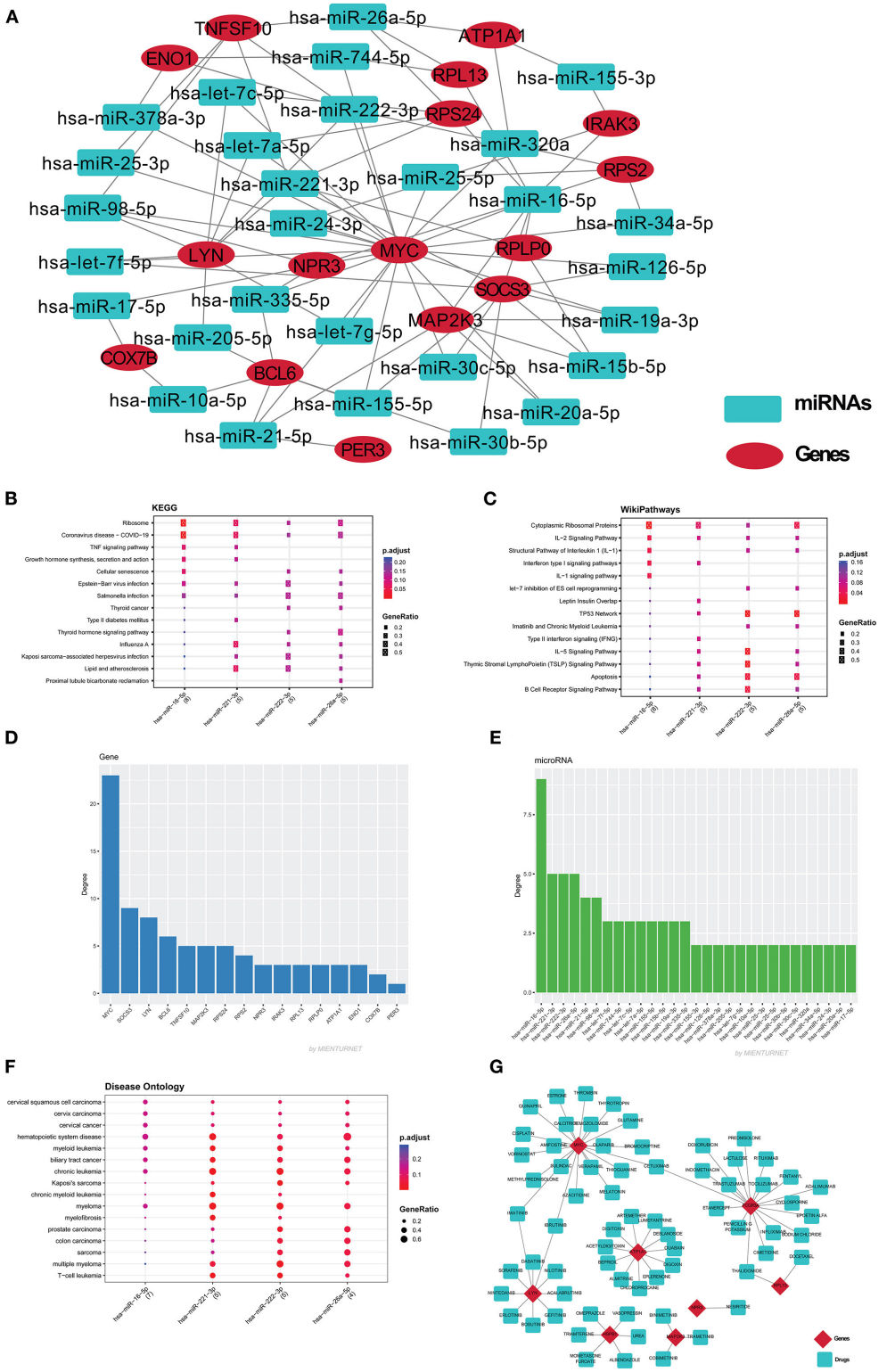

FIGURE 7 | (A) The miRNAs-mRNA network contains 47 nodes and 85 edges. Red color eclipse indicates genes, whereas, cyan color rectangle indicates their associated miRNAs. The mienturnet database also analyzes the major miRNAs pathways of key miRNAs. The degree of these four miRNAs was plotted against the KEGG pathways **(B)**, WikiPathways **(C)**, and disease ontology **(F)**. The bar plot shows the genes **(D)** and miRNA **(E)** based on degree centrality. **(G)** The gene-drug network was build using drug gene interaction database, which build the network of 78 nodes and 72 edges. Red color diamond for genes and cyan color for their drugs.

TABLE 5 | The scores of the 19 seed genes in the native network were determined.

Sr. No.	Gene	IVI score	Gene	SPD score	Gene	Hubness score
1	RPS24	45.82538	RPS24	49.77075	RPS2	81.57813
2	MYC	26.69248	RPS2	46.32048	RPS24	79.5567
3	RPL13	25.10682	RPL13	41.60822	RPL13	64.30335
4	RPS2	20.43554	RPLP0	41.56268	RPLP0	64.30078
5	RPLP0	18.87599	LYN	8.263571	MYC	16.28468
6	BCL6	6.661571	MYC	6.925186	LYN	12.20791
7	LYN	6.297702	MAP2K3	5.662946	SOCS3	8.827513
8	TNFSF10	4.720607	BCL6	5.502842	HSPB1	5.966899
9	SOCS3	3.093086	TNFSF10	5.278298	MAP2K3	5.497646
10	HSPB1	2.515714	SOCS3	3.546049	TNFSF10	4.816811
11	ENO1	2.15667	HSPB1	3.370381	BCL6	4.770602
12	MAP2K3	2.067014	COX7B	2.702907	COX7B	3.981947
13	IRAK3	1.913351	FCGR3A	2.099974	ENO1	2.789033
14	FCGR3A	1.432519	ENO1	2.067738	IRAK3	2.3437
15	PER3	1.328185	IRAK3	2.014448	FCGR3A	2.182645
16	NPPB	1.24651	PER3	1.614294	PER3	2.082526
17	ATP1A1	1.15923	ATP1A1	1.031002	ATP1A1	1.611522
18	COX7B	1.088852	NPPB	1	NPPB	1.19186
19	NPR3	1.030828	NPR3	1	NPR3	1.19186

RPS24 has the greatest score in the table, while NPR3 has the lowest.

signal transduction (GO:1902532) while the least suggested function is negative regulation of apoptotic signaling pathway (GO:2001234) (see **Figure 5A** for seed gene pathways), with circles indicating modules. The different pathways are indicated by the color of interaction between nodes. If a gene has multiple colors, it suggests that it plays multiple roles in different pathways. Genes that play a key role in the pathophysiology of various diseases could be useful biomarkers in future research. In cluster 5, the gene MYC has many colors and various connections via edges. Thus, it may be a more important gene as compared to others. While some seed genes, like RPS24 and RPS2, show only one type of color that suggests a unique function that also plays a key role (see **Figures 5B,C** for molecular functions and cellular location of seed genes). Following the PPIN and Gene enrichment analyses, we tried to find the most influential nodes, also known as hub nodes, using the IVI-value and other associated scores. The IVI values, hubness score, spreading score, and local HI index of the 19 seed nodes are displayed in the network. The non-seed genes, such as RPS27A and FAU, have the greatest values. In **Figure 6**, the size of the nodes and colors indicates higher to lower IVI value. If the nodes have a higher value than 100, the color will be yellow and circle size enlarge. The exact IVI-value of nodes is mentioned in **Table 4**. The spreader nodes are projected to have the largest impact on the flow of information throughout the network because they have high connections with other nodes inside the network. We took these influential nodes to add one more intermediate layer of information in the networks that reveal the interaction of genes and proteins through the intermediate miRNA that regulate the genes (**Figure 7**). Thus, giving us a glimpse of the underlying physiology of these two conditions that were cumulatively called CRS.

Furthermore, we used various other available tools for identifying the most influential nodes with IVI like based on its centrality measurements (9, 10). The DC is the simplest local centrality measure for a graph (degree centrality). Two global centrality measures, betweenness centrality, and collective influence, are among the most extensively used for identifying network influencers. Betweenness is the tendency of a node in a graph to be on the shortest path between nodes (1). Influencers of information flow inside a network are nodes with a high betweenness (11). The collective number of nodes that may be reached from a given node is measured by collective impact, a new global centrality metric. Neighborhood connectedness is a network's semi-local centrality measure that considers node connectivity (number of neighbors). It's called a semi-local measure because it's not limited to a node's immediate neighbors and considers the entire environment. The average connectivity of all neighbors of a vertex I is defined as its neighborhood connectivity. It is also said that a node's prominence in the network is determined by not only the number of first connections (degree centrality), but also the amount to which the nodes near neighbors are connected to each other and other nodes (neighborhood connectivity). The greatest value h such that there are at least h neighbors of a degree greater than or equal to h is defined as the H index of node i. The local H index is a semi-local centrality metric, despite its name, because it applies the H index centrality to a node's second order neighbors. All these centrality metrics (Hubness Score, Spreading Score, Degree Centrality, ClusterRank, local H index, neighborhood connectivity, betweenness centrality, and collective influence)

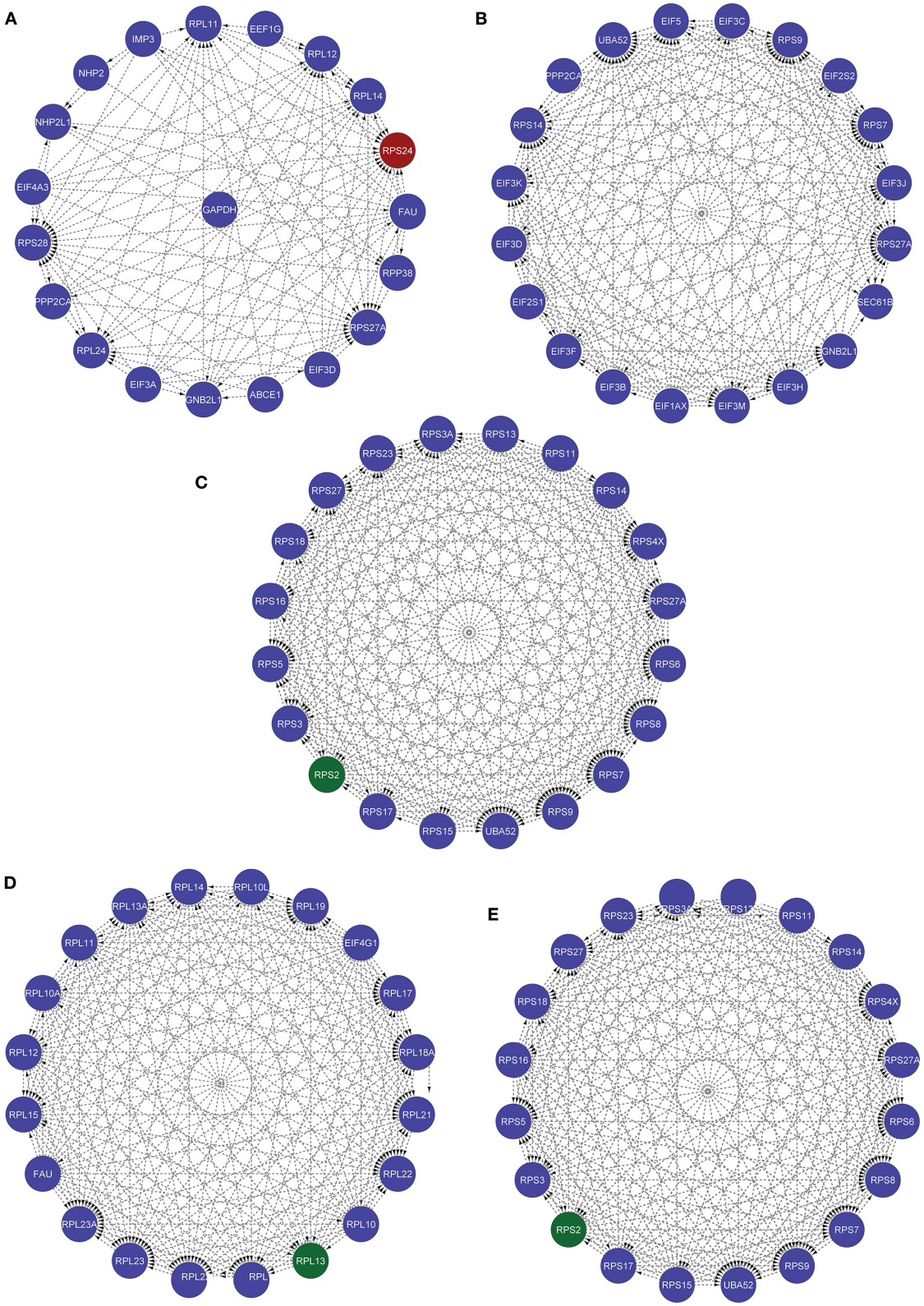

FIGURE 8 | These five networks containing the top 20 nodes were extracted from the native network using five centrality approaches. **(A)** Based on IVI method, RPS24 seed genes is present. **(B)** According to the Spreading Score, there are no seed genes in the top 20 nodes. **(C)** Local H index network, **(D)** collective influence network, **(E)** hubness score network with RPS2 seed gene.

are critical for identifying a network's most significant nodes (**Table 5**). Based on five centrality top 20 genes network extract from native network (**Figure 8**).

These results offer DEGs that may act as therapeutic targets for CVD and CKD in the future. This study reveals many aspects of CVD and CKD, such as gene-gene interaction, gene enrichment analysis, and pathways of hub genes. The hub genes may be the biomarker of the two conditions (CVD and CKD) need to be validated further but there are limitations such as few genes may be up-regulated and downregulated in the separate entity (means either in CVD or CKD). Maybe those genes are the key genes in CVD or CKD further research will reveal this gap. The study mainly focuses only on overlapped genes, despite all up and down genes. The non-seed genes are the most influential nodes in the network, not related to CVD and CKD. Because of the PPIN networks from the String database construct, the gene-gene interaction network using the source selected (human) and not disease specific genes interact with the seed genes. So, the study focuses only on the seed genes or related genes with the disease, but the results show the IVI -score, hubness score, and Spreading score, etc., of the non-seed genes (**Table 4**).

Our computational approach offers a comprehensive study, revealing the biomarkers of CVD and CKD using network approach and IVI methods (centrality measures), signifying the importance of nodes in the network, which help in Discover and understanding the various aspects of this disease. CKD Patients exhibit a pronounced risk for CVD events, utmost 50% of patients with CKD (stage 4 to 5) have CVD.

CONCLUSION

Evidence-based approach has always been the center of clinical studies, while *in-silico* approaches focus to produce that potential evidence based on past knowledge, thus making this integrated process fast and efficient. On the other hand, there is great efforts are ongoing with the aim of reducing CVD residual risk by developing reliable prognostic and predictive biomarkers. Apart from many challenges, finding seed genes is one of the first challenges and we have proposed a very simple and efficient way to do that using set theory. The resulting 43 seed genes (that defines the molecular relationship between CVD and CKD) can then be used to construct the GGiN (gene-gene interaction network) to uncover the possible biological and functional meaning. On the other hand, we have used IVI method to calculate the influence of the nodes in the network, which further minimizes the gene list to a more realistic one (that can be tested *in-vivo* or *vitro*). Our study finds 19 genes out of many for being more prominent in the CRS (published data), whereas many other genes show a good expressions level. Although, RPS27A, a non-seed gene, was found to be the most influential node in the network followed by RPS2 and MYC. Based on these findings, new validation experiments can be constructed to further prove these as markers or good drug targets. Thus, giving us an opportunity to reduce the risks of CKD and CVD.

DATA AVAILABILITY STATEMENT

The datasets presented in this study can be found in online repositories. The names of the repository/repositories and accession number(s) can be found in the article/**Supplementary Material**.

AUTHOR CONTRIBUTIONS

MA and RI conceptualized the work. MA and AA did data curation. MA, RA, SH, and AS prepared the figures. MA, RA, ST, AA, SA, and RI wrote the manuscript. HB, SA, MA, RI, and RB revised the manuscript. All authors contributed to the article and approved the submitted version.

FUNDING

MA, ST, and RA were financially supported by the Indian Council of Medical Research, Government of India under Senior Research Fellow. FTS No. ISRM 11/(04)/2019. AA financially was supported by the Department of Health and Research, (DHR) Ministry of Health and Family Welfare, Government of India under young scientist F.No. 12014/06/2019-HR.

SUPPLEMENTARY MATERIAL

The Supplementary Material for this article can be found online at: https://www.frontiersin.org/articles/10.3389/fcvm.2021.755321/full#supplementary-material

Supplementary Table 1 | In cardiovascular disease (CVD) and chronic kidney disease (CKD), total DEGs were gathered from 11 GSE series, as well as up and down common genes.

Supplementary Table 2 | All genes rank order via Integrated Value of Influence (IVI) values.

REFERENCES

1. Jankowski J, Floege J, Fliser D, Böhm M, Marx N. Cardiovascular disease in chronic kidney disease: pathophysiological insights and therapeutic options. *Circulation.* (2021) 143:1157–72. doi: 10.1161/CIRCULATIONAHA.120.050686
2. Webster AC, Nagler EV, Morton RL, Masson P. Chronic kidney disease. *Lancet.* (2017) 389:1238–52. doi: 10.1016/S0140-6736(16)32064-5
3. Rysz J, Gluba-Brzózka A, Rysz-Górzyńska M, Franczyk B. The role and function of HDL in patients with chronic kidney disease and the risk of cardiovascular disease. *Int J Mol Sci.* (2020) 21:601. doi: 10.3390/ijms21020601
4. Carracedo J, Alique M, Vida C, Bodega G, Ceprián N, Morales E, et al. Mechanisms of cardiovascular disorders in patients with chronic kidney disease: a process related to accelerated senescence. *Front Cell Dev Biol.* (2020) 8:185. doi: 10.3389/fcell.2020.00185
5. Saritas T, Floege J. Cardiovascular disease in patients with chronic kidney disease. *Herz.* (2020) 45:122–8. doi: 10.1007/s00059-019-04884-0

6. Kelly DM, Rothwell PM. Does chronic kidney disease predict stroke risk independent of blood pressure? A systematic review and meta-regression. *Stroke.* (2019) 50:3085–92. doi: 10.1161/STROKEAHA.119.025442
7. Pálsson R, Patel UD. Cardiovascular complications of diabetic kidney disease. *Adv Chronic Kidney Dis.* (2014) 21:273–80. doi: 10.1053/j.ackd.2014.03.003
8. Murray CJL. The state of US health, 1990-2010: burden of diseases, injuries, and risk factors. *JAMA.* (2013) 310:591–606. doi: 10.1001/jama.2013.13805
9. Romagnani P, Remuzzi G, Glassock R, Levin A, Jager KJ, Tonelli M, et al. Chronic kidney disease. *Nat Rev Dis Primer.* (2017) 3:17088. doi: 10.1038/nrdp.2017.88
10. Wang X, Gulbahce N, Yu H. Network-based methods for human disease gene prediction. *Brief Funct Genomics.* (2011) 10:280–93. doi: 10.1093/bfgp/elr024
11. Simpson SL, Bowman FD, Laurienti PJ. Analyzing complex functional brain networks: fusing statistics and network science to understand the brain. *Stat Surv.* (2013) 7:1–366. doi: 10.1214/13-SS103
12. Joshi A, Rienks M, Theofilatos K, Mayr M. Systems biology in cardiovascular disease: a multiomics approach. *Nat Rev Cardiol.* (2021) 18:313–30. doi: 10.1038/s41569-020-00477-1
13. Salavaty A, Ramialison M, Currie PD. Integrated value of influence: an integrative method for the identification of the most influential nodes within networks. *Patterns.* (2020) 1:100052. doi: 10.1016/j.patter.2020.100052
14. Meghanathan N. Neighborhood-based bridge node centrality tuple for complex network analysis. *Appl Netw Sci.* (2021) 6:47. doi: 10.1007/s41109-021-00388-1
15. Ashtiani M, Salehzadeh-Yazdi A, Razaghi-Moghadam Z, Hennig H, Wolkenhauer O, Mirzaie M, et al. A systematic survey of centrality measures for protein-protein interaction networks. *BMC Syst Biol.* (2018) 12:80. doi: 10.1186/s12918-018-0598-2
16. Devarbhavi P, Telang L, Vastrad B, Tengli A, Vastrad C, Kottureshetti I. Identification of key pathways and genes in polycystic ovary syndrome via integrated bioinformatics analysis and prediction of small therapeutic molecules. *Reprod Biol Endocrinol.* (2021) 19:31. doi: 10.1186/s12958-021-00706-3
17. Prashanth G, Vastrad B, Tengli A, Vastrad C, Kottureshetti I. Investigation of candidate genes and mechanisms underlying obesity associated type 2 diabetes mellitus using bioinformatics analysis and screening of small drug molecules. *BMC Endocr Disord.* (2021) 21:80. doi: 10.1186/s12902-021-00718-5
18. Fajarda O, Duarte-Pereira S, Silva RM, Oliveira JL. Merging microarray studies to identify a common gene expression signature to several structural heart diseases. *BioData Min.* (2020) 13:8. doi: 10.1186/s13040-020-00217-8
19. Mou T, Zhu D, Wei X, Li T, Zheng D, Pu J, et al. Identification and interaction analysis of key genes and microRNAs in hepatocellular carcinoma by bioinformatics analysis. *World J Surg Oncol.* (2017) 15:63. doi: 10.1186/s12957-017-1127-2
20. Afroz S, Giddaluru J, Vishwakarma S, Naz S, Khan AA, Khan N. A comprehensive gene expression meta-analysis identifies novel immune signatures in rheumatoid arthritis patients. *Front Immunol.* (2017) 8:74. doi: 10.3389/fimmu.2017.00074
21. Pavlopoulos GA, Kontou PI, Pavlopoulou A, Bouyioukos C, Markou E, Bagos PG. Bipartite graphs in systems biology and medicine: a survey of methods and applications. *GigaScience.* (2018) 7:giy014. doi: 10.1093/gigascience/giy014
22. Szklarczyk D, Morris JH, Cook H, Kuhn M, Wyder S, Simonovic M, et al. The STRING database in 2017: quality-controlled protein–protein association networks, made broadly accessible. *Nucleic Acids Res.* (2017) 45:D362–8. doi: 10.1093/nar/gkw937
23. Niu X, Zhang J, Zhang L, Hou Y, Pu S, Chu A, et al. Weighted gene co-expression network analysis identifies critical genes in the development of heart failure after acute myocardial infarction. *Front Genet.* (2019) 10:1214. doi: 10.3389/fgene.2019.01214
24. Udhaya Kumar S, Thirumal Kumar D, Siva R, George Priya Doss C, Younes S, Younes N, et al. Dysregulation of signaling pathways due to differentially expressed genes from the B-cell transcriptomes of systemic lupus erythematosus patients – a bioinformatics approach. *Front Bioeng Biotechnol.* (2020) 8:276. doi: 10.3389/fbioe.2020.00276
25. Koh GCKW, Porras P, Aranda B, Hermjakob H, Orchard SE. Analyzing protein–protein interaction networks. *J Proteome Res.* (2012) 11:2014–31. doi: 10.1021/pr201211w
26. Gao L, Sun P-G, Song J. Clustering algorithms for detecting functional modules in protein interaction networks. *J Bioinform Comput Biol.* (2009) 07:217–42. doi: 10.1142/S0219720009004023
27. Shih Y-K, Parthasarathy S. Identifying functional modules in interaction networks through overlapping Markov clustering. *Bioinformatics.* (2012) 28:i473–9. doi: 10.1093/bioinformatics/bts370
28. Bernot G, Comet J-P, Richard A, Chaves M, Gouzé J-L, Dayan F. Modeling analysis of gene regulatory networks. In Cazals F, Kornprobst P, editors. *Modeling in Computational Biology Biomedicine*. Berlin; Heidelberg: Springer (2013). p. 47–80. doi: 10.1007/978-3-642-31208-3_2
29. Dubovenko A, Nikolsky Y, Rakhmatulin E, Nikolskaya T. Functional analysis of OMICs data small molecule compounds in an integrated 'knowledge-based' platform. In: Tatarinova TV, Nikolsky Y, editors. *Biological Networks Pathway Analysis Methods in Molecular Biology*. New York, NY: Springer (2017). p. 101–124. doi: 10.1007/978-1-4939-7027-8_6
30. Gao Y, Zhang S, Zhang Y, Qian J. Identification of microRNA-target gene-transcription factor regulatory networks in colorectal adenoma using microarray expression data. *Front Genet.* (2020) 11:463. doi: 10.3389/fgene.2020.00463
31. Bindea G, Mlecnik B, Hackl H, Charoentong P, Tosolini M, Kirilovsky A, et al. ClueGO: a Cytoscape plug-in to decipher functionally grouped gene ontology and pathway annotation networks. *Bioinformatics.* (2009) 25:1091–3. doi: 10.1093/bioinformatics/btp101
32. Zhou Y, Zhou B, Pache L, Chang M, Khodabakhshi AH, Tanaseichuk O, et al. Metascape provides a biologist-oriented resource for the analysis of systems-level datasets. *Nat Commun.* (2019) 10:1523. doi: 10.1038/s41467-019-09234-6
33. Jia Z-Y, Xia Y, Tong D, Yao J, Chen H-Q, Yang J. Module-based functional pathway enrichment analysis of a protein-protein interaction network to study the effects of intestinal microbiota depletion in mice. *Mol Med Rep.* (2014) 9:2205–12. doi: 10.3892/mmr.2014.2137
34. Haider S, Ponnusamy K, Singh RKB, Chakraborti A, Bamezai RNK. Hamiltonian energy as an efficient approach to identify the significant key regulators in biological networks. *PLoS ONE.* (2019) 14:e0221463. doi: 10.1371/journal.pone.0221463
35. Wang X, Yang Q, Liu M, Ma X. Comprehensive influence of topological location and neighbor information on identifying influential nodes in complex networks. *PLoS ONE.* (2021) 16:e0251208. doi: 10.1371/journal.pone.0251208
36. Kim H, Davies P, Walker SI. New scaling relation for information transfer in biological networks. *J R Soc Interface.* (2015) 12:20150944. doi: 10.1098/rsif.2015.0944
37. Li Z, Ren T, Ma X, Liu S, Zhang Y, Zhou T. Identifying influential spreaders by gravity model. *Sci Rep.* (2019) 9:8387. doi: 10.1038/s41598-019-44930-9
38. Jalili M, Gebhardt T, Wolkenhauer O, Salehzadeh-Yazdi A. Unveiling network-based functional features through integration of gene expression into protein networks. *Biochim Biophys Acta BBA Mol Basis Dis.* (2018) 1864:2349–59. doi: 10.1016/j.bbadis.2018.02.010
39. Ozgur A, Vu T, Erkan G, Radev DR. Identifying gene-disease associations using centrality on a literature mined gene-interaction network. *Bioinformatics.* (2008) 24:i277–85. doi: 10.1093/bioinformatics/btn182
40. Bashan A, Bartsch RP, Kantelhardt JW, Havlin S, Ivanov PCH. Network physiology reveals relations between network topology and physiological function. *Nat Commun.* (2012) 3:702. doi: 10.1038/ncomms1705
41. Bindea G, Galon J, Mlecnik B. CluePedia Cytoscape plugin: pathway insights using integrated experimental and *in silico* data. *Bioinformatics.* (2013) 29:661–3. doi: 10.1093/bioinformatics/btt019
42. Bezabih G, Cheng H, Han B, Feng M, Xue Y, Hu H, et al. Phosphoproteome analysis reveals phosphorylation underpinnings in the brains of nurse and forager honeybees (*Apis mellifera*). *Sci Rep.* (2017) 7:1973. doi: 10.1038/s41598-017-02192-3
43. Bohler A, Wu G, Kutmon M, Pradhana LA, Coort SL, Hanspers K, et al. Reactome from a WikiPathways perspective. *PLoS Comput Biol.* (2016) 12:e1004941. doi: 10.1371/journal.pcbi.1004941

44. Meunier D, Lambiotte R, Bullmore ET. Modular and hierarchically modular organization of brain networks. *Front Neurosci.* (2010) 4:200. doi: 10.3389/fnins.2010.00200
45. Finc K, Bonna K, He X, Lydon-Staley DM, Kühn S, Duch W, et al. Dynamic reconfiguration of functional brain networks during working memory training. *Nat Commun.* (2020) 11:2435. doi: 10.1038/s41467-020-15631-z
46. Ali S, Malik MDZ, Singh SS, Chirom K, Ishrat R, Singh RKB. Exploring novel key regulators in breast cancer network. *PLoS ONE.* (2018) 13:e0198525. doi: 10.1371/journal.pone.0198525
47. Mistry D, Wise RP, Dickerson JA. DiffSLC: a graph centrality method to detect essential proteins of a protein-protein interaction network. *PLoS ONE.* (2017) 12:e0187091. doi: 10.1371/journal.pone.0187091
48. Qiao T, Shan W, Zhou C. How to identify the most powerful node in complex networks? A novel entropy centrality approach. *Entropy.* (2017) 19:614. doi: 10.3390/e19110614
49. Singh A, Singh RR, Iyengar SRS. Node-weighted centrality: a new way of centrality hybridization. *Comput Soc Netw.* (2020) 7:6. doi: 10.1186/s40649-020-00081-w

Conflict of Interest: The authors declare that the research was conducted in the absence of any commercial or financial relationships that could be construed as a potential conflict of interest.

The reviewer MA declared a shared affiliation, with six of the authors MA, ST, RA, MS, AA, and RI to the handling editor at the time of the review.

Advantages of publishing in Frontiers

OPEN ACCESS
Articles are free to read for greatest visibility and readership

FAST PUBLICATION
Around 90 days from submission to decision

HIGH QUALITY PEER-REVIEW
Rigorous, collaborative, and constructive peer-review

TRANSPARENT PEER-REVIEW
Editors and reviewers acknowledged by name on published articles

Frontiers
Avenue du Tribunal-Fédéral 34
1005 Lausanne | Switzerland

Visit us: www.frontiersin.org
Contact us: frontiersin.org/about/contact

REPRODUCIBILITY OF RESEARCH
Support open data and methods to enhance research reproducibility

DIGITAL PUBLISHING
Articles designed for optimal readership across devices

FOLLOW US
@frontiersin

IMPACT METRICS
Advanced article metrics track visibility across digital media

EXTENSIVE PROMOTION
Marketing and promotion of impactful research

LOOP RESEARCH NETWORK
Our network increases your article's readership